Italian National Agency for New Technologies, Energy and Sustainable Economic Development

SFERA III Project

ENEA activities on CSP technology

On-site training for industries Molten Salt Systems CSP plants

7ht – 11th November 2022

Walter Gaggioli walter.gaggioli@enea.it

ENEA RESEARCH & DEVELOPMENT: 4 DEPARTMENTS

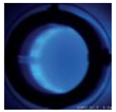

Fusion & Nuclear safety

- Fusion
- Fission (new gen)
- Radiation protection
- Nuclear safety & security
- Ionizing/non ionizing radiation applications

Energy technologies

- CSP and thermal solar energy, including thermal energy storage
- Photovoltaics
- Smart grids (incl HVDC)
- Efficient conversion and use of energy, electric energy storage, fuel cells
- Bioenergy, biorefinery and green chemistry
- Smart energy & smart cities
- Sustainable mobility
- Sustainable use of fossil fuels
- ICT

Sustainability of territorial systems

- Resource efficiency
- Environmental technologies
- Climate change: modeling, adaptation and mitigation
- Prevention and Recovery
- Seismic and natural hazards assessment and prevention
- Bio and nanotechs
- Agrifood
- Circular economy

Energy Efficiency

- Building diagnoses
- NZEB
- Energy efficiency in industry, public and private buildings
- Covenant of Mayors
- Diffusion of energy efficiency consciousness

Solar Thermal and Smart Network Division (TERIN STSN)

The division works under *supervision of the Department Energy Technologies and Renewable Sources (TERIN)*

The infrastructures are distributed among three ENEA research centers: **Casaccia, Portici and Trisaia**

Responsible of division: PhD Walter Gaggioli (walter.gaggioli@enea.it)

Main Challenge: support the decarbonisation process of energy networks and industrial processes

3 laboratories:

Solar Technology Engineering Laboratory (TERIN-STSN-ITES) – Responsible ***PhD Valeria Russo*** (valeria.russo@enea.it)

Components development laboratory for solar systems TERIN-STSN-SCIS) – Responsible ***PhD Michela Lanchi*** (michela.lanchi@enea.it)

Smart Grid and Energy Networks Laboratory (TERIN-STSN-SGRE) – Responsible ***PhD Maria Valenti*** (maria.valenti@enea.it)

Work force of the division: 70 people

Solar Thermal and Smart Network Division (TERIN STSN)

Laboratory TERIN-STSN-ITES - Solar Technology Engineering Laboratory: development and validation of models for CSP applications, management of experimental CSP plants, design and managinig of experimental tests; Advanced engineering services for CSP commercial plants, characterization and quality control of the optics of solar concentrators, accredited laboratory for Qualification and certification solar components)

Laboratory TERIN-STSN-SCIS – Solar Components and Plants Development Laboratory: study, analysis, research and development of materials, components and methodologies for solar systems: receiver tubes and mirrors (coatings), thermal storage systems (sensible and latent heat materials), thermochemical storage (metal oxide and carbonates), solar chemistry systems (hydrogen and solar fuels production), development and validation of models for CSP applications.

Laboratory TERIN-STSN-SGRE - Smart Grid and Energy Networks Laboratory: study, analysis, research and development of technologies, methodologies and devices for applications in the Smart Grid sector and energy grids and micro-grids in the presence of distributed power generation and energy storage, and for the integration of renewable sources into the grid, flexible management of production and demand and the provision of ancillary services.

Solar Thermal and Smart Network Division (TERIN STSN)

Research

Design

Development

Test & Validation

Research activities

Research Infrastructures (Casaccia, Portici, Trisaia)

Materials, components and systems for CST plants (improvement of energy performance and economic competitiveness; integration with energy networks)

Thermal storage systems serving electrical and thermal networks (improvement of dispatchability and smart grid integration)

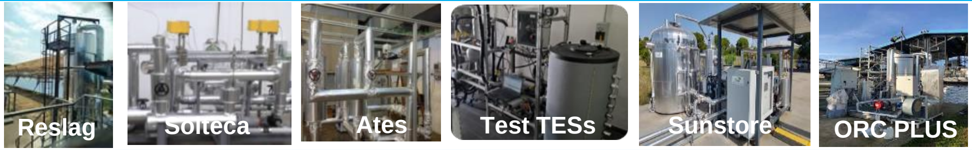

Components and systems for the production of **solar fuels and heat supply at medium and high temperatures for industrial processes**

Components and systems for **smart multi-vector energy networks** (smart networks for energy communities, CST serving the networks)

Support to the industrial system: **component qualification and advanced engineering services**

ENEA

Solar Thermal and Smart Network Division (TERIN STSN)

Main running projects

SOLAR GRID (PON)

Development of innovative solutions for CSP and PV plants (**cogeneration and grid flexibility**)

SALTOPOWER (HORIZON EUROPE)

Development of molten salt solar technology, solar chemistry (networking, training, research)

Advanced engineering services

ENI: Development of high temperature thermal storage systems - FATA: Engineering services for the construction of CSP plants

RdS

MINISTERO DELLA TRANSIZIONE ECOLOGICA

Project 1.9: Solar Thermodynamic
Project 1.3: WP Hydrogen Production
Project 1.2: WP Thermal storage
Project 2.1: Cybersecurity for energy systems
Project 2.3: New models for improving adequacy, security and resilience of power systems

PIANO NAZIONALE DI RIPRESA E RESILIENZA

Participation in PNRR projects: Rome Technopole, RAISE

ENEA

PNRR H2

PIANO NAZIONALE DI RIPRESA E RESILIENZA

LA 1.1.33: Thermochemical cycles; LA 1.2.1: Development of high temperature hydrogen separation membranes

EuroPaTMoS (ERANET)

Development of new components and operating procedures for molten salt solar plants.

eNeuron (H2020)

Development of innovative tools for the optimal management of energy communities.

SFERA III (H2020)

Collaboration with the European industrial system and development of joint research

HYROGEN PROJECT (POR)

WP1: production

LA1.2.3 Development of non-programmable renewable energy production forecasting models.

WP4: Integration of hydrogen into networks

LA 4.1.1, LA 4.1.2; LA 4.2.1; LA 4.3.1, LA 4.3.7: Development of technologies, systems and guidelines for the smart management of hydrogen generation, storage and use equipment interfaced with energy networks.

MISSION INNOVATION

Study of the potential and role of smart multienergy microgrids for enabling energy transition.

HEXERGY RdS bando B

Sviluppo e validazione accumuli termici basati su vapore/zeolite per calore processi industriali.

ENEA's ACTIVITIES ON CSP/CST TECHNOLOGY

ENEA Facilities (Casaccia Research Centre – Rome)

Molten salts tecnology

PCS Test facility, MoSE plant Chemical Solar laboratory, corrosion test facility

Thermal Storage systems

Molten salt (Low , high temperatures) thermocline with and without filler, PCM, concrete, thermochemical storage (RESLAG, ORC-PLUS; ATES, SOLTECA facilities)

Heat for Industrial Processes

PCS, MoSE, OMSoP,ENEA Ship plant

Components qualification

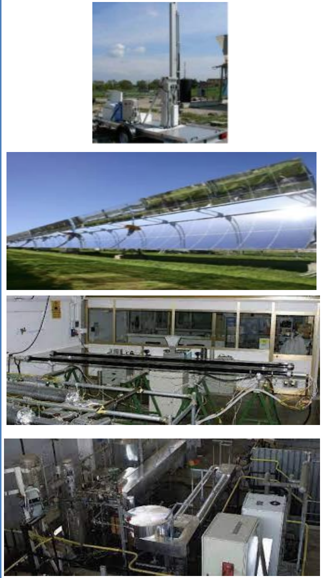

PCS, MoSE plants, Optical test bench facilities, test bench Receiver tubes

Solar Chemistry

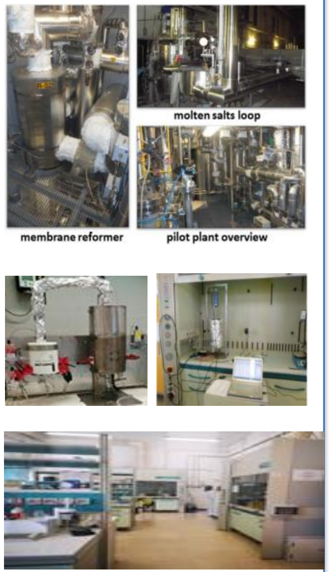

Comethy plant, Chemical Solar laboratory

The ENEA approach to CSP technology

Test facility PCS

Lab R&D

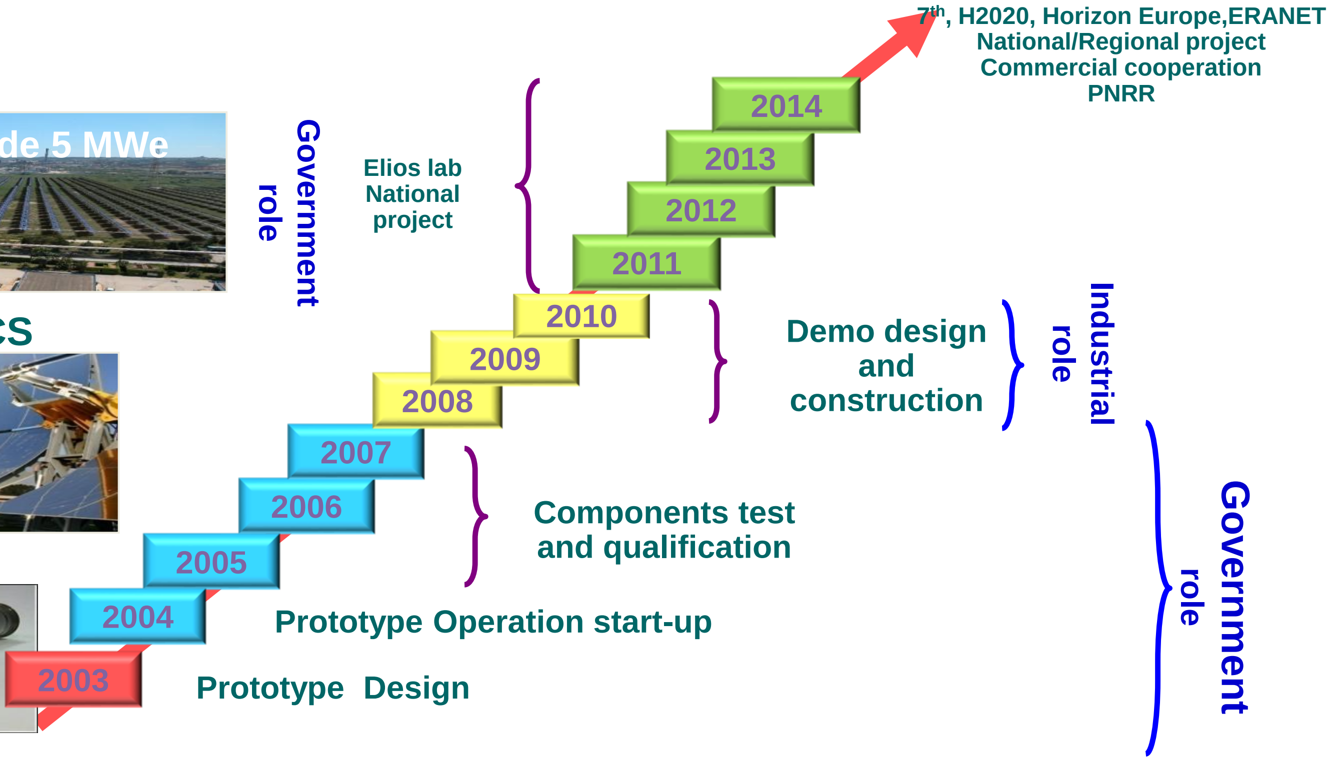

ENEA's innovation on the use of MS in linear CSP

ENEA innovation since 2000: Double tanks using molten salts as HTF and HSM

ENEA technology

Commercial plants based on oil as HTF and MS as HSM

CSP oil + MS

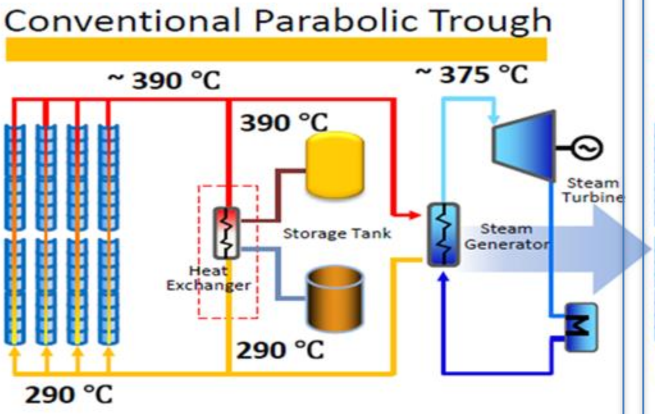

HTF: oil
HSM: molten salt
Min-Max T: 290-390°C
ΔT: 100°C

ENEA concept CSP MS + MS

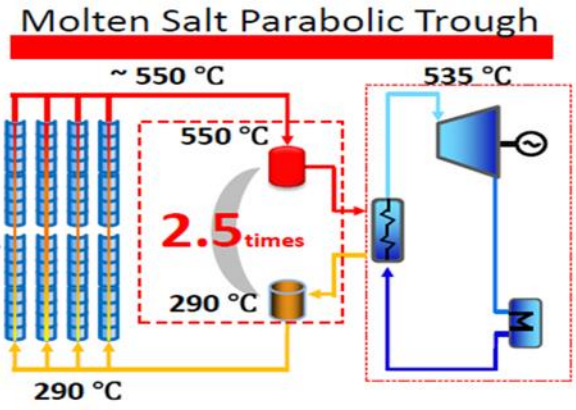

HTF: molten salt
HSM: molten salt
Min-Max T: 290- 550°C
ΔT: 260°C

Achievements:

- **Reduction of the size** of the thermal storage system by increasing the ΔT of the thermal cycle **(2,5 times)**;
- **Removal of the heat exchanger** between the HTF and the storage system.
- Realization of real scale **experimental facilities in Italy**

PCS FACILITY

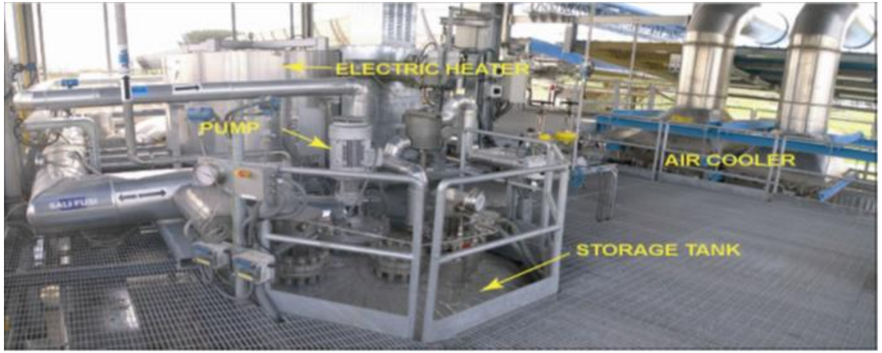

- Built at ENEA Casaccia National Labs (Rome) technologies at 2003-2004
- 10 years of operation
- Experimental tests of various components
- 55,000+ hr operation in hot stand by condition
- 1400+ filling/draining cycles
- 9500+ hr operation with circulation of molten salts
- 2014 – PCS has got renew of operating license

The PCS has exceeded the ten-year tests for pressure vessels of the Italian National Agency for the safety of work

PCS FACILITY

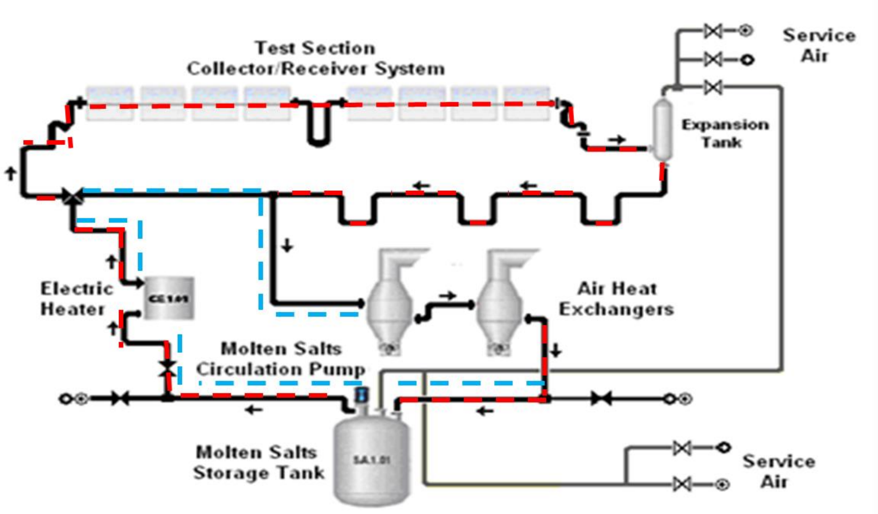

Description	values	u.m.
Fluid Type	Salts mixture	
40% KNO3 – 60% NaNO3		
Flow rate min / max	4,5 / 6,5	kg/s
Temperature min / max	270 /550	° C
Pressure pump delivery side	0,8	MPa
Storage tank:		
diameter	2	m
height	2,8	m
design pressure	0,2	MPa
electric heaters power	100	KW
stored salts quantity	12000	Kg
Heater max electric power	400	kW
Air exchangers max thermal power	400	kW
Test Section nominal length	100	m
Test Section mirrors surface	540	m^2

Electric heating systems

- Electric heater: Joule effect (400kW)
- Piping, valves, flanges: Mineral Insulated cable (26kW)
- Heat collecting Element : Joule effect 150 kW
- Air coolers: Joule effect (100 kW)
- Storage tank: internal heaters: 50kW - External heaters: MI cable (16 kW)

OMSoP FACILITY

Coupling Dish/MGT

PILOT PLANT (5 kWe) – ENEA Casaccia Research Centre

Innovative system for greater reliability, compactness, low costs

Commercial target: Domestic applications and small commercial users (3-10 kW) / modular approach for higher capacities

Main innovation:

- Replacement of the Stirling engine with Micro Gas Turbine (from automotive sector): original design, high T, recuperative Brayton cycle;
- Receiver: high temperature (800° C), compact design, possible heat storage

Objectives: *I*ntegration of Micro Gas Turbine technology (MGT) with concentrated solar systems to produce electricity, but also thermal energy (cogeneration)

ENEA ACTIVITIES ON CSP

Focus: centralized and distributed generation and cogeneration

Objective 1. Innovative solutions development for increasing efficiency and reducing energy production cost

Activity lines

a. Development and testing of innovative components & Systems (receiver tube, coating, mirror surfaces, new heat transfer fluids, industrial plants technical advisor)

b. Development of solar fuels production processes (hydrogen through solar source, thermochemical, hybrids)

c. Development and qualification of CST technology for the provision of Solar Heat for Industrial Processes (agro-food, iron and steel, textile, chemical, etc.)

ENEA

ENEA ACTIVITIES ON CSP

Focus: centralized and distributed generation and cogeneration

Objective 2. Innovative solutions development related to solar thermal energy storage for dispatchability and provision of ancillary network services.

Activity lines:

d. **Research and development of technologies, methodologies and devices for applications in the Smart Grid sector and energy grids and micro-grids also in presence of high levels of renewable energy sources and for the integration of CSP into the grid + Forecast of solar radiation**

e. **Study, development and testing of smart advanced techniques, methods and devices to facilitate a secure, reliable, and efficient operation of energy systems, R&D on components, materials and processes for low-medium-high temperature Thermal energy storage advanced systems:**

- **sensible heat (double tanks with Molten Salt as HTF & HSM, thermocline, concrete)**
- **Phase Change Materials (PCM);**
- **Tthermochemical storage (in view of a seasonal storage too);**

ENEA

ENEA ACTIVITIES ON CSP

Activity line A: Development of innovative components/systems

International cooperation & industrial transfer technology

ENEA as Technical advisor for commercial projects

Partanna Plant mid-size Molten salt CSP plant (4MWe + 16h thermal storage)

Stromboli Plant mid-size Molten salt CSP plant (4MWe + 16h thermal storage)

ENEA as coordinator of EU projects

MATS plant – Borg el Arab in Egypt (2018)

1 MWe + 250 m^3/d of desalinated water

Involvement of Egyptian Government, agencies and Italian companies. Budget of about 22 M€)

ORC-PLUS plant – Green Energy Park in Morocco (2019)

1 MWe + 4h thermal storage

Involvement, agencies and Italian companies. Project was coordinated by ENEA (budget of about 7 M€)

ENEA

ENEA ACTIVITIES ON CSP

Activity line A: Development of innovative components/systems

Solar Collector Optics Laboratory

main activities
characterization and quality control of solar concentrators for producers and users of CSP systems. The measurements are carried out in compliance with state-of-the-art international procedures and guidelines, using advanced and innovative methods and tools.

Regarding the characterization of the mirrors, the main parameters investigated are:
1) solar reflectance; 2) the 3D shape of the reflective surface.

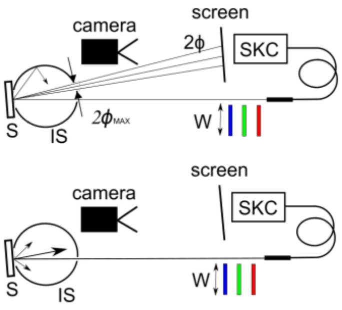

SMQ2 measurement system

VIS field measurement in field measurement setup

ENEA ACTIVITIES ON CSP

Activity line A: Development of innovative components/systems

Test Bench for the heat loss measurements

- **Characterization** and quality control receiver tubes for high temperature;
- **Evaluation of the heat loss** measuring the electric power per unit length (W/m), required to maintain at steady state the temperature of the steel tube;
- **Evaluation of the emittance** of the absorber coating as function of the steel tube temperature;
- Round Robin tests

Test bench Receiver tubes

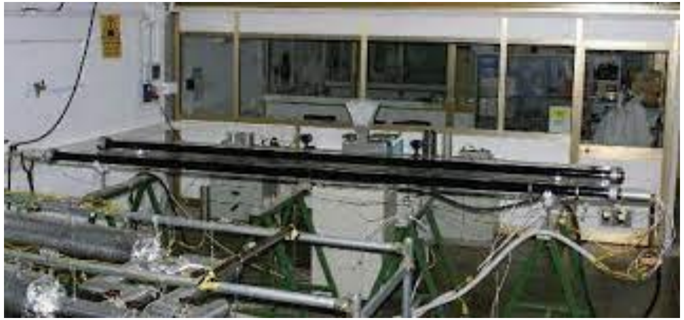

Test Bench for melting/freezing tests

- **Evaluation of the time range** necessary for the complete solidification/melting of the mixture
- Analysis of the **receiver behavior during abnormal operating conditions** and in case of blocking of molten salts circulation
- **Definition of the operating procedures** in order to prevent damage

ENEA

ENEA ACTIVITIES ON CSP

Activity line A: Development of innovative components/systems

Test Bench for melting/freezing tests

- **Evaluation of the time range** necessary for the complete solidification/melting of the mixture;

- Analysis of the **receiver behavior during abnormal operating conditions** and in case of blocking of molten salts circulation;

- **Definition of the operating procedures** in order to prevent damage caused by the natural expansion of the salt volume

Test bench Receiver tubes

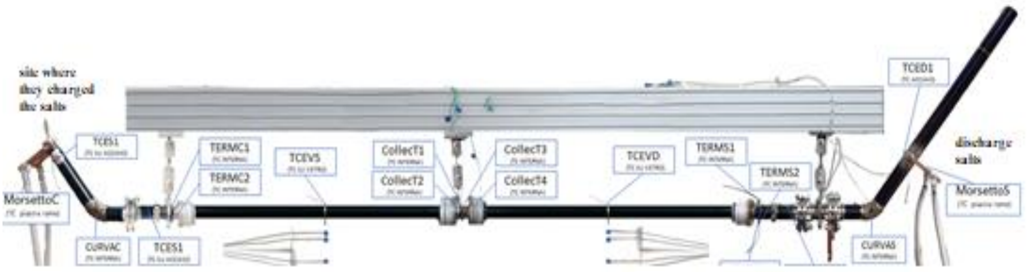

SOLAR PLANT COMPONENTS

Activity line A: Development of spectrally selective coatings

ENEA Past activities

Development of high performance solar coatings for **medium (400°C)** and **high (550°C)** temperature applications under vacuum based on the double-nitride cermet.

ENEA technology of the double-nitride cermet

- ✓ Simple, repeatable and robust deposition processes
- ✓ High deposition rate/ low cost fabrication process suitable for ind. production

Photothermal performance for evacuated receiver tube operating at 400 °C:

$\alpha_s \geq 96.0\%$ and $\varepsilon_{th} \leq 8.5\%$ at 400°C

Installed on "DUBA 1" in Saudi Arabia

Photothermal performance for evacuated receiver tube operating at 550 °C:

$\alpha_s \geq 95.0\%$ and $\varepsilon_{th} \leq 10.5\%$ at 550°C

Installed on "AKESAI" in China,
"MATS" in Egypt, "Partanna" in Italy

ENEA

SOLAR PLANT COMPONENTS

Activity line A: Development of spectrally selective coatings

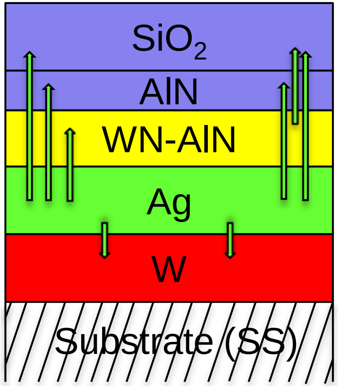

ENEA Future activities

Development of "new solar coating" for applications at high temperature **(550 °C)** with Ag as infrared reflector

- ✓ **Improved photo-thermal performance** thanks to higher reflectance of silver than tungsten one in the infrared region
- ✓ **Improved long-term thermal stability** thanks to:

1. Introduction of barrier layers above and below the Ag layer to block the high diffusivity of Ag atoms that undermines the structural and chemical stability at high temperature of the ENEA/ASE coating with Ag as infrared reflector

2. More efficient surface pre-treatments of stainless steel (SS) substrate

3. High energy sputtering process to deposit more compact and uniform layers above and below the Ag infrared reflector

SOLAR PLANT COMPONENTS

Activity line A: Development of self cleaning solar mirrors

Objectives:

Developing self cleaning coatings that preserve optical properties of reflectors, in order to reduce costs of the O&M processes without an impact on production costs (by means of scalable and economic solutions).

Tailoring coatings on geographic location, climate zone and integrated dust sensors feedback.

Funded Projects: **RdS MiTE (National), SOLARGRID**

Current activities: Fabrication and characterization of two kind of auxetic metamaterials:

1. 2D aluminum nitrides (**AlN**) doped with metals (like Aluminum or Silver) and non-metals (like Oxygen or Nitrogen) by means of reactive sputtering deposition;
2. POSS-PMMA nanostructured hybrid polymers by means of Sol-Gel and polymers processing techniques usable in front surface (polymeric or metallic reflectors) and back surface (silvered glasses) mirrors architecture.

1

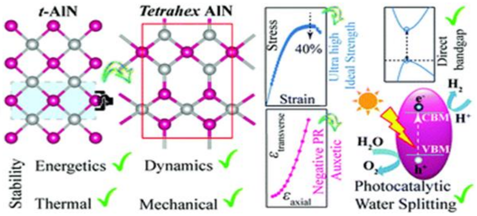

2

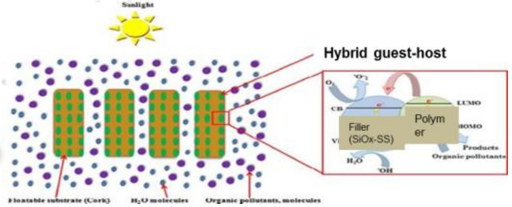

ENEA

SOLAR PLANT COMPONENTS

Activity line A: Development of heat transfer fluids

State of the art: use of **binary molten salt mixtures for PT applications** (ENEA's technology)

Challenges: **reduction of HTF solidification temperature** (from 240°C to about 100°C) in order to:

- simplify the start-up / shutdown procedures and reduce the cost of the O&M processes;
- extend the application to thermal cycles at low / medium temperature (i.e: ORC cycles);
- improve the scalability of the concentrating solar systems technology (small size plants).

Funded Projects: RdS MISE (National), IN-POWER (EU), SFERA III

Experimental characterization of ternary and quaternary mixtures (including alkaline and alkaline earth metal nitrates) to individuate promising fluids in terms of:

- Freezing point
- Chemical stability (upper temperature)
- Thermophysical properties (ρ, μ, cp, k)
- Environmental safety and toxicity
- Cost
- Construction materials compatibility

Thermal stability tests

Corrosion tests

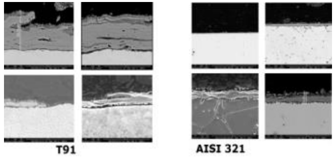

ENEA

SOLAR CHEMISTRY

Activity line B: Solar fuels and sustainable hydrogen production

Possible pathways for hydrogen production ppowered by solar energy

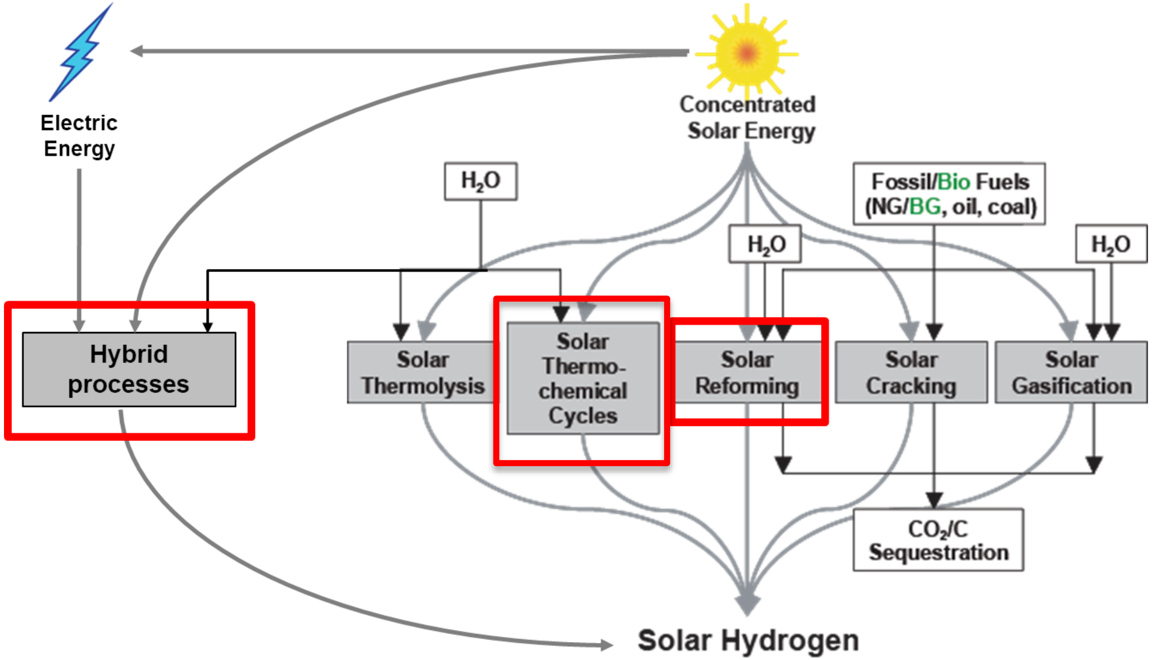

SOLAR CHEMISTRY: EU past projects

Activity line B: Solar fuels - Sustainable hydrogen production

H_2 through carbon source, fed by solar energy

CoMETHy project

Objectives **i)** Development of an innovative Reformer (fully integrated membrane reactor) assisted by solar energy; **ii)** Reduction in feed and fuel consumption and CO_2 emissions.

Achievements **i)** New catalysts and a "membrane reactor" to reduce the temperature (<565 ° C); **ii)** Demonstrative plant at Casaccia RC (~3 Nm^3/h di H_2)

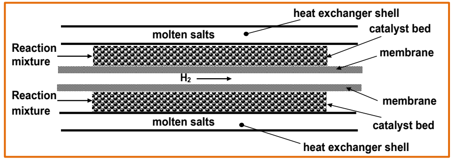

H_2 from water splitting processes

Sol2Hy2 project

Objectives: Development of a fully integrated, sustainable thermo/electrochemical processes based on a modification of the Sulphur/Iodine cycle powered by solar energy and electricity

Achievements **i)** new materials (catalysts, membrane) components (reactor, separator)

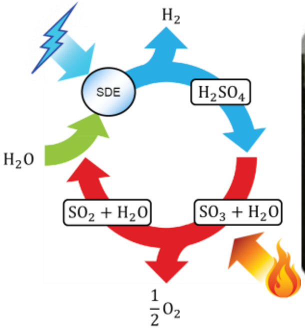

SOLAR CHEMISTRY: Overview of on-going projects

Solar Chemistry activities in ENEA are currently mainly implemented in the framework of the *Electric System Research Program and PNRR project*

Projects	- Electric System Research Program: Project 1.3 - Hydrogen Technologies (Overall ENEA budget: 11.2 M€) - PNRR Project: Research and development of Hydrogen Technologies (Overall ENEA budget: 75 M€)
Short description of STSN Division activities	Developing technologies to support the energy transition, including: 1) **Thermochemical Hydrogen production from renewable carboneaceous feedstocks (1 M€)** 2) **Thermochemical water splitting for hydrogen production (0.6 M€)**
Involved institutions	ENEA, RSE, CNR and Italian Universities
Time-line	2022-2024

Solar furnace

The solar furnace, installed at ENEA Portici Research Centre, is a research platform for testing components and systems for the production and utilization of medium and high temperature heat obtained by using concentrated solar energy.

It is a two-stage Solar Furnace including a heliostat and an off-axis primary collector. A thermal circuit, namely the solar cavity receiver and the high temperature packed bed sensible heat storage system, will complete the furnace.

SOLAR THERMAL TESTING AND QUALIFICATION

Activity line C: Solar thermal qualification and certification test laboratory

Challenge: development of standard technologies, easily repeatable and integrable

Objective:

- Qualification and certification of solar thermal collectors and systems according to European and International standard for accessing to national incentives.
- Thermal performance characterization of small-scale concentrating solar collectors according to European and International Standard (EN 12975 – ISO 9806)

Activities:

- **Efficiency tests** on solar collectors (FPC, ETC, CST, Dish systems) according to European (EN 12975) and international (ISO 9806) standards
- **Reliability and durability tests** according the same standards
- **Assessment of daily and annual performance** of solar thermal systems according to EN 12976 and ISO 9459 standards
- **Support to the industrial sector**
- **On-site testing** of concentrating solar plants for accessing to national incentives

ENEA

Accredited Laboratory

ACCREDIA
L'ENTE ITALIANO DI ACCREDITAMENTO

Laboratory is member of the **Solar Keymark** Network

The Solar Keymark
CEN Keymark Scheme

HEAT FOR INDUSTRIAL PROCESSES

Activity line C: Development and qualification of CST technology for the provision of Solar Heat for Industrial Processes

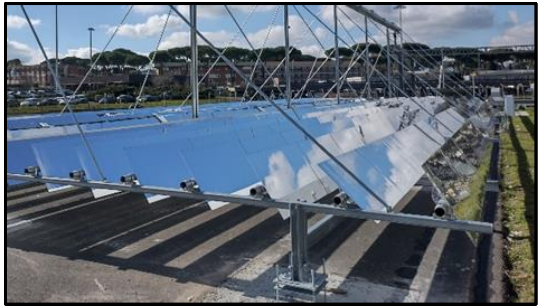

Objective:

Definition and optimization of the solar field management strategies in order to satisfy the heat process request by the end user

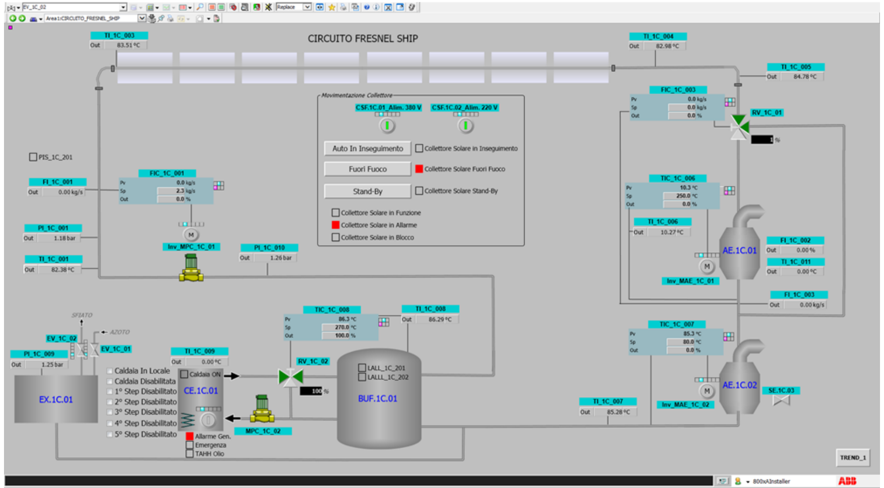

ENEA

Activity line D: Smart Grids, energy grids and microgrids

- ✓ Development and implementation of **multi-objective strategies for the optimal management of smart grids** including DG from RES.
- ✓ **Modeling and energy analysis of grids and microgrids**, where RES and energy storage systems are involved, through simulation platforms (Digsilent PowerFactory 15, Neplan, Homer Energy, TRNSYS).
- ✓ Feasibility studies and preliminary design of **demonstrators** of electrical distribution networks for the transition to smart grids.
- ✓ Development and implementation of methodologies for predictability (**forecasting**) of production and consumption (ANN, neuro-fuzzy, etc.
- ✓ Modeling of framework for strengthening the energy systems **resilience** as well as to **increase production and consumption from renewable sources**

ENEA's SMART GRID & ENERGY NETWORK ACTIVITIES

Activity line D: Smart Grids, energy grids and microgrids

- ✓ Design, development and characterization of **energy storage systems** for residential and industrial uses and for sustainable mobility.
- ✓ Production and consumption monitoring systems (**advanced multimetering**)
- ✓ **Advanced Metering Infrastructures** (AMI) design architectures and functional tests (comparison among communication protocols, synchronization mechanisms, problem of security in data exchange, implementation of experimental architecture and testing).
- ✓ Development of solutions for the use of RES in the context of **Virtual Power Plants** and **Energy Communities**.

Study, development and testing of smart advanced techniques, methods and devices to facilitate a secure, reliable, and efficient operation of energy systems, also in presence of high levels of renewable energy sources.

ENEA

Smart Energy Microgrid

Activity line D: Smart Grids, energy grids and microgrids

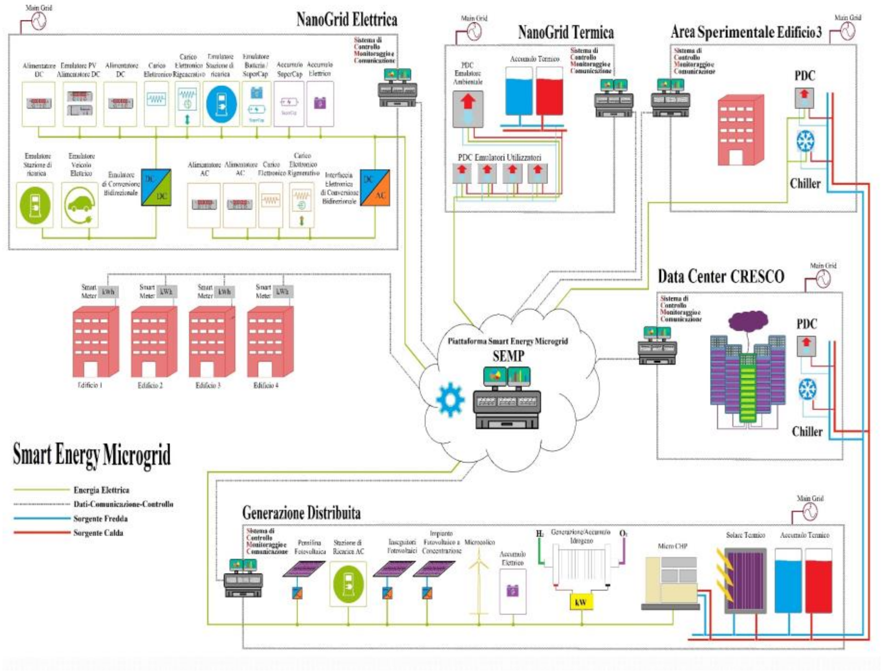

Smart Energy Microgrid is a prototype of advanced multi-energy systems which will allow the 'intelligent' coordination of energy vectors and of the various sources of renewable and conventional energy production, according to demand and generation forecasts.

SMART GRIDS AND ADVANCED ENERGY SYSTEMS

Activity line D: Smart Grids, energy grids and microgrids

Funded by several Italian and European Projects

Objective:

Advanced Energy Management Systems (EMSs) - in the context of smart energy networks and grids, local multi-carrier energy systems, local and renewable energy communities.

Innovative SW/HW technologies and applications for enabling energy system integration (smart management and control of several networks and multiple energy carriers as a unique energy system) and energy transition

Power Systems and Energy Networks Software

NEPLAN, IBM CPLEX, python, DIgSILENT PowerFactory, Typhoon HIL, National Instruments LabVIEW

Eelctric Nanogrid - Research Infrastructure

ThermalGRID Research Infrastructure

ESTIMATION AND FORECAST OF SOLAR RADIATION

Activity line D: Forecast of solar radiation

Objective: accurately predicting GHI and DNI in order to forecast the thermal energy production and to manage thermal storage

Funded by several Italian and international Project

FORECST

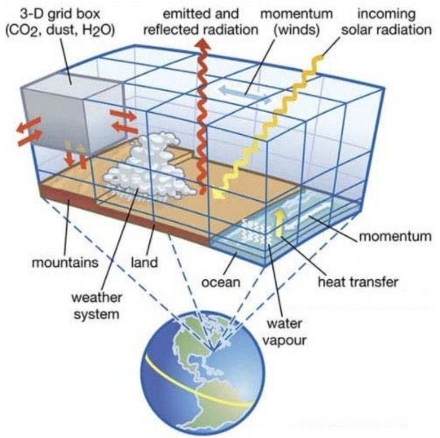

Outputs from NWP (physical) models + Empirical model for Solar Irradiance

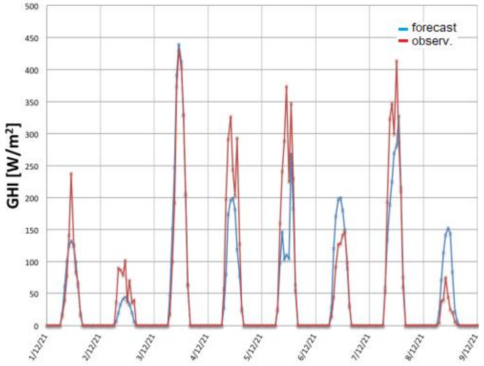

Numerical Weather Forecast models + GHI and DNI forecast for specific location

DESIGN AND VALIDATION ENVIRONMENT

Activity line D: Smart Grids, energy grids and microgrids

Objectives: Development of solutions for the use of RES in the context of **Virtual Power Plants** and **Energy Communities** (Simulations, emulation and C-Hil stations)

PiCON-RET Smart Converter Design and Optimization Platform

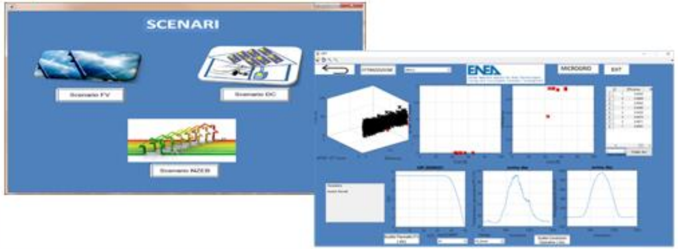

Power System Simulation Tool Stations

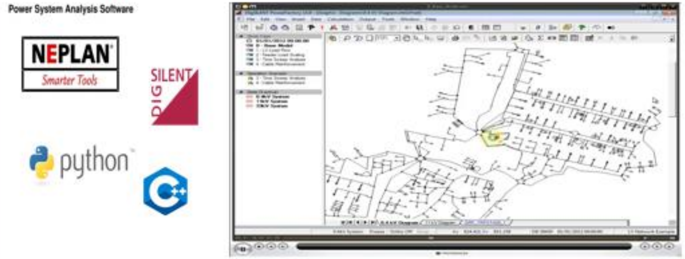

Multiobjective Optimization Environment

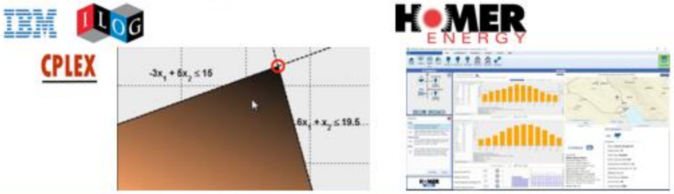

Controller hardware in the loop (C-HIL)

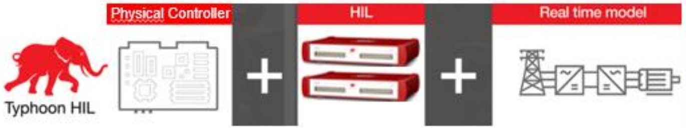

ENEA

Nanogrid AC/DC

Activity line D: Smart Grids, energy grids and microgrids

Objectives: Development and implementation of multi-objective strategies for the optimal management of smart grids including DG from RES

TES CLASSIFICATION - ENEA ACTIVITIES

THERMAL STORAGE CONCEPT

- **ACTIVE SYSTEMS** — *Circulating thermal storage media*
  - **DIRECT SYSTEMS** — *Heat thermal fluid (HTF) and heat storage media (HSM) media are the same*
    - *Double tank using molten salts/thermal oil*
    - *Single thermocline tank using molten salts with integrated SG*
    - *Packed bed thermocline tank using oil or molten salts as HTF*
  - **INDIRECT SYSTEMS** — *HTF and HSM are separated*
    - *Single thermocline tank using molten salts/oil with integrated HEXs*
- **PASSIVE SYSTEMS** — *Confined thermal storage media*
  - *Solids (e.g.: concrete)* — *HTF/concrete (mainly sensible heat)*
  - *Solids/Liquid (PCMs, eg: molten salts also with nanoparticles)* — *HTF/PCM (mainly latent heat)*
  - *Thermo Chemical Materials (e.g.: C or Mn oxides)* — *HTF/TCM (mainly heat of reaction)*

THERMAL ENERGY STORAGE ACTIVITIES

Activity line E: Thermal Energy Storage Systems

Sensible heat storage through thermocline systems (single tank)

Objective: storage energy density improvement and cost reduction by compact single tank systems, also integrated with a vapour generator (VG).

MATS, OPTS EU projects

Storage integrated with SG (direct)

Patent nr. 102017000129902

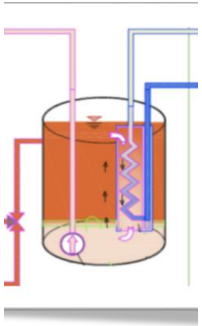

RESLAG project

Storage with bed packed with slag (direct)

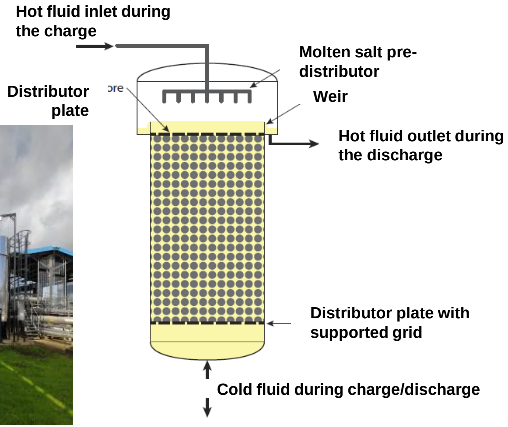

ORC-Plus project

Storage with a confined fluid (indirect)

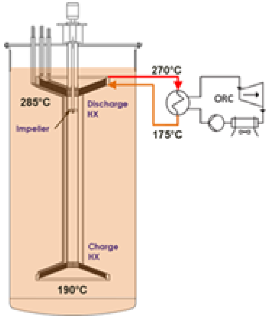

THERMAL ENERGY STORAGE ACTIVITIES

Activity line E: Thermal Energy Storage Systems

Thermal storage by solid materials (concrete)

Objective: development of low-cost storage systems, using readily available materials (including waste) for applications up to 400 ° C

Basic concrete

- Developed formula to produce high conductibility and conductivity concrete including recycled materials.

- Realized pilot plant of SOLTECA3 and SOLTECA Air at Casaccia RC

Concrete with PCM stabilized in shape (up to 5 $_{wt}$%)

Patent nr. 102017000129902. Thermal Storage Device, Modular System Incorporating the Device and Relative Method of Implementation (102017000129902).

THERMAL ENERGY STORAGE ACTIVITIES

Activity line E: Thermal Energy Storage Systems

Enhanced thermal storage with PCM

Objective: Increase of the storage energy density of sensible heat systems

- Realized ATES facility for testing different kind of exchange area and different uses (integration to concrete / thermocline tank matrices)

- Tested PCM (solar salt) as it is and with inclusions of nanostructured materials (SiO_2), also by capsules system.

THERMAL ENERGY STORAGE ACTIVITIES

Activity line E: Thermal Energy Storage Systems

TES systems for local smart thermal energy grid

Objective: support decarbonisations of local heat process

Development of innovative SW/HW technologies to enable energy integration at the level of resources and networks and promote the energy transition.

Design & developing :

- Advanced solutions for the control of new heat thermal networks
- advanced strategies for the integrated management of heat and electricity

Thermal nanogrid and storage laboratory

THERMOCHEMICAL STORAGE ACTIVITIES

Activity line E: Thermal Energy Storage Systems

Thermo-chemical storage

Implementation of thermochemical systems integrated with solar systems to increase efficiency and duration of the storage.

ENEA activities for thermochemical storage at high temperatures

- **Testing of promising material** (calcium carbonate supported on mayenite, mixed manganese oxides)

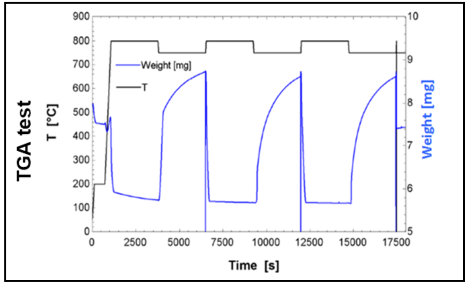

- **Developing of kinetic models** for the dynamic simulation of charging/discharging

- **Analysis of different integration schemes** solar plant/storage unit

- Development of **experimental equipments (fixed bed and fluidized bed reactor) for kinetic characterization of pellets at different pressures**

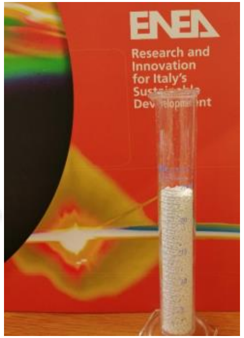

THERMOCHEMICAL STORAGE ACTIVITIES

Activity line E: Thermal Energy Storage Systems

- **National Program PTR 2019-2021 : Thermal storage/Selection and development of innovative TCS (HT)**
- **Partner: Sapienza University of Rome**

2019

Experimental screening on TCS systems based on

Metal oxides **Carbonates**

Selection of the **optimal synthesis processes**

2020

Realization of **a lab scale apparatus** for exp. tests in **realistic conditions** (P, T)

Development of kinetic models to be integrated into the **dynamic TCS unit model**

2021

Experimental characterization of systems in **real pressure condition**

Experimental validation of TCS reactor models

Application of TCS model

actual storage density evaluat. **techno-econ.** analysis

ENEA

THERMAL ENERGY STORAGE ACTIVITIES

Activity line E: Thermal Energy Storage Systems

R&D activity on adsorption thermal storage at low-medium temperature

Adsorption thermal storage for solar applications and waste-heat recovery

Objective: Development and testing of a thermo-chemical storage, based on vapour and zeolite 13X working-pair, for solar-cooling and process heat applications at medium temperature (100-200°C)

Activities:

- Modeling implementation of adsorption/desorption kinetics for the simulation of charging and discharging processes
- Implementation of lab-scale prototype for analyzing and testing the thermo-chemical storage
- Design, construction and testing of a technology demonstrator (LFR solar field, TES system and controlled dissipation system) for the performance assessment of the thermo-chemical storage

Realized testing plant at Trisaia Research Centre

Thanks for your kind attention

SFERA-III

Solar Facilities for the European Research Area

4th Training for Industries

7-11 November 2022, Cr ENEA Casaccia Rome (Italy)

Electric heating systems for molten salt circuits (I): introduction

Walter Gaggioli (ENEA, Head of STSN Division)

JOINT RESEARCH ACTIVITIES

THIS PROJECT HAS RECEIVED FUNDING FROM THE EUROPEAN UNION'S HORIZON 2020 RESEARCH AND INNOVATION PROGRAMME UNDER GRANT AGREEMENT NO **823802**

Joule electric heating

Cable electric tracing

Joule electric heating

Joule electric heating

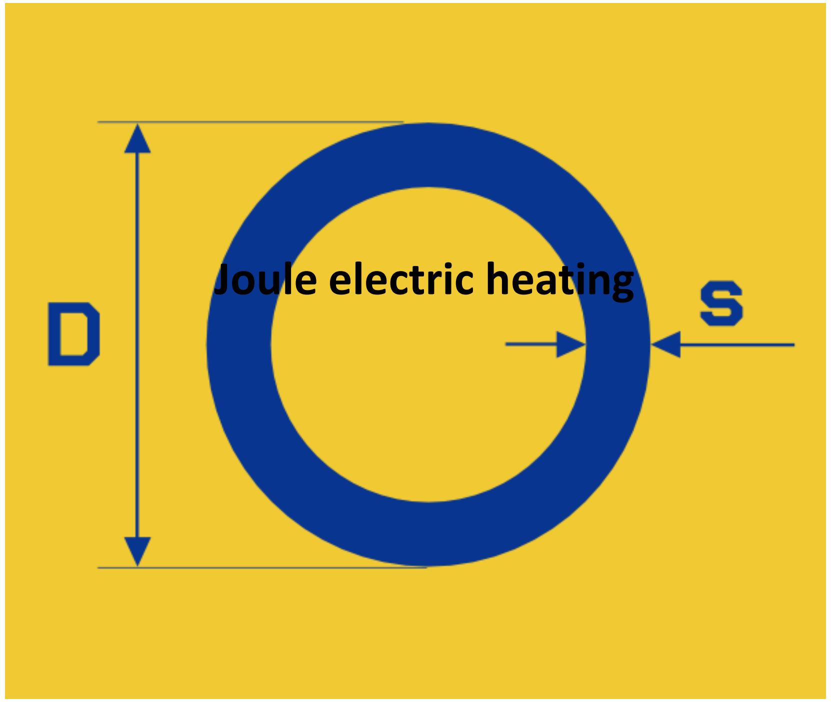

Joule electric heating

As a heating element it offers a large surface area and consequently a greater and more effective thermal radiation

resistivity of AISI 316 an average temperature of 380 ° C), $\rho tot = \sim 4x10^{-3}\ \Omega$

$S = \Pi/4(D^2-d^2)$

$d= D-2s$

$R= SL\rho tot$

Joule electric heating

	W_{tot} =	30.000	Watt		
numero sezioni =		2			
	π =	3,14			
	L_{tot} collettori =	100	m		
Dati singolo Collettore	$\rho_{300°C}$ =	96,68	µΩ x cm	0,9668	µΩ x m
	de =	7,00	cm	70,00	mm
	di =	6,40	cm	64,00	mm
	S =	6,31	cm^2	6,31E-04	m^2
	L =	5.000	cm	50,0	m
	$R_{50mcoll}$ =	76.554	µΩ	76.554	µΩ
	$R_{50mcoll}$ =	0,077	Ω		
	W_{util} =	15.000	Watt		
	I collett =	443	A		
	Rtot =	3,828E-02	Ω		
	Itot =	885,31	A		
	W =	30.000	Watt		
	V =	33,89	volt		

mm^2	m Ω / m
120	0,1880
150	0,1530
185	0,1230
240	0,0943
300	0,0761
400	0,0607
500	0,0496
630	0,0402

7065

Pay attention to:

- at value of Electric resistances of the junction cable between power unit and electrical loads in the field (reduce the DC, correct size of the cables);
- Resistance of contacts (point of local overheating);

Collettore	Linea	I linea	Lunghezza	Sezione		n° cavi	totale	R linea	W linea	ΔV
N°		A	m	mm^2	m Ω / m	-	m Ω / m	Ω	Watt	
1	1	442,65	40,0	120,0	0,1880	1,0	0,188	7,520E-03	1473,48	3,3287
1 2	2	885,31	90,0	630,0	0,0402	1,0	0,040	3,618E-03	2835,66	3,2030
3	3	442,65	140,0	185,0	0,1230	2,0	0,062	8,610E-03	1687,05	3,8112

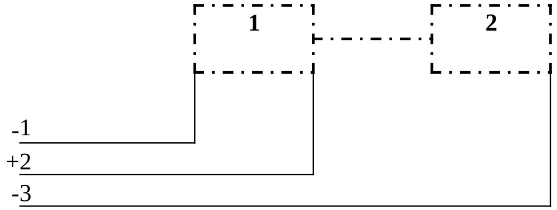

Joule electric heating

shunts: Element placed in parallel with a section of circuit, in order to decrease the electric current that circulates there

The electric resistance of flexible hole is more higher then the pipe

To have a correct heating of all piping element present in line of hydraulic circuit the have a similar resistivity, other way the element with major electric resistance they will get hot and will have local thermal crisis of component. One solution at this issue is that to install a local shunt to have a correct distribution of the electric currents.

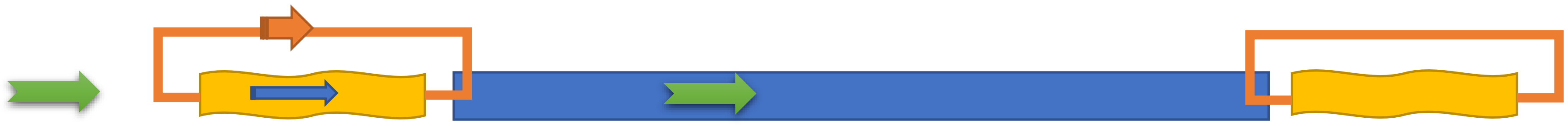

Pay attention:

1) Valves (safety issues)
2) Instrumentations must be insulated
3) potential issues of local electric corrosion if the electrical connections they are not designed, realized and installed correctly
4) Pipe/component supports must be insulated

Joule electric heating

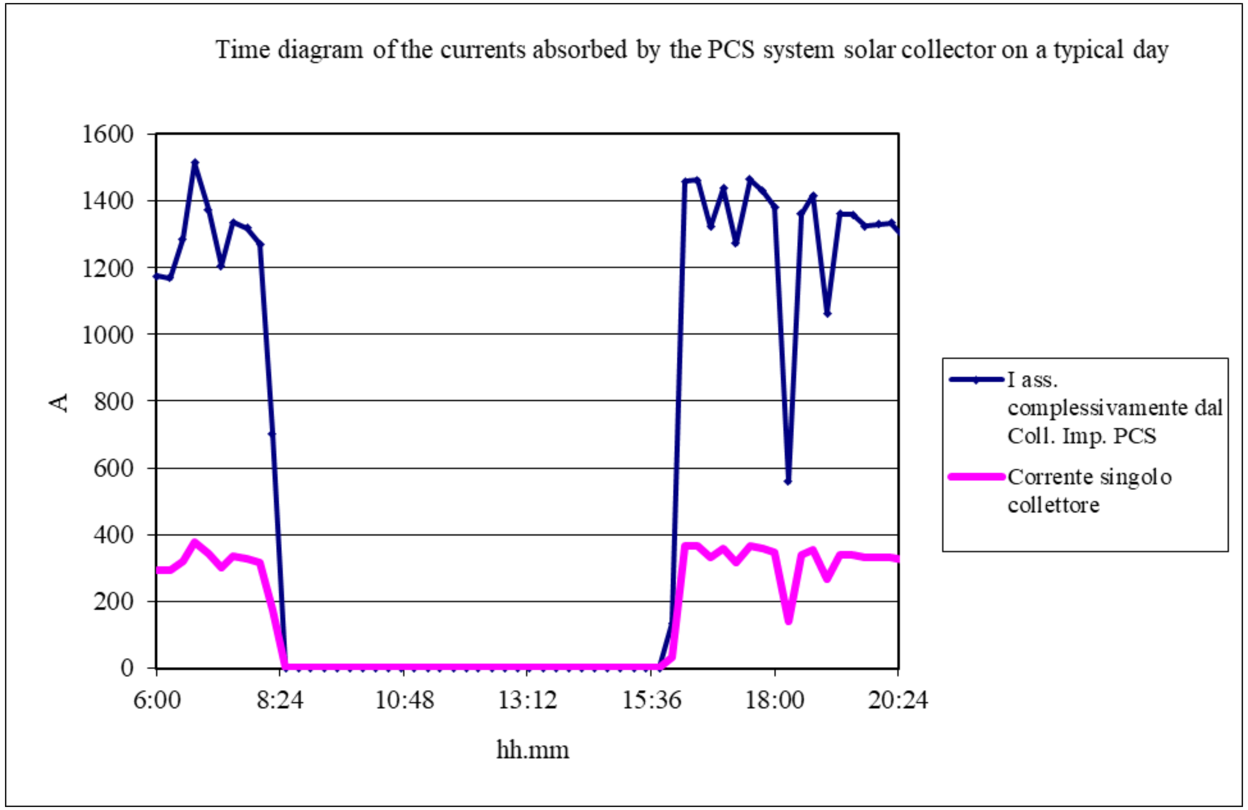

safety criterion to avoid the onset of the thermal crisis

$$q''_{max}/G_{min} < 0{,}11 \text{ kJ/kg}$$

q''_{max} maximum heat flow

G_{min} minimum flow rate

Cable electric tracing

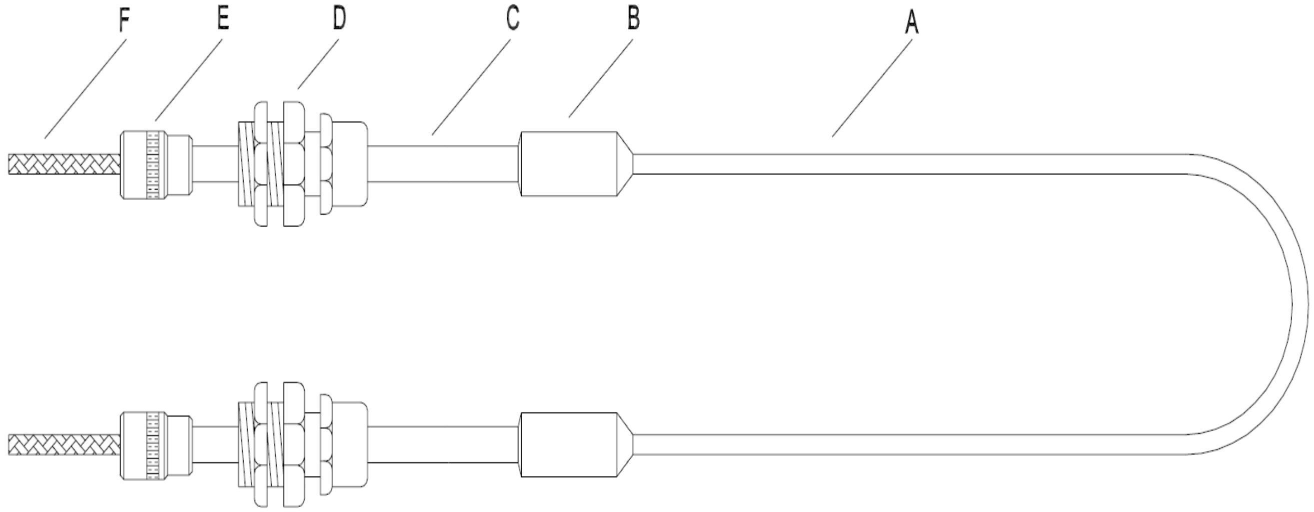

A) Heating cable
B) Junction of cast cable - cold cable
C) Mineral oxide cold cable
D) Brass cable gland with gasket
E) GIF termination cold cable - flexible cable
F) Flexible cable

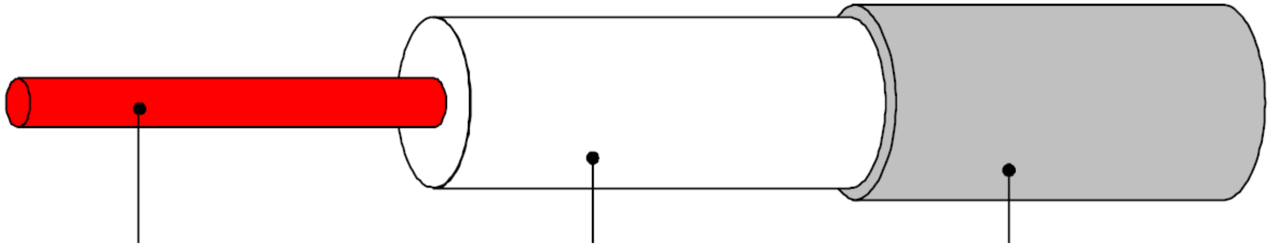

Conductor resistive

Insulating (MgO)

Conductor resistive

HEATING CABLES

Hints on dimensioning of heating with heating cables

Sizing requires calculations of the following thermal powers for:

→ **Maintaining** (at a certain temperature)

→ **Heating** (metal and any internal fluid)

→ **Latent heat of fusion** (in case of unfreezing)

Maintaining Thermal Power

$$Q_m = 2 \cdot \pi \cdot \lambda_{ins} \cdot (T_m - T_r) / (E \cdot \ln((D_e + 2 \cdot s_{ins}) / D_e))$$

Q_m: maintaining thermal power, W/m

λ_{ins} : insulating thermal conductivity, W/m°C

T_m : maintaining temperature, °C

T_r : room temperature, °C

D_e : external pipe diameter, mm

s_{ins} : insulation thickness, mm

E : system safety factor (between 0.8 ÷ 0.9)

Heating Thermal Power (without considering thermal losses)

→ it depends on the time required to complete the operation

$$Q_{heat} = (M_{steel} \cdot cp_{steel} + M_{salt} \cdot cp_{salt}) \cdot (T_f - T_i) / (E \cdot \Delta t \cdot 3{,}6)$$

Q_{heat} : heating thermal power , W/m

M_{steel} : mass of steel, kg/m

M_{salt} : mass of salt, kg/m

cp_{steel} : specific heat of steel, kJ/kg°C

cp_{salt} : specific heat of salts, kJ/kg°C

T_f : maintaining temperature (final), °C

T_i : room temperature (initial), °C

Δt : time interval, h

E : system safety factor

Heating Thermal Power (considered the thermal losses)

$$Q_{tot} = Q_{heat} + 2/3 \cdot Q_m$$

Q_{tot}: total heating thermal power, W/m

Q_{heat}: heating thermal power, W/m

Q_m: maintaining thermal power, W/m

Latent heat of fusion

$$Q_{fus} = M_{salts} \cdot H_{fus} / \left(E \cdot \Delta t \cdot 3{,}6 \right) W/m$$

Q_{fus}: thermal power of fusion, W/m

M_{salts} : mass of salts

H_{fus} : heat of fusion of salts, kJ/kg

E : system safety factor

Cable electric tracing

The DN80 pipe reaches the maintenance temperature after about 6.9 hours, while the DN100 reaches it after 11.3 hours.

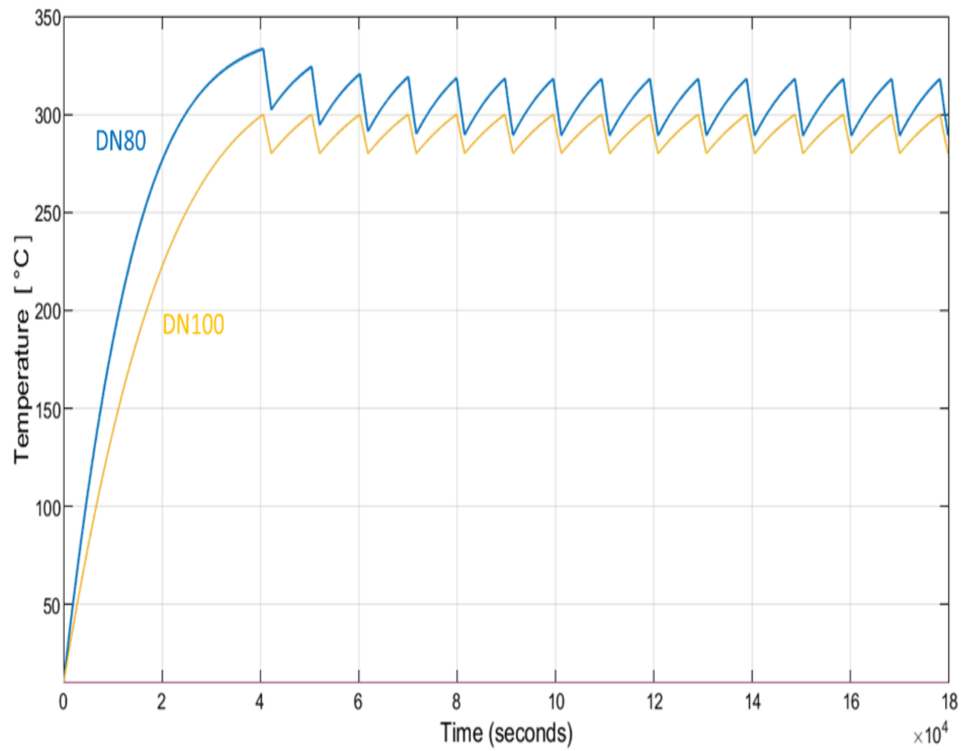

Pipe heating in the absence of internal salt with control

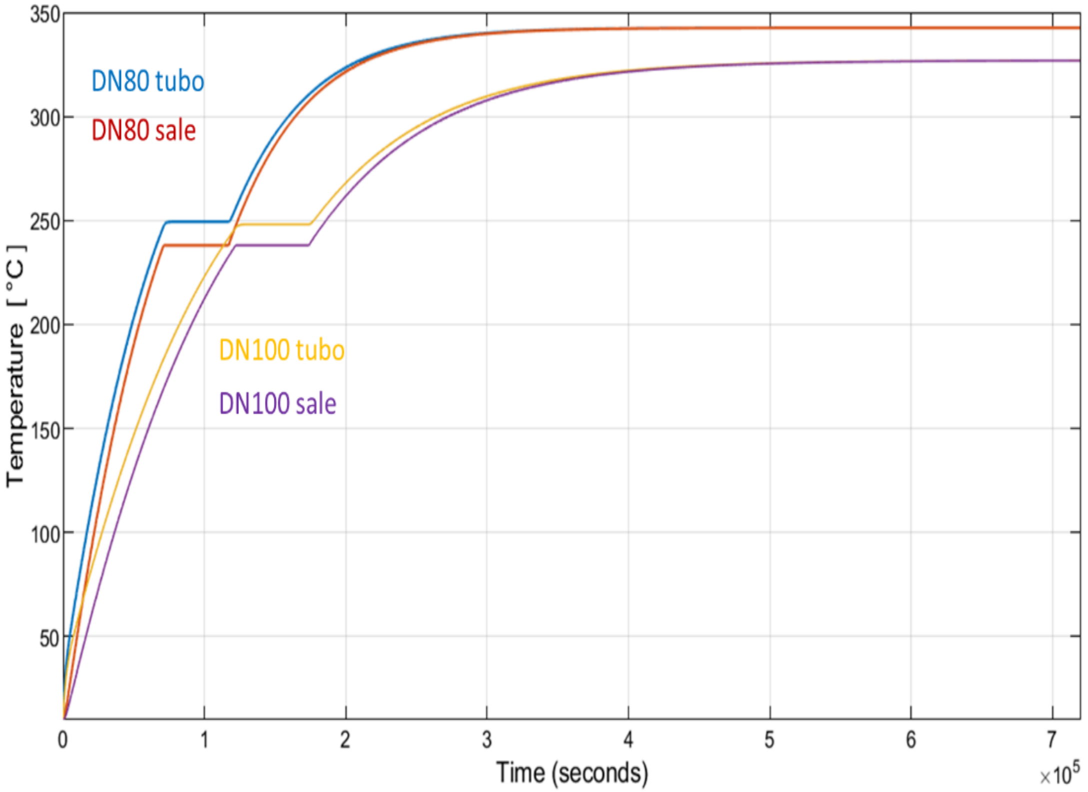

Pipe heating in presence of internal salt with control

The melting start temperature is reached after about 20.5 h, for the DN80 pipe, complete melting occurs after 32.7 h, in 12.2 h.

In the case of the DN100 pipe, the melting start temperature is reached after about 34.3 h, while the complete melting occurs after 48 h, in 13.7 h.

The mineral insulated heating cable consists of a resistive conductor insulated with Oxide of Magnesium and a continuous and seamless metal outer sheath

To meet the different application needs and to have a range of resistivity values as much as wide as possible, the resistive conductor is made of Copper or its alloys; the outer sheath can be made in Copper, Cupronickel 70/30, AISI 321 and, on request, Inconel 600.

They can be powered both at very low voltage (24 V AC and 48 V AC) and in low voltage (110 V a.c., 230 V a.c. and 400 V a.c.) based on system requirements and power heaters that must be installed on the various pipes, choosing the appropriate resistivity

Mineral insulated cables are constant power cables as they deliver power regardless of the external temperature to which the heating cable is subjected. They are series circuit cables in which the conductor itself, when powered, produces an effect Joule, a dissipation of electrical power.

PRINCIPLE OF OPERATION

Mineral insulated cables are constant power cables as they deliver power regardless of the external temperature to which the heating cable is subjected. They are series circuit cables in which the conductor itself, when powered, produces an effect … r.

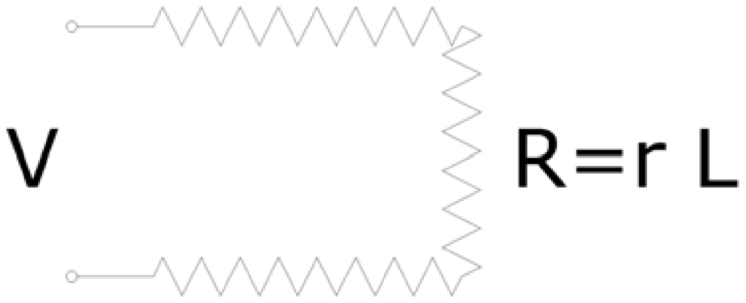

the power supplied is determined by the well-known Joule formula $W= V^2 / r L$

V = it is the supply voltage in volts

W = it is the power in Watts supplied by the heating circuit

r = it is the resistivity in ohms per meter of the heating cable used

L = it is the length of the heating circuit created

R = iit s the resistivity in ohms of the heating circuit

CHOICE OF THE HEATING CABLE

It is necessary to proceed with the choice of the heating cable as follows:

- calculate the power needed
- calculate the ohmi resistance R of the cable necessary to obtain the required power,
- divide the R value by the length of the heating element to obtain the specific resistance (Ω / m);
- choose the heating cable with the specific resistance that is closest to the value found.
- Check that at the operating temperature the power dissipated by the heating element is that required; otherwise, choose the heating cable with the immediately lowest specific resistance and repeat the procedure

$R = V^2/W$

V: supply voltage
W: Power requested

DETERMINATION OF THE SHEATH TEMPERATURE OF THE HEATING ELEMENT

The sheath temperature of the heating elements under insulation can also be determined, in an approximate way, with the following relationship:

Tg= Tm + (9,33 x W) / d

Tg = sheath temperature (° C);
Tm = temperature of the environment surrounding the cable and which can be considered equal to the maintenance temperature (° C);
W = power dissipated by each meter of cable (W / m);
d = outer diameter of the heating cable

Mineral insulated cables are constant power circuits only as a function of the operating temperature and not as a function of the length of the heating circuit.

When dimensioning the heating circuit it is necessary know the operating conditions, the exact geometry of the component (pipe, tank, etc.) on which it will be installed

CHECKS BEFORE INSTALLATION

- To Check that the thermal calculation sheet supplied with the offer shows the dimensional values and operating hours required;

- To Check that the heating circuits supplied are those shown in the offer and in the order and that the label applied to each heating circuit supplied shows the following data:
  a. The type of heating cable
  b. The length of the heating cable
  c. The power of the heating circuit
  d. The power supply voltage

  ➢ Carefully keep this labels which must subsequently be fixed on the cold tail near the power box.

  ➢ On the back of the label must be affixed, a care of the installer, the exact installation position of the heating element on the pipe, tank, pump, etc.

CHECKS AFTER ASSEMBLY

1. Visual check of the good condition of the sheaths of the heating cables, of the cold cables and of all the joints and terminations.
2. Measurement of the insulation resistance (it must be higher than 50-100 Megaohm applying a voltage of 500V DC- at 20 ° C).
3. Measurement of ohmic resistance; a tolerance of +/- 10% with respect to the theoretical one is allowed.
4. Measurement of absorbed current and supplied power; a tolerance of +/- 10% with respect to the theoretical one is allowed.
5. Check that the cable does not touch at any point: the minimum distance between the two sections of cable heating must be about 10/15 mm.
6. Check that the minimum bending radius equal to 6 times the cable diameter is respected in all points.

it is recommended to repeat the checks 2,3 and 4 also after that the insulation works they have been completed

Walter GAGGIOLI, PhD
ENEA
TERIN-STSN
walter.gaggioli@enea.it

THANK YOU FOR YOUR ATTENTION!
ANY QUESTIONS?

SFERA-III

Solar Facilities for the European Research Area

4th Training for Industries

7-11 November 2022, Cr ENEA Casaccia Rome (Italy)

Components for molten salt circuits

PhD Walter Gaggioli

JOINT RESEARCH ACTIVITIES

THIS PROJECT HAS RECEIVED FUNDING FROM THE EUROPEAN UNION’S HORIZON 2020 RESEARCH AND INNOVATION PROGRAMME UNDER GRANT AGREEMENT NO **823802**

MS pump: type centrifugal & immerged; body and single components in AISI321H

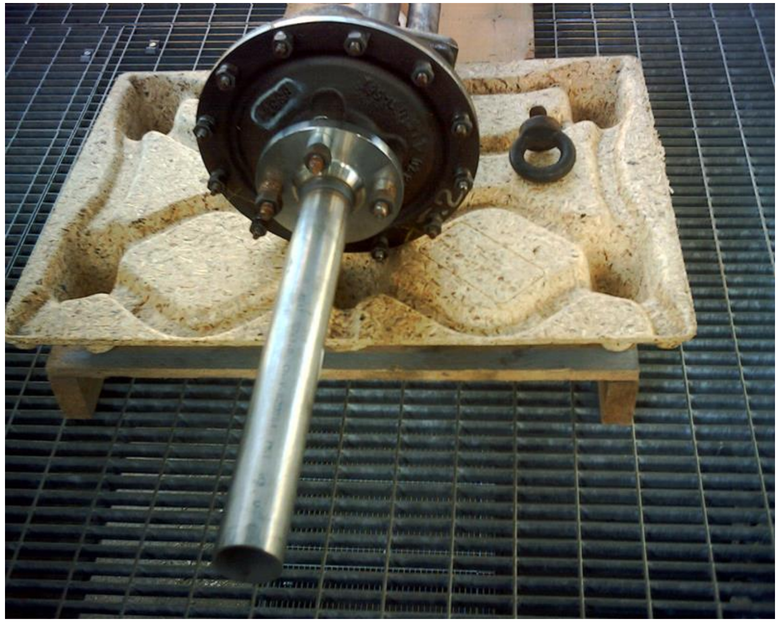

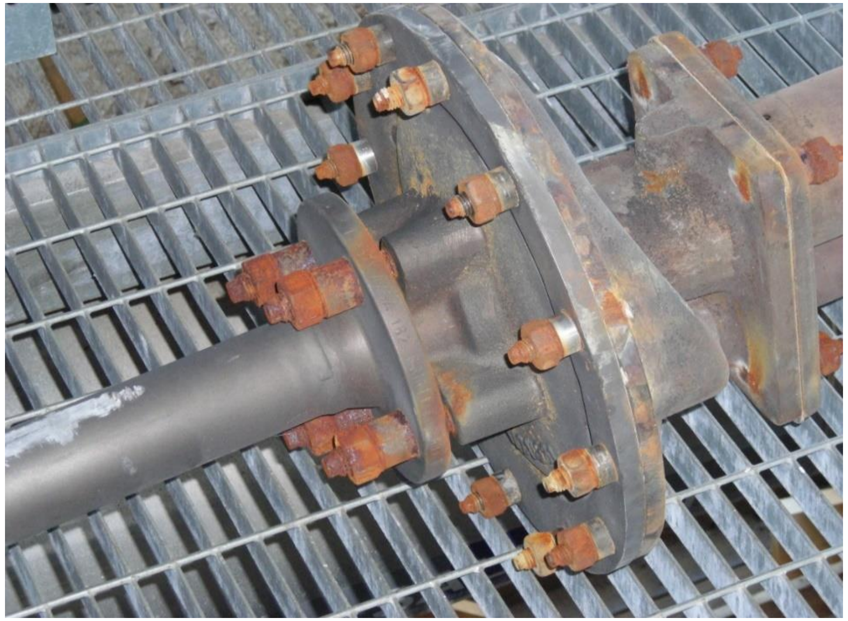

pump: case of use not AISI bolts after 1000 h

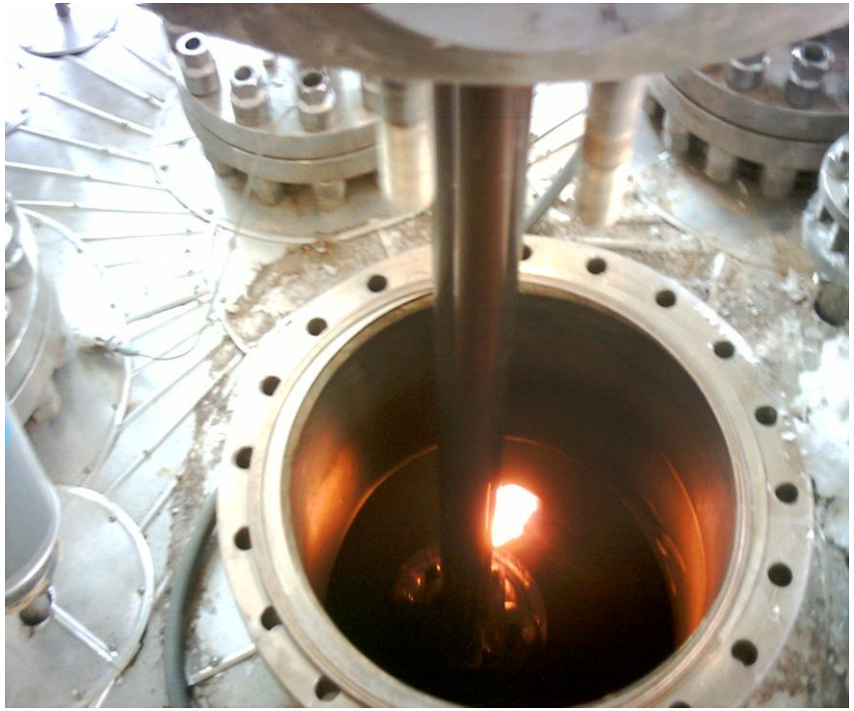

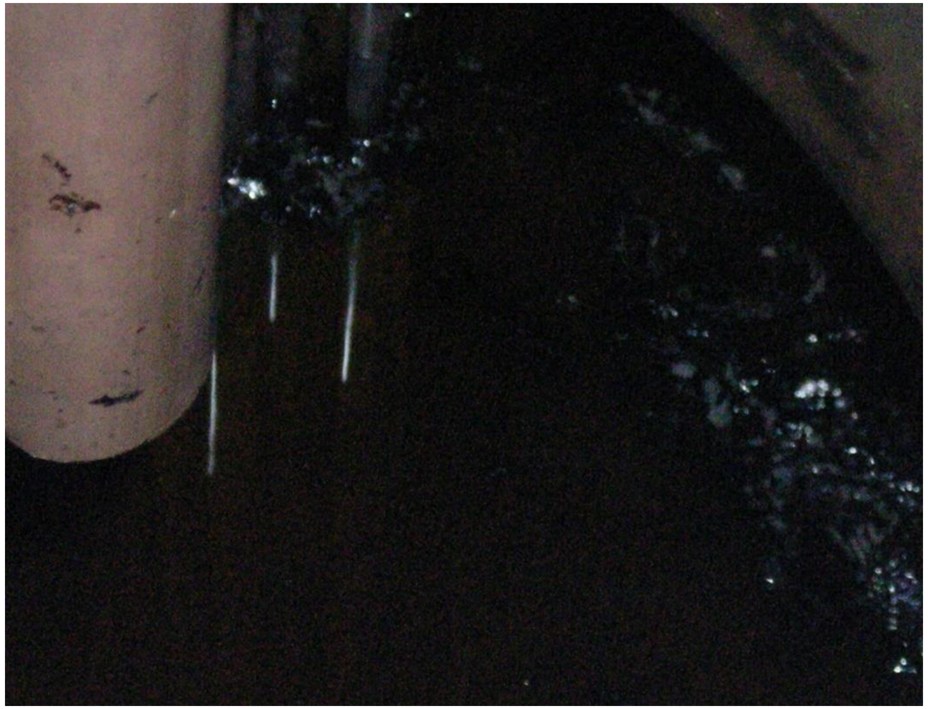

accidental spillage of oil into the PCS molten salt tank (atmospheric vented tank)

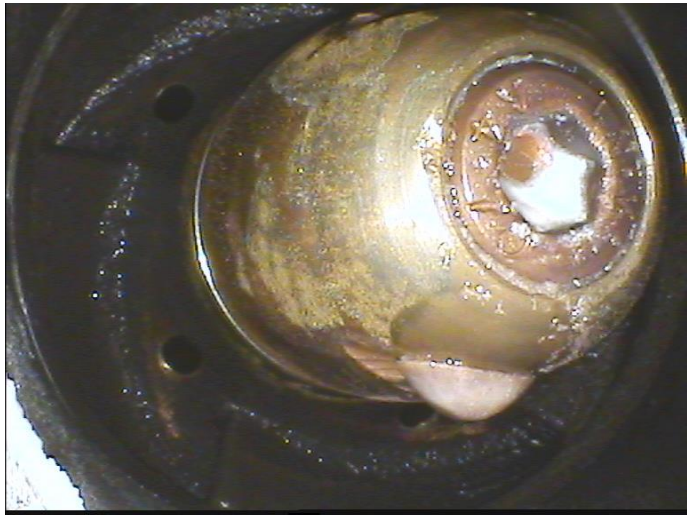


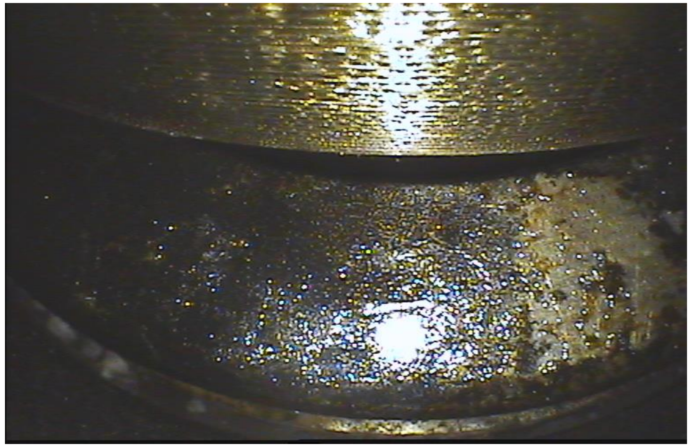

Internal MS pump AISI 321H body inspection after 4000 working hours

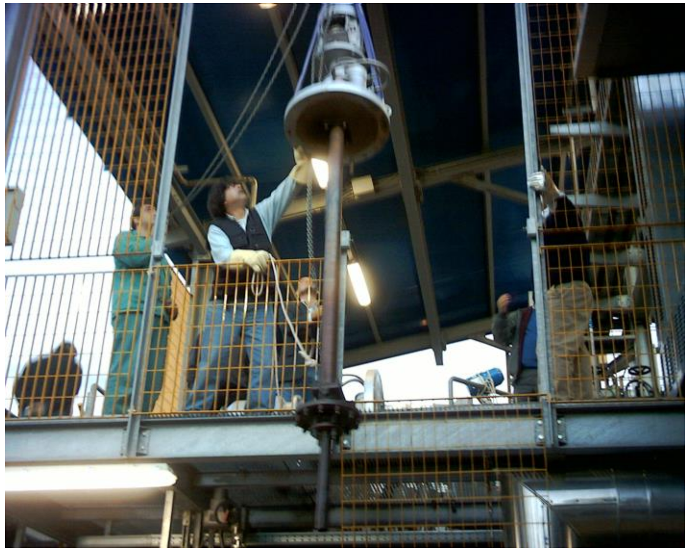

pump extraction from PCS molten salt tank

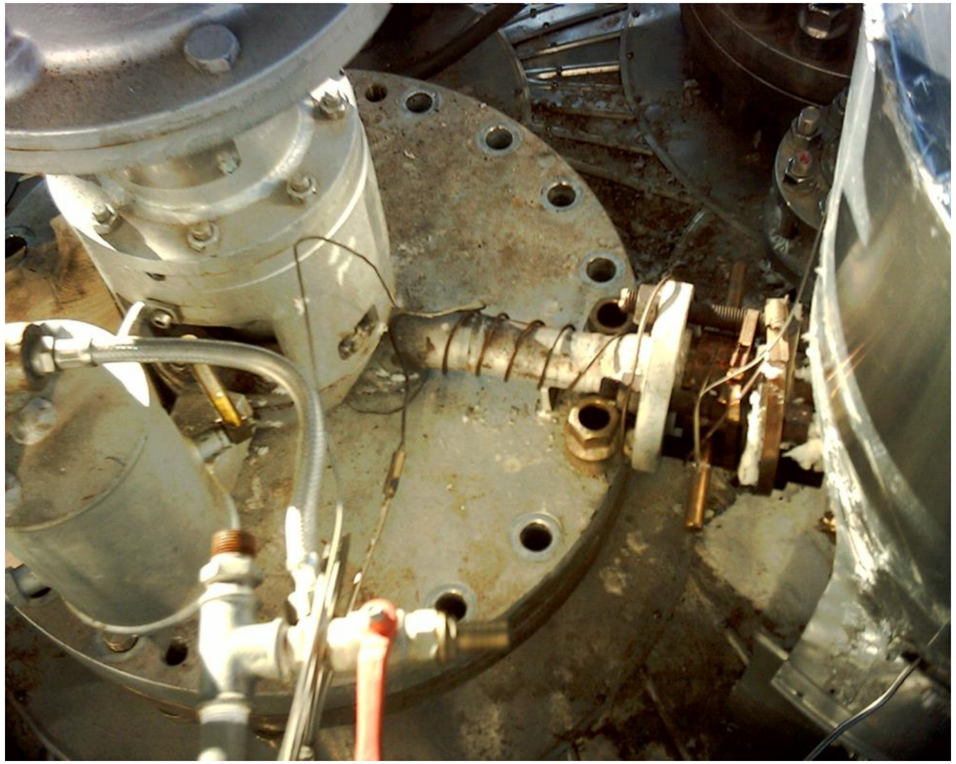

cold point of PCS molten salt tank pump

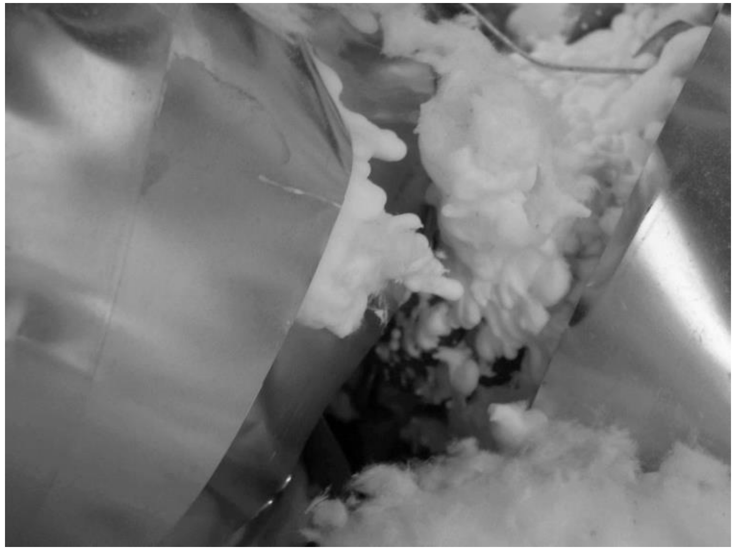


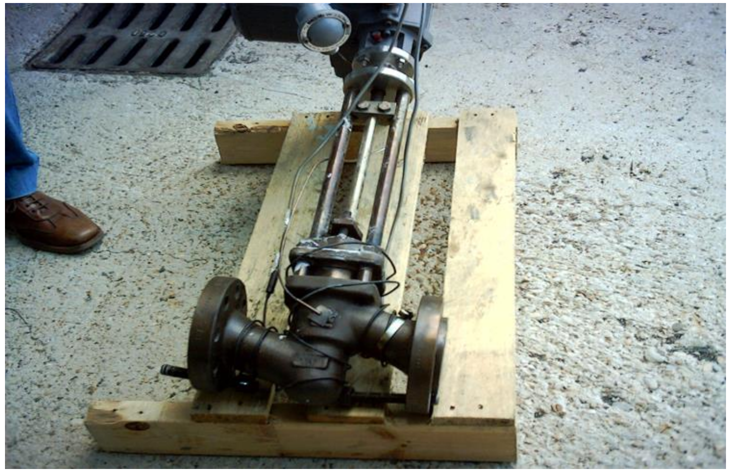
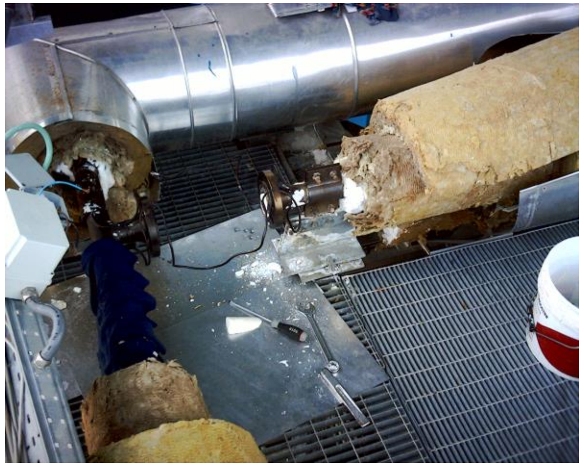

GLOBE VALVE
Main seal: BELLOWS
Material: AISI 321H

MS leakage from
valves without bellows

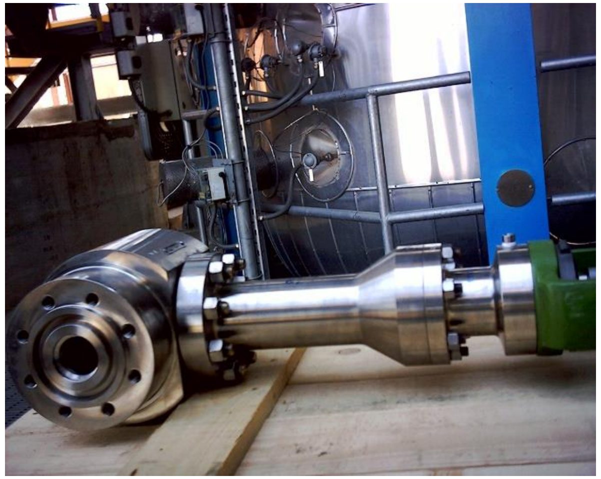
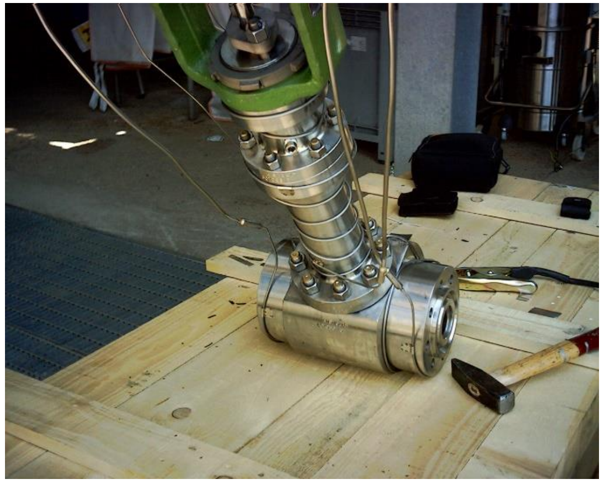
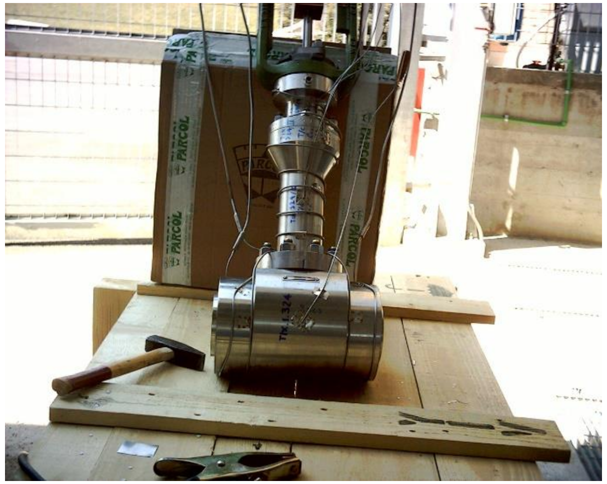


MS valves with bellows

Teflon gasket for instrumentation fittings after 100 working hours : leakage of MS

Pipe support

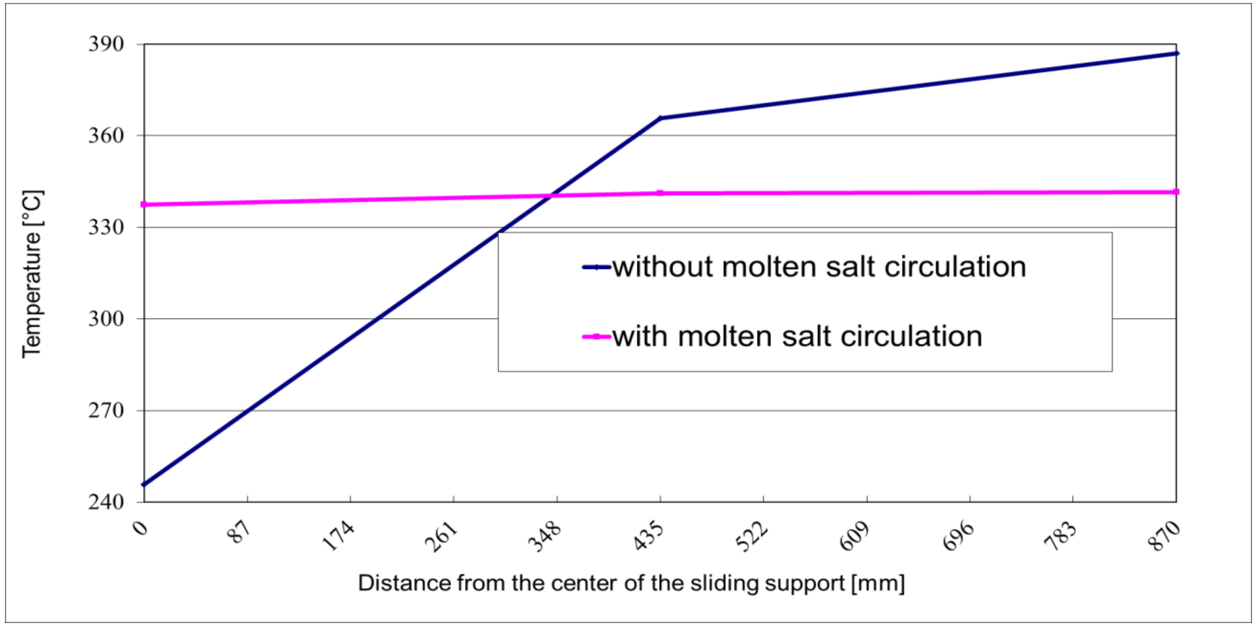

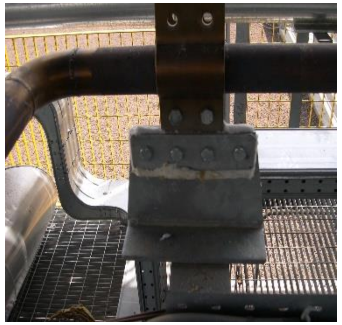

Temperatures profile on the sliding support and at the distances of 430 mm and 870 mm from it, in the conditions of non-circulating fluid (heating with heating cables) and circulating fluid.

Walter GAGGIOLI, PhD
ENEA
TERIN-STSN
walter.gaggioli@enea.it

THANK YOU FOR YOUR ATTENTION!
ANY QUESTIONS?

SFERA-III

Solar Facilities for the European Research Area

Solar Facilities for the European Research Area

4th Training for Industries

7-11 November 2022, Cr ENEA Casaccia Rome (Italy)

ELECTRIC HEATING SYSTEMS FOR MOLTEN SALT CIRCUITS

Giuseppe PETRONI (ENEA, TERIN-STSN-ITES)

JOINT RESEARCH ACTIVITIES

THIS PROJECT HAS RECEIVED FUNDING FROM THE EUROPEAN UNION'S HORIZON 2020 RESEARCH AND INNOVATION PROGRAMME UNDER GRANT AGREEMENT NO **823802**

→ Melting temperature of Salts = 240°C

→ A **higher temperature** must be guaranteed in all the components crossed by the salts by implementation of **specific systems**

→ **Heating systems** are necessary in the phases of:

First salts circulation → to **pre-heat** the components

Drainage → to **maintain** the temperature

After accidental salts freezing → to **melt** the salts

<u>**Heating represents one of the biggest critical issues**</u>

COMMON HEATING SYSTEMS:

1. Tracing with **HEATING CABLES**
2. Heating by **JOULE EFFECT**
3. Heating by **ARMORED RESISTANCE**

R

I

V

$$P = V \times I = R \times I$$

HEATING CABLES

Hints on dimensioning of heating by heating cables

Sizing requires calculations of the following thermal powers for:

→ **Maintaining** (at a certain temperature)

→ **Heating** (metal and any internal fluid)

→ **Latent heat of fusion** (in case of unfreezing)

Maintaining Thermal Power

$$Q_m = 2 \cdot \pi \cdot \lambda_{ins} \cdot (T_m - T_r) / (E \cdot \ln((D_e + 2 \cdot s_{ins}) / D_e))$$

Q_m: maintaining thermal power, W/m

λ_{ins} : insulating thermal conductivity, W/m°C

T_m : maintaining temperature, °C

T_r : room temperature, °C

D_e : external pipe diameter, mm

s_{ins} : insulation thickness, mm

E : system safety factor (between 0.8 ÷ 0.9)

Heating Thermal Power (without considering thermal losses)

→ it depends on the time required to complete the operation

$$Q_{heat} = (M_{steel} \cdot cp_{steel} + M_{salt} \cdot cp_{salt}) \cdot (T_f - T_i) / (E \cdot \Delta t \cdot 3{,}6)$$

Q_{heat} : heating thermal power , W/m

M_{steel} : mass of steel, kg/m

M_{salt} : mass of salt, kg/m

cp_{steel} : specific heat of steel, kJ/kg°C

cp_{salt} : specific heat of salts, kJ/kg°C

T_f : maintaining temperature (final), °C

T_i : room temperature (initial), °C

Δt : time interval, h

E : system safety factor

Heating Thermal Power (considered the thermal losses)

$$Q_{tot} = Q_{heat} + 2/3 \cdot Q_m$$

Q_{tot}: total heating thermal power, W/m

Q_{heat}: heating thermal power, W/m

Q_m: maintaining thermal power, W/m

Latent heat of fusion

$$Q_{fus} = M_{salts} \cdot H_{fus} / (E \cdot \Delta t \cdot 3{,}6)\, W/m$$

Q_{fus}: thermal power of fusion, W/m

M_{salts} : mass of salts

H_{fus} : heat of fusion of salts, kJ/kg

E : system safety factor

HEATING CABLES

→ Most commonly used have:
- ☐ Mineral Insulation
- ☐ Stainless Steel sheath
- ☐ Single conductor

Main features

Conductor material ………..	Nickelcrome
Isolating material …………..	Magnesium Oxide
Sheat material ..……………	Stainless Steel 321
Voltage ……………………..Up to 500V, Alternate Power	
Isolating resistance ………..	1000MOhm/1000m; tested in factory
Isolating voltage …………..2.0KV rms ac	
Max. sheat temperature ….	600°C
Min. installation temperature -60°C	
Min. bending radius ……….	6 times the cable diameter
Min. laying pace …………..	50mm

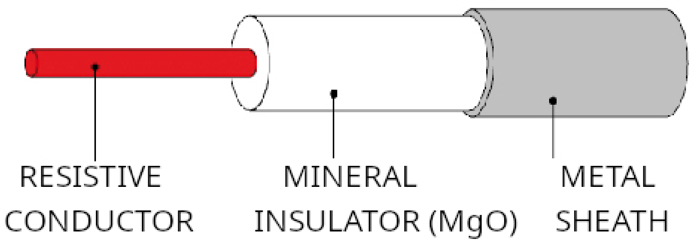

HEATING CABLES ON PIPING

HEATING CABLES ON VALVES

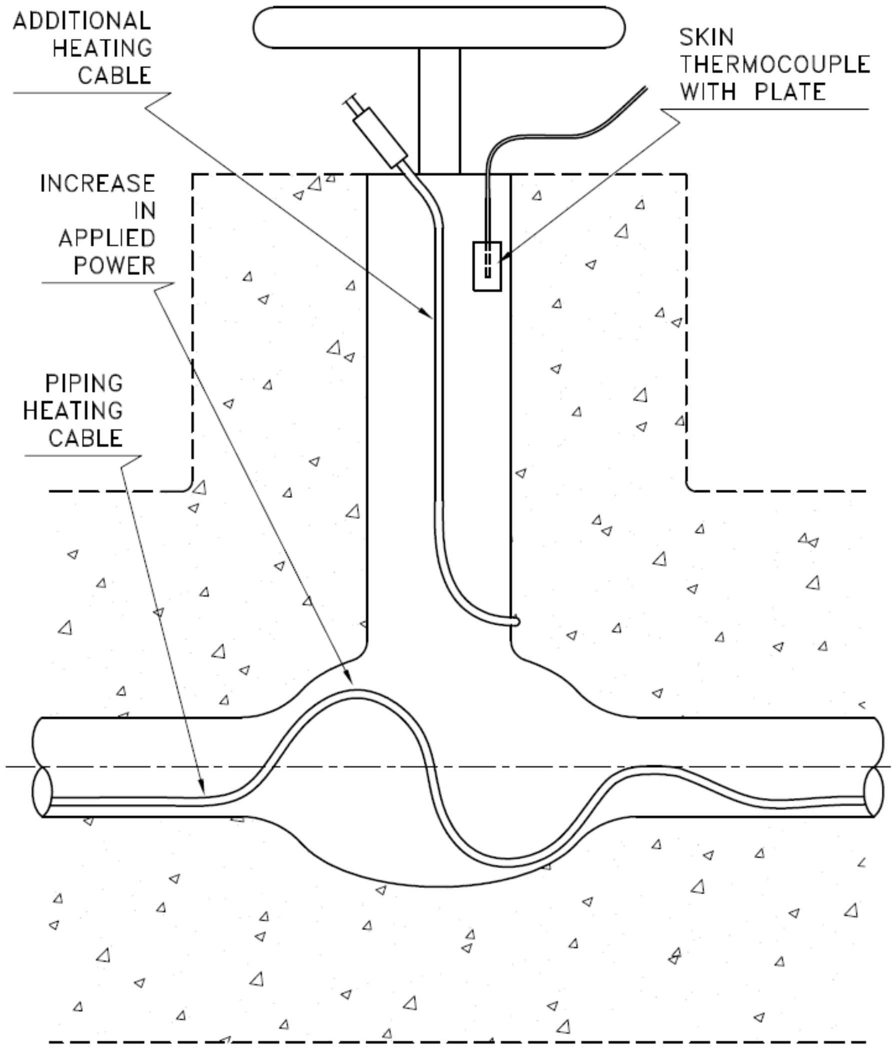

HEATING CABLES ON VENTS

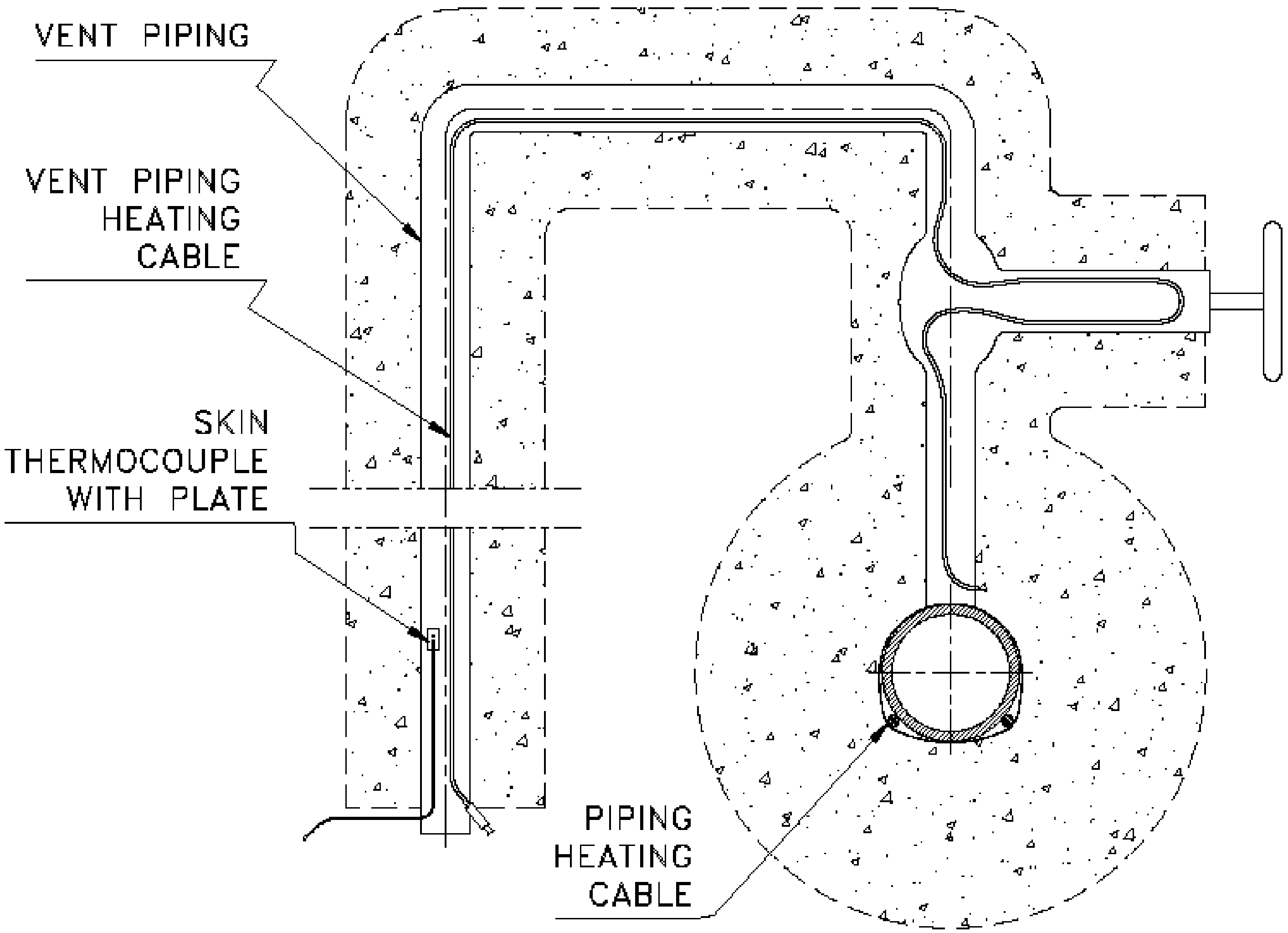

HEATING CABLES ON DRAINS

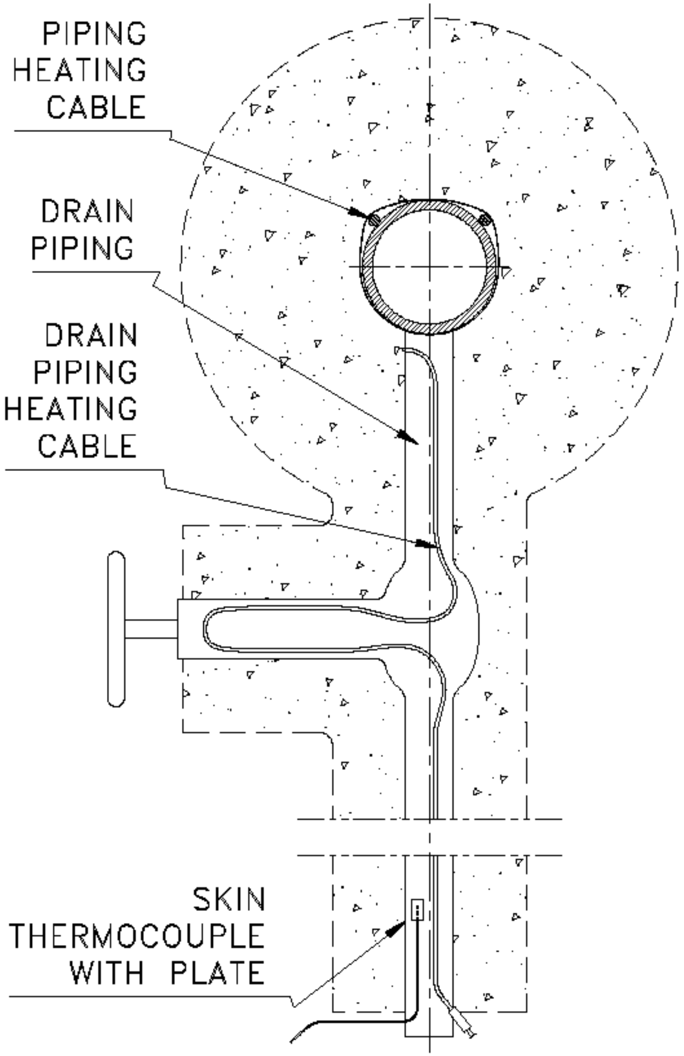

HEATING CABLES ON PRESSURE DERIVATION

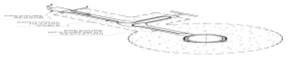

HEATING CABLES ON PIPING PRATICAL EXEMPLES

Heating cables
fixed by metal clamps

HEATING CABLES ON PIPING PRATICAL EXEMPLES

Heating cables covered by stainless-steel sheet fixed by steel-wire

This solution serves two purposes:

- Avoid contact between cable and insulation to avoid damage due to overheating of the cable
- Create an oven-like effect to better distribute the heat

HEATING CABLES ON PIPING PRATICAL EXEMPLES

Heating cables with the hot end part (not in contact with the pipe) covered with a metal sheet to prevent overheating of the cable

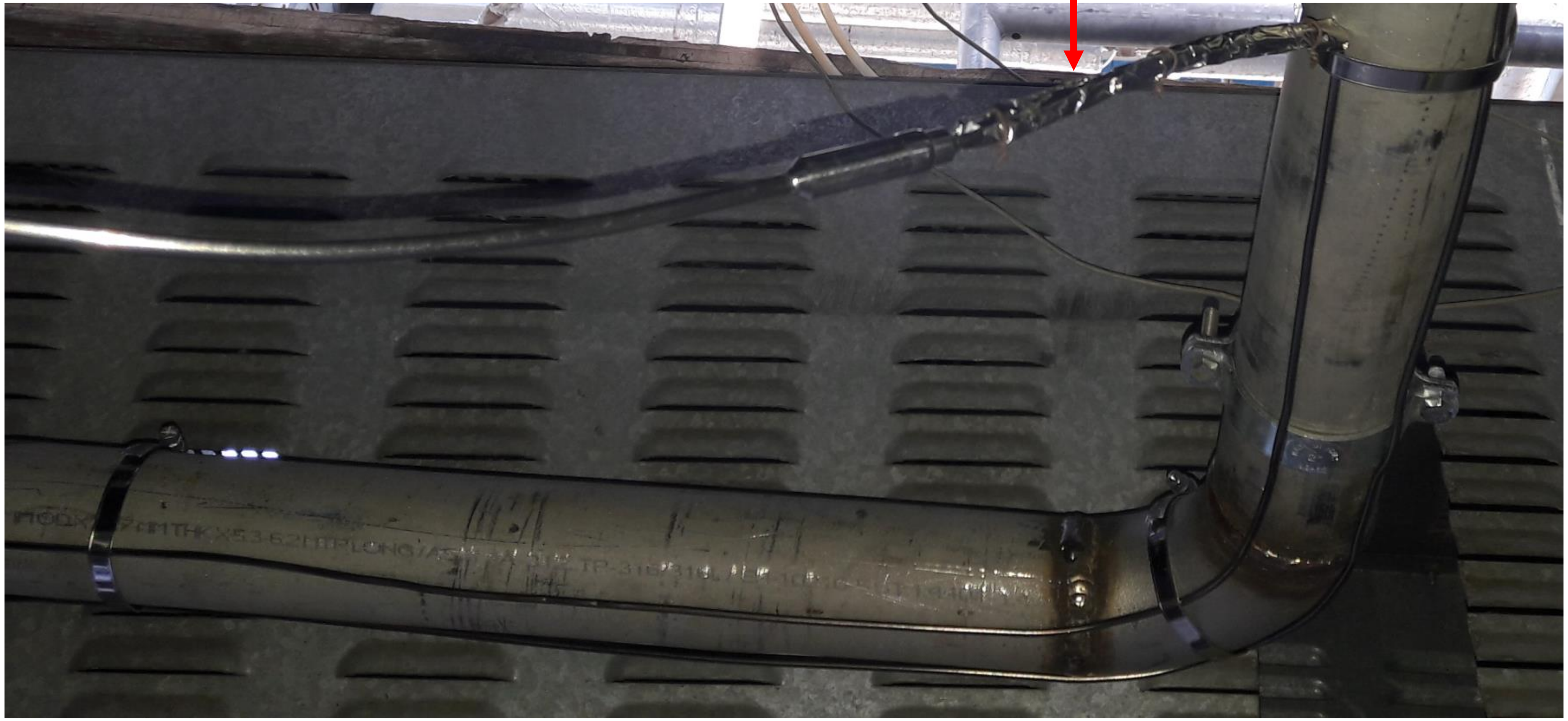

HEATING CABLES ON PIPING PRATICAL EXEMPLES

Hot end part of the cable at the end of insulation (almost optimal realization...)

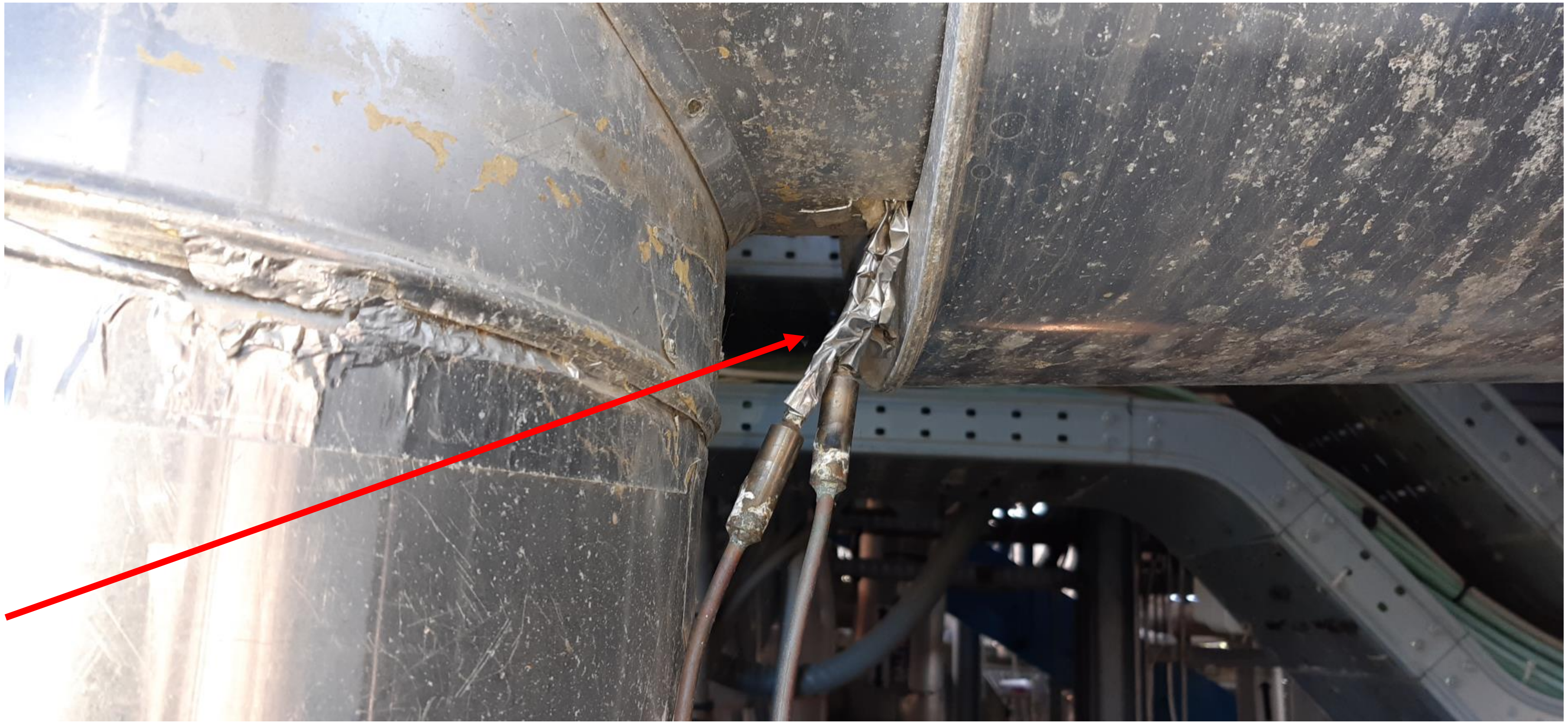

HEATING CABLES ON PIPING PRATICAL EXAMPLES

Correct arrangement of the cable around a pair of flanges

HEATING CABLES ON VESSELS

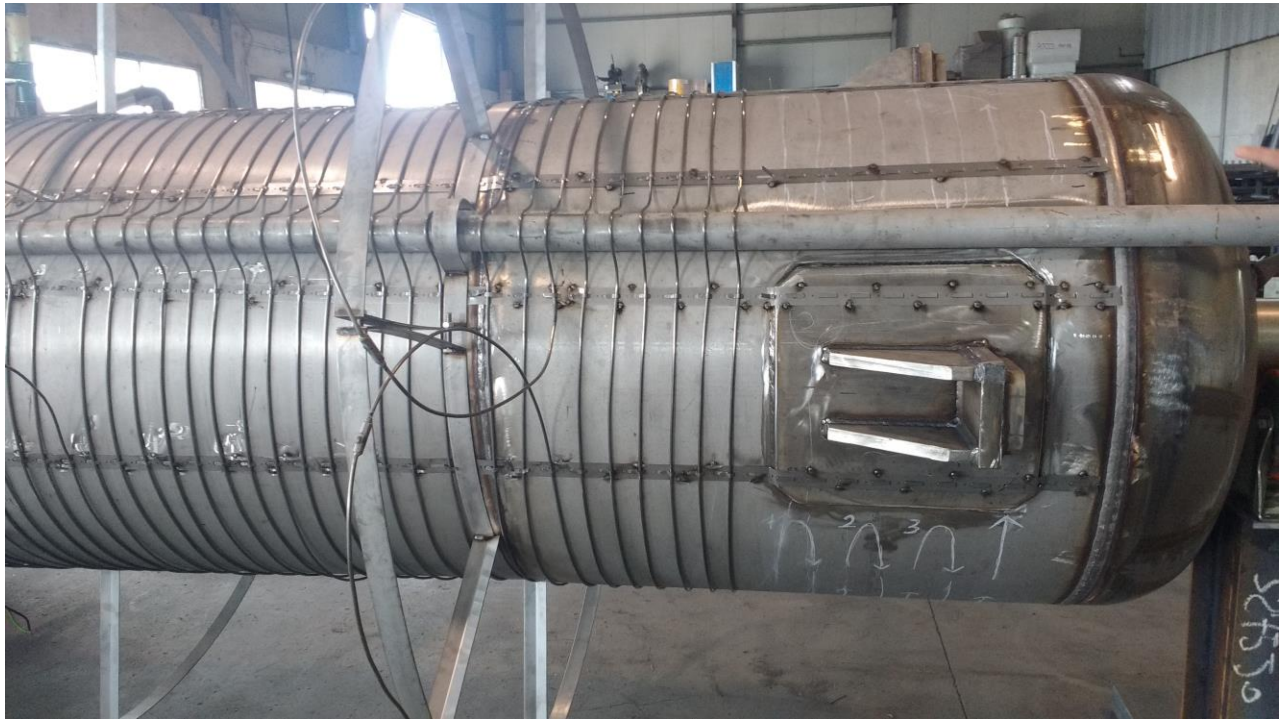

Arrangement of the cable around the wall of a vessel

Arrangement of the cable on the bottom of a vessel

HEATING BY JOULE EFFECT

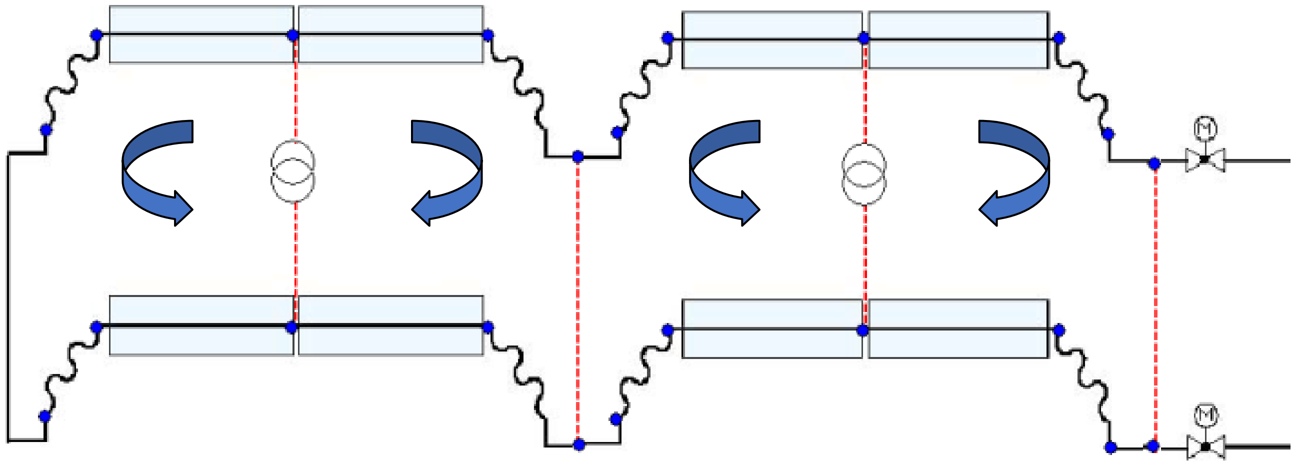

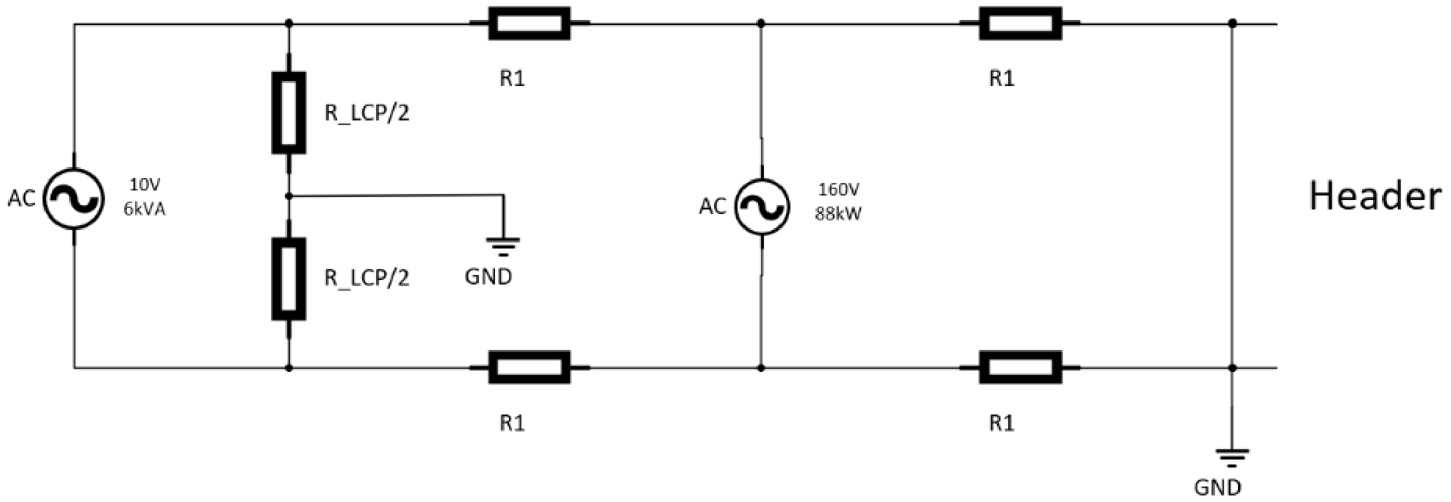

HEATING BY JOULE EFFECT

Electrical clamp

Aluminium plate and Electrical terminal

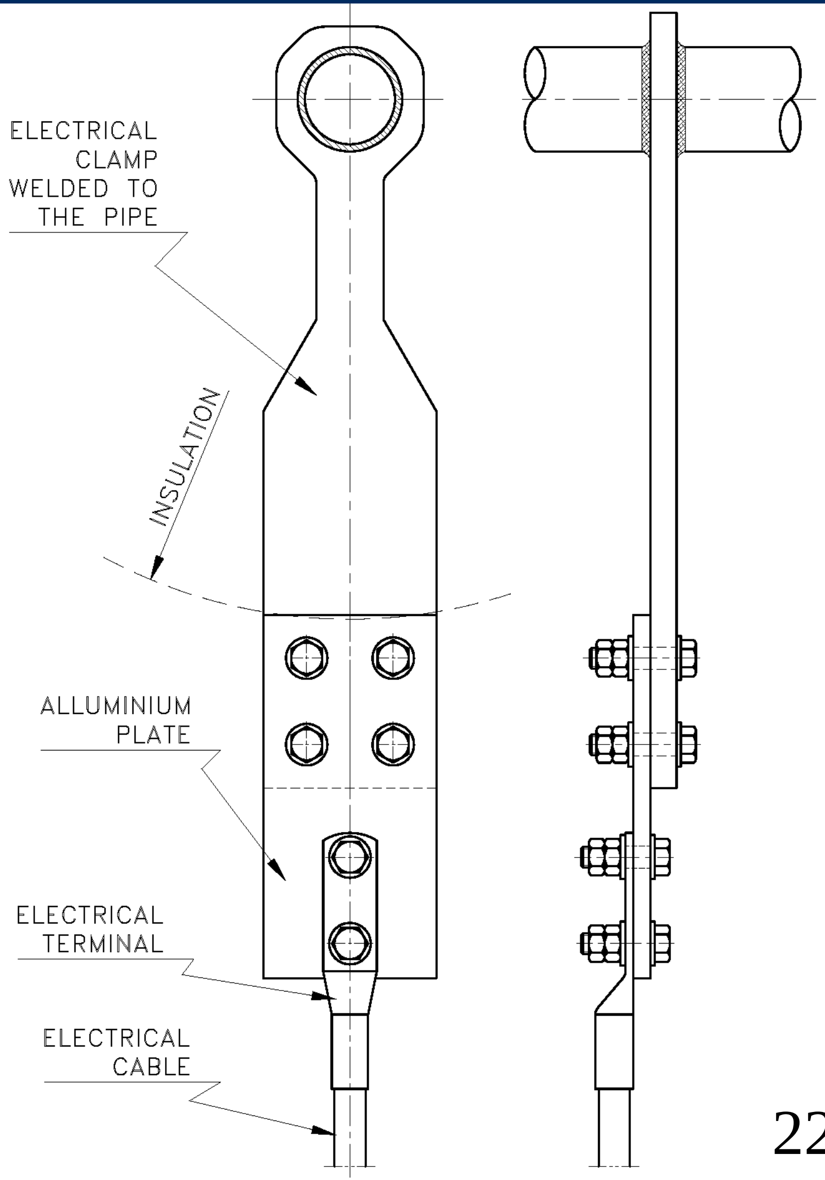

HEATING BY JOULE EFFECT

Exemples of complete electrical clamp

HEATING BY JOULE EFFECT

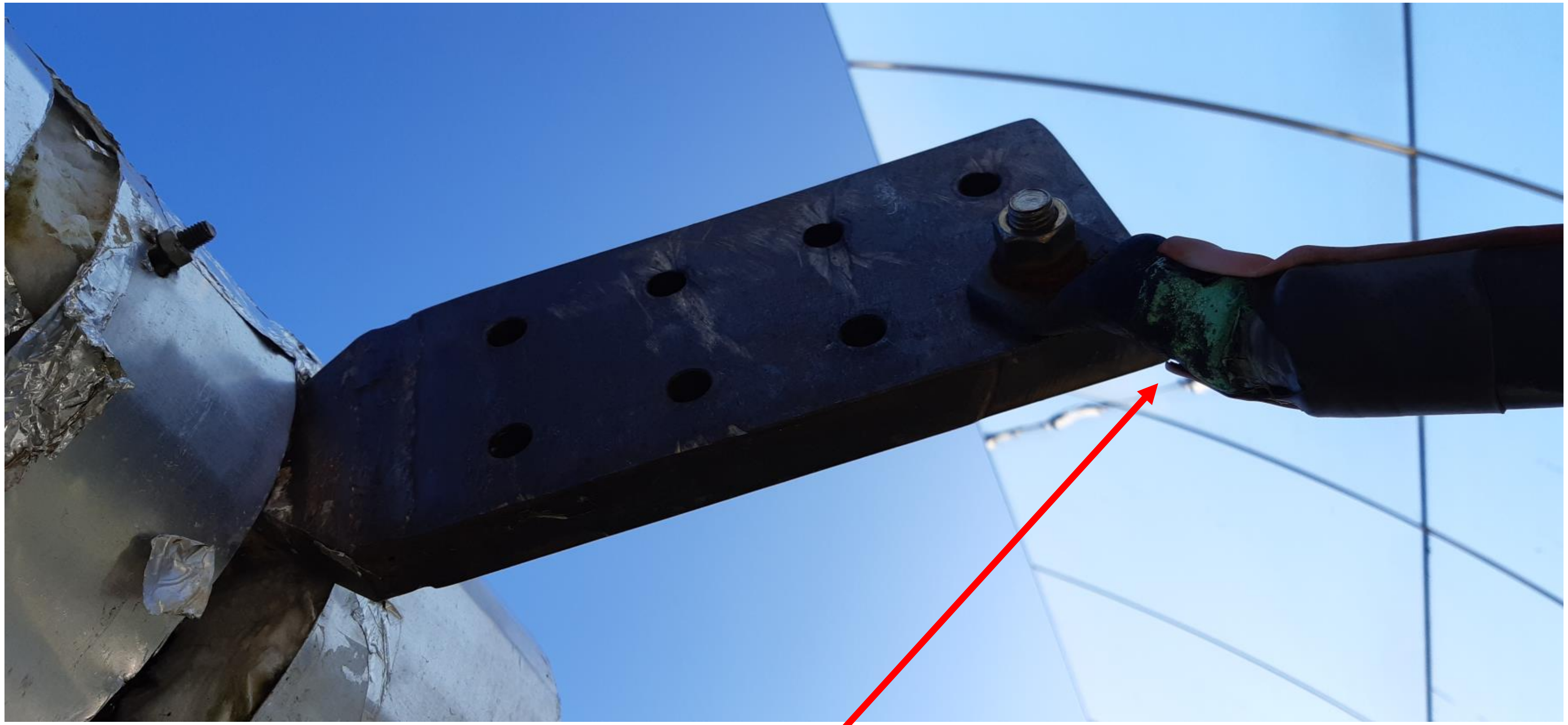

Exemples of bad electrical clamp

Overheated terminal

HEATING BY JOULE EFFECT

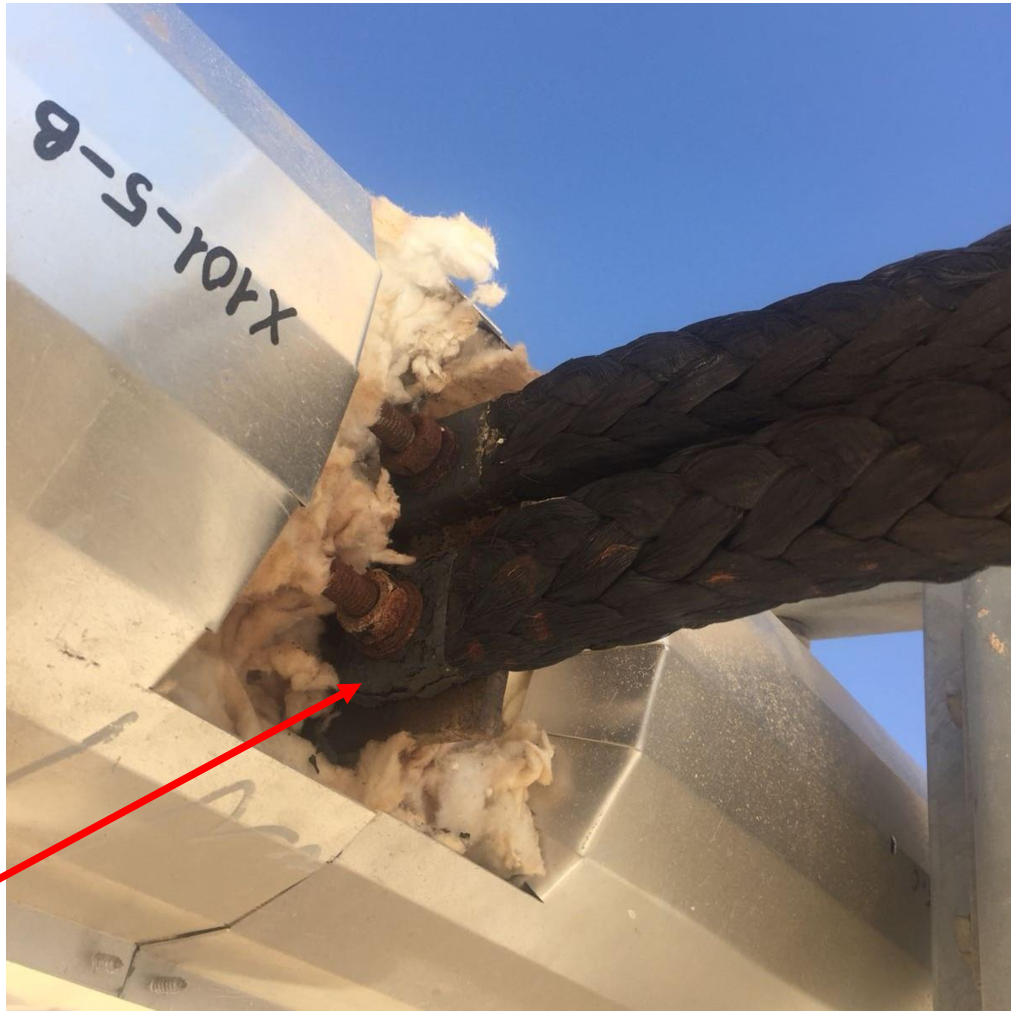

overheated terminals

HEATING BY JOULE EFFECT

HEATING BY JOULE EFFECT

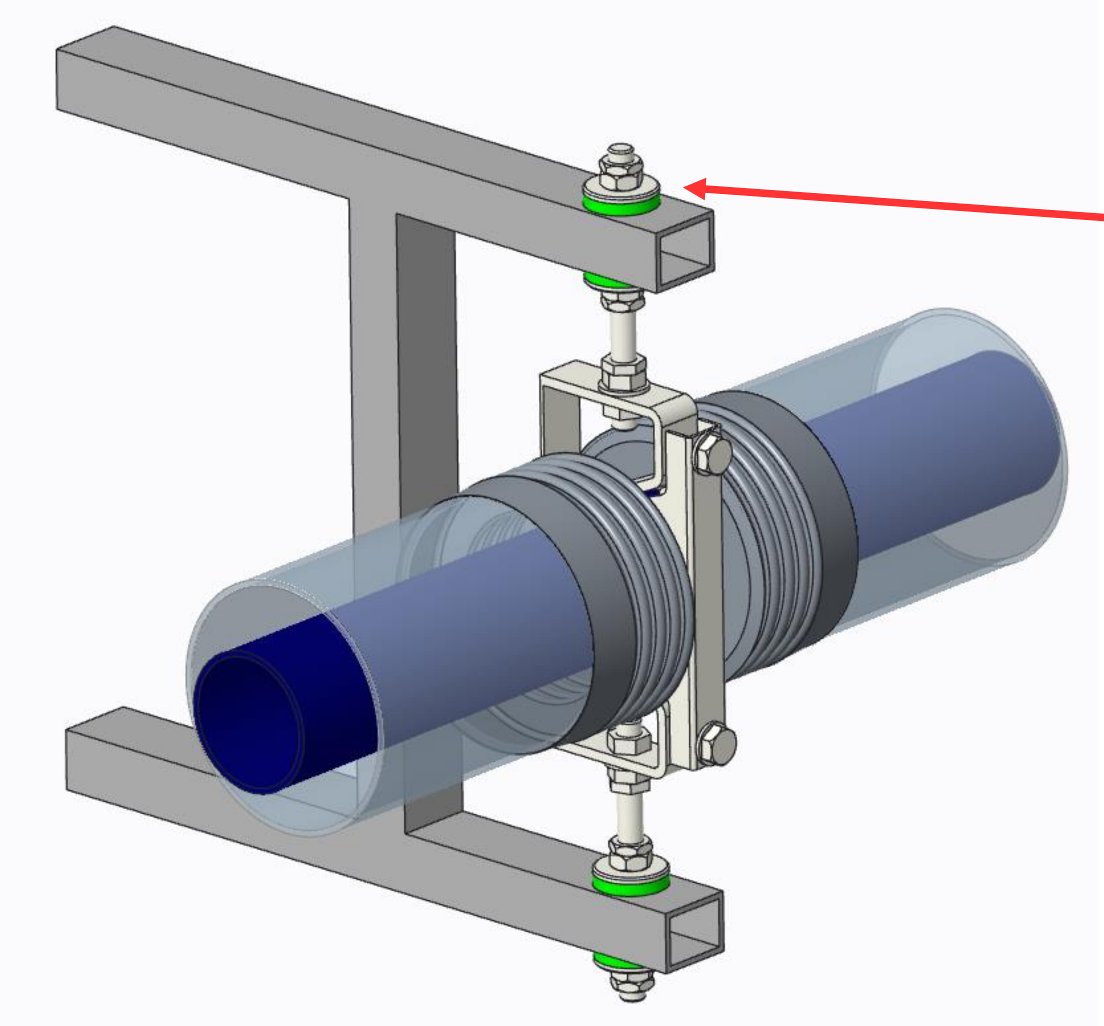

Insulating material discs (in green)

Electrically insulated receiver tube supports

HEATING IN TANKS

Well

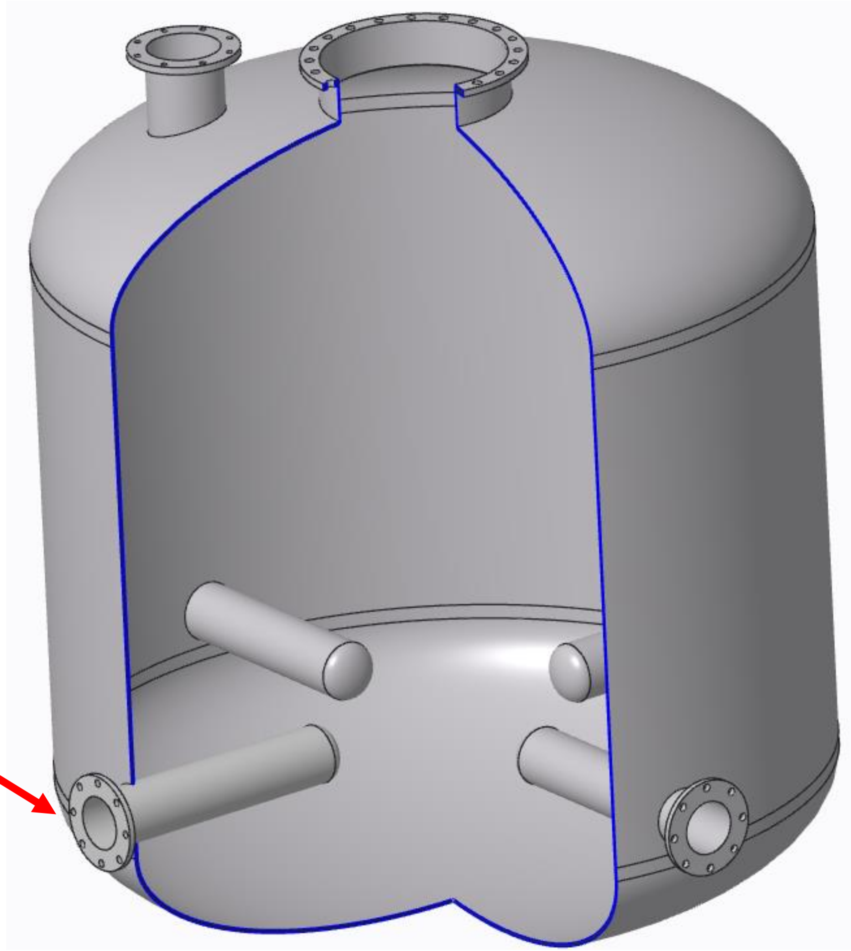

HEATING IN TANKS

Armored resistance with flange

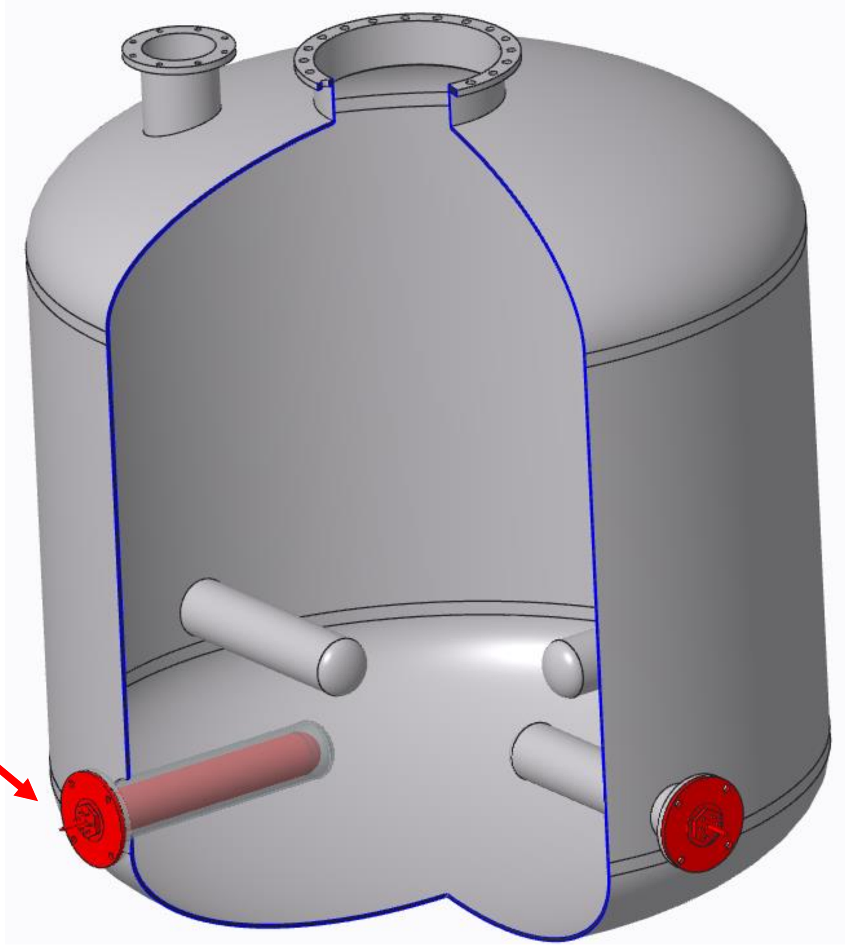

HEATING INSIDE TANKS

Pump

Well

Flange

Armored resistance (external head)

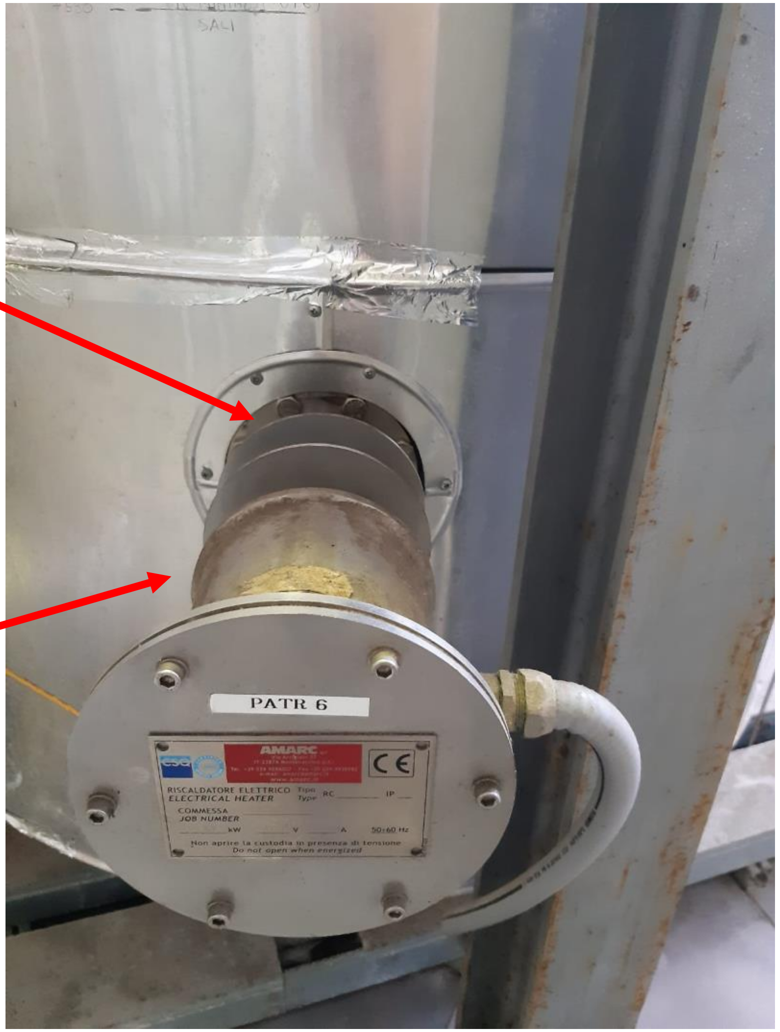

HEATING INSIDE TANKS

→ In small tank this system can be used for melt the salts

HEATING INSIDE TANKS

Salts melting operations
directly inside a 95m tank
(MATS Plant)

Giuseppe PETRONI
ENEA
TERIN-STSN-ITES
giuseppe.petroni@enea.it

THANK YOU FOR YOUR ATTENTION!
ANY QUESTIONS?

SFERA-III

Solar Facilities for the European Research Area

Solar Facilities for the European Research Area

4th Training for Industries

7-11 November 2022, Cr ENEA Casaccia Rome (Italy)

Lessons learned from operation of MS TES Systems

Giuseppe Canneto (ENEA, TERIN-STSN-SCIS)

JOINT RESEARCH ACTIVITIES

THIS PROJECT HAS RECEIVED FUNDING FROM THE EUROPEAN UNION'S HORIZON 2020 RESEARCH AND INNOVATION PROGRAMME UNDER GRANT AGREEMENT NO **823802**

Content

1 Historical background: SOLAR TWO plant (California, 1994) and ANDASOL plant (Spain, 2007)

First PT plant with direct two-tank TES: ARCHIMEDE project (2010, Sicily)

2 MATS Project: Demonstrative PT plant with a thermocline MS storage tank (2016, Egypt)

PARTANNA Project: first commercial LF Plant with a direct two-tank MS TES (2021,Sicily)

Some projects with the participation of ENEA

TES: Best Practices

3 Considerations on failures in the hot salt tanks of commercial plant

Passive cooling system in tank foundation : experimental data vs. results of numerical simulations.

Historical background: ***Solar Two plant***

(Google image)

Historical background: *Solar Two plant*

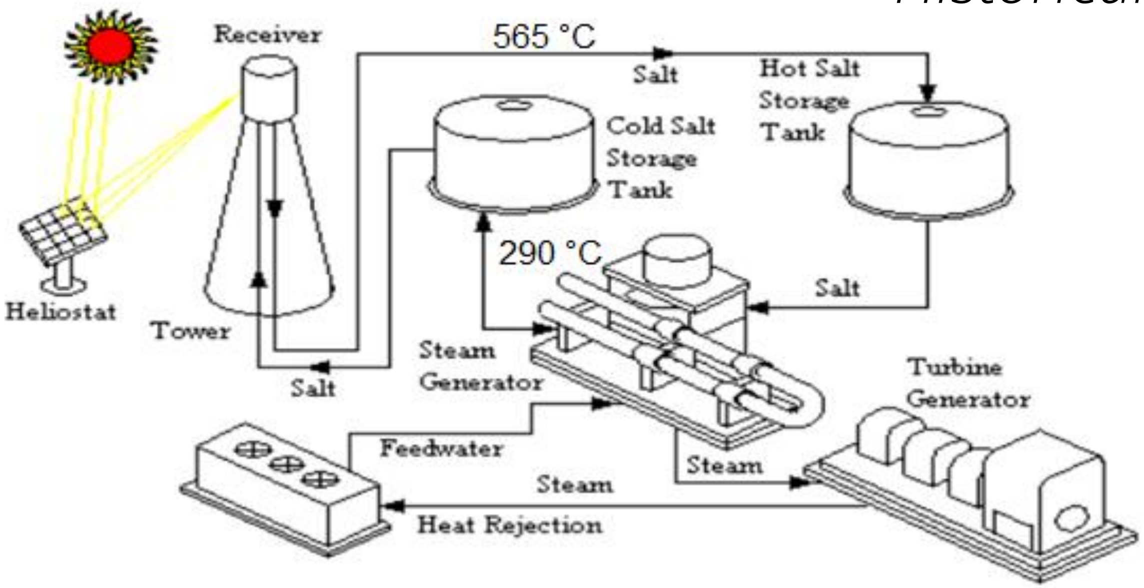

Solar Two: first plant using Molten Salts

Operative period: 1994-1999

Storage technology system: two-tanks direct storage system

HTF and HSM : molten salt

Storage Capacity: 107 MWhth

Storage duration: 3 h

Andasol plant

(Google image)

Andasol plant

(Source: Andasol 3)

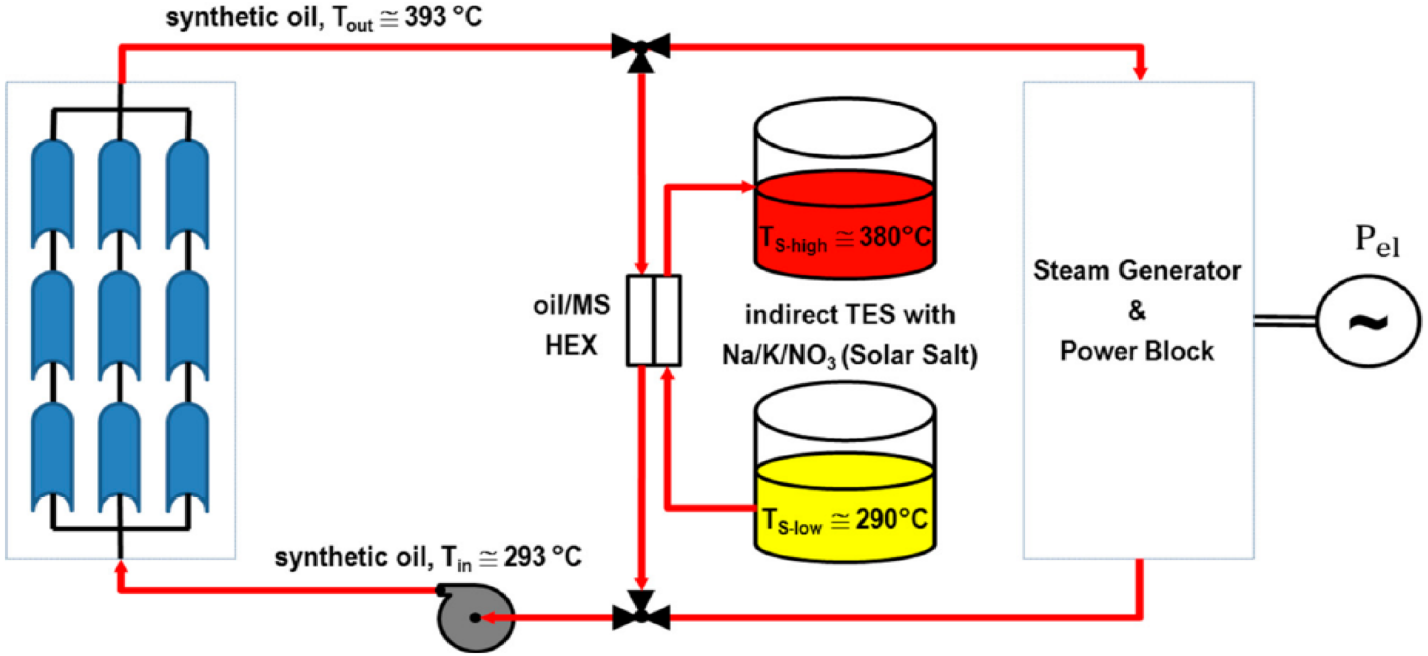

Storage Technology system: indirect two-tank storage systems
Storage Capacity: 1100 MWhth
Storage duration: 7.5 h.

Differences between the two plant schemes

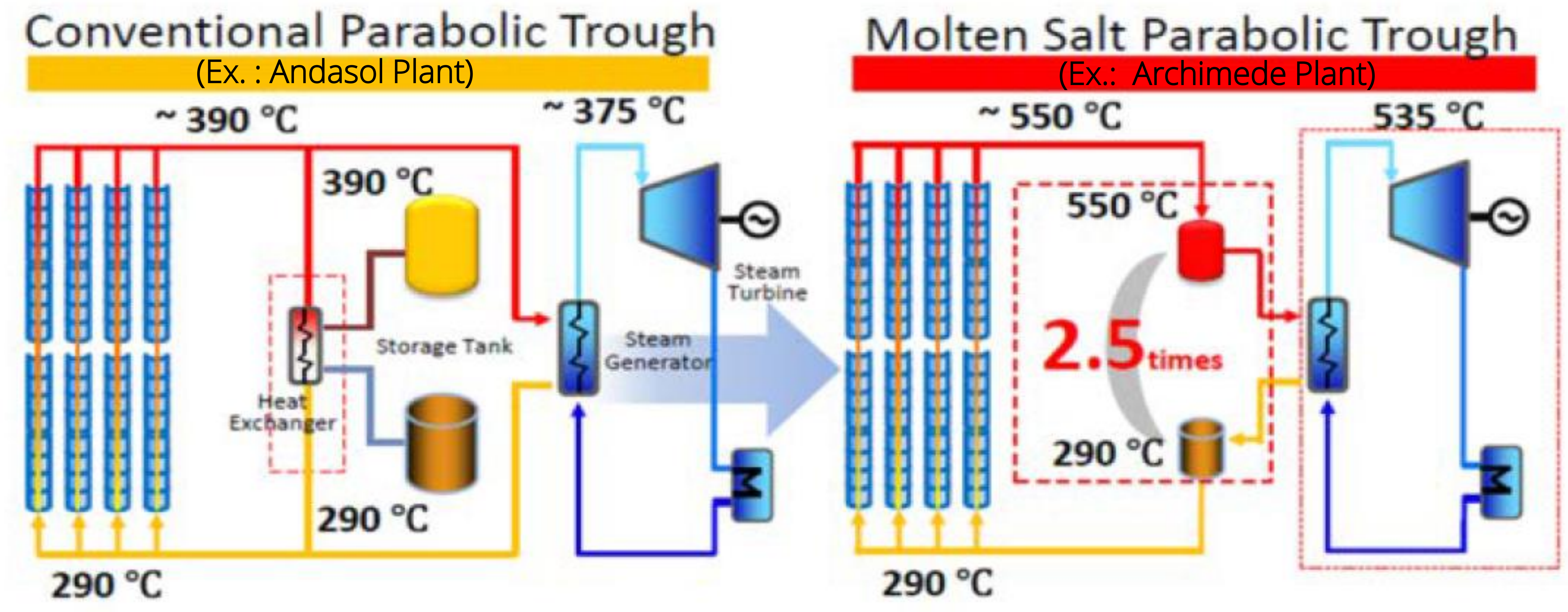

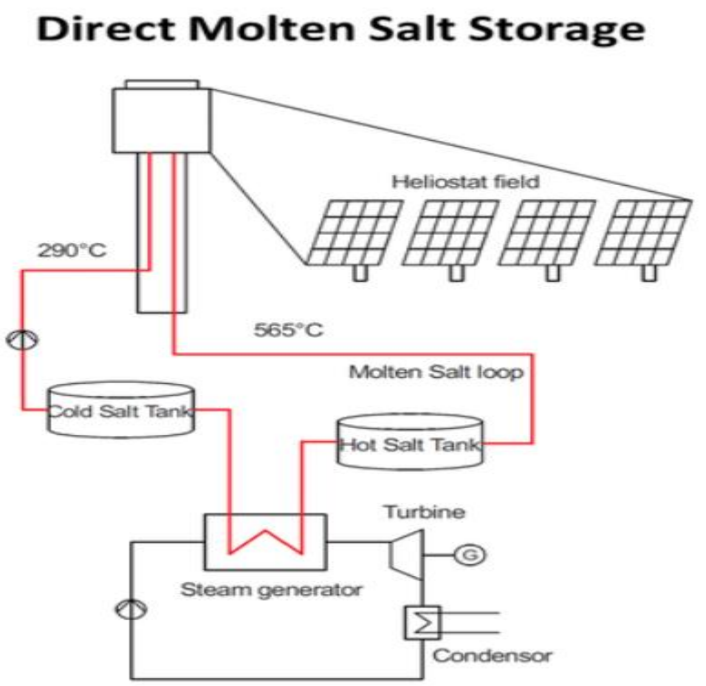

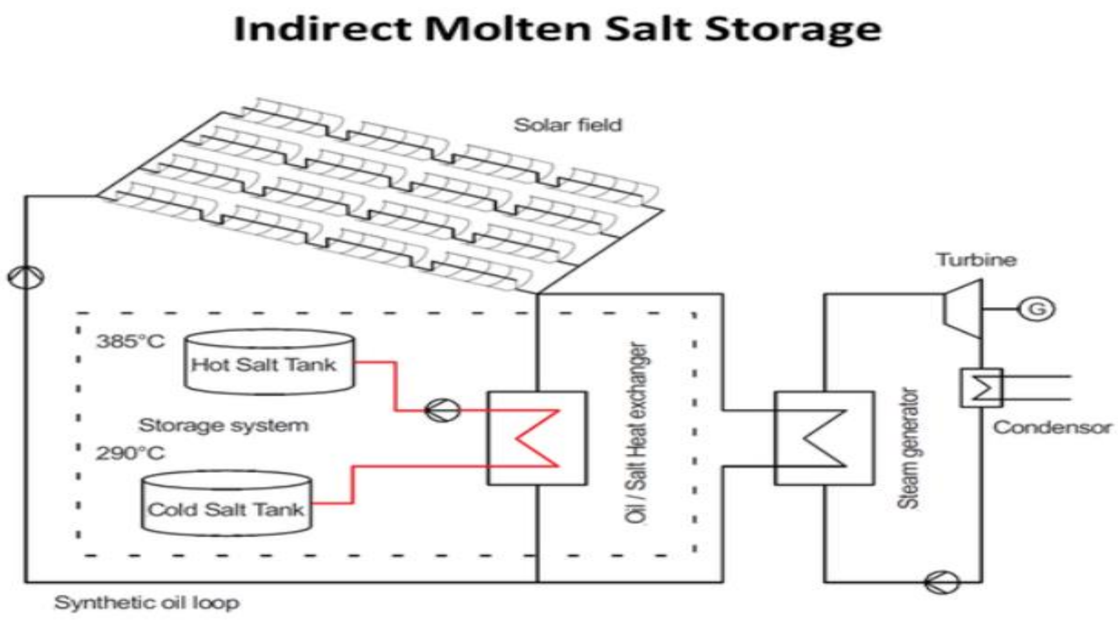

	Direct Two-tank system	Indirect Two-tank system
Plant	Gemasolar	Andasol
Cold Tank Temperature	290 °C	290 °C
Hot Tank Temperature	565 °C	385 °C
Inventory	8500 tons	28500 tons
Thermal Capacity	~ 1000 MWh	~ 1100 MWh

(**Source: Overview of molten salt storage systems and material development for solar thermal power plants** ,T. Bauer, et al. 2012)

The Archimede project

(Google image)

*The **Archimede plant: basic data***

ISCC type **plant**

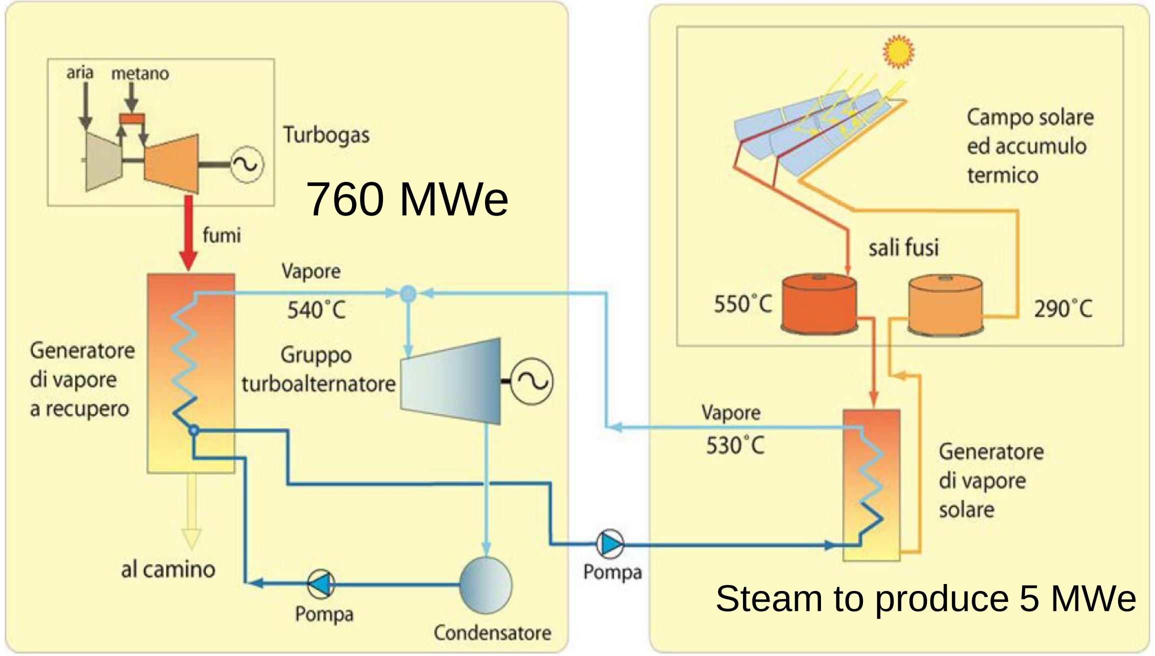

Commissioning: 2010
ISCC Plant
Storage system: direct 2-tank storage system
HTF, HSM: Molten Salt
Storage duration : 6.5h

*The **Mats project***

(Google image)

The *Mats plant: basic data*

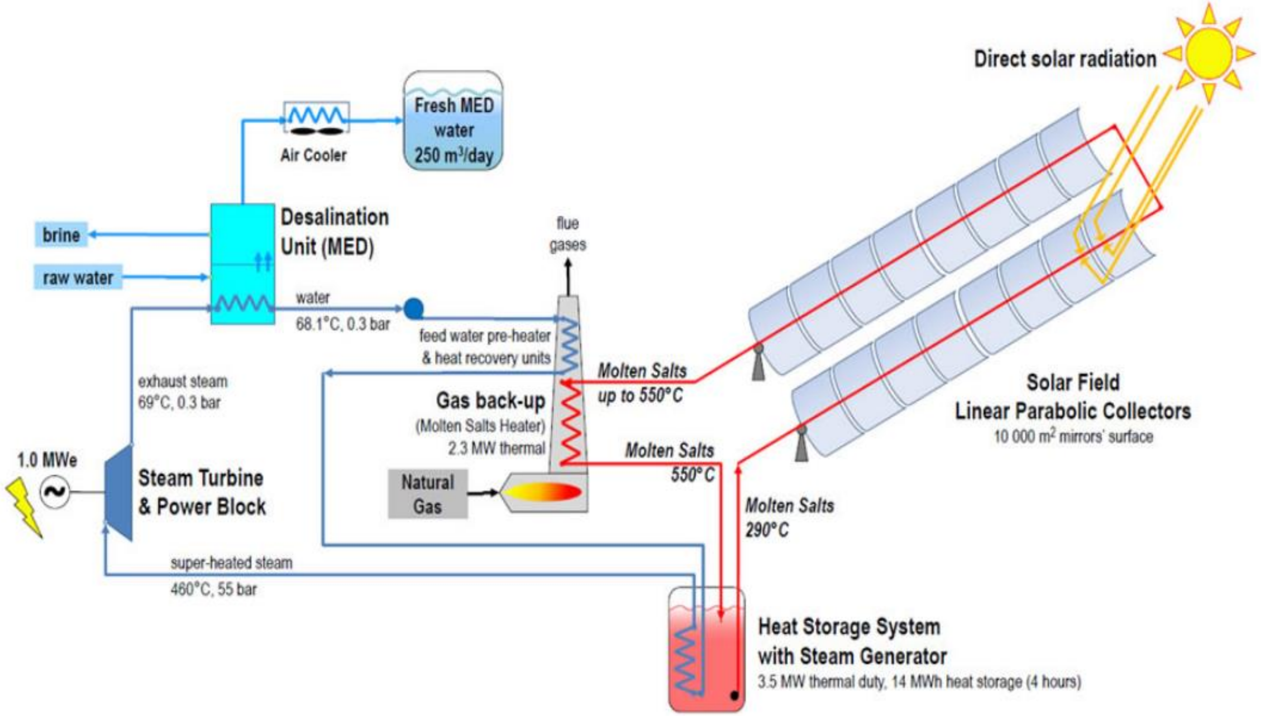

Storage Technology: single tank thermocline storage system with "once through" steam generator inside the tank
Storage Capacity: 14 MWhth
Storage duration: 4 h.

The Partanna project

(Google image)

The Partanna plant: basic data

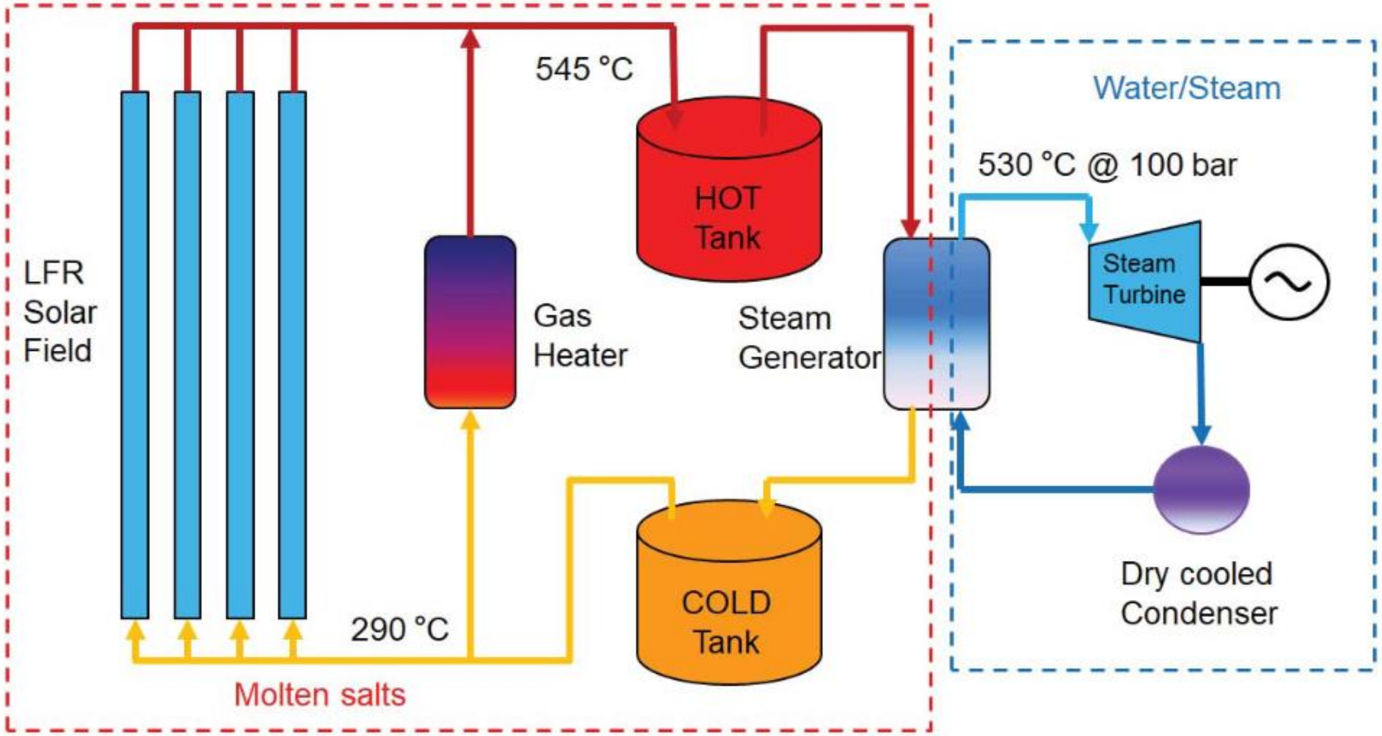

Power: 4.2 MWe
HTF and HSM: Solar Salt
Storage thermal Capacity=180 MWhth
Storage duration = up to 15 h
Synchronized with the national high voltage grid in 2021

Best practices for solar storage tanks

- Storage tanks are unique: there are no dedicated **standards** for their calculation
- Tanks design according to **API** Standard 650 combined with **ASME** Code
- Tanks are sized to hold the **full inventory** of salt
- **Minimum heel level** of salt to keep the impeller of the salt pumps submerged
- **Material expansion**: the floor and the foundation must be designed to handle the normal expansion of the tanks
- **Buckling**: the thickness of the floor must provide adequate resistance to buckling
- **Friction** between the tank and the foundation
- Tanks are manufactured on site: quality control of all the **weldings** is essential.
- **Passive cooling system**: the concrete under the tank does not overheat.

Considerations on failures in the hot salt tanks of commercial plant (Solarpaces, 2022)

- *Design Basis Document / Owner's Technical Specification for Nitrate Salt Systems in CSP Projects Hypothesis of Hot Tank Failure-* Bruce Kelly et al. SolarPaces 2022

- *Effect of welding parameters on residual stress and distortion of molten salt hot tank floors for concentrated solar power applications* - Julian D. Osorio, et.al. SolaPaces 2022

-API 650 and ASME Section II standards: these standards seem to be limited for CSP hot tanks (large capacity, high temperatures, thermal cycling, and transient conditions).

-5 **failures** (occurred sooner than the expected low cycle fatigue life)

-**Transient operation** conditions rapidly change the temperature increasing thermal stresses in the tank's floor and shell.

-The combination of **thermal stresses and friction** can compromise the integrity of the tank

Hypothesis on failures in the hot salt tanks of commercial plant: the welding process

(*Effect of welding parameters on residual stress and distortion of molten salt hot tank floors for concentrated solar power applications* - Julian D. Osorio, et.al. SolaPaces 2022)

The tank floor is usually fabricated by welding thin rectangular plates): residual stresses and plastic deformation may be introduced into the floor after welding

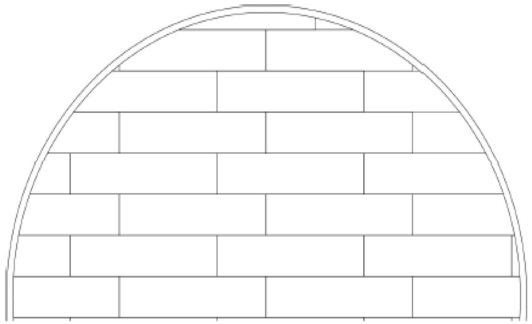

a) horizontal plates (small tanks)

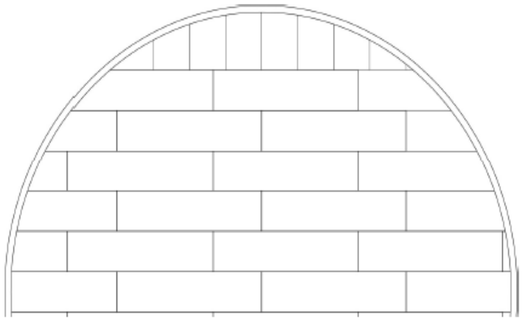

b) horizontal and vertical plates (large diameter tanks)

Fabrication of a molten salt storage tank*

Distorsion of the floor: possible effect after the welding process

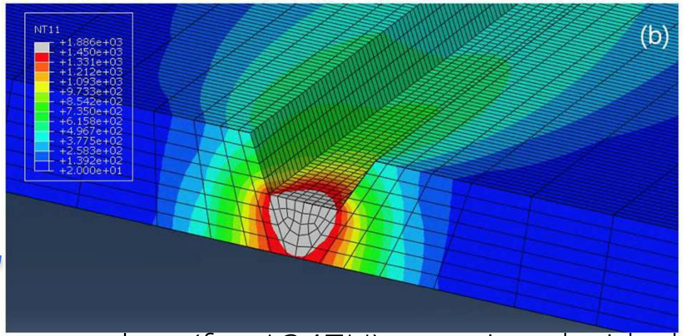

Tensile stress contour plots (for A347H) associated with the welding procedure

*The Partanna Project: A First of a Kind Plant Based on Molten Salts in LFR Collectors M. Falchetta et al. SolarPaces 2019

Hypothesis on failures in the hot salt tanks of commercial plant: the radial gradient of temperature 1/2

(*Design Basis Document / Owner's Technical Specification for Nitrate Salt Systems in CSP Projects - Hypothesis of Hot Tank Failure-* Bruce Kelly et al. SolarPaces 2022)

Near the **center of the tank**, thermal resistance to heat transfer from the floor to the foundation can be greater than the thermal resistance at the **perimeter of the tank**

Heat flux from the floor is **greater at the tank perimeter than at the tank center.**

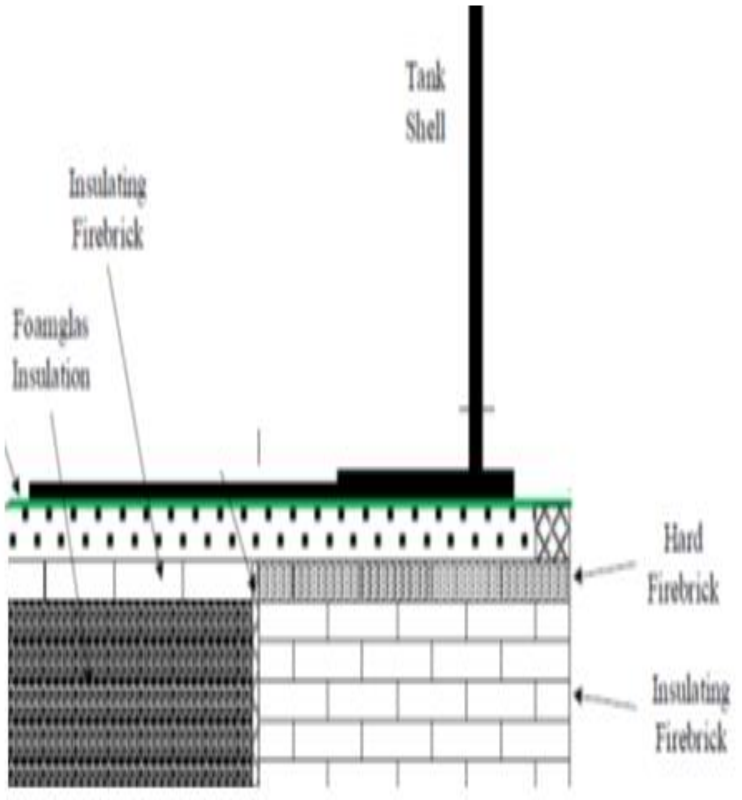

Cross-section of a tank foundation

Hypothesis on failures in the hot salt tanks of commercial plant: the radial gradient of temperature 2/2

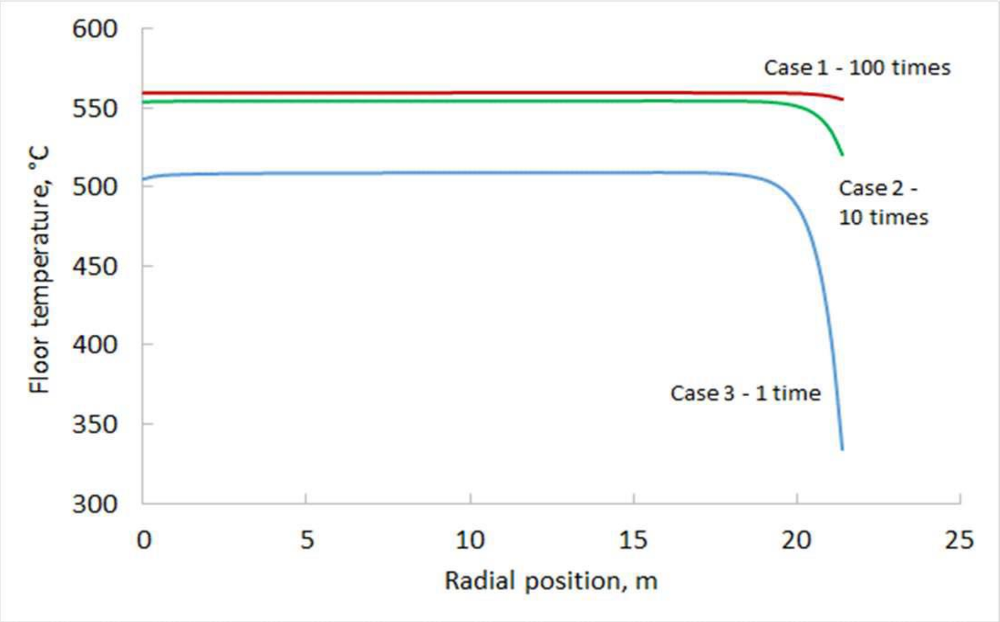

Floor Temperature vs radial position

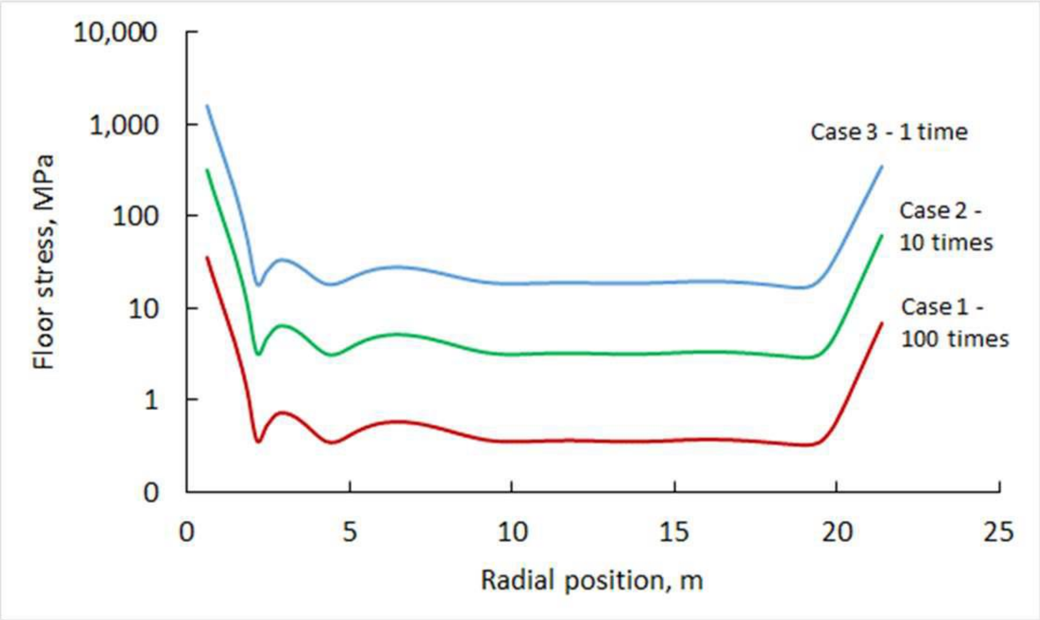

Floor stress vs radial position

"Calculations show that any radial temperature gradient above about 35 °C is sufficient to permanently damage the floor".

Passive cooling system in tank foundation: comparison experimental data vs. numerical simulations 1/11

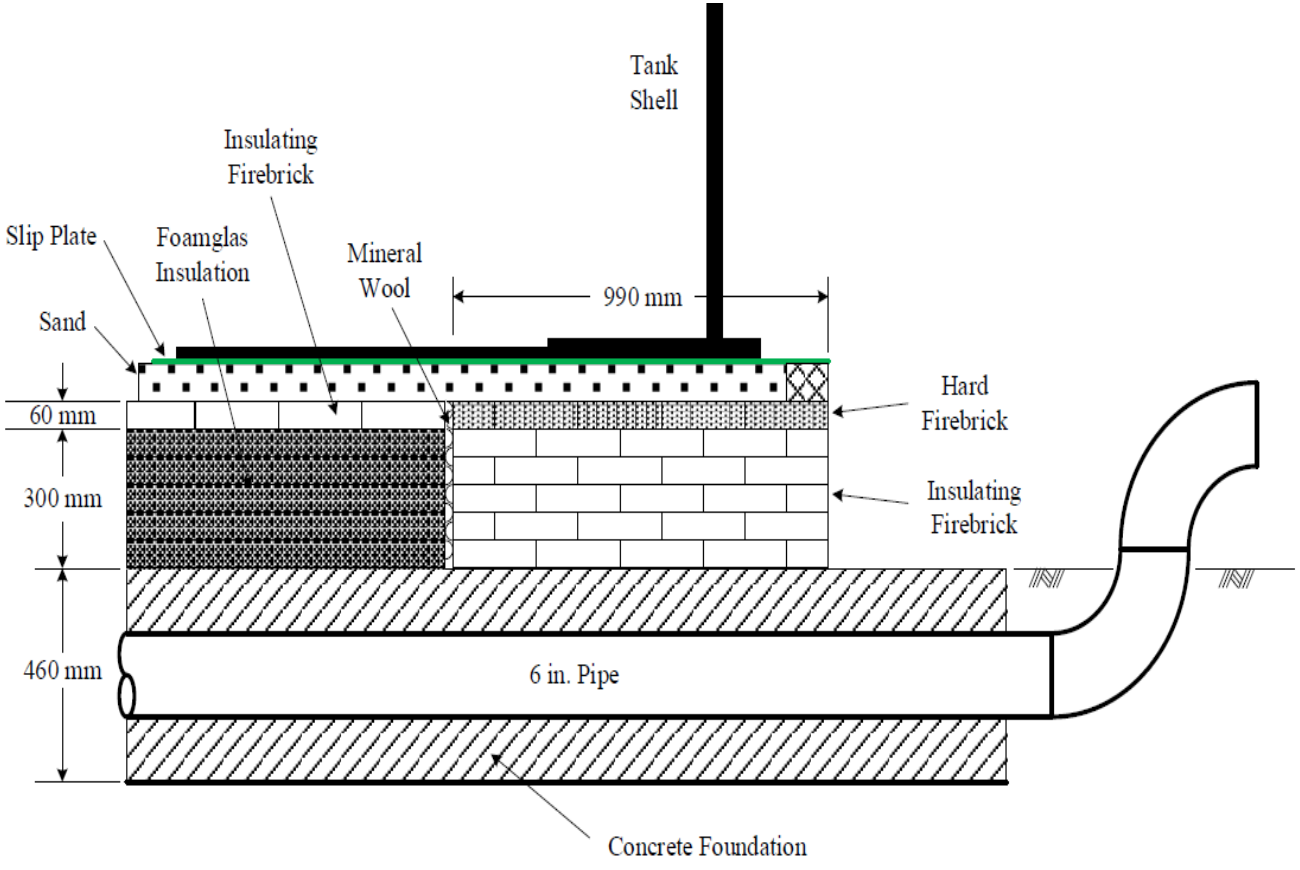

Cross-section of the hot-tank foundation at Solar Two plant

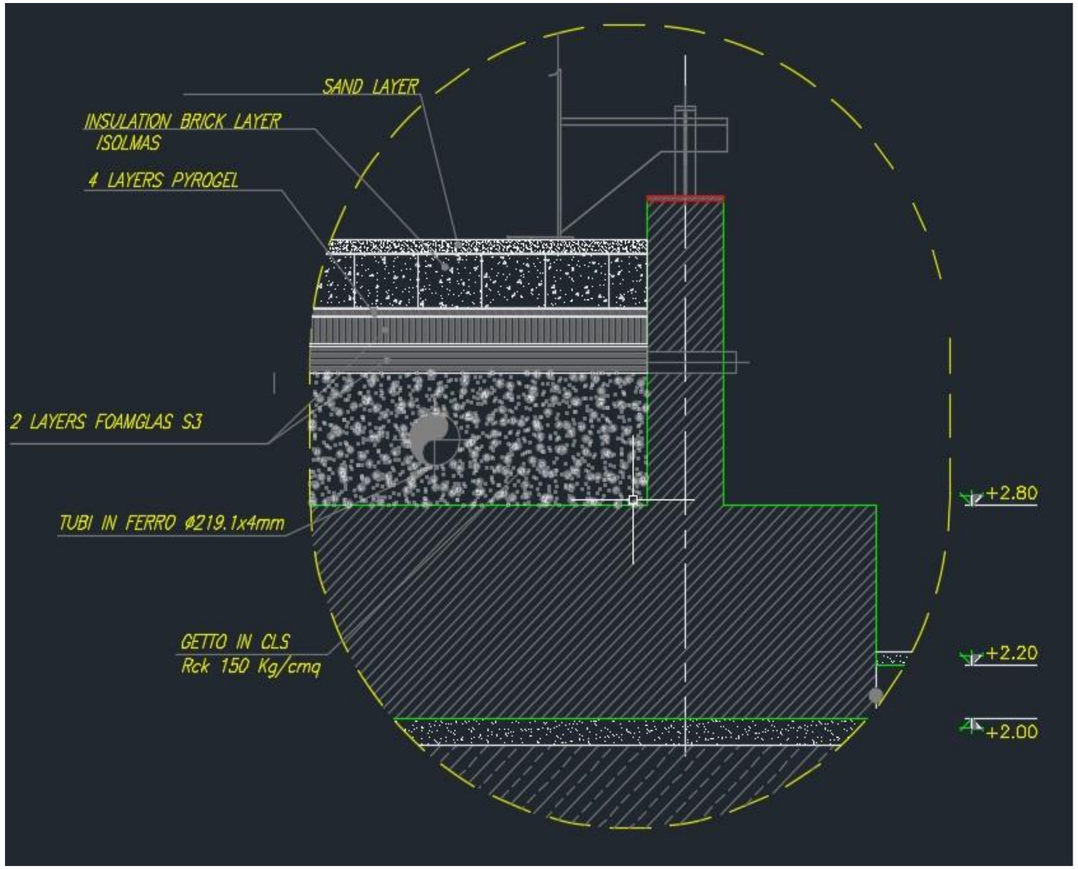

Cross-section of the hot-tank foundation at Archimede plant with 8 inches cooling pipes

Passive cooling system in tank foundation: comparison experimental data vs. numerical simulations 2/11


Fabrication of the tanks at the Archimede plant


Cooling pipes into the concrete of the hot tank at the Archimede plant

Passive cooling system in tank foundation: comparison experimental data vs. numerical simulations 3/11

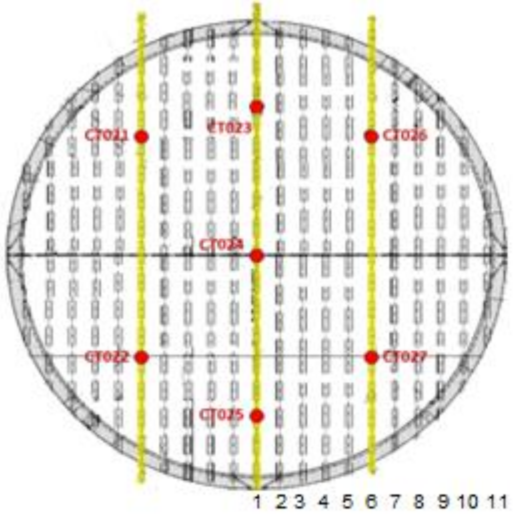

Layout of the cooling pipes and temperature sensors inside the tank foundation

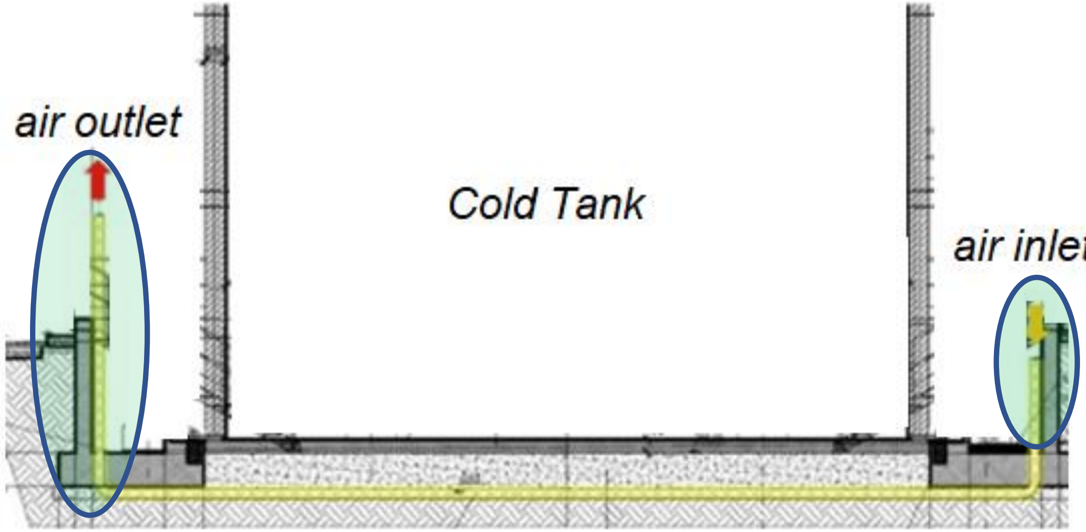

Height of the pipes on one side is greater than the height on the other side

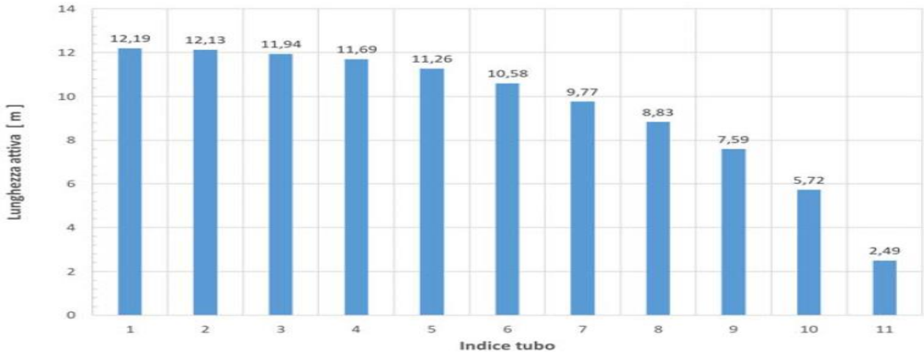

Active lengths of the cooling pipes

- -21 stainless steel pipes (A304) di=150 mm
- -Active length for heat removal is different for individual pipes
- -Height of the pipes on one side is greater than the height on the other side
- -Air movement inside the pipes is due to buoyancy force

Passive cooling system in tank foundation: comparison experimental data vs. numerical simulations.4/11

Wind could affect hot air escaping from the cooling tubes

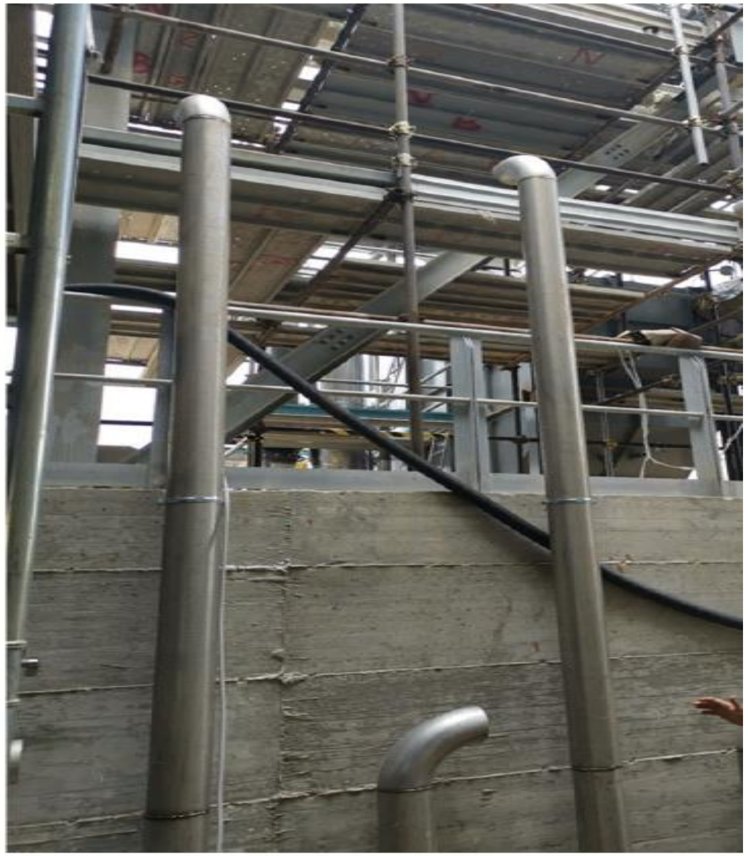

Half in the north direction half south direction.

Passive cooling system in tank foundation: comparison experimental data vs. numerical simulations 5/11

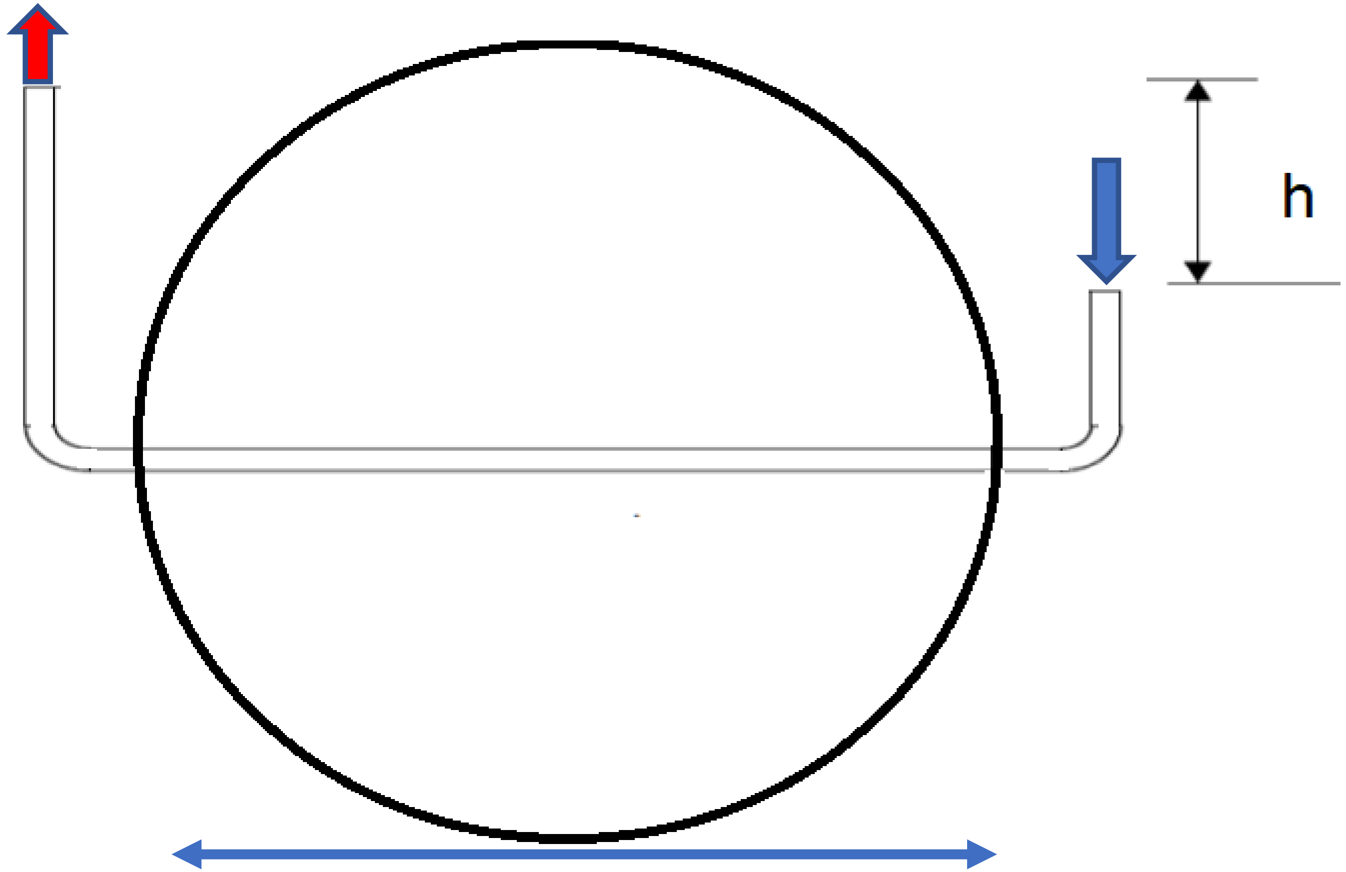

Active lenght of the central pipe

-Air natural circulation

-Buoyancy force

$$P = g\ h\ (rho_{in} - rho_{out}) \quad \text{(Pa)}$$

-Iteratively calculation for velocity

Calculated velocities into the pipes *

pipe	L (m)	V (m/s)	flow (kg/s)
1	12,19	0,7228	0,01402
2	12,13	0,7220	0,01400
3	11,94	0,7194	0,01395
4	11,69	0,7153	0,01387
5	11,26	0,7100	0,01377
6	10,58	0,7003	0,01358
7	9,77	0,6886	0,01335
8	8,83	0,6735	0,01306
9	7,59	0,6491	0,01259
10	5,72	0,6008	0,01165
11	2,49	0,4490	0,00871

* D. Mazzei Internal report ENEA 2020

Passive cooling system in tank foundation: comparison experimental data vs. numerical simulations 6/11

One of the geometric configuration and mesh considered in the simulations

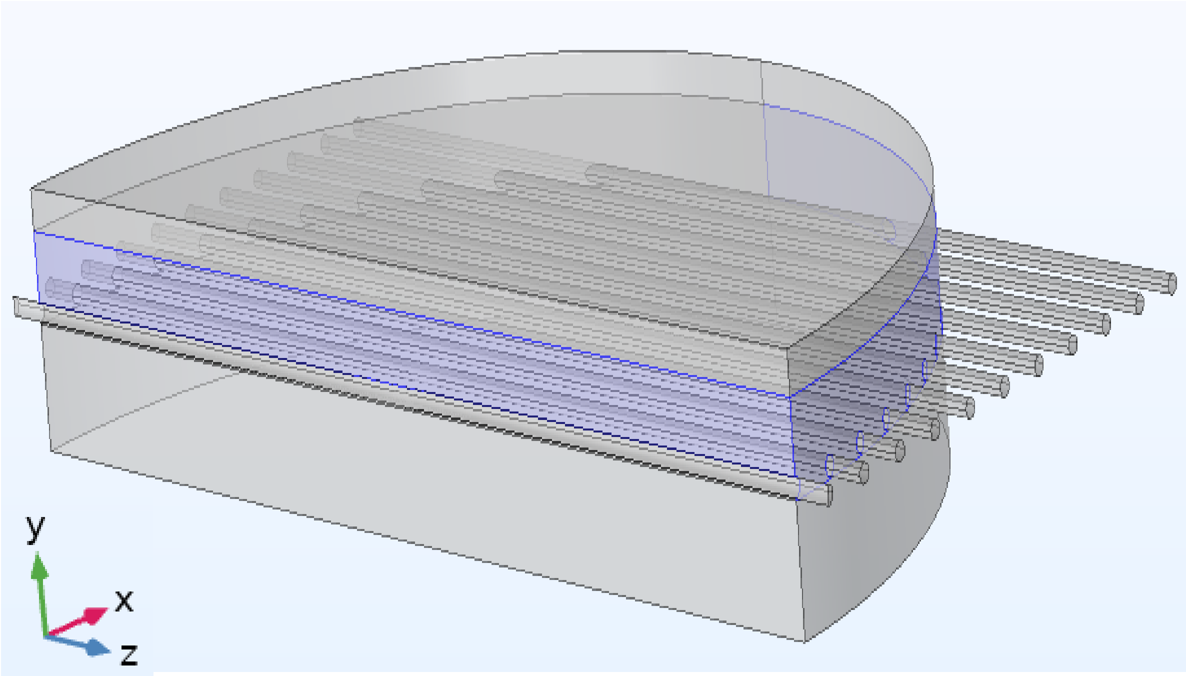

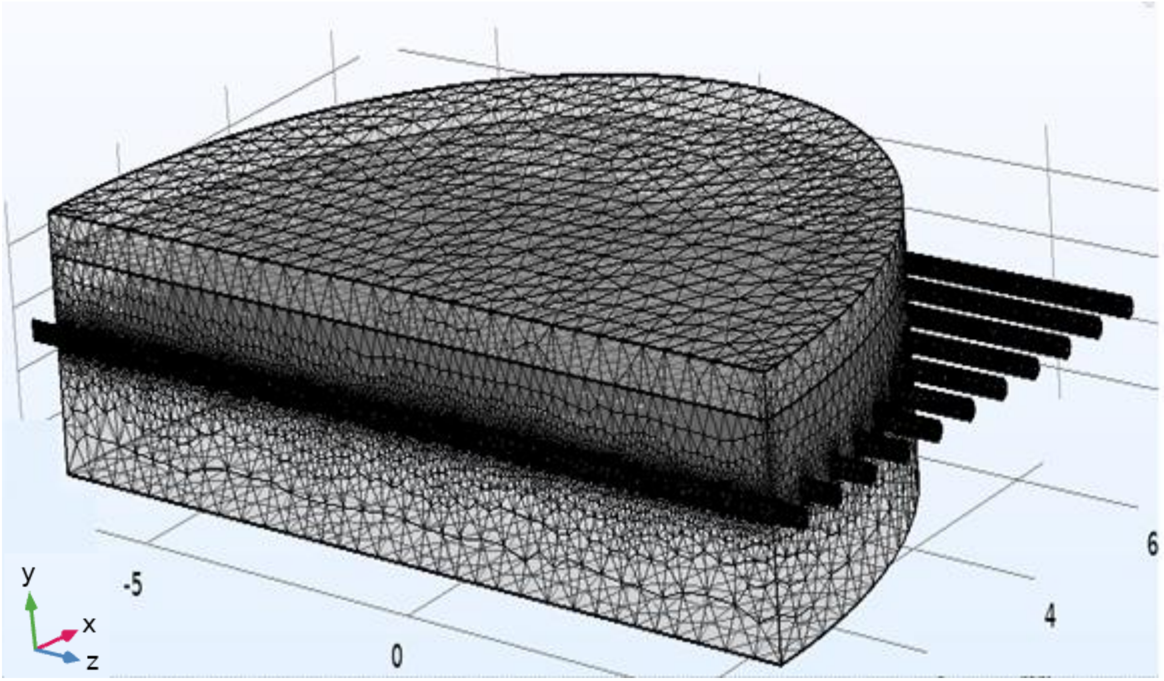

Passive cooling system in tank foundation: comparison experimental data vs. numerical simulations 7/11

Materials

- Materials
  - Promaboard (mat1)
  - soil (mat2)
  - Air (mat4)
  - Concrete_ (mat5)

Thermal conductivity 200 °C 400 °C 600 °C 800 °C	(ASTM C182-98)	W/m K	0,09 0,10 0,12 0,15

Dynamic viscosity	mu	eta(T[1/K])[Pa*s]	Pa·s
Ratio of specific heats	gamma	1.4	1
Heat capacity at consta...	Cp	Cp(T[1/K])[J/(kg*K)]	J/(kg·K)
Density	rho	rho(pA[1/Pa],T[1/K])[k...	kg/m³
Thermal conductivity	k_iso ; ki...	k(T[1/K])[W/(m*K)]	W/(m·K)

Design thermal values for materials in general building applications

Material group or application		Density ρ kg/m³	Design thermal conductivity λ W/(m·K)	Specific heat capacity c_p J/(kg·K)	Water vapour resistance factor μ dry	wet
Asphalt		2 100	0,70	1 000	50 000	50 000
Bitumen	Pure	1 050	0,17	1 000	50 000	50 000
	Felt/sheet	1 100	0,23	1 000	50 000	50 000
Concrete [a]	Medium density	1 800	1,15	1 000	100	60
		2 000	1,35	1 000	100	60
		2 200	1,65	1 000	120	70
	High density	2 400	2,00	1 000	130	80
	Reinforced (with 1 % of steel)	2 300	2,3	1 000	130	80
	Reinforced (with 2 % of steel)	2 400	2,5	1 000	130	80

	k_concrete	k_calcium silicate T>350 °C	k_calcium silicate T<350 °C	k_soil (clay)	T_salts	T_soil	Soil Depth
Parameter values used in the simulations	1.15-2.5 W/(m K)	0.11 W/(m K)	0.09 W/(m K)	1.5-2 W/(m K)	290 Cold 545 Hot °C	20-40 °C	1-10 m

Passive cooling system in tank foundation: comparison experimental data vs. numerical simulations 8/11 Results

Temperature trend along lines parallel to the y axis and contained in the yz plane across the center of the tank (cold tank)

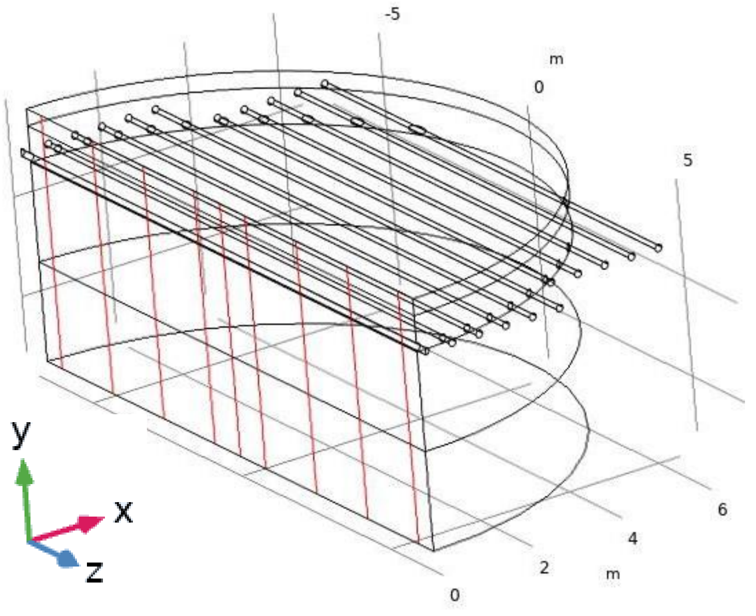

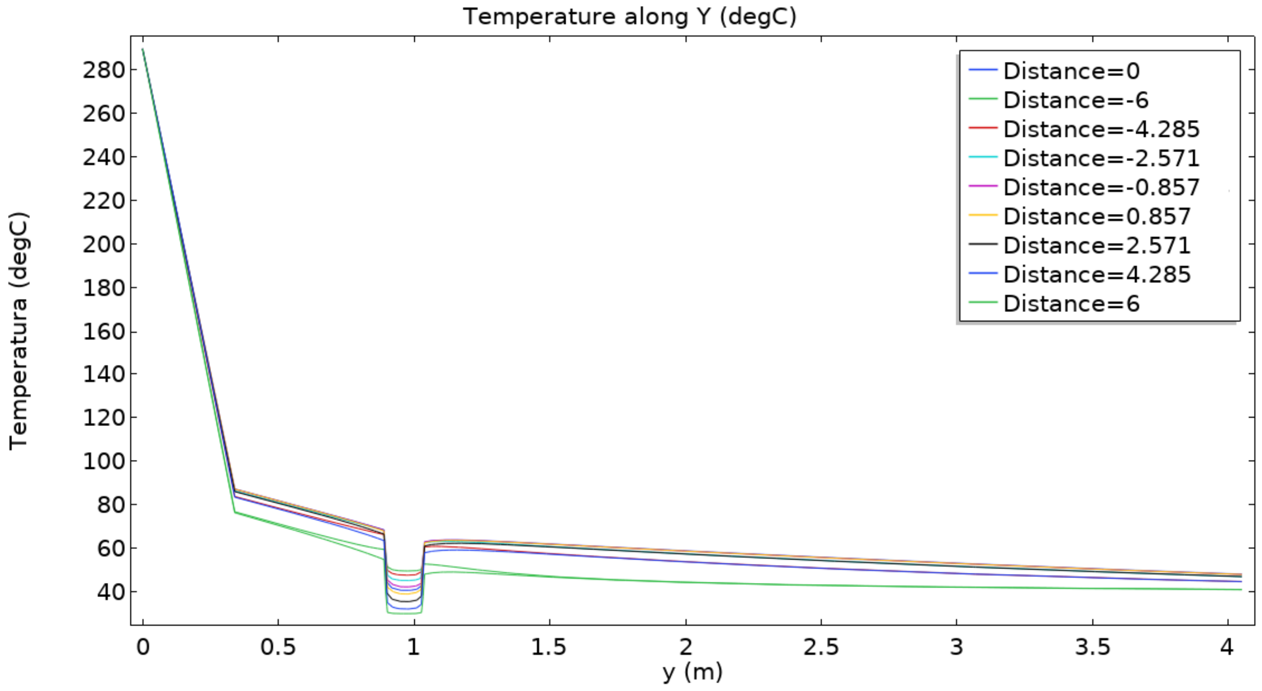

Passive cooling system in tank foundation: comparison experimental data vs. numerical simulations 9/11 Results

Temperature trend along lines parallel to the x axis and contained in the xz plane (at the interface between the insulation and the concrete) (cold tank)

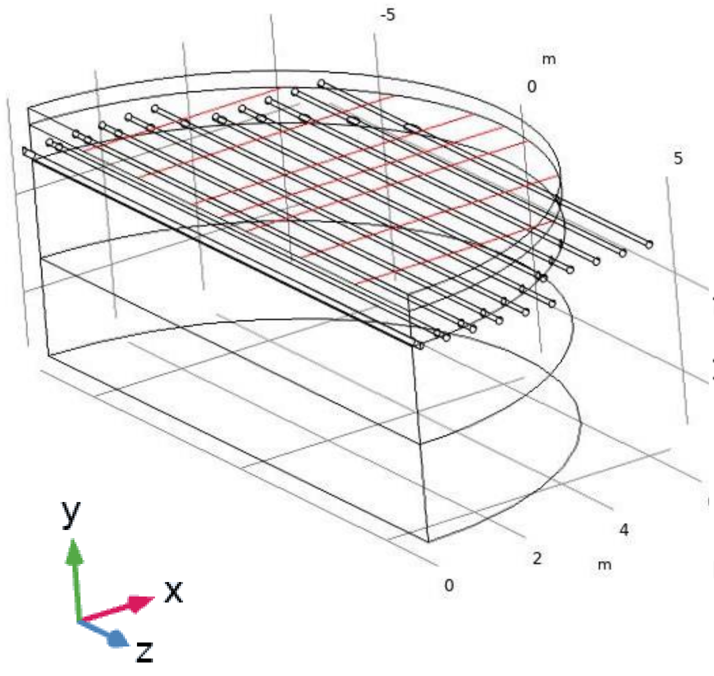

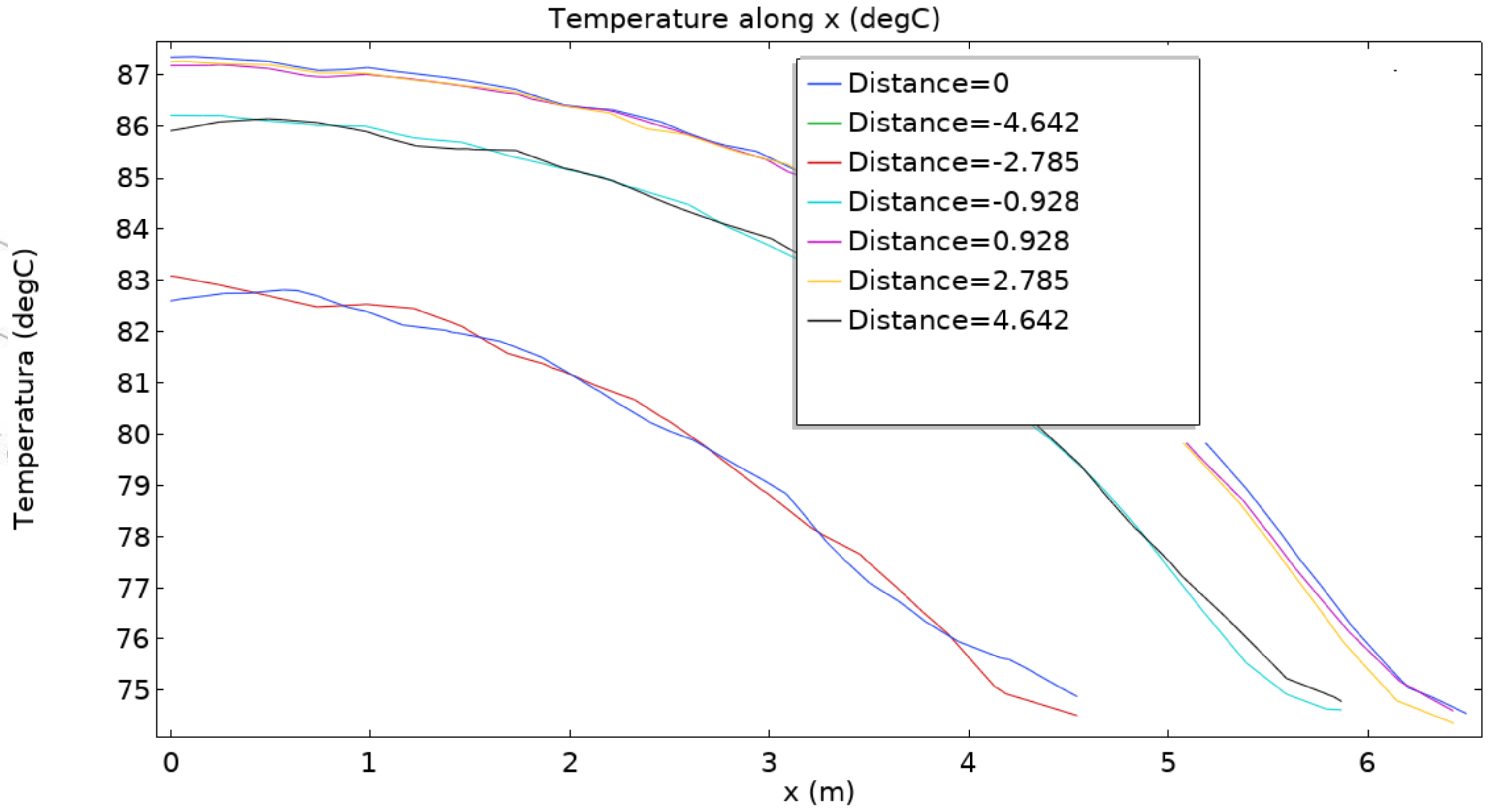

Results

Passive cooling system in tank foundation: comparison experimental data vs. numerical simulations 10/11

Temperature trend along lines parallel to the z axis
at the interface plane between insulation and concrete and comparison with experimental data (cold tank)

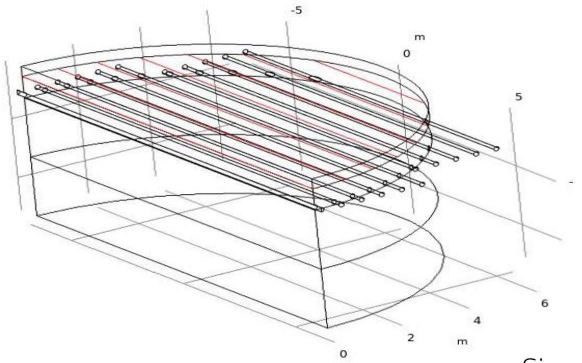

Simulation data

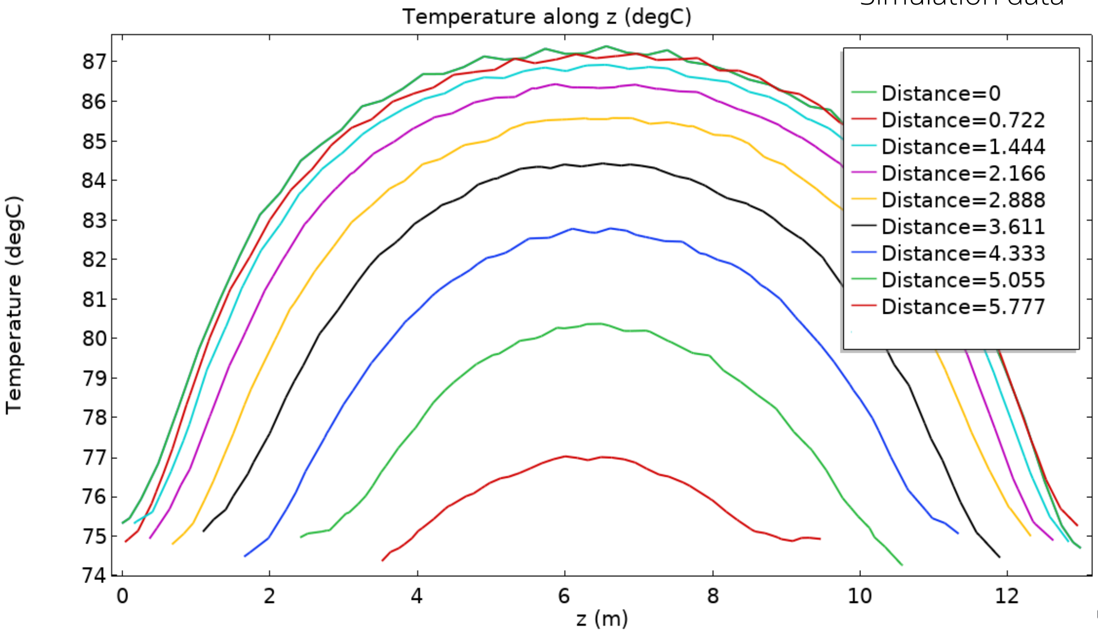

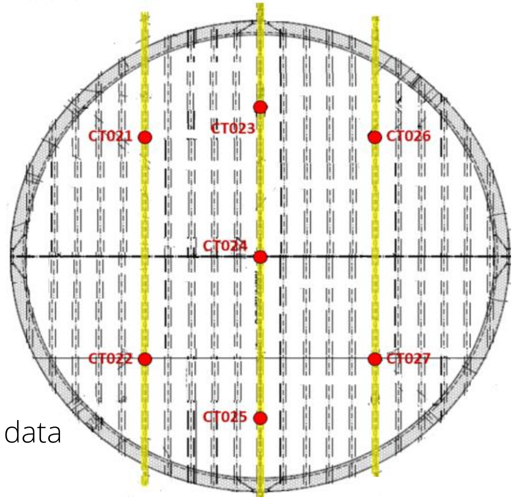

Experimental data

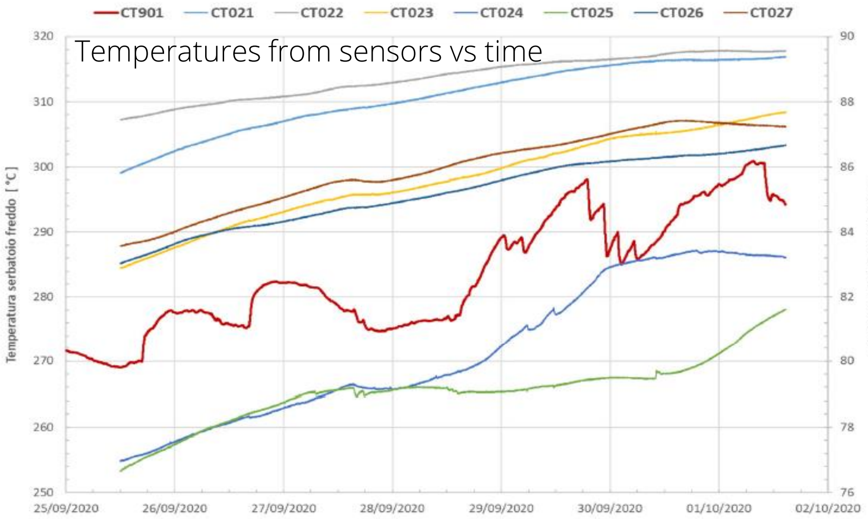

Passive cooling system in tank foundation: comparison experimental data vs. numerical simulations 11/11

Results

Temperature contours plots along section planes parallel to the xy and yz planes (Hot tank)

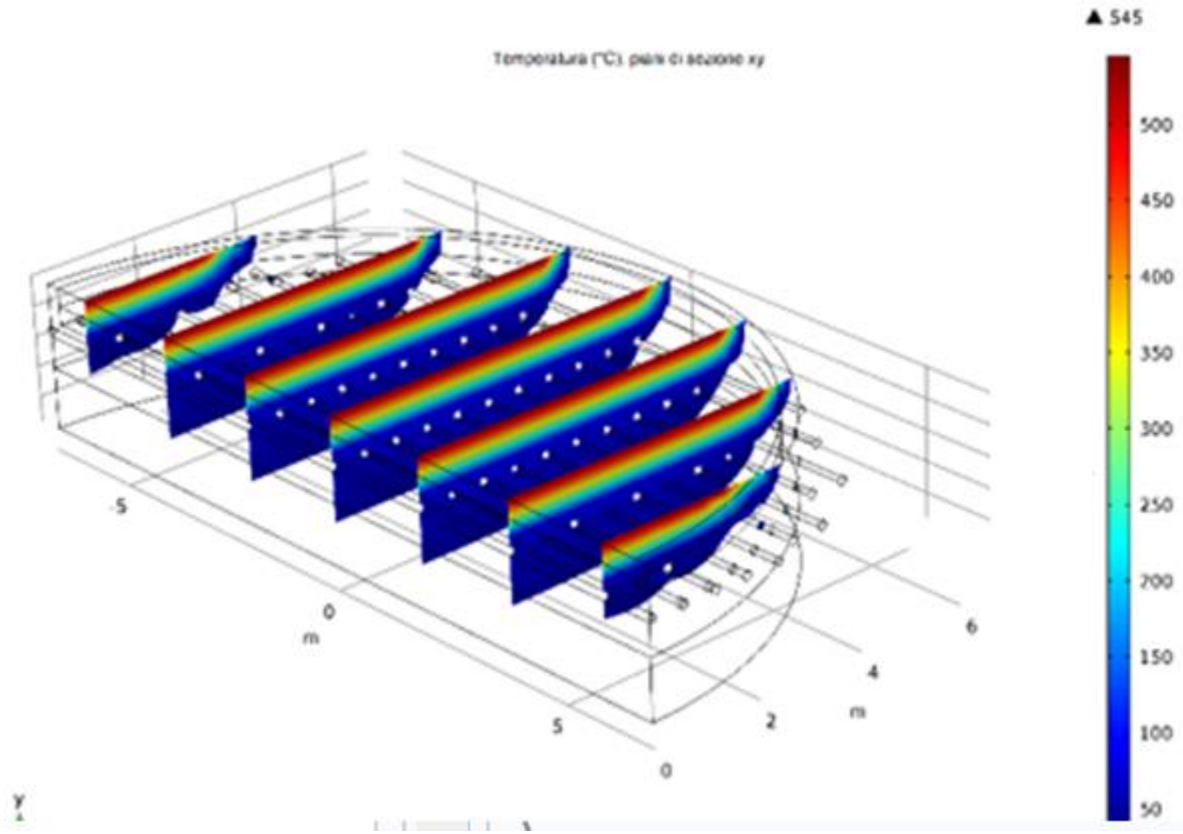

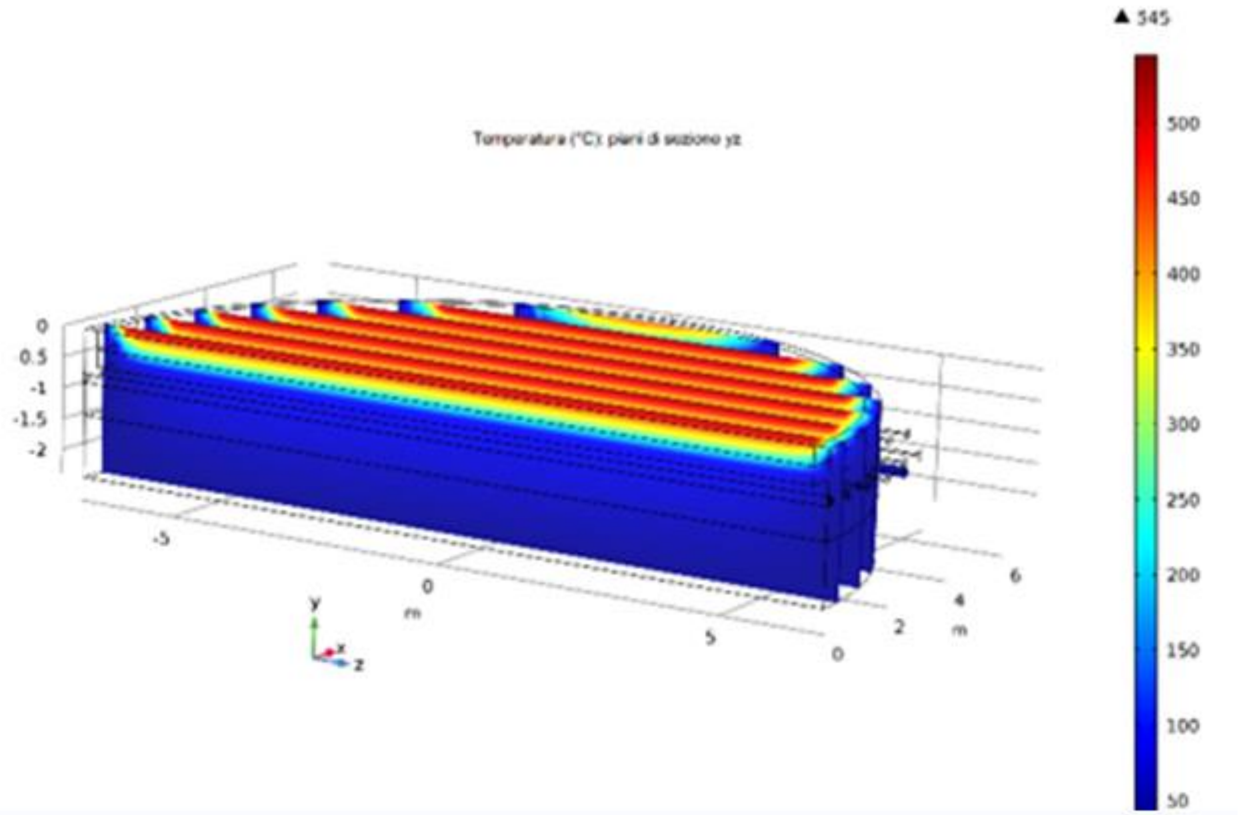

References

- *Design Basis Document / Owner's Technical Specification for Nitrate Salt Systems in CSP Projects Hypothesis of Hot Tank Failure-* Bruce Kelly et al. SolarPaces 2022

- *Effect of welding parameters on residual stress and distortion of molten salt hot tank floors for concentrated solar power applications* - Julian D. Osorio, et.al. SolaPaces 2022

- *Analytical approach to ground heat losses for high temperature thermal storage systems*

  C. Suárez , J. Pino , F. Rosa , J. Guerra *Int J Energy Res*. 2019 DOI: 10.1002/er.4278

- *Heat loss from thermal energy storage ventilated tank foundations*

  C. Suarez , F.J. Pino , F. Rosa , J. Guerra Solar Energy · 2015 DOI: 10.1016/j.solener.2015.09.045

Giuseppe Canneto
ENEA
TERIN-STSN-ITES
giuseppe.canneto@enea.it

THANK YOU FOR YOUR ATTENTION!
ANY QUESTIONS?

SFERA-III

Solar Facilities for the European Research Area

Solar Facilities for the European Research Area

4th Training for Industries

7-11 November 2022, Cr ENEA Casaccia Rome (Italy)

LESSONS LEARNED FROM THE COMMISSIONING/MANAGEMENT OF THE CSP PLANT OPERATIONS

Giuseppe PETRONI (ENEA, TERIN-STSN-ITES)

JOINT RESEARCH ACTIVITIES

THIS PROJECT HAS RECEIVED FUNDING FROM THE EUROPEAN UNION'S HORIZON 2020 RESEARCH AND INNOVATION PROGRAMME UNDER GRANT AGREEMENT NO **823802**

→ Molten salts have their own peculiarities, so you need:

→ accurate checks on compliance with the construction specifications of particularly important aspects such as **tracing** and **insulation**

→ periodic checks on critical parts such as the solar collector, the hydraulic seal (salt leaks), the electrical terminals, etc.

Each of these failures can cause serious damage

PLANT WASHING

→ Use demi-water (to avoid chemical corrosion) pumped by a dedicated external pump

- Clean up processing residues (flushing and discharging the dirty water)
- Drain the water (using vent and drain pipes)
- Dry any residual water very carefully to avoid dangerous flash-evaporation during the first start-up of the salts (flushing dry air and turning the tracing on)

PLANT START-UP OPERATION

- Turn the tracing on – temperature set-point = 290°C
- Check the correct positioning of the valves
- When the set-point temperature is reached, gradually start the pump
- When the rated flow range is reached, focus the mirrors

OPERATIONS IN RATED OPERATING CONDITIONS

- The plant works automatically, no operations needed, only supervision is required

PLANT-STOP OPERATION

- Turn the vents, drains and drain tank tracing on
- Defocus the mirrors
- Stop the pump
- When the tracing set-point is reached, gradually open the drain and vent valves
- Wait for the correct level on the drainage tank to be reached

SAME EXAMPLE OF DAMAGE CAUSED BY BAD WASHING

Processing residues

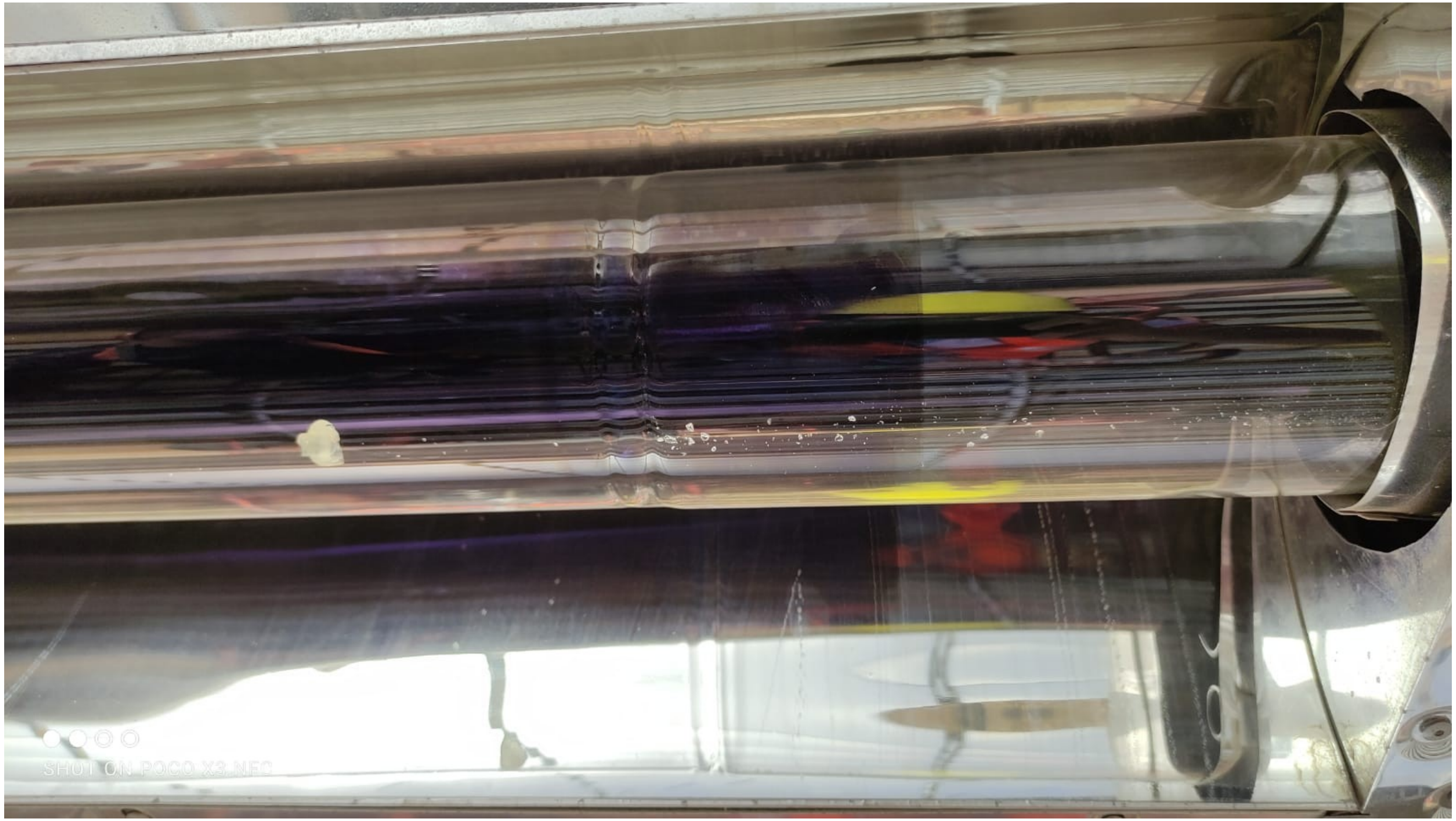
SHOT ON POCO X3 NFC

The worst case: tube fracture following an attempt to melt a cork

Example of drainage pipe completely plugged: need to cut the pipe for repair

CONCLUSIONS

The molten salts have their own peculiarities.
They must be very carefully treated.
If treated correctly, they can perform their task without problems

SFERA-III

Solar Facilities for the European Research Area

Giuseppe PETRONI
ENEA
TERIN-STSN-ITES
giuseppe.petroni@enea.it

THANK YOU FOR YOUR ATTENTION!
ANY QUESTIONS?

SFERA-III
Solar Facilities for the European Research Area

Solar Facilities for the European Research Area

4th Training for Industries
7-11 November 2022, Cr ENEA Casaccia Rome (Italy)

Characterization of receiver tubes and experimental testing of MS cooling/freezing in receiver

Valeria RUSSO (ENEA, TERIN-STSN-ITES)

JOINT RESEARCH ACTIVITIES

THIS PROJECT HAS RECEIVED FUNDING FROM THE EUROPEAN UNION'S HORIZON 2020 RESEARCH AND INNOVATION PROGRAMME UNDER GRANT AGREEMENT NO **823802**

Characterization of the receivers

In the ENEA Casaccia Center there are two facilities for the **indoor receivers characterization**

Test Bench for the heat loss measurements

Test Bench for melting/freezing tests

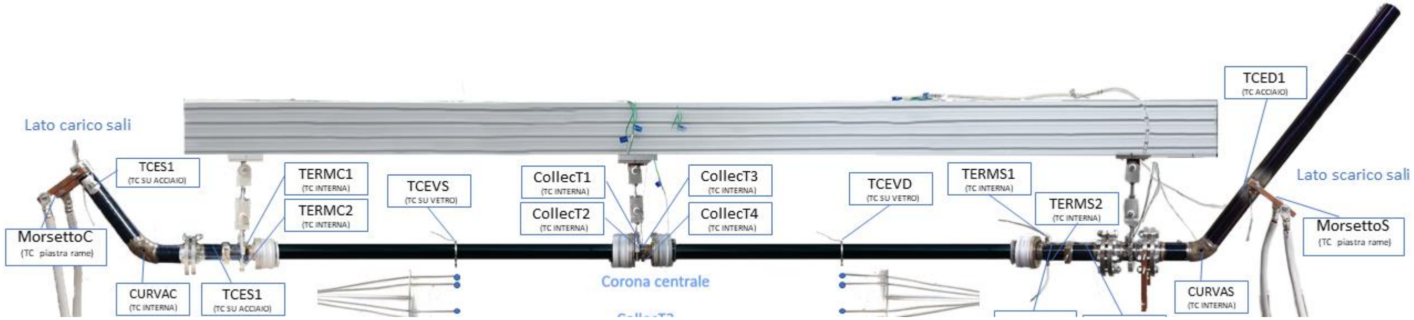

Test bench for heat loss measurements (1)

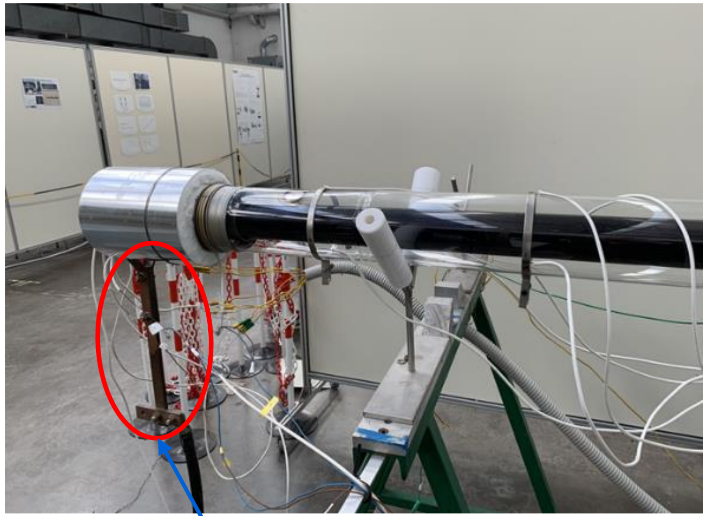

The steel tube is heated directly by an electric generator by the Joule effect

Clamps of the Joule heating system

Clamps of the Joule heating system

Test bench for heat loss measurements (2)

LABVIEW Software is used for:

- To regulate the electric power
- To acquire the measured data with a frequency of 0.2 s^{-1}

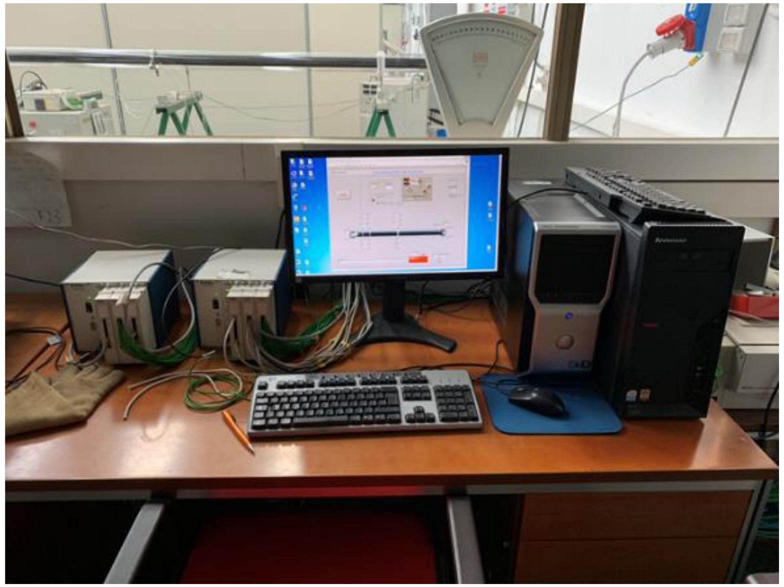

The steel tube is heated **regulating the voltage** applied at the ends as a function of the **maximum temperature** measured in the middle

Test settings and measurements

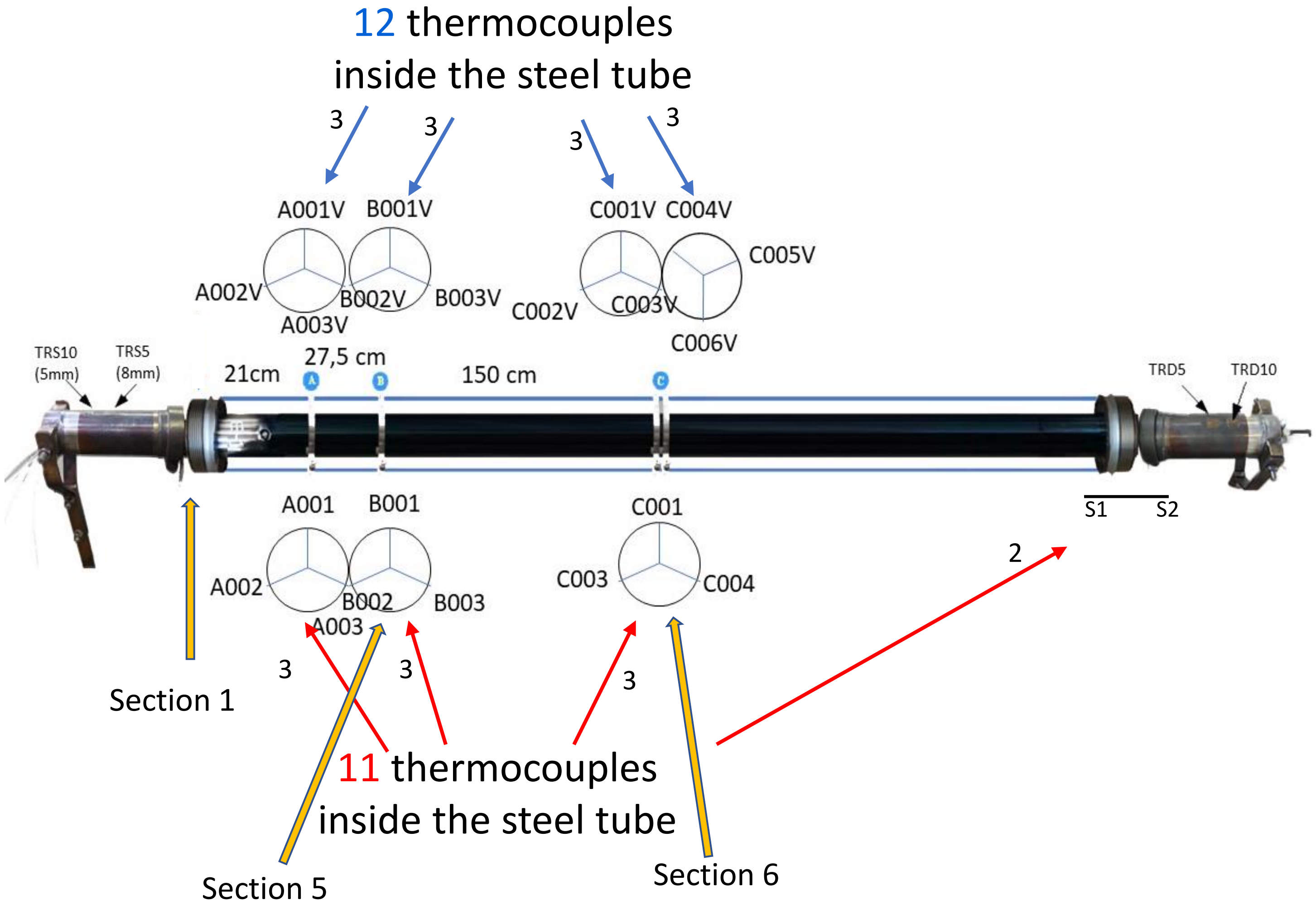

- ✓ Voltage is measured among sections 1 and 5 (Vl), sections 5 and 6 (Vc), and at the ends of the steel tube (V), for checking V= 2(Vl+Vc).
- ✓ Electric current is measured in real time by the amperemeter of the electric power generator
- ✓ All data of voltage, electric current and temperatures, are collected and stored by the acquisition data system
- ✓ Voltage is automatically adjusted according to the temperature measured in section 6

Heat loss test procedure

Main objective of indoor test

- Measurement of the heat loss
- Evaluation of the emittance of the absorber coating as function of the steel tube temperature

Test procedure

- Steel tube is heated directly by the electric generator
- Reference steel temperatures: **300-550°C with a step of 50°C**
- **3 tests** for each temperature (minimum number for statistic)

Heat loss evaluated measuring the electric power per unit length (W/m), required to maintain at steady state the temperature of the steel tube

Heat loss evaluation

Example of temperature distributions measured on steel tubes

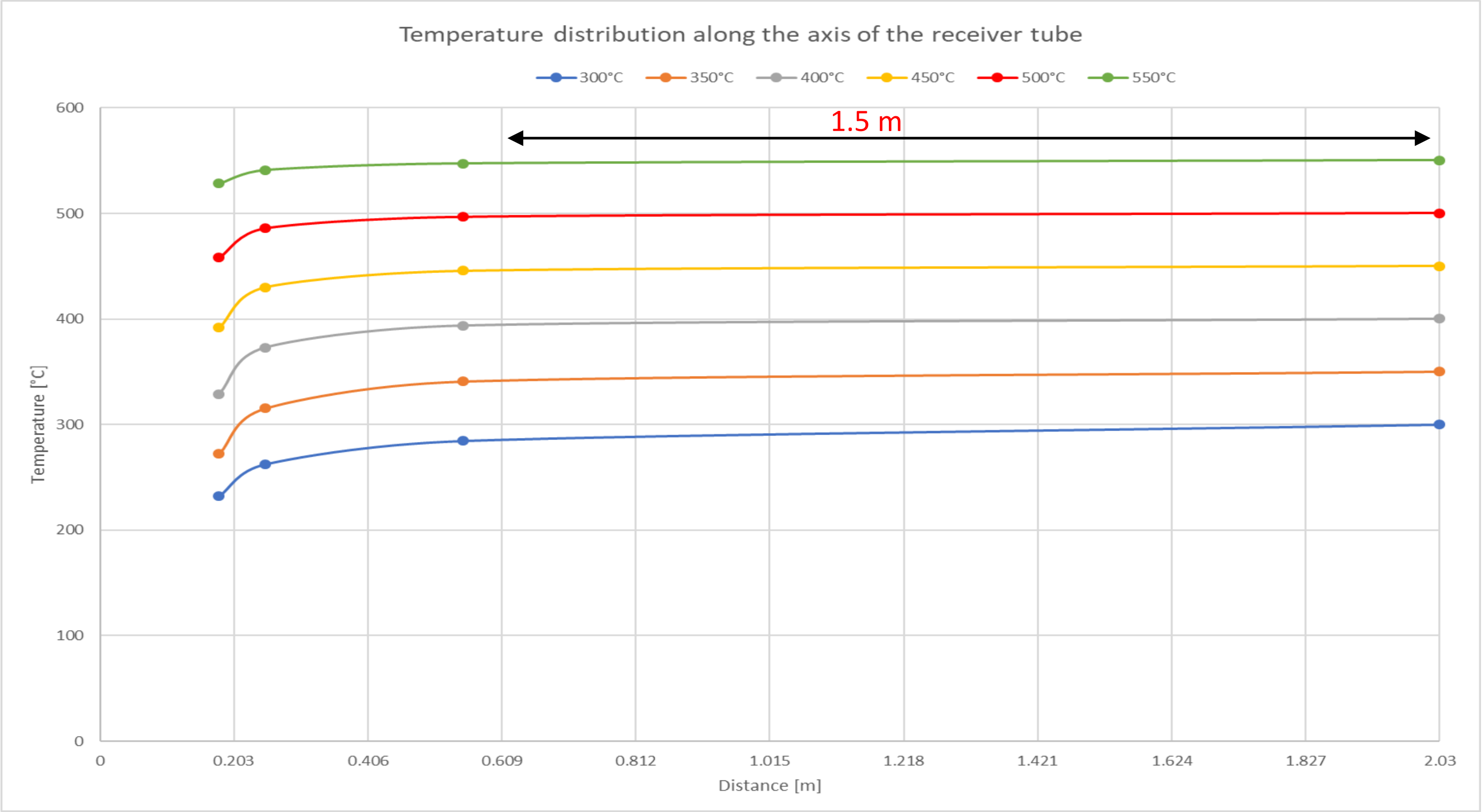

- Temperature of the steel tubes can be assumed constant in an interval of about 1.5 m from the middle section of the receiver.

Heat Loss per unit length of the receiver

$$HL(T_{s,i}) = P_{c,i} = \frac{V_{c,i}}{l_{5-6}} I_i$$

Statistical Data Processing (1)

- To evaluate the accuracy of the measurements, the standard deviation of is calculated for all the 18 tests performed and quantities acquired

Standard deviation of heat loss measurements

$$\sigma_{P_{2,1}} = \frac{1}{l_{5-6}} \sqrt{I_i^2 \sigma_{V,c,i}^2 + V_{c,i}^2 \sigma_{I,i}^2} \qquad \text{for i=1,…,18}$$

- The tube temperature is quite uniform in each cross section, so the mean values can be evaluated as the average value of the three measured temperatures.

Standard deviation of the average steel temperature in section 6

$$\sigma_{T_{s,i}} = \frac{1}{3}\left[\sigma_{T_{ca1,i}}^2 + \sigma_{T_{ca2,i}}^2 + \sigma_{T_{ca3,i}}^2\right]^{\frac{1}{2}}$$

Statistical Data Processing (2)

N of Test	T_amb [°C]	T_steel [°C]	SD_Tsteel	T_ste-T_amb [°C]	T_g [°C]	SD_Tg	DVC_tubo [V]	SD_DVC_tubo	DV_Tubo [V]	SD_DVTubo	I_Alim [A]	SD_Ialim	HL_Ctubo [W/m]	HL_Tubo [W/m]
1	13,56	299,95	0,029	286,38	54,33	0,055	0,73	0,0102	1,93	0,0200	351,21	0,034	169,80	168.92
2	13,24	349,86	0,004	336,62	64,34	0,121	0,88	0,0065	2,32	0,0075	415,43	0,010	244,98	239.11
3	11,08	399,89	0,005	388,81	80,42	0,118	1,08	0,0043	2,83	0,0068	491,37	0,011	352,53	345.01
4	12,53	449,88	0,004	437,36	97,50	0,134	1,30	0,0020	3,43	0,0059	579,20	0,009	503,04	492.83
5	13,34	499,89	0,174	486,55	123,00	0,130	1,55	0,1705	4,09	0,4493	673,97	0,741	706,45	692.67
6	20,30	549,89	0,009	529,59	155,40	0,163	1,88	0,0029	5,00	0,0078	799,01	0,012	1002,21	992.21
7	13,08	299,87	0,004	286,79	52,27	0,232	0,72	0,0093	1,88	0,0104	346,69	0,013	165,72	161.54
8	18,71	349,77	0,006	331,05	71,66	0,086	0,91	0,0067	2,43	0,0085	428,49	0,012	260,19	257.98
9	19,57	399,75	0,009	380,18	84,98	0,182	1,10	0,0044	2,95	0,0095	504,74	0,015	371,40	369.36
10	19,44	449,79	0,009	430,35	109,03	0,541	1,32	0,0027	3,52	0,0077	588,97	0,012	519,01	514.68
11	20,20	499,85	0,007	479,65	130,74	0,528	1,58	0,0026	4,20	0,0078	686,53	0,012	723,25	715.88
12	24,53	549,91	0,009	525,37	163,38	0,136	1,87	0,0038	5,00	0,0102	795,56	0,017	992,92	986.15
13	17,82	299,79	0,005	281,97	58,09	0,149	0,74	0,0083	1,98	0,0096	361,02	0,012	179,08	177.22
14	21,17	349,75	0,007	328,59	72,66	0,288	0,90	0,0025	2,43	0,0065	426,45	0,012	256,80	257.33
15	22,44	399,74	0,007	377,30	90,76	0,131	1,10	0,0022	2,94	0,0067	501,68	0,012	366,27	365.82
16	23,46	449,81	0,005	426,35	112,19	0,090	1,32	0,0023	3,52	0,0064	587,17	0,012	515,72	512.18
17	24,04	499,87	0,007	475,82	135,89	0,164	1,57	0,0029	4,20	0,0081	684,21	0,014	718,13	712.74

Heat Loss evaluation

Heat Loss as a function of the average temperature measured in the middle section of the steel tube

The fitting model of the radial heat loss is:

$$HLT_{so}-T_{amb}=a\,(T_{so}-T_{amb})^4+b\,(T_{so}-T_{amb})$$

a, b : Constant evaluated by elaboration of the experimental data
T_{so} : Temperature of the outer surface of the absorber coating

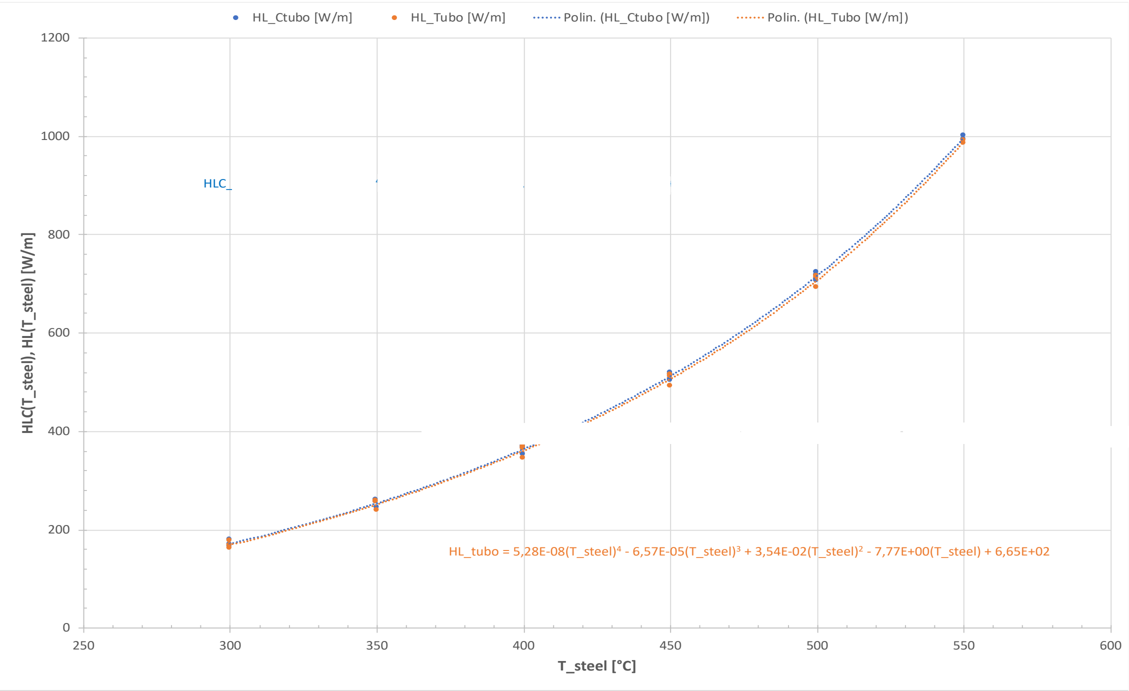

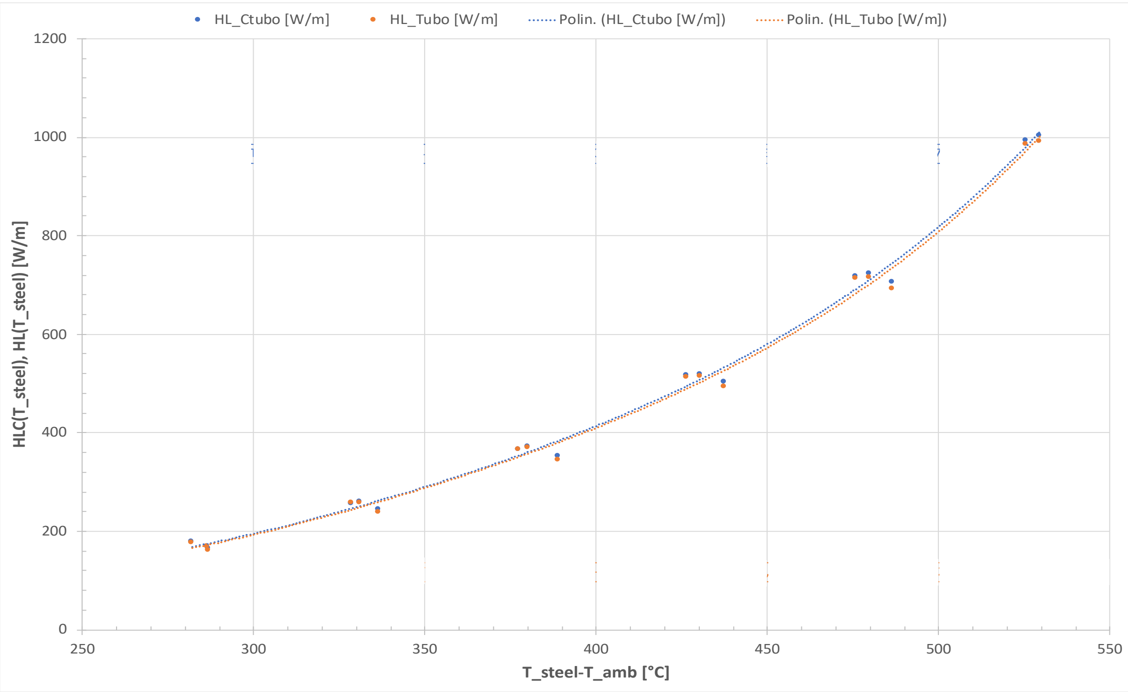

Emittance evaluation

Thermal power exchanged by radiation per unit length of the steel tube (W/m)

$$HL(T_{steel}) = \frac{2\pi r_{steel}\sigma_0(T_{steel}^4 - T_g^4)}{\frac{1}{\varepsilon_{s(T_{steel})}} + \frac{r_{steel}}{r_g}\left[\frac{1}{\varepsilon_g} - 1\right]}$$

$\varepsilon_s(T_{steel})$: Emittance of the cermet coating
$\varepsilon_g(T_g)$: Emittance of the glass

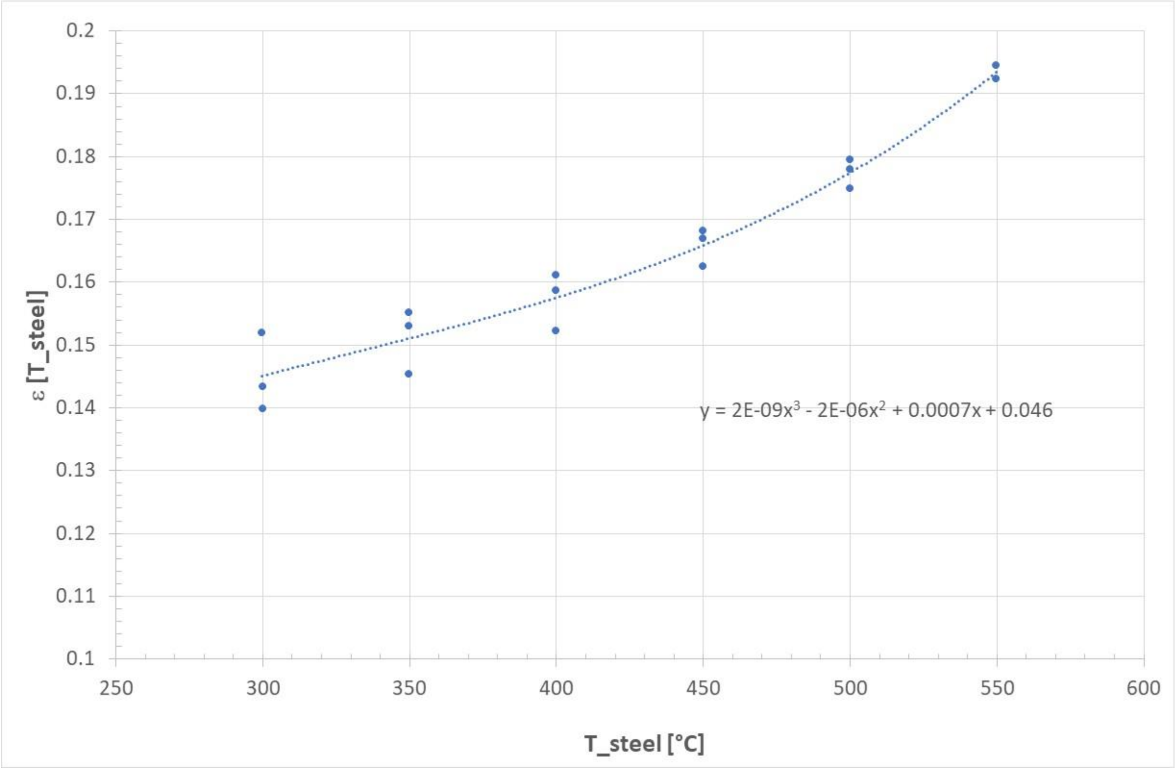

$$\varepsilon_s(T_{steel}) = \frac{HL(T_{steel})r_g}{2\pi r_{steel}r_g\sigma_0\left(T_{steel}^4 - T_g^4\right) - r_{steel}HL(T_{steel})\left[\frac{1}{\varepsilon_g} - 1\right]}$$

Receiver tube of infinite length, made with the same steel, the same cermet and in the same vacuum conditions

Heat exchange with the environment would occur only by radiation

Electric power (Pe) needed to keep the receiver at a constant temperature would only be a function of resistivity and electric current

$$P_e = \rho(T)\frac{I^2}{S} = P_{irr} = P_{HL}$$

Hypothesis

- the variation of the electrical resistivity is linear with the temperature
- resistivity is related to resistance by the following relationship: $\rho(T) = R(T)\frac{S}{l}$

Data analisys

Resistivity curve

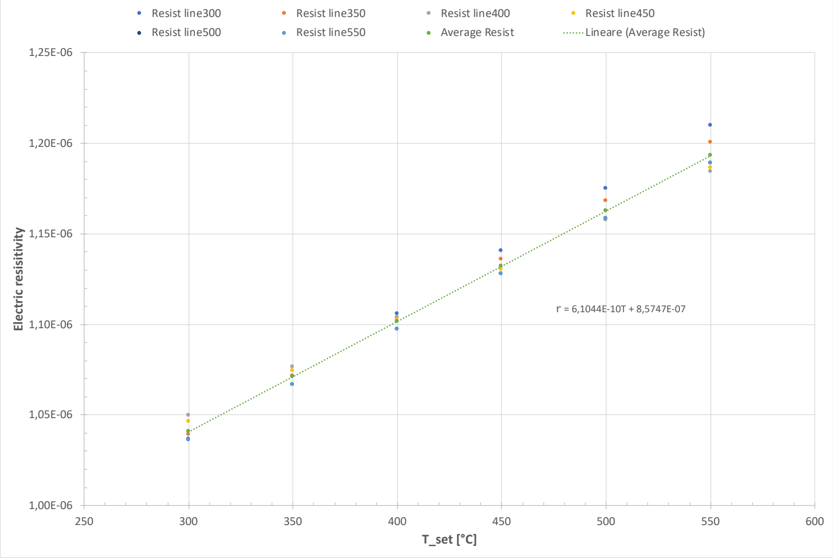

Comparison between pheat loss calculated by resistivity curve and the experimental one

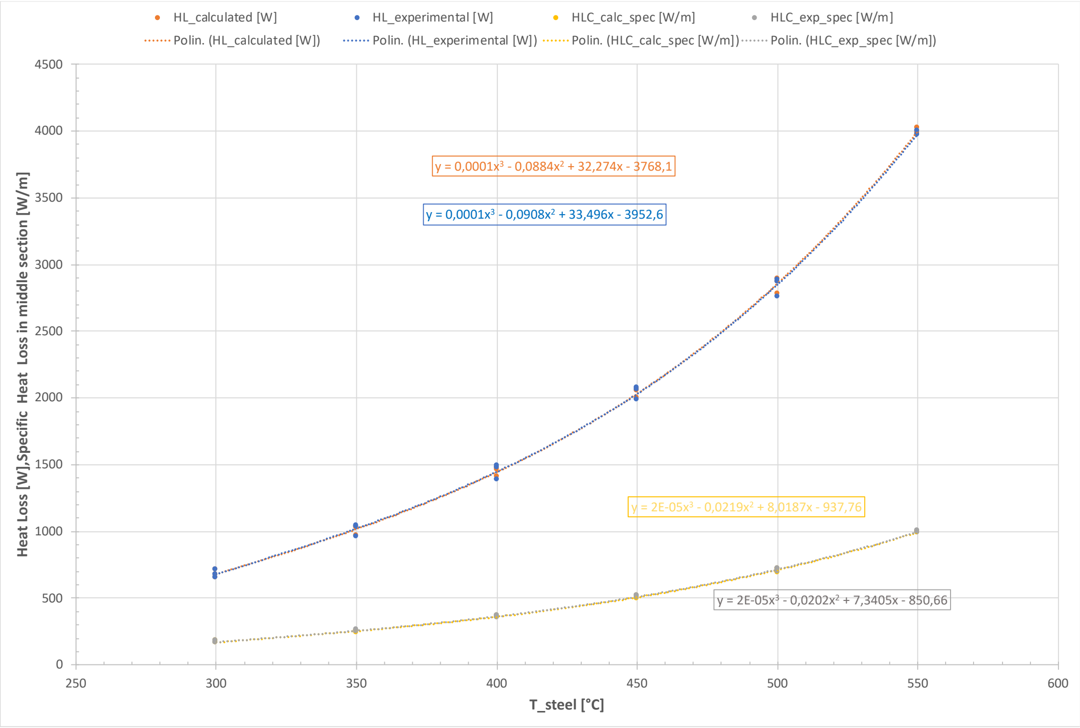

Very low percentage error on average about 1%.

Test bench for freezing/melting test

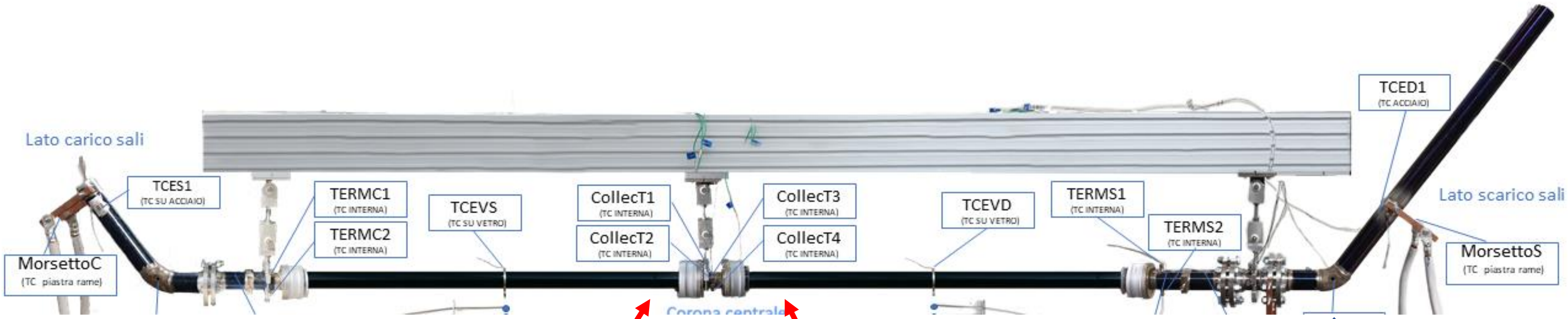

Two receivers tubes were joined together by welding

Two curves with a system of flanges were positioned at the ends for the operations of loading and unloading of salts.

The heating inside the tube should be uniform

An impedance system was used to heat the receivers

Due to the presence of the glass envelope it is impossible to install heat tracing

Test bench for freezing/melting test: instrumentation position

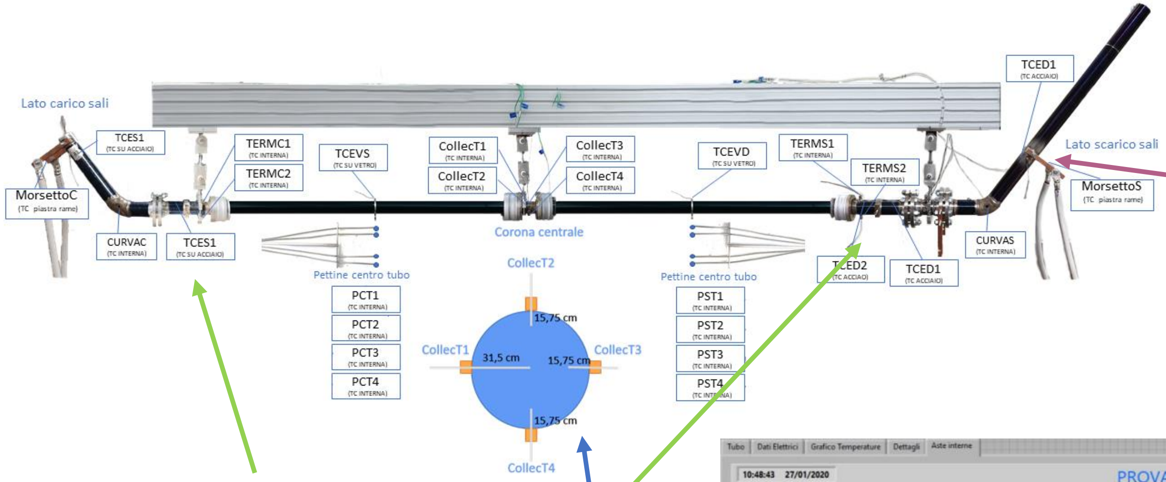

2 thermocouples have been positioned in correspondence with the terminals of the electric heating system (Terminal C and Terminal S)

2 thermocouples immersed in the fluid are positioned at the inlet and outlet of the receivers’ tubes

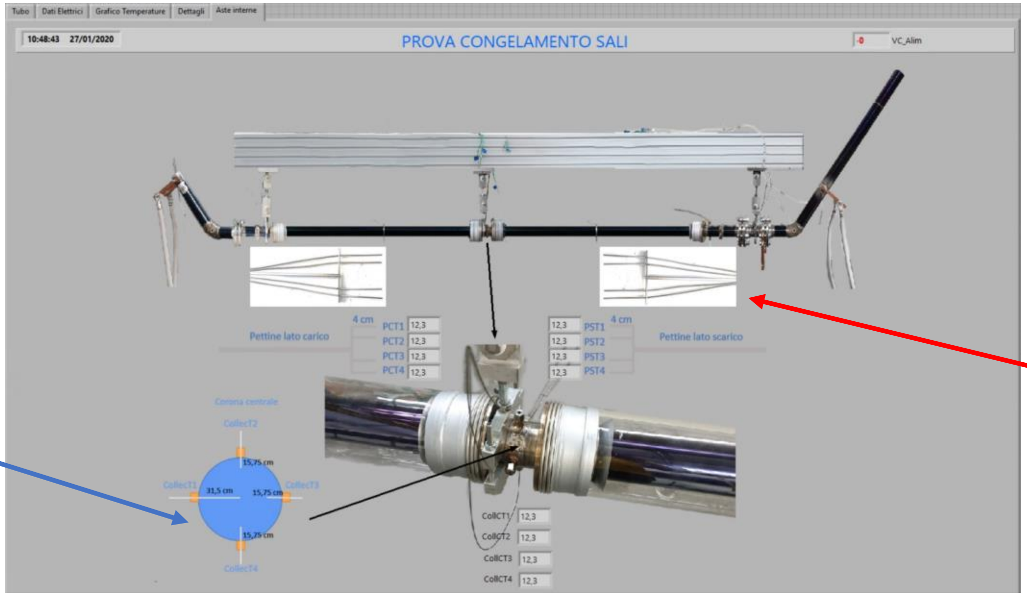

4 thermocouples have been positioned in a radial pattern in the joint between the two pipes

4 thermocouples immersed have been positioned along the vertical diameter, in correspondence with the central section of each of the two receiver tubes

The trend of the acquired magnitudes is visible on a screen

Solar Facilities for the European Research Area

freezing/melting test: set up

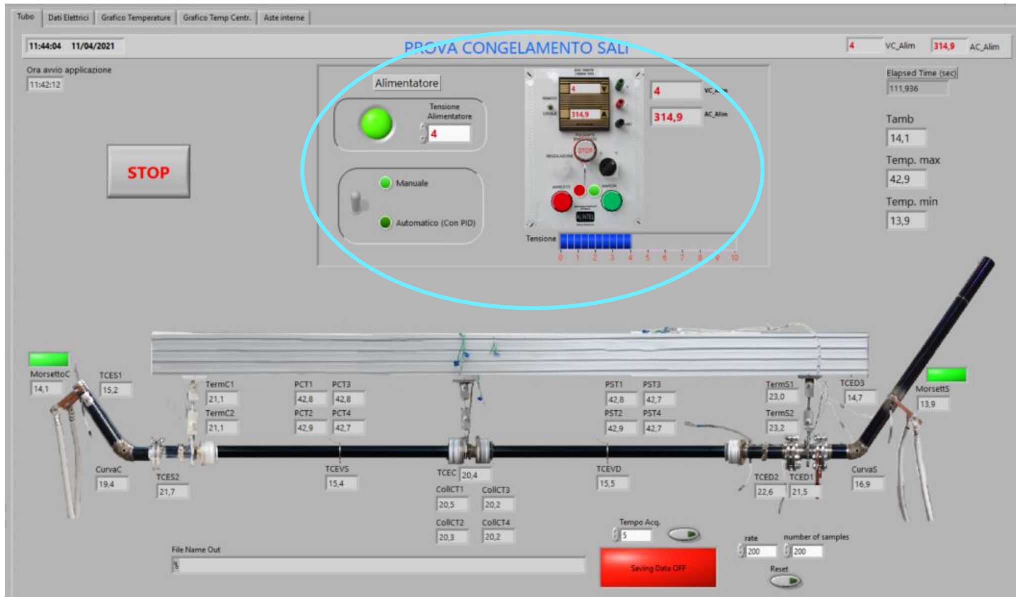

- ✓ A 10 kW power supply (0-10V 1000A) was used to heat the receivers
- ✓ A variable voltage from 0 to 10V and a variable current are applied at the ends of the two receivers

- ✓ The system is controlled and adjusted automatically through a software developed with LabView
- ✓ The trend of the acquired magnitudes is visible on a screen

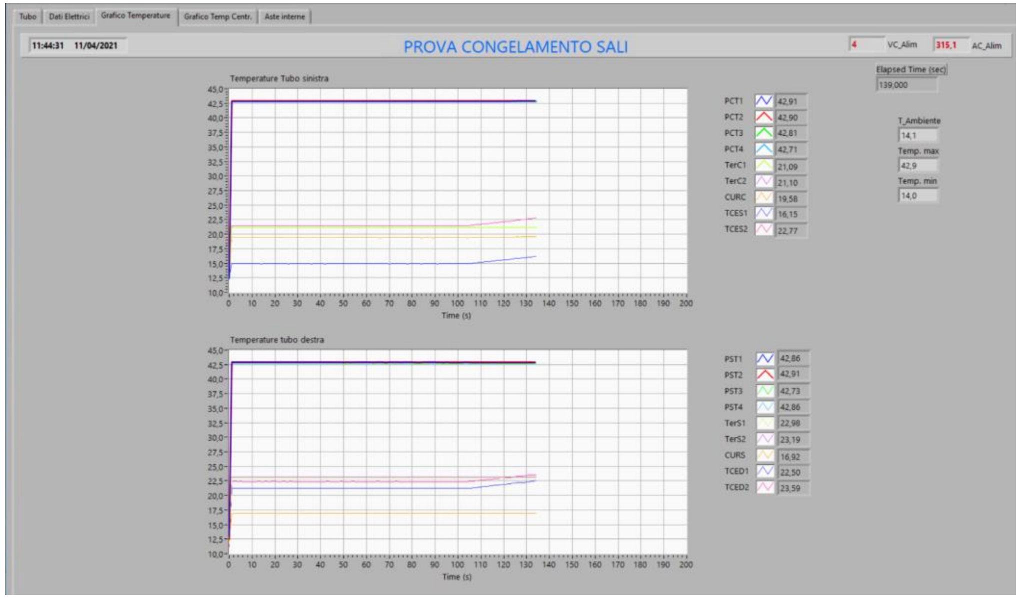

Test Procedure

Main objective of melting/freezing test

- Evaluation of the time range necessary for the complete solidification/melting of the mixture
- Analysis of the receiver behavior during abnormal operating conditions and in case of blocking of molten salts circulation
- Definition of the operating procedures in order to prevent damage caused by the natural expansion of the salt volume

Test condition

- Solidification: start from a constant and uniform temperature of 270°C that simulates an emergency condition with the plant in night circulation
- Melting: starts from ambient temperature untill the completed phase change

- This evaluation is important for the definition of the management strategies of a CSP plant
- It is possible to know the time available for a complete drainage of the solar filed

Melting test (1)

Test Conditions

- the binary salt is heated by the power supply
- maximum temperature reached: 270°C
- output voltage applied: 4,5V

The whole process takes about 5.5 hours

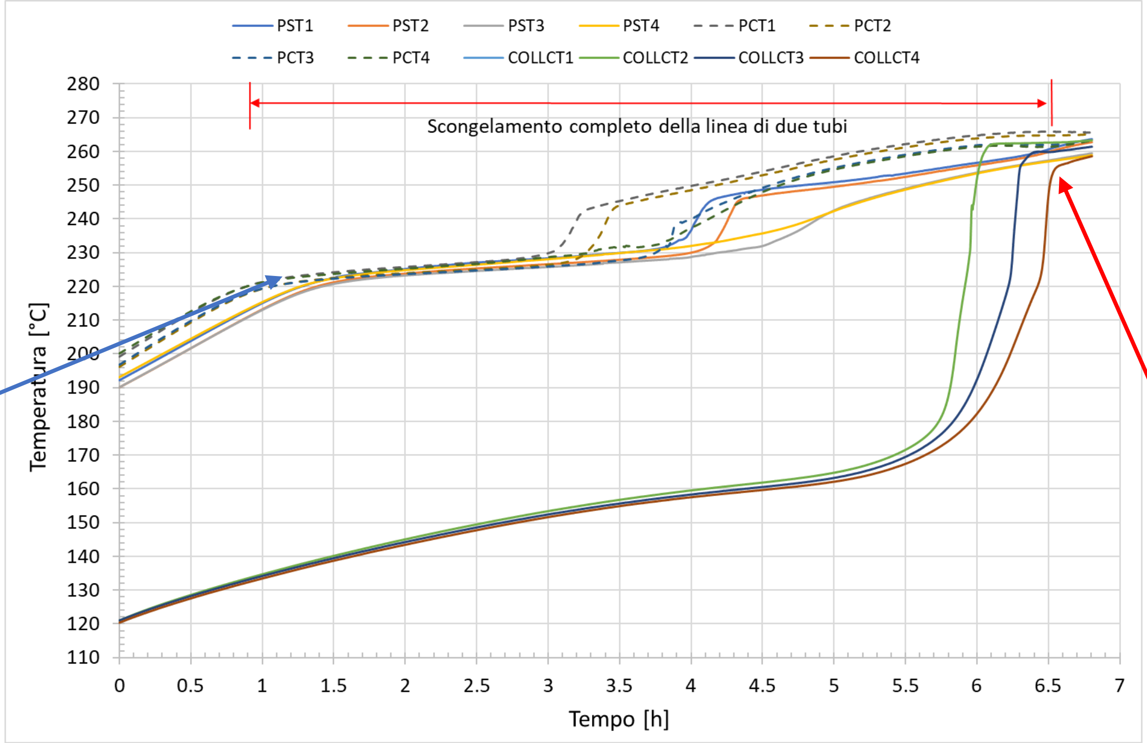

Melting process starts at a temperature of about 221°C

Melting completed at temperature of about 250°C.

Melting test (2)

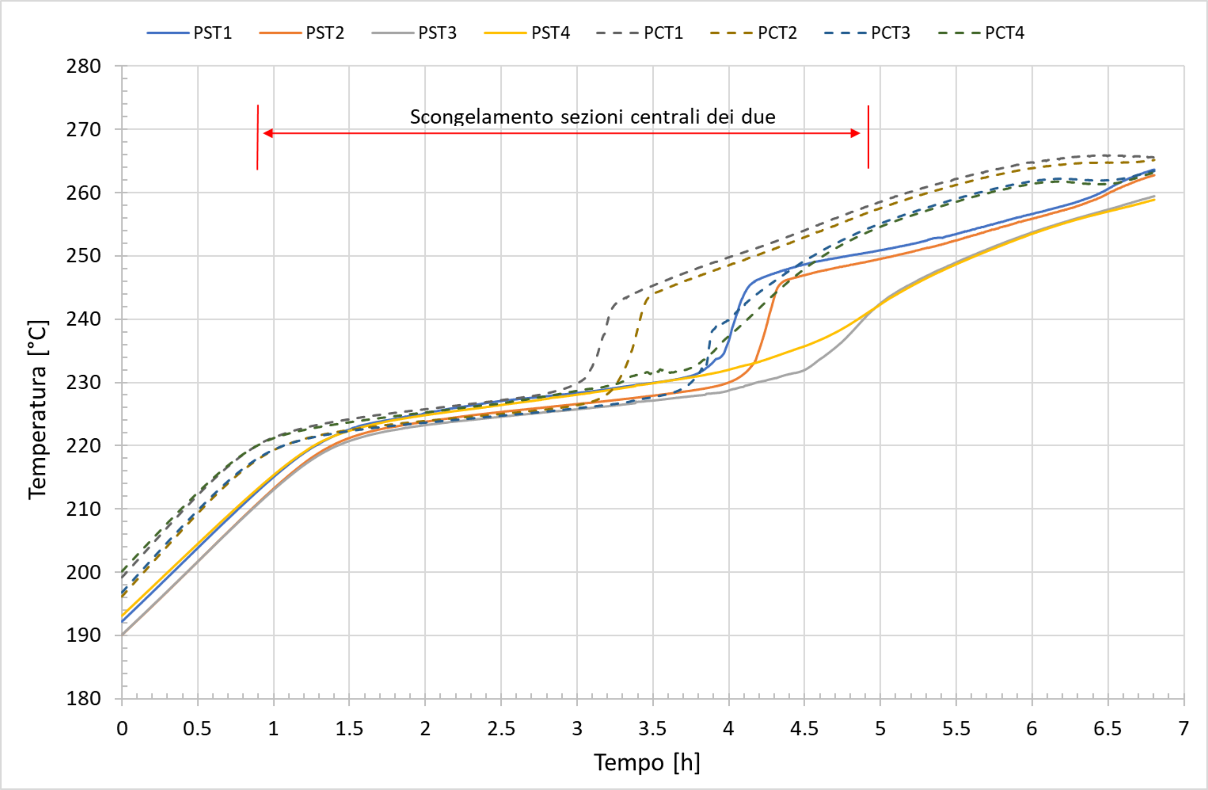

Central section of the receivers

- Melting process in the two different receivers takes place with a delay of about 30 minutes each other
- Thermocouples positioned in the upper part measures value of temperature higher than the value measured by the thermocouple positioned in the bottom part of the same section

- Slow initial rise temperature (from 220°C to 230°C)
- Sudden increase after 230°C

Salt is in mostly liquid, so facilitates the process melting the remaining solid part.

Melting test (3)

Central collar welded between the two receivers

- In correspondence with the central collar there are high heat losses caused by the supports of the pipes
- The temperature rises very slowly
- The mixture is solid until the temperature undergoes a sudden increase

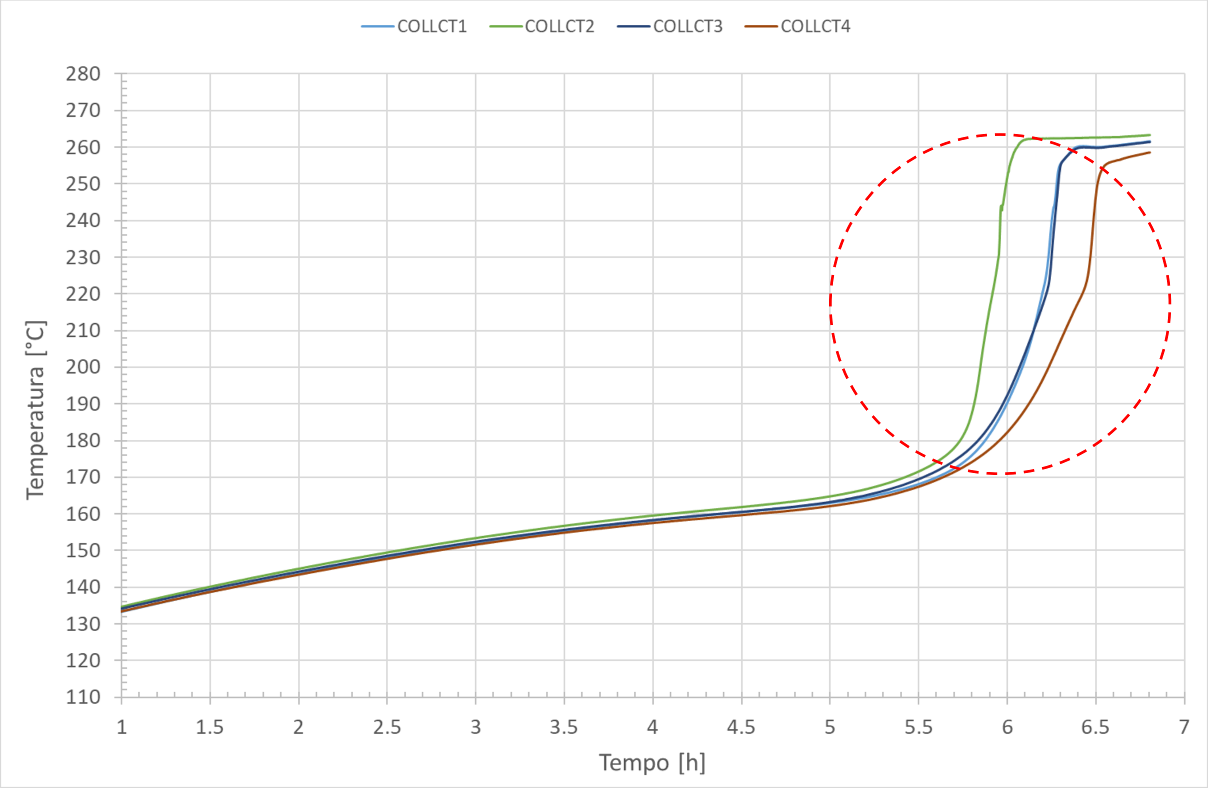

Melting process is not clearly visible

The process occurs very quickly and after the complete melting of the salts inside the receivers

Freezing test (1)

Test Conditions

- freezing tests were carried out under the same real operating condition as in night circulation
- inlet temperature: 290°C
- outlet temperature: 270°C, the minimum temperature condition was considering during the test in order to be more conservative

Test procedure

- after the melting process the heating continues until reaching the stationary condition of T=270 ° C
- the stationary condition is maintained for one hour
- the Joule heating system was switched off

The whole process takes about 3.5 hours

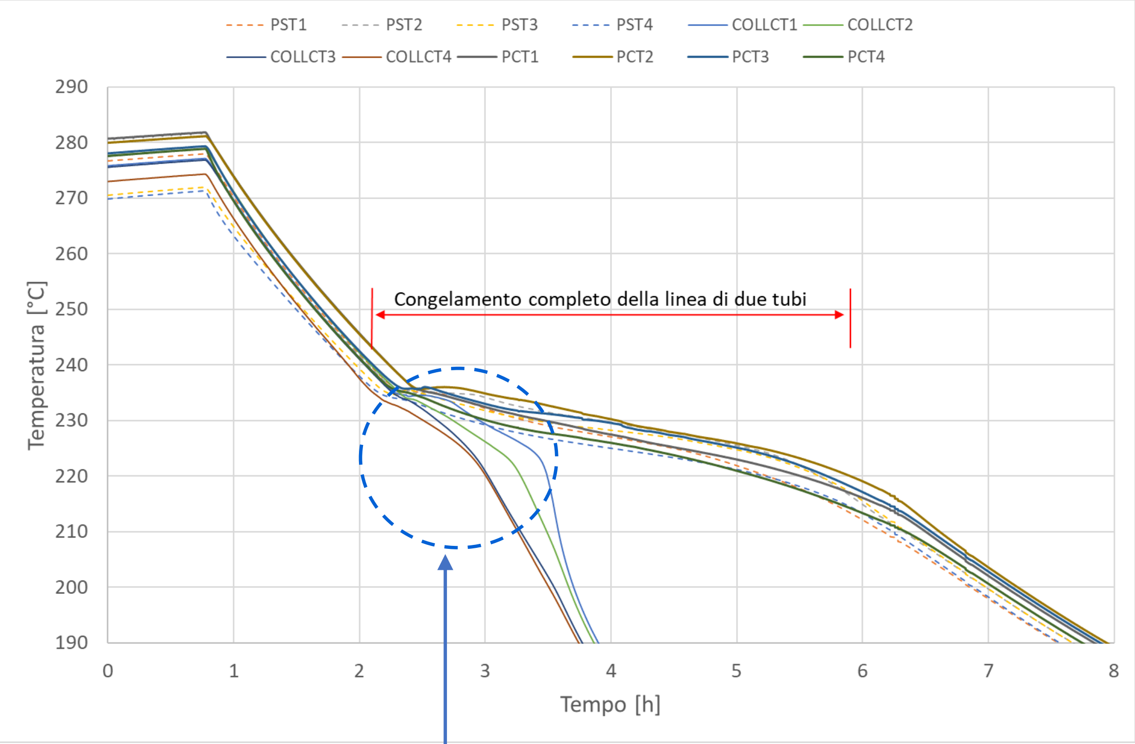

The area that cools first coincides with the collar welded between the two receiver tubes

Freezing test (2)

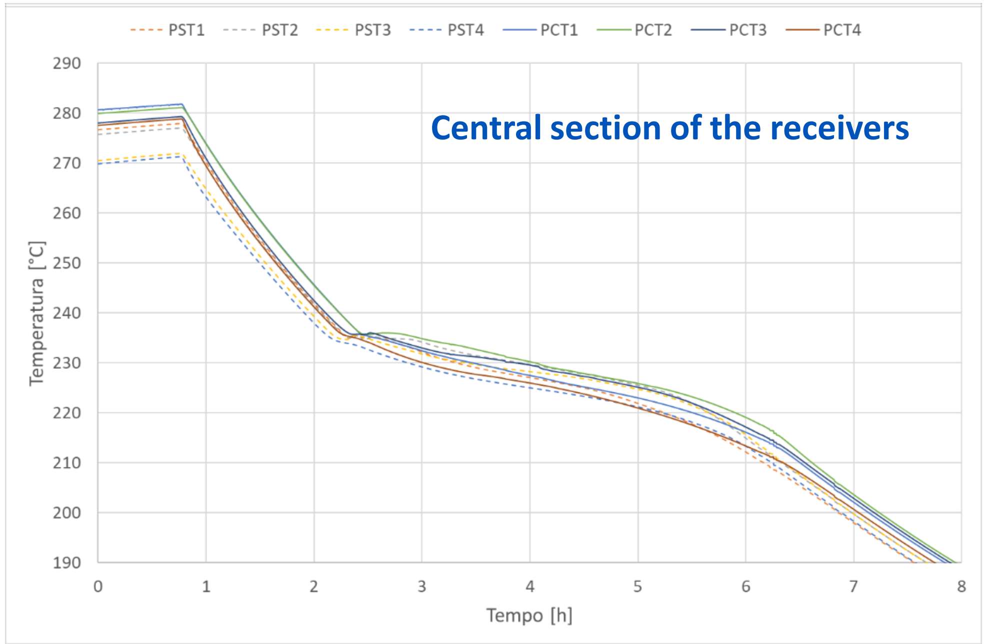

solidification process begins on the external walls of the tube (PCT1, PCT4) and continues towards the inside (PCT2, PCT3)

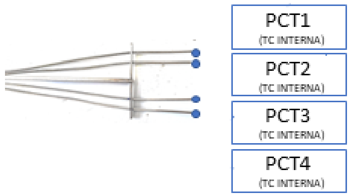

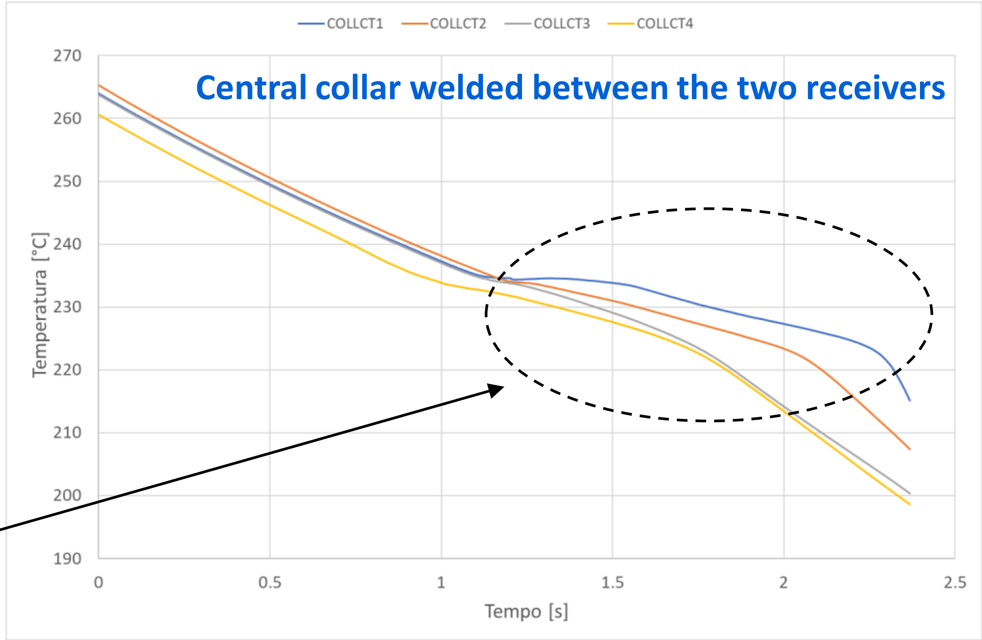

- ✓ solidification process begins almost simultaneously both in the collar and in the central sections of the tubes
- ✓ process is much faster in the collar ending in about 1 hour

Final consideration

- For the melting process the electric generator supplies a constant voltage of 4.5V
- The power supplied during the melting test is about 6.26kW
- The whole melting process takes about 5.5 hours
- Starting from a stationery condition at a temperature of about 270°C, the salt present inside two receiver tubes takes about 3.5 hours to solidify without circulating
- The tests indicate that the beginning of the phase change (liquid to solid) occurs at the coldest points and continues radially from the surface of the pipes towards the inside of the same

SFERA-III

Solar Facilities for the European Research Area

Valeria RUSSO, PhD
ENEA
TERIN-STSN-ITES
valeria.russo@enea.it

THANK YOU FOR YOUR ATTENTION!
ANY QUESTIONS?

SFERA-III

Solar Facilities for the European Research Area

Solar Facilities for the European Research Area

4th Training for Industries

7-11th November 2022, ENEA Casaccia Research Center, Rome (Italy)

Molten salts as heat transfer fluids for chemical reactors

Luca TURCHETTI (ENEA, TERIN-STSN-SCIS)

JOINT RESEARCH ACTIVITIES

THIS PROJECT HAS RECEIVED FUNDING FROM THE EUROPEAN UNION'S HORIZON 2020 RESEARCH AND INNOVATION PROGRAMME UNDER GRANT AGREEMENT NO **823802**

Concentrating solar thermal energy: much more than electricity!

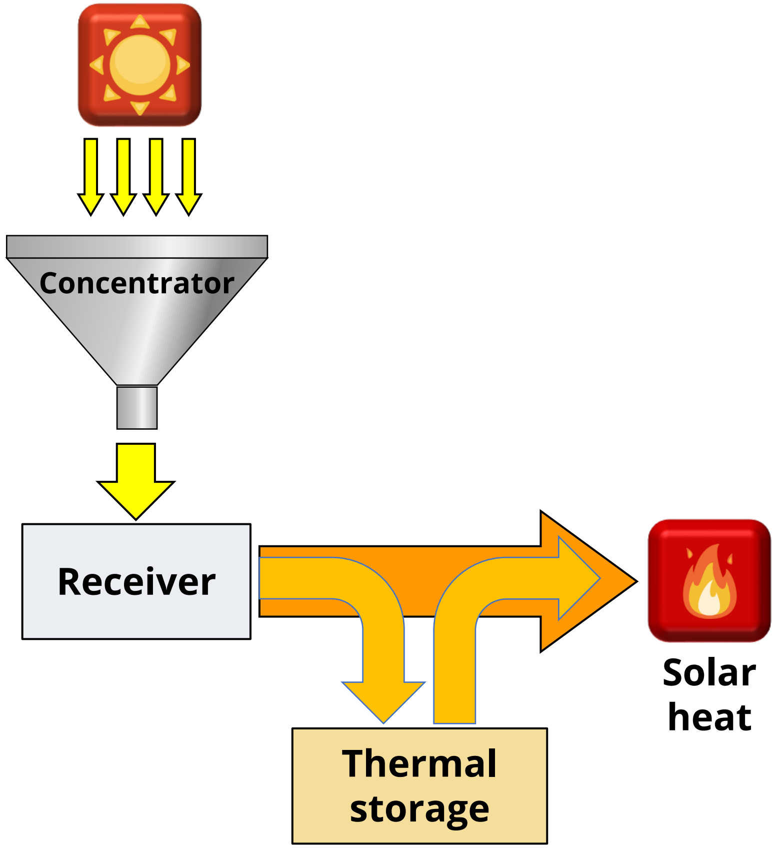

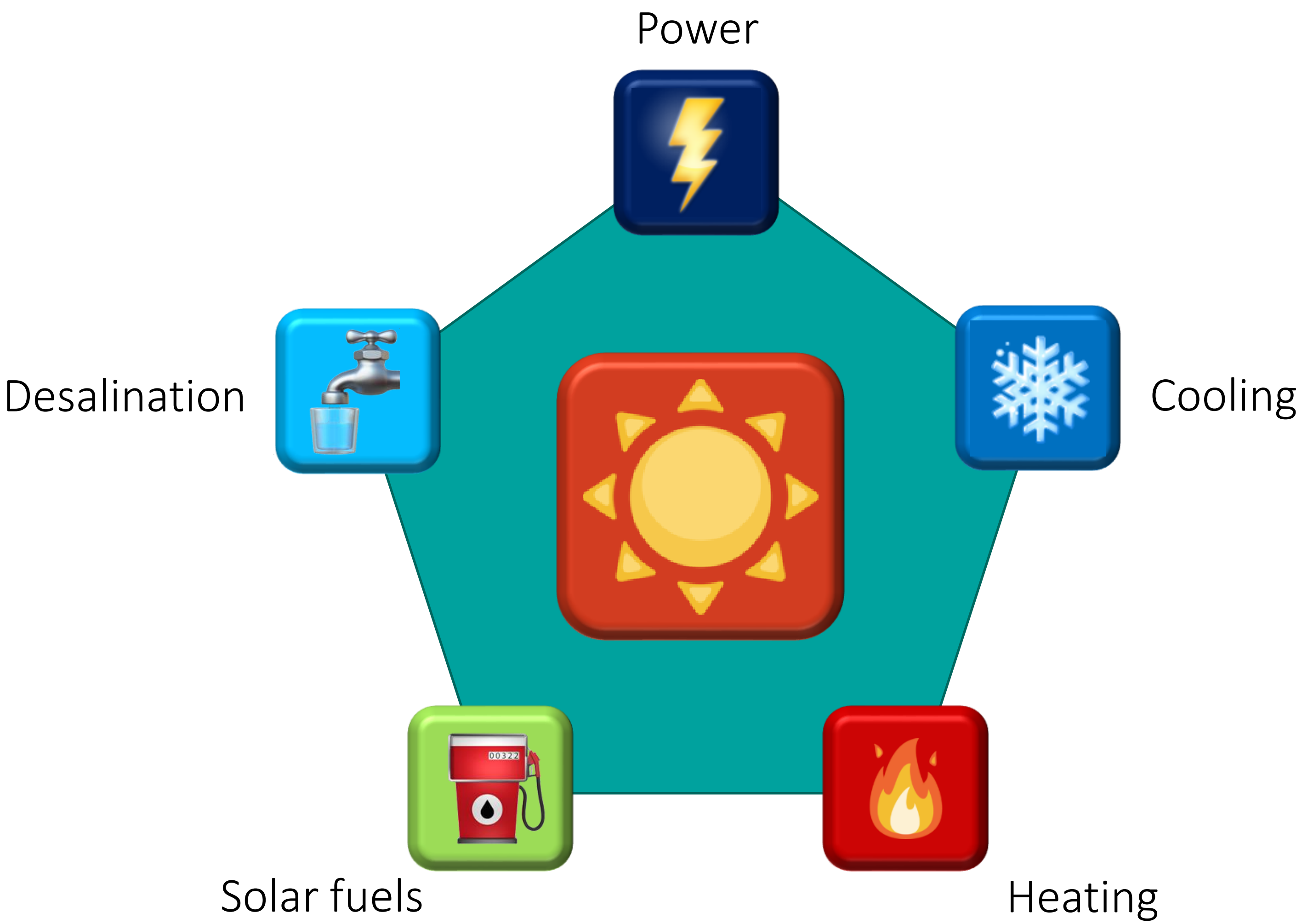

Is renewable electricity the only key to industrial decarbonization?

TOTAL FINAL ENERGY CONSUMPTION IN 2014: 360 EJ

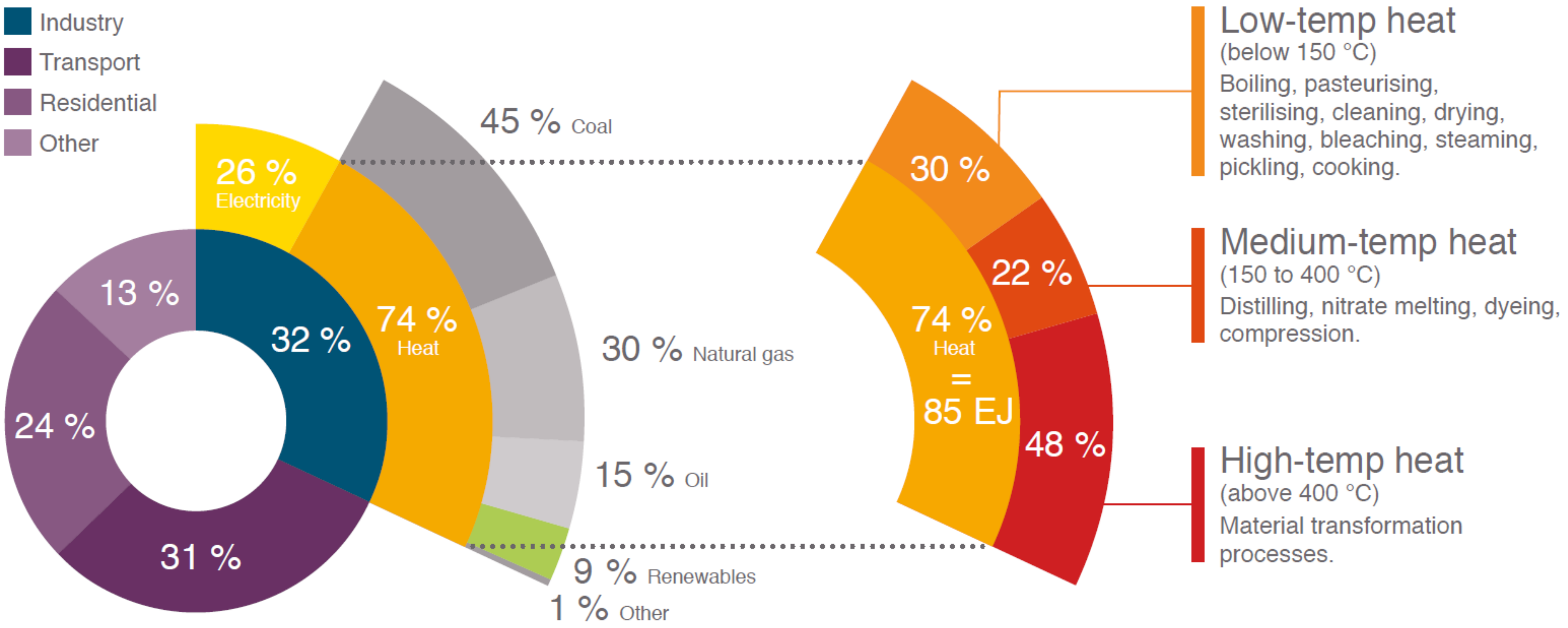

Image source: SolarPayback (https://www.solar-payback.com/)
Data Source: IEA and IRENA

Low- and medium-temperature solar heat for industrial processes

Demand

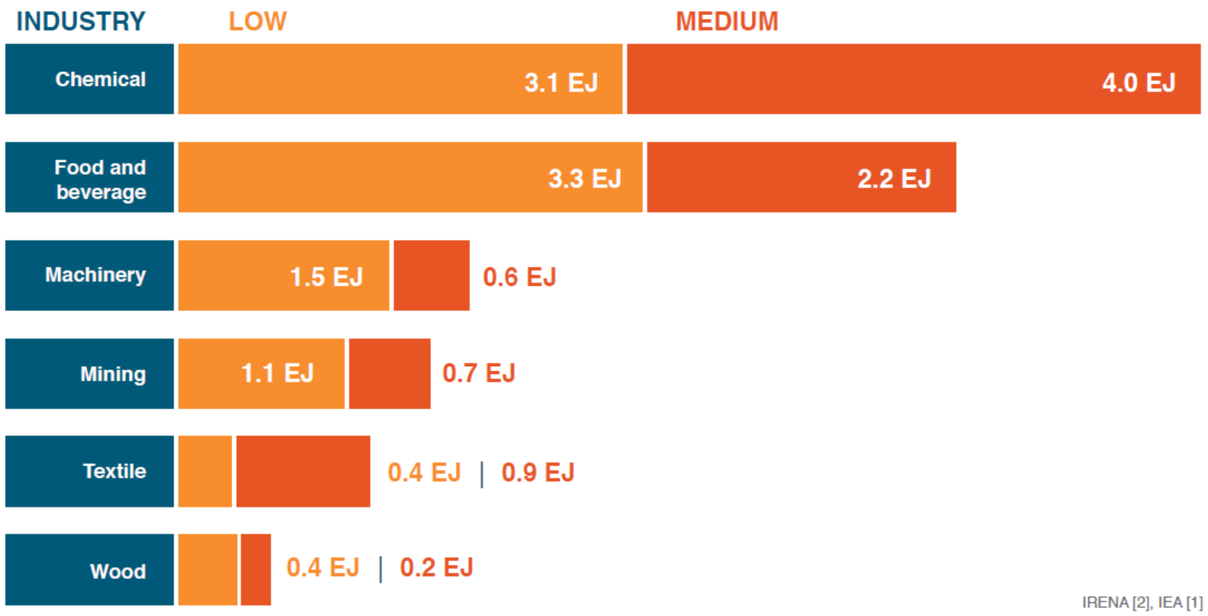

Technologies

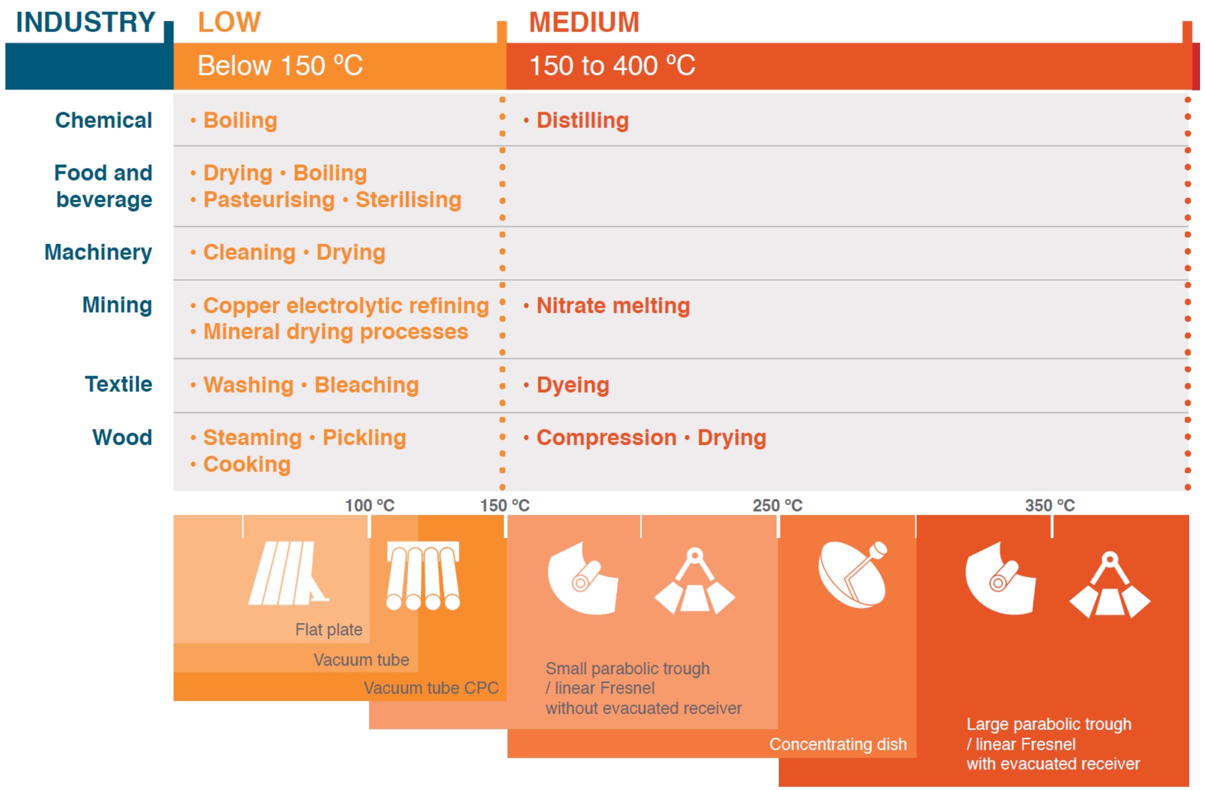

Image source: SolarPayback (https://www.solar-payback.com/)
Data Source: IEA and IRENA (2014)

Solar heat supply to chemical processes (I):
Direct/indirect irradiation (without HTF)

Directly irradiated reactors

Indirectly irradiated reactors

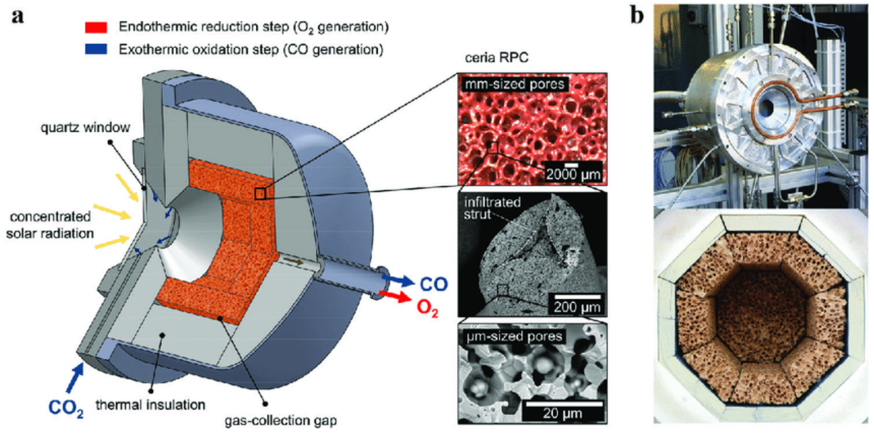

Source: Marxer et al., energy & Environmental Science, 10 (2017), 1142

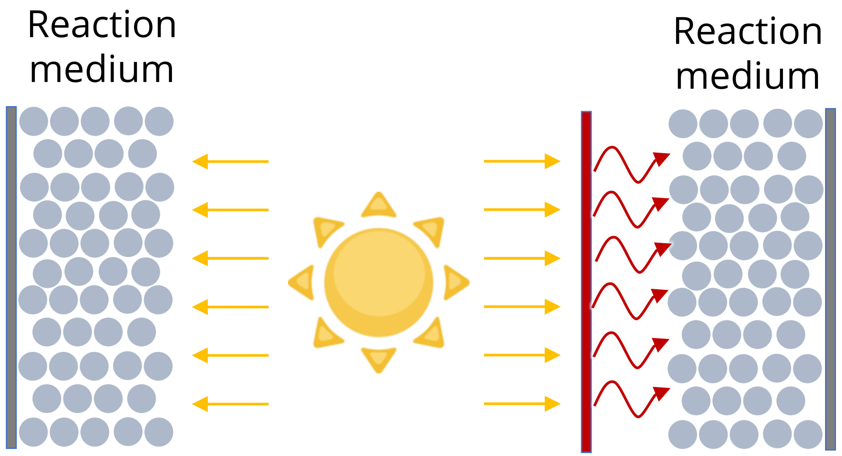

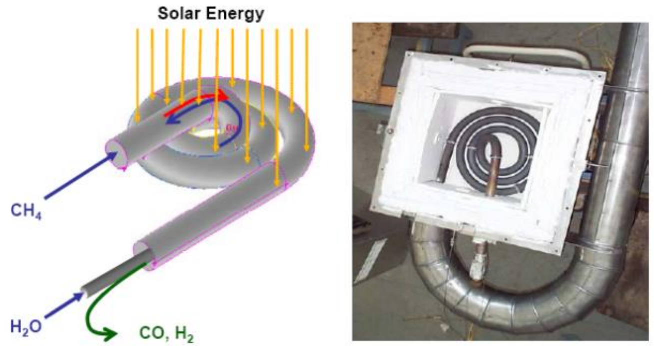

Source: Roeb et al., Int. J Nuclear Hydrogen Production and applications, 2 (2011), No. 3, 202-226

Direct/indirect irradiation can also be applied to process streams, e.g., pre-heating of the feed stream upstream of an adiabatic reactor.

Solar heat supply to chemical processes (II):
Use of heat transfer fluids

Integration points for solar heat in industrial processes

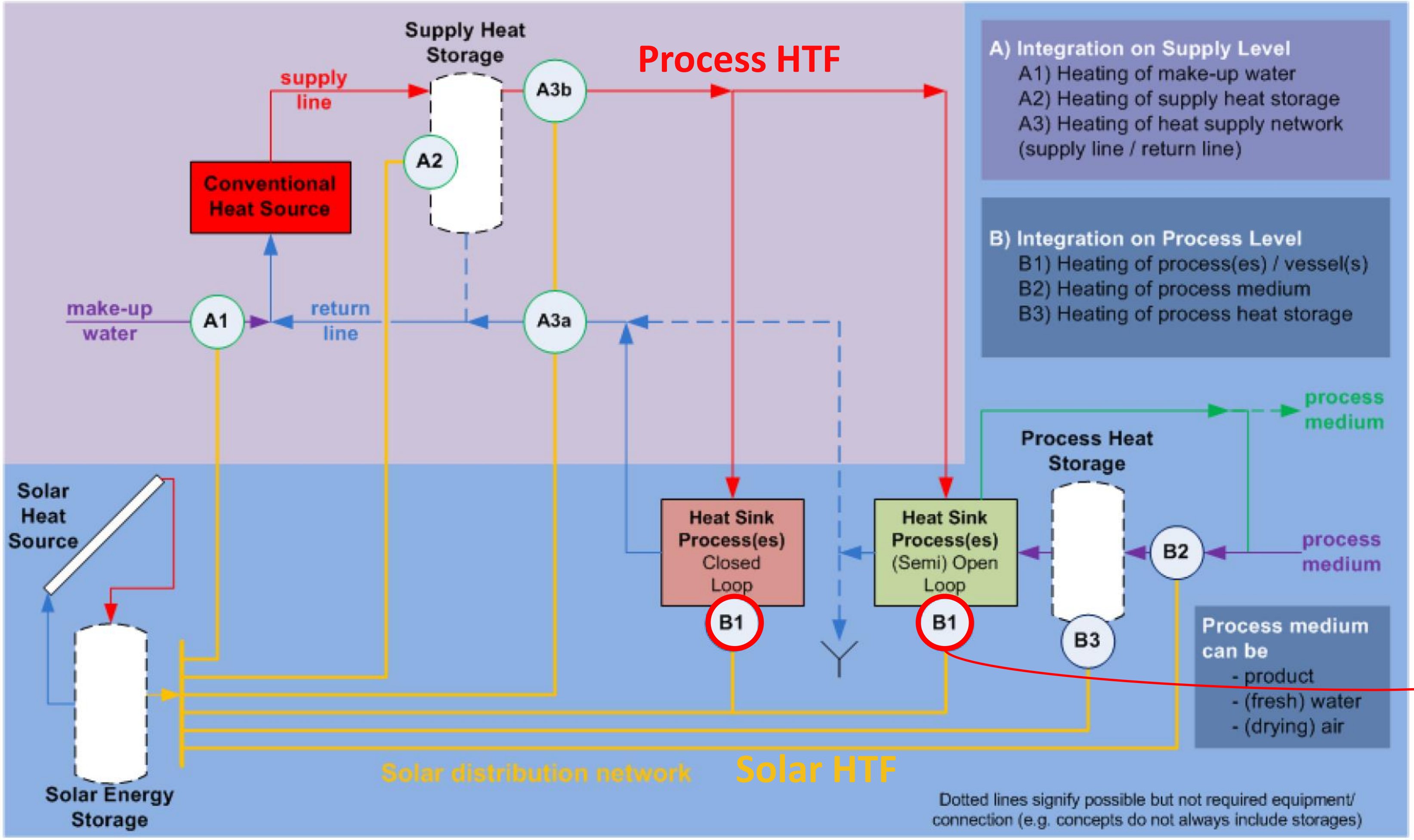

For chemical processes, integration at the reactor level is especially challenging, because it requires the development of integrated heat exchangers/reactors

Image source: AEE INTEC

Solar heat supply to chemical processes (III):
Direct/indirect irradiation vs use of HTF

Direct/indirect irradiation	Use of HTF
Very high maximum operating temperatures (>1000 °C)	Maximum temperature limited by HTF: • Liquid HTF: <600 °C (Solar salt) • Gaseous HTF: no temperature limit, but worse heat transfer behaviour • Solid HTF: high T possible; heat exchange equipment more complex
Complex coupling with TES systems. Very high-T TES solutions not yet commercially available.	Easy coupling with comercially available TES technologies if liquid HTF is used
More efficient heating of solids (catalysts, reactants) in properly designed directly irradiated reactors	Solids in the reactor are indirectly heated through the reactor wall or by process streams
Receiver-reactor design can be challenging	Reactor design closer to conventional process equipment
Complex management of cloud transients	HTF buffers fluctuations of the solar resource
Complex startup-shutdown	Hot stand-by makes startup easier

Molten salts as an interface for the steady supply of renewable high-temperature heat to chemical processes

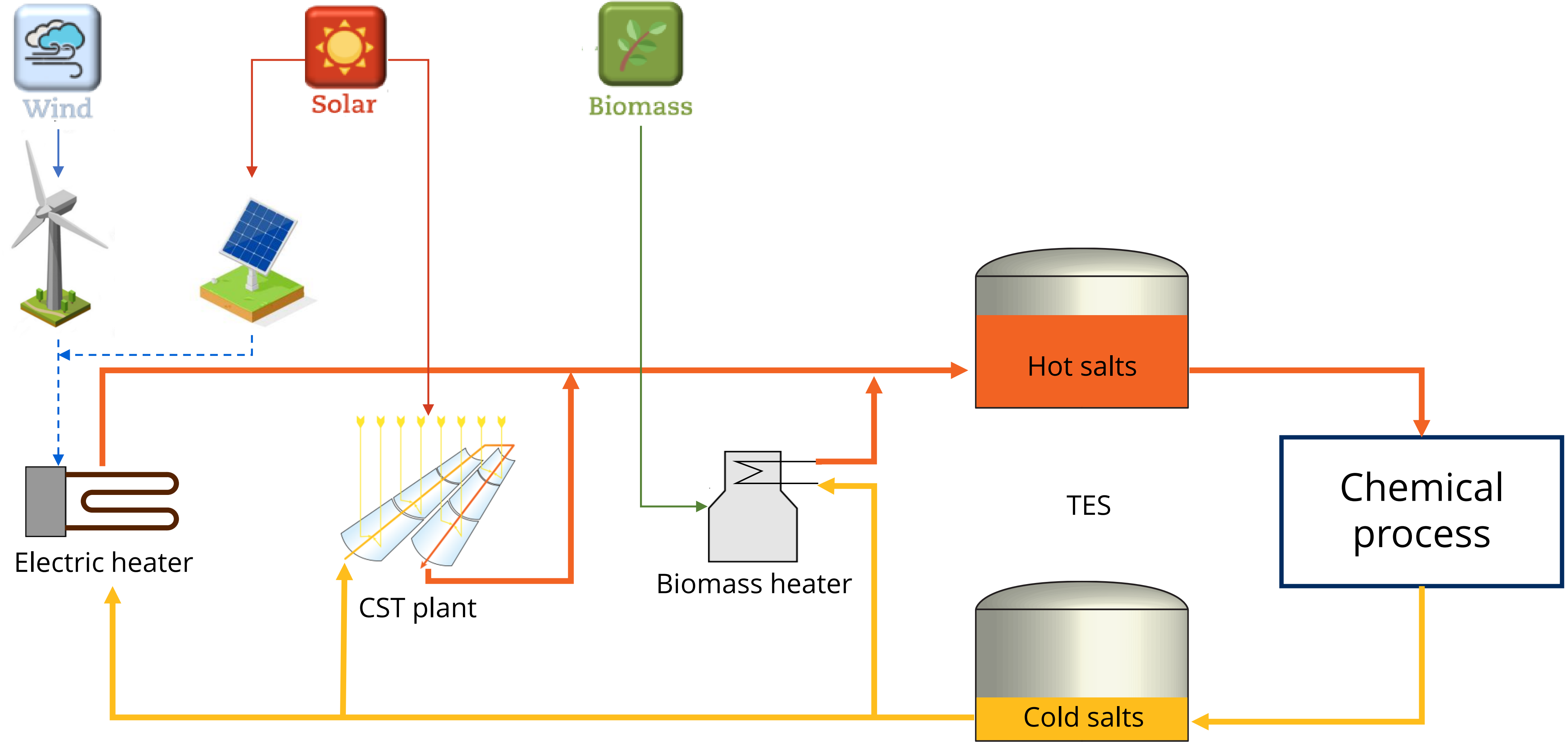

Case study:
Hydrogen production by steam methane reforming

Methane steam reforming (grey hydrogen): conventional process

$CH_4 + H_2O \leftrightarrows CO + 3H_2$	$\Delta H_{500°C} = 221{,}6 \ \frac{kJ}{mol}$	(SR)
$CO + H_2O \leftrightarrows CO_2 + H_2$	$\Delta H_{500°C} = -37{,}4 \ \frac{kJ}{mol}$	(WGS)
$\boxed{CH_4 + 2H_2O \leftrightarrows CO_2 + 4H_2}$	$\Delta H_{500°C} = 184{,}2 \ \frac{kJ}{mol}$	(OSR)
$CH_4 + CO_2 \leftrightarrows 2CO + 2H_2$	$\frac{kJ}{mol}$	(DR)

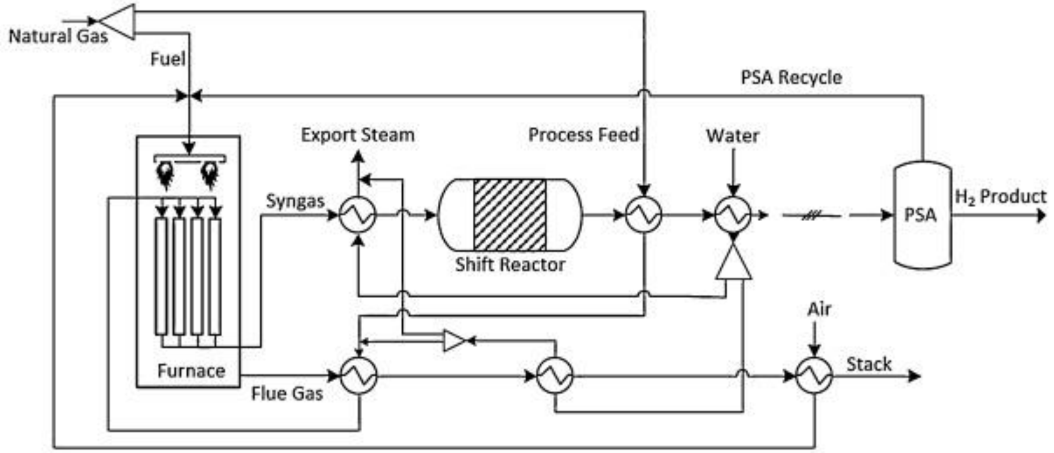

Conventional process:

- Carried out in externally heated (furnace) tubular reactors
- Operating conditions: T = 700-1000 °C; P = 10-40 bar; S/C = 3-6
- Downstream of the reformer, 1 or 2 WGS reactor(s) (500-600°C)
- About 12 t of CO_2 per t of H_2
  - From the chemical reaction
  - From combution
- H_2 production cost: 1-2 $/kg, strongly depending on gas price

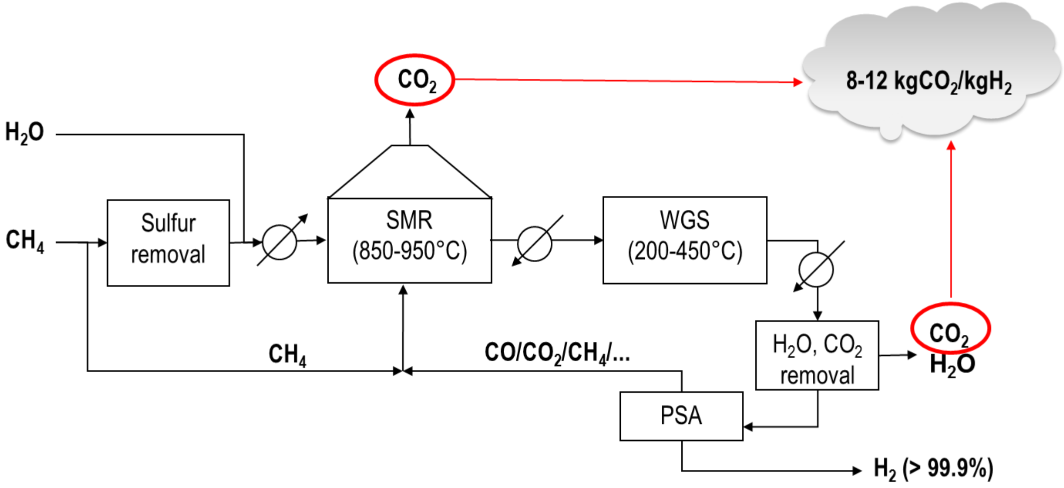

Low-temperature molten-salt-heated methane steam reforming: the CoMETHy project

Conventional SMR → **CoMETHy project**

T = 700 - 1000 °C → T = 450 - 550 °C

Advantages:

- Lower-grade materials
- Higher safety
- Single reactor for SR and WGS
- **Use of solar power from CSP with MS**

→

- Up to 100% H_2 from renewables
  - Solar upgrading of fossil fuels
  - Reforming of renewable feedstocks
- NO CO_2 from fuel gas combustion

Drawbacks:

- Low hydrogen yield → Membrane reactor
- Slow reaction kinetics → Active and stable catalysts
- Low catalyst bed exploitation → Monolithic solid foam catalyst carriers

The membrane reactor concept

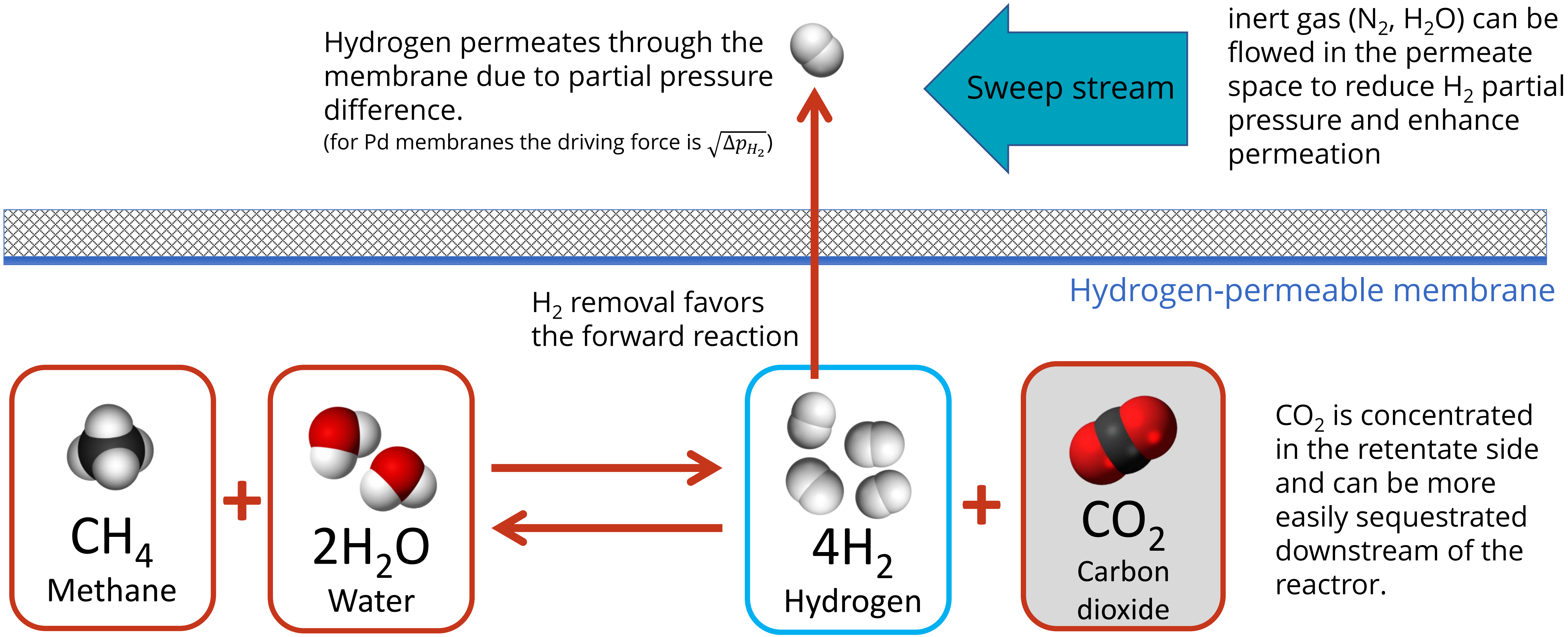

CoMETHy plant concept

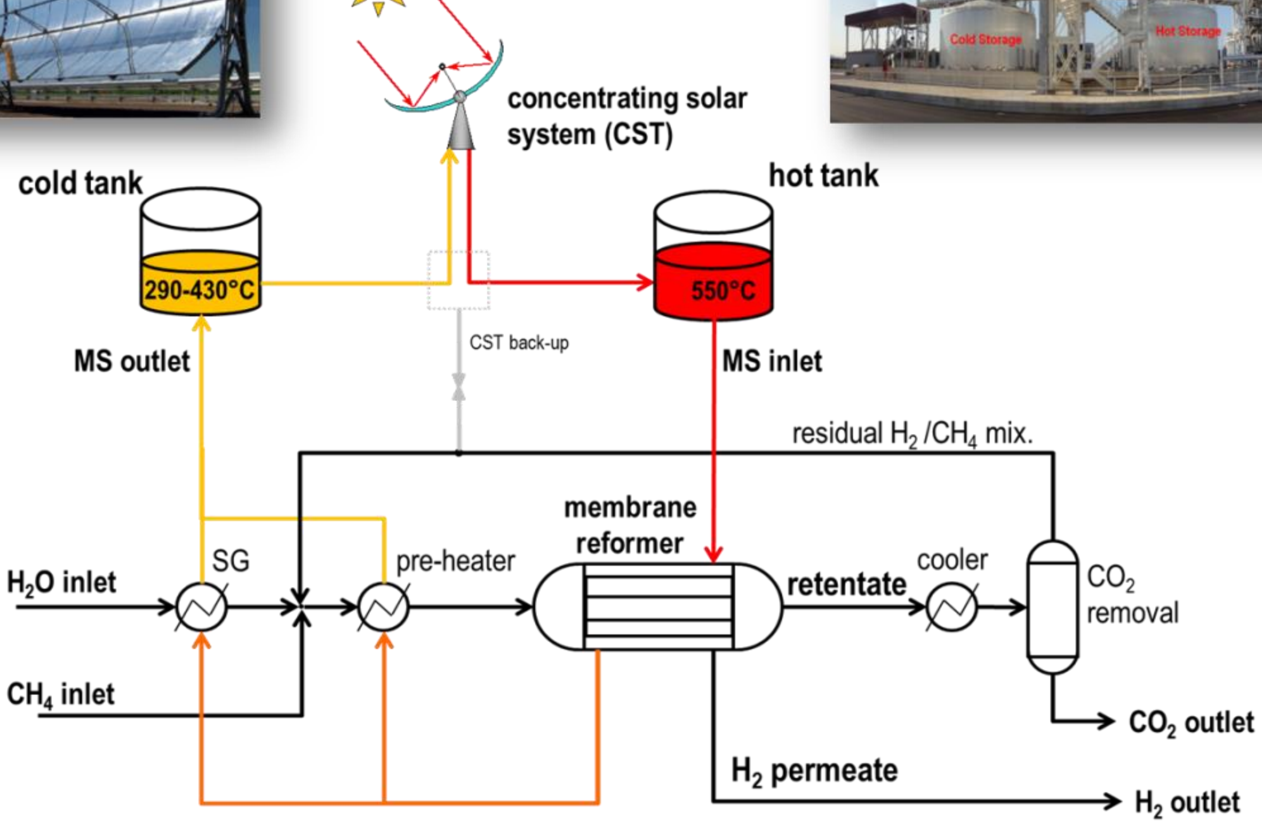

CoMETHy molten-salt-heated membrane reactor

MS-heated membrane reformer
(2Nm³/h pure hydrogen)

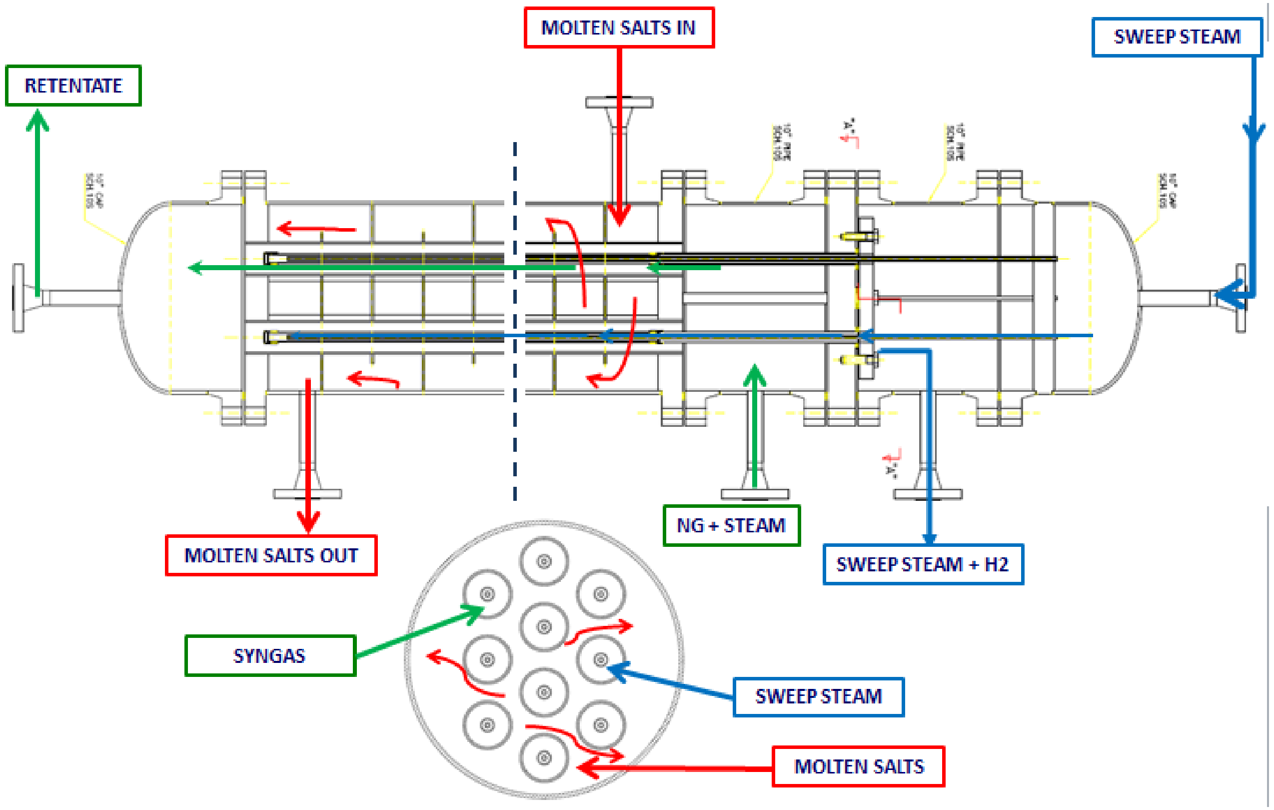

Selective membranes for hydrogen separation

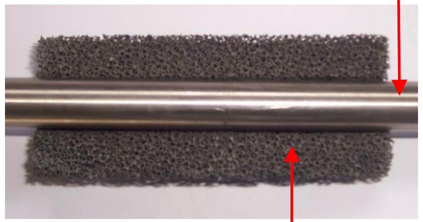

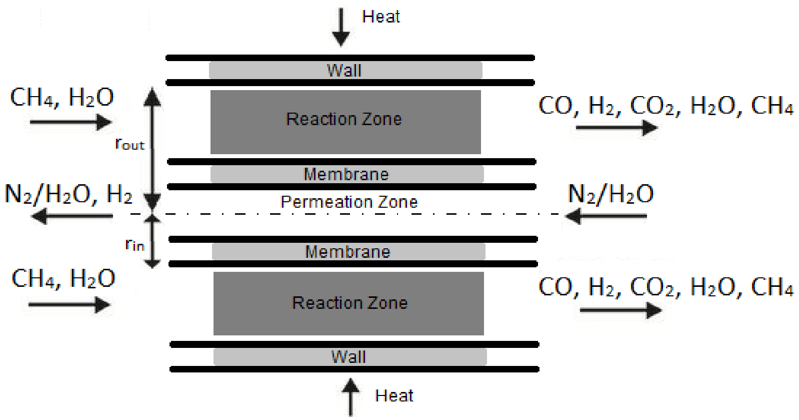

Advanced catalysts for low-temperature steam reforming (NG, biogas, ethanol)

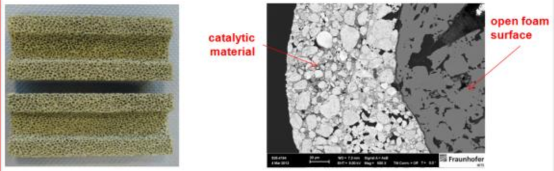

CoMETHy molten-salt-heated membrane reactor

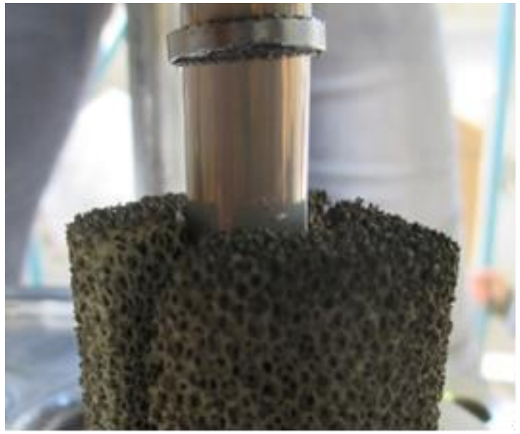

(a)

(b)

(c)

(d)

CoMETHy pilot plant

Membrane reactor

ENEA MoSE loop

Overview of chemical section

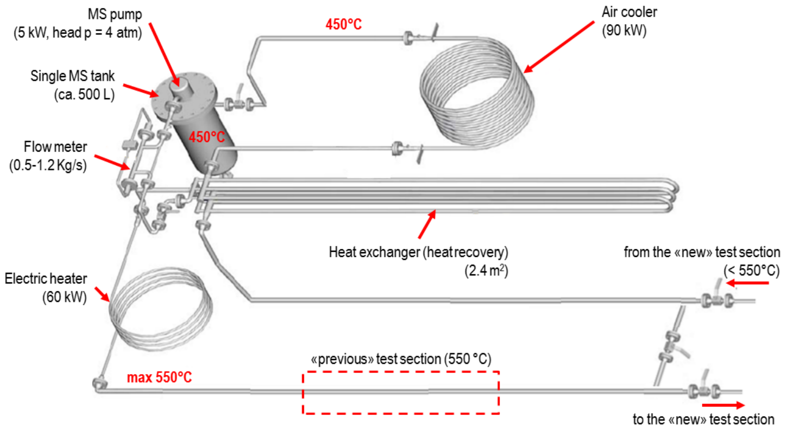

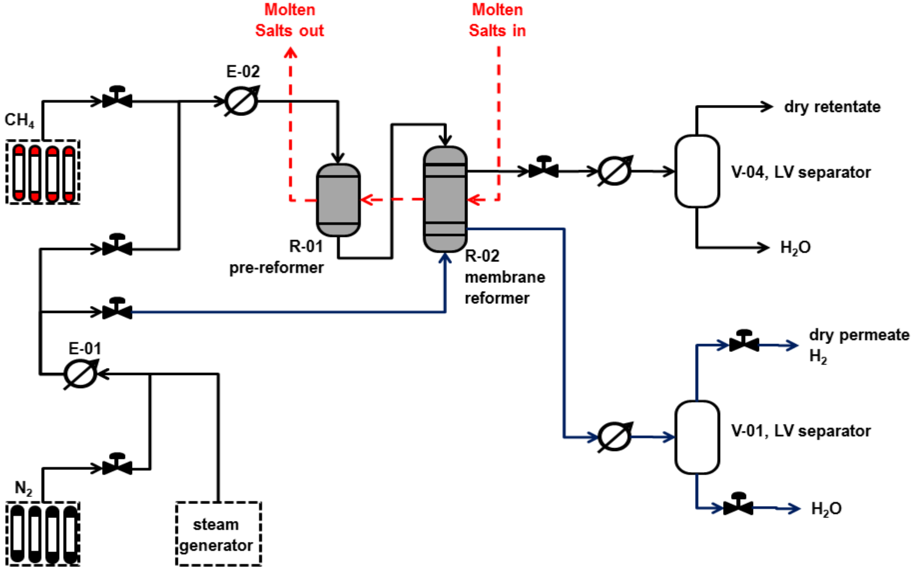

CoMETHy pilot plant: testing results

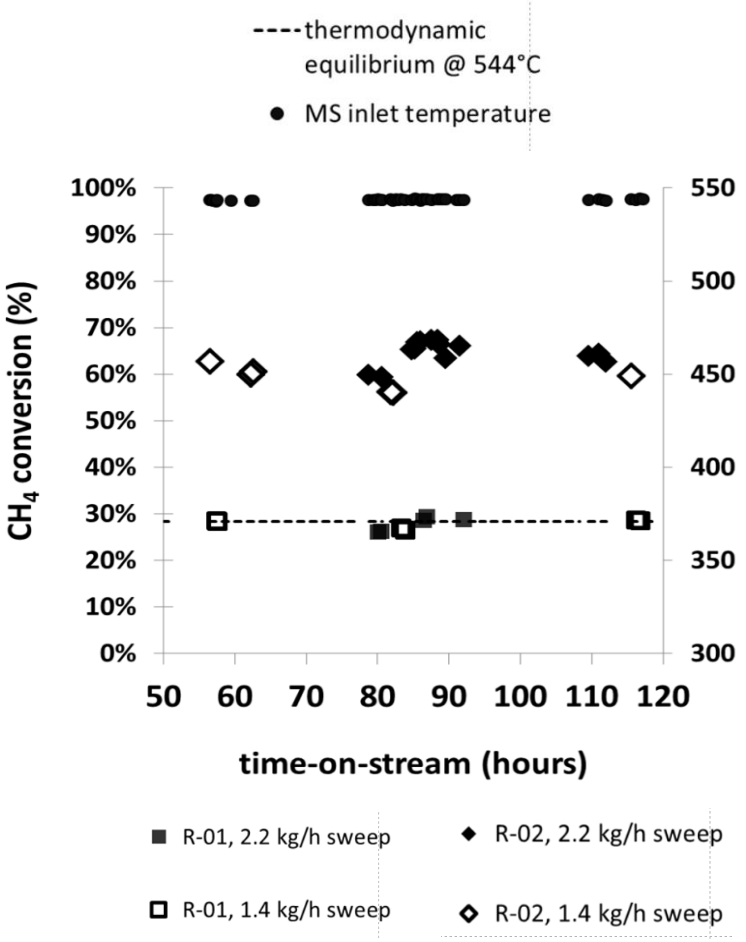

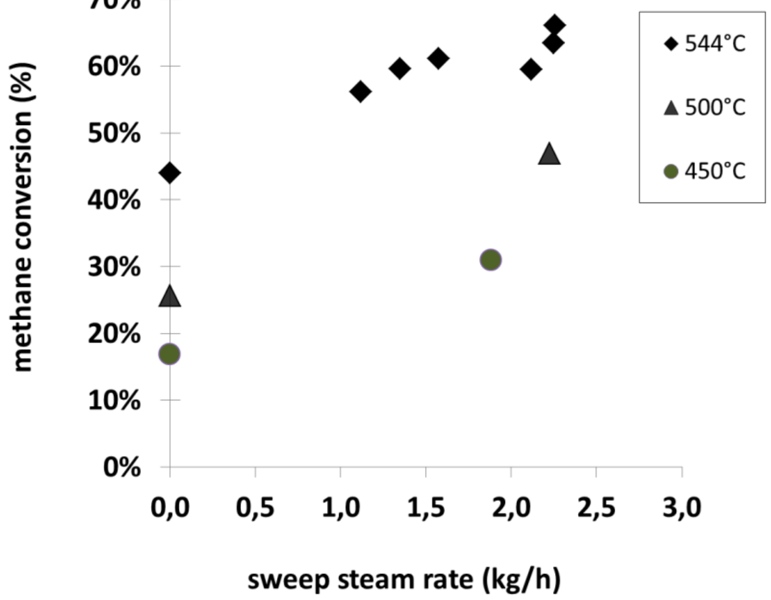

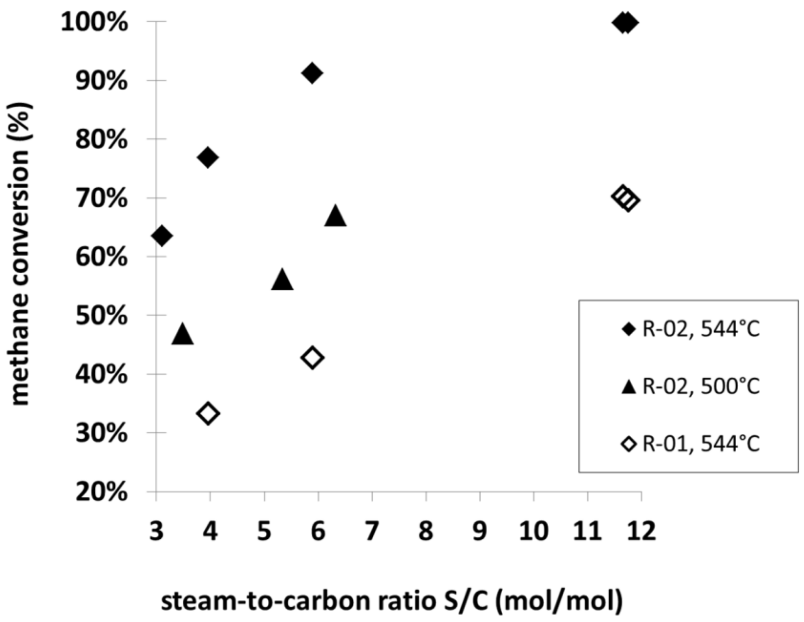

Source: doi:10.1016/j.ijhydene.2020.09.070

CoMETHy followup:
Investigation of a new planar reactor configuration

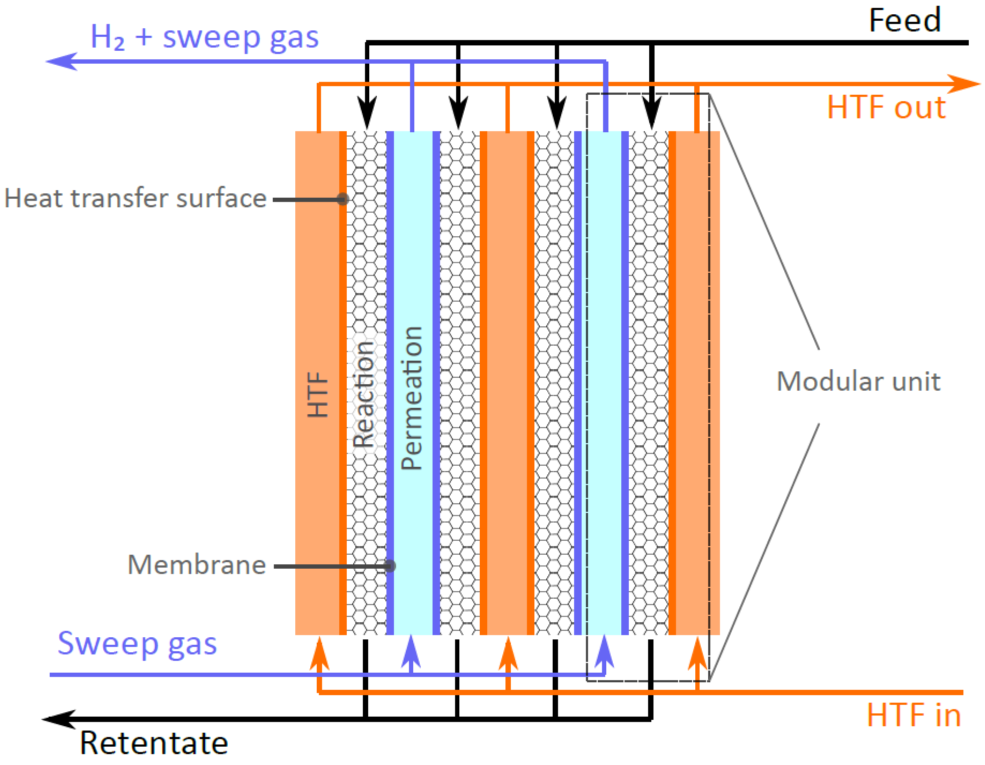

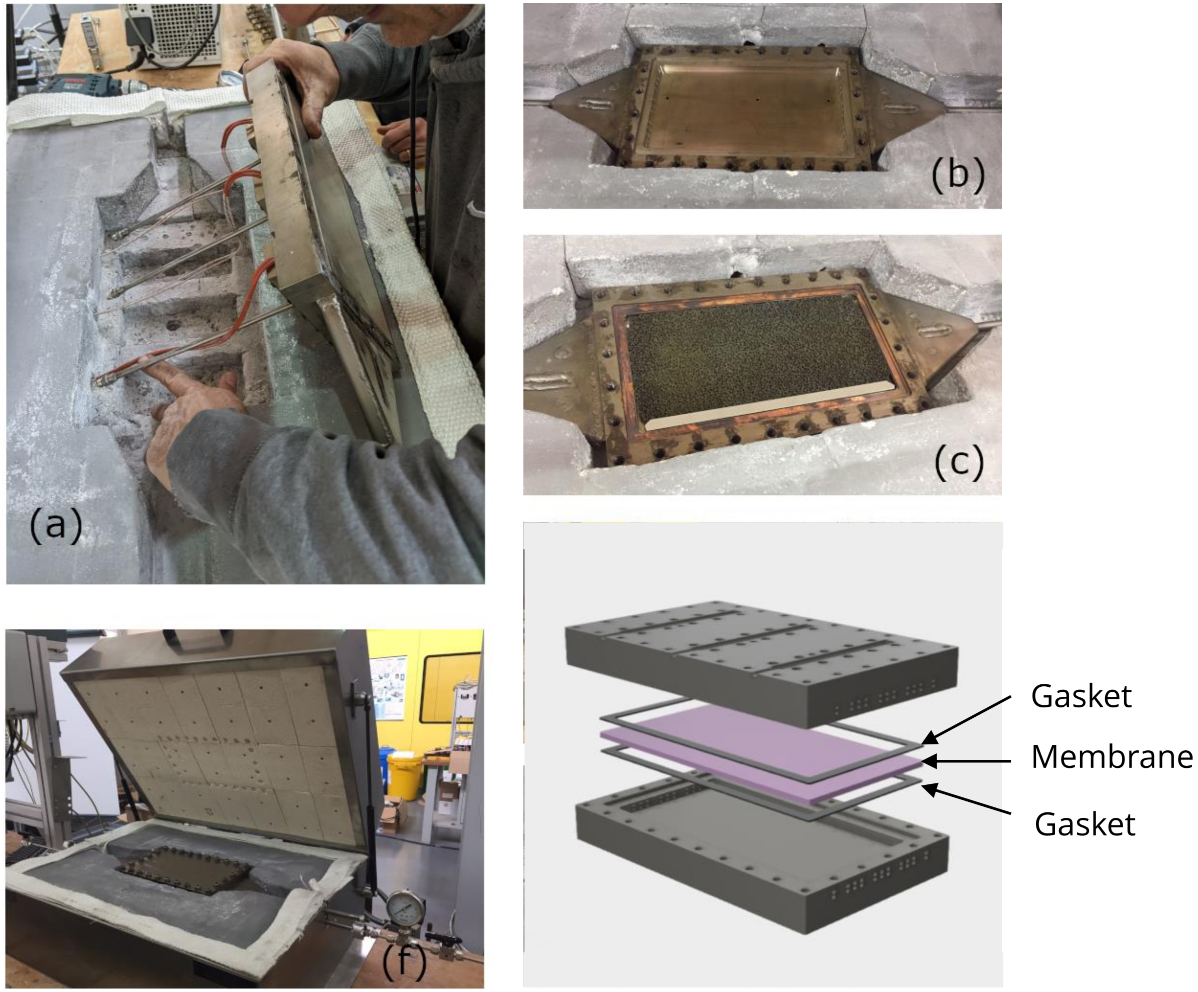

RdS RICERCA DI SISTEMA

This work was funded by the
Italian Ministry of Economic Development
though the «Electric System Research» programme
2019-2021 implementation plan

Reactor simulation: definition of baseline case

In order to understand how the close interplay of reaction, permeation and heat exchange phenomena determine the behavior of the reactor (and its design), reactor simulations can be carried out; the following baseline case can be considered:

- Biogas reforming in a planar reactor
- Catalyst: Ni/CeZrLa deposited on SiC foam (CoMETHy project); loading: 140 g/L

Parameter	Units	Value
Feed stream temperature	°C	500
Molten salt temperature	°C	500
Pressure in reaction space (retentate)	bar	9
Pressure in permeate space	bar	1
Steam to methane ratio (mol/mol) in the feed stream	-	3
CO2 to methane ratio (mol/mol) in the feed stream	-	1
Sweep gas to feed methane ratio (mol/mol)	-	1,5
Reaction space thickness	cm	1
Length to thickness ratio of the reaction space	-	30

Reactor simulation:
effect of membrane and heat exchanger integration

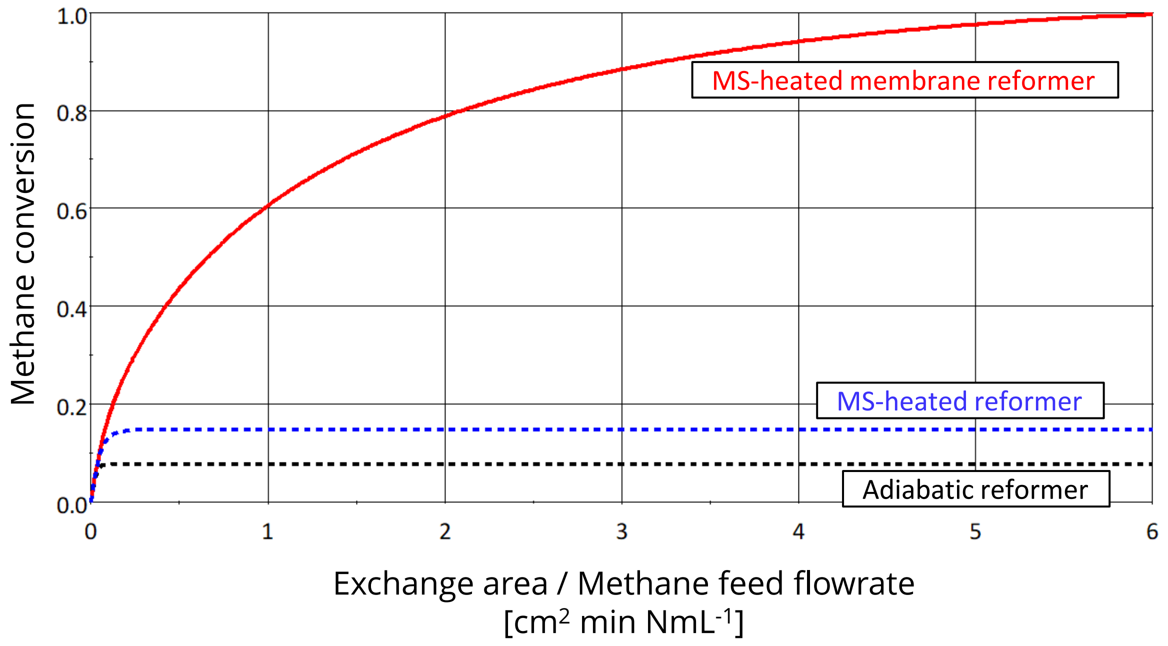

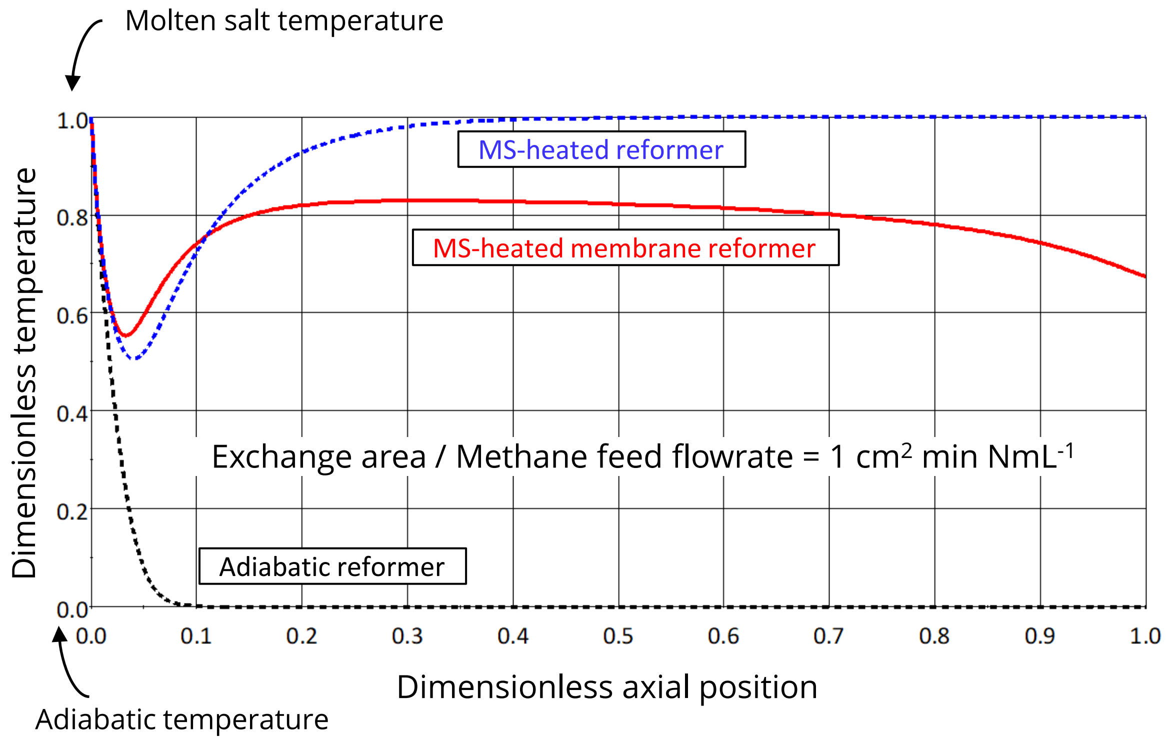

Reactor simulation:
effect of reaction, permeation and heat exchange kinetics

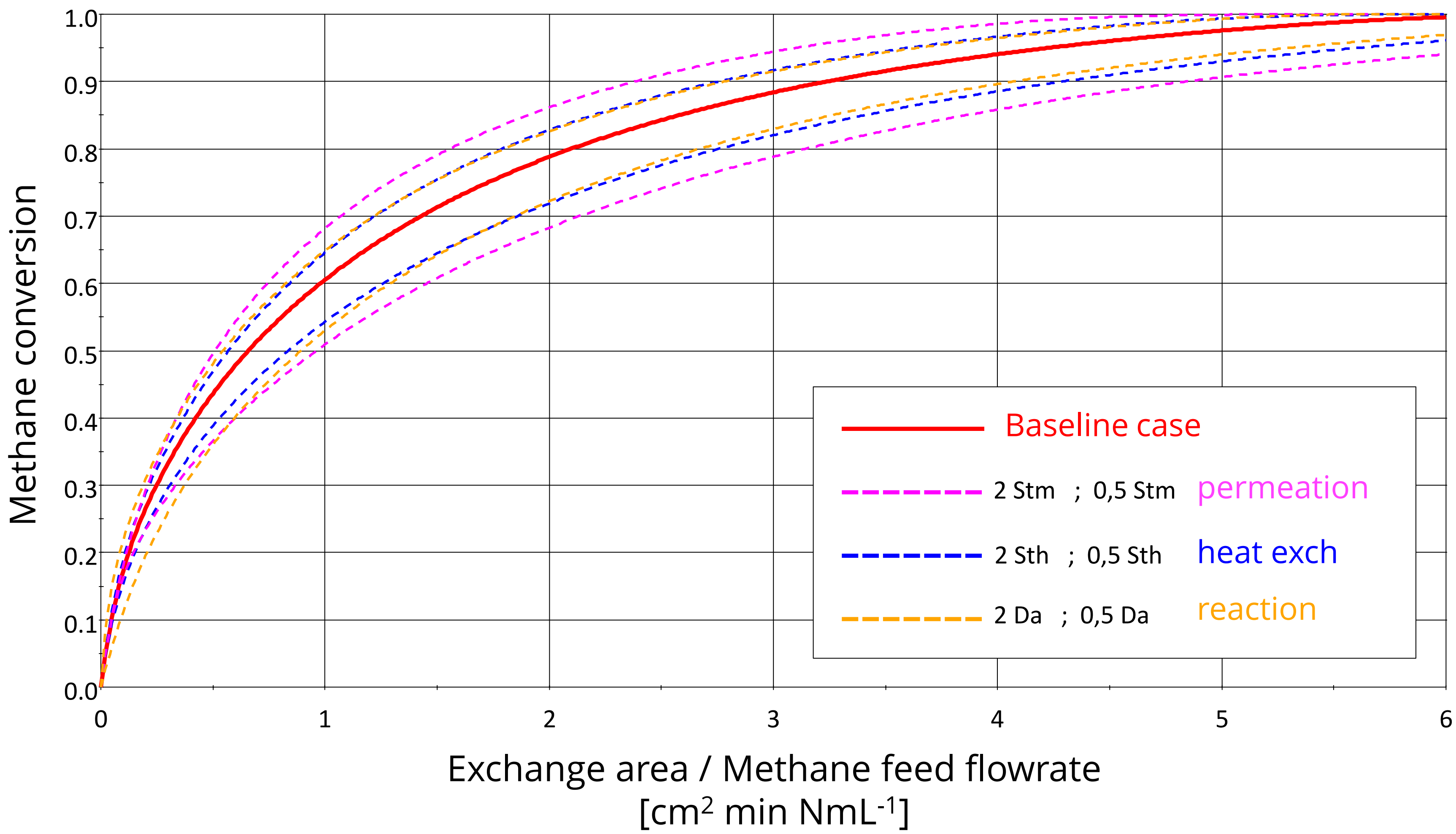

Reactor simulation:
effect of sweep gas flowrate and molten salt temperature

Effect of sweep gas flowrate

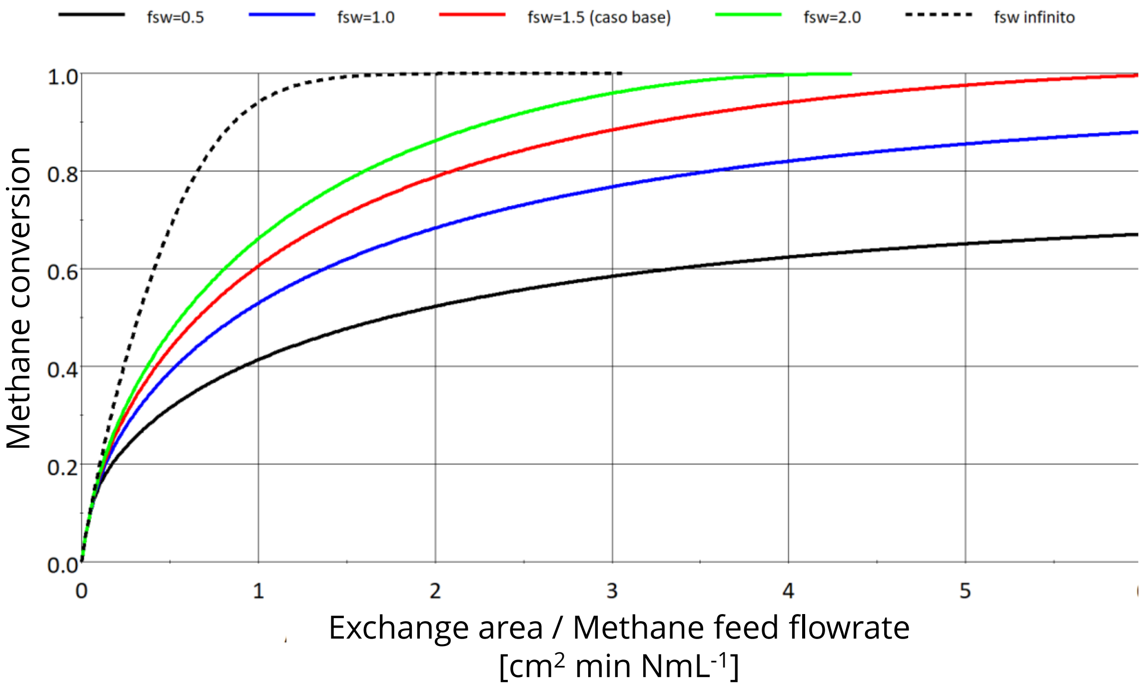

Effect of molten salt temperature

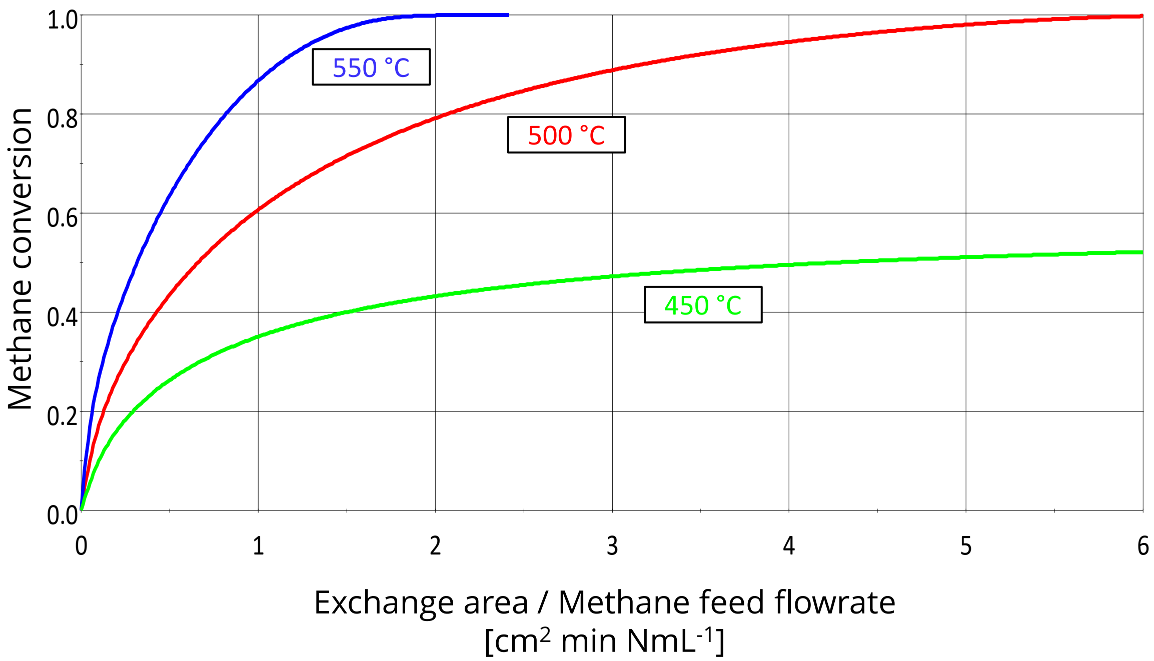

Luca TURCHETTI, PhD
ENEA
TERIN-STSN-SCIS
luca.turchetti@enea.it

THANK YOU FOR YOUR ATTENTION!
ANY QUESTIONS?

References

- *Experimental validation of a pilot membrane reactor for hydrogen production by solar steam reforming of methane at maximum 550 °C using molten salts as heat transfer fluid.*
  International Journal of Hydrogen Energy, 45(58), 33088-33101. doi:10.1016/j.ijhydene.2020.09.070
- *Techno-economic assessment of solar steam reforming of methane in a membrane reactor using molten salts as heat transfer fluid*.
  International Journal of Hydrogen Energy, 46(71), 35172-35188. doi:10.1016/j.ijhydene.2021.08.096
- *Kinetic assessment of Ni-based catalysts in low-temperature methane/biogas steam reforming*.
  International Journal of Hydrogen Energy, 2016, 41(38), 16865-16877. doi:10.1016/j.ijhydene.2016.07.245

SFERA-III

Solar Facilities for the European Research Area

4th Training for Industries

7-11th November 2022, ENEA Casaccia Research Center, Rome (Italy)

Use of molten salts in biomass gasification processes

Raffaele Liberatore (ENEA , TERIN-STSN-SCIS)

JOINT RESEARCH ACTIVITIES

THIS PROJECT HAS RECEIVED FUNDING FROM THE EUROPEAN UNION’S HORIZON 2020 RESEARCH AND INNOVATION PROGRAMME UNDER GRANT AGREEMENT NO **823802**

Outline:

Biomass gasification main aspects

Process analysis

Reactor configuration

Integrated heat exchanger

Gasifier coupling with parabolic trough CSP

Conclusions

Biomass gasification main aspects

Solid fuel + Thermal energy = Gaseous fuel

Biomass → Agro-forestry wastes

- Pyrolysis: thermal degradation with no oxygen
- Gasification:
  - ↓ Tar
  - ↑ LHV

→ ICE, gas turbine, fuel cell

Equivalent ratio effect

Equivalent Ratio

$$ER = \frac{Air_{in}}{Air_{stoich}}\ [\%]$$

$ER \uparrow$:
- $\uparrow \eta_c$
- $\uparrow \eta_g$
- $\uparrow T$
- $\downarrow Tar$

Carbon conversion efficiency

$$\eta_{carbon} = \frac{12(CO_2 + CO + CH_4 + nC_nH_m)}{22.4 \cdot C} \cdot V_g \cdot 100\ [\%]$$

No LHV!

Cold gas efficiency

$$\eta_g = \frac{LHV_g \cdot V_g}{LHV_b \cdot G_b}$$

G_b: mass flow rate [kg/s]
V_g: Gas flow [SNm^3]

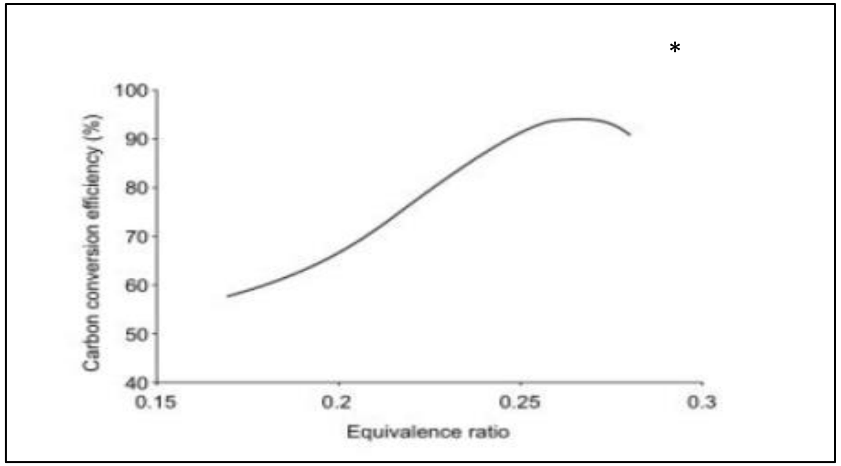

*Basu P. In Biomass Gasification and Pyrolysis, Practical Design and Theory, pages 65 -96. Academic Press, Boston, 2010

SFERA-III
Solar Facilities for the European Research Area

Up draft reactor for test campaign

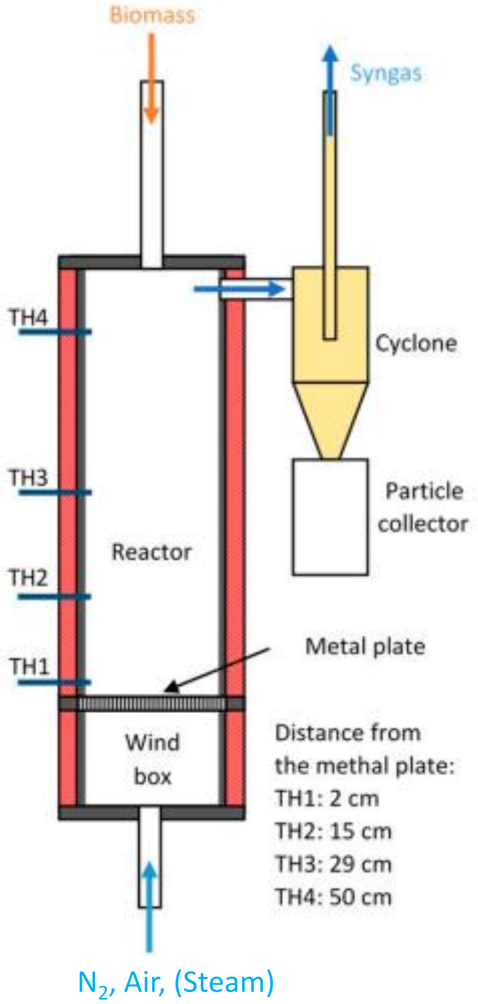

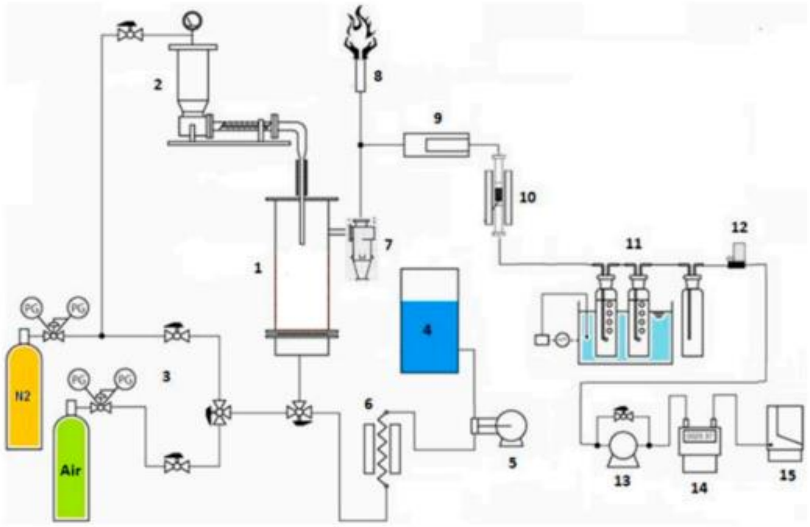

Equivalent ratio effect

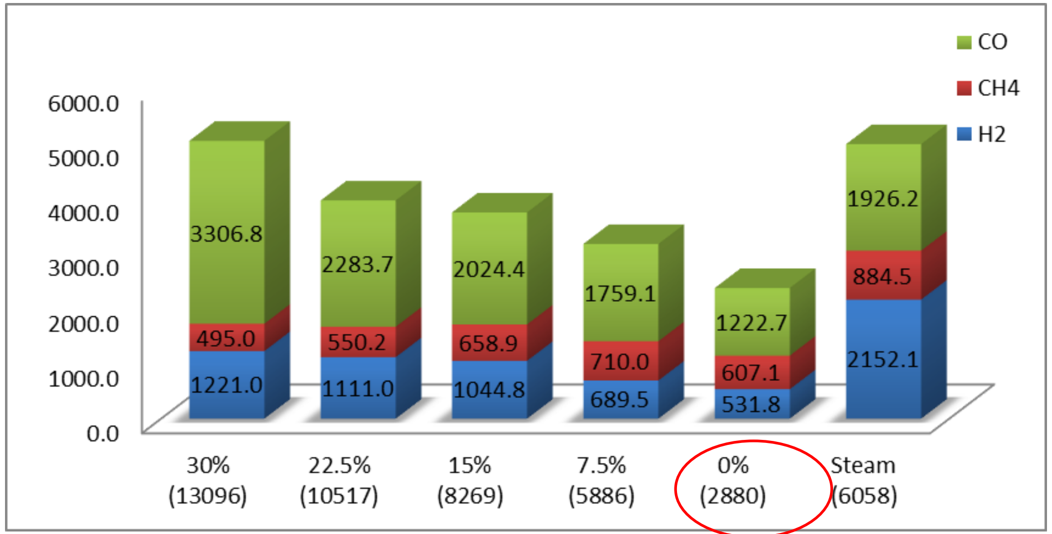

pyrolysis

Used biomass: hazelnut shell

Electric heater power: 850-900 °C

Influence of oxidant agents on syngas quality

Feeding rate: 5.3 g/min + 0.4 NL/min N_2 to avoid clogging

Air: 8.4-0 NL/min; steam: 2.7 g/min

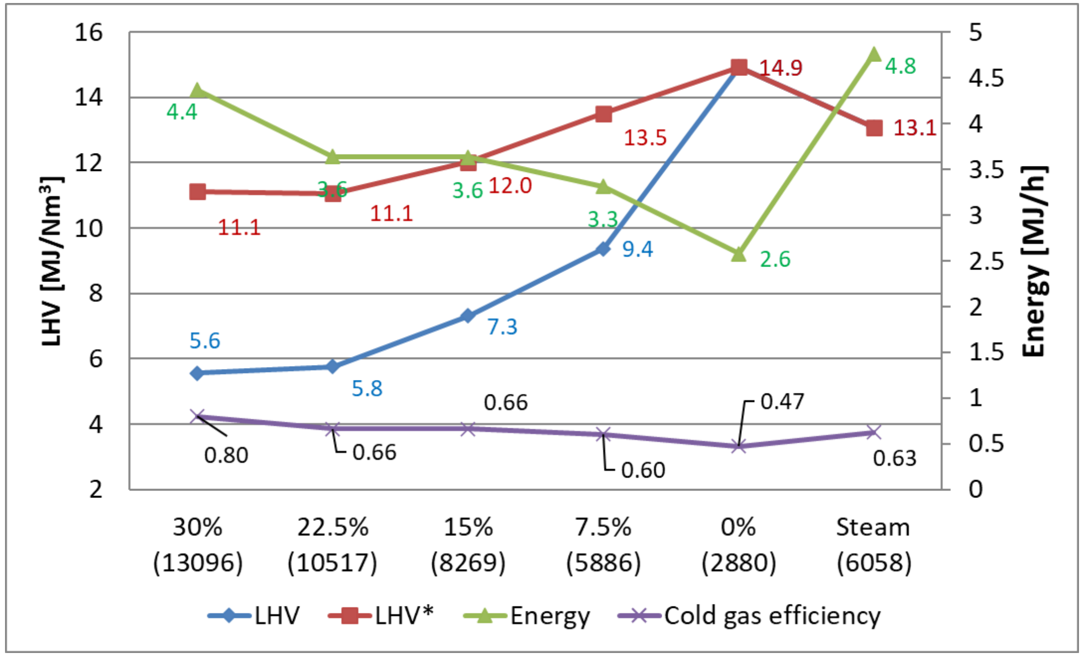

Gasification + CSP

Solar Central Receiver (tower)

(direct energy supply)

- Plant difficulties
- Internal thermal transients
- Unstable operation

*
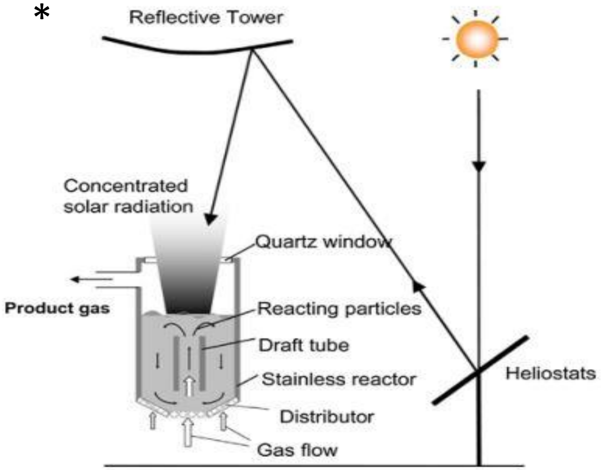

Parabolic trough with MS

- Thermal storage
- Stability and continuity operation

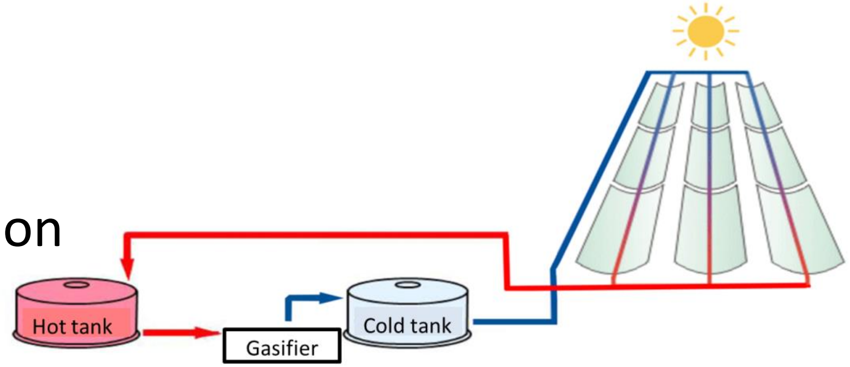

* Puig Arnavat M. State of art on reactor designs for solar gasification of carbonaceous feed. Solar energy, 2013: 67-84.

** Juelich Solar tower (DLR-Germany).

Pyrolysis zone temperature range

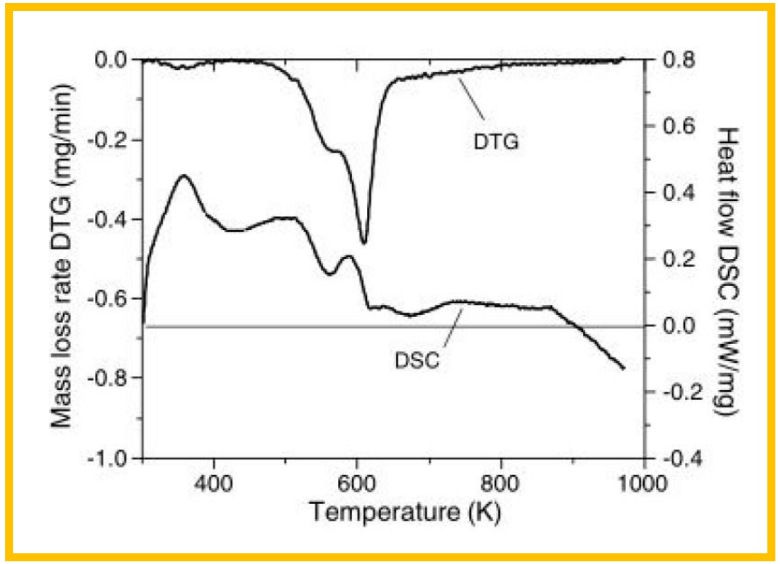

DSC curve caloric requirement by integrating DSC for straw and

different kind of biomass

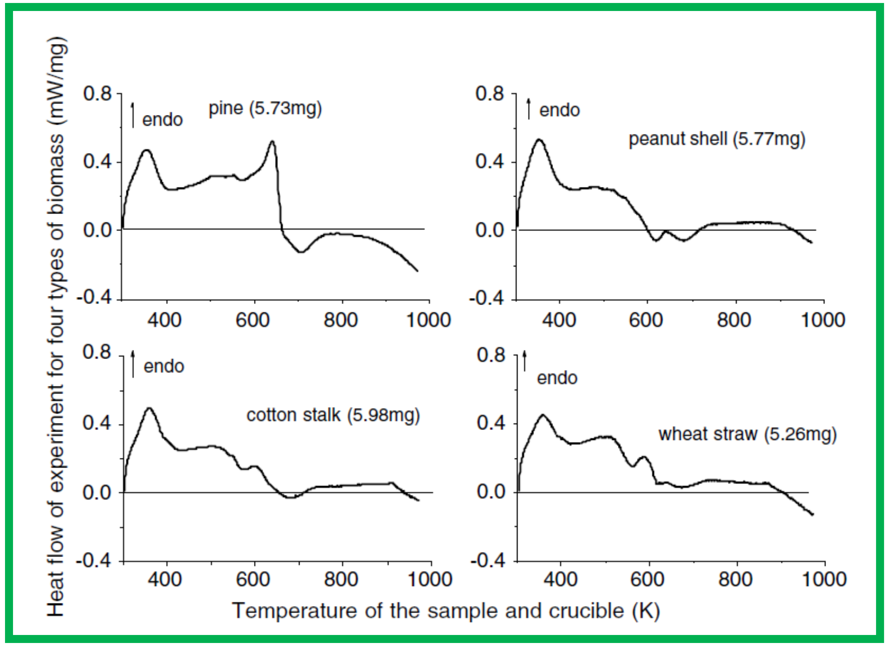

He et al. Energy Conversion and Management 47 (2006) 2461–2469

- 25-170 °C [298-443 K]: the energy required accounts for the sensible heat to cover the temperature range and, the latent heat for vaporization of the fuel moisture.
- 170-260 °C [443-533 K]: here, warm up of dry biomass and steam are the only processes taking place
- 260-400 °C [533-673 K]: in this range the complex degradation reactions must be considered, with the simultaneous and competitive development of char and biomass devolatilization reactions. Solid mass reduction increases to a total of 56.4 wt% (on wet basis).
- 400-600 °C [673-873 K]: in this temperature range, a further char increase in temperature and a reduction of the solid fraction (about 8.7%) occurs, thus the biomass degradation is almost completed.

Consumption

Step	DT [°C]	Solid residue [%]	Energy demand [kJ/kg]
1 (sensible part-liquid)	25-100	100	106
1 (latent part)	100	100	341
1 (sensible part-vapor)	100-170	85	120
2	170-260	82	188
3	260-400	34	152
4	400-500	31	67
5	500-600	27	66
Total	25-600	27	1040

Energy supply main aspects

Conventional energy source:

Combustion

By external source:

Solar energy + Combustion

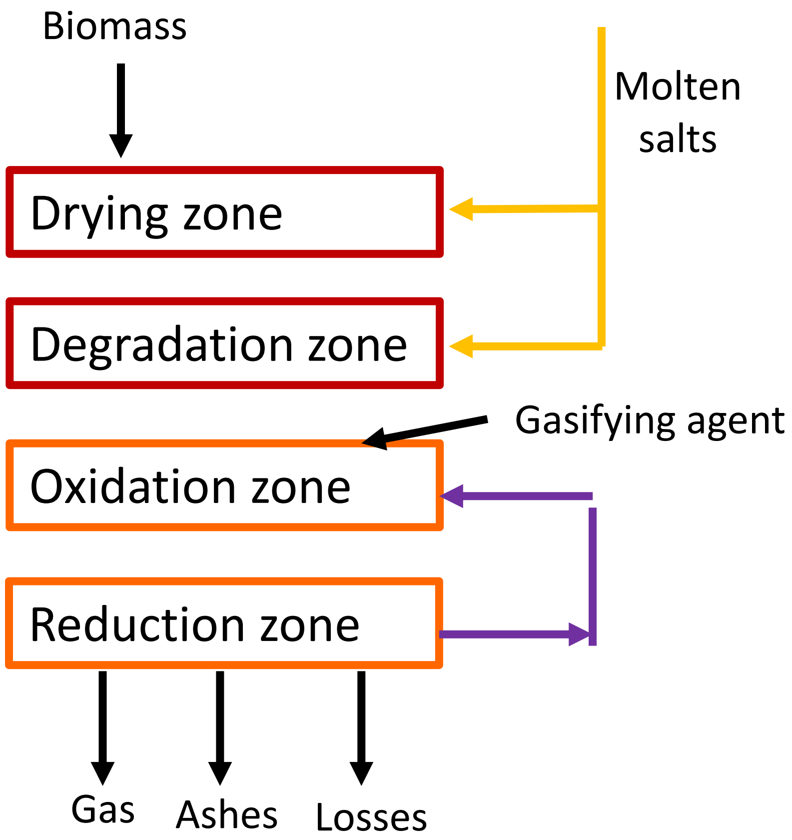

Reactor choice

Fluidized bed reactors: constant T > 700-800 °C

Moving bed reactors: variable T

Crossdraft

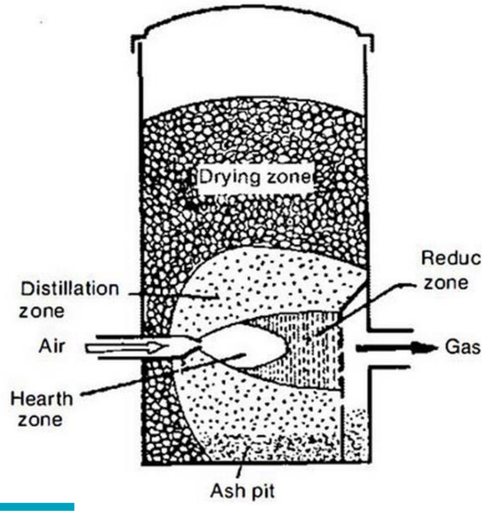

Downdraft

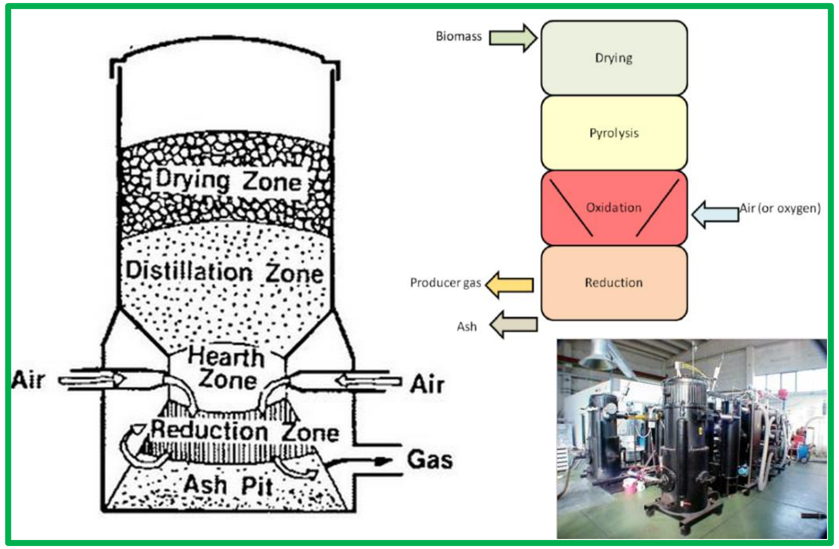

Updraft

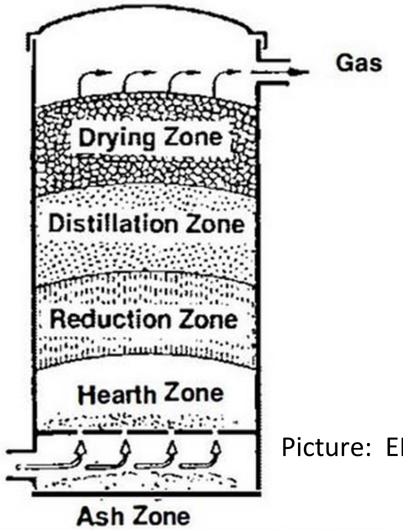

Figures source: Rado I. Biomass downdraft gasifier chp systems. 2013.

Picture: ENEA Trisaia downdraft reactor.

Integrated heat exchanger

- *14 circoular plats*
- $U_d = 16.56\ ^{W}/_{m^2 \cdot K}$
- $A_0 = 20.95\ m^2$
- $\omega_{bio} = 0.25\ rpm$
- $h_r = 9\ ^{K}/_{min}$
- $t_r = 52\ min$
- $p = 25\ atm$
- $\Delta T_{sali} = 295 - 550\ °C$
- $\Delta T_{bio} = 25 - 500\ °C$
- $\Delta p_{loss} = 0.152\ atm$
- $NTU = 0.5$
- $Q = 59.15\ kW$

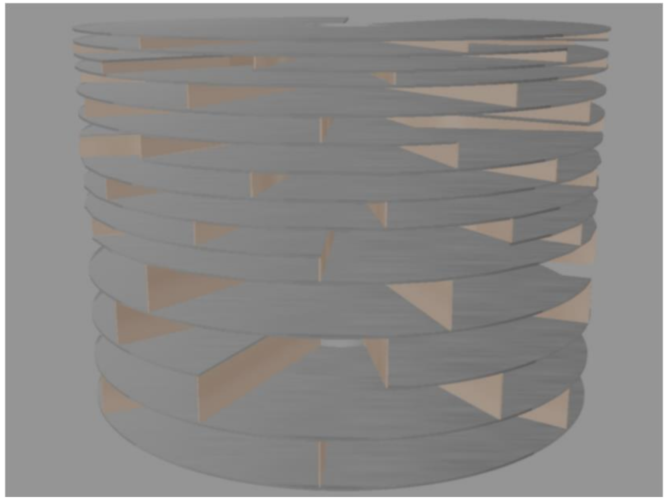

Biomass

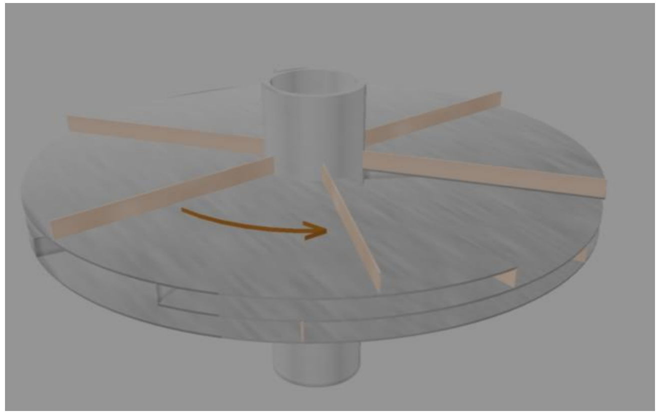

Molten salts

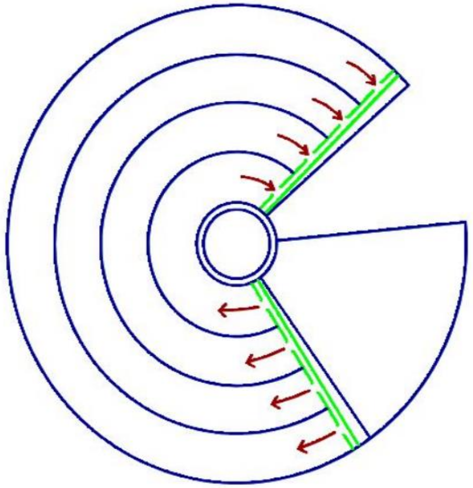

Syngas production considerations

Downdraft (classic) ***ER = 30% → DH = -3828 kJ/kg 1100 °C***

Downdraft using MS

ER = 20%
DH = -2850 kJ/kg

N_2 in ↓33%

LHV ↑20%

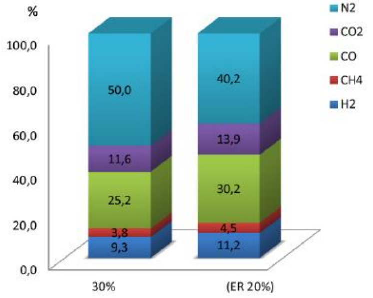

Trisaia (classic at HT) ***ER = 33% T = 1300 °C***

Downdraft using MS

ER = 25%

N_2 in ↓17%

LHV ↑ 10%

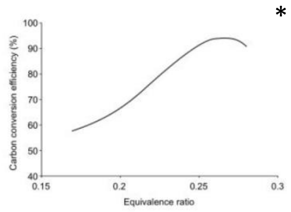

Tar ↓

Tar < → easy cleaning → dry cleaning → water savings

*Basu P. In Biomass Gasification and Pyrolysis, Practical Design and Theory, pages 65 -96. Academic Press, Boston, 2010.

Syngas production considerations

Water content 15% → 22%

$$CO + H_2O \rightarrow CO_2 + H_2$$ Shift reaction

$$C + H_2O \rightarrow CO + H_2$$ H_2O-gas gasification

$$C_6H_{6,2}O_{0,2} + 5,8H_2O \rightarrow 6CO + 8,9H_2$$

Vapour gasification
S/B = 0.5

ER = 25%

N_2 in 17%

% N_2 ↓ 10%

% H_2 ↑ ≈ 30%

LHV ↑ 50%

Tar ↓

CSP design

Hypothesis

Storage time: 16 hours, assuming 8 hours of daily direct irradiation to ensure continuity of the gasifier operation.

Thermal power producible by a gasifier: 800 kW_t. This size can ensure temperature homogeneity and correct blending of air in the process where this is the only gasification agent.

η_g = 0.8

LHV = 17 MJ/kg

Biomass flow = 215 kg/h

Energy required up to 500 °C (drying and almost the whole pyrolysis) = is 974 kJ/kg.

Thermal losses = 3%

Solar power = 60 kW_t

Site: Italy (Priolo Gargallo-SR: 37.1N; 15.1E; DNI: 1936 $kWh/m^2/y$ corresponding to 5.3 $kWh/m^2/d$);

η_{gl} = 0.46 (assessed by the SW SAM®)

$$Q = A \cdot DNI \cdot \eta_{gl}$$

Plant operation: 24h/d - 8000 h/y →1440 kWh/d kWh/y →A: 590,2 m^2 corresponding to just more than one collector for commercial PT.

CSP design

Storage (double tank)

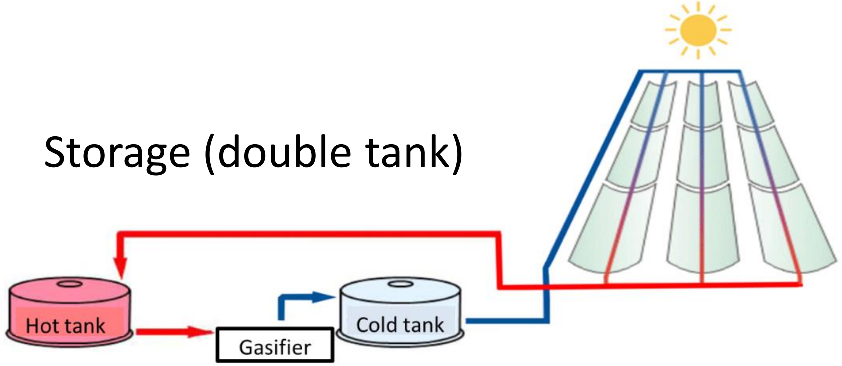

$Qs = Mms \cdot \int cp \cdot dT$
Qs = 60x16 = 960 kWh/d → TES volume: 6 m^3 for each of the 2 tanks

To ensure continuity also during winter →
November characteristic (DNI: 3.06 kWh/m^2/d, η_{gl}: 31%) ⇒ A:1518 m^2

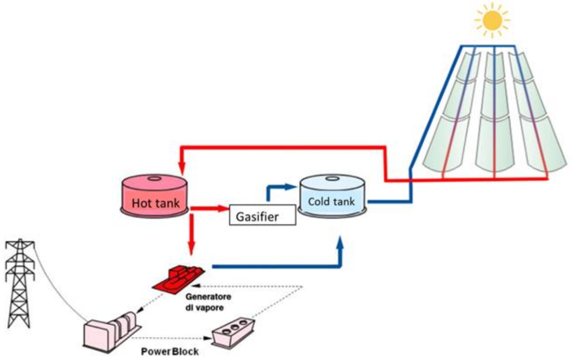

For a 50 MW_e CSP-ST, if 4 downdraft gasifiers producing 800 kW_t were installed in parallel, the necessary mirror surface devoted to the gasifiers would be only about 5.6‰ of the total area (yearly average) and at a maximum of 1.43% (in November) → they can compensate the heat loss with no fossil fuel usage.

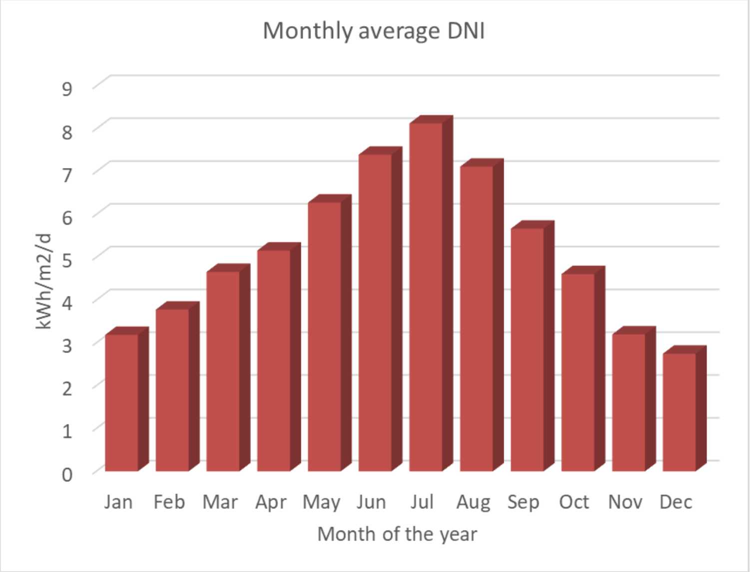

Conclusions

Coupling is technically feasible and beneficial for both technologies.

Thermal storage with a produced gas containing 11 times the energy provided by solar plants through MS.

Gases of high quality in terms of LHV and Tar Content

Using gas by renewable source with consequent elimination of fossil fraction and increase of Capacity Factor of CSP plant.

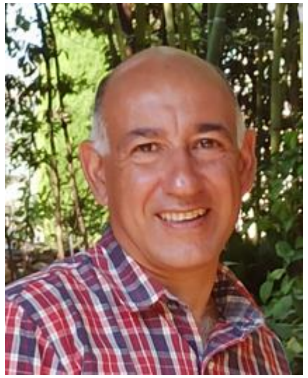

Raffaele LIBERATORE
ENEA
TERIN-STSN-SCIS
raffaele.liberatore@enea.it

THANK YOU FOR YOUR ATTENTION!
ANY QUESTIONS?

References

This work was published in these articles:

Gallucci F, Liberatore R, Sapegno L, Volponi E, Venturini P, Rispoli F, Paris E, Carnevale M , Colantoni A
Influence of Oxidant Agent on Syngas Composition: Gasification of Hazelnut Shells through an Updraft Reactor. [2019]
https://doi.org/10.3390/en13010102
Energies 2019, 13(1), 102

Liberatore R, Crescenzi T, Sapegno L, Volponi E, Venturini P, Rispoli F, Paris E, Carnevale M, Gallucci F.
Analysis on the coupling of biomass gasification process with a parabolic trough concentrating solar plant. [2019]
European Biomass Conference and Exhibition Proceedings 2019 (May 27-30 Lisbon) pp. 1804-1808.

Gallucci F, Liberatore R, Sapegno L, Volponi E, Venturini P, Paris E, Carnevale M, Rispoli F.
Biomass gasification: the effect of equivalence ratio on syngas quality in the case of externally heated reactor. [2019]
European Biomass Conference and Exhibition Proceedings 2019 (May 27-30 Lisbon) pp. 913-917.

SFERA-III

Solar Facilities for the European Research Area

Solar Facilities for the European Research Area

4th Training for Industries
7-11 November 2022, Cr ENEA Casaccia Rome (Italy)

Molten Salt CSP plants and photovoltaic plants: examples of technological hybridization

Valeria RUSSO (ENEA, TERIN-STSN-ITES)

JOINT RESEARCH ACTIVITIES

THIS PROJECT HAS RECEIVED FUNDING FROM THE EUROPEAN UNION’S HORIZON 2020 RESEARCH AND INNOVATION PROGRAMME UNDER GRANT AGREEMENT NO **823802**

Global Energy Market

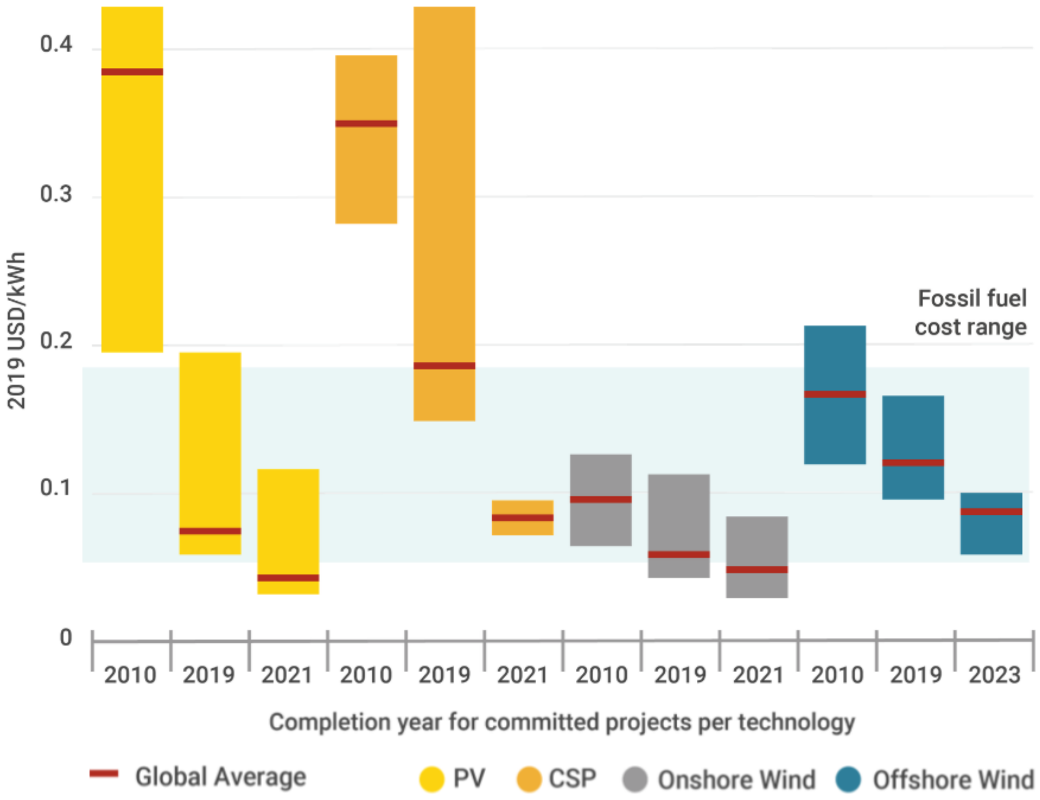

[IRENA – International Renewable Energy Agency]

Research focus:

- Increase in efficiency
- Cost reduction
- Energy dispatching
  - Energy storage system
  - Technologies integration

SOLAR TECHNOLOGIES:

- **PV**: 8 c€/kWh; 578 GW
- **CSP**: 12-30 c€/kWh; 6 GW

CSP-PV Comparison

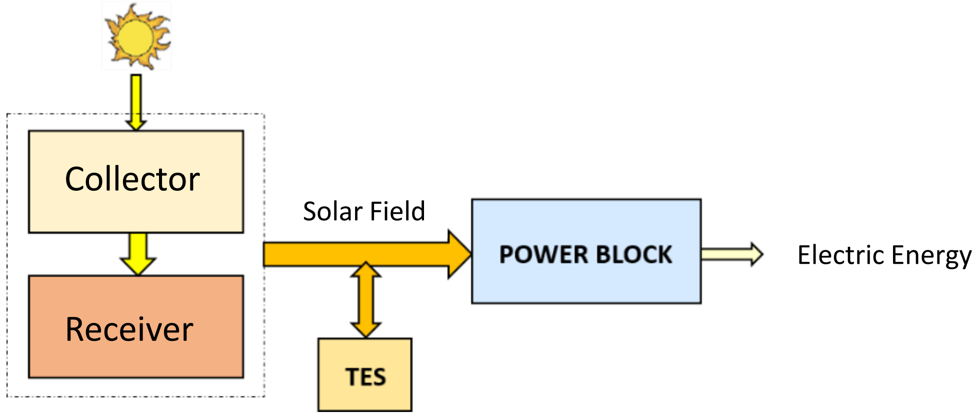

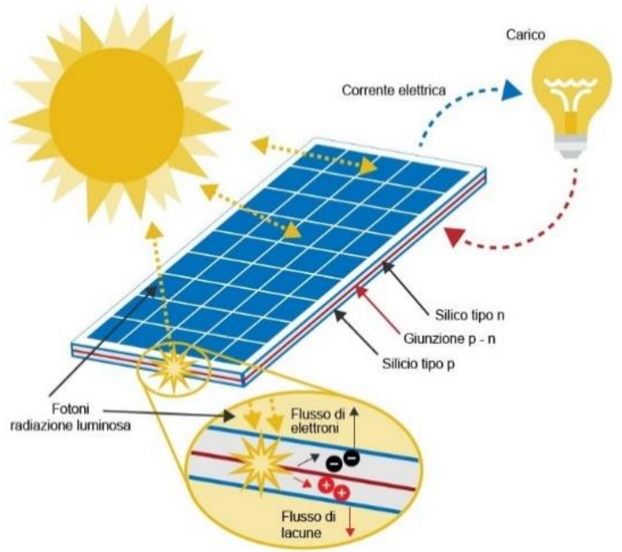

- ✓ High Thermal Storage Capacity
- ✓ Greater Capacity Factor
- ✓ Constant performance over time
- Higher costs
- Only direct radiation is used

- ✓ Lower costs
- ✓ Simplicity of operation
- ✓ Less seasonal effect
- Limited Storage Capacity
- Minor Capacity Factor
- Greater performance degradation

PV-CSP Hybridization Objective

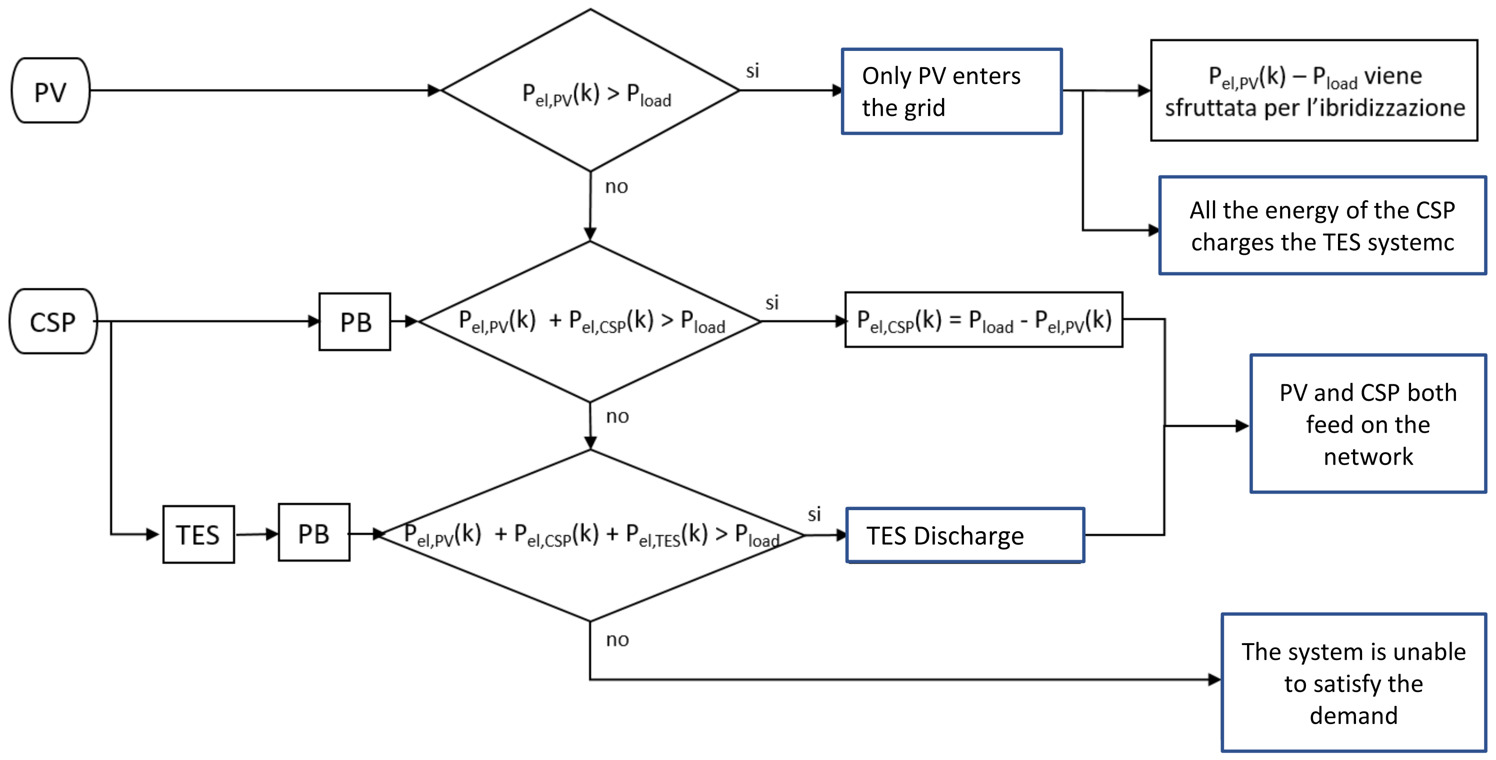

- Maximize the fraction of solar energy used
- Satisfy energy demand as much as possible by stabilizing the electricity grid
- Reduce the production costs (CSP size reduction)

Hybridization logic:

PV and CSP section connected **upstream** of electricity production.

Hybrid configurations studied

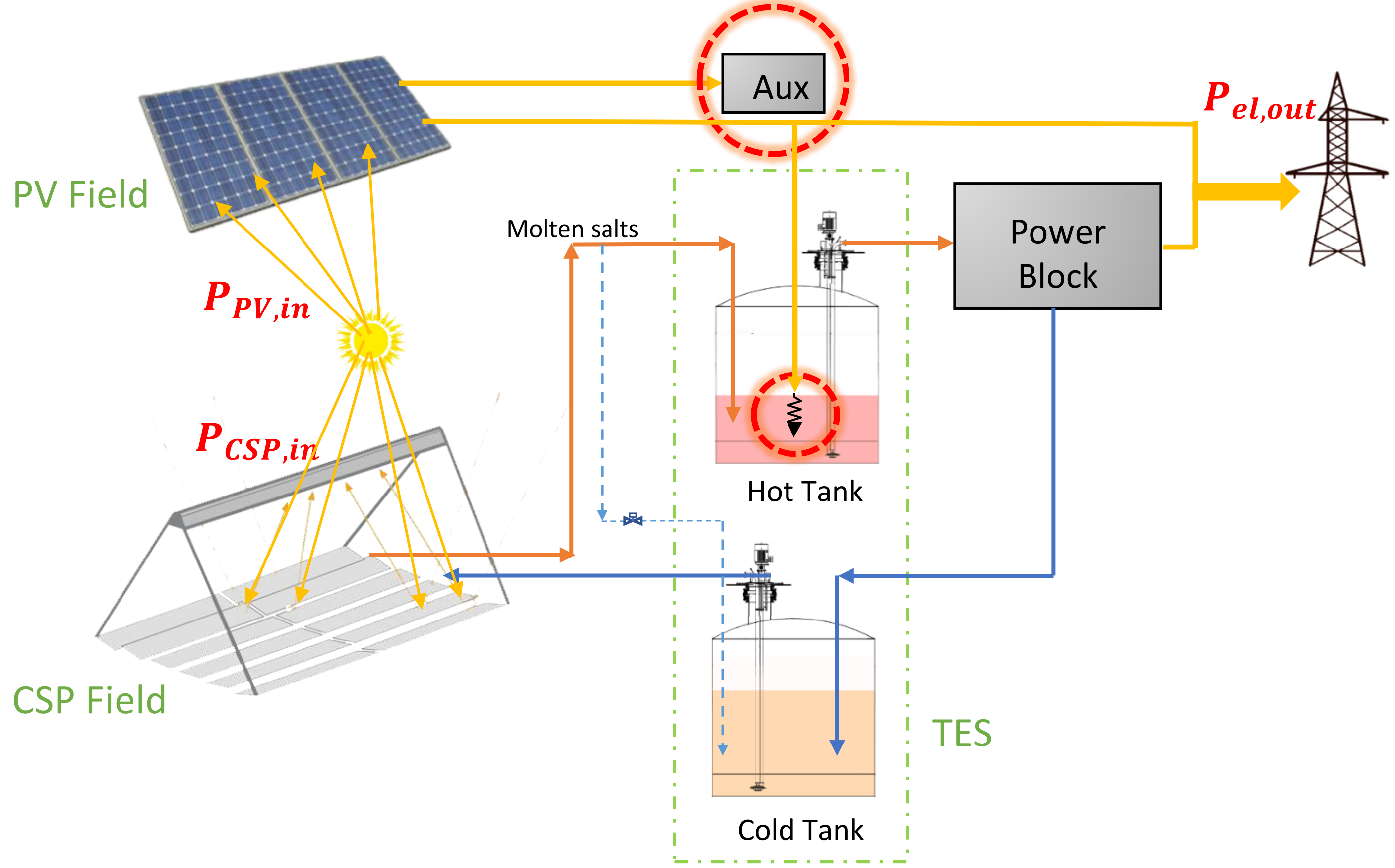

Sizing hypothesis: CSP

Sizing hypothesis: CSP

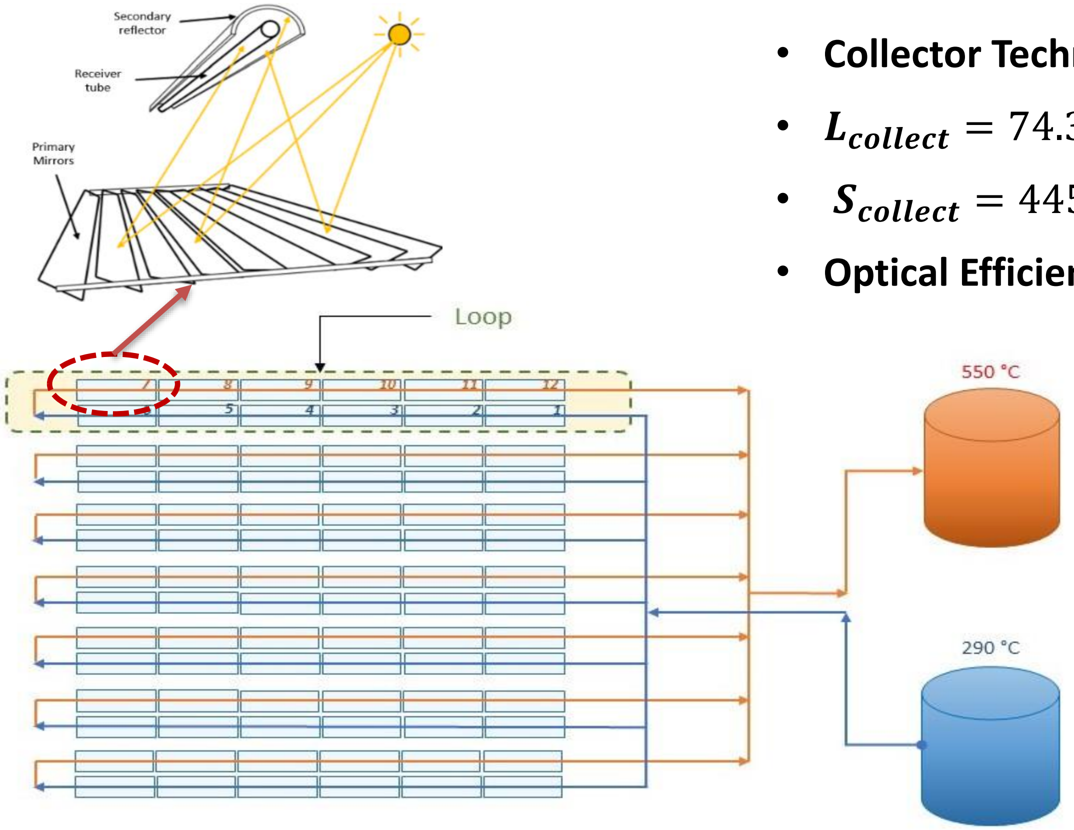

- **Nominal Power**: $5\ MWe$
- **Collector Technology**: Linear Fresnell Collector
- $\boldsymbol{L_{collect}} = 74.34\ m;$
- $\boldsymbol{S_{collect}} = 445.5\ m^2$
- **Optical Efficiency**: $\eta_{ott} = 66\%$

- **HTF**: binary mixture of molten salt (40% KNO3 - 60% NaNO3)
- $\boldsymbol{T_{max}} = 545\ °C;\ \ \boldsymbol{T_{min}} = 290\ °C$
- **Loop Number**: 7
- **Collectors per loop**: 12
- **Direction:**N-S
- $\boldsymbol{L_{loop}} = 892\ m$
- $\boldsymbol{\dot{m}_{loop}} = 2 \div 13.7\ kg/s$
- $\boldsymbol{S_{CSP}} = 37422\ m^2$

Sizing hypothesis: TES

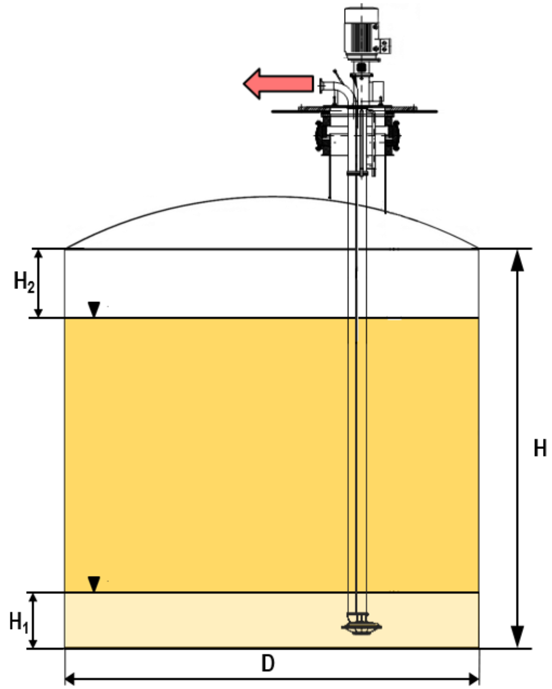

Direct storage system with two tanks and molten salt as heat storage medium:

- **Heat storage medium**≡ HTF
- $\boldsymbol{h_{TES}} = 15\ h$
- $\boldsymbol{C_{TES}} = 187500\ KWh_{th}$
- $\begin{cases} \boldsymbol{D} = 10.80\ m \\ \boldsymbol{H} = 11.65\ m \end{cases}$
- $H_1 = 0.75\ m$
- $\boldsymbol{M_{TES,max}} = \dfrac{C_{TES} \cdot 3600}{\Delta h} = 1747\ t$

Sizing hypothesis: PV

- **Nominal Power**: $8\ MWe$
- **Technology**: Monocrystalline silicon cell, n-type (LG–NEON2)
- **Module dimensions**(L x P x H) = 1686 x 1016 x 40 $[mm]$
- **Peak Power**: $W_p = 350\ W$
- **Nominal efficiency**: $\eta_{module} = 20.4\%$

- $\boldsymbol{S_{PV}} = 39330\ m^2$
- **Module number**: 22960
- **Modules per looop**: 20
- **Loop number**: 1148 (82 group of 14 100kW multi-strings inverters)
- **Direction:** Sud
- **Tilt** = 30°

Curve caratteristiche

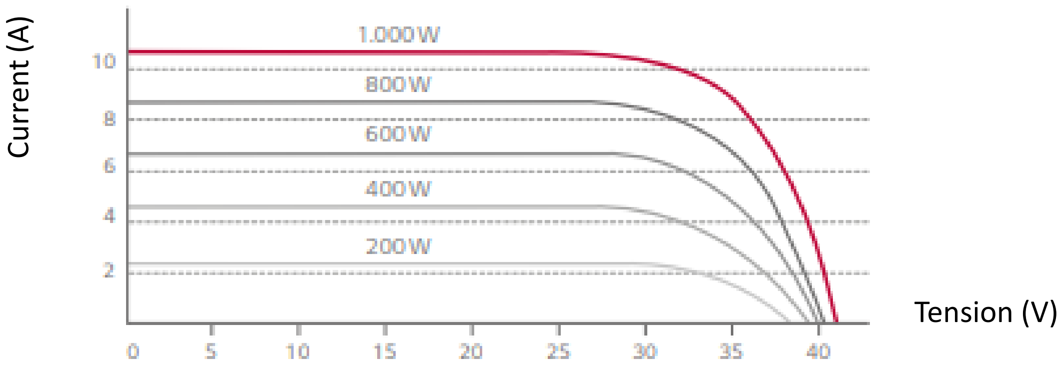

Solar radiation for PV modules

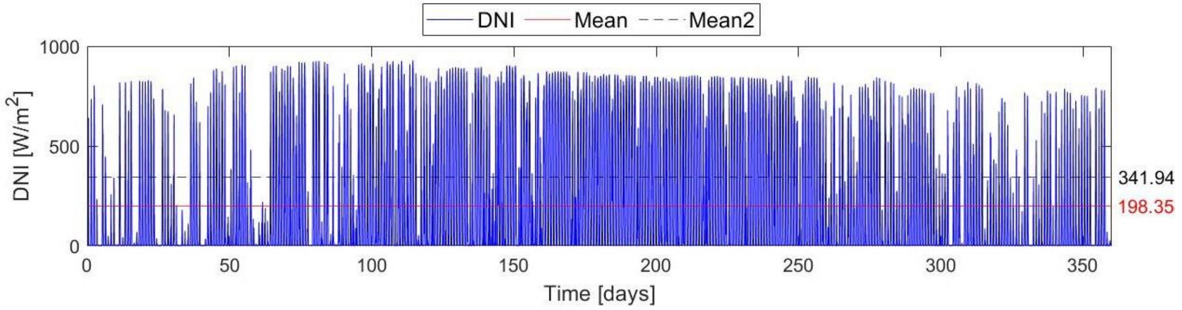

$$\begin{cases} DNI \cdot \cos\vartheta_z \cdot \cos\vartheta = Radiazione\ diretta\ sulla\ superficie\ del\ modulo\ fotovoltaico \\ DHI \cdot \left(\dfrac{1+\cos\beta}{2}\right) = Radiazione\ diffusa\ sulla\ superficie\ del\ modulo\ fotovoltaico \\ GHI \cdot Albedo \cdot \left(\dfrac{1-\cos\beta}{2}\right) = Riflessione\ sulla\ superficie\ del\ modulo\ fotovoltaico \end{cases}$$

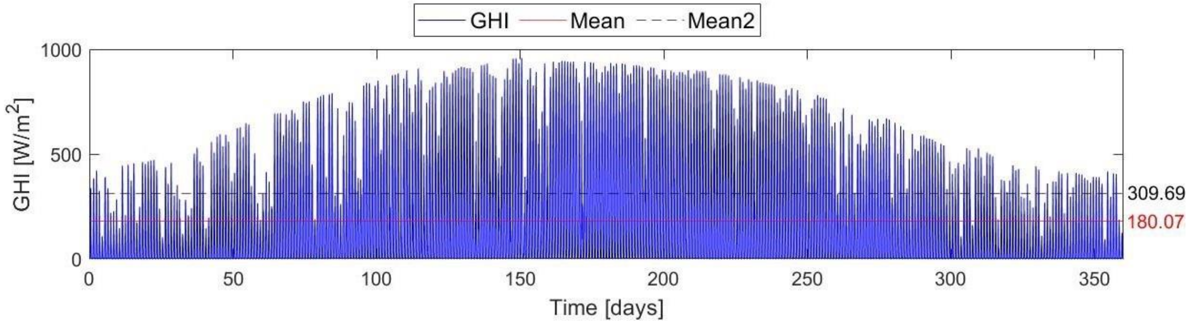

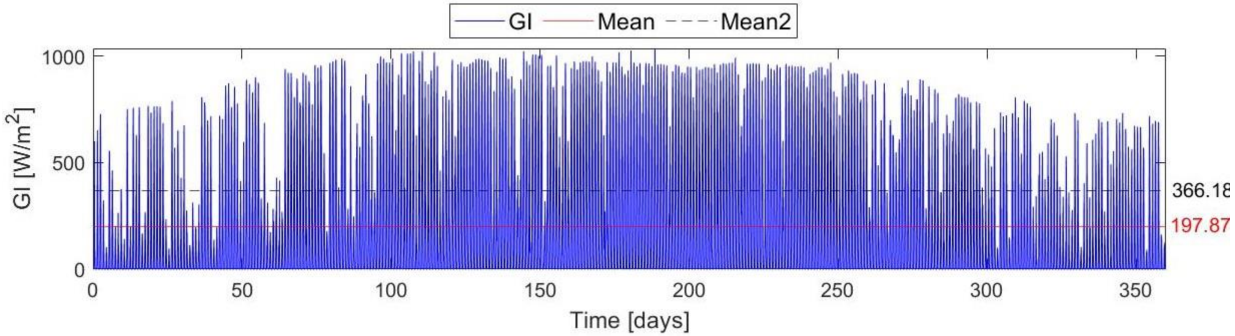

Solar radiation for CSP collector

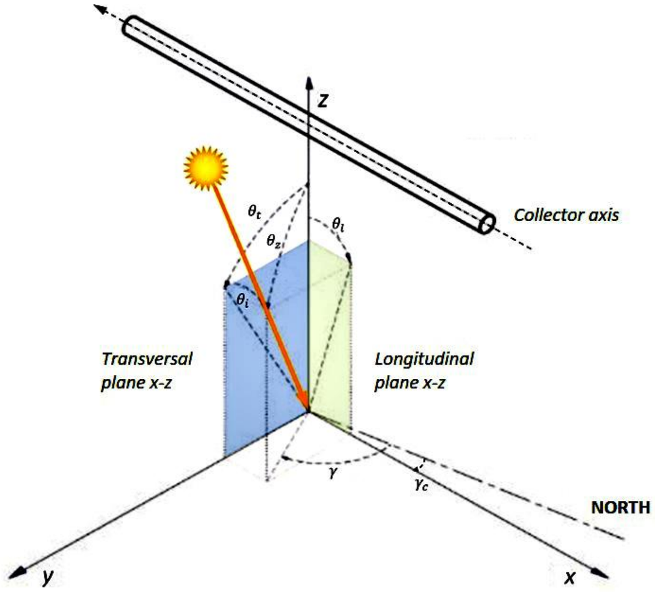

$$\vartheta_t = arctan(\sin(\gamma - \gamma_c) \cdot \tan(\vartheta_z))$$
$$\vartheta_l = arcsin(\cos(\gamma - \gamma_c) \cdot \sin(\vartheta_z))$$

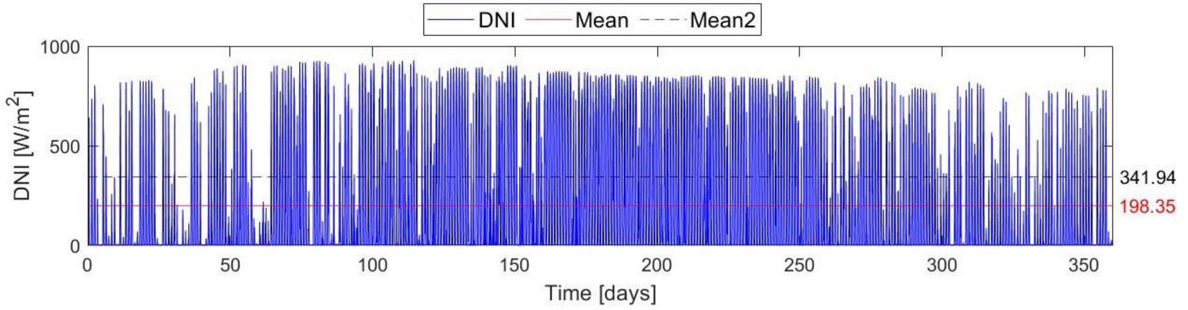

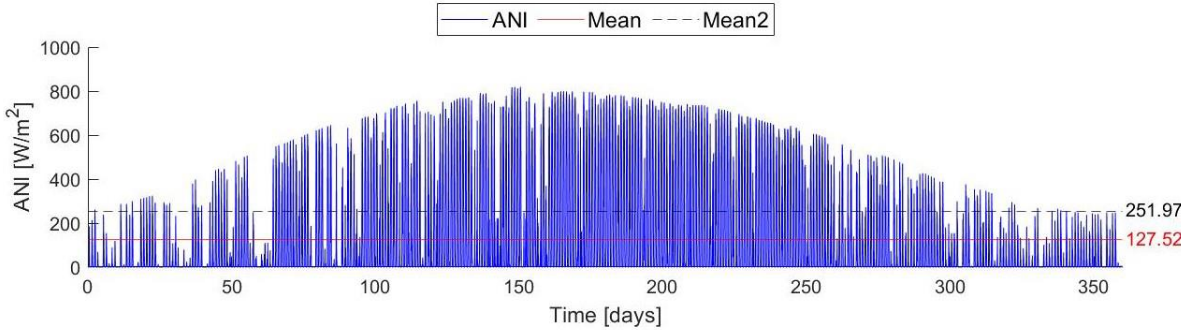

$ANI = DNI * IAM_l(\vartheta_l)\ IAM_t(\vartheta_t)$

Hypothesis of the Matlab Model

- **Quasi- steady state simulation** (neglected dynamics,no thermal inertia and transients);
- **Time step**: $\Delta t_{year} = 300\ s, \Delta t_{day} = 5\ s$;
- **Energy and mass balances** of the various components for each Δt;
- **Ideal heat exchange** in SG and perfectly adiabatic tanks
- **Initial Condition** for all the simulation:
  Hot tank empty and cold tank full both at $290°C$;
- **Radiation** Enea – «Casaccia» (TMY):
  $DNI_y = 1738\ kWh/m^2; DNI_{max} = 928\ W/m^2$

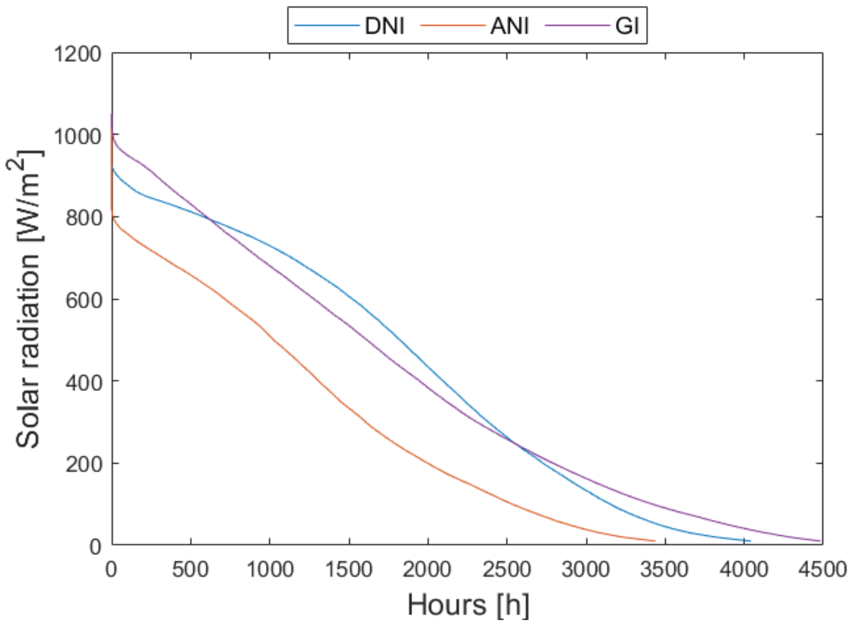

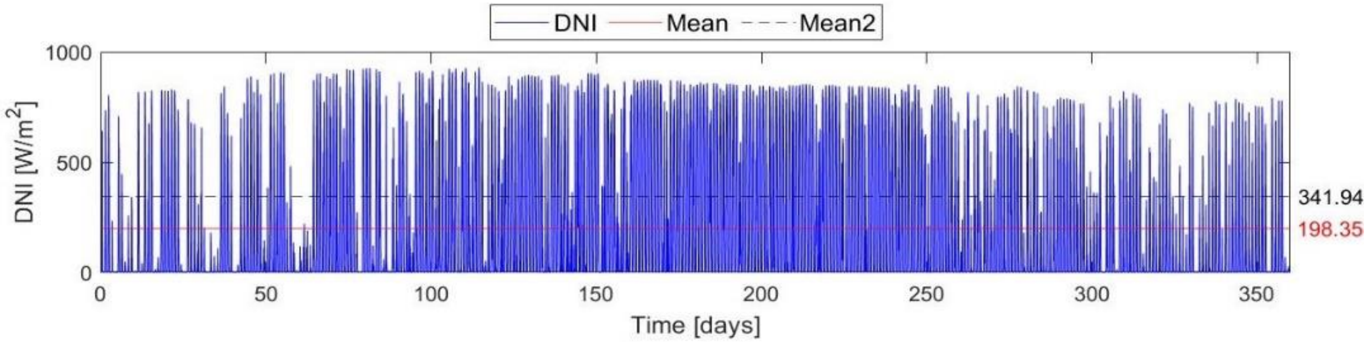

Components models: operational maps for CSP

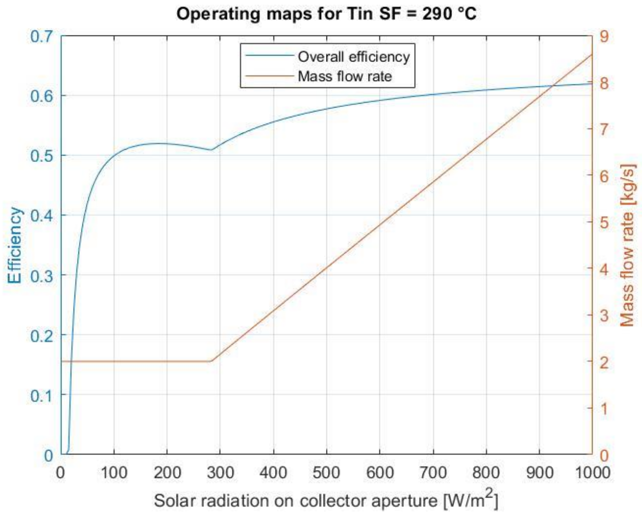

- $\boldsymbol{ANI} = DNI \cdot IAM_l(\theta_l) \cdot IAM_t(\theta_t)$
  Aperture Normal Irradiance

$$P_{SF} = ANI \cdot S_{CSP} \cdot \eta_{SF}$$

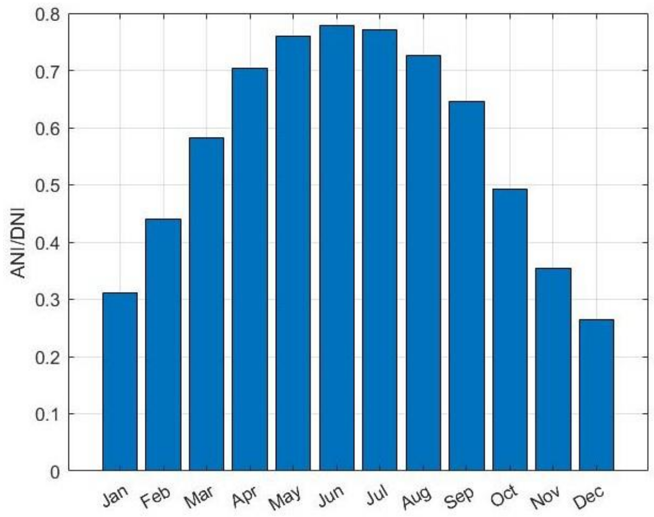

- **Operational maps**

$$\begin{cases} \dot{m}_{SF}(T_{in,SF}, ANI) \\ \eta_{SF}(T_{in,SF}, ANI) \end{cases}$$

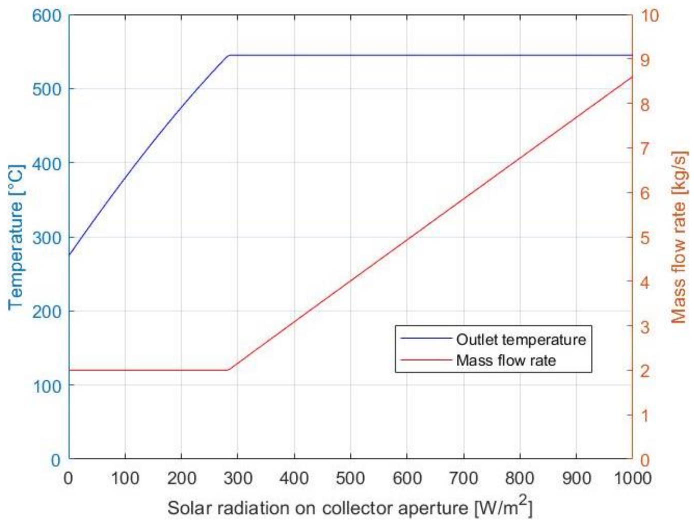

- **Power block model:**

$$x(k) = \frac{P_{th,PB}}{P_{max}}$$

$$\eta_{PB}(k) = \eta_0 \cdot f(x(k)); f\text{: } polinomiale$$

$$\dot{m}_{PB}(k) = \frac{P_{th,PB}(k)}{h_{in,PB}(k) - h_{out,PB}(k)}$$

Components models: operational maps for PV

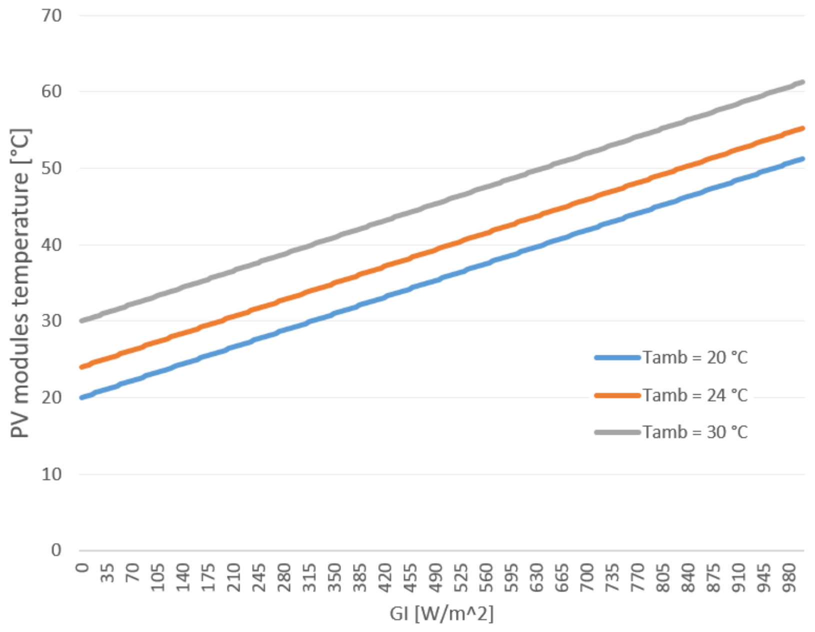

- $$T_{modulo}(k) = T_{amb}(k) + (NOCT - 20) \cdot \frac{GI(k)}{800}$$
  $NOCT = 45\,°C$ (T nominale celle)
- $$P_{GI}(k) = GI(k) \cdot S_{PV}/1000 \ \ [\text{kW}]$$

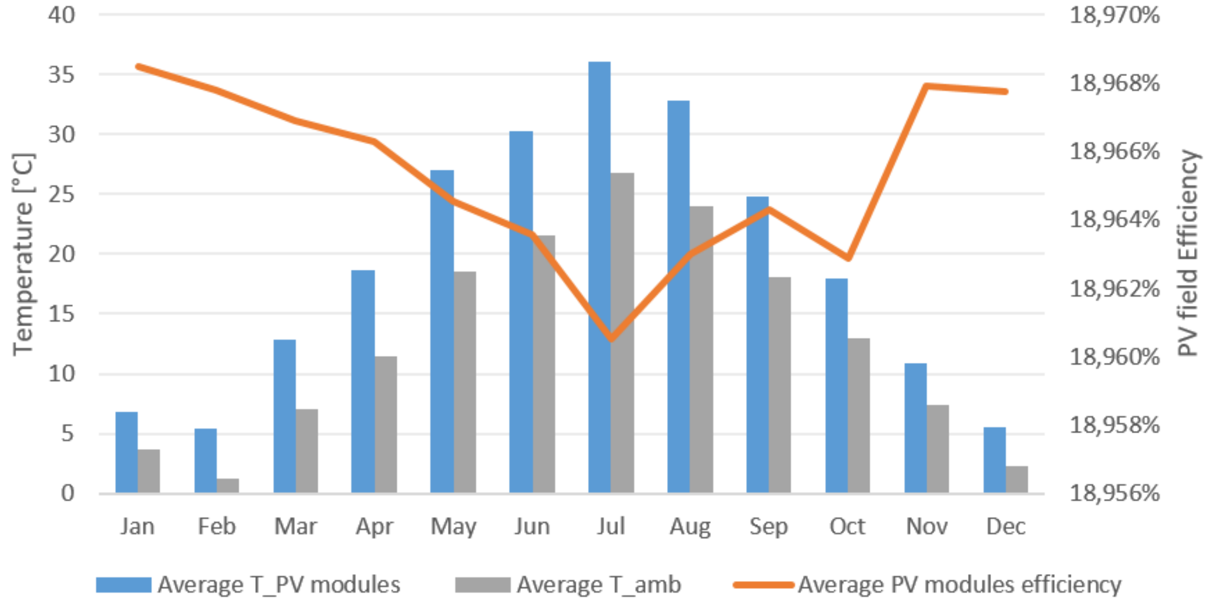

- $$\eta_{PV} = \frac{P_{el,PV,tot}(k)}{P_{GI}(k)} = \eta_{moduli} \cdot \eta_{BOS}$$

System operation logic : controls

- ✓ T_{switch}
- ✓ T_{ht}
- ✓ $SOC_H(k) = \frac{H_{utile}(k)}{H_{max}}$
- ✓ $M_{utile} \rightarrow m_{PB}$

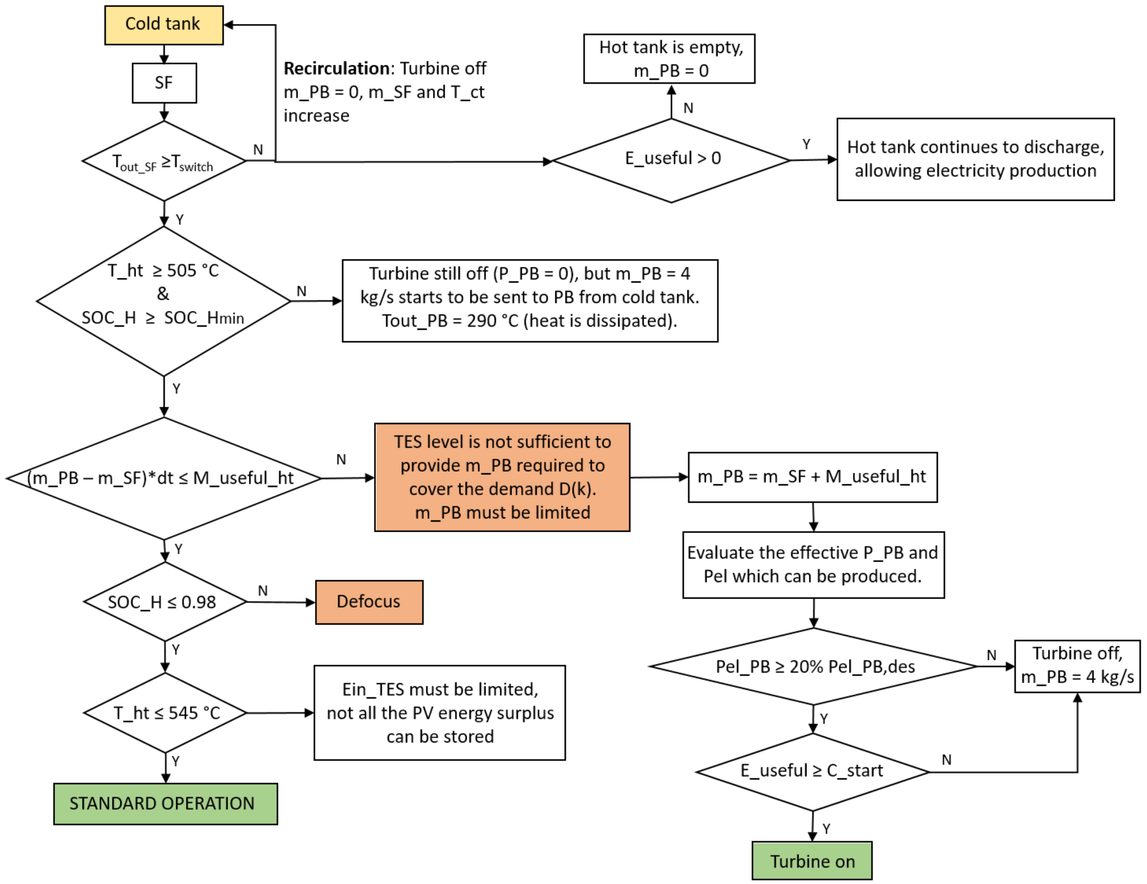

Annual simulation results

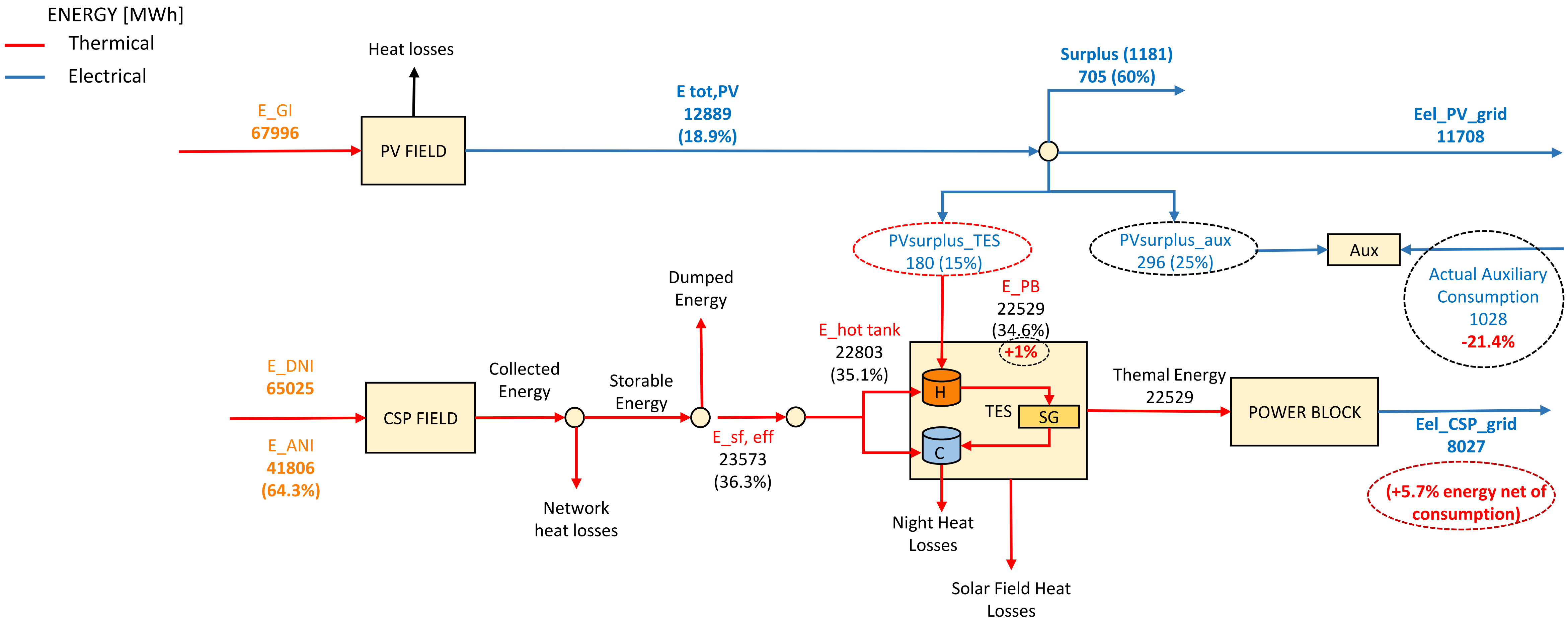

Electric Power Produced

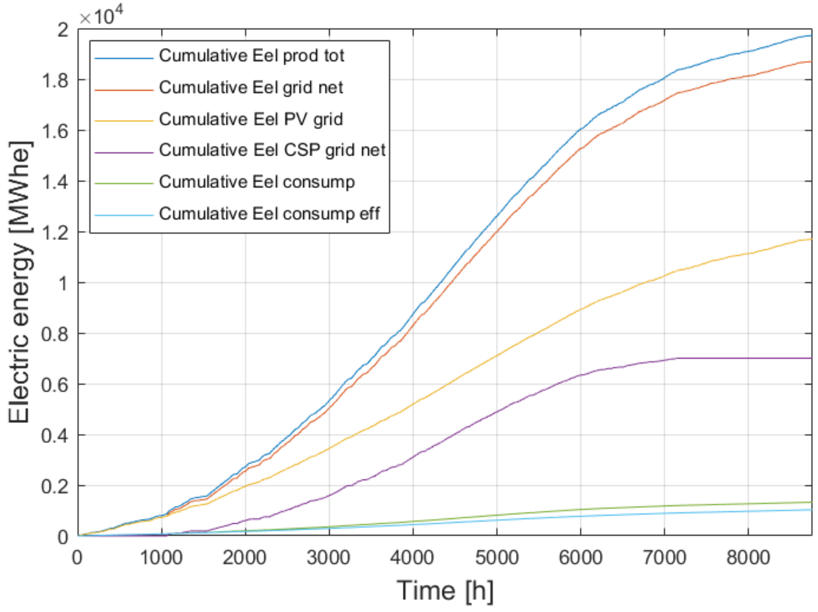

Breakdown of the cumulative electricity produced

$$P_{tot} = 5\ MWe$$

for 34% of the annual hours

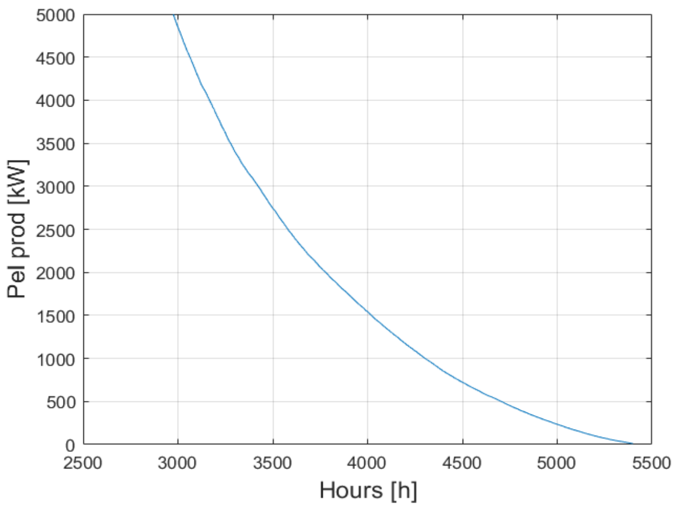

Monthly Distribution

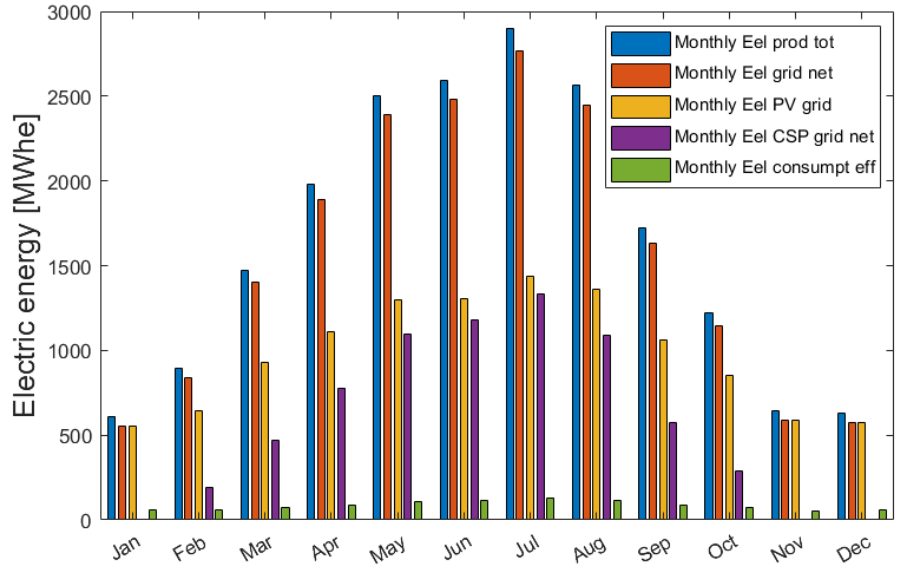

Comparison of average monthly results

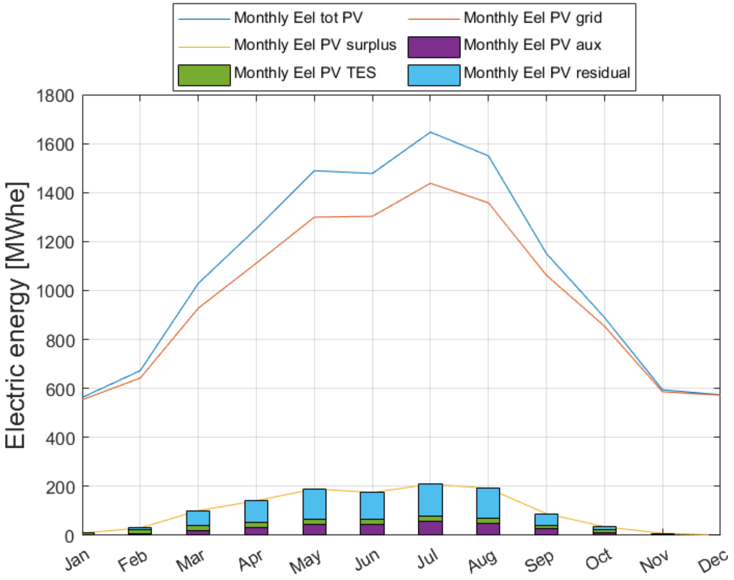

Monthly breakdown of the PV energy surplus

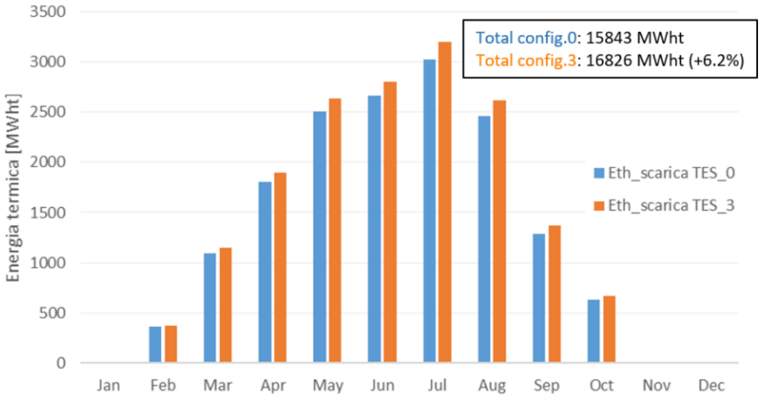

$$CF = \frac{E_{el,grid}}{E_{el,teorica}} = 0.43$$

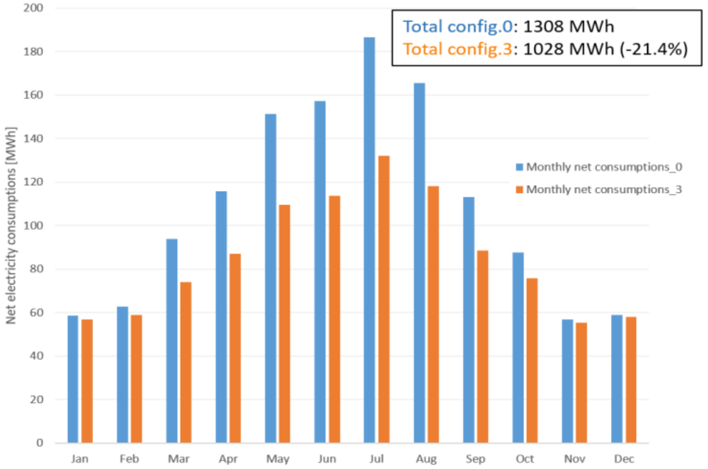

Daily simulation

1th of July

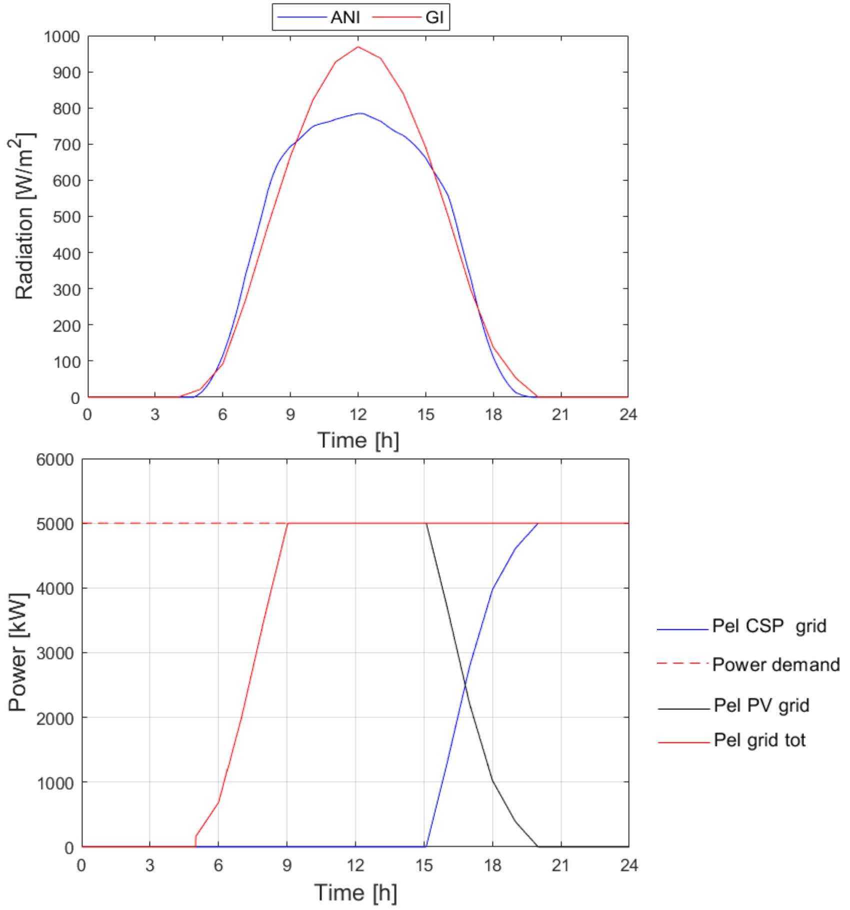

21th of March

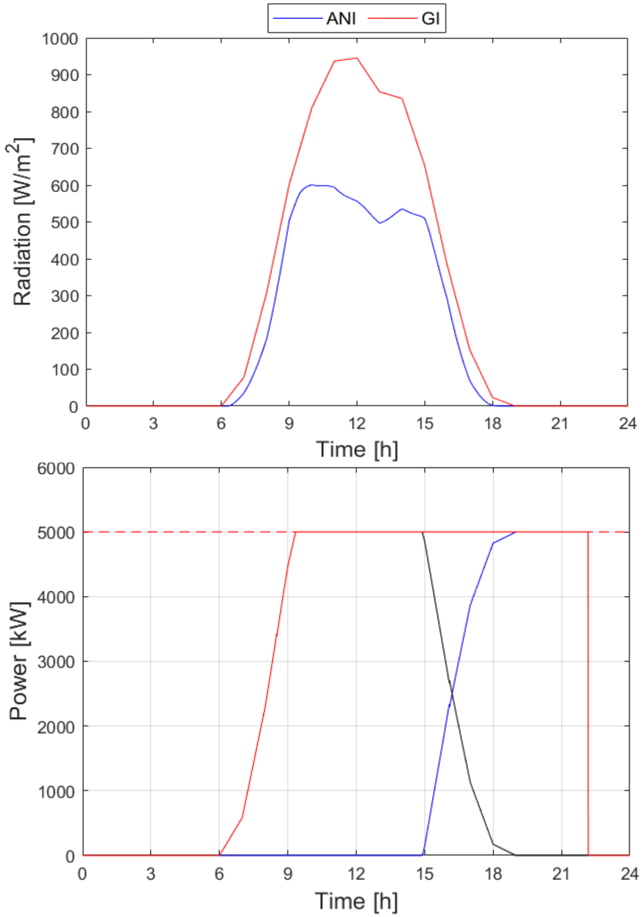

	July 1st	March 21th	
E_{DNI}	343.36	273.29	MWh_e
E_{ANI}	268.07	162.68	MWh_e
E_{GI}	301.95	258.00	MWh_e

Power output of the final hybrid configuration

	July 1st	March 21th	
$E_{el,\,grid\,net}$	83.97	70.86	MWh_e
$E_{el,\,PV\,grid}$	48.68	41.57	MWh_e
$E_{el,\,CSP\,grid\,net}$	35.10	29.29	MWh_e
$E_{el,\,PV\,aux}$	1.63	0.97	MWh_e
$E_{el,\,PV\,TES}$	6.87	6.38	MWh_e
$E_{el,\,PV\,residual}$	0	0	MWh_e
CF	70%	59%	

Daily simulation: hybrid configuration

1th of July

21th of March

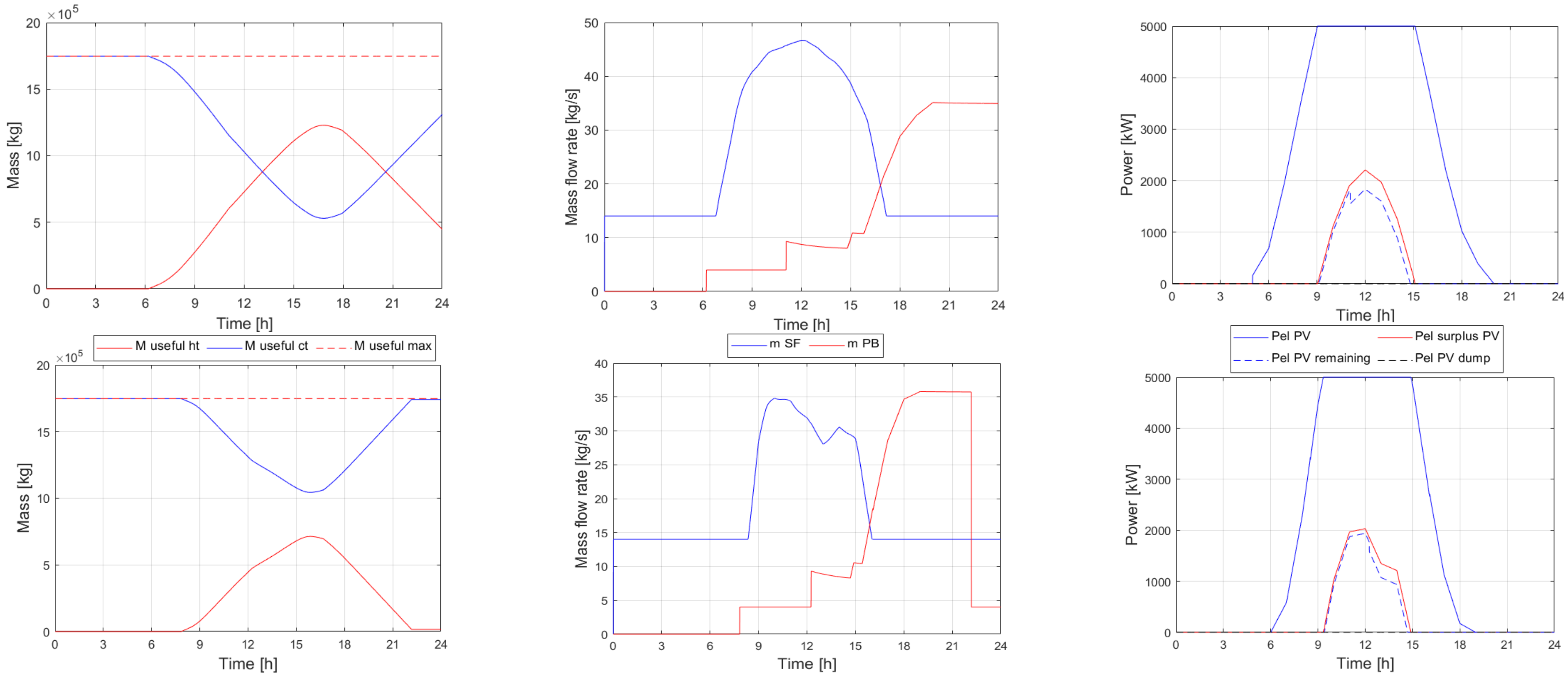

Daily simulation: comparison results for July

Base configuration

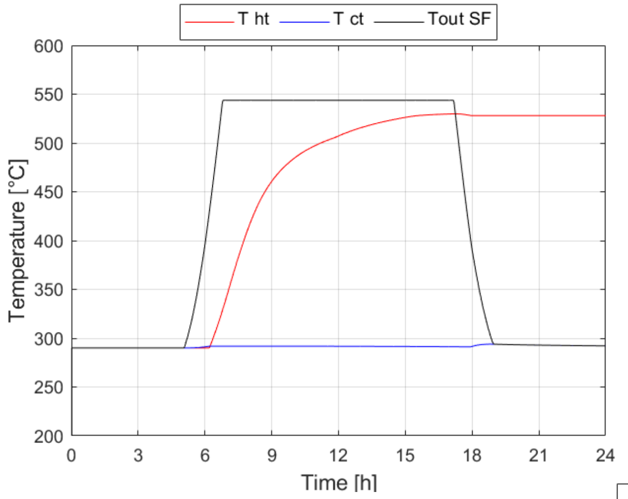

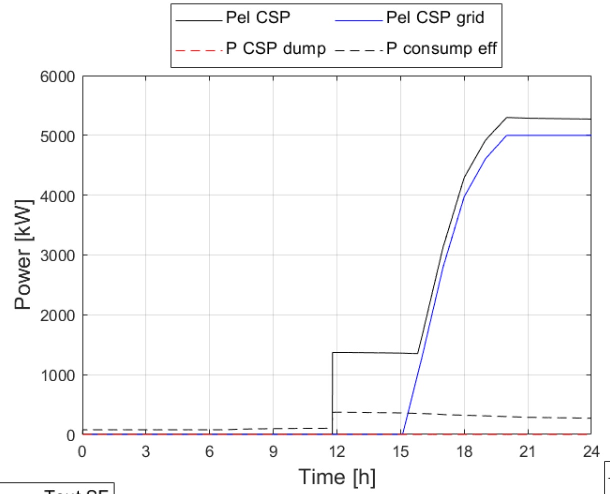

CSP Electric Power and Consumption

Temperature

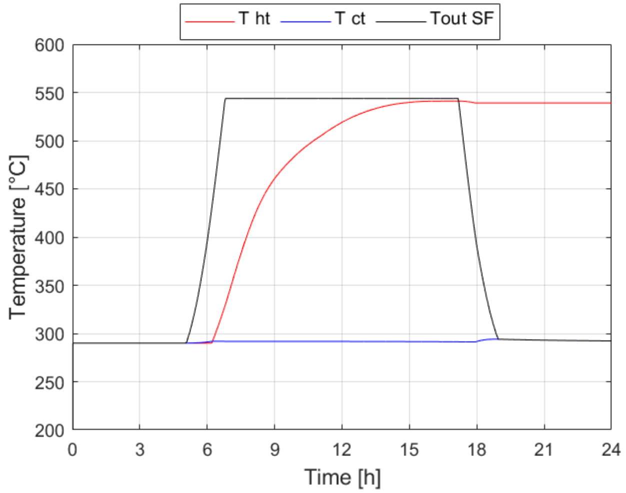

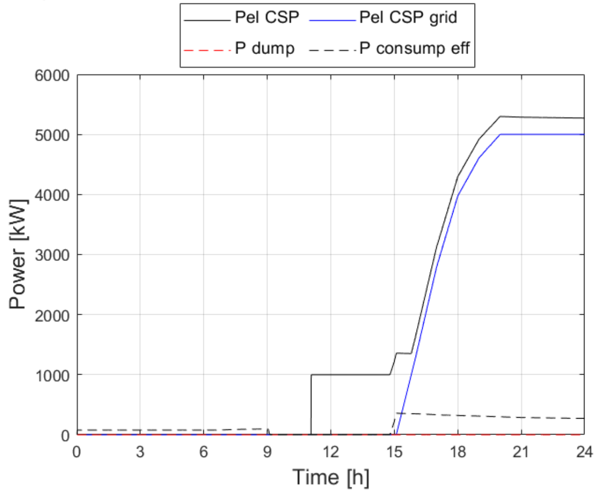

Final hybrid configuration

Preliminary economic analysis

- **Initial Investment**: IC = 29.4 M€
  - CSP: 19.96 M€ (3993 €/kWh)
  - PV: 9.44 M€ (1180 €/kWh)
- **O&M** = 1.5% IC
- **Useful life**: 25 anni

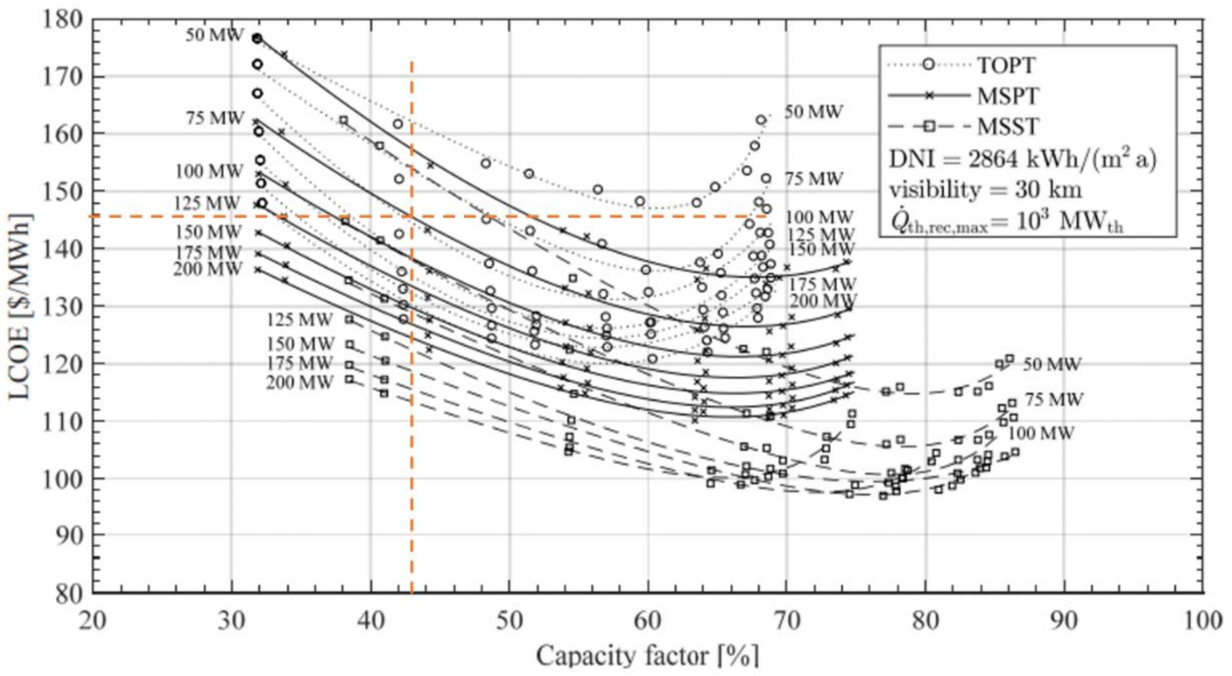

LCOE: 13.51 c€/kWh (-2%)

PBP: 10-11 years

Conclusions and future developments

Main Objectives Achieved

- Better exploitation of solar energy
    - +5.7% energy sent to the grid by the CSP net of consumption
    - + 6.2% energy supplied by TES
    - + 1-2% CF, considering only solar source
- CSP field size reduction
- LCOE reduction and greater market competitiveness

Future Objectives

- Optimization of integration between the two solar fields (exploitation of the PV surplus)
- Verification of the benefits for larger plants and in higher radiation conditions
- Optimization of integration with non-solar source

Valeria RUSSO, PhD
ENEA
TERIN-STSN-ITES
valeria.russo@enea.it

THANK YOU FOR YOUR ATTENTION!
ANY QUESTIONS?

SFERA-III

Solar Facilities for the European Research Area

Solar Facilities for the European Research Area

4th Training for Industries

7-11th November 2022, Cr ENEA Casaccia Rome (Italy)

Coating for molten salt receiver tube

Gabriella Rossi and Salvatore Esposito - (ENEA, TERIN-STSN-SCIS)

JOINT RESEARCH ACTIVITIES

THIS PROJECT HAS RECEIVED FUNDING FROM THE EUROPEAN UNION'S HORIZON 2020 RESEARCH AND INNOVATION PROGRAMME UNDER GRANT AGREEMENT NO **823802**

SCIS laboratory of the ENEA Research Centre of Portici

Research team of Portici

- works in the context of ENEA laboratory for the development of solar components and plants (SCIS)
- started at the beginning of 2000 with the **mission** to develop **absorber coatings for solar applications**
- gained **skills** in the field of:
  - deposition process technologies for fabrication of innovative materials
  - optical, morphological and structural characterization of materials
  - optical design of solar coating
  - concept design of deposition plants for thin film fabrication

RESEARCH TEAM OF PORTICI

Salvatore Esposito
(Team leader – Electronic Engineer)

Antonio Guglielmo
(Senior Researcher – Mechanical Engineer)

Antonio D'Angelo
(Researcher – Industrial Chemist)

Claudia Diletto
(Researcher – Industrial Chemist)

Gabriella Rossi
(Researcher – Chemical Engineer)

OUR EXPERTISE

Development of materials and process technologies for solar applications

- ✓ **Thin film fabrication:**
  - ✓ metal, ceramic, ceramic-metal nanocomposite (CERMET) deposited by sputtering vacuum technology
  - ✓ ceramic deposited by sol-gel method
- ✓ **Surface plasma treatment:** physical or chemical plasma etching
- ✓ **Durability test:** Accelerated ageing tests by high temperature cycles performed in tubular ovens operating in vacuum or in air
- ✓ **Salt mist corrosion test, humidity freeze test, damp heat test, condensation test**: impact of environmental factors on stability of solar coating stored or operating in air

MRC-643 sputtering plant

OUR EXPERTISE

Techniques for optical characterization of materials

- ✓ UV-Vis-NIR Spectrophotometry
- ✓ FTIR Spectroscopy
- ✓ Ellipsometry

Vase Ellipsometer

Techniques for morphological and structural characterization of materials

- ✓ Scanning Electron Microscopy (SEM) coupled with Energy Dispersive X-Ray Analysis (EDX)
- ✓ X-ray Fluorescence Spectroscopy (XRF)
- ✓ Raman Spectroscopy
- ✓ FTIR Spectroscopy
- ✓ Atomic Force Microscopy (AFM)
- ✓ X-ray Diffraction (XRD)
- ✓ Differential Scanning Calorimetry and ThermoGravimetric Analysis (DSC-TGA)
- ✓ Profilometry
- ✓ Adhesion Test

OUR EXPERTISE

Optical design of solar coating

- ✓ Simulation software developed in ENEA (MATLAB environment)
- ✓ Commercial simulation software (Macleod)

Concept design of deposition plants for thin film fabrication

ENEA-1 pilot sputtering plant

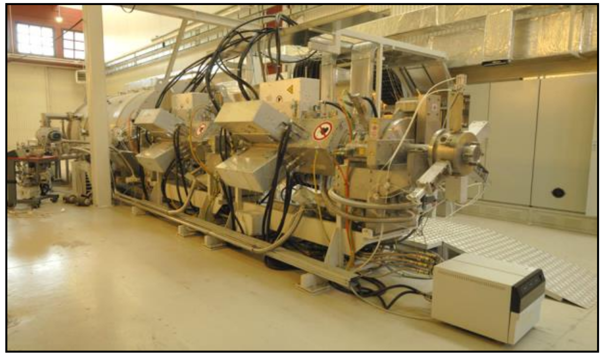

ENEA-2 R&D sputtering plant

Concentrated Solar Power (CSP) Technologies

Direct Solar Radiation ▶ Concentration (reflector) ▶ Collection (receiver) ▶ Thermodynamic cycle (from thermal to electrical energy)

Point Focusing Systems

Central Tower Systems

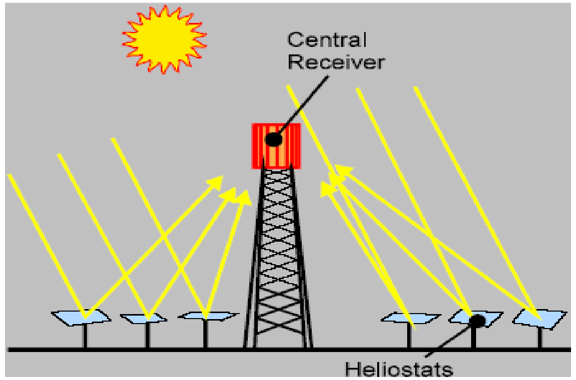

Dish-Stirling Systems

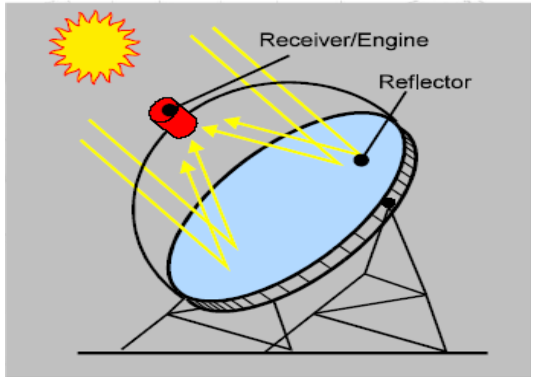

Linear Focusing Systems

Parabolic Through

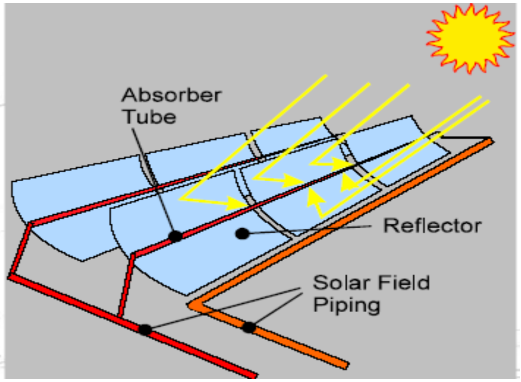

Linear Fresnel

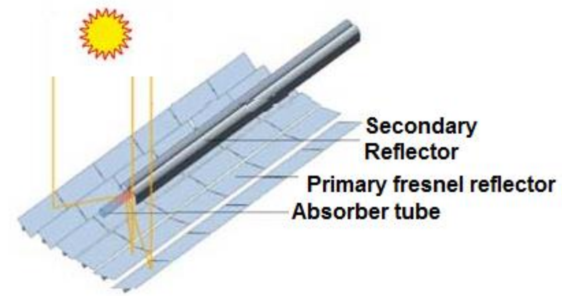

KEY COMPONENT: SOLAR RECEIVER

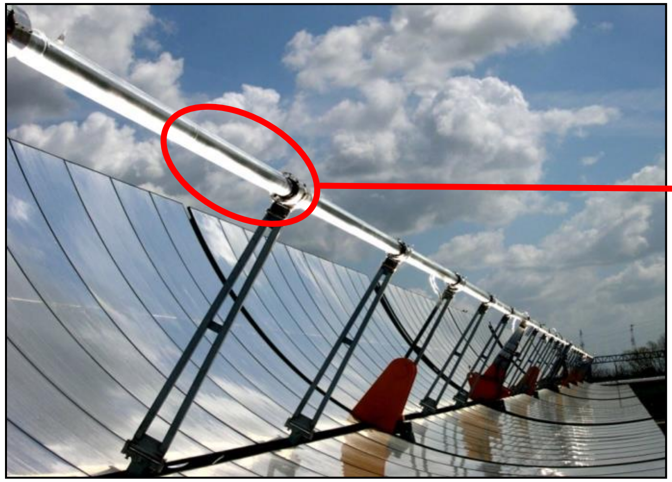

- The receiver tube is the Heat Collector Element (HCE) placed along the focal line of parabolic mirrors
- It is one of the solar field components with the highest technological content
- Concentrated Solar Plant (CSP) yield strongly depends on the receiver performance

KEY COMPONENT: SOLAR RECEIVER

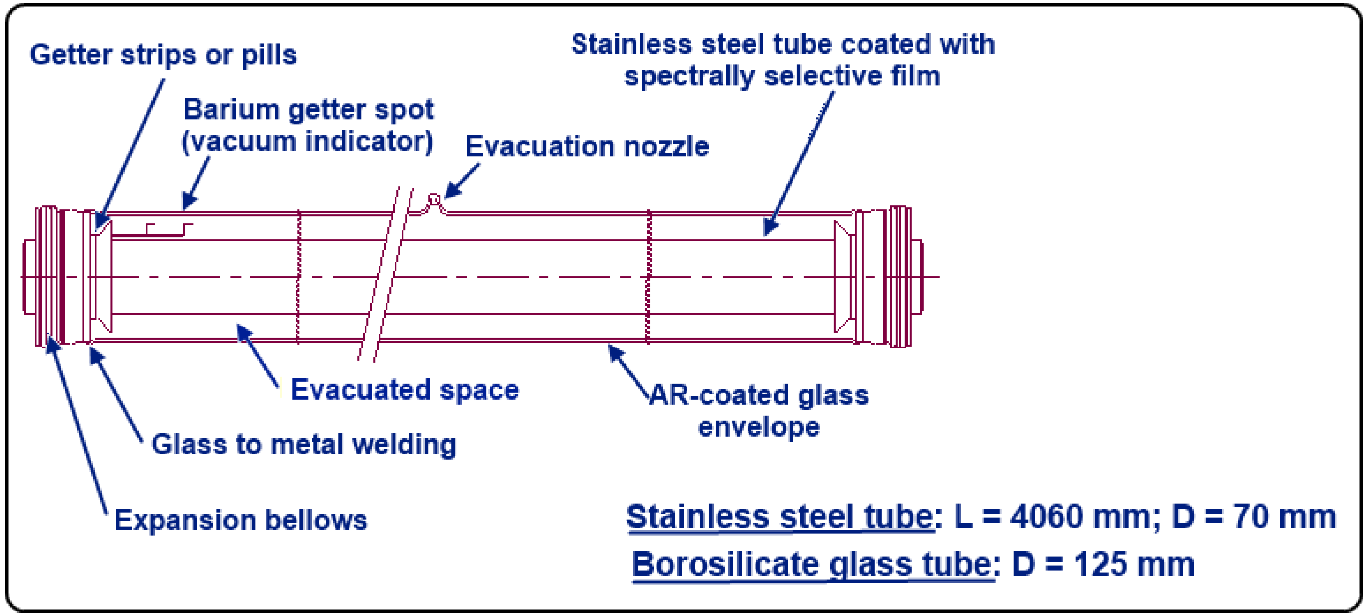

- An innovative solar selective coating on stainless steel tube (4 m long, 70 mm diameter)
- Anti-reflective evacuated 125-mm diameter glass tube to maximize the solar transmittance
- An advanced glass-to-metal (COVAR) seal and metal bellows to compensate the different thermal expansions of tube and glass envelop

- A new getter designed to absorb gases that permeate into the vacuum annulus over time
- Barium getter spot as vacuum indicator
- Enclosure in vacuum-tight (10^{-4} mbar) to reduce heat losses at high-operating temperatures and to protects the solar selective coating from oxidation

SPECTRALLY SELECTIVE COATINGS FOR RECEIVER TUBE

Main features

- High photothermal conversion efficiency of direct solar radiation concentrated on receiver tube
  - ✓ High absorptance (α_s) of solar radiation
  - ✓ Low thermal emissivity (ε_{th}) at operating temperatures (limited heat loss)
- Chemical-structural stability at high temperature in vacuum for receiver reliability and durability
- Low manufacturing costs: high-throughput deposition processes, deposition plants with low investment and operating costs

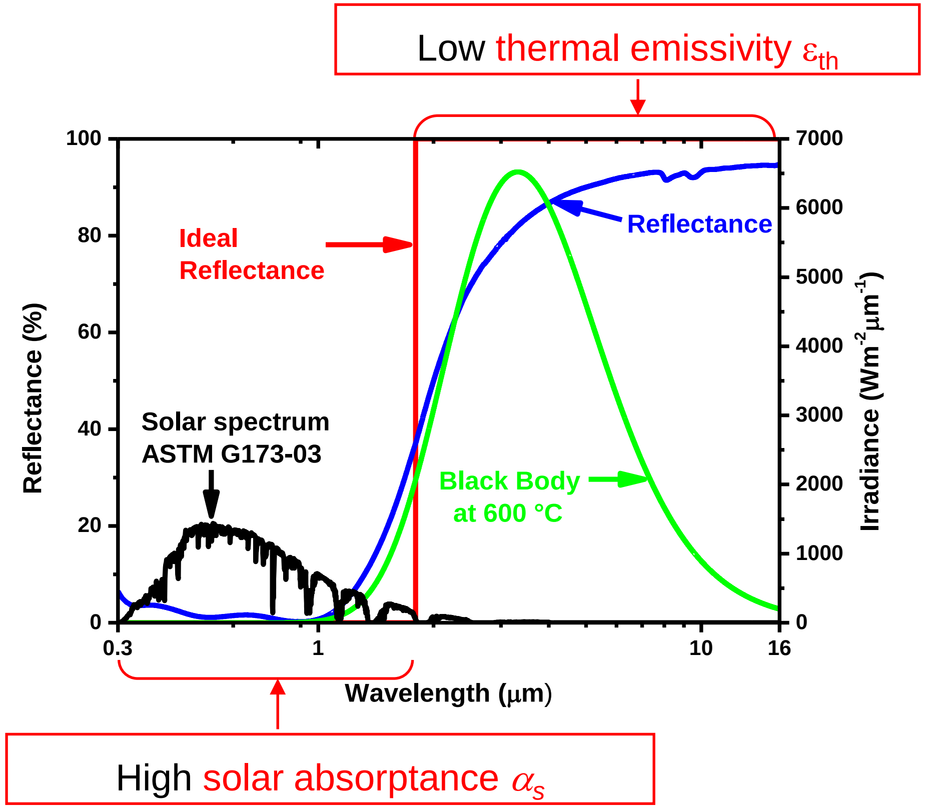

SPECTRALLY SELECTIVE COATINGS FOR RECEIVER TUBE

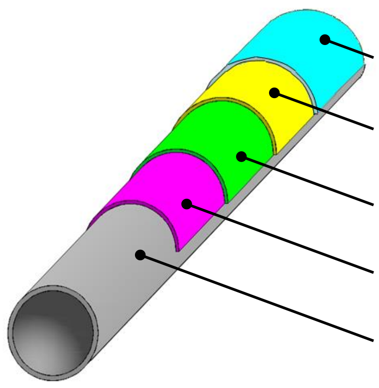

Typical structure of solar coating

1. Antireflection filter (one or more ceramic layers)
2. Solar absorber layer (CERMET multilayer)
3. Infrared reflector (metallic layer)
4. Adaptive layer (ceramic/metallic/ CERMET layer)
5. Substrate: Stainless steel tube

- **CERMET:** ceramic-metallic nanocomposite absorbing in the solar wavelength range and transparent in the infrared region
- SEM image (cross section view) of a solar coating with W-Al_2O_3 CERMET

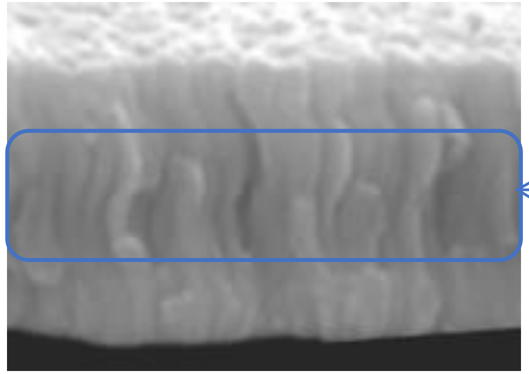

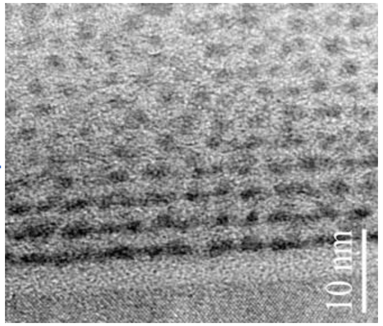

- High Resolution TEM image of a W-Al_2O_3 CERMET
- CERMET consists of metallic nanoparticles (3 nm) dispersed in a ceramic matrix

DEPOSITION TECHNOLOGY: MAGNETRON SPUTTERING

Process requirements

- High deposition rate
- Low fabrication cost
- Good repeatability
- Stable and robust
- Suitable for large area deposition

Sputtering is a physical vapor deposition (PVD) process for thin film deposition able to fulfil all process requirements

Atoms and molecules are ejected from solid target through the impact of energetic noble gas ions on the target

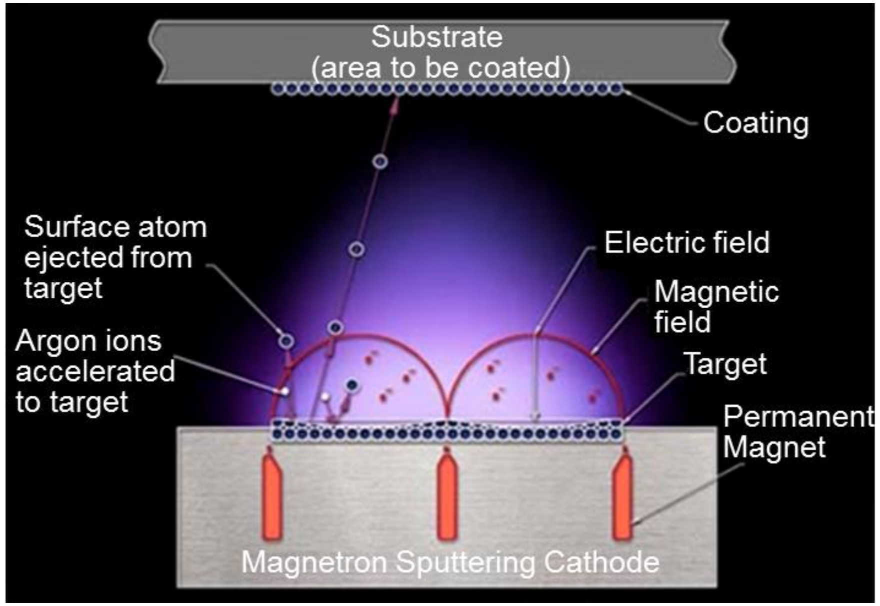

Fabricated by sputtering processes:

- Ceramic and metallic layers
- CERMET layers (by co-sputtering process, confocal or in sequence sputtering sources)
- Adaptive and/or barrier layer

PROCEDURE FOR SOLAR COATING FABRICATION

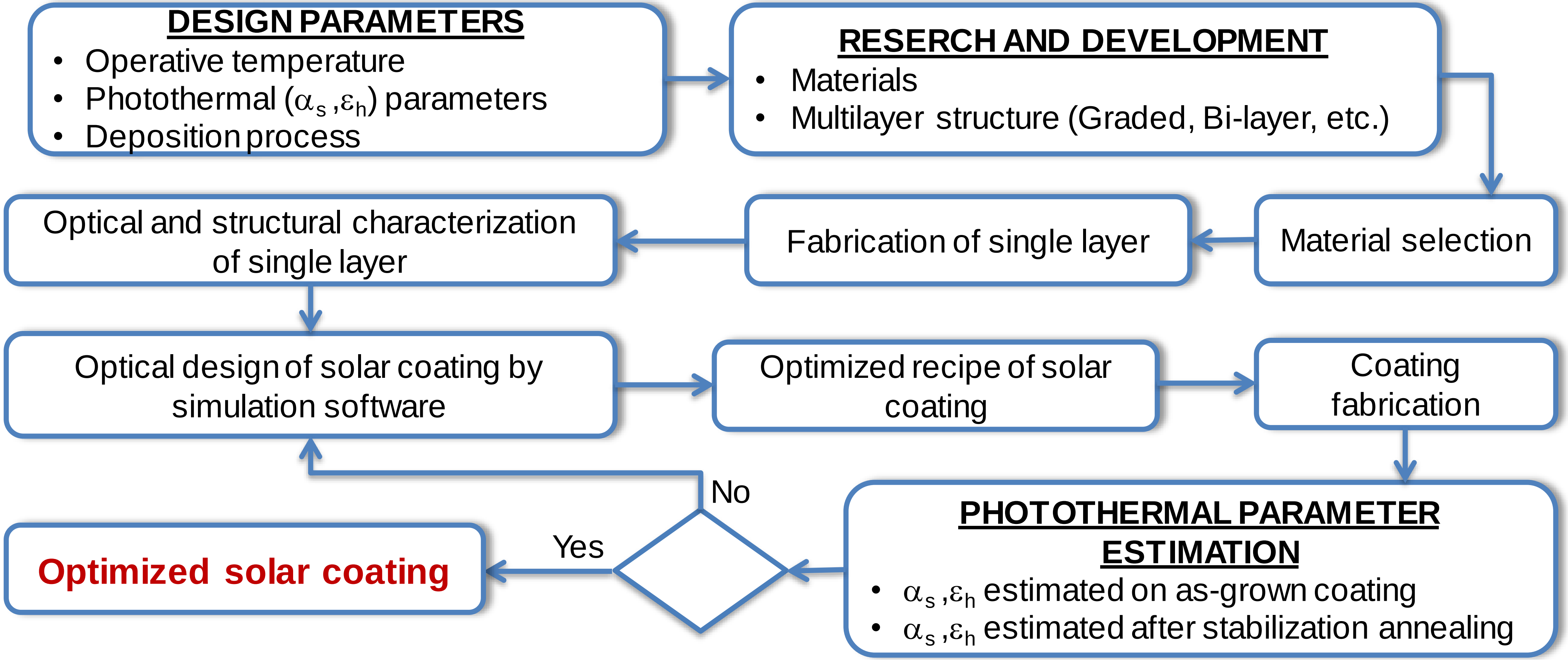

2008: ENEA PATENT BASED ON W-Al_2O_3 CERMET

Solar coating based on W-Al_2O_3 CERMET for high temperature (550 °C) applications

Solar coating materials

- Antireflection filter: aluminium oxide
- Solar absorber layer:
  - graded type CERMET consisting of nanoparticles of tungsten dispersed in an aluminium oxide matrix
  - tungsten content decreasing from infrared reflector to antireflection filter
- Infrared reflector: crystalline tungsten
- Adaptive layer: CERMET layer with constant content of tungsten and alumina

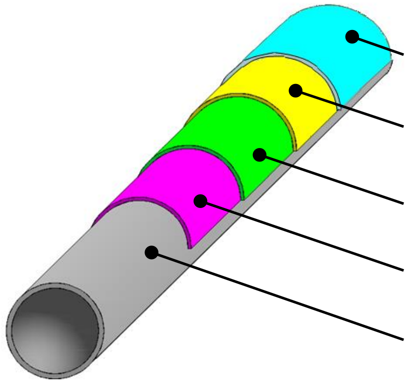

DEPOSITION PROCESS	
Antireflection filter (Al_2O_3)	Sputtering (RF)
Absorber layer (W-Al_2O_3)	Co-sputtering (DC/RF)
Infrared Reflector (W)	Sputtering (DC)
Adaptive layer (W-Al_2O_3)	Co-sputtering (DC/RF)

ENEA 1

1. General view

2. Load lock and revolver

- Sputtering plant for production of solar receiver coatings
- Manufactured by Kenosistec in 2005
- Plant developed around the tubular geometry of receiver
- Estimated production capability: up to 12.000 receivers/year
- Manufactured one tube at a time
- Processes for coating fabrication developed by ENEA
- Design of solar coating performed by ENEA

Solar coating performance

- $\alpha_s \geq 94.6\%$ and $\varepsilon_h < 14\%$ at 550°C
- High chemical and structural stability under vacuum ($<10^{-4}$ mbar) up to 600°C
- Coating lifetime 25 years for a Sun illumination of 8 hours per day
- High chemical and structural stability in air up to 300°C

ARCHIMEDE PROJECT

- ENEA-1 was acquired by Archimede Solar Energy (ASE) in 2007
- ENEA-1 was employed to deposit the solar coating of the receiver tubes for Archimede ENEL Plant at Priolo Gargallo (Sicily)
- Archimede is the first example of combined cycle power plant with the CSP section at high temperature (550 °C)
- The CSP is a 5 MWe plant with molten salts as HTF

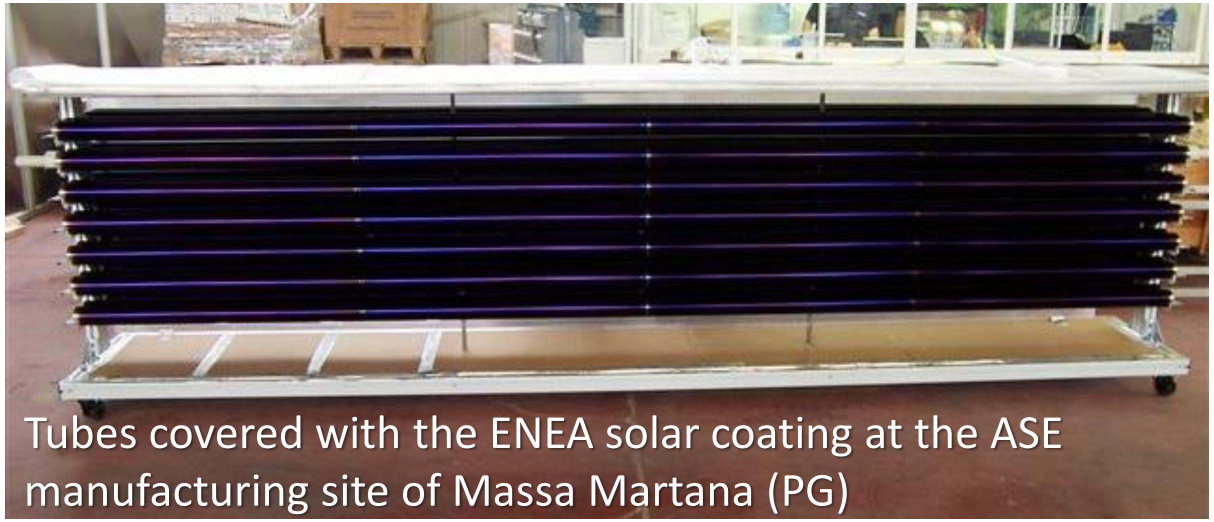

2011: ENEA patent based on double nitride cermet

Solar coating based on WN-AlN CERMET for medium (400 °C) and high (550 °C) T applications

Solar coating materials

- Antireflection filter: silicon dioxide and aluminium nitride
- Solar absorber layer:
  - graded type cermet consisting of nanoparticles of tungsten nitride and aluminium nitride
  - tungsten nitride content decreasing from infrared reflector to antireflection filter
- Infrared reflector: silver for applications up to 400°C, crystalline tungsten for applications up to 550°C
- Adaptive layer of W in case of Ag infrared reflector

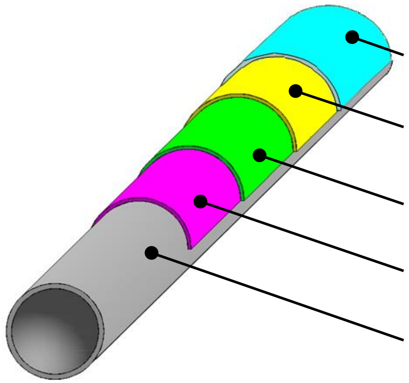

Antireflection filter (SiO2 +AlN)	
Antireflection filter (SiO2 +AlN)	Sputtering (MF reactive)
Absorber layer (WN-AlN)	Co-sputtering (DC/MF reactive)
Infrared Reflector (W, Ag)	Sputtering (DC)
Adaptive layer (W)	Co-sputtering (DC/MF reactive)

ENEA 2

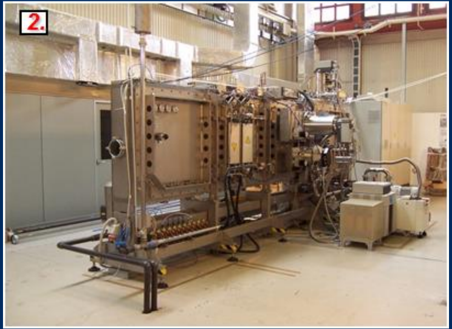

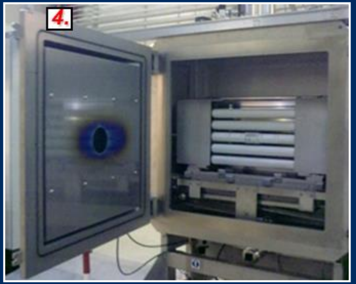

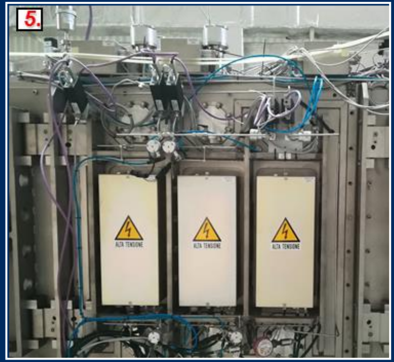

1. Front side
2. Back side
3. Plasma image
4. Load-lock with the carrier
5. Sputtering cathodes

MAIN FEATURES

- Deposition plant for R&D on spectrally selective coating for receiver tubes
- ENEA concept design
- Design based on a concept of scalable plant for industrial production
- Experimental machine
- High flexibility
- Deposition on planar and tubular substrate
- Scansion system
- Substrate transported by carrier
- Sputtering and co-sputtering processes
- Suitable to design and fabricate solar coatings based on the ENEA technology of double nitride CERMET

ENEA-2 SPUTTERING PLANT

Load-Lock Chamber

- Substrate pre-treatment: heating and plasma etching
- Tube rotation during pre-treatment processes

Deposition Chamber

- Six cathodes arranged in pairs on two opposite sides
- Carrier translation and tube rotation during deposition process
- Deposition processes:

  Metals → sputtering (DC)

  Ceramics → sputtering (Bipolar DC-Pulsed or MF reactive)

  CERMET → co-sputtering (DC/Bipolar DC-Pulsed or MF reactive)

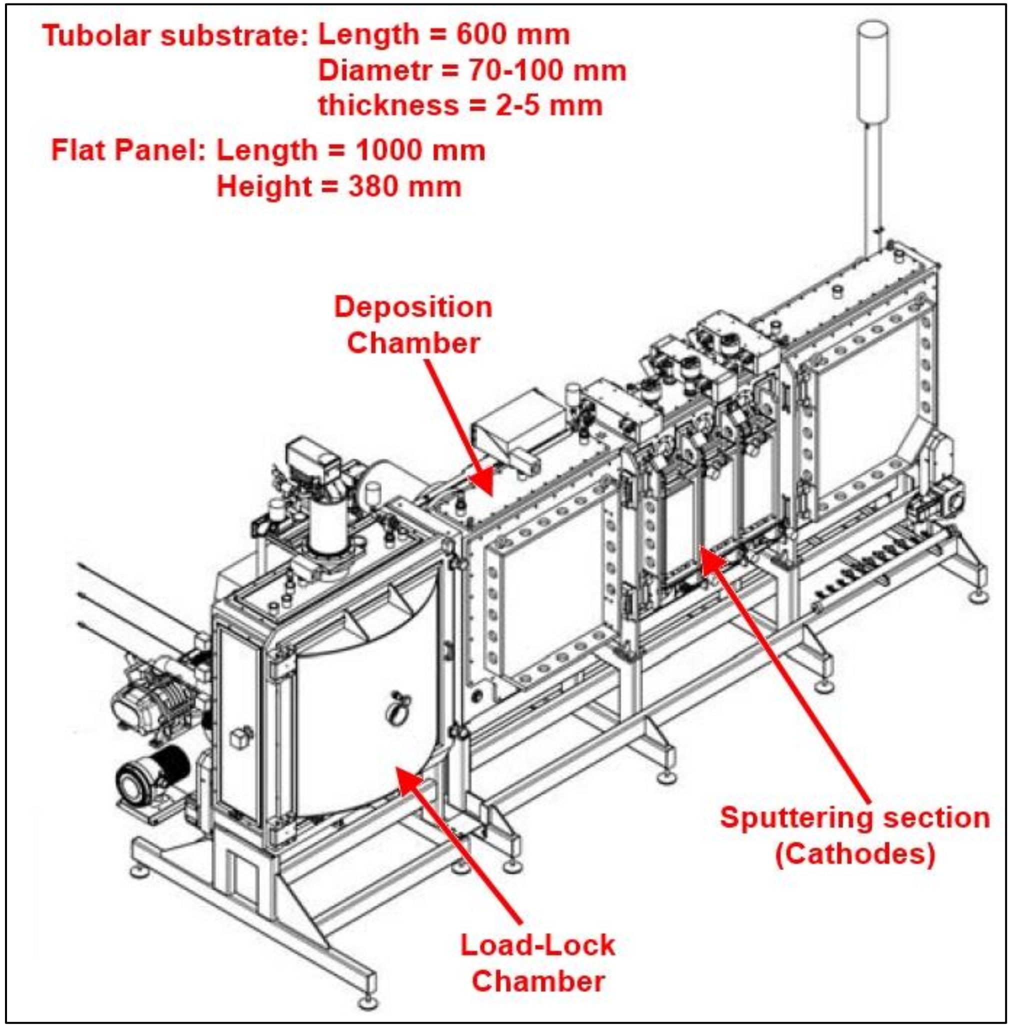

ASE MANUFACTURING SITE

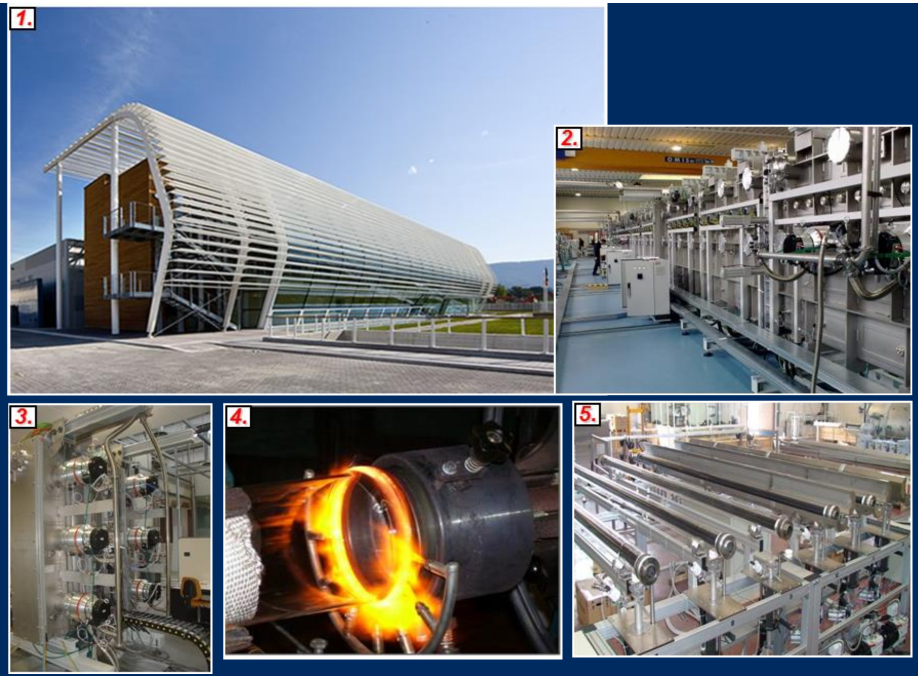

1. ASE headquarter
2. Sputtering plant overview
3. Cathode pumping system detail
4. Glass to metal welding system
5. Solar receiver degassing system

INDUSTRIAL PRODUCTION

- Deposition plant for R&D on spectrally selective coating for receiver tubes
- ASE sputtering plant was designed and fabricated to deposit solar coatings based on the ENEA technology of double nitride cermet
- Full capacity 75.000 receivers/year
- All tubes for medium and high temperature were produced by ASE under ENEA license

Solar coating performance

at medium temperature (400 °C):

- $\alpha_s \geq 95.0\%$ and $\varepsilon_h < 10.5\%$ at 550°C
- High chemical and structural stability under vacuum ($<10^{-4}$ mbar) up to 450°C
- Coating lifetime 25 years for a Sun illumination of 8 hours per day

at high temperature (550 °C):

- $\alpha_s \geq 95.0\%$ and $\varepsilon_h < 10.5\%$ at 550°C
- High chemical and structural stability under vacuum ($<10^{-4}$ mbar) up to 600°C
- Coating lifetime 25 years for a Sun illumination of 8 hours per day

ASE SOLAR RECEIVERS

ASE Solar receiver installed on commercial parabolic through plants

- ✓ Receivers operating at medium temperature (400 °C) / PLUS-type
  2016-2017: receivers supplied by ASE for DUBA-1 Integrated Solar Combined Cycle (ISCC) plant – Saudi Arabia – diathermic oil - 43 MWe power

- ✓ Receivers operating at high temperature (550 °C) / Molten Salt type
  2015-2016: receivers supplied by ASE for AKESAI Solar Thermal Power Plant (ASTPP, molten salts) – China - 55 MWe power and equipped with 15 hours thermal storage

ASE SOLAR RECEIVERS

ASE Solar receiver installed on demonstrative plants

- ✓ Receivers operating at high temperature (550 °C) / Molten Salt-type 2022: receivers supplied by ASE for Partanna CSP plant – Italy- molten salts – 4,26 MWe power

- ✓ Receivers operating at high temperature (550 °C) / Molten Salt-type 2018: receivers supplied by ASE for the integrated "MATS" CSP – Egypt molten salts –1 MWe power


SOLINPAR CSP plant in Partanna (Sicily, Italy)


MATS CSP plant in Borg El Arab (Egypt)

SOLAR COATING IN AIR – NEEDS AND CHALLENGES

- **Current receiver tube technology - in absence of atmosphere (vacuum)** → **Maximum operating T = 550 °C**
- **Overcoming this temperature barrier implies the need of solar coatings operating in air**

SOLAR COATING IN AIR – OBJECTIVES

To develop **highly selective absorber coating** for receiver tubes of Linear Collector Plants able to work in **open air** atmosphere at **high temperature** (>550°C), showing:

- **satisfactory optical properties** (solar absorptance ≥ 70%, thermal emissivity < 25%)
- **thermal stability** (photothermal performance reduction < 5% in 25 years)

SOLAR COATING IN AIR – MULTILAYER STRUCTURE

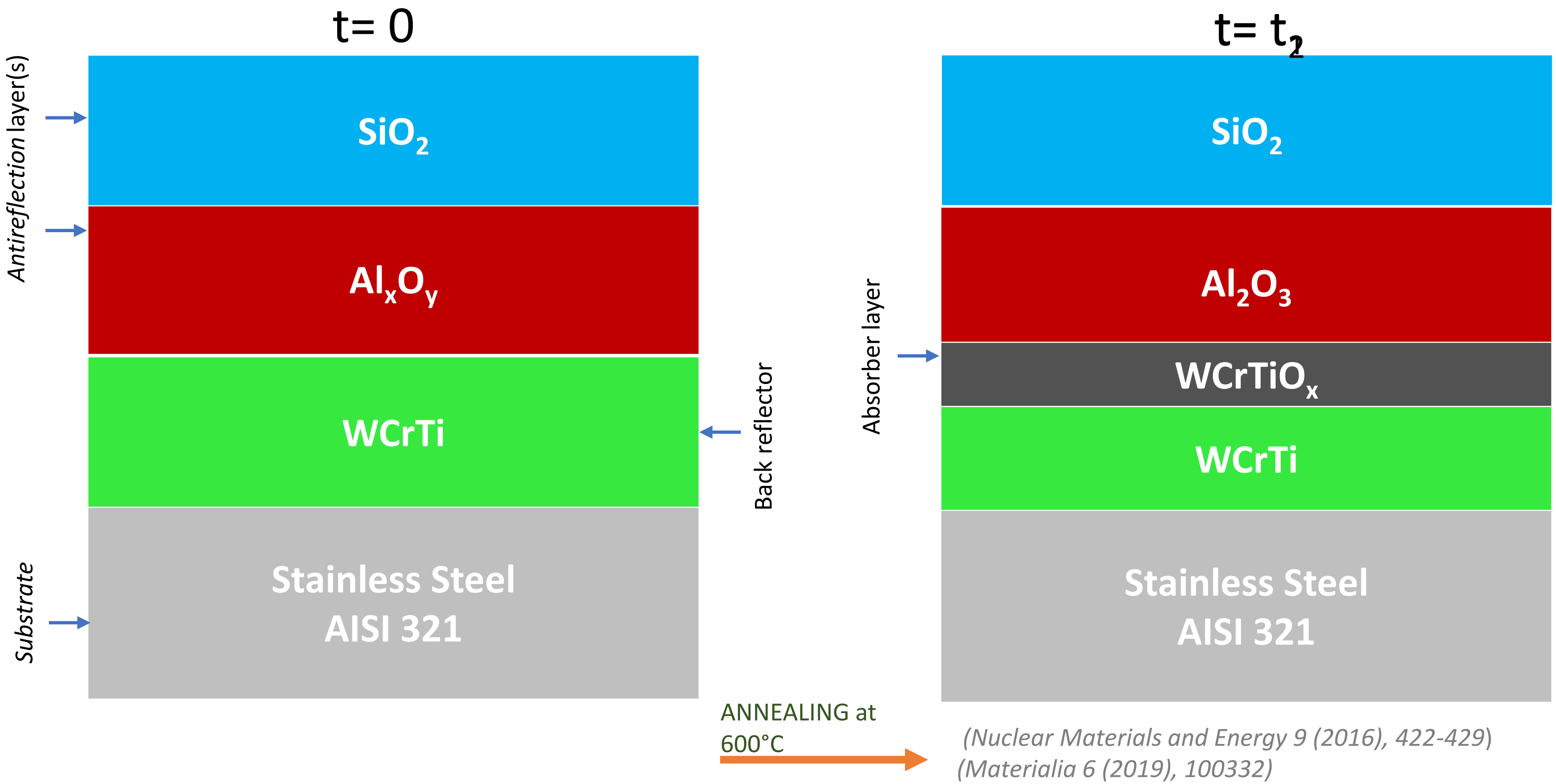

(Nuclear Materials and Energy 9 (2016), 422-429)
(Materialia 6 (2019), 100332)

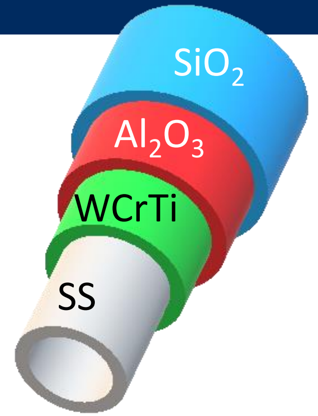

Thermal oxidation of WCrTi

Mixed metal oxides formation (chromium oxide prevailing)

Both absorber and barrier layer

ENHANCED STABILITY

SOLAR COATING IN AIR – EXPERIMENTAL APPROACH

1. self-passivating layer of WCrTi is deposited on stainless steel substrate (AISI 321) by DC sputtering technique, to act as back reflector (500 nm thickness)

2. a first antireflection layer of Al_xO_y deposited through reactive sputtering in transition mode (≈ 120 nm thickness)

3. a second final antireflection layer of SiO_2 is added with uniform and compact sealing method (spin coating at 3500 rpm for 30 s)

4. 10 annealing cycles at 600°C in air for 1904 hours overall duration

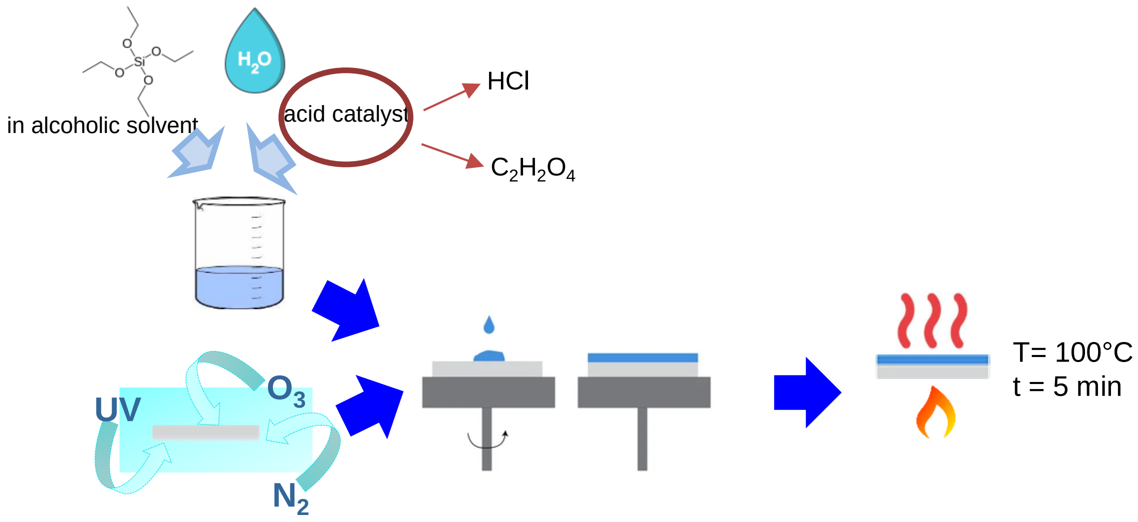

SOLAR COATING IN AIR - PHOTOTHERMAL PROPERTIES

Optical Parameters before and after aging in air at 600°C

	Solar Absorptance (α)		Thermal Emissivity (ε_{th}) at 600°C	
	as grown	*1904 hours aging*	*as grown*	*1904 hours aging*
$WCrTi/Al_2O_3/SiO_2$	78,17	72.96%	18,09%	18.54%

as grown *aged*

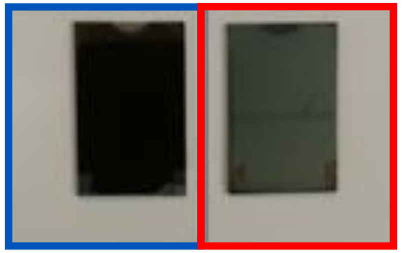

- sample shows an α reduction of 6% and an ε_{th} increase of 2%
- for high temperature applications **thermal emissivity is crucial** and should remain as low as possible ➡ ***$WCrTi/Al_2O_3/SiO_2$ is a suitable solution***

NEXT STEPS

- ENEA patent on innovative solar coatings under vacuum with improved photo-thermal performance and durability at high temperature (550 °C)

- ENEA patent on innovative solar coatings in air with high photo-thermal performance and long durability in the temperature range 600 -800 °C

Gabriella ROSSI, PhD
ENEA
TERIN-STSN-SCIS
gabriella.rossi@enea.it

THANK YOU FOR YOUR ATTENTION!
ANY QUESTIONS?

SFERA-III

Solar Facilities for the European Research Area

4^{th} Training for Industries

7-11^{th} November 2022, Cr ENEA Casaccia Rome (Italy)

CSP Plant Model & CSP Performance Simulation

Valeria RUSSO (ENEA, TERIN-STSN-ITES), Marco D'Auria (ENEA, TERIN-STSN-SCIS)

JOINT RESEARCH ACTIVITIES

THIS PROJECT HAS RECEIVED FUNDING FROM THE EUROPEAN UNION'S HORIZON 2020 RESEARCH AND INNOVATION PROGRAMME UNDER GRANT AGREEMENT NO **823802**

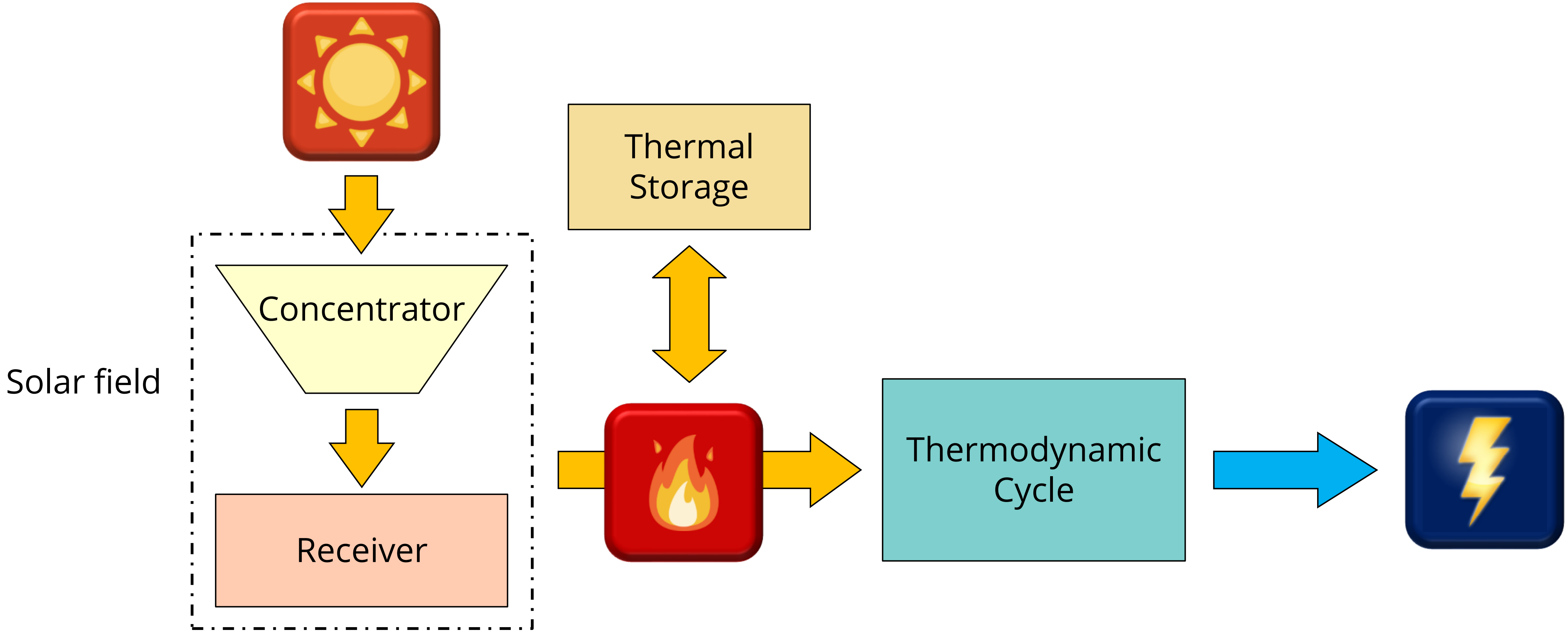
Thermal Storage
Concentrator
Solar field
Receiver
Thermodynamic Cycle

Not only electricity generation: potential CST applications

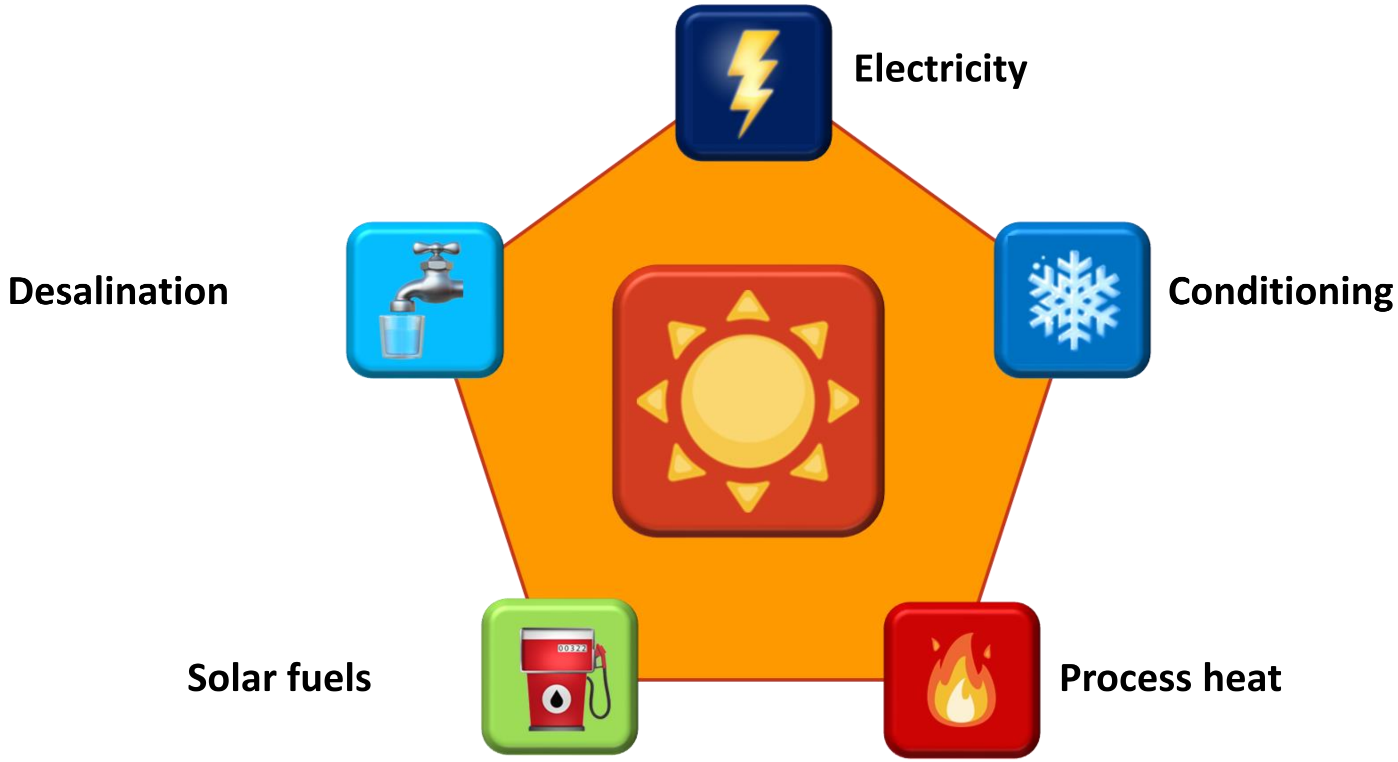

CSP technologies

PUNCTUAL CONCENTRATION

LINEAR CONCENTRATION

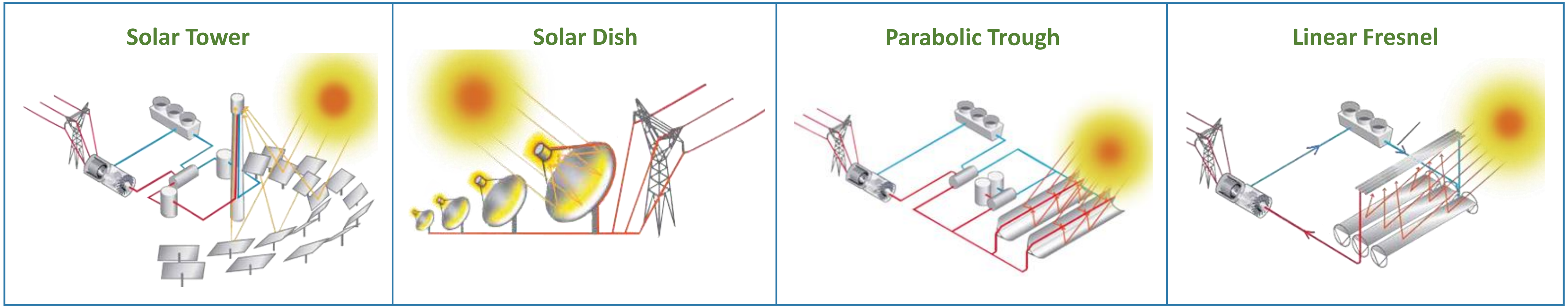

	Solar Tower	Dish	Parabolic Trough	Fresnel
Concentration Ratio	300 - 1000	300 - 2000	70 - 80	25 - 100
Power [MW_e]	10 - 400	0.003 - 0.3	10 - 300	0.001 - 200
Peak Effciency [%]	22-24	24-26	24-28	20-24
Average Efficiency [%]	16-18	13-16	12-16	9-11

CSP technologies

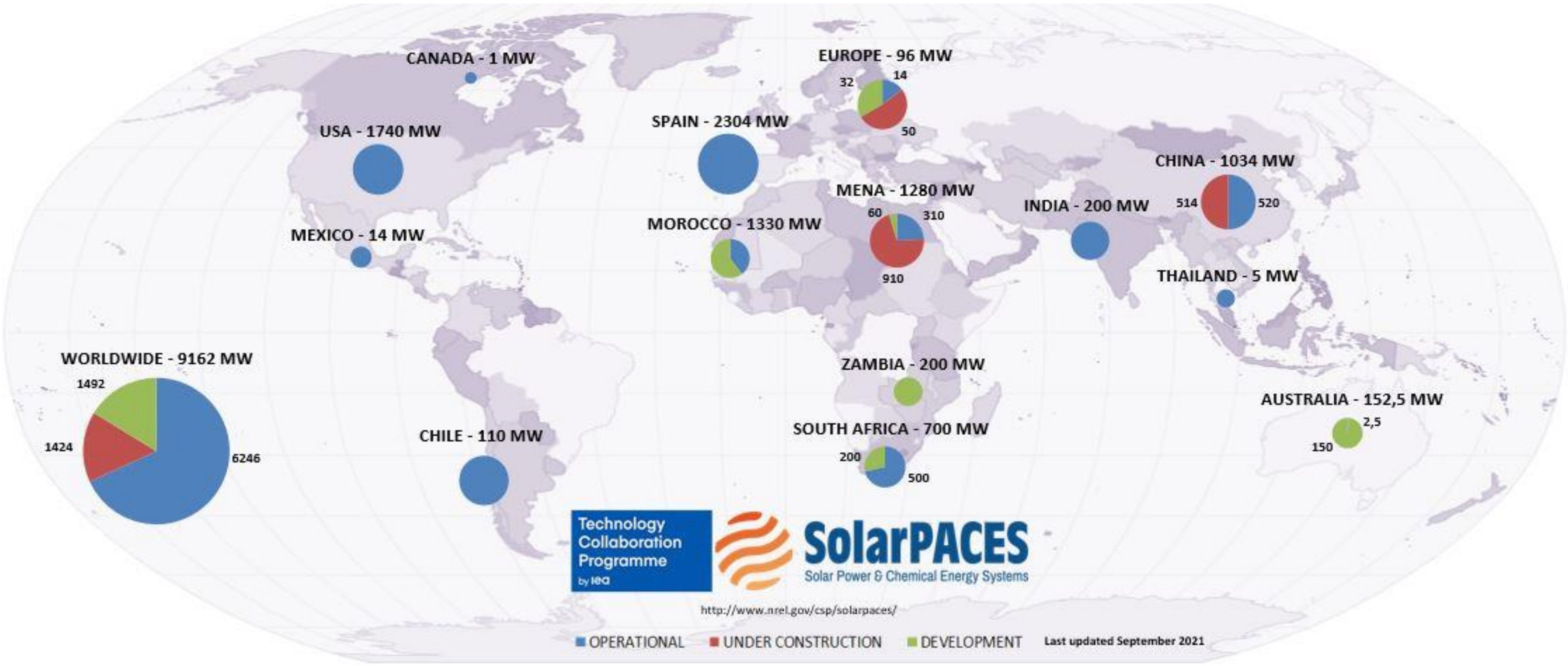

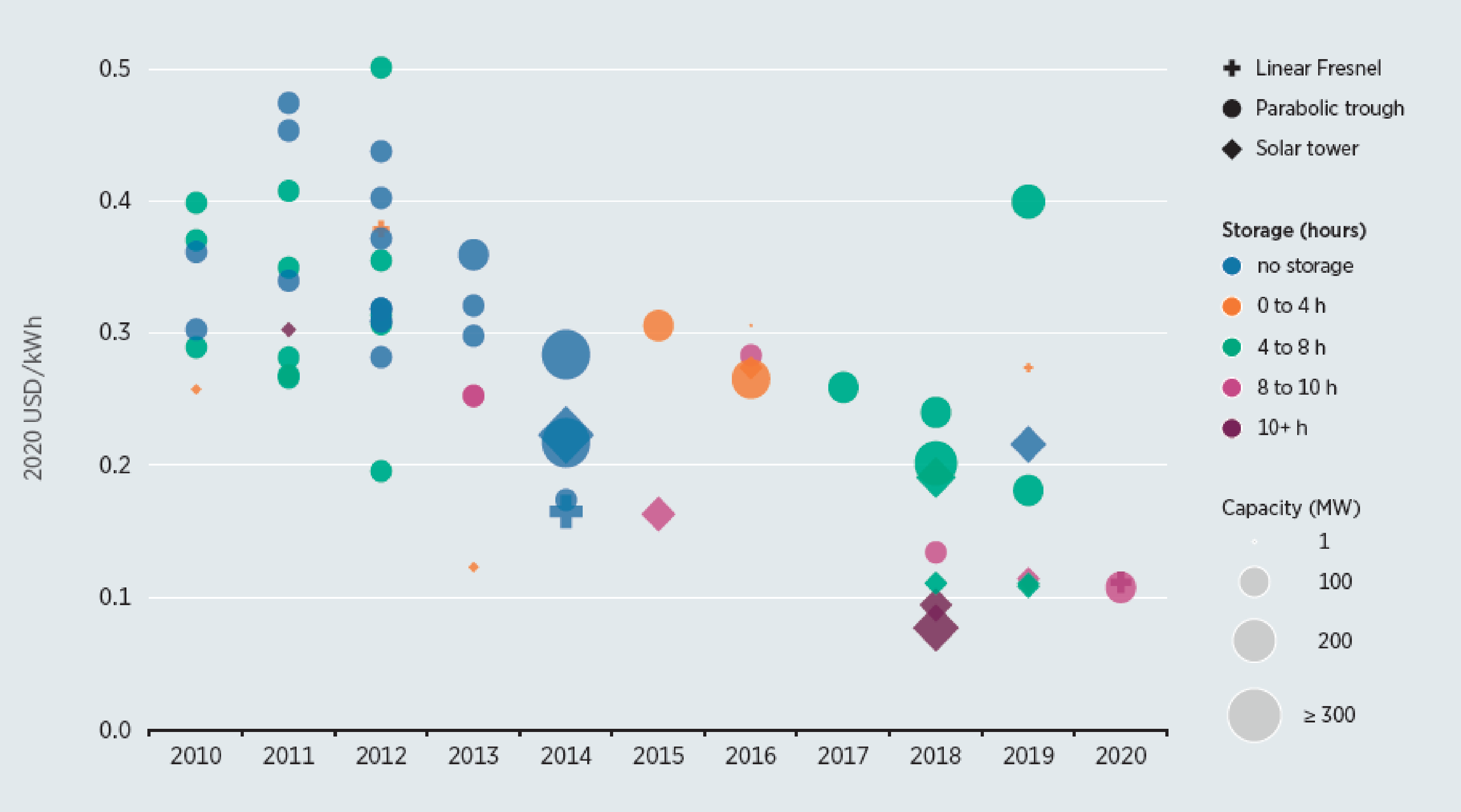

Source: IRENA Renewable Cost Database.

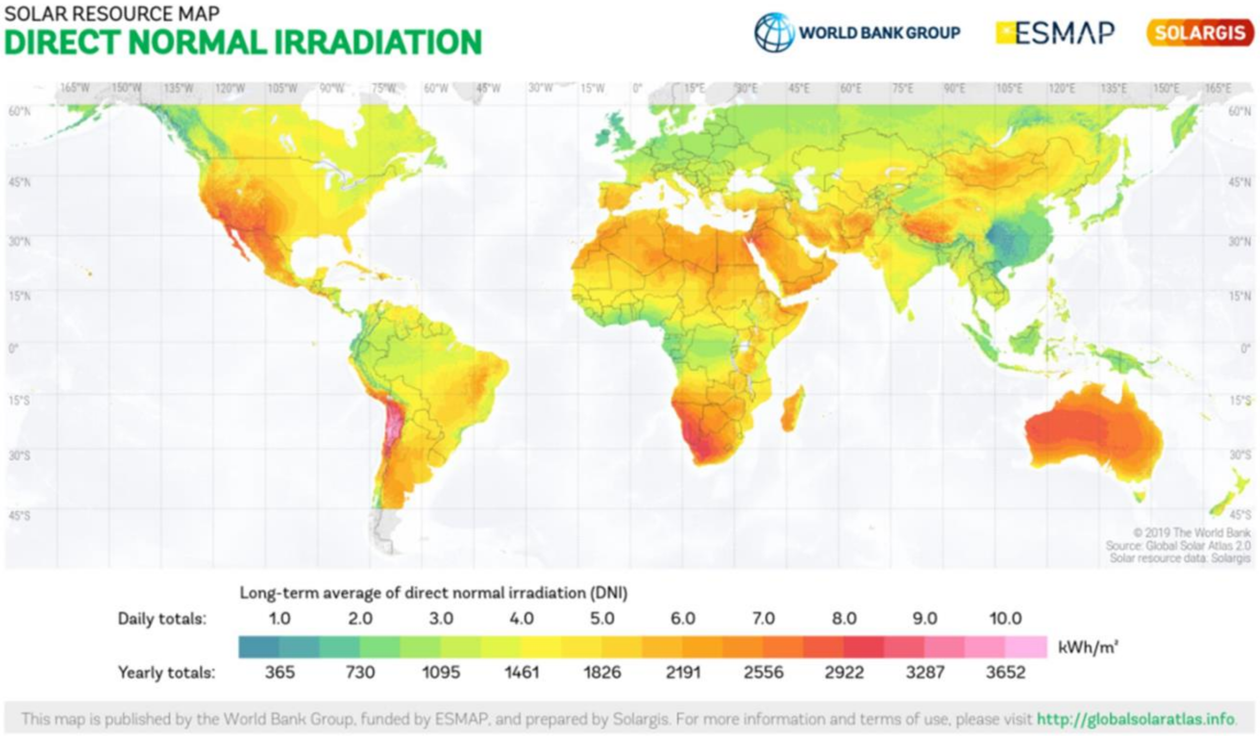
SOLAR RESOURCE MAP
DIRECT NORMAL IRRADIATION
WORLD BANK GROUP
ESMAP
SOLARGIS
© 2019 The World Bank
Source: Global Solar Atlas 2.0
Solar resource data: Solargis
Long-term average of direct normal irradiation (DNI)
Daily totals: 1.0 2.0 3.0 4.0 5.0 6.0 7.0 8.0 9.0 10.0
kWh/m²
Yearly totals: 365 730 1095 1461 1826 2191 2556 2922 3287 3652
This map is published by the World Bank Group, funded by ESMAP, and prepared by Solargis. For more information and terms of use, please visit http://globalsolaratlas.info.

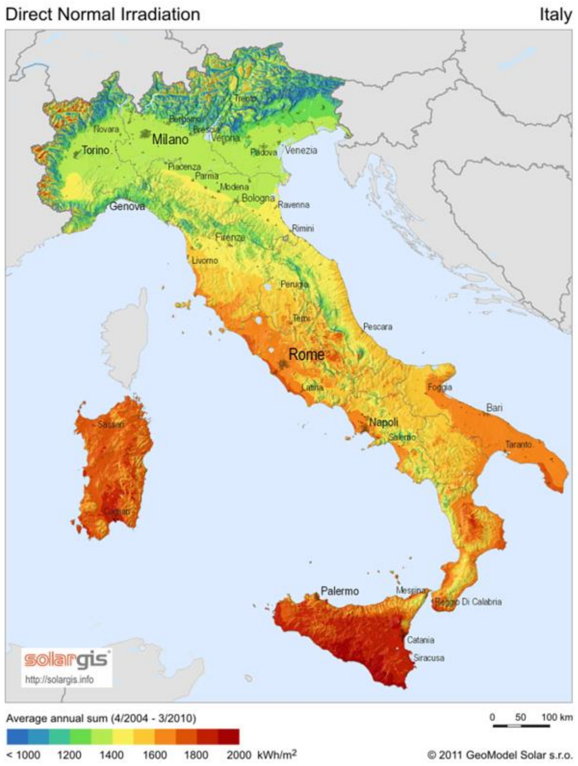
Direct Normal Irradiation
Italy
Milano
Torino
Genova
Venezia
Bologna
Rome
Napoli
Bari
Palermo
solargis
http://solargis.info
Average annual sum (4/2004 - 3/2010)
< 1000 1200 1400 1600 1800 2000 kWh/m²
0 50 100 km
© 2011 GeoModel Solar s.r.o.

CSP Plant Model

A CSP Plant consists of the following main systems:

- Solar Field (Concentrator + Receiver)
- Piping
- Storage
- Interface Equipment and Power block

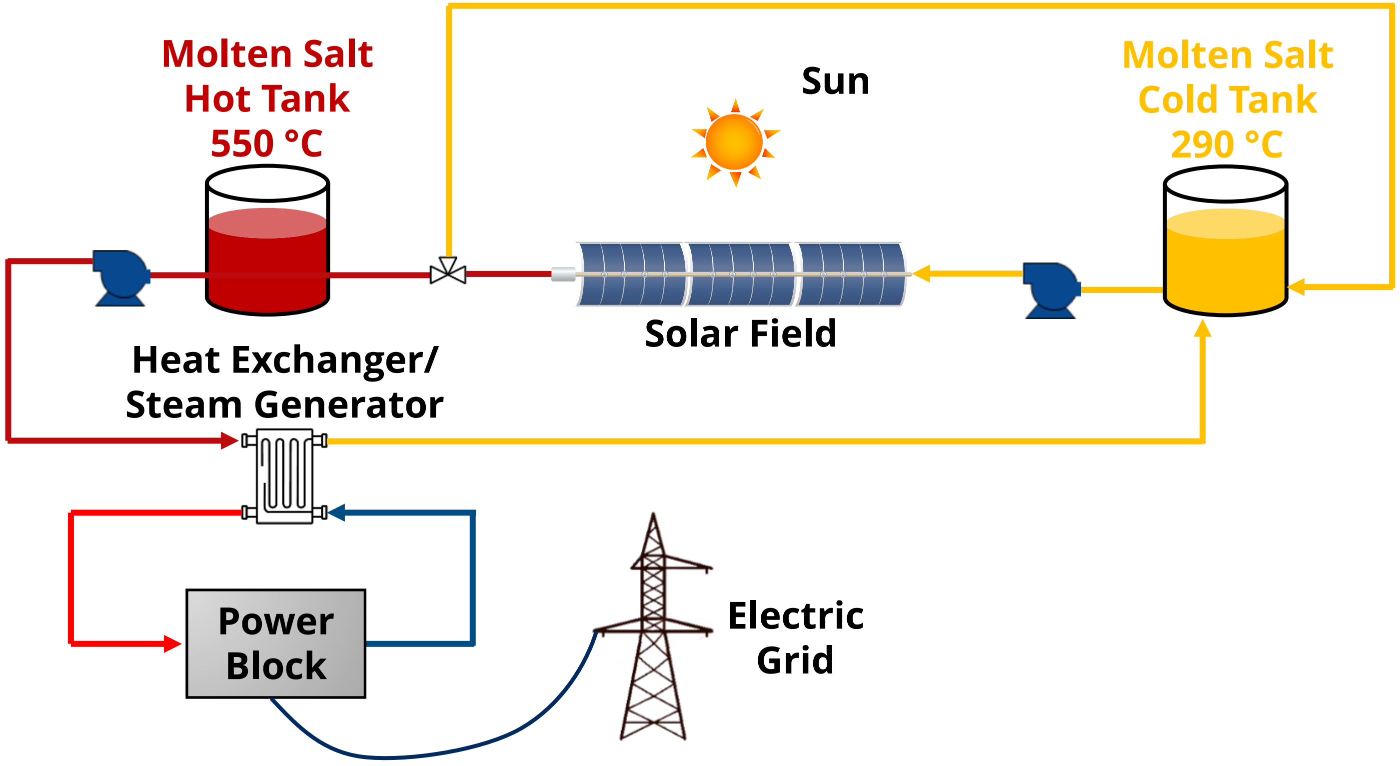

CSP Plant Model

Every system can be described by a physical/mathematical model:

- Solar Concentrator (Optical Model)
- Solar Receiver (Thermal Model)
- Piping (Piping Model)
- Storage (Storage Model)
- Interface Equipment and Power block (Power Block Model)

$$\eta_{plant} = \eta_{optical} \times \eta_{thermal} \times \eta_{piping} \times \eta_{storage} \times \eta_{powerblock}$$

$$\eta_{plant} = \frac{P_{EL}}{P_{SOL}}$$

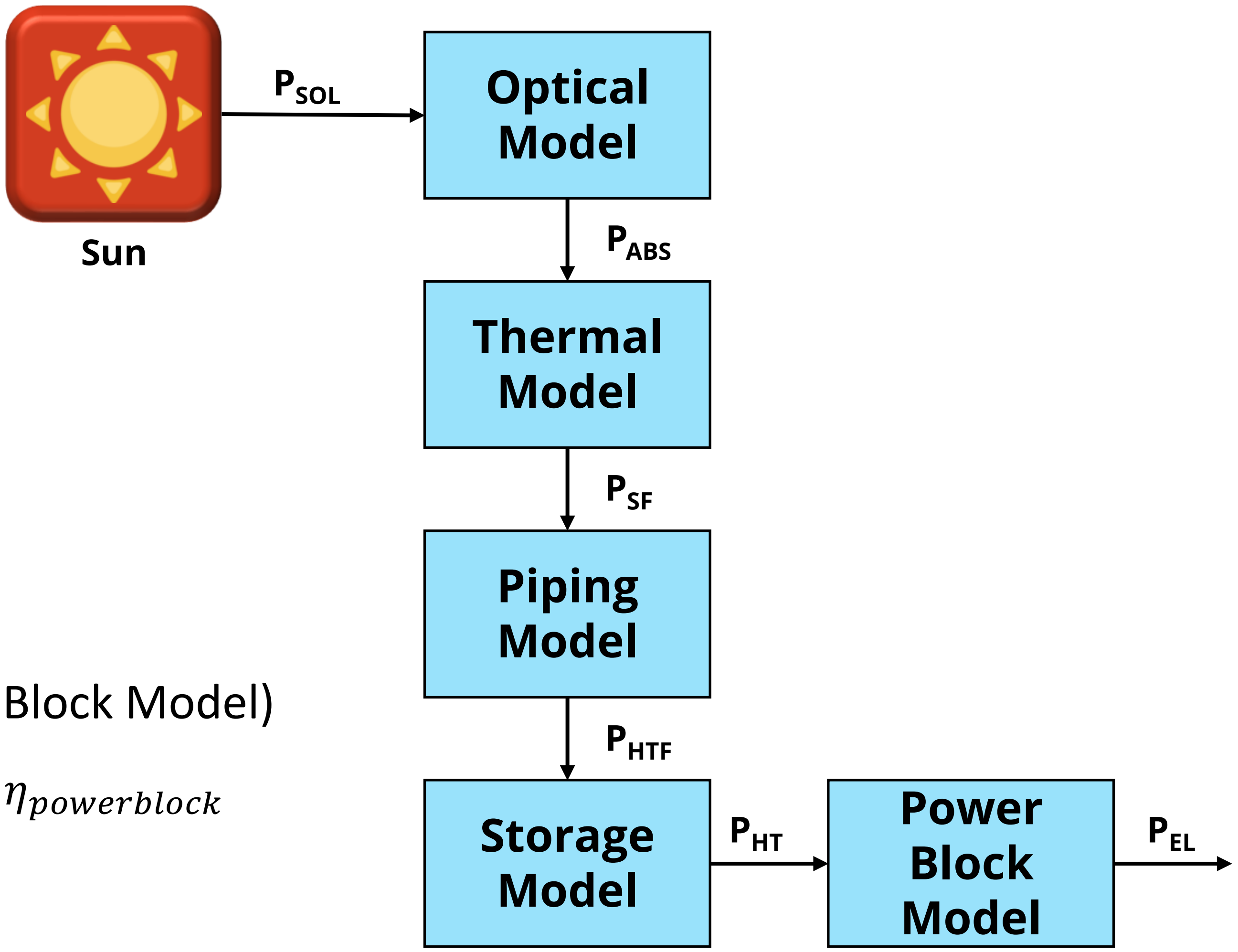

Optical model: Sun's position

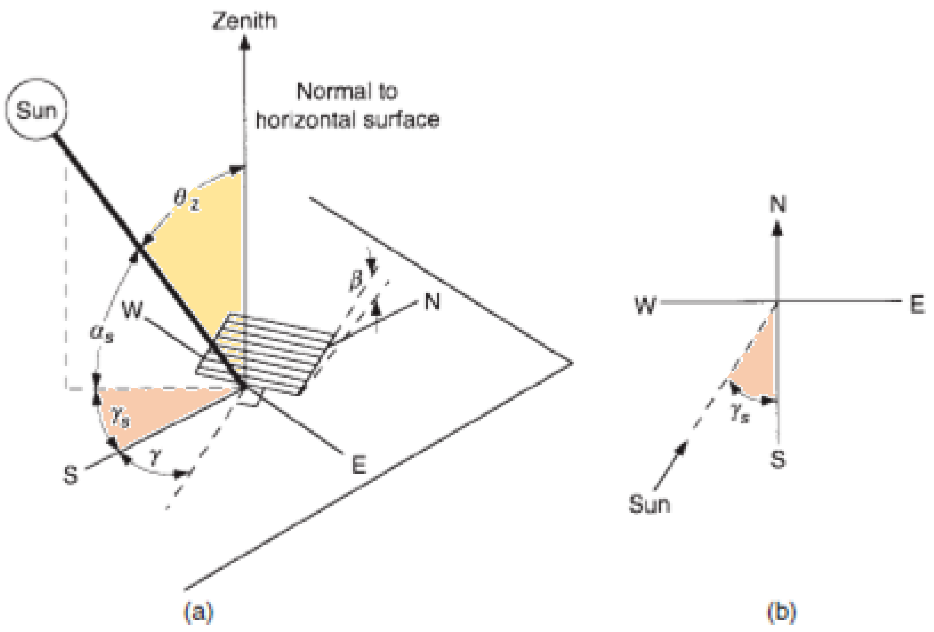

Zenith angle, ϑ_z, the angle between the vertical line and the line to the Sun. It coincide with the angle of incidence, that is the angle between the beam radiation on a surface and the normal to that surface.

Azimuth angle, γ_S, the angular displacement from south of the project beam radiation on the horizontal plane.

Optical model

Optical losses are associated with the following parameters:

- **Reflectivity**, ρ, of the collector reflective surface. Only a fraction of the incident solar flux is reflected towards the receiver tube. Typical solar spectral reflectivity values of clean, rear-silvered low iron glass mirrors are around 0.93–0.94.
- **Intercept factor**, γ. A fraction of the direct solar radiation reflected by the mirrors does not reach the active surface of the receiver pipe due to either microscopic imperfections of the reflectors, macroscopic errors in the parabolic-trough concentrator shape mechanical deformation of the PTC, flexible bellows, or shadowing by the receiver tube supports. Typical values within the range of 0.91–0.93 for high-quality PTCs.
- **Transmissivity** of the glass cover, τ. The steel receiver tube is inserted in a glass cover to reduce thermal losses. A fraction of the direct solar radiation reflected by the mirrors onto the glass cover of the receiver pipe is unable to penetrate it. The ratio of the radiation passing through the glass cover to the total incident radiation on it is the transmissivity of the glass. It is typically in the range 0.93-0.96.
- **Absorptivity** of the receiver selective coating, α. This parameter quantifies the amount of energy absorbed by the steel receiver pipe over the total radiation reaching its outer wall. This parameter is typically 0.95-0.96 for receiver pipes with a cermet selective coating.
- For a clean, good-quality PTC, the nominal (peak) optical efficiency is usually in the range 0.74–0.79 and it is equal to

$$\eta_{optical,nom} = \rho \times \gamma \times \tau \times \alpha$$

- Other parameters: Cleanliness, Tracking error, Cosine losses, End losses, Row shadowing, etc…

Optical model: Parabolic Trough

IAM (Incidence Angle Modifier). The incidence angle of the beam solar radiation, *ϑ*, affects the optical parameters mentioned earlier and the useful aperture area of the collector. This effect is quantified by the incidence angle modifier, *K(ϑ)*, which includes all-optical and geometric losses in a PTC due to an incidence angle greater than 0°. The effective percentage of the beam solar radiation reaching the PTC aperture plane with the incidence angle *ϑ* that is finally absorbed by the receiver tube is

$$\eta_{optical}(\vartheta) = \eta_{optical,nom} \times K(\theta)$$
$$= cos(\vartheta) - 5.25097 \cdot 10^{-4} \cdot \vartheta - 2.859621 \cdot 10^{-5} \cdot \vartheta^2$$

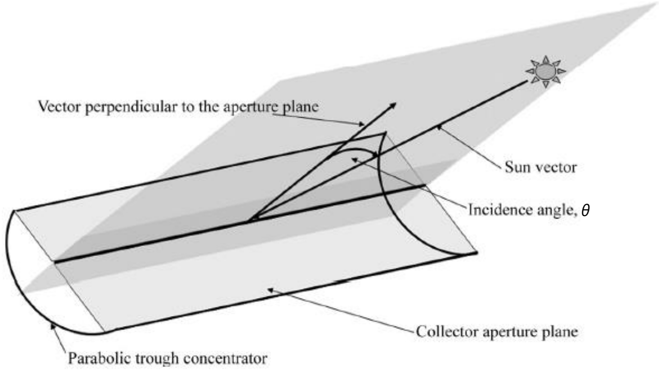

Row shadowing. Shadowing between rows generally occurs at extreme solar positions when the shadow cast by a collector closer to the sun obscures a portion of an adjacent collector. The shadowing effect is derived by considering the geometry of the two adjacent collector rows. The shadowing efficiency is equal to the ratio of the non-shadowed aperture to the total aperture width.

$$\eta_{shadow} = \frac{w_a}{w} = |\cos(\omega_{col})| \frac{L_{spacing}}{w}$$

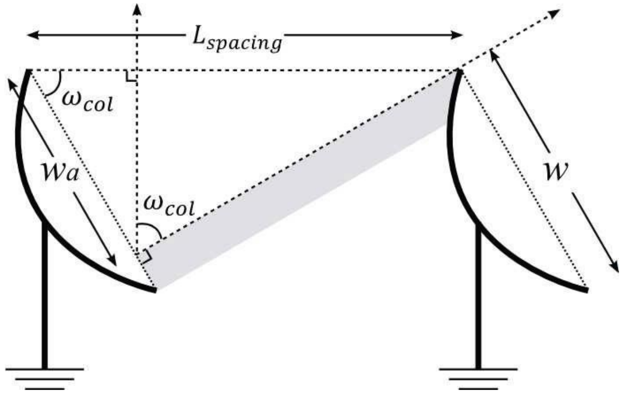

Optical model: Linear Fresnel

Secondary reflector. It allows a better Intercept factor; additional reflection losses occur.

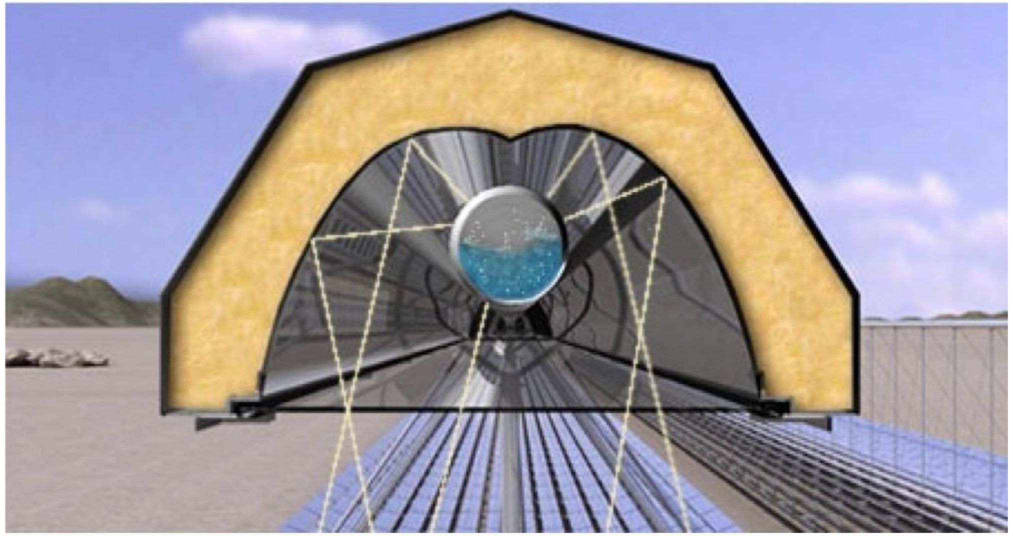

Losses in the longitudinal direction.

- **Cosine Effect**: the ratio between the solar radiation absorbed by the receiver tube and the solar radiation collected by aperture area, *cos*(ϑ_L)*;*
- **End Losses**: due to the occurrence of a non-illumintating area (the "shaded" area):

$$f_{endlosses} = \frac{L_{shaded}}{L}$$

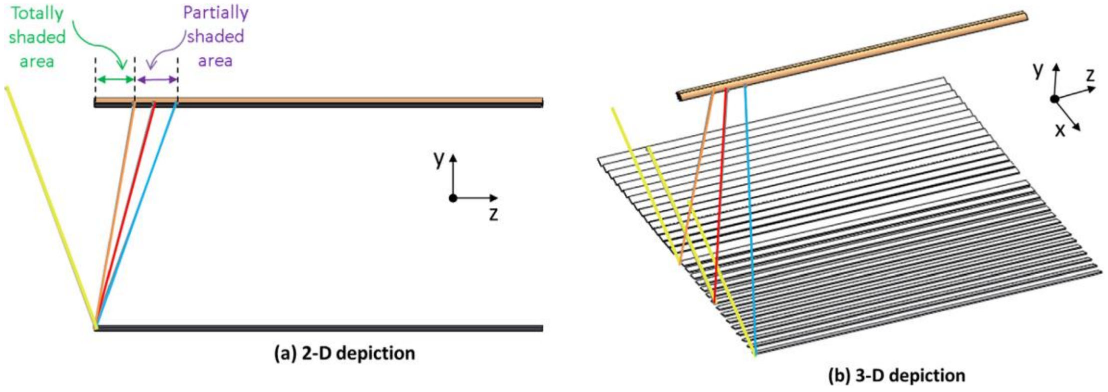

Optical model: Linear Fresnel

Losses in the transversal direction.

- **Rotation optical losses**: The mirrors rotate in order to follow the sun and to concentrate properly the solar irradiation on the receiver. During the rotation the effective mirror width changes.

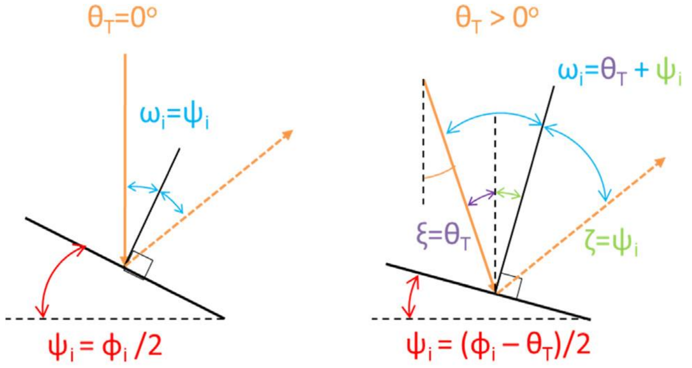

(a) (b)

- **Mirror Shading and blocking effect**: Shading optical losses between contiguous mirrors generally occurs at extreme solar positions.

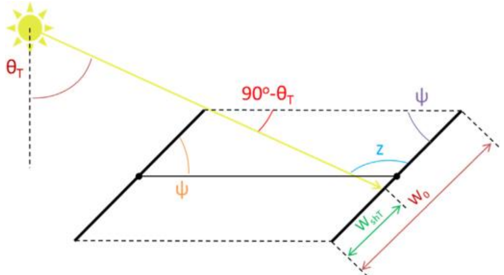

- **Row shading effect:** Shading optical losses due to the shadow of the secondary reflector falling on the primary reflector surface

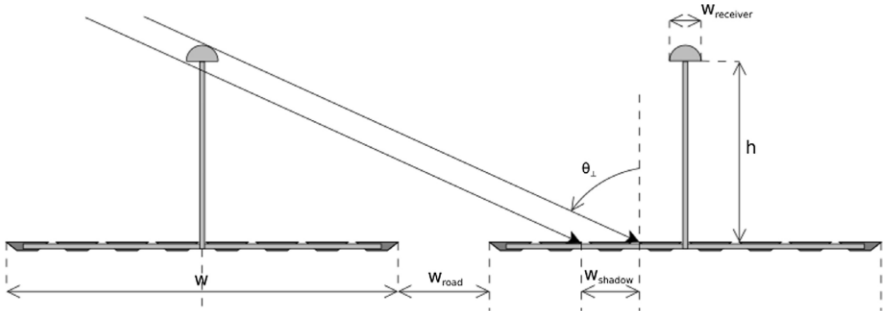

Optical model: Linear Fresnel

$$ANI = DNI * IAM_l(\vartheta_l)\ IAM_t(\vartheta_t)$$

$$\vartheta_t = arctan(\sin(\gamma - \gamma_c) \cdot \tan(\vartheta_z))$$
$$\vartheta_l = arcsin(\cos(\gamma - \gamma_c) \cdot \sin(\vartheta_z))$$

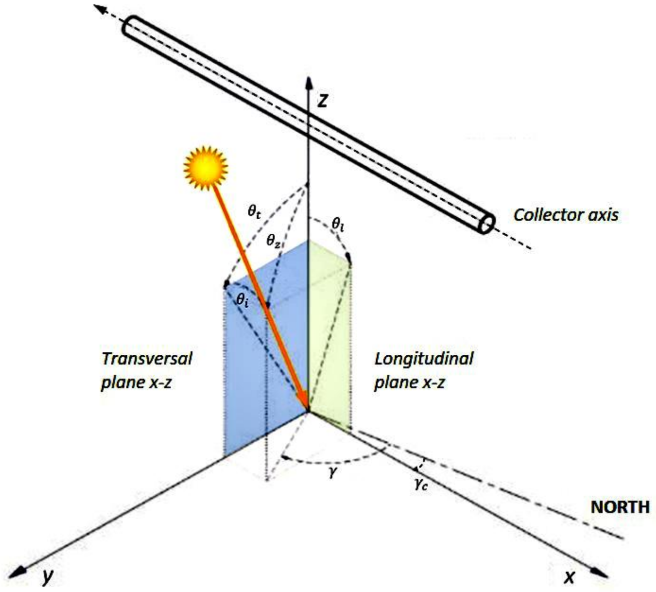

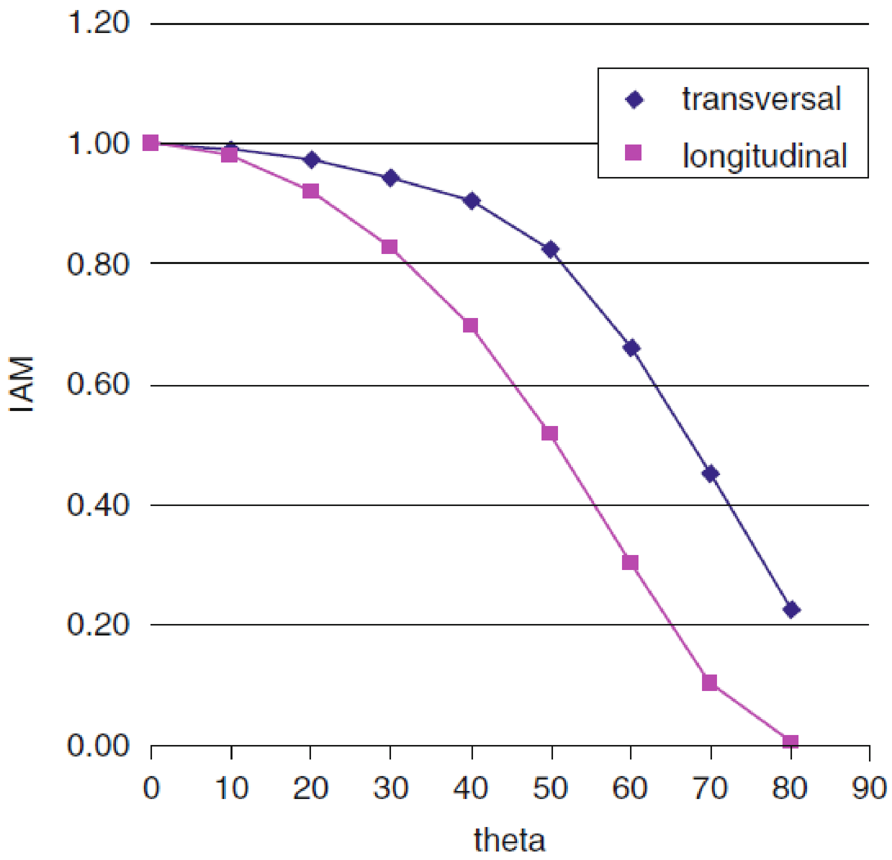

Optical model: Parabolic Trough vs Linear Fresnel

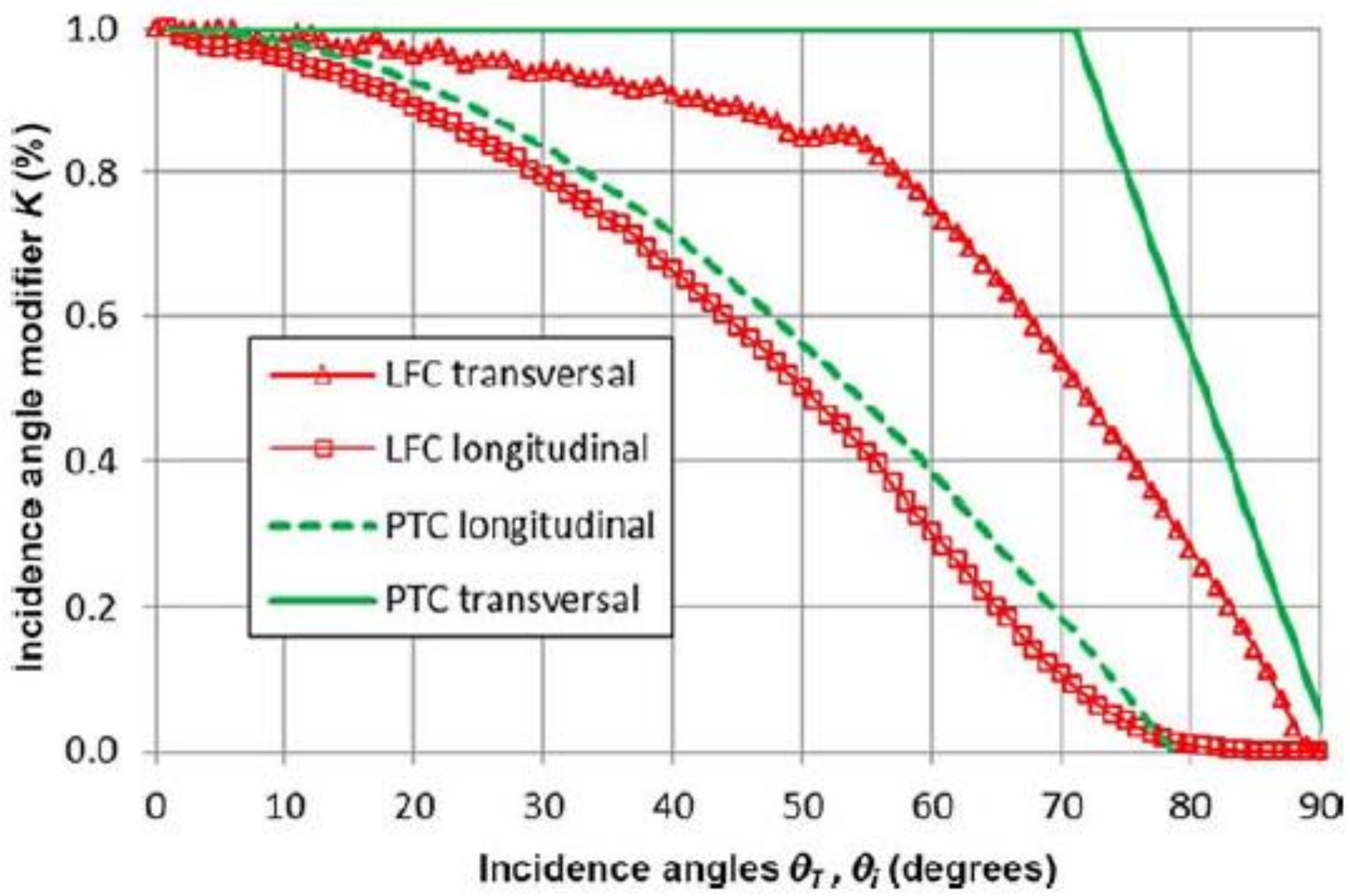

Thermal model

Thermal losses are due to radiative, convective, and conductive heat losses from the receiver tube to environment.

The heat losses can be experimentally determined by operating the collector under real solar conditions at several temperature.

These experimental results can be formulated as

$$P_{loss} = \underbrace{a_1 \cdot (T_m - T_{amb})}_{\text{Conduction + Convection}} + \underbrace{a_2 \cdot (T_m - T_{amb})^4}_{\text{Radiation}}$$

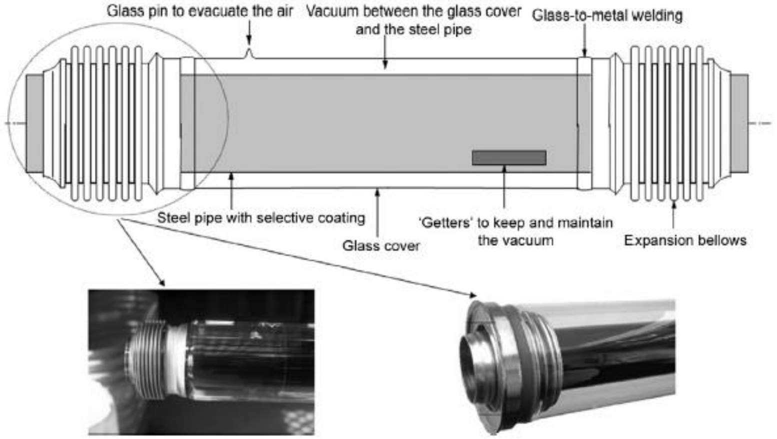

a_1, a_2: coefficients obtained from the experimental data
T_{amb}: ambient temperature
T_m: average temperature of the metal

Thermal model

Hypothesis: Quasi-steady state condition

In the longitudinal direction, we can write:

- Heat balance on the external surface of the absorber tube
$$P_{ABS} = P_{SF} + P_{loss}$$
- First law of thermodynamics,
$$P_{SF} = \Delta\dot{H} + \Delta\dot{E}_k$$
- Relation for the conservation of mass,
$$\rho \cdot u = CONST$$
- Conservation of mechanical energy
$$\int_{in}^{out} v\,dp + \frac{u_{out}^2}{2} - \frac{u_{in}^2}{2} + Y = 0$$
- Convection heat transfer from inside surfaces of the absorber tube to the HTF,
$$P_{SF} = 2\pi D \cdot h_{conv} \cdot (T_m - T_{out})$$

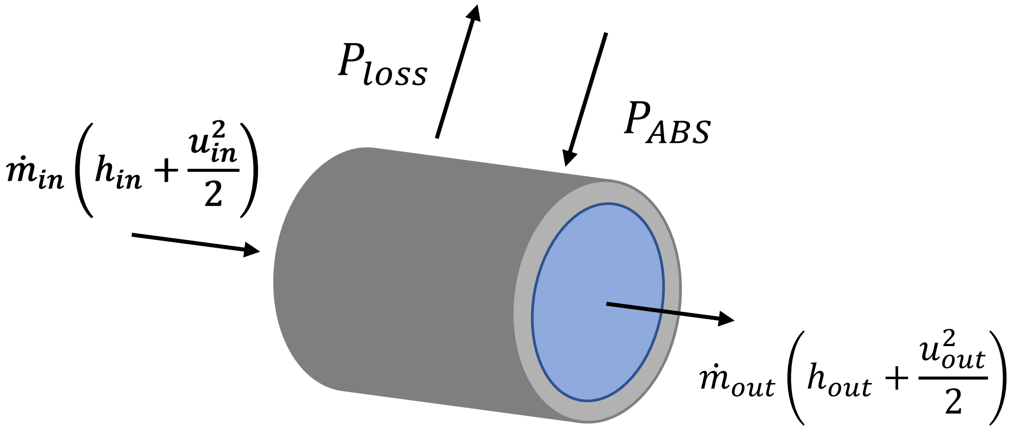

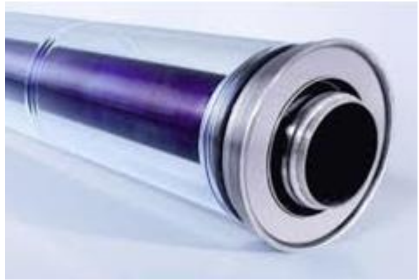

Hypothesis: Quasi-steady state condition

In the transversal direction, for a glass-enveloped receiver tube we can refer to the following figure and to the relative thermal resistance model:

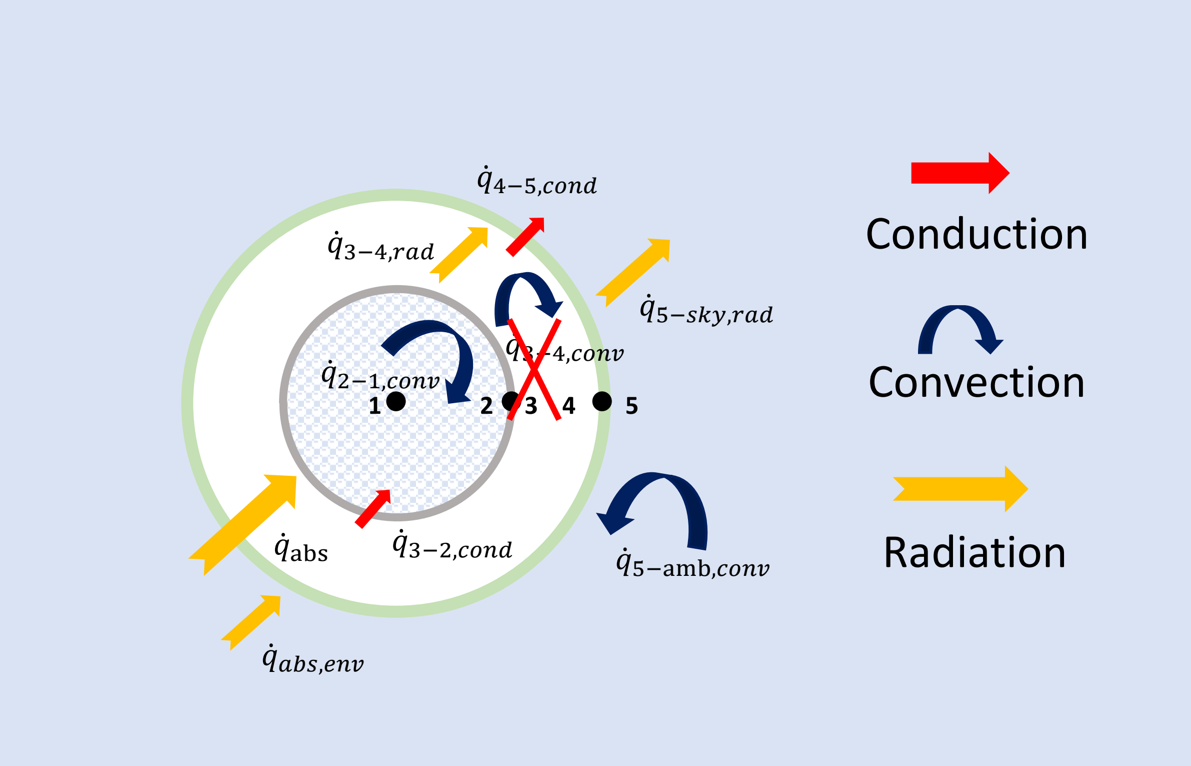

In the case of an evacuated tube receiver

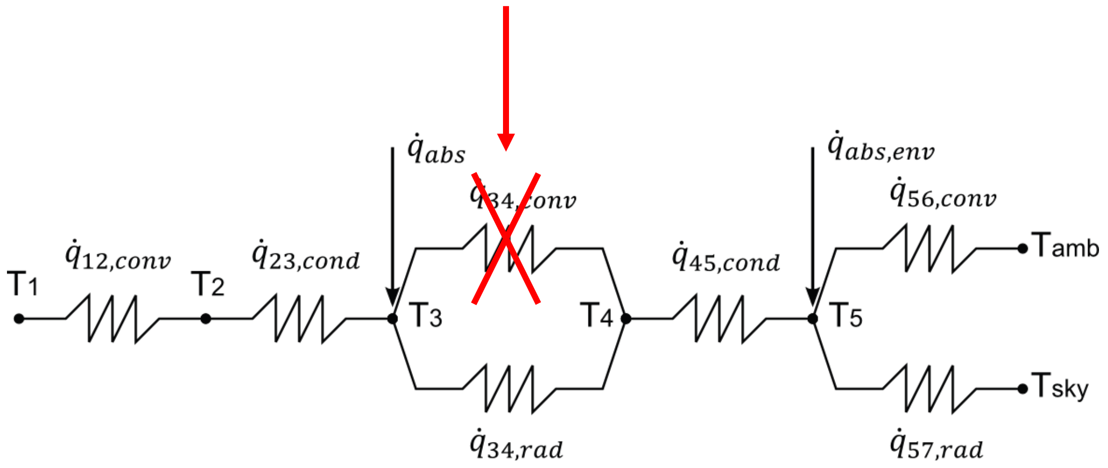

Hypothesis: Quasi-steady state condition

In the transversal direction, for an evacuated receiver tube with a secondary reflector we can refer to the following figure:

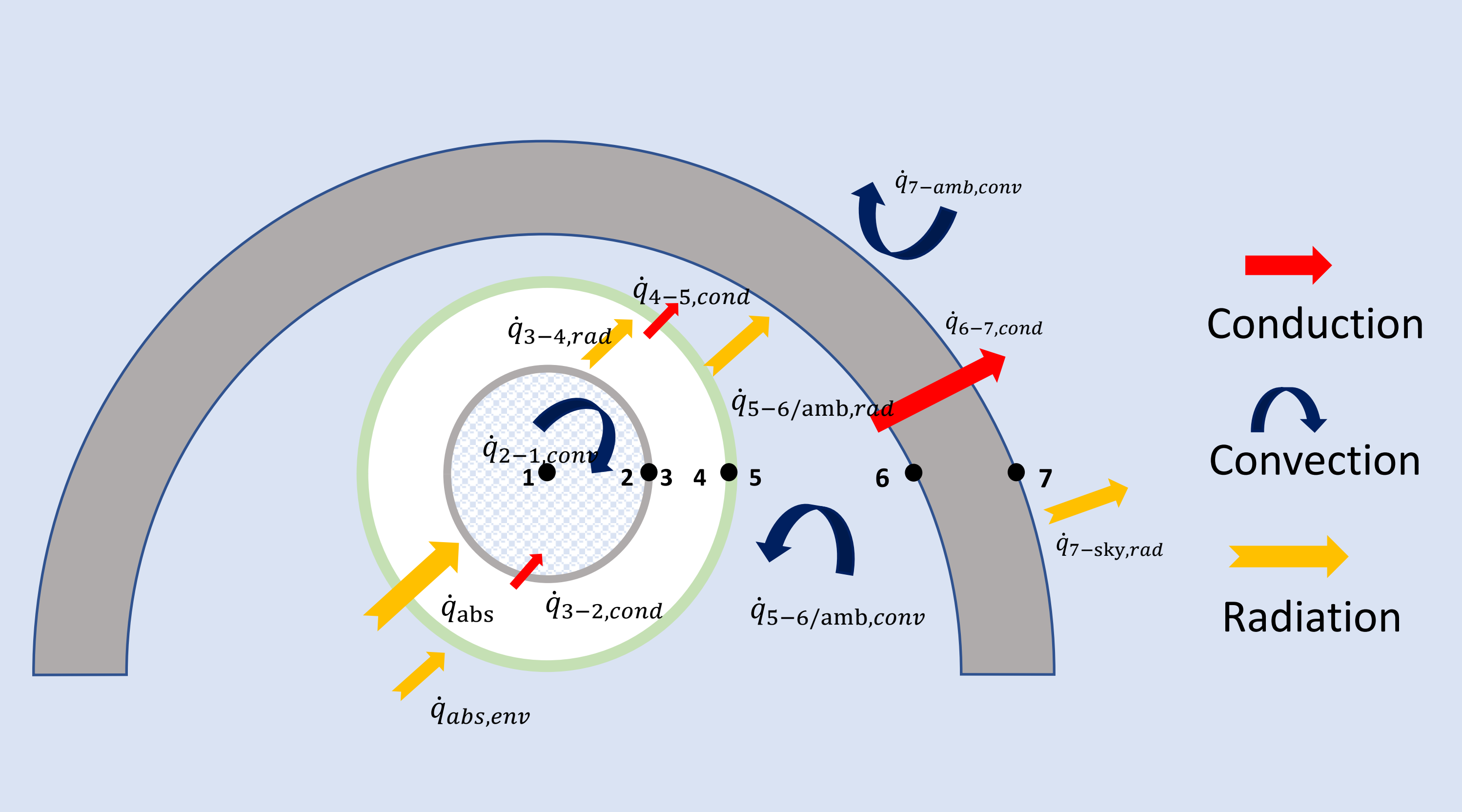

Optical and Thermal (Solar Field) model

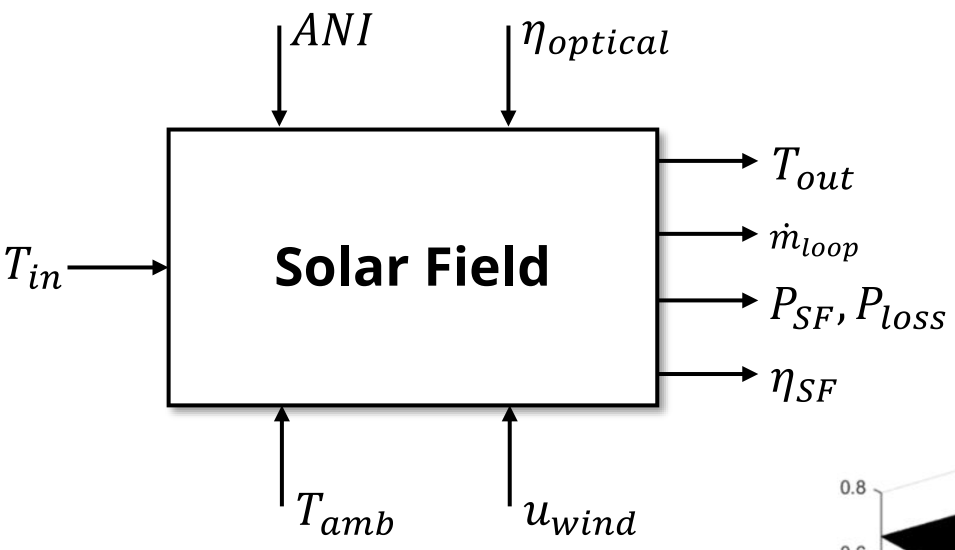

$$ANI = DNI \cdot IAM$$

$$\eta_{optical} = \eta_{optical,nom} \cdot f_{end} \cdot f_{shading} \cdot f_{cleanliness}$$

$$\eta_{SF} = f1(ANI, \eta_{optical}, T_{in}, u_{vento}, T_a)$$

$$\dot{m}_{loop} = f2(ANI, \eta_{optical}, T_{in}, u_{wind}, T_{amb})$$

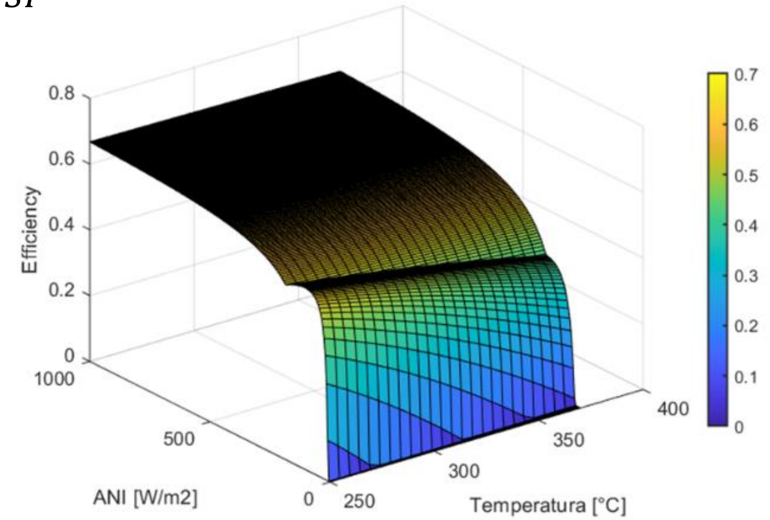

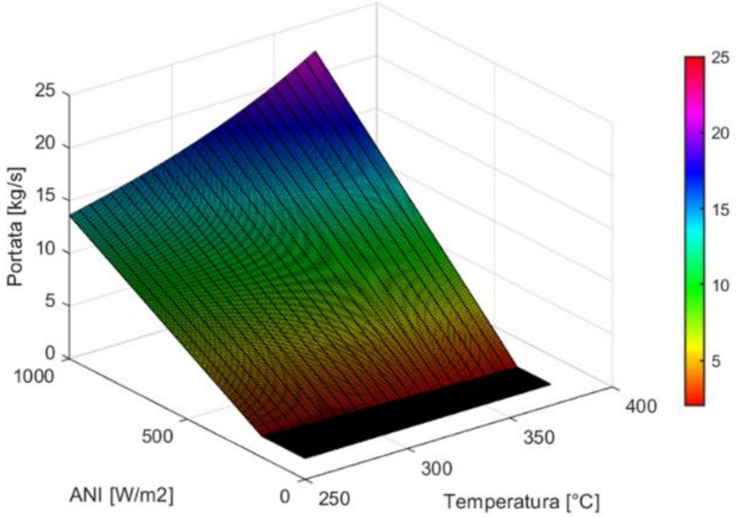

Piping model

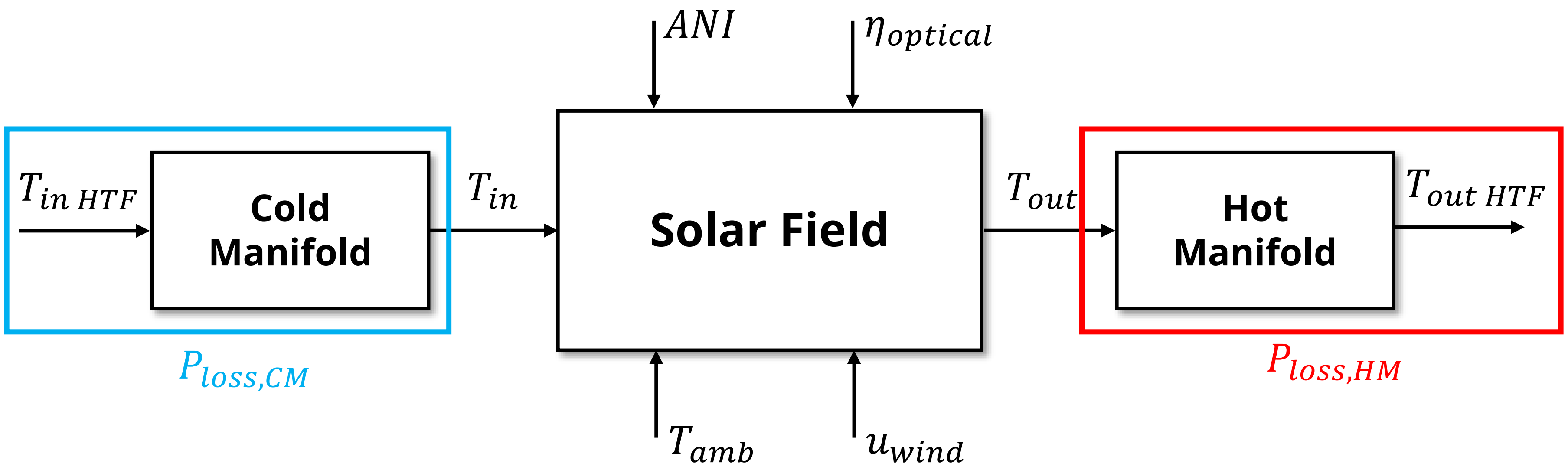

The heat losses in the piping system can be evaluated as:

$$P_{SF,CM} = U_{CM} \cdot (T_{in} - T_{amb})$$

$$P_{SF,HM} = U_{HM} \cdot (T_{out} - T_{amb})$$

$$U = \frac{1}{R_{HTF,conv} + R_{insul,cond} + R_{amb,rad+conv}}$$

Optical, thermal and piping model for a Parabolic Trough

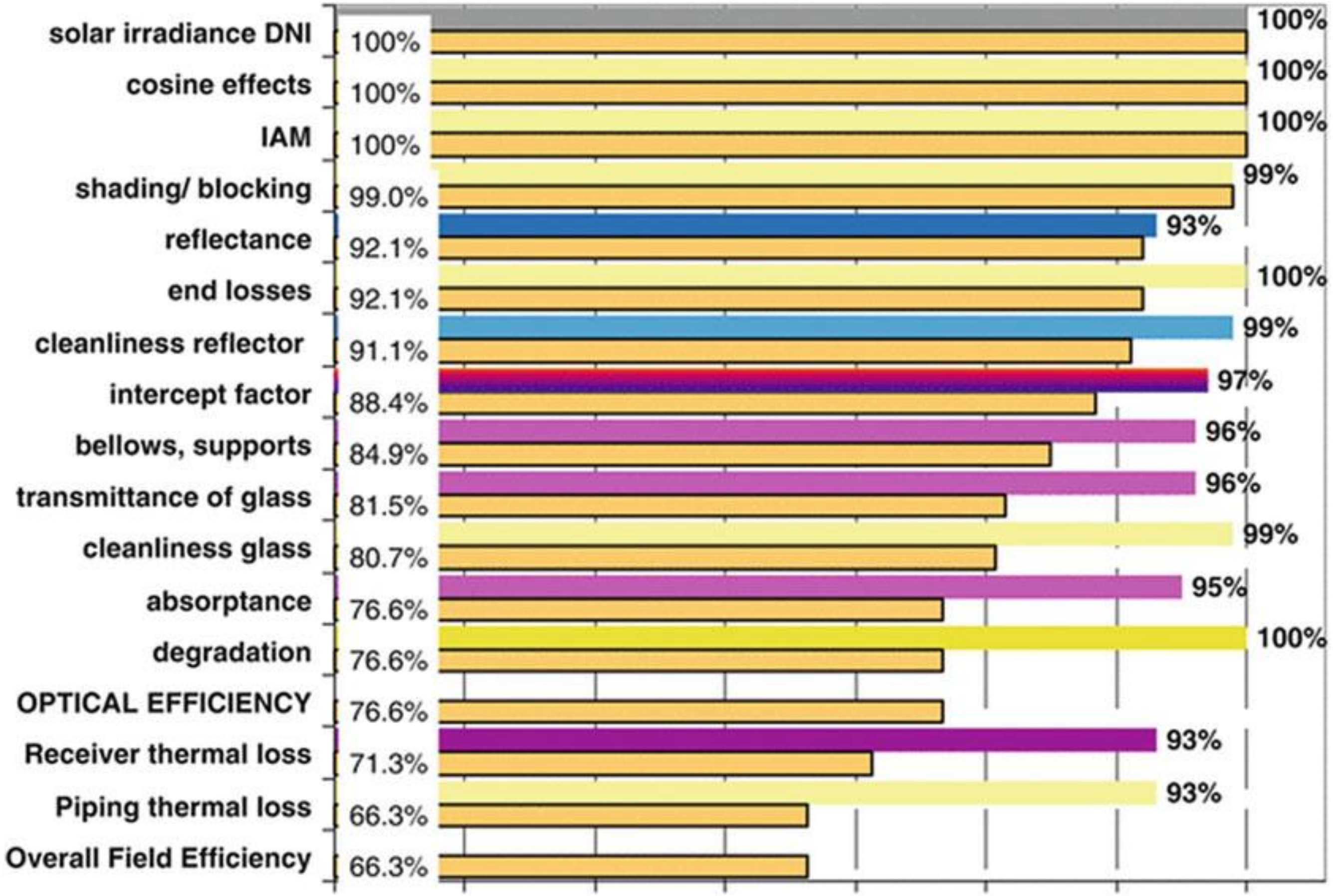

For each tank, we can write:

- First law of thermodynamics, $$\frac{dE_{TES}}{dt} = \sum \dot{Q}_{in,n} - \sum \dot{Q}_{out,n} - \dot{Q}_{loss,TES}$$

- Relation for the conservation of mass, $$\frac{dm_{TES}}{dt} = \sum \dot{m}_{in,n} - \sum \dot{m}_{out,n}$$

- Heat loss formula, $$\dot{Q}_{loss,TES} = U_{TES} \cdot (T_{TES} - T_{amb})$$

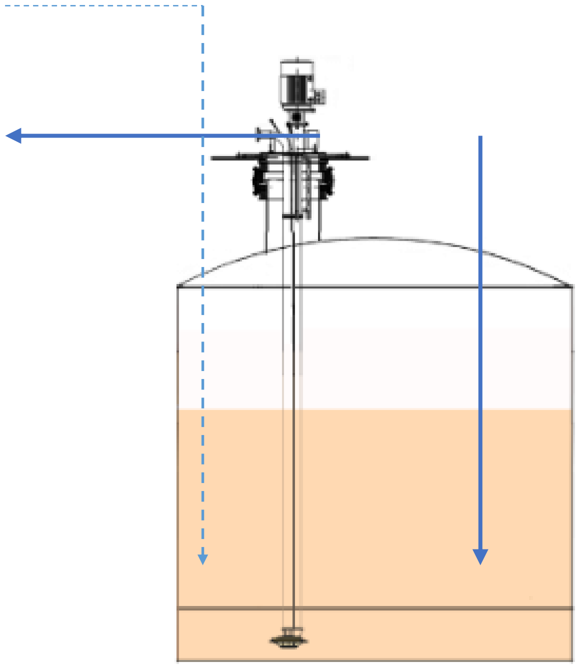

Power Block model

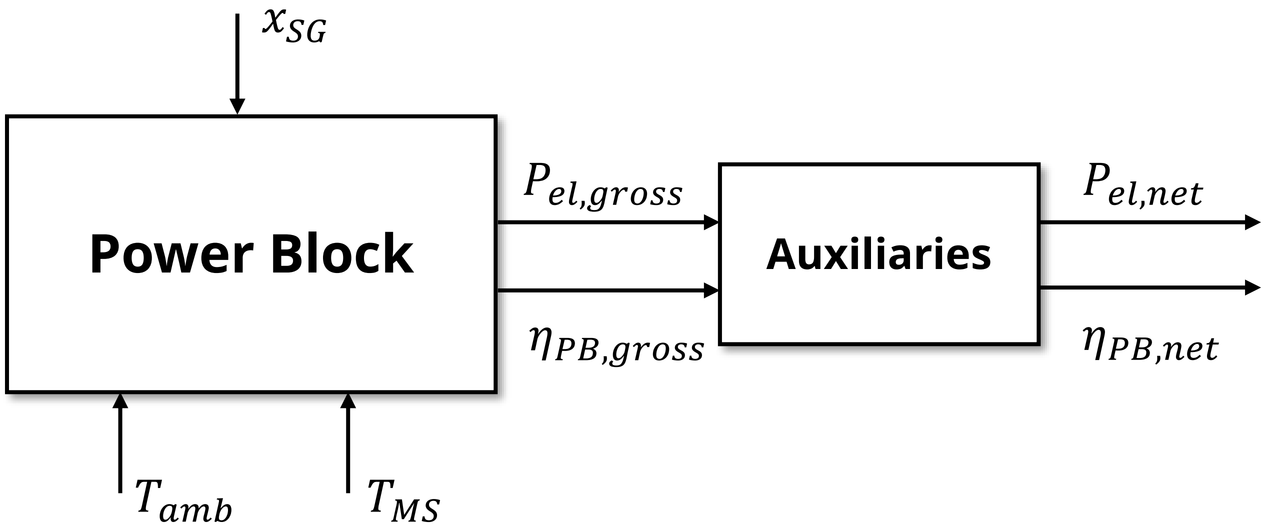

$$x_{SG} = \frac{P_{th,PB}}{P_{th,max}}$$

$$\eta_{PB} = \eta_{PB,nom} \cdot f(x) \qquad f: polynomial$$

$$\dot{m}_{PB} = \frac{P_{th,PB}}{\eta_{PB}\left(h_{in,PB} - h_{out,PB}\right)}$$

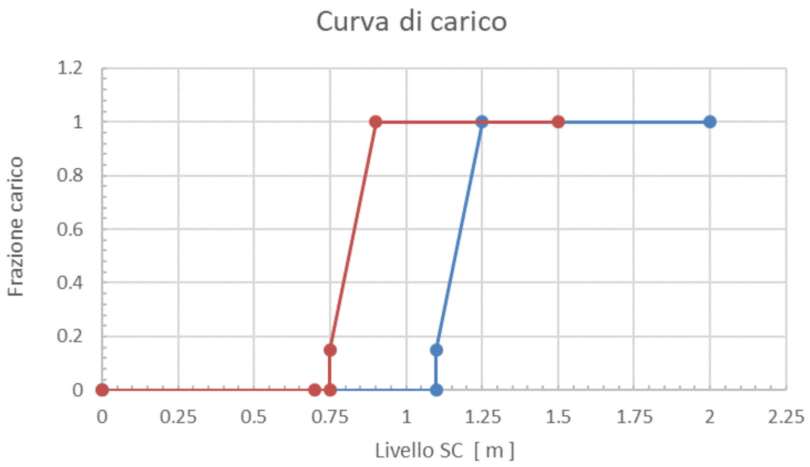

Control logic CSP Plant

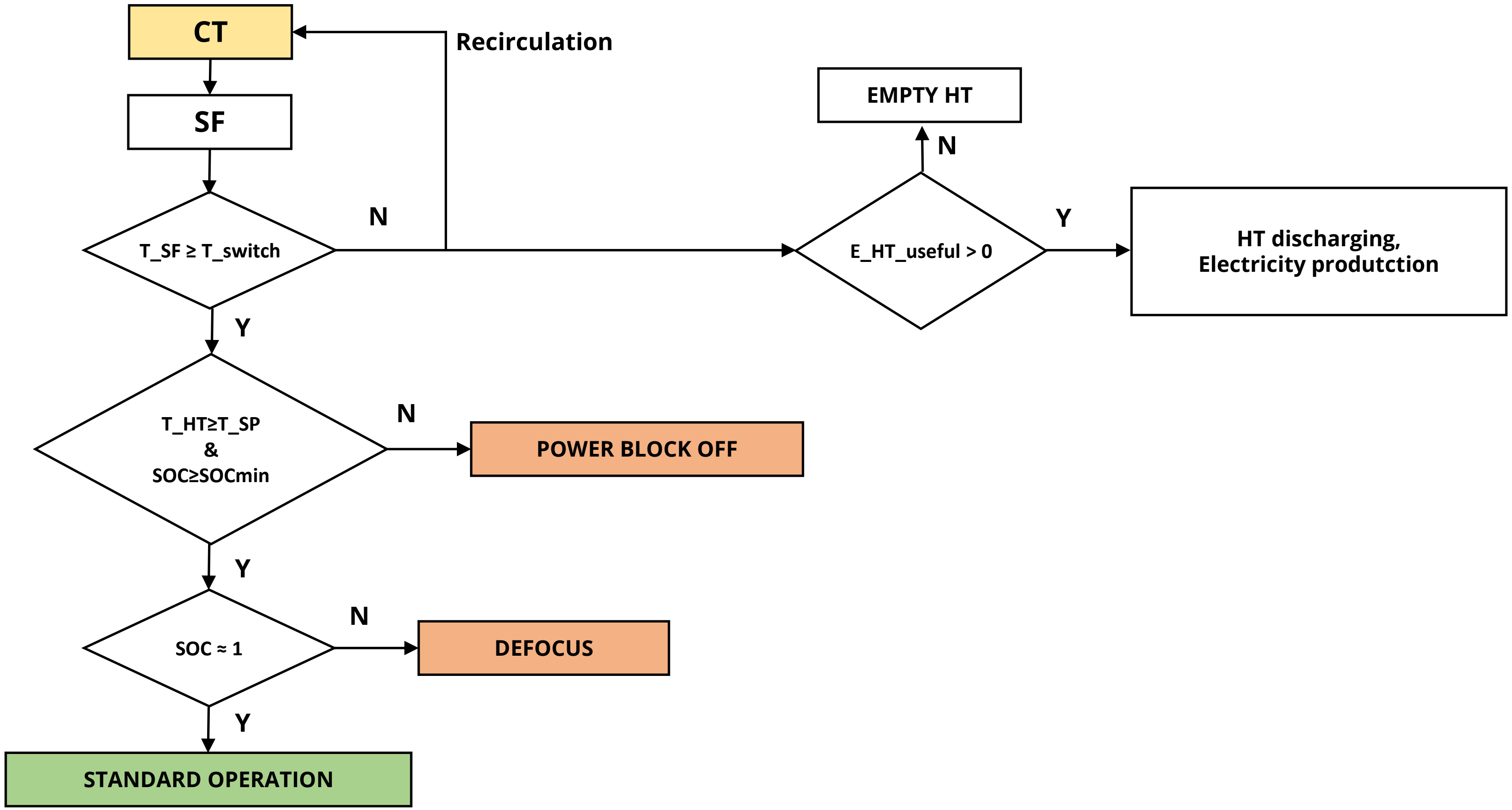

CSP Performance Simulation: Design Parameters

- **Nominal Gross Power**: $4.6\ MWe$
- **Nominal Power block Efficiency**: $\eta_{PB,gross} = \%$
- **Collector Technology:** Linear Fresnell Collector
- **Direction:** N-S
- $\boldsymbol{L_{loop}} = 800\ m$
- **Loop Number**: 7
- **Nominal Optical Efficiency**: $\eta_{optical,nom} = 70\%$
- **HTF**: binary mixture of molten salt (40% KNO_3 - 60% $NaNO_3$)
- $\boldsymbol{T_{max}} = 545\ °C$; $\boldsymbol{T_{min}} = 290\ °C$
- $\boldsymbol{\dot{m}_{loop}} = 2.0 \div 13.7\ kg/s$
- **TES**: Direct storage system with two tanks
- **HSM** ≡ HTF
- $\boldsymbol{h\_TES}$ = 12 h

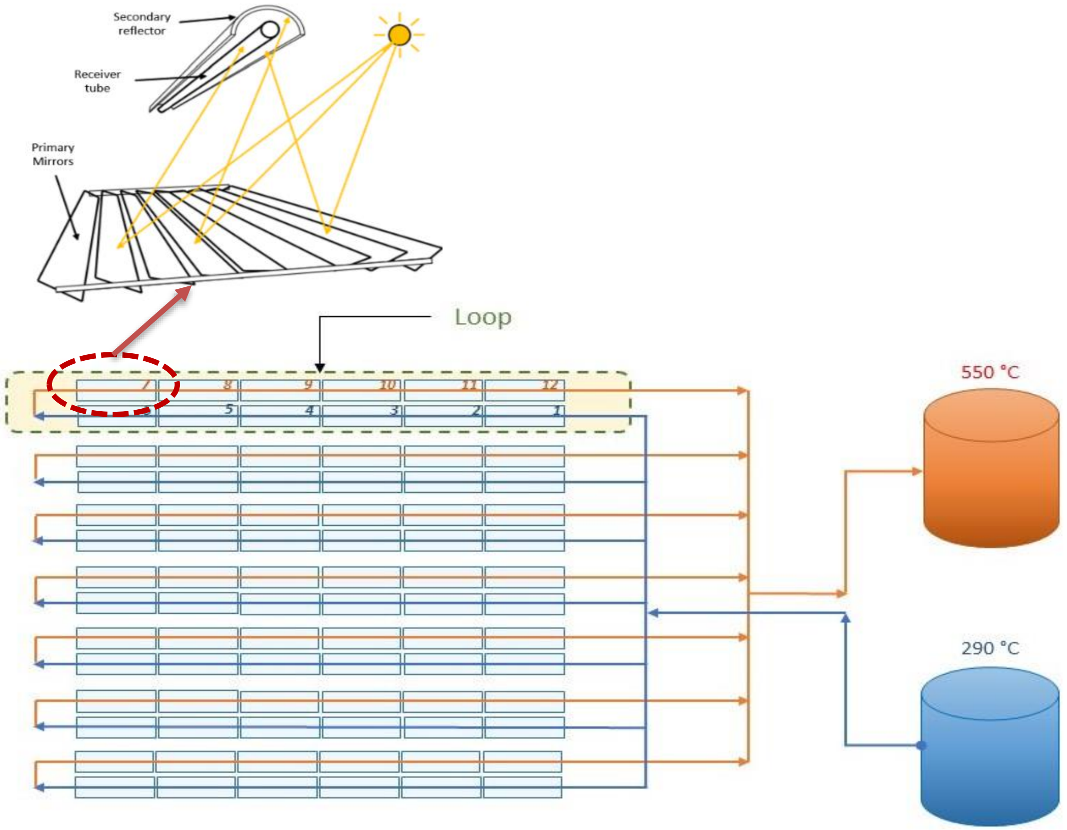

Daily Simulation: Solar Field

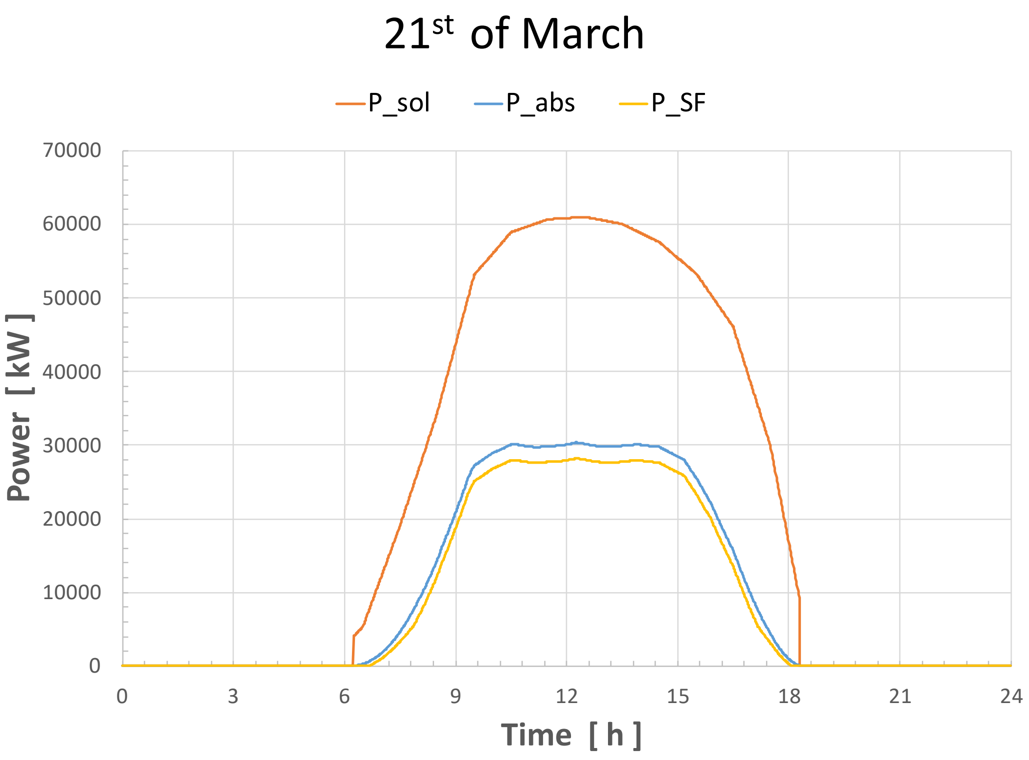

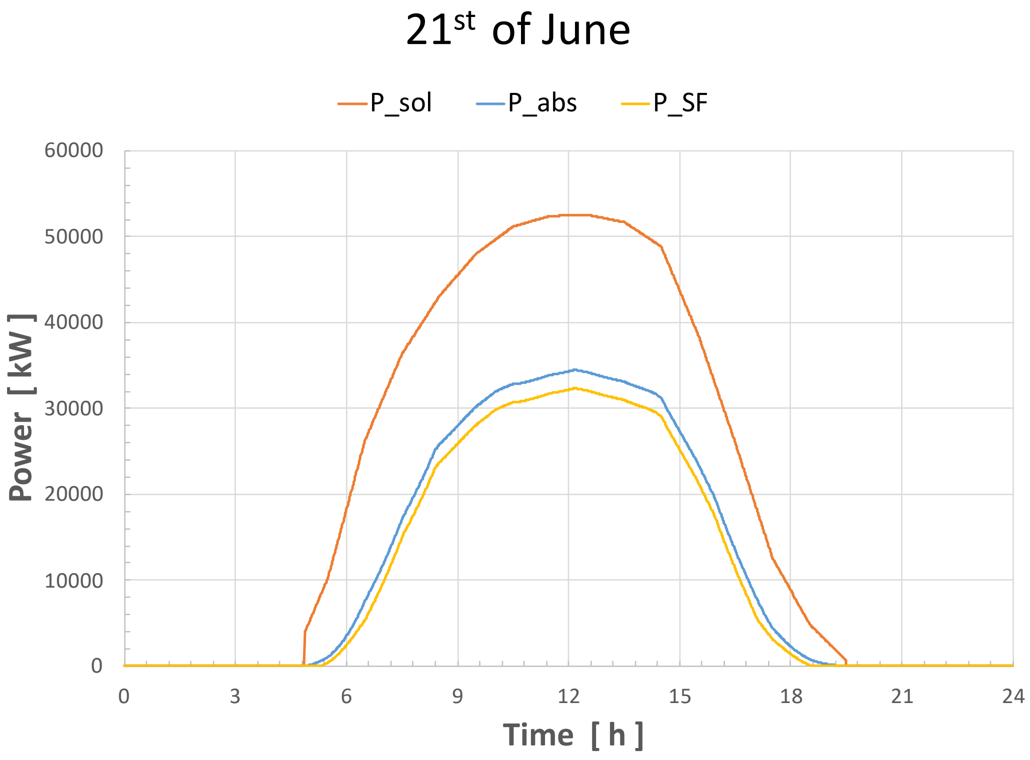

Daily Simulation: Thermal Storage

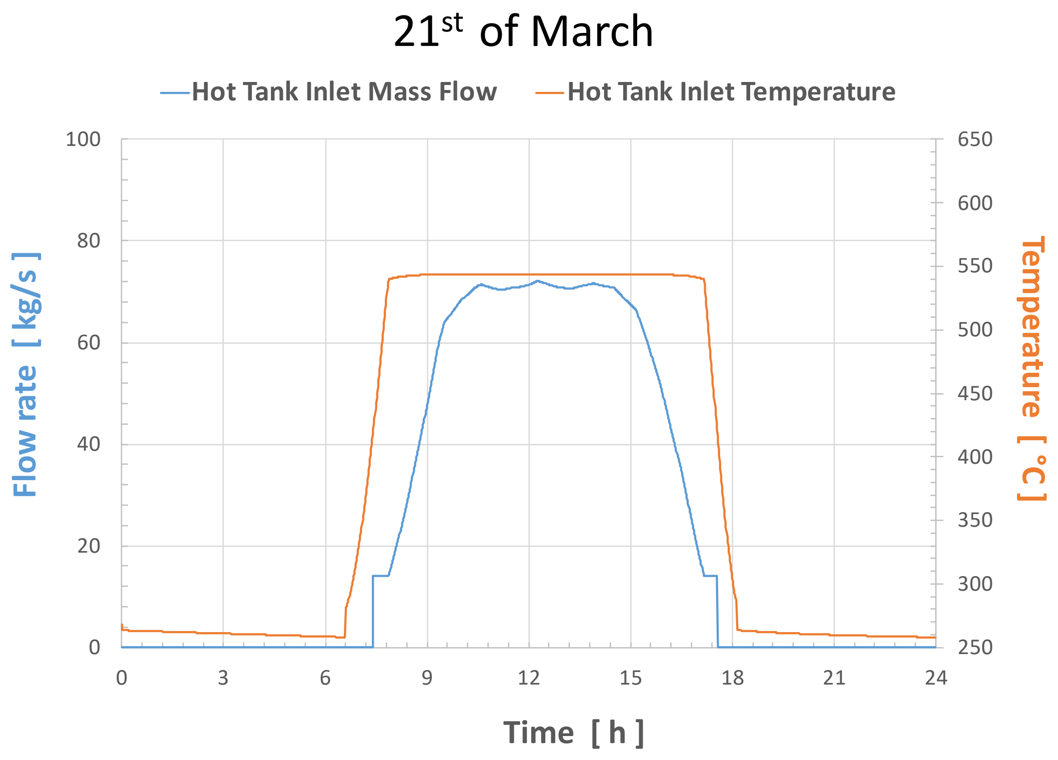

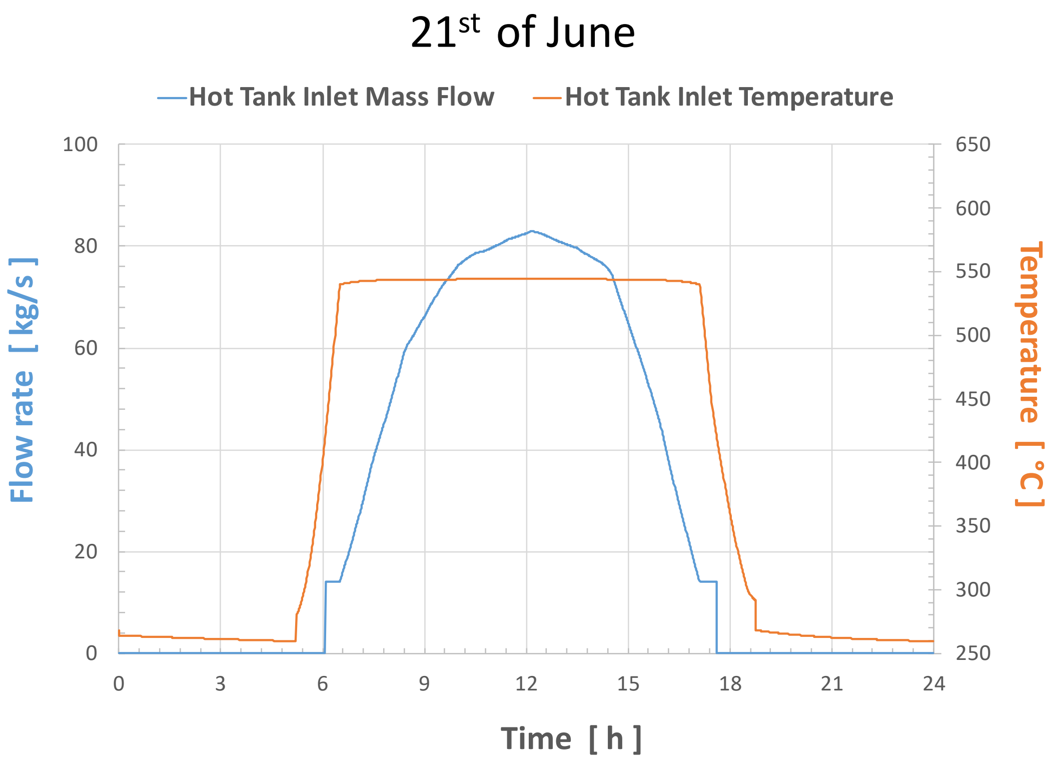

Daily Simulation: Thermal Storage

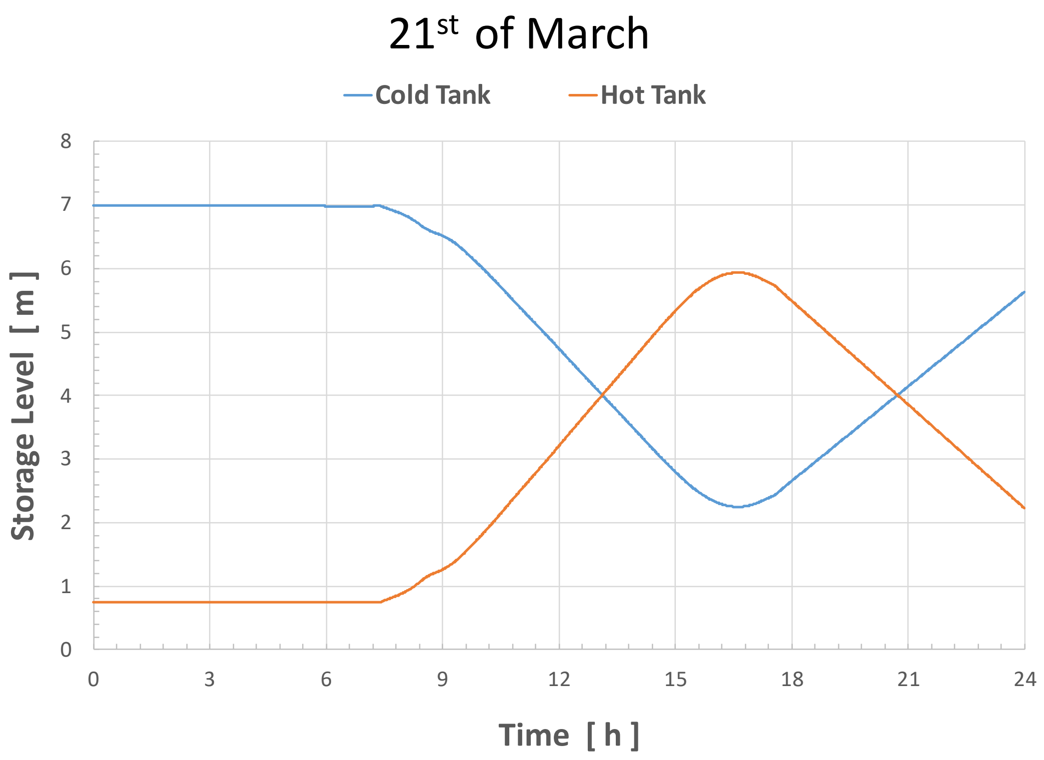

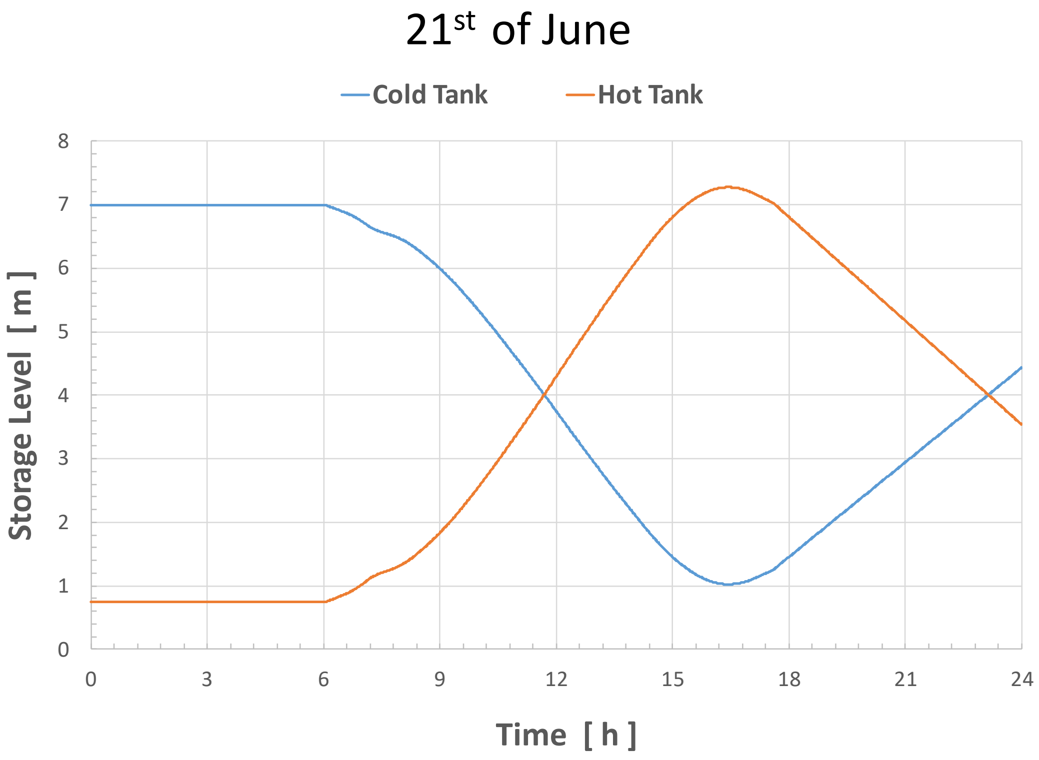

Daily Simulation: Power Block

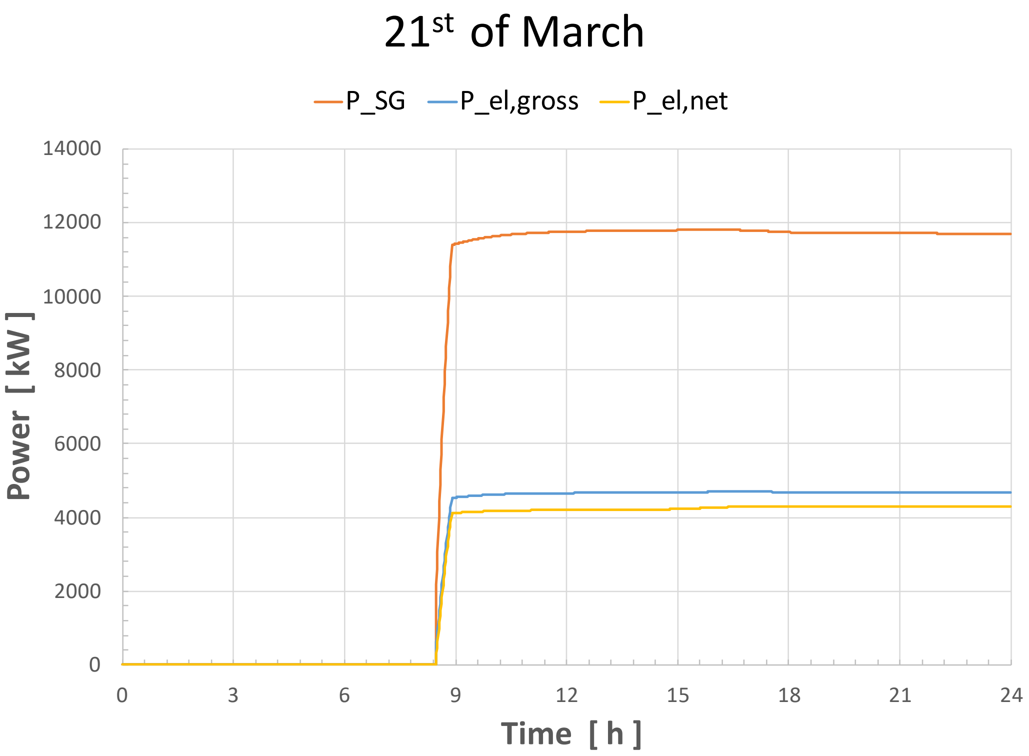

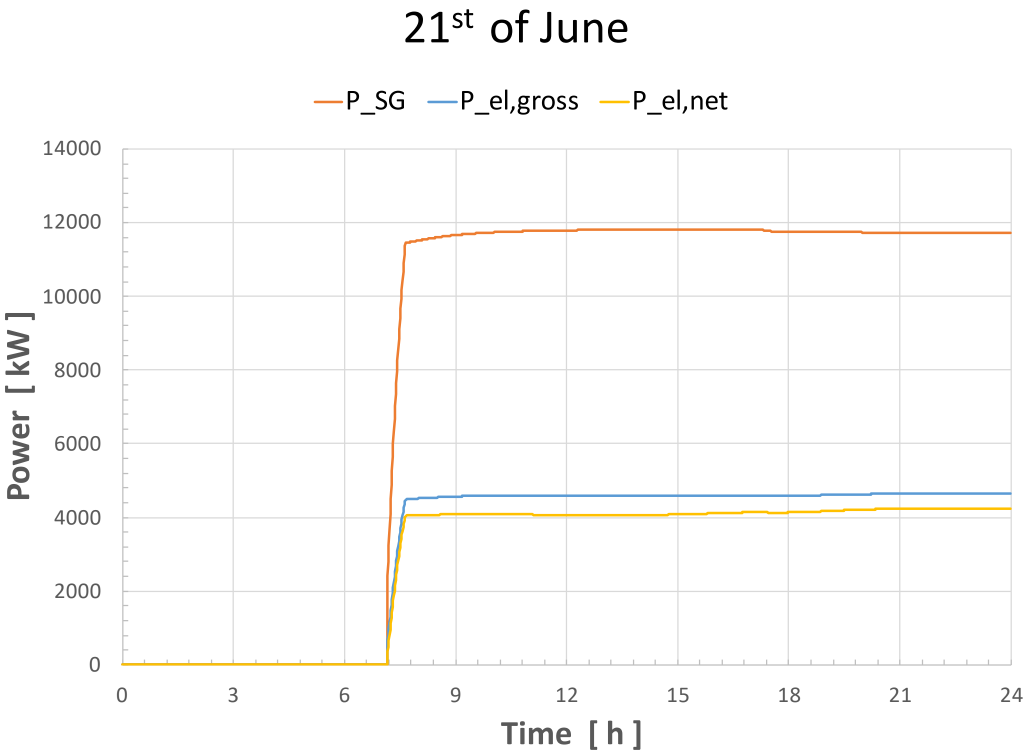

Daily Simulation: Summary Results

Energy (MWh)	21st March	21st June
Solar	543.2	503.7
Absorbed	240.9	288.3
Solar field net to HT	216.7	260.3
PB thermal	180.2	195.8
Gross Electric	71.7	76.6
Net Electric	64.4	68.1

Annul Simulation: Monthly Distribution

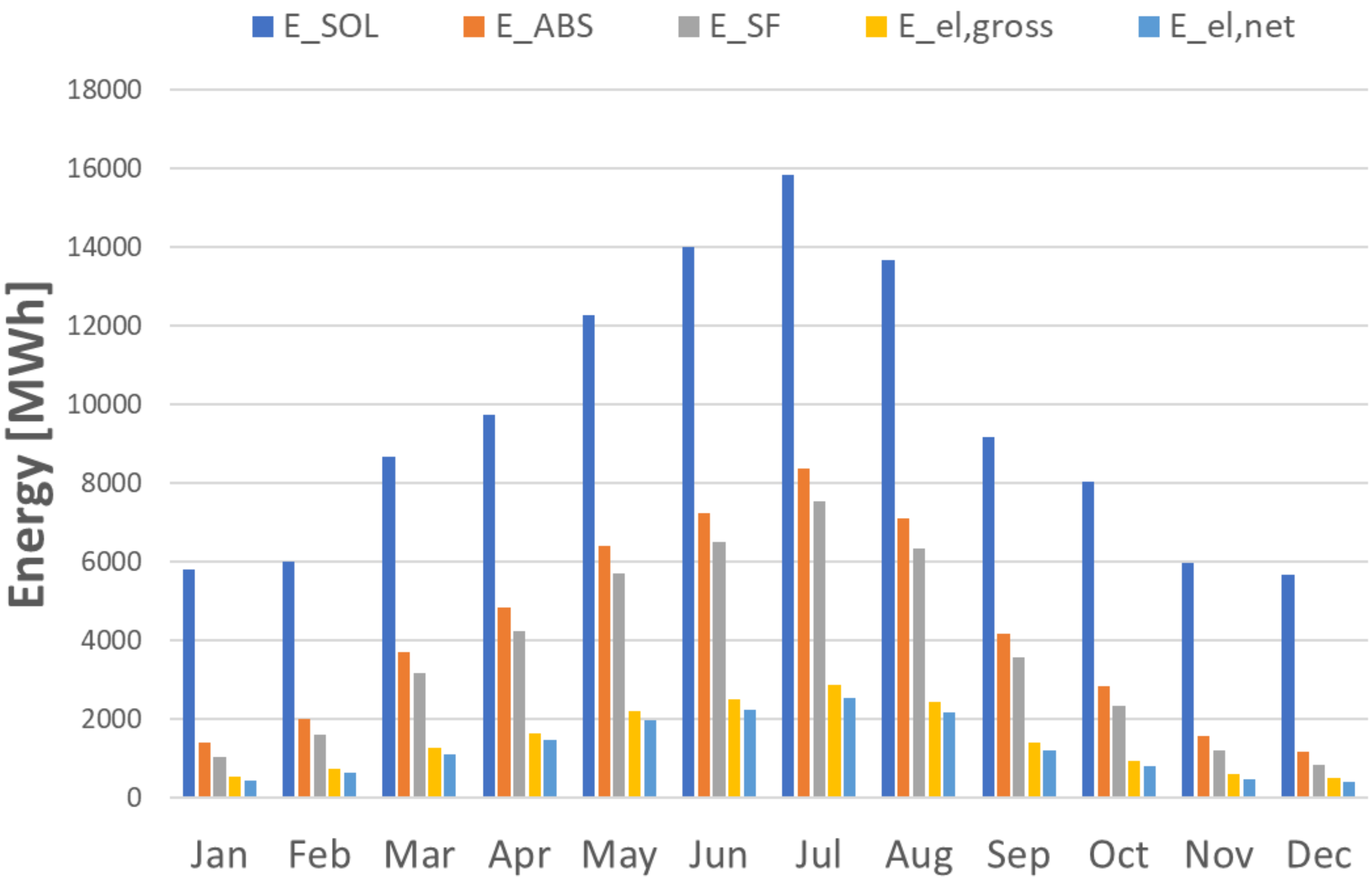

Annual Simulation: Summary Results

Energy	MWh
Solar	114873
Absorbed	50795
Solar field net to HT	45887
PB thermal	44984
Gross Electric	17645
Net Electric	15436

Efficiency	%
Optical	44.2
Thermal	90.3
Solar field (Optical+Thermal)	39.9
Power Block net	34.3
Overall	13.4
Capacity Factor	38.3

Valeria RUSSO, PhD
ENEA
TERIN-STSN-ITES
valeria.russo@enea.it

THANK YOU FOR YOUR ATTENTION!
ANY QUESTIONS?

SFERA-III
Solar Facilities for the European Research Area

4th Training for Industries
7-11th November 2022, Cr ENEA Casaccia Rome (Italy)

Low maintenance reflective surfaces for CSP plants

ANNA CASTALDO (ENEA, TERIN-STSN-SCIS)

JOINT RESEARCH ACTIVITIES

THIS PROJECT HAS RECEIVED FUNDING FROM THE EUROPEAN UNION'S HORIZON 2020 RESEARCH AND INNOVATION PROGRAMME UNDER GRANT AGREEMENT NO **823802**

OUTLINE

- **REFLECTIVE SURFACES: mirrors and reflectors architecture, materials and durability, solar weighted hemispherical reflectance.**
- **LCOE and MAINTENANCE COSTS.**
- **SOILING and CLEANING.**
- **«WETTABILITY» : hydrophobic, hydrophylic and SELFCLEANING surfaces, Wetting Contact Angle (WCA°) measurement.**
- **COATINGS or TREATMENTS? Experimental considerations.**
- **AUXETIC OPTICAL METAMATERIALS: INORGANIC Aluminum nitride politypoids; POLYMERS: Hybrid nano-composites.**
- **From lab to industrial scale.**
- **NEXT GOAL: «smartization of solar field» by means of adding sensor performance to coatings.**

Reflective surfaces introduction


For the use of solar energy on an industrial scale concentrating solar power technology offers a valid solution to capitalize the enormous potential coming from the Sun. The original Archimede's idea of focalizing sun light by means of reflecting surfaces for burning enemies approaching ships was used by Siracusa's state-city to repel Romans attack during the second Punic war. Nowadays, although it differs in terms of the components and the variety of reflector configurations used, this technology shares the same idea for the production of energy from a solar source.




Optical concentrators are **REFLECTIVE SURFACES** used in a variety of solar collectors in order to REDIRECT sunlight onto a receiver surface. The active reflecting element is a SOLAR **MIRROR** supported by a backing structure which maintains its shape, both constitute the **REFLECTOR**. The reflector quality in a CSP system directly influences the amount of solar radiation that can be converted into power.



flat
curved with one dimensional curvature as in a parabolic trough
curved with two dimensional curvature as in a parabolic dish

Reflective surfaces: optics

The ability to REFLECT the majority of the incident sunlight can be quantified by the ***solar-weighted* hemispherical** reflectance.***
The ability to re-direct the incident sunlight to the receiver with minimal loss can be quantified by the ***specularity.*** *Typically $\varphi \leq 20$ mrad, therefore the reflectance concerning CSP can be referred to as* ***near-specular.***

**solar weighted because not all parts of the solar spectrum have the same amount of energy.* Solar weighting of the reflectance parameters is *calculated with the currently valid standard solar spectrum ASTM G173 for direct irradiance and the appropriate Air Mass (i.e. for Europe and USA it is AM 1.5).*
*** hemispherical because the reflection properties can change depending on the incidence angle of the incident radiation*

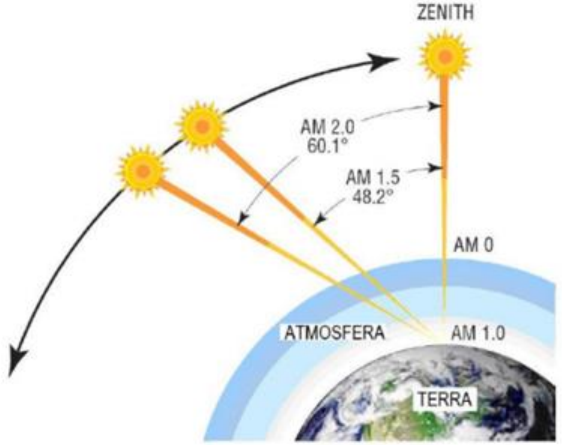

$$\alpha+\tau+\rho = 1$$

$$\rho_{\lambda,\phi}(\lambda,\theta_i,\phi) = \rho_{\lambda,h}(\lambda,\theta_i,h)\cdot\left[1-\sum_{j=1}^{M}K_j\exp\left[\frac{-\phi^2}{2\sigma_j^2(\lambda,\theta)}\right]\right]$$

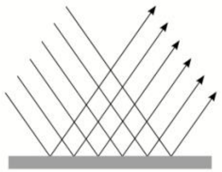

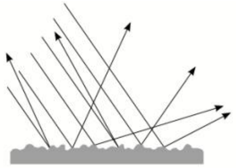

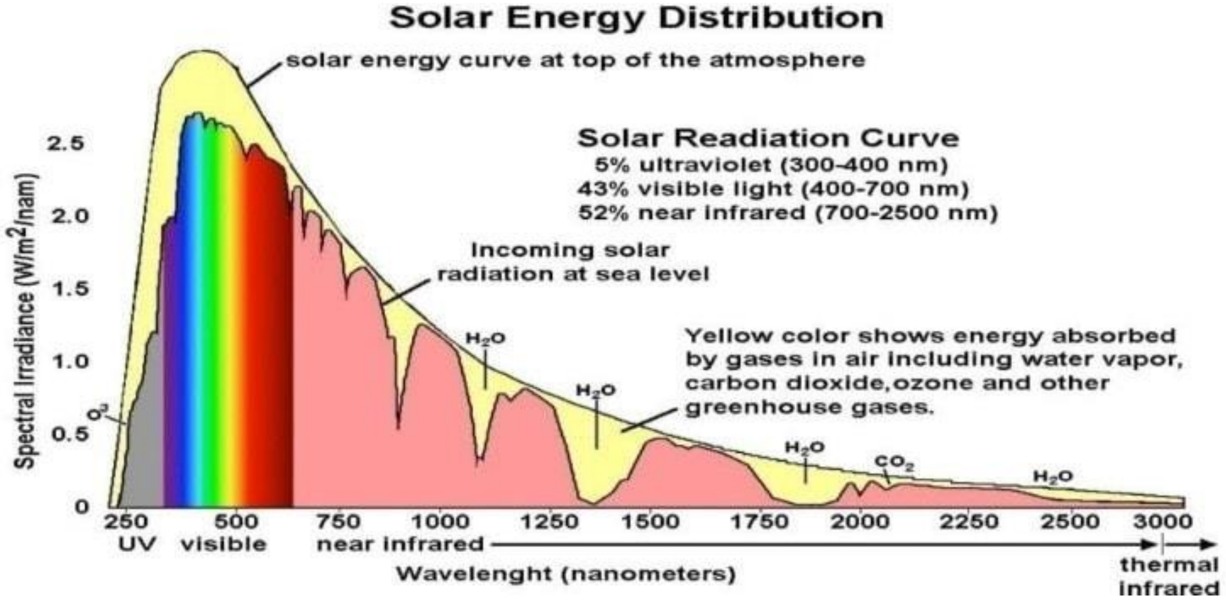

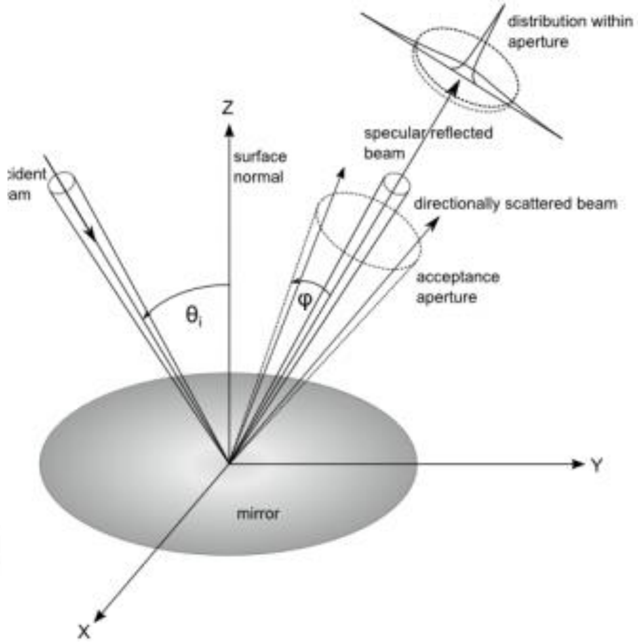

SOLAR MIRRORS
Typology

- **SOLAR AVERAGED REFLECTANCE PROPERTIES SHOULD BE AS CLOSE TO UNITY AS POSSIBLE**

Reflectance is dependent on the wavelength, λ, the angle of incidence, ϑ_i, between the incoming light and the normal to the mirror surface, light polarization, the angle of acceptance, φ.

- **DURABILITY/ROBUSTNESS**

At least 10 years in field exercise conditions.

BSM
Back surface mirror.
Second surface mirror.

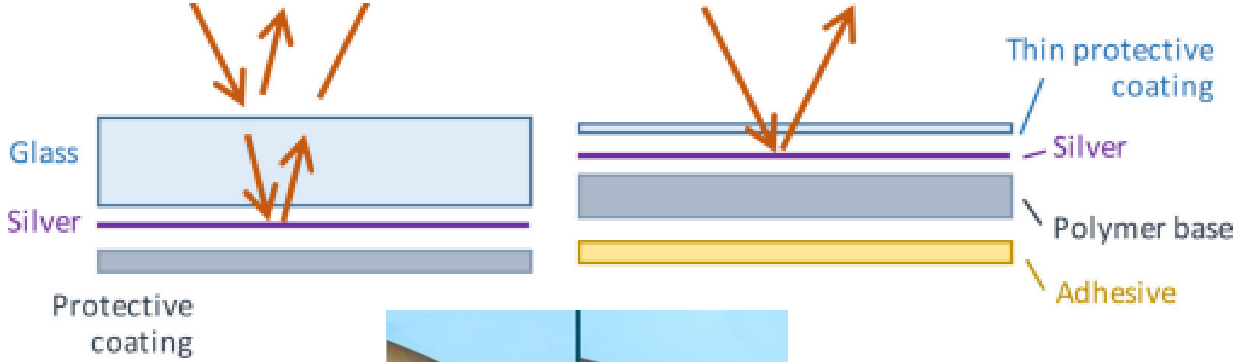

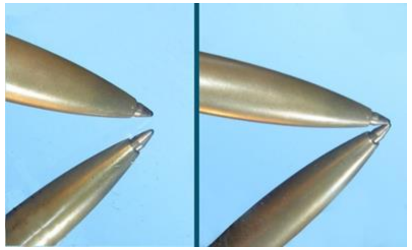

FSM
Front surface mirror.
First surface mirror.

SOLAR MIRRORS production

Mirror making

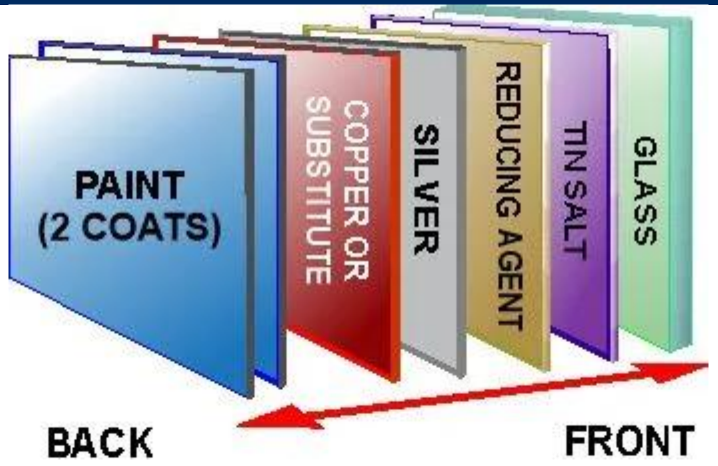

Production line for mirror making – The silvering process takes place on giant production lines, starting with sheets of glass at one end and finished mirrors at the other.

Low-iron Glass (1-mm to 4-mm thick)
Reflective Layer (wet – silver)
Back Layer (Cu) (Cu –less)
1st Coat Paint Layer (20% Pb ⟶ 2.5% Pb) (lead – free <0,15% Pb or < 5 ppm BP)
2nd Coat Paint Layer (20% Pb 2.5% Pb) (lead – free <0,15% Pb or < 5 ppm BP)
UV / Moisture / Adhesive Barrier Layer
Adhesive (PS, spray)
Substrate (SS, Al)

PMMA superstrate
Reflective Layer (100 nm Ag)
Pressure Sensitive Adhesive (PSA)
Substrate

Anti-soiling Layer
PMMA superstrate
Adhesion Promoting Layer (1-10 nm)
Reflective Layer (100 nm Ag)
Metal Back Layer (30- 50 nm Cu)
Pressure Sensitive Adhesive (PSA)
Substrate

Abengoa

SOLAR MIRRORS materials properties

Table 1
Reflective and semi-transparent solar materials considered in this study [1].

Sample name	Product description	Thickness	Intended environment	Performance reported by manufacturer	
Back-silvered glass				$R_{direct,solar}$ [2]	
AgGlass4 mm	Flat glass mirror (2014)	4 mm	Outdoor	≥ 0.945 [3]	
AgGlass2 mm	Flat glass mirror (2013)	2 mm	Outdoor	≥ 0.945 [3]	
AgGlass1 mm	Flat glass mirror (2008)	1 mm	Outdoor	≥ 0.945 [3]	
Metallized polymer films				$R_{h,solar}$	$R_{specular, 660\ nm, 15°, 25\ mrad}$
AgFilm1	Silvered acrylic film	117 μm	Outdoor	0.94	> 0.95 [4]
AgFilm2	Silvered polymer film	100 μm	Outdoor	0.93	0.94 [5]
AlFilm	Aluminized boPET	23 μm	Indoor	[6]	
Metallized aluminum sheets				$R_{h,solar/light}$	$R_{specular, 60°\ ISO\ 7668}$
AgSheet1	Silvered aluminum sheet	0.5 mm	Indoor	≥ 0.95	≥ 0.92 [7]
AgSheet2	Silvered aluminum sheet	0.4 mm	Indoor (lighting)	≥ 0.98	≥ 0.93 [8]
AgSheet3	Silvered aluminum sheet	0.3 mm	Indoor (lighting)	≥ 0.98	≥ 0.93 [9]
AlSheet	Aluminized aluminum sheet	0.4 mm	Outdoor	≥ 0.89	≥ 0.88 [10]
Transparent polymer films					
ETFE100 μm	ETFE film	100 μm	Outdoor	[11]	
FEP100 μm	FEP film	100 μm	Outdoor	[12]	
Transparent glass				$T_{normal,solar}$	
Borosilicate3.3 mm	borosilicate substrate	3.3 mm	Outdoor	0.92 [13]	
BorosilicateAR3.3 mm	AR-coated borosilicate	3.3 mm	Outdoor	0.97 [14]	

SOURCE: P. Good, T. Cooper, M. Quercia, N. Wiik, G. Ambrosetti, A. Steinfel, “Spectral reflectance transmittance, and angular scattering of materials for solar concentrators”, Sol. Energy Mater. Sol. Cells, n.144 (2016), pp. 509-522.

CONSIDERATIONS:

- Ag better than Al
- BSM better than FSM

Problems to solve: operating life, corrosion, abrasion, soiling, photo-degradation.

Degradation types of reflector materials used in concentrating solar thermal systems

Defect type	Damaging agent	Example	Defect type	Damaging agent	Example
Abrasion	Contact cleaning		Corrosion spots	Humidity, chlorides, pollutant gases	
Erosion	Airborne particles	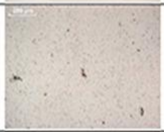	PVD-layer corrosión (observed for aluminum reflectors only)	Humidity, chlorides	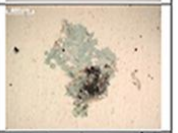
Stains on the glass	Humidity and chemicals		Micropitting (observed for aluminum reflectors only)	Humidity, chlorides	
Deposits	Airborne particles and humidity	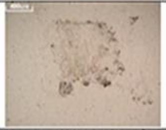	Tarnishing	Temperature, humidity	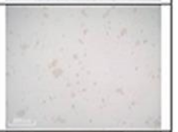
Paint deterioration	UV radiation		Blisters	Humidity	
Edge corrosion	Humidity, chlorides, pollutant gases		Delamination	Thermal cycling	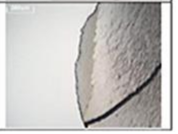

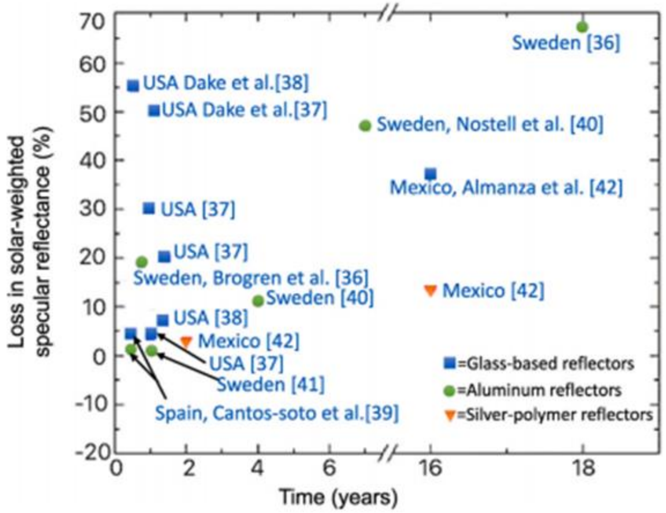

Common durability tests used to assess mechanical hardness and robustness of coating for cover glass of solar systems.

Water Jet Erosion	ASTM G73	For erosion studies, creates simulated impingement conditions between high-speed rotating blades and liquid droplets.
Rain Test	MIL 810 (Procedure 3) Rain drip test	Applicable for mild rain condition or falling of water from condensation or leakage from upper surface
	MIL 810 (Procedure 1) Blowing rain	Actual rain condition with varied aggressiveness
Damp Heat Test	–	Surfaces are exposed to ~85 °C and 85% relative humidity (RH) for several thousand hours
Temperature Tolerance	–	Several heating and cooling cycles at temperatures ranging from −10 to 100 °C
Solution/Solvent Immersion Test	–	Aqueous solutions: DI water, 3.5 to 5 wt% NaCl in water, acidic and alkaline solvent with pH varying from 0 to 14, in either hot or cold conditions. Organic solvents: Ethanol, acetone, isopropanol,

SOURCE:García-Segura, F. Sutter, L. Martínez-Arcos, T.J. Reche-Navarro, F. Wiesinger, J. Wette, F. Buendía-Martínez, A. Fernández-García,
Degradation types of reflector materials used in concentrating solar thermal systems, Renewable and Sustainable Energy Reviews,143, 2021,110879,
ISSN 1364-0321,
https://doi.org/10.1016/j.rser.2021.110879.

SOLAR MIRRORS costs

- **COSTS**

Solar field costs represent 30-50% of the initial capital investment for solar power plants depending on the energy policy and economic framework in the location country. It is of interest to design as less expensive as possible mirrors for large-scale manufacturing.

d ~1.1 Mm^2 solar field
Silvered glass, 4mm
Reflectivity: 93.5%

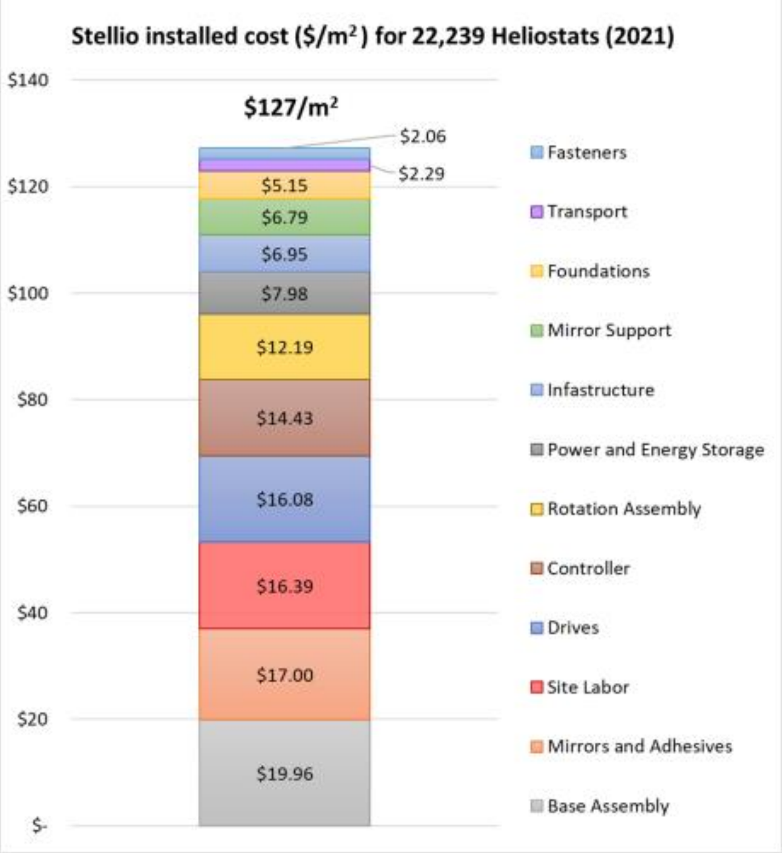

). Installed cost for the Stellio assuming 22,239 heliostats yielding 1,078,592 m^2 of aperture area

Total installed cost is estimated at $127/$m^2$.
Chart by Stephen Glynn and Sertac Akar, NREL

__The Stellio heliostat deployed at commercial scale by Schlaich Bergermann und Partner (sbp) sonne GmbHand is being used at the 50-megawatt electric (MW_e) Hami Concentrating Solar Power (CSP) power tower plant in China.__ For the Stellio solar field of 1,078,592 m^2 that was comprised of 22,239 heliostats, the estimated installed cost was $127/$m^2$.

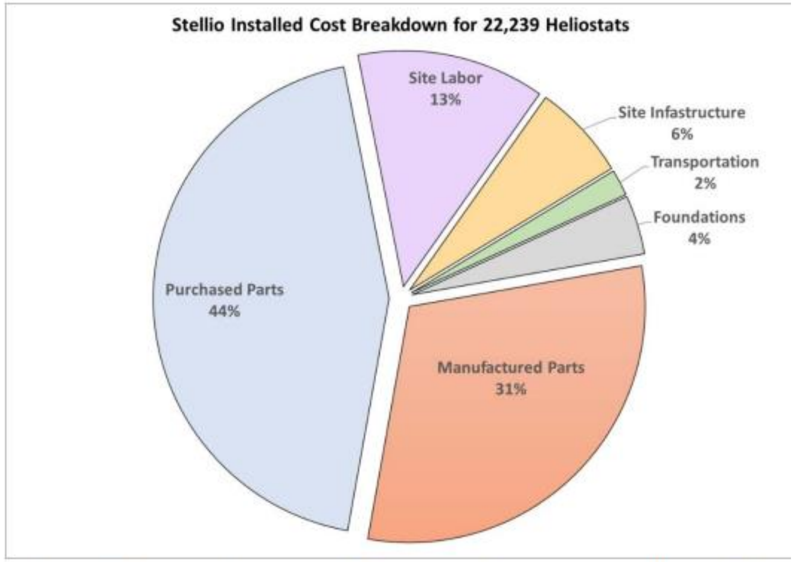

Figure 11 Total installed cost breakdown by category for sbp Stellio heliostat

Chart by Stephen Glynn and Sertac Akar, NREL

SOURCE: *Technical Report NREL/TP-7A40-80482 February 2022*

LCOE and maintenance costs

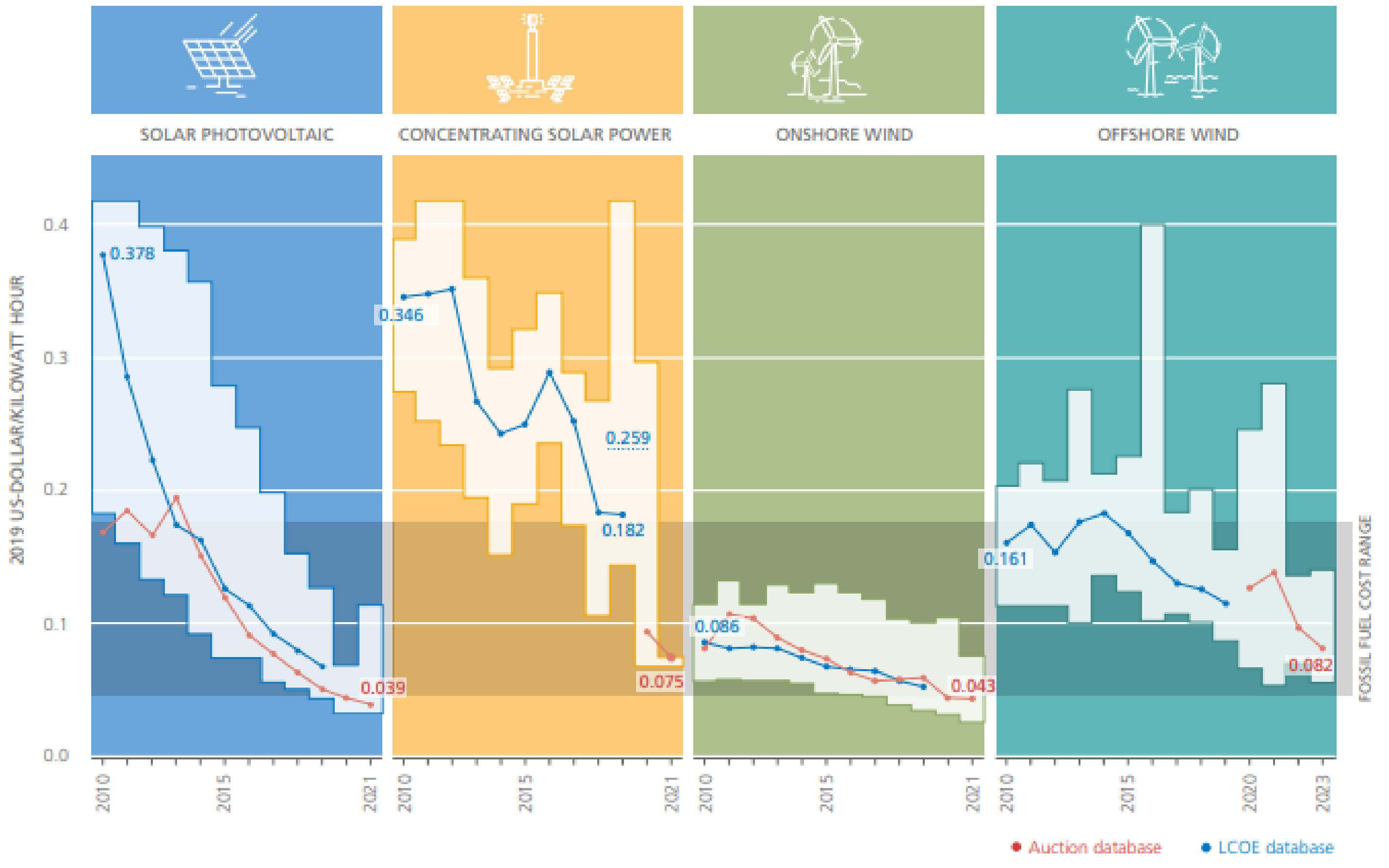

Cost development of energy generation using renewable sources since 2010. The grey shaded area shows the range of costs for fossil power generation. (IRENA 2020: Renewable Power Generation Costs)

Utility-scale solar power plants are currently being proposed at numerous sites.
The **LCOE** for new solar power plants into operation in 2020 and 2021 are between **0.073 US dollars and 0.094 US dollars per kilowatt-hour** that is 48 to 59 % below the calculated costs for 2019. While there are obvious local, regional, and global environmental benefits of large-scale solar power (e.g. jobs, low pollution, low fossil-fuel consumption, domestic resource, etc.), local environmental impacts must also be considered. The greatest local impacts relate to **the use** of land and **water.**

$$LCOE = \frac{\text{Present value of total investment over plant life (USD)}}{\text{Present value of total energy generated over plant life (kWh)}}$$

$$OPEX(i) = 0.02 \times CAPEX \times (1 + ir)^{i-1}$$

The Operation and maintenance EXpenditure per year (OPEX (i) is estimated to be 2% of the CAPEX, where i is the year of operation, starting from 1 (first year) to 25 (plant lifetime) and ir is the inflation rate per annum estimated to be 5%.

CSP trend, LCOE and maintenance costs

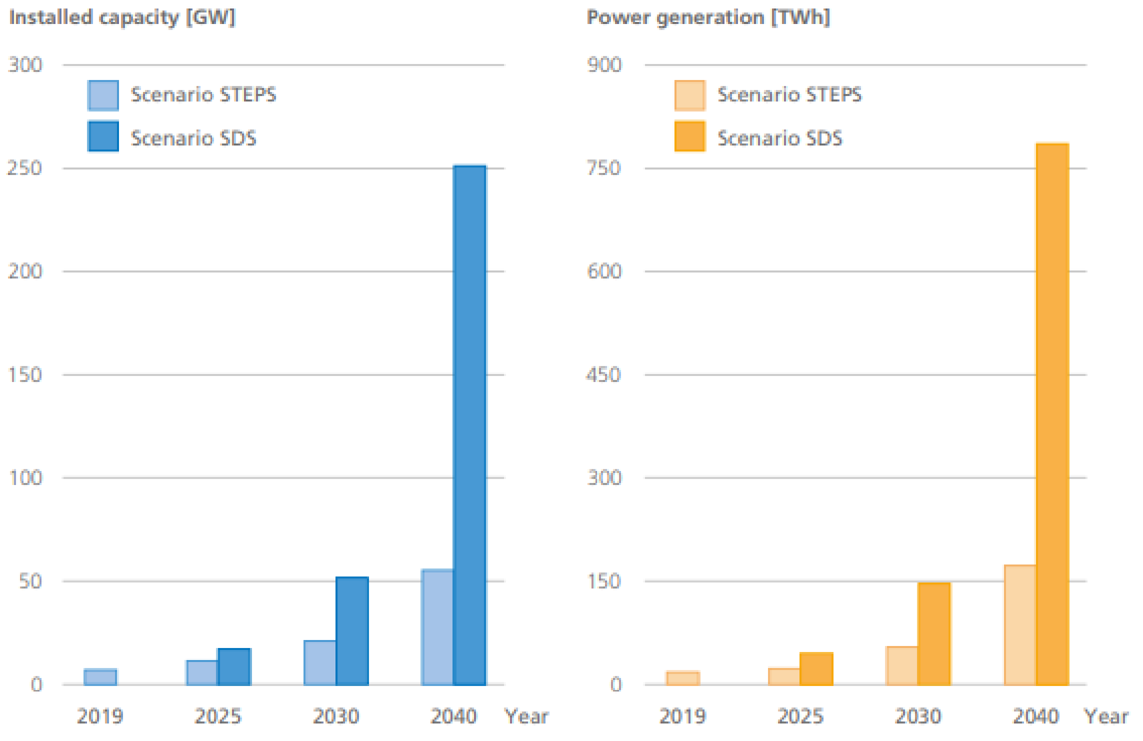

Possible expansion scenarios for CSP according to the International Energy Agency's World.
STEPS: Stated Policies Scenario) (status 2020);
SDS: Sustainable Development Scenario(necessary measures to achieve the UN sustainability goals, in particular limiting global warming to 1.5 °C if possible, in any case to below 2 °C).

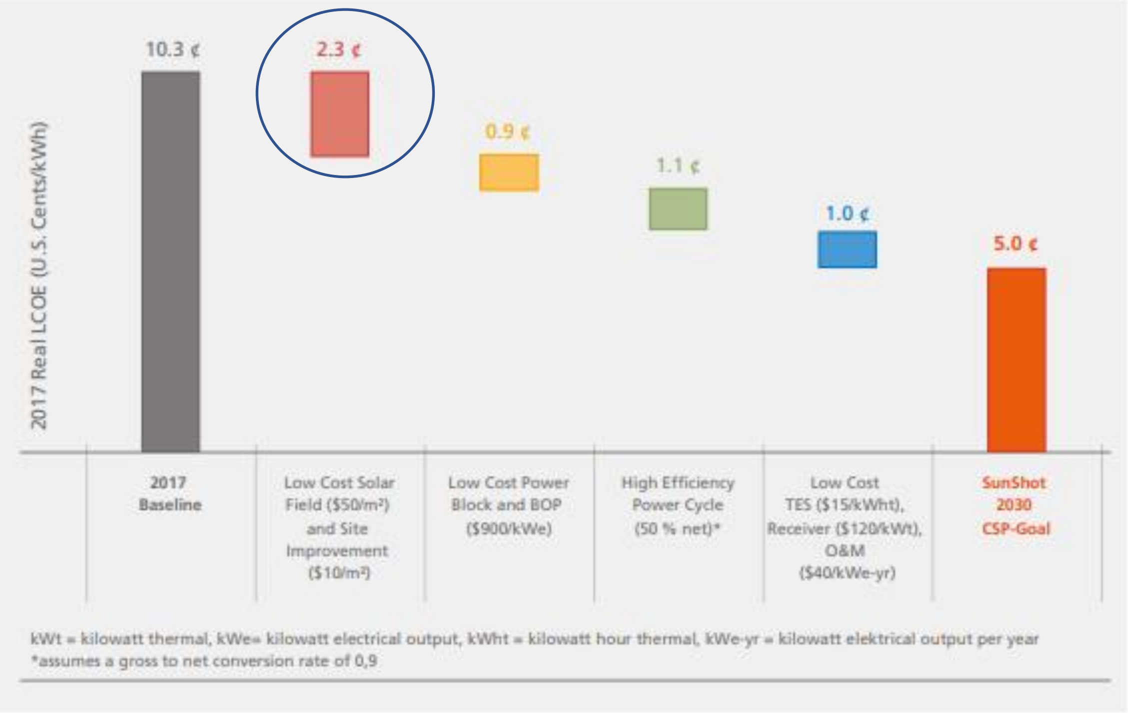

Example of a development path towards five US cents / kWh for base load-capable CSP electricity (Solar Energy Technologies Office 2017)

Reducing the annual **operating and maintenance costs** from the current level of 60 to 40 US dollars per kilowatt-hour of electricity generated (see graphic, O&M - operation & maintenance) requires improvements in regulation and control. This involves the precise recording of all operating states with extensive operation automation. The detailed knowledge of the condition of the system makes it possible, for example, to carry out maintenance in advance and to save water by cleaning the mirrors only when necessary – not at fixed intervals as before.

The role of cleaning in maintenance costs

MAINTENANCE OPERATIONS COSTS

CSP plants consume billions of liters of water per year for different purposes. Because steam-cycle cooling accounts for over 90% of water consumption in a typical wet-cooled CSP power plant, minimizing cooling water use is the most important step in water conservation. Switching from wet to dry cooling not solve entirely the problem, because soiling problems requires mirrors washing. Research work is devoted to develop new technologies for optimizing cleaning processes and minimizing water use. No solution has already found that reached commercial penetration in the CSP sector.

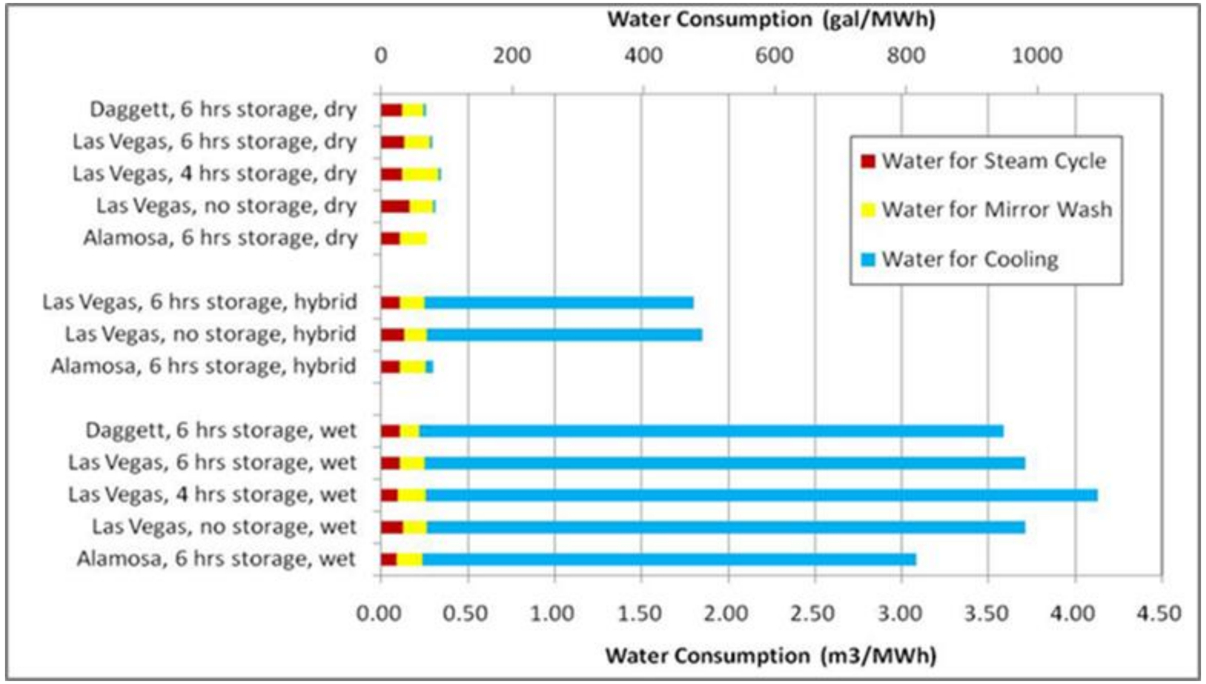

SOILING and CLEANING

$$\zeta_{\lambda,\phi}(\lambda,\theta_i,\varphi) = \frac{\rho_{\lambda,\phi,soil}(\lambda,\theta_i,\varphi)}{\rho_{\lambda,\phi}(\lambda,\theta_i,\varphi)}$$

CLEANLINESS or SOILING factor, or SOILING ratio

A CSP plant requires:
-0.3 m³ /MWh (dry), 3.5 m³ /MWh (wet)
-120L for m² of reflective surface
-30L for m² of installed solar plant

E.g. grain cultivation in Morocco requires around 1600 L/m² of cultivated area per year.

Andasol 3 (50MW) dimensions : 200 hectares (280 football field)
1 hectare=10000 m²

Soiling as fallen dust tons/Km^2

SOILING

Country	Location	Fallen dust tons/km^2/year
Iraq	Khur Al-Zubir	75.92
Iraq	Um Qasir	193.47
Oman	Al-Fahal	89
Saudi Arabia	Riyadh	392
Palestine	Dea Sea	45
Chad	North Dianena	142
Nigeria	Kano	137-181
Greece	Crete	10-100
USA	Arizona	54
USA	Nevada	4.3-15.7
USA	California	6.8-33.9
Libya	Libya	155
Marocco	Tan Tan	175
Marocco	Boujdour	219
Mauritania	Dakhla	191
Mali	Niger River	913-10446
Australia	Namoy Valley	16.9-58.2
China	Shapotu	372

«WETTABILITY»

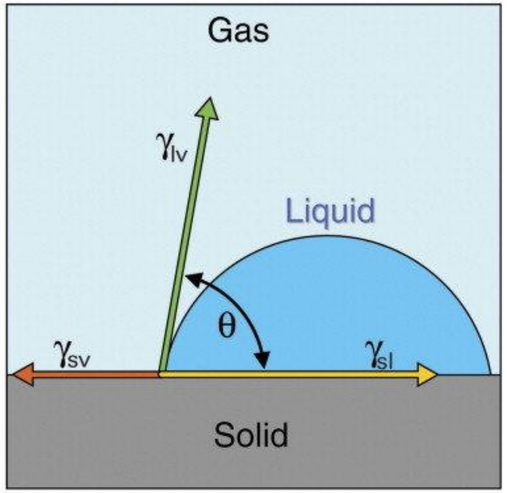

YOUNG 'S EQUATION (ideal solid surface)

For a drop of liquid lying on a perfectly flat, smooth and dry surface the degree of wetting is quantified using equilibrium angle of contact that liquid/vapour interface makes with solid surface at three phase contact line given by equation:

$$cos\theta = \frac{\gamma_{SG} - \gamma_{SL}}{\gamma_{LG}}$$

$$\Delta\theta = \theta_a - \theta_r.$$

CAH, Contact Angle Hysteresis

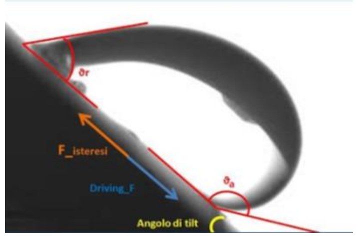

WCA°, wetting contact angle measurement
SESSIL DROP METHOD

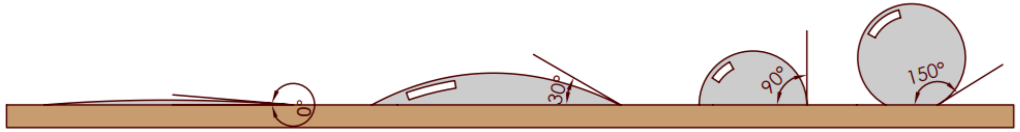

WCA	Definition
θ ≤90°	Hydrophilic
90° < θ ≤ 150°	Hydrophobic
θ > 150°	Super hydrophobic

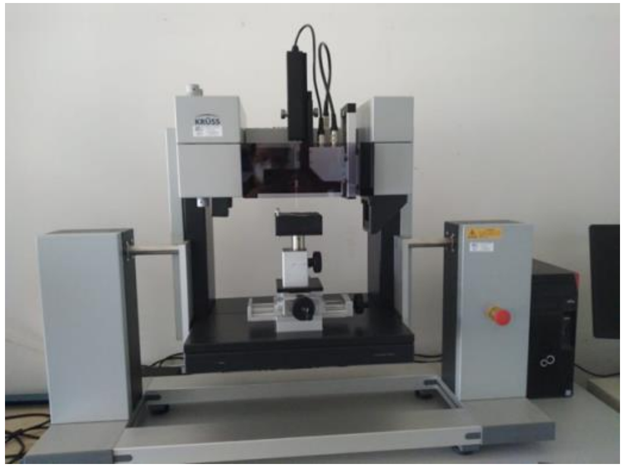

WENZEL state, CASSIE-BAXTER state (non ideal with roughness)

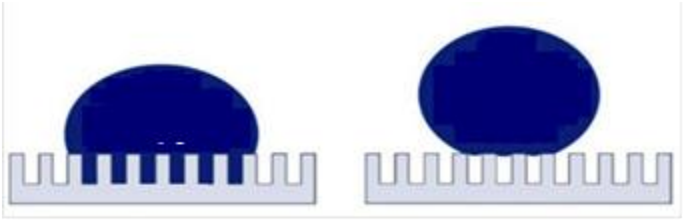

$$cos\theta = r\ cos\theta_{eq}$$

r is roughness ratio

$$cos\theta = f_{sl}\ cos\theta_1 + f_{lv}\ cos\theta_2$$

KRUSS DSA 100

«SELF-CLEANING effects»

SELFCLEANING effect
ROLLING (ob)
K/A *capillary effect*
K capillary work, A adhesion work

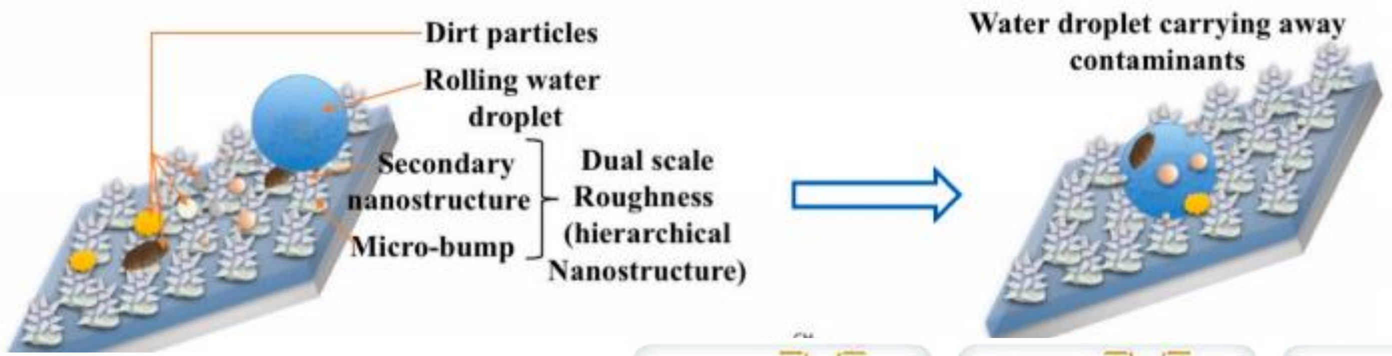

LOTUS effect

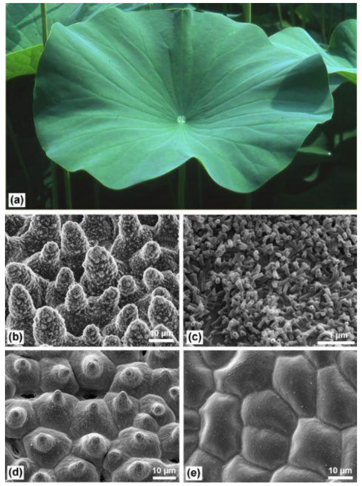

SLIDING (il)
Photo-redox
Photo-induced superhudroplilicity of TiO_2

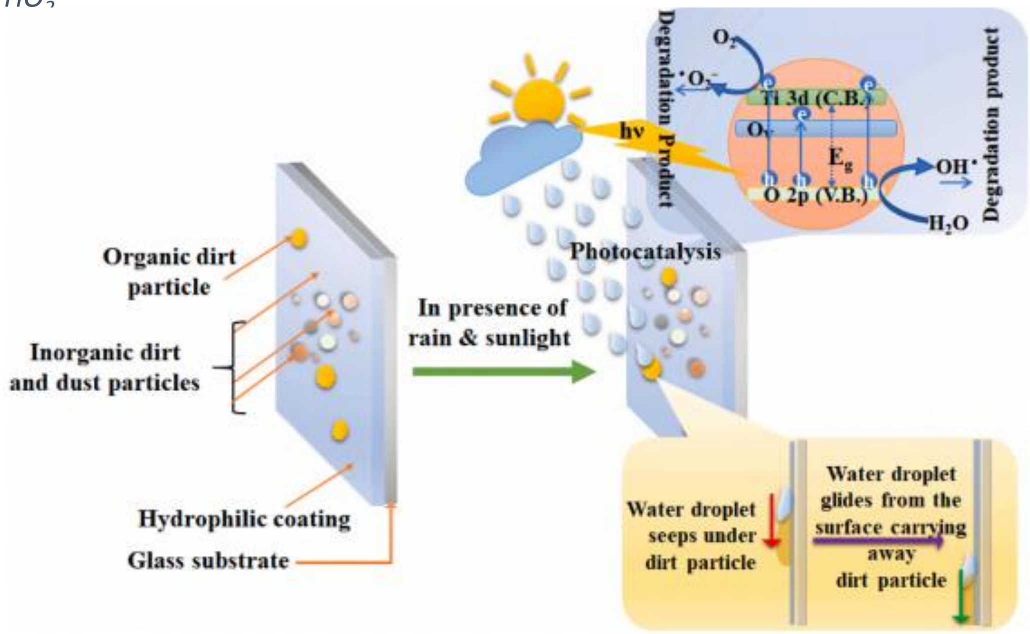

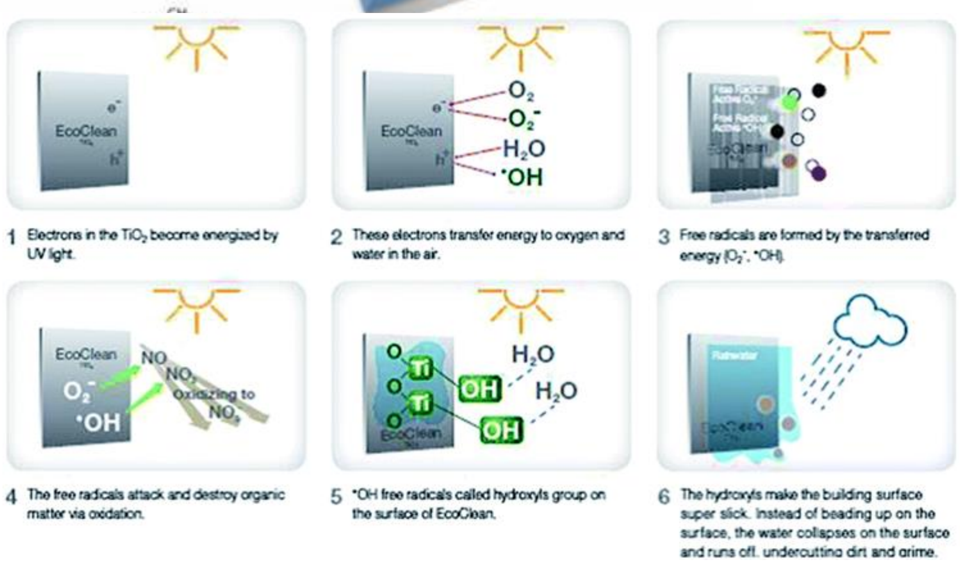

WETTABILITY: COATINGS or TREATMENTS?

✓ Selfcleaning coating as a strategy to reduce solar mirrors soiling, water consumption, operation and maintenance costs.

MAJOR CHALLENGES

in producing transparent, durable and robust self-cleaning surfaces:

1) Fragile nanostructures.
2) Adhesive strength between the coating and the substrate.
3) Resistance against environmental abrasion.
4) Non uniformity.
5) Unwanted haze.
6) Cost effective technique.

OUR APPROACH:

1. **Different mirrors architectures last layer IDENTIFICATION as working substrate**

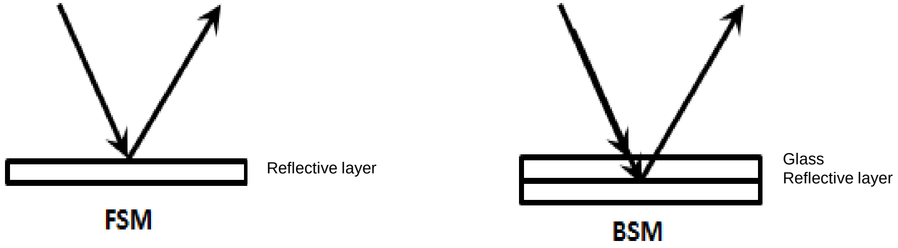

2. **TREATMENTS or COATINGS «compatible» with mirrors fabrication steps with two main requisites: hardness and optical clarity.**

Alumina, and/or optical polymers as PMMA

«Wetting modification: tratments or coatings?»

TREATMENTS

Several types of plasma generation processes were considered and one of them exhibited very promising results, but…

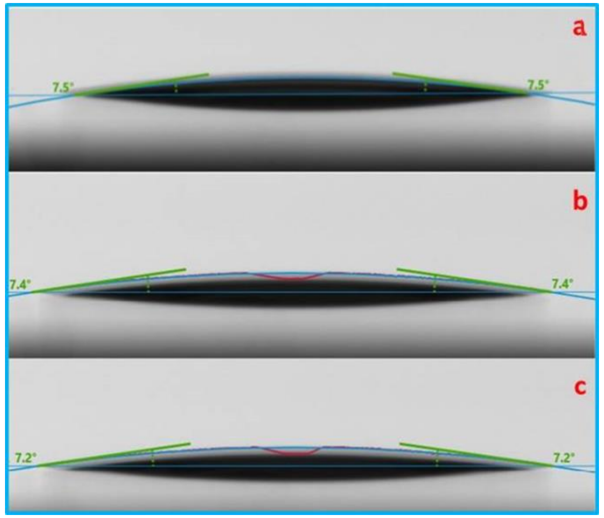

Plasma Oxygen

- Purge in N_2 di 60'
- $P_{processo}$: [1.9-2.3] 10^{-1} mbar
- O2 flux: 10sccm
- P: 160W
- Frequency: 13,56MHz
- Time: 1s (a), 5s (b), 10 s(c)

…transient effect.

In facts, plasma based cleaning procedures (robotic) were performed in PV /CSP dry cleaning 2 times a week.

COATINGS

OPTICAL METAMATERIALS

Fabrication and characterization of two kind of auxetic* metamaterials:

1. 2D aluminum nitrides (AlN) doped with metals (like Aluminum or Silver) and non-metals (like Oxygen or Nitrogen) by means of reactive sputtering deposition
2. Nanostructured hybrid polymers by means of Sol-Gel and polymers processing techniques

that both result transparent, hydrophobic, photocatalytic and usable in front surface (polymeric or metallic reflectors) and back surface (silvered glasses) mirrors architecture.

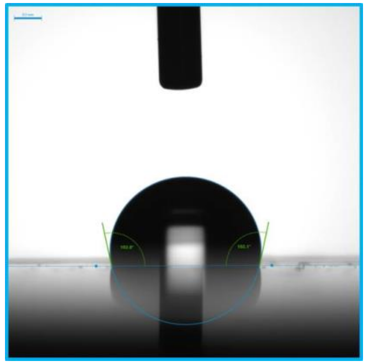

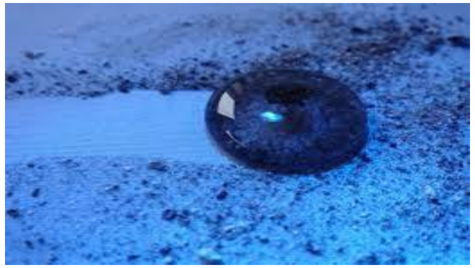

AUXETIC MATERIALS

Auxetic materials (from the Greek word 'αὐξητικός', whose meaning is 'tending to increase') show a negative Poisson's ratio (the ratio between the transverse and the longitudinal strain produced by the application of a load orthogonal to its section). Most materials get thinner when stretched, but "auxetics" do the opposite and get thicker. By virtue of the auxetic behavior, mechanical properties such as fracture toughness, indentation resistance, shear properties, wettability, can be improved, opening the way to several potential applications in medical, sports, automobile, defense, etc. Even though the existence of auxetic materials has been admitted for more than 150 years only a few natural examples have been found from some biological tissues (cat skin, cow teat, butterfly wings). *Despite common sense, partial auxetics are quite common, as 69 % of cubic elemental metals present an auxetic behavior in at least one direction. Design, modeling and fabrication of novel auxetic materials and structures is still on the way.*

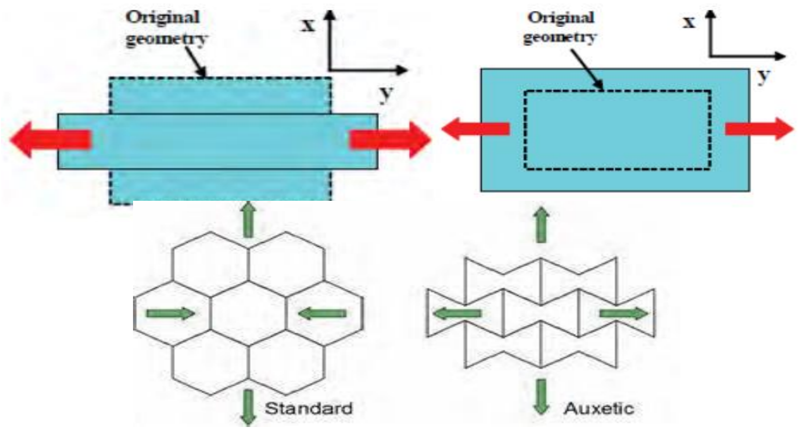

Idealized reentrant unit cells can be produced by the symmetrical collapse of a polyhedron with cubic symmetry

Poisson's ratio

$$\nu_{lt} = -\frac{\varepsilon_t}{\varepsilon_l}$$

Material properties can be tailored through modification of their geometry or architecture at all scales ranging from macroscopic objects to molecular level.

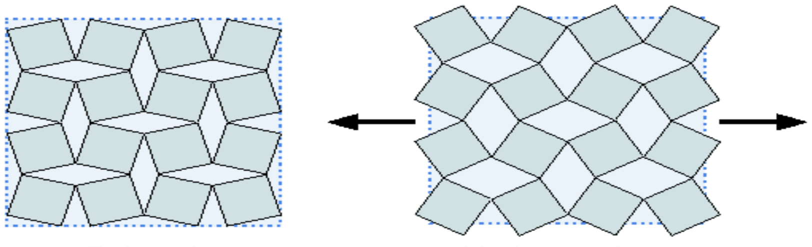

«AUXETICS in other sectors»

expanded polytetrafluoroethylene (ePTFE), Goretex

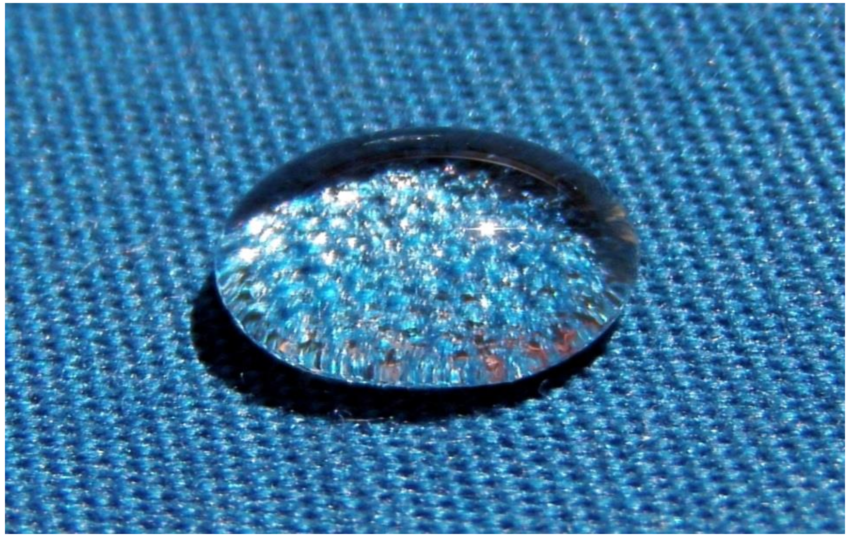

…«Goretex fibers if strained resemble to an opened umbrella»

SFERA-III

Solar Facilities for the European Research Area

«How to obtain an auxetic? »

2D honeycomb topologies

RE-ENTRANT STRUCTURES

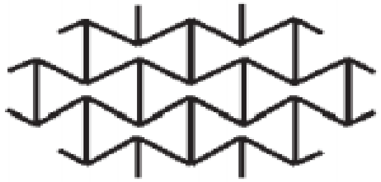

3D bucklicrystals

ROTATING POLYGONAL STRUCTURES

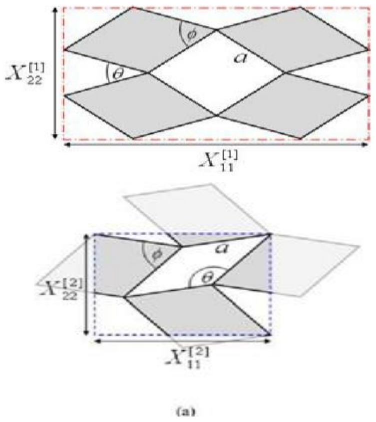

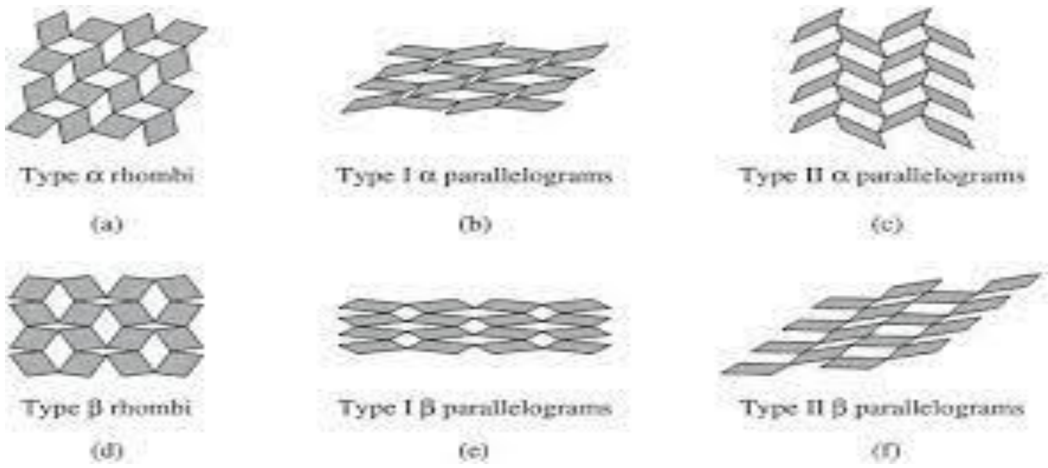

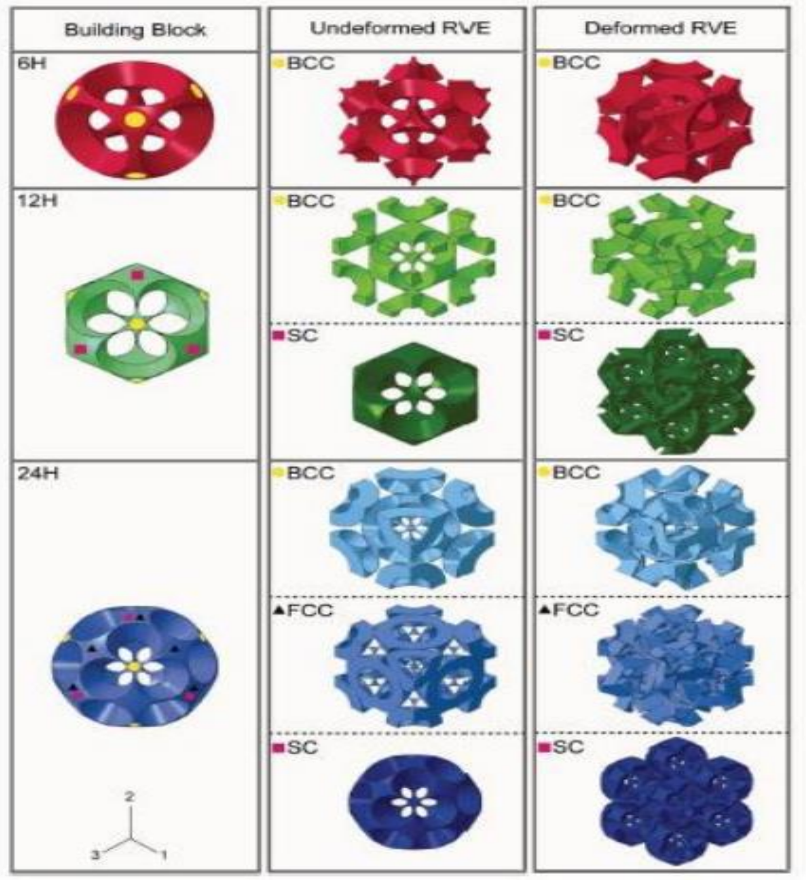

CHIRAL STRUCTURES

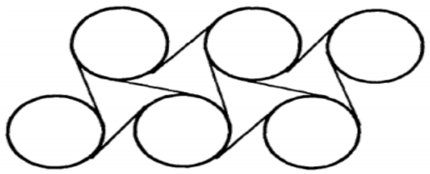

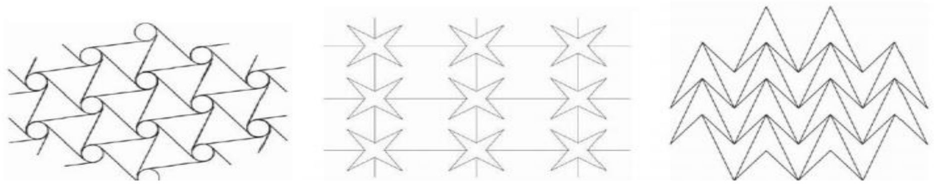

Auxetics in the nanoscale

NANOTECHNOLOGY
Nanoscience and nanotechnology are the study and application of extremely small things (10^{-9} m) and can be used across all the other science fields, such as chemistry, biology, physics, materials science, and engineering. At the nanoscale, the physical, chemical and biological properties of materials differ in foundamental and valuable ways from bulk matter. Nanotechnology R&D is direct toward understanding and creating improved materials, devices and systems that exploit these new properties.

Challenges of this scale

A critical iussue for nanotechnology is that components, structures and systems are in a size regime where they are:

- ✓ TOO SMALL for direct measurements
- ✓ TOO LARGE to be described by means of rigorous first principle theoretical and computational methods;
- ✓ TOO MUCH fluctuating to be treated monolithically in time and space;
- ✓ TOO FEW PARTICLES based to be described as a statistical ensemble.

The major part of their atoms are in surficial state with uncompletely saturated bonds.

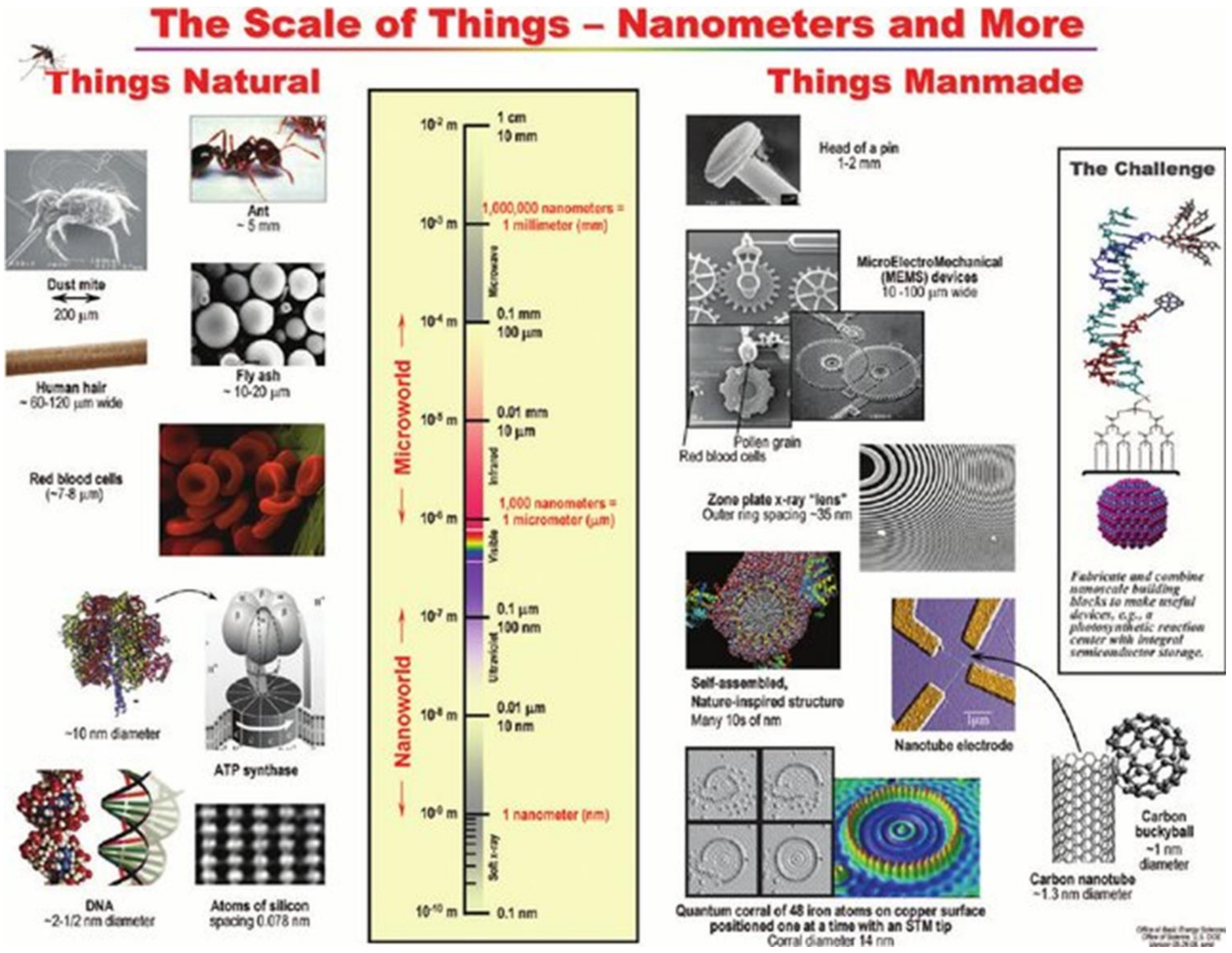

Auxetics by means of nanotechnology: chemical approach

TECHNOLOGY FOCUS

Thin film nanotechnology is pervasive in many applications, including microelectronics, optics, magnetic, hard resistant coatings, micro-mechanics, etc. Progress in each of these areas depends upon the ability to selectively and controllably deposit thin films - thickness ranging from tens of ångströms to micrometer - with specified physical properties. It requires control - often at the atomic level - of film nanostructure and nanochemistry. There are a vast number of deposition methods available and in use today. All methods have their specific limitations and involve compromises with respect to process specifics, substrate material limitations, expected film properties, and cost. This makes it difficult to select the best technique for any specific application.

1. Depositions that happen because of a **chemical** reaction:

   Chemical Vapor Deposition (CVD)
   Electrodeposition
   Epitaxy
   Thermal oxidation
   SOL GEL

*These processes exploit the creation of solid materials directly from **chemical reactions in gas and/or liquid compositions** or with the substrate material. The solid material is usually not the only product formed by the reaction. Byproducts can include gases, liquids and even other solids.*

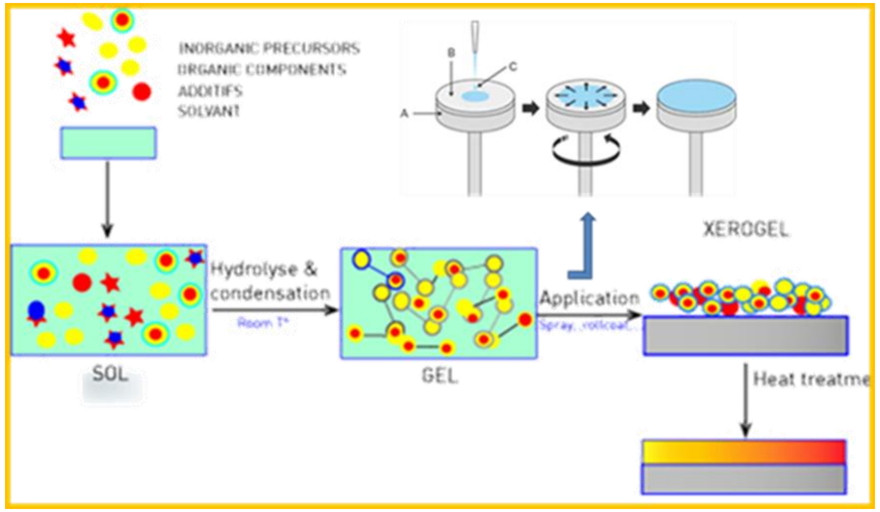

Auxetics by means of nanotechnology: physical approach

2. Depositions that happen because of a **physical** reaction:

- Physical Vapor Deposition (PVD)
- Evaporation
- **Sputtering**
- Casting

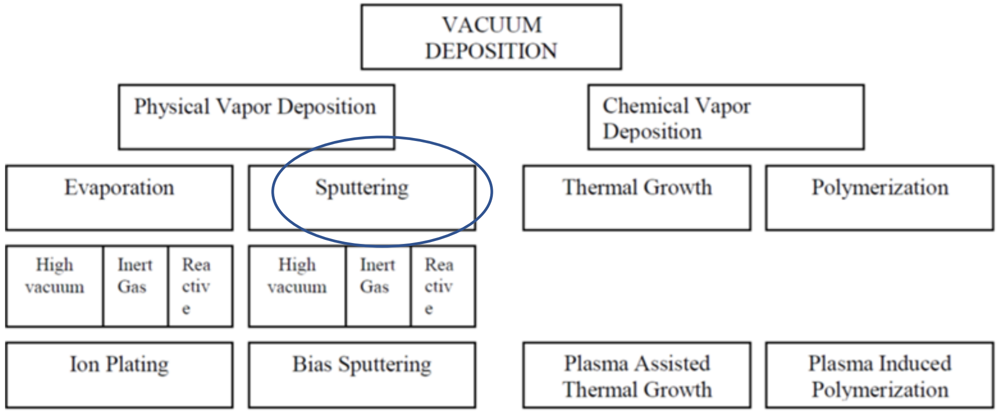

*Common for all these processes are that the material deposited is **physically moved** on to the substrate. In other words, there is no chemical reaction which forms the material on the substrate. This is not completely correct for casting processes, though it is more convenient to think of them that way.*

S P U T T E R I N G

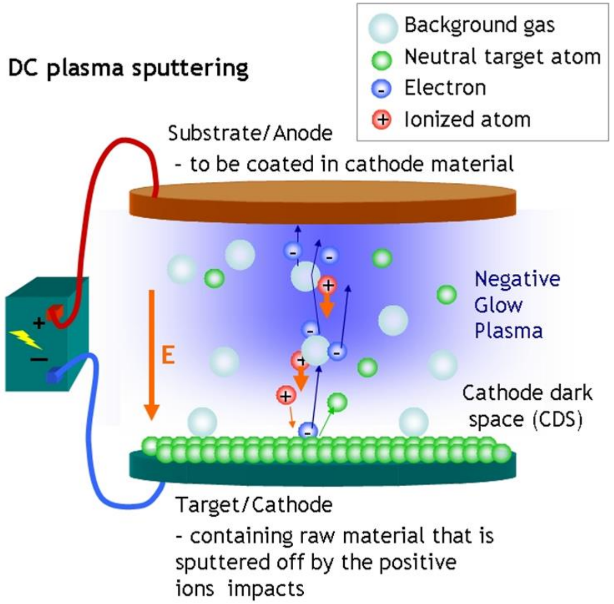

Electric field accelerates electrons in the glow region causing ionization of argon.

Argon ions are accelerated toward cathode while some electrons are accelerated toward anode.

Ions toward cathode and electrons toward anode give rise to net current flux that circulates in the circuit.

Chemically reactive gases introduced in the process chamber can react with ejected target materials to form oxides, nitrides, carbides.

Reactive sputtering can be defined as the sputtering of elemental targets in the presence of chemically reactive gases, that mass react with both the ejected target material and the target surface

- ***A mixture of inert + reactive gases used for sputtering***

oxides – Al_2O_3, SiO_2, Ta_2O_5 (O_2)
nitrides – TaN, TiN, Si_3N_4 (N_2, NH_3)
carbides – TiC, WC, SiC (CH_4, C_2H_4, C_3H_8)

Advantages:
- It is capable of producing thin compound films of controllable stoichiometry and composition at high deposition rates.
- Elemental targets are usually more easily purified, and hence, high-purity films can be produced.
- The complexity and expense of RF systems can be avoided, since metallic targets are generally electrically conductive, and hence, DC power can be applied.
- Metallic targets are thermally conductive, which makes the cooling of these targets more efficient thus, the range of the applied power can be extended e.g. up to 50 W/cm² and higher, without the fear of being cracked.

Inorganic metamaterials: AlN, theory

Aluminium nitride poli-typoids

The choice of aluminium nitride, AlN, a hard covalent semiconductor with a bandgap of 6.2 eV, whose common crystalline hexagonal phase is a wurtzite-type structure starts from the consideration of preserving the overall mirror fabrication process architecture changing only few steps relative to the alumina last layer (Al_2O_3, an aluminum oxide neither hydrophilic nor hydrophobic (WCA 52°) utilized as transparent barrier layer to preserve stability and reflectivity of metallized mirrors) with a wetting tailorable aluminum compound, more hydrophobic than alumina (Al_2O_3) by virtue of covalent character of Al-N bond and potential auxetic properties.

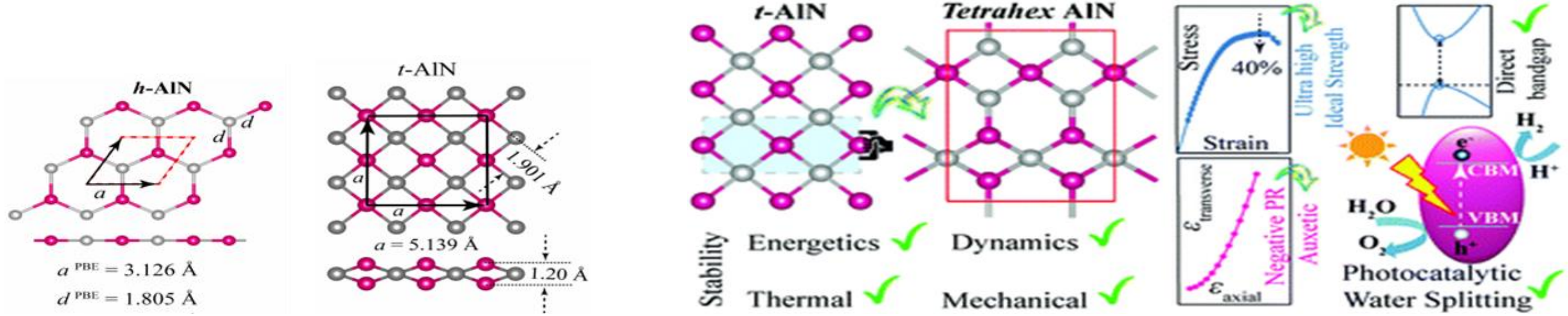

From a structural point of view, honeycomb structure of AlN (h-AlN) is not the only 2D structure made up of Al and N atoms. There is a spatial arrangement of atoms with multiple bonds between neighbors due to the valence electron pairs repulsion rule, recently discovered* and named tetra-hexagonal 2D structured AlN (th-AlN), constituted by perfectly ordered hexagonal and tetragonal rings with unprecedented properties (anysotropy, negative Poisson’s ratio, ultrahigh ideal strength, photocatalytic properties, tunable wettability, etc.)

*M.E. Kilic et al, J.Mater. Chem. C. 2021, 9. 4971-4977

Inorganic metamaterials: AlN, experimental results

It is possible to change wettability (from 52° to around 100° WCA), promoting AUXETIC and photocatalytic properties in sputtered AlN based metamaterials, by means of nitride 2D growth and doping with metals (like aluminium, silver) and non-metals (like nitrogen and oxygen), preserving optical clarity in visible solar range.

Sample	P_0 [mbar]	I [A]	ΔV [V]	Flux (sccm)	Pres-Pos µbar (%)	Thick, [nm]
AlNx_1	9.3*10-7	10.4	303	50Ar+28N2+1O2	10.6 (32)	106
AlNx_2	5.1*10-7	10.0	307	50Ar+28N2+2O2	10.8 (32)	120
AlNx_3	5.7*10-7	9.7	317	50Ar+28N2+3O2	10.9 (32)	124
AlNx_4	5.2*10-7	9.2	332	50Ar+28N2+4O2	11 (32)	100
AlNx_5	7.0*10-7	9.4	317	50Ar+28N2+3O2	10.7 (32)	121
AlNx_6	6.0*10-7	11.6	292	400Ar+2O2+80N2	10.4 (43)	128
AlNx_7	4.4*10-7	10.6	307	400Ar+7O2+50N2	10.0 (43)	97
AlNx_8	1.9*10-7	10.2	317	400Ar+11O2+45N2	10.0 (43)	99
AlNx_9	1.,5*10-7	11.2	296	400Ar+4O2+70N2	10.2 (43)	129
AlNx_10	8.7*10-7	11.4	291	400Ar+3O2+75N2	10.4 (43)	126
AlNx_11	4.7*10-7	11.5	289	400Ar+2O2+80N2	10.5 (43)	123
AlNx_12	3.8*10-7	11.6	287	400Ar+7O2+80N2	10.5 (43)	127

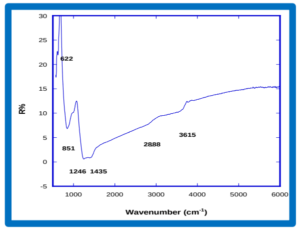

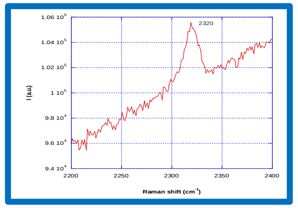

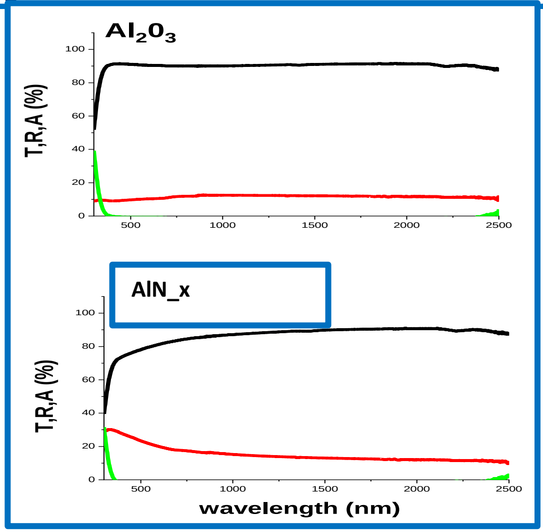

Doped 2D AlN_x

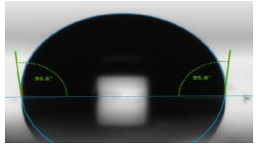

Sample	WCA
AlNx_1	98 ± 3°
AlNx_2	96.3±0.5°
AlNx_3	96±2°
AlNx_4	98.6±1.5°
AlNx_4bis	96.0±0.8°

PROTOTYPE 20cm x 30cm

POLYMERS: Hybrid nano-composites

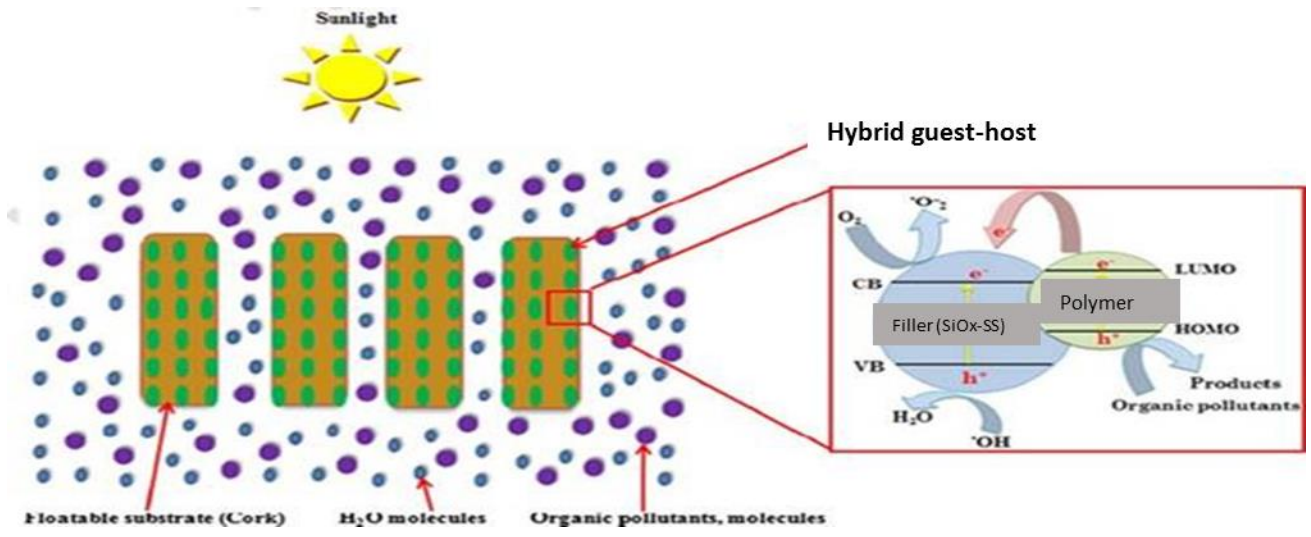

Photo-catalysis of organic pollutants.

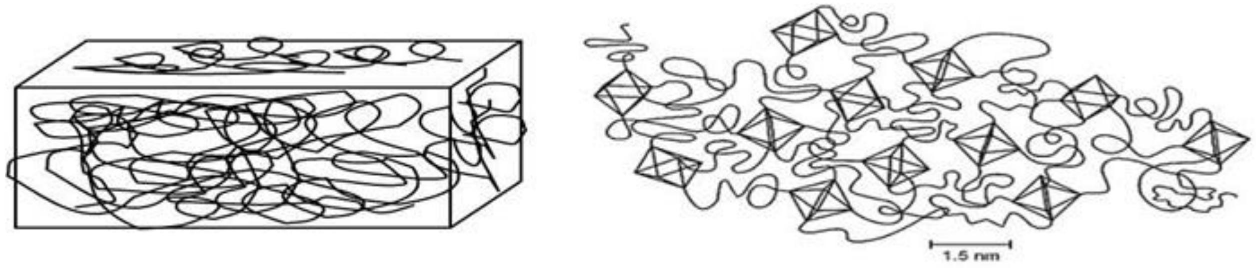

Amorphous guest-host polymer scheme.

Hybrid polymers

Inorganic nano-sized guests insertion into polymers for optic, by means of copolymerization and/or doping, and/or plasma etching treatments has been utilized for influencing chain folding and modifying wetting properties.

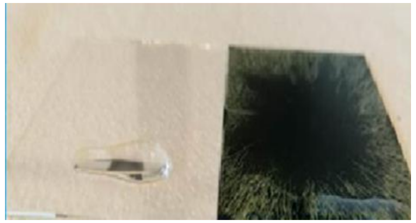

Example of PANi + TiO_2

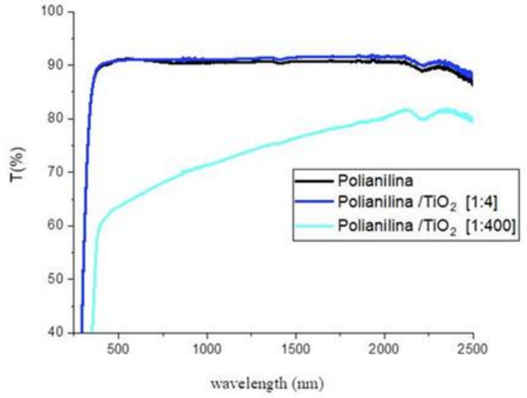

By proper mixing of components it is possible to obtain self-cleaning superhydrophilic hybrid polymers. The content of TiO_2 can be modulated as trade-off between WCA° and optical transmittance.

POLYMERS: Hybrid nano-composites experimentals

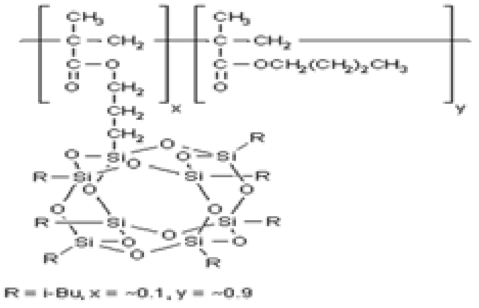

Polymeric structure.

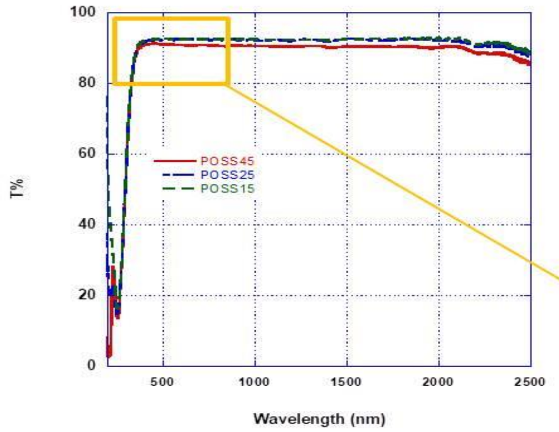

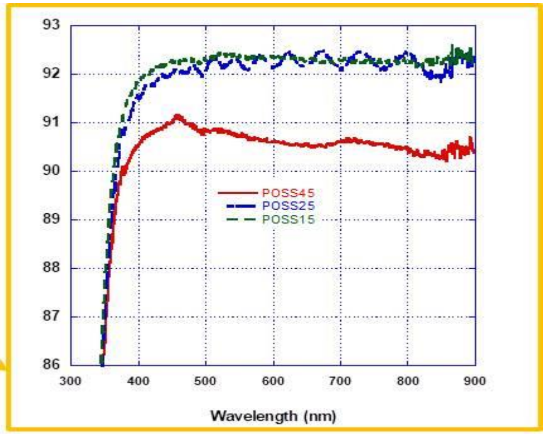

Optical properties: transmittance, T% of composites containing a different amount of filler, deposited on an optical glass.

Wetting contact angle measurements.

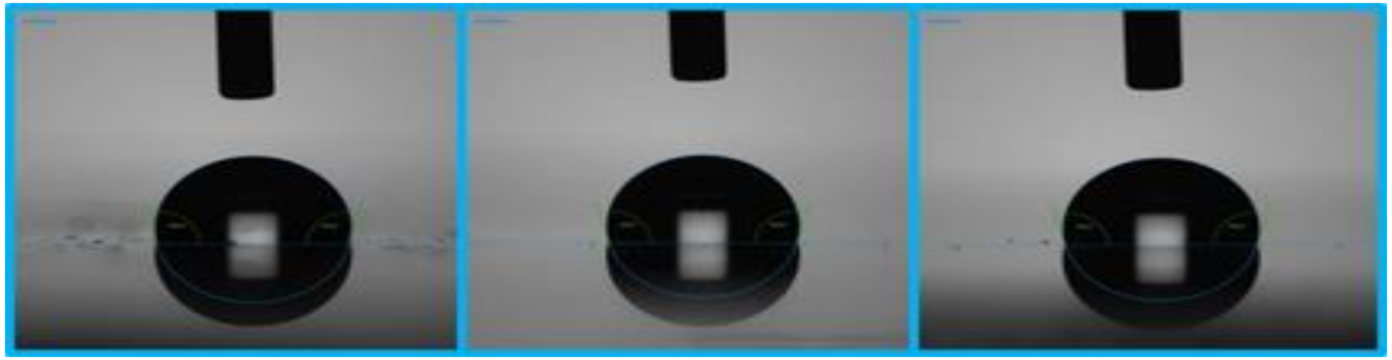

P15 (WCA° = 102°±1) **P25(WCA° = 103.7°±0.2),** **P45 (WCA° = 102.5°±0.7)**

TRADE-OFF between optical clarity and wettability.

INCREASE of TRL

From lab to industrial scale

Spin coating

R2R processing

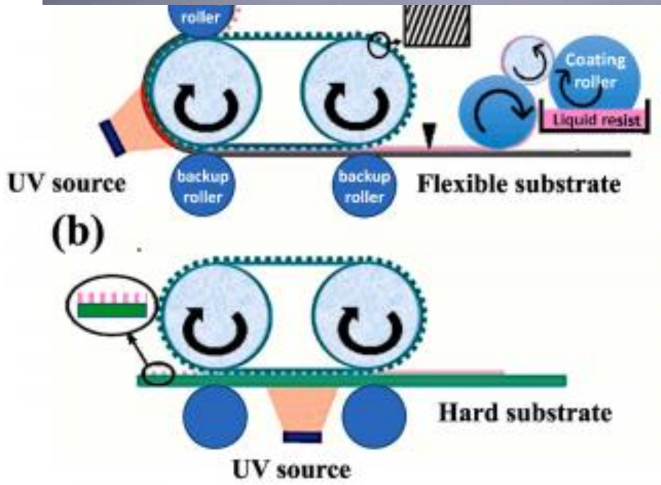

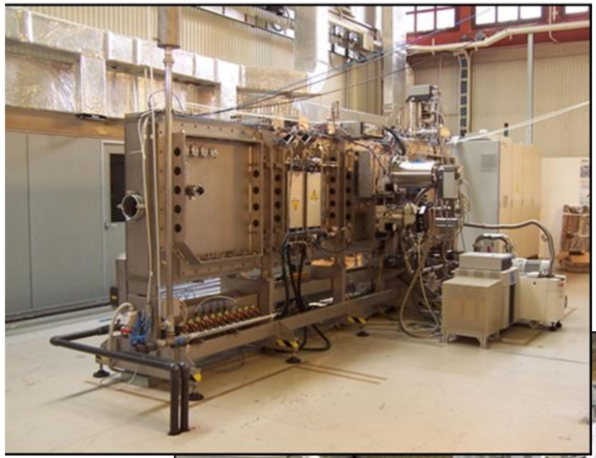

ENEA 2 lab equipment

ASE production line

HVLP SPRAY

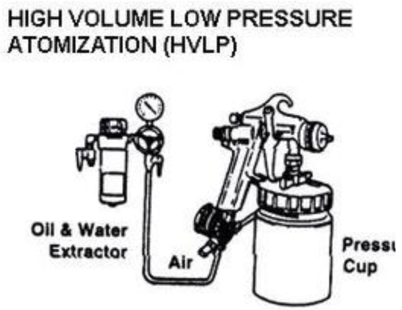

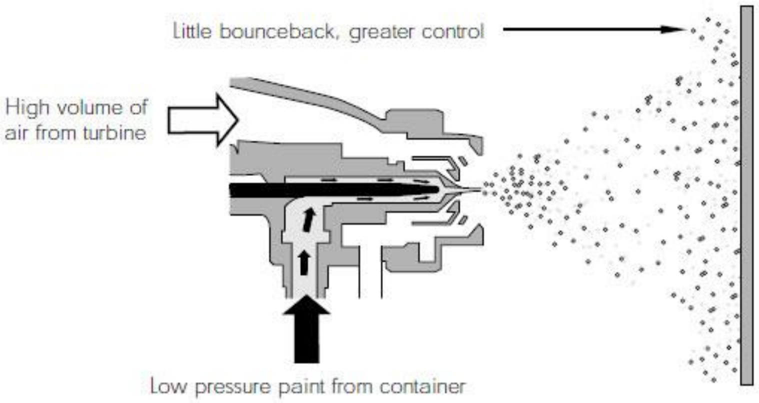

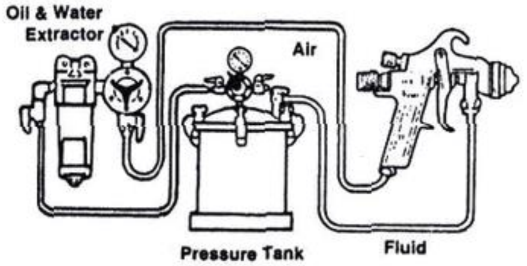

Choosing The Right Nozzle Size

High volume low pressure atomization can be fully framed in the additive manufacturing technologies.
Worldwide concern over increased air pollution has necessitated numerous changes, including how we finish our products. HVLP air atomization, Air Assisted Airless and electrostatics are now the only accepted methods of production spraying in certain parts of the country. Although all HVLP spray guns operate with the same objective in mind, how they accomplish this goal may differ. First, air used in the atomization process reaches the HVLP spray gun's nozzle in one of four ways: (1) standard high-pressure compressed air, which has its pressure restricted within the gun body; (2) standard high-pressure compressed air, which is assisted with a venturi feed and then filtered ambient air prior to its pressure restriction within the gun's body; (3) standard externally fed HVLP turbine air; and (4) compressor-assisted externally fed turbine air. Items 1 and 3 have seen the most growth and ultimate acceptance in recent years and we have selected them.
The benefits of HVLP atomization are improved transfer efficiency, often approaching 65%, compliance with local finishing regulations, a softer spray that penetrates easily into recesses or cavities, reduced material (costs) consumption as well as reduced spray booth maintenance and reduced hazardous waste. Turbine-operated HVLP systems enjoy great portability and ease of operation where compressed air is not available. HVLP spray guns with internal restrictors use existing air supplies, are easy to operate, and are lower in cost than turbine HVLP.

SPRAY

- Step 1 — Nanocomposite formulation (dissolution, suspension, sonication, temperature, etc.).
- Step 2 — Viscosity measurement and choice of proper nozzle and pressure for optimal deposition.
- Step 3 — Feeeding the container and defining geometry (distance, angular positioning, etc.).
- Step 4 — Spray deposition.
- Step 5 — Drying (Solvent evaporation in an oven (T <80°C), vacuum steps?).
- Step 6 — Sample's morphology characterization.

GOAL: to get «uniform» coverage!

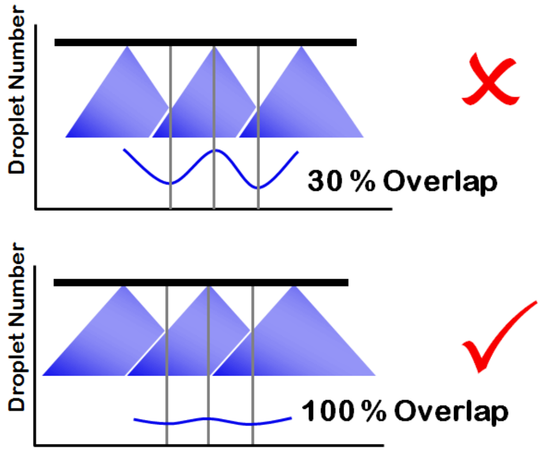

PROTOTYPE: 50cm x 50cm

S. Esposito, A. D'Angelo, A. Antonaia, A. Castaldo, M. Ferrara, M. L. Addonizio, A. Guglielmo		"Optimization procedure and fabrication of highly efficient and thermally stable solar coating for receiver operating at high temperature" Solar Energy Materials and Solar Cells (2016), pp. 429-437.
A. Castaldo, M. Ferrara, A. Antonaia		Low emission sputtered coatings for smart glazing" IET Digital library 18th Italian National Conference on Photonic Technologies (Fotonica 2016), 2016 page 93 (4.) 2016 10.1049/cp.2016.0953
Anna Castaldo		ENERGIES Special Issue "Solar Thermodynamic Materials Overview" in the section "D1: Advanced Energy Materials". (ISSN 1996-1073).
Anna Castaldo		"Room side low emission sputtered coatings for smart glazing how to reduce thermal discomfort of insulating windows" ADVANCED BUILDING SKINS 2018
Anna Castaldo, Emilia Gambale; Giuseppe Vitiello		Aluminium Nitride Doping for Solar Mirrors Self-Cleaning Coatings, Energies 2021 14(20), 6668; https://doi.org/10.3390/en14206668
A. Castaldo, G. Vitiello, E. Gambale, M. Lanchi, M. Ferrara, M. Zinzi.		Mirroring Solar Radiation Emitting Heat Toward the Universe: Design, Production, and Preliminary Testing of a Metamaterial Based Daytime Passive Radiative Cooler. *Energies* **2020**, *13*(16), 4192; https://doi.org/10.3390/en13164192
Anna Castaldo		"Auxetic metamaterials for changing solar mirrors wettability", ORAL SolarPACES2021, ONLINE CONFERENCE, 27-29/09/2021
Anna Castaldo, Emilia Gambale, Giuseppe Vitiello.		Thermal stability of sputtered tungsten nitrides for solar thermal applications, APPLIED SCIENCES 2022, 12, 10208. https://doi.org/10.3390/app122010208
Anna Castaldo, Emilia Gambale, Michela Lanchi, Luca Turchetti, Giuseppe Vitiello.		Sensing properties of metamaterials utilized as self-cleaning coating for solar mirrors SolarPACES2022, Albuquerque USA.

References, projects and acknowledgments

The results illustrated in this presentation have been obtained in the framework of the project "Concentrating Solar Power", under the "Electric System Research" Program 2019-2021, with the financial support of Italian Ministry Ecological Transition, in the project SOLARGRID and work is in progress for the "Electric System Research" Program PTR 2022-2024.

OUTLOOK
towards the talking mirror

There is a lot of efforts on reducing the Operating Expenses (OPEX) of concentrated solar power systems. One of the way regards the performance of reflector/mirror key component invalidated from soiling and it is based on the development of self-cleaning reflectors (mirrors coated with self-cleaning thin transparent films), that can be washed with the lowest quantity of water, granting savings particularly significant for countries with high labor or resource (water, etc.) costs (e.g. desert areas). Moreover, the role of self-cleaning coatings to maintain adequate cleanliness of all varieties of the solar mirrors and the ability to withstand degradation due to environmental factors over time, without compromising the optical transparency/reflectivity of the component is of great importance. Therefore, an emerging trend for sustaining performance of the solar mirrors throughout their entire service life requires ***integration of an autonomous and smart operational quality control in addition to self-cleaning technologies****.*
Providing a solar field with intelligence and automating processes means to know the dirty level, or the failure of a single mirror (or the entire field) and program cleaning operations or component substitution. From practical point of view this means adding SENSING properties to mirrors. How?
In our labs we demonstrated that is possible to change wetting properties of solar mirrors by applying transparent and auxetic metamaterials on reflectors surfaces by means of scalable processes, to the purpose of reducing water consumption in cleaning procedures. In particular, auxetic aluminum nitrides obtained by means of sputtering deposition on metallized low iron glasses have been proposed as self-cleaning solution ideal for back surface mirrors and hybrid organic-inorganic nanocomposites deposited on a lab scale by spin coating and on a pre-industrial scale by spraying for front surface mirrors. Both coatings are transparent, hydrophobic, versatile and can be applied by means of cheap and scalable techniques onto large substrates. In the future work we propose of extending coatings requisites, formulating self-cleaning metamaterials that can act as ***sensors of mirrors performance*** *failure due to dust, or excessive humidity, or other selected parameters (e.g. break events, ageing, corrosion, erosion, etc.) and hence furnish, by means of a proper electronic interface and IoT, information about the soiling and about the correct functioning both of the single component and/or the entire solar field. To reach a similar ambitious goal, the first step will be to make conductive the metamaterials, in manner of tailoring resistive sensors, that can change their conductivity in function of a failure (or a desired information). Once obtained this result, it will be possible covering (in toto or in part) solar mirrors with such a "intelligent" metamaterial, fabricated by means of an unique step of solar mirrors production process, where it is possible to modulate conductivity by simple addition of metallic nanostructures tailored for a specific sensor requirement.*

CONCLUSIONS

- **REFLECTIVE SURFACES description and requirements for decreasing LCOE : LOW MAINTENANCE in restoring optical properties affected by soiling reducing water consumption.**
- **Development of SELF-CLEANING solutions tailored for BSM and FSM solar mirrors: METAMATERIALS with optical properties.**
- **Materials Science and Engineering of HYBRID organic-inorganic NANOCOMPOSITE formulation: nitrides and polysilsesquioxanes.**
- **From lab to pre-industrial PROTOTYPE: scaling-up by means of simple and cheap fabrication methods.**
- **CSP smartization trend: new research projects and goals.**

Anna CASTALDO, PhD
ENEA
TERIN-STSN-SCIS
anna.castaldo@enea.it

THANK YOU FOR YOUR ATTENTION!
ANY QUESTIONS?

References

- *Aluminum Nitride Doping for Solar Mirrors Self-Cleaning Coatings,* Energies 2021 14(20), 6668, https://doi.org/10.3390/en14206668
- *Solar Thermodynamic materials overview,* Energies 2021 Special issue D1: Advanced Energy Materials (ISSN 1996-1073)
- *Auxetic metamaterials for changing solar mirrors wettability*, Proceedings of Solar PACES2021.
- *Thermal Stability of Sputtered Tungsten Nitrides for Solar Thermal Applications*. Applied Science. 2022, 12, 10208. https://doi.org/10.3390/app122010208
- *Highly performing low emission sputtered coatings stable in air for energy saving glazing units,* Advanced Buildings Skins Conference Proceedings (ISBN 978-3-9524883-4-8).

SFERA-III
Solar Facilities for the European Research Area

4th Training for Industries
7-11th November 2022, Cr ENEA Casaccia Rome (Italy)

Chemical and physical characteristic of different MS mixtures

Annarita Spadoni / Anna Chiara Tizzoni (ENEA, TERIN-STSN-SCIS)

JOINT RESEARCH ACTIVITIES

THIS PROJECT HAS RECEIVED FUNDING FROM THE EUROPEAN UNION'S HORIZON 2020 RESEARCH AND INNOVATION PROGRAMME UNDER GRANT AGREEMENT NO **823802**

Outline- contents

Contents:

❖ **Part I: Thermal Energy Storage: general considerations**

❖ Part II: MS molten salts mixtures: selection criteria

SFERA-III
Solar Facilities for the European Research Area

Overview

Concentrated Solar Power (CSP) systems are emerging technologies:

- for **carbon free energy production**
- to **produce high temperature heat** for industrial processes, i.e water desalination
- to **store the sun's energy** in the form of heat, using low cost and stable materials

TES, thermal energy storage: decoupling of energy supply and demand; no intermittency of solar resources, grid stability, enhancement of global process efficiency and cost.

A proper storage systems is a crucial point for the economic dispatchability of CSP technology.

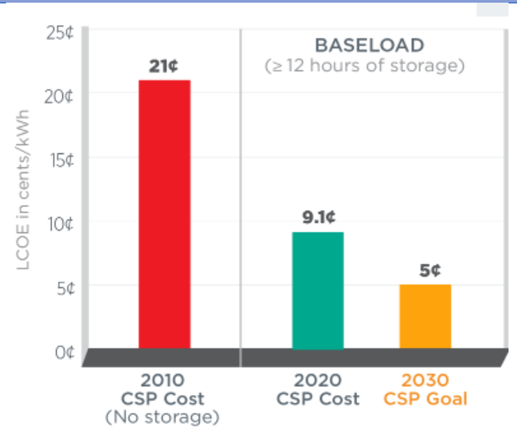

Source: https://www.energy.gov/eere/solar/concentrating-solar-thermal-power

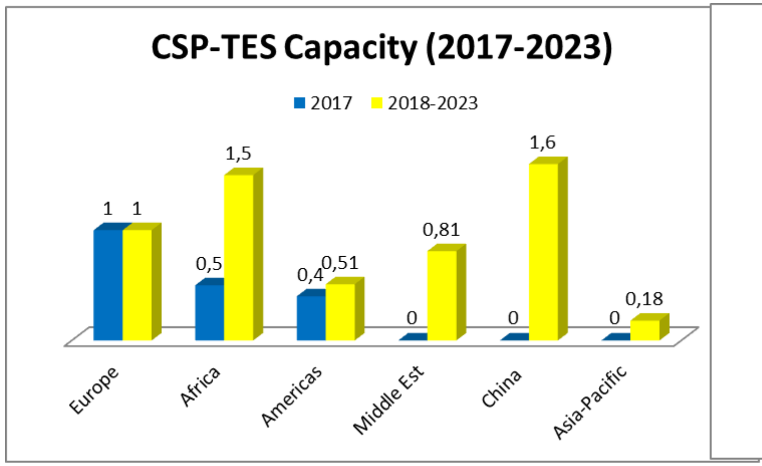

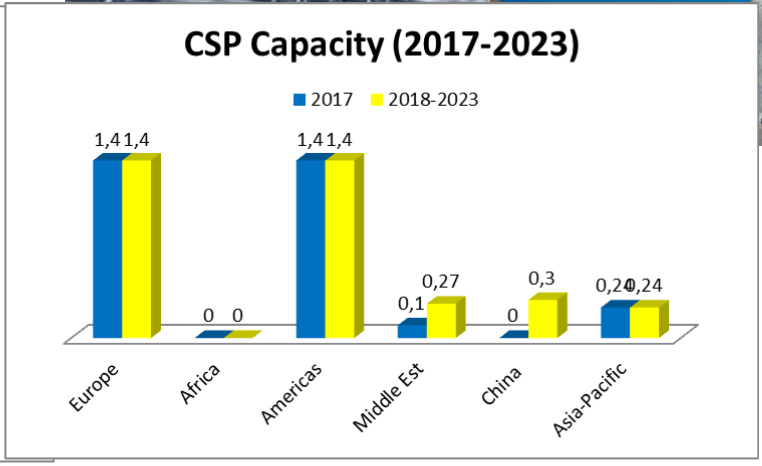

source: https://www.iea.org/data-and-statistics/charts/csp-capacity-by-technology-2017-2023, IEA.

Outline-Topics

Molten salts can be used as heat transport fluids (HTF) and heat storage materials (HSM) in these types of installations.

CSP-TES Technology

Heat Tranfert Fluids (HTF)

Heat Storage Materials (HSM)

The binary mixture of $NaNO_3$-KNO_3, indicated as "**solar salt**" is currently the most employed molten nitrate, used as reference material. (280-565°C)

Solar salt drawback: high melting point, operative issues (an external heating system is necessary during the startup such as the tracing of pipelines, and the electrical heaters are expected to provide for the minimum storage temperature tank)

Useful to investigate other mixtures with low melting points, which can be employed both as HTF or HSM.

- **Predictive modelling methods for the design of new inorganic low melting fluids.**
- **Experimental characterization of their thermal, chemical and physical properties**

Topic of this lesson: define a proper selection criteria and summarize the state of the art about the main molten salt HTFs HSMs for real life CSP applications at **medium temperatures (100-600 °C).**

Thermal Energy Storage (TES)

All kinds of <u>TES</u> can be classified in four categories:

- **Active/Passive systems**
- **Direct/Indirect systems**

✓ In an **active** system the HSM directly transfers the thermal heat to a working fluid in a power block.

✓ In a **passive** system another fluid it is employed for transferring the thermal energy from the HSM to the power block.

✓ In **direct** storage systems, the HTF and HSM are the same, while, in an **indirect** configuration, the two fluids are different, and the heat is transferred between them by an intermediate heat exchanger (HX).

- TES is natural storage option for CSP
- Basic working principle without storage:

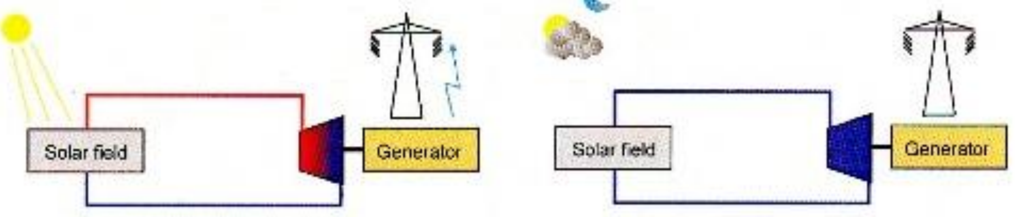

- Basic working principle with storage:

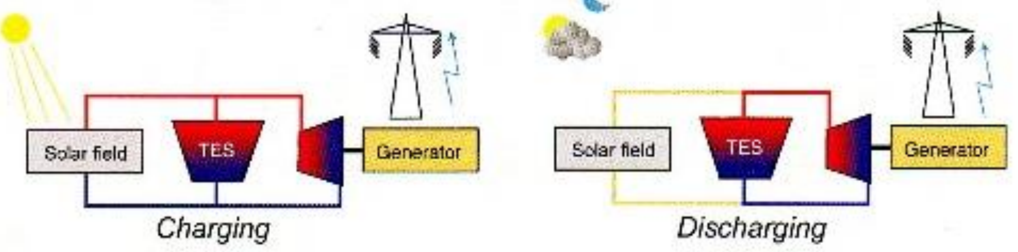

Storage Modes and Materials

According to the different types of heats, different materials can be used to obtain thermal energy storages.

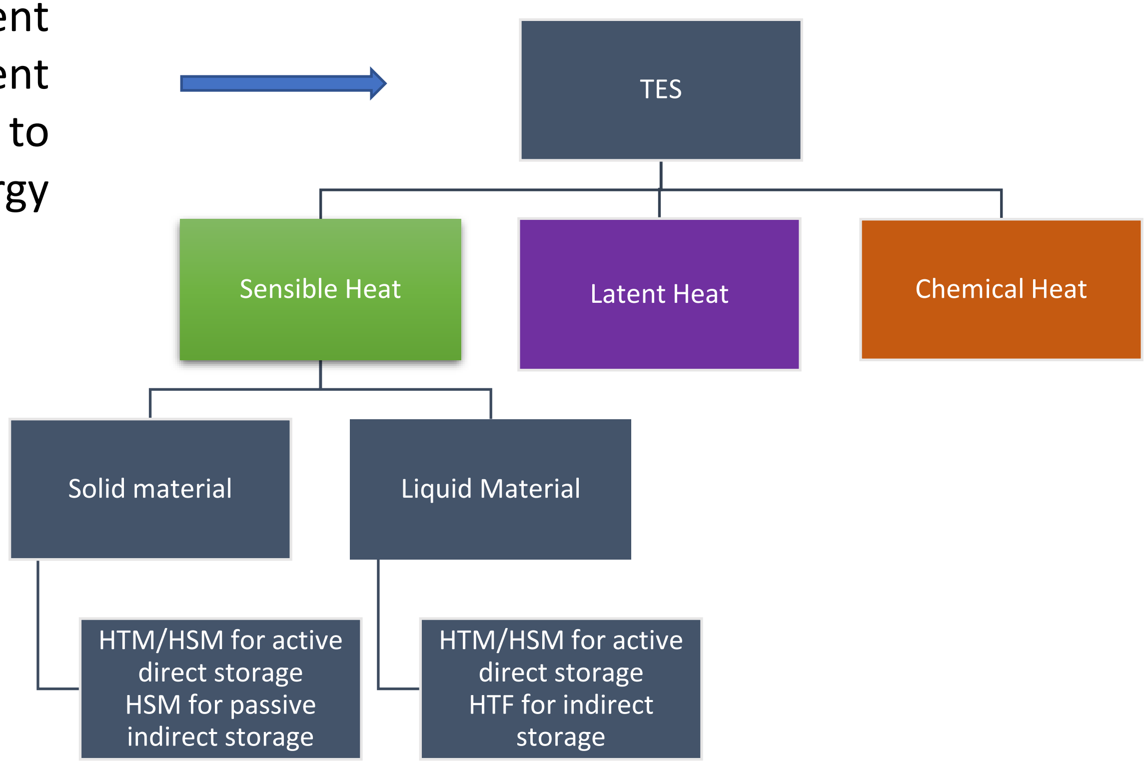

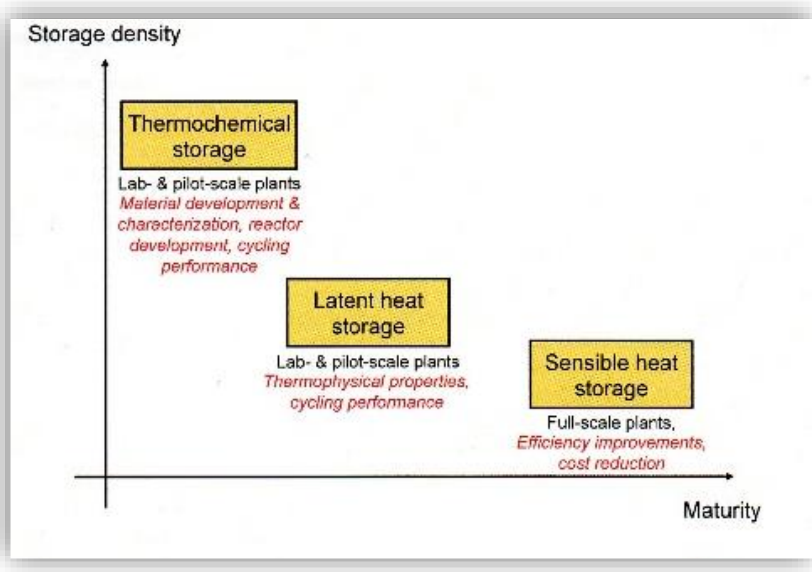

The choice of feasible thermal fluids (TES) is a crucial point for the dispatchability and economic effectiveness of CSP technology!

Sensible heat storage

Liquid materials

✓Diathermic oils as HTF, that are composed by a mixture of organic compounds, mostly diphenyl and diphenyl oxides.

✓Nitrate alkaline mixtures are generally used as HSMs.

Solid materials

✓An intermediate HTF is necessary in order to ensure the contact with the HX.

✓It must mantain a thermocline stratification.

✓ Can be less costly (per weigh and volume) than molten nitrates.

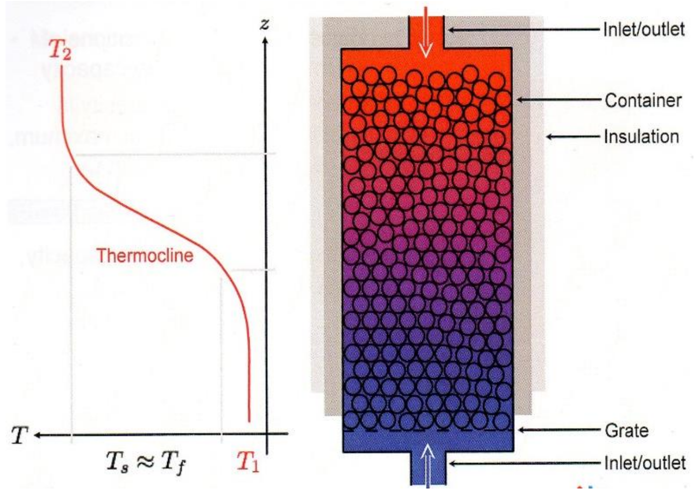

Latent heat storage

Phase change materials (PCMs)

- ✓ energy storage density is high per volume
- ✓ possibility to discharge it at constant temperature
- ✓ problems of designing a proper heat exchanger, given the change in volume during phase transition.

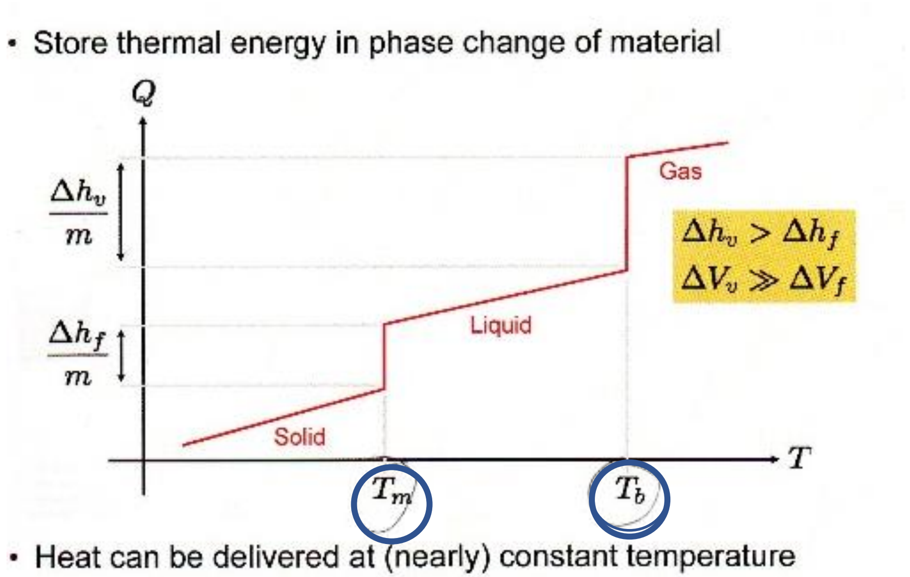

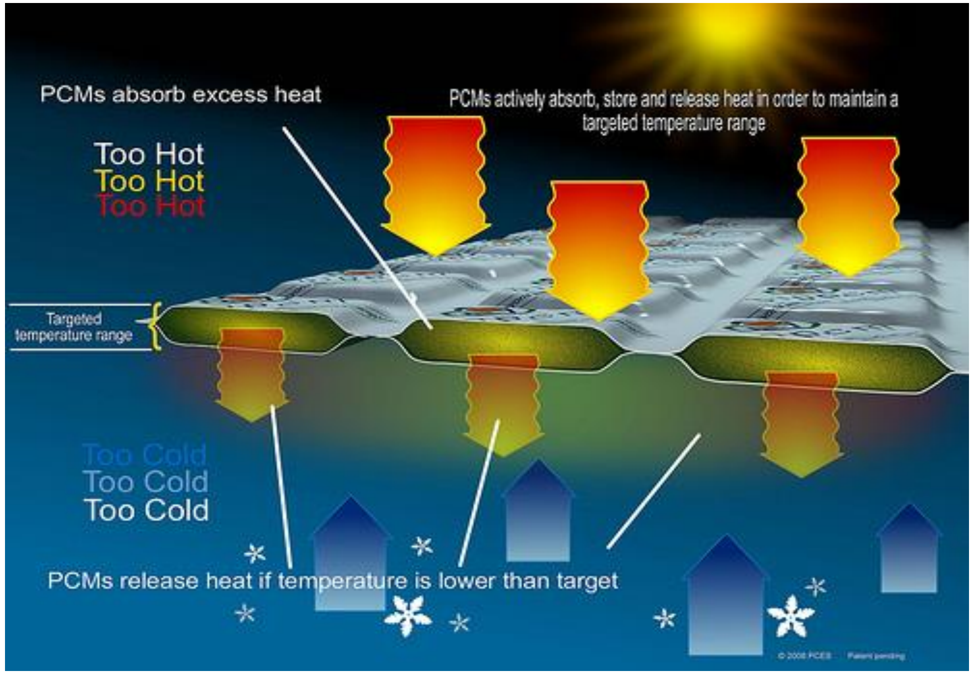

Chemical heat storage

Possibility to accumulate the solar heat in the energy of a single reversible reaction

The most common systems use a solid-gas reaction:

R (s) + Heat = P1 (s)+ P2 (gas)

✓ By this method can be possible to carry out seasonal heat storage.

Reaction type	Example of Reaction	$T_{charging}$(°C)	$T_{discharging}$(°C)	ΔH_{reaz} (Kj/mol reagent)	Energy density (Gj/m^3)
Hydroxides	$Ca(OH)_2 = CaO + H_2O$	550	450	104.4	1.6
Carbonates	$CaCO_3 = CaO + CO_2$	850-950	550-700	178	2.5
	$MgCO_3 = MgO + CO_2$	510-750	na	125	2.0
	$CaCO_3/CaO/Ca_{12}Al_{14}O_{33}$	850-950	750	178	not available
Oxides	$2BaO_2 = 2\ BaO + O_2$	650-850	450-580	77	1.2
	$2Co_3O_4 = 6CoO + O_2$	915-920	835-850	354.6	1.1
	$6Mn_2O_3 = 4Mn3O_4 + O_2$	920-1000	500-650	202.8	1.2

The whole process can be divided into three parts:

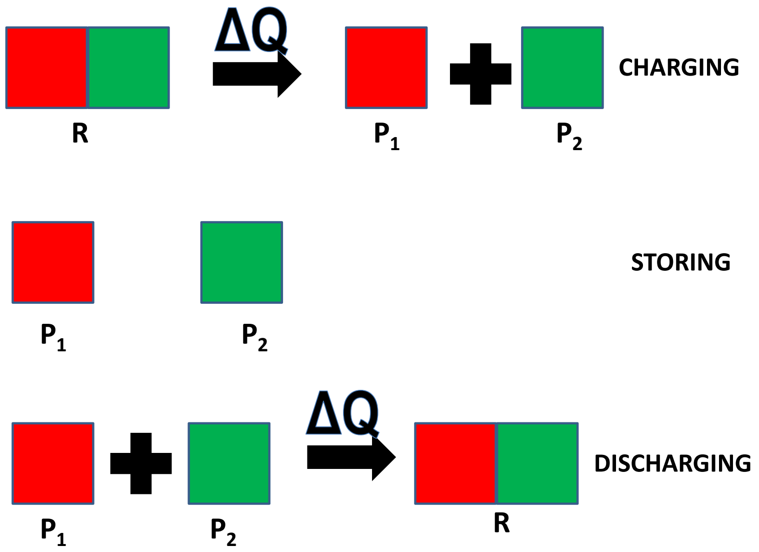

Q= m ΔHreact

MS as HSM- State of art

- **Molten salts mixtures** are known to exhibit satisfactory thermal and physical features, both for heat exchange and storage, in the temperature range concerned, together with low corrosion properties and a relatively low cost .

Advantages of molten salts (nitrates/nitrites) :

- *safe*
- *non-toxic*
- *available at low cost*
- *stable at relatively high temperatures*

T liquidus(°C)	238
Cp(J/ K g)	1.6 (238-600 °C)
Viscosity (cP)	4.5-1.6(238-600 °C)
Density (gr/ml)	1.95 – 1.70 (238-600 °C)
Thermal conductivity(W / K m)	0.50 – 0.55 (320-550 °C)

"Solar Salt" ($NaNO_3$-KNO_3 60-40 % w/w corresponding to 64/36 mol/mol) is currently the most employed material both as HTF and HSM.

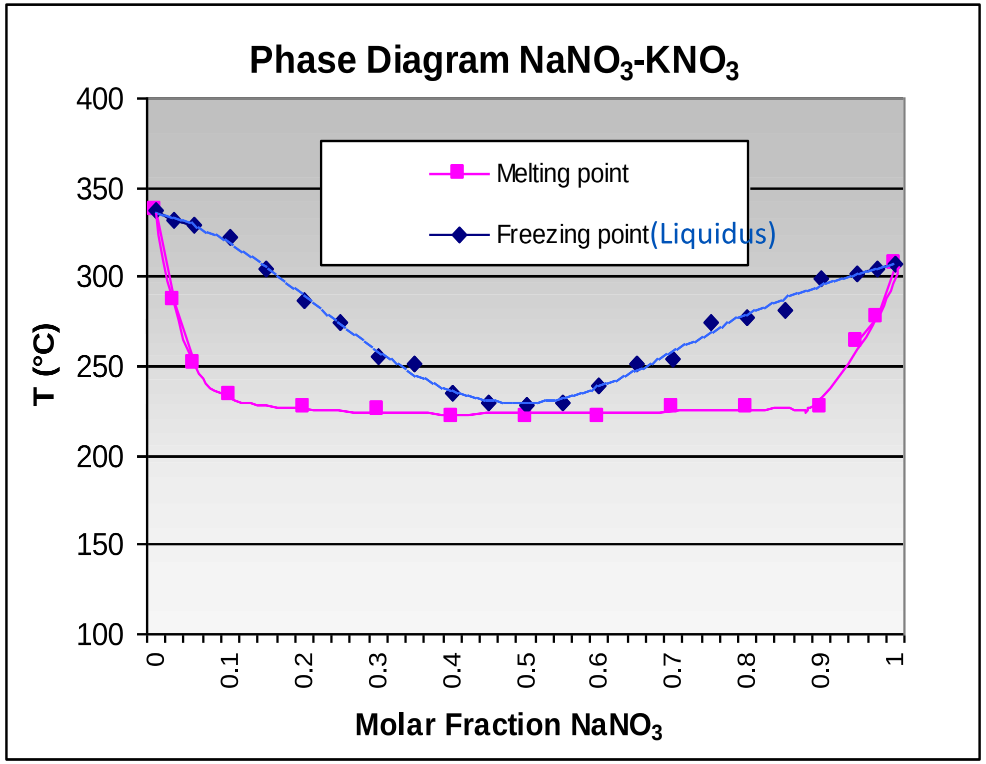

Diathermic oils vs MS

Advantages

DIATHERMIC OIL

- ✓ low freezing point (-18÷12 °C), which avoids the HTF solidification in the plant receiver tube and pipelines;
- ✓ No necessity for a heating system to maintain the plant lines at a temperature higher than the one in the external ambient.

SOLAR SALT

- ✓ quite inexpensive
- ✓ not flammable
- ✓ high thermal stability point (≈ 600 °C)
- ✓ low viscosity
- ✓ high heat capacity
- ✓ Rankine electric power generating block is slightly affected by a decrease of the lower operative point of the thermal fluids below 270 °C , the “solar salt” formulation can be considered the only realistic choice.

Disadvantages

DIATHERMIC OIL

- ❑ expensive, toxic for humans and environment;
- ❑ relatively low thermal stability, they can be employed up to about 250 °C at atmospheric pressure, and under pressure from nitrogen or inert gases up to around 440 °C.
- ❑ Above this temperature they undergo an irreversible degradation and are also very flammable materials.

SOLAR SALT

- ❑ Compatibility with materials up to 600°C (but expensive 347H-321H stainless steels are to be used at least above about 500°C)
- ❑ relatively high freezing point (238 °C)

Considerable attention must be paid to avoid salt freezing in the CSP plant, which can seriously affect the power plant's operating conditions, by plugging valves and pipes, and reducing heat transfer surface.

Novel mixtures: selection criteria

The **key factors** to be considered are:

- ✓ heat transport
- ✓ storage efficiency
- ✓ cost effectiveness
- ✓ environmental friendliness

The following characteristics are to be evaluated:

1) **Working temperatures** (freezing temperature, upper thermal stability point, and range of operating temperature)
2) **Thermophysical properties** (density, viscosity, heat capacity, and thermal conductivity)
3) **Environmental safety and risk for human health**
4) **Material cost**
5) **Construction materials compatibility and corrosion** resistance of alloys

Novel mixtures: selection criteria

Considerations

- Molten salts (MS), which in general consist of NO_3^-/NO_2^- mixtures are mostly considered, but only salts deriving from Na/K/Li/Ca are taken into account, because other salts are rare and more expensive.

- Carbonates, chlorides o other salts are little soluble in molten nitrates, so their addition results not interesting.

- $NaNO_2$ cannot be coupled with $Ca(NO_3)_2$ because of metathetical reaction ($Ca(NO_2)_2$ which leads to $Ca(NO_3)_2$).

- Mixtures must be stable in air to avoid inert storage systems.

Solar Salt	
Chemical composition (%wt)	$NaNO_3/KNO_3$ (60/40)
Density $\left[\frac{kg}{m^3}\right]$ vs. temperature [°C]	$\rho = 2090 - 0.63 \cdot T$
Dynamic Viscosity [cP] vs. temperature [°C]	$\mu = 71,645 \cdot T^{-1.763}$
Thermal conductivity $[\frac{W}{°C*m}]$ vs. temperature [°C]	$k = 0.3804 + 3.452 \cdot 10^{-4} \cdot T$
Heat capacity $[\frac{kJ}{°C*kg}]$ vs. temperature [°C]	$cp = 1.5404 + 3.0924 \cdot 10^{-5} \cdot T$
Thermal stability (max operation temperature)	600 °C
Liquidus temperature (initial solidification point)	238 °C

Hitec® (Na/K nitrate/nitrite)	
Chemical composition (%wt)	$NaNO_3/KNO_3/NaNO_2$ (7/53/40)
Density $\left[\frac{kg}{m^3}\right]$ vs. temperature [°C]	$\rho = -0.9 \cdot T + 2269.4$
Dynamic Viscosity [cP] vs. temperature [°C]	$\mu = 146,452 \cdot T^{-1.903}$
Thermal conductivity $[\frac{W}{°C*m}]$ vs. temperature [°C]	$k = 0.5843 \mp 0.0006 \cdot T$
Heat capacity $[\frac{kJ}{°C*kg}]$ vs. temperature [°C]	$cp = 1.55 - 0.0001 \cdot T$
Thermal stability (max operation temperature)	450 under air; 530 °C under inert gas
Liquidus temperature (initial solidification point)	141 °C

Giaconia, A.; Tizzoni, A.C.; Sau, S.; Corsaro, N.; Mansi, E.; Spadoni, A.; Delise, T. Assessment and Perspectives of Heat Transfer Fluids for CSP Applications.
Energies 2021, 14, 7486. https://doi.org/10.3390/en14227486

Hitec XL® (Na/K/Ca nitrate)	
Chemical composition (%wt)	$NaNO_3/KNO_3/Ca(NO_3)_2$ (15/43/42)
Density $\left[\frac{kg}{m^3}\right]$ vs. temperature [°C]	$\rho = 2240 - 0.827 \cdot T$
Dynamic Viscosity [cP] vs. temperature [°C]	$\mu = 509,611 \cdot T^{-2.072}$
Thermal conductivity $[\frac{W}{°C*m}]$	~0.519 (constant in the operative range)
Heat capacity $[\frac{kJ}{°C*kg}]$ vs. temperature [°C]	$cp = 1.542 - 0.000322 \cdot T$
Thermal stability (max operation temperature)	≤425 °C
Liquidus temperature (initial solidification point)	~125 °C
Na/K/Li nitrate	
Chemical composition (%wt)	$NaNO_3/KNO_3/LiNO_3$ (18/45/37)
Density $\left[\frac{kg}{m^3}\right]$ vs. temperature [°C]	$\rho = 2051 - 0.6639 \cdot T$
Dynamic Viscosity [cP] vs. temperature [°C]	$\mu = 58,725 \cdot T^{-1.69}$
Thermal conductivity $[\frac{W}{°C*m}]$	$k = 0.0005 \cdot T + 0.4$
Heat capacity $[\frac{kJ}{°C*kg}]$ vs. temperature [°C]	$cp = 1.5395 + 0.0003 \cdot T$
Thermal stability (max operation temperature)	600 °C
Liquidus temperature (initial solidification point)	120 °C

* data obtained by ENEA in the framework of the "Concentrating Solar Power" project under the "Electric System Research" Programme 2019–2021.

Outline- contents

Contents:

- ❖ **Part I: Thermal Energy Storage: general considerations**

- ❖ **Part II: MS molten salts mixtures:**
    - ❖ **selection criteria**
    - ❖ **characterization techniques**
    - ❖ **results and comparison between the most commercial MS mixtures**

[1] *Giaconia, A.; Tizzoni, A.C.; Sau, S.; Corsaro, N.; Mansi, E.; Spadoni, A.; Delise, T. Assessment and Perspectives of Heat Transfer Fluids for CSP Applications. Energies 2021, 14, 7486.*

[2] *Delise, T., Tizzoni, A.C., Ferrara, M., Corsaro, N., D'Ottavi, C., Sau, S., Licoccia, S. Thermophysical, environmental, and compatibility properties of nitrate and nitrite containing molten salts for medium temperature CSP applications: A critical review (2019)*
Journal of the European Ceramic Society, 39 (1), pp. 92-99.

Selection criteria

- It is necessary to narrow the candidates **by simulating multicomponent systems** with thermodynamic models;
- The results are generally **low melting composition zones** from which it is possible to synthetize promising mixtures;
- Then, the selected materials **are characterized** against their thermophysical and stability properties.

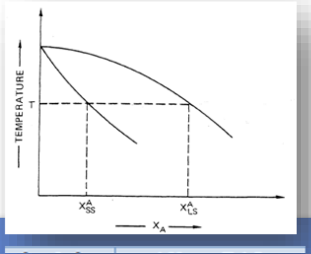

Models can be used to predict properties of different compounds, without the need to perform long and expensive experimental campaigns.

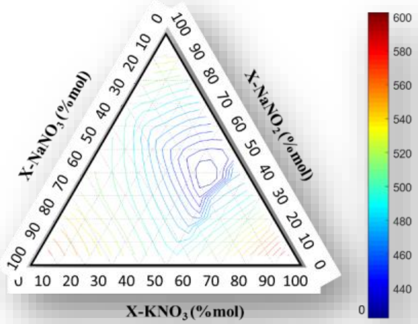

Multi-components Phase diagrams: individuation of a low melting zone

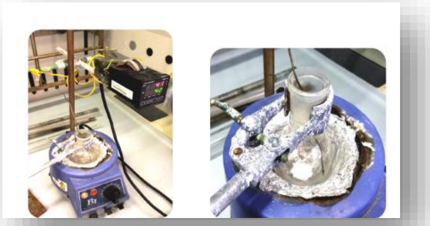

Novel promising mixtures to be synthetized

Experimental validation

Properties
Purity
phase diagrams
Thermal stability
Specific heat
viscosity
density
heat conductivity

LOCAL COMPOSITION MODELS (Wilson, NRTL…)

Chemical thermodynamics formulates the equilibrium condition between phases **equating the chemical potentials** (or fugacity) of each component in contact phases.

$$f_i^\alpha = f_i^\beta$$

Fugacity can be expressed in terms of temperature, pressure and composition, describing the behaviour of the system.
The **non-ideality** of the system can be expressed by:

Equations of state $\ln \frac{\hat{f}_i}{P} = \int_0^P \frac{1}{P}\left(\frac{\bar{v}_i P}{RT} - 1\right) dP \,,$ $\hat{f}_i = \boldsymbol{\gamma_i} x_i f_i^0$ $\boldsymbol{RT\ln\gamma_i = \left(\frac{\partial G^E}{\partial n_i}\right)_{P,T,n_{j\neq i}}}$

Where $x_i f_i^{\,0}$ is the fugacity of a considered ideal system and is **γ_i is the activity coefficient**.

These models assume that the **local composition around a molecule is different** from the medium composition of the mixture. The advantage consists in the possibility of predicting the behaviour of MULTICOMPONENT system,

with only few experimental data of binary systems required.

Study and modeling of multicomponent mixtures
modelling

Local composition models: example of the procedure using Wilson theory

INPUT: Enthalpy and T melting of pure components and L12 and L21 values of binary salts

Initialization of variables x1=0.1;x2=0.1;x3=0.1

$$T_i = \frac{\Delta H_i^{fus}}{\frac{\Delta H_i^{fus}}{T_{im}} - R[\ln x_i + \ln \gamma_i]} \qquad i = 1,2,3,4$$

$$\ln\gamma_i = -\ln\left(\sum_{j=1}^{m} x_j \Lambda_{ij}\right) + 1 - \sum_{k=1}^{m} \frac{x_k \Lambda_{ki}}{\sum_{j=1}^{m} x_j \Lambda_{kj}}$$

$$T_{min} = \max\{T_1, T_2, T_3, T_4\}$$

Minimum temperature and molar fraction values of the quaternary salt

OUTPUT: Ternary plot of mixture of alt by keeping one molar fraction constant

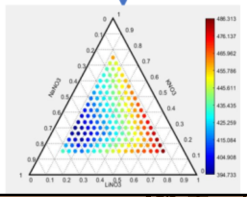

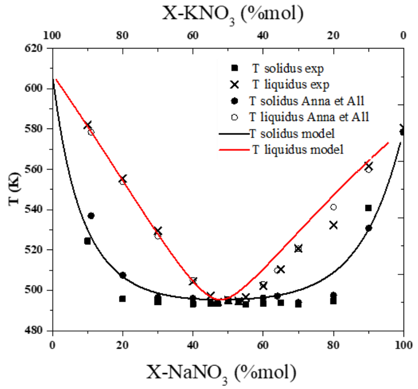

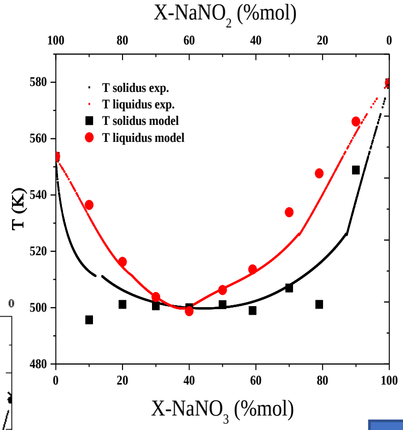

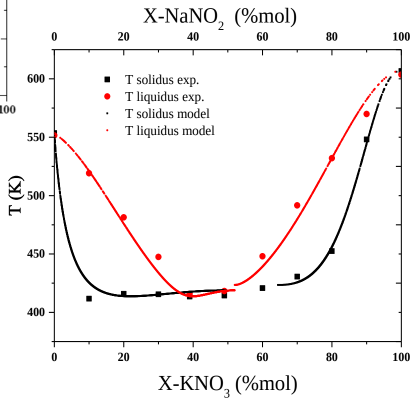

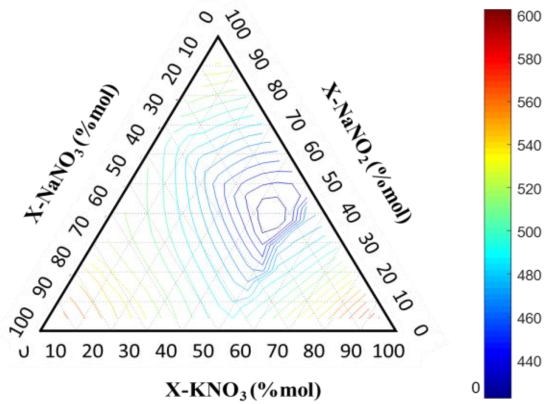

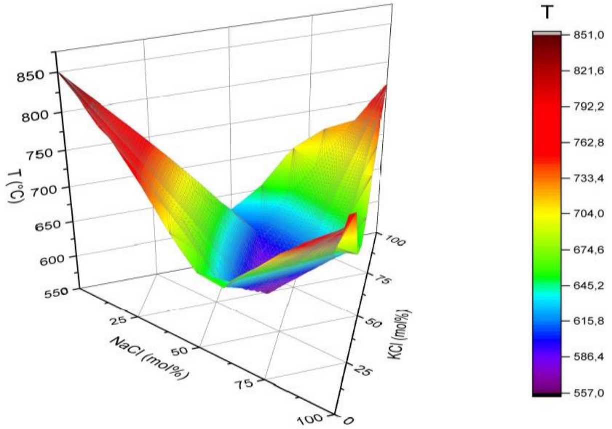

2) Thermophysical properties
MS Purity

Ion Chromatography (IC)

Ion chromatography (IC) is an analytical technique for the determination of major constituents in the ionic form in aqueous samples.

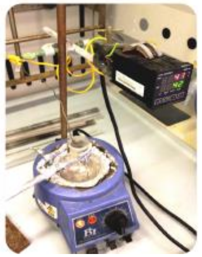

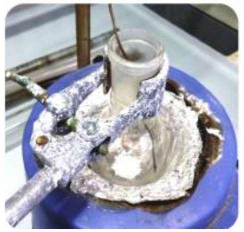

MAX PERCENTAGE OF IMPURITIES	
Chloride	0,20%
Carbonates	0,03%
Sulfates	0,05%
Alkalinity hydroxyls	0,15%
Perchlorates	0,04%
Magnesium	0,04%
Calcium	0,04%
Insoluble	0,04%
	0,06%
It is not accepted the use of anticaking agents.	

MICROWAVE PLASMA ATOMIC EMISSION SPECTROMETRY *(MP- AES)*

MP-AES allows to measure the presence of **metals**, even in small percentages.

Properties
Purity
phase diagrams
Thermal stability
specific heat
viscosity
density
heat conductivity

SFERA-III

Solar Facilities for the European Research Area

Study and modeling of binary and ternary mixtures

Phase diagrams

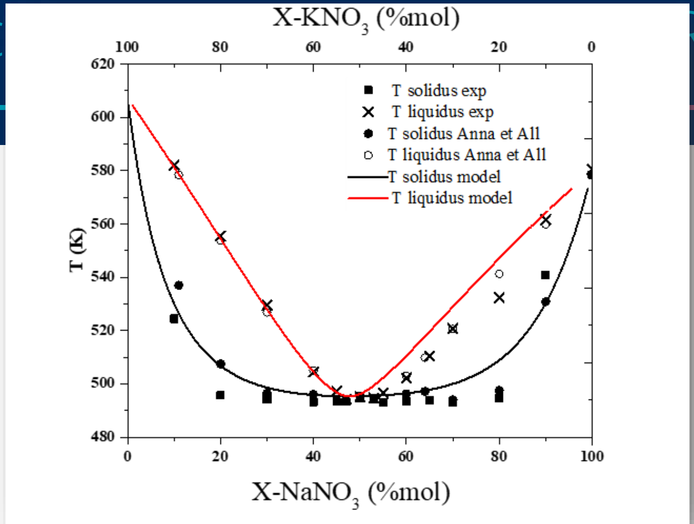

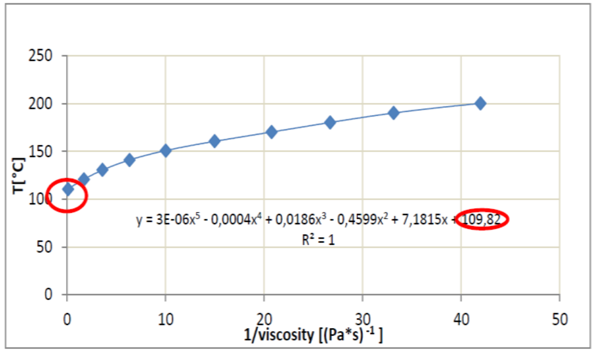

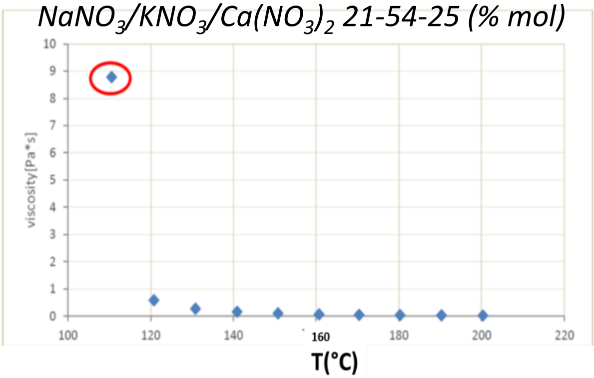

TGA/DSC

Applying a controlled temperature ramp, allowing the salt to melt and then to solidify it is possible to detect **"onsets**" of solidification and melting (Tliq and Tsol)

Rheometer

The dynamic viscosity of a Newtonian fluid (such as a molten nitrate) is directly dependent on the materials temperature.

$$\log_{10} \mu = A + \ BT - \ T0$$

Properties
Purity
phase diagrams
Thermal stability
specific heat
viscosity
density
heat conductivity

Study and modeling of binary and ternary mixtures

Thermal stability

By increasing the temperature of the molten nitrate salts, these undergo a **degradation mechanism** which, in general, can be divided into two steps:

Firstly, nitrites and oxygen are produced

1 step. $$\mathbf{MNO_3 \rightleftarrows MNO_2 + \frac{1}{2}\,O_2}$$ **where M= Na, K, Li**

This reaction is reversible. In turn, nitrites can lead to a second reaction:

2 step. $$\mathbf{2MNO_3 \rightarrow M_2O + N_2 + \frac{5}{2}O_2}$$

This process is not expected to be easily reversible, so alkaline oxides can:

- accumulate and **increase the melting point** of the mixture
- react **producing alkaline hydroxides (very corrosive) and carbonates**
- **precipitate** leading to problems with valves and pipeline occlusions due to limited solubility

The presence of nitrites: **Ion chromatography.**

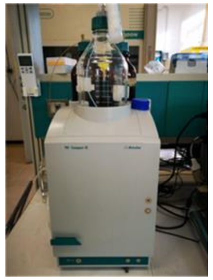

The presence of oxides: **acid-base titration**.

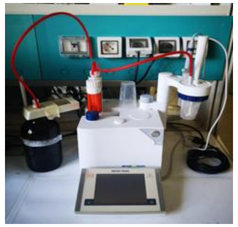

The formation of oxides is the factor that determines the upper temperature limit at which is possible to use a nitrate/nitrite salt.

Specific heat

It is possible to estimate **heat capacity** values of molten salts with the use of a known heat capacity substance as reference (high purity sapphire).

$$W_z = Cp_z \cdot m_z \cdot \beta \cdot \Delta T$$

$$W_{salt} = Cp_{salt} \cdot m_{salt} \cdot \beta \cdot \Delta T$$

$$\Downarrow$$

$$Cp_{salt} = \frac{Cp_z \cdot m_z \cdot W_{salt}}{m_{salt} \cdot W_z}$$

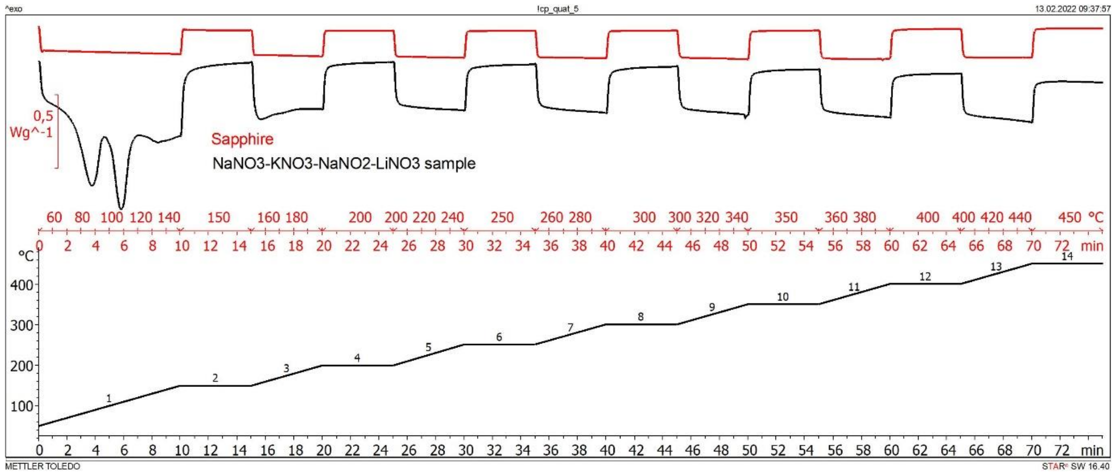

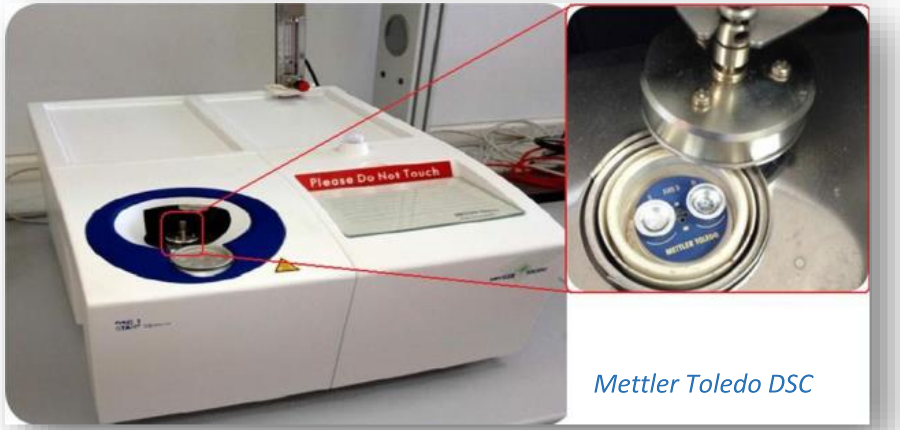

Mettler Toledo DSC

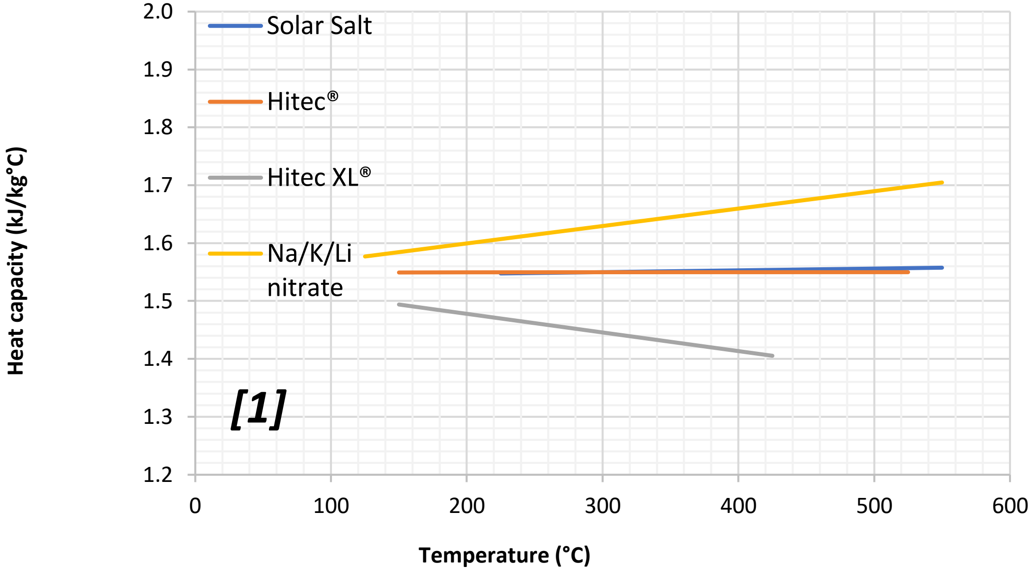

Properties
Purity
Phase diagrams
Thermal stability
Specific heat
viscosity
density
heat conductivity

2) Thermophysical properties
Viscosity

Viscosity, **measured by a viscometer, is a measure of the resistance of a fluid to deform under shear stress.**

Considering a model in which a fluid is delimited between two parallel planes and being force and surface parallel, their relationship represents a **shear stress**:

$$\tau_{xy} = \frac{\vec{F}}{\vec{A}}$$

The shear stress is proportional to the velocity $\vec{u}$ and inversely proportional to the distance of the two plans. This dependence is called Newton's law for viscous fluids:

$$\tau_{xy} = \mu \frac{du_x}{dy}$$

in which the coefficient of proportionality μ takes the name of **dynamic viscosity** for a fluid [Pa*s].

Properties
Purity
phase diagrams
Thermal stability
specific heat
viscosity
density
heat conductivity

2) Thermophysical properties
Viscosity

The gradient of velocity **(shear rate)** is uniform between the two planes :

$$\gamma = \frac{du_x}{dy} = \frac{u_x}{dy}$$

Then the **viscosity** is defined as:

$$\mu = \frac{shear\ stress}{shear\ rate} = \frac{\tau}{\gamma}$$

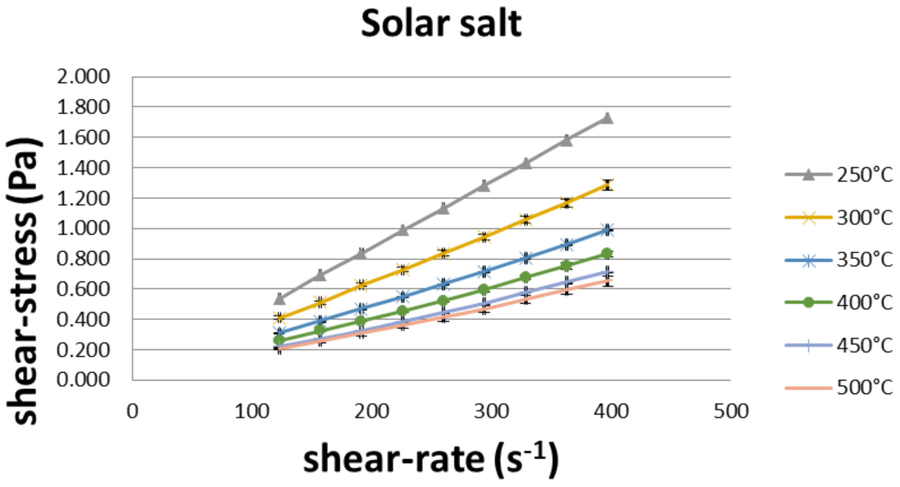

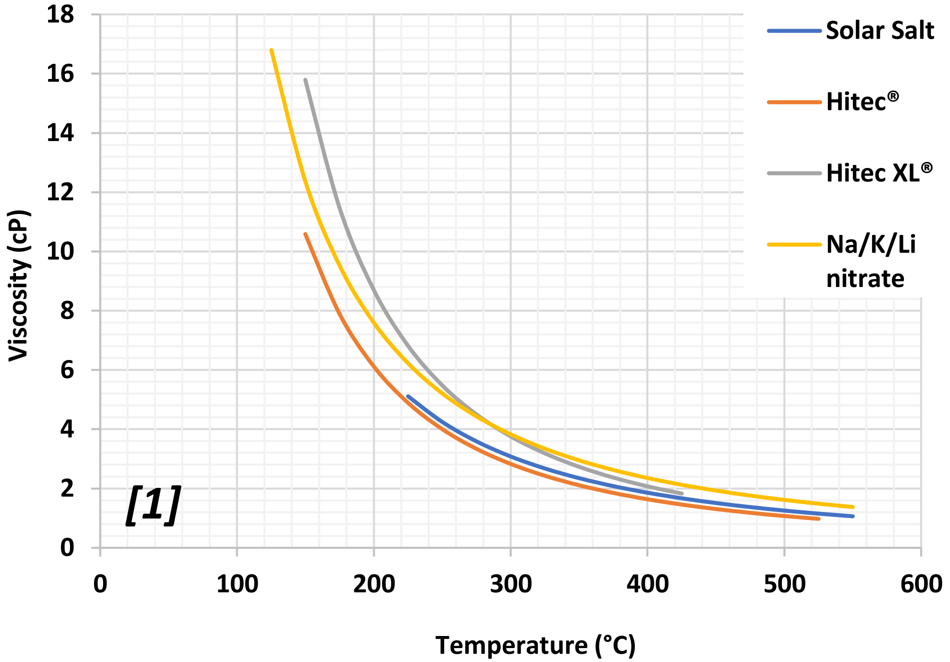

If the relationship between shear stress and shear rate is **a straight line passing through the axis origin**, the fluid is defined Newtonian and the slope is the Viscosity

2) Thermophysical properties
Density

Density measurements of the mixtures are performed with an *Archimedean* based test.

The equipment consists of a **thermoregulated stainless steel container** where the salt mixture is placed and heated; the system is kept under air at atmospheric pressure.

The temperature is regulated by an external PID controller.

The salt is then vigorously stirred, and a steel cylinder connected to the dynamometer is immersed; the weight loss due to the Buoyancy effect was noted.

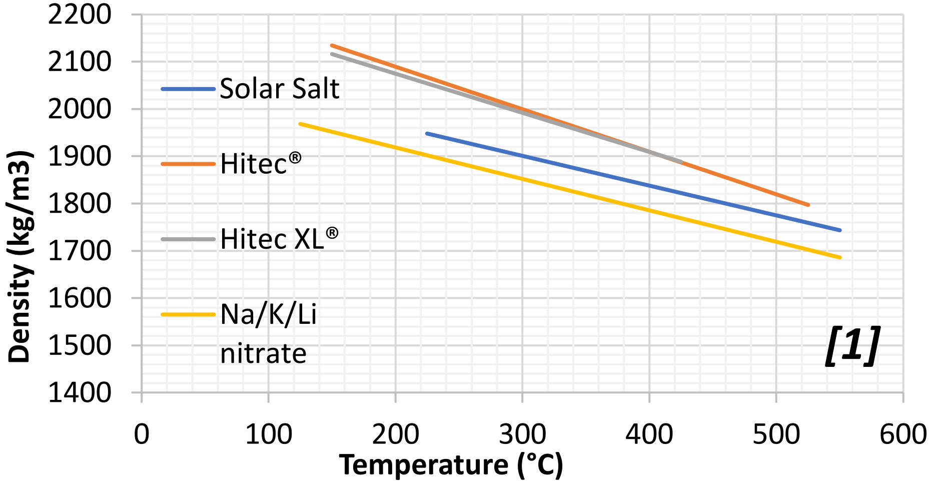

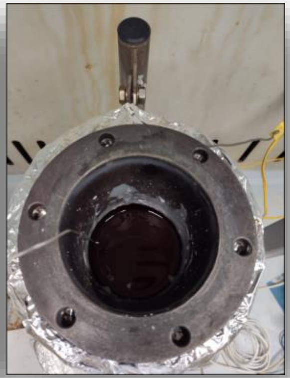

Properties
Purity
phase diagrams
Thermal stability
specific heat
viscosity
density
heat conductivity

2) Thermophysical properties

Heat conductivity

Heat conductivity : instrument based on the "hot wire" method (only for solid)

Transient Plane Source (TPS) element is used as both heat source and temperature sensor, and the measurement is made by recording the voltage change over the TPS-element while its temperature is slightly heated by an electrical current pulse .

- HOT DISK 2500 s (TPS technique)

TPS element

SAMPLE

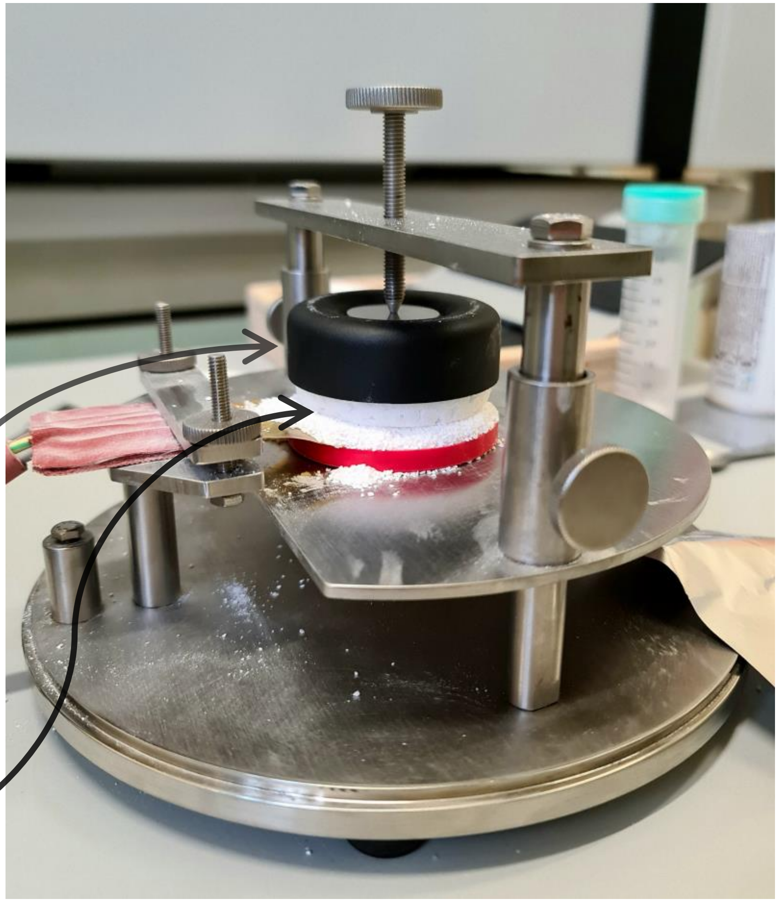

Properties
Purity
phase diagrams
Thermal stability
specific heat
viscosity
density
heat conductivity

2) Thermophysical properties

Properties	Interest for HTF	Interest for HSM
Purity	Required purity for CSP applications	Required purity for CSP applications
phase diagrams	Determination of the lowest Tliq	Determination of the lowest Tliq
Thermal stability	Maximum operative T	Maximum operative T
specific heat	Capacity of solar heat tranfer to the storage system	Capacity of heat storage
viscosity	Determination of the necessary pumps hydraulic head	It depends on the storage system. In“Archimede “configuration HTF and HSM are the same fluid.
density	Related to heat capacity; capability of heat storage per volume	Related to heat capacity; capability of heat storage per volume
heat conductivity	Necessary parameter to determine the heat exchange surfaces	Necessary parameter to determine the heat exchange surfaces

3) Environmental safety and risk for human health

	Risk Phrases
Solar salt	May intensify fire - H272
Ternary Li/Na/K//NO3	May intensify fire - H272 Causes serious eye irritation -H319
Ternary Ca/Na/K//NO3	May intensify fire - H272
Hitech® ($NaNO_3$/KNO_3/$NaNO_2$)	May intensify fire - H272 Causes serious eye irritation -H319 Eye Irrit. - H319 Very toxic to aquatic life-H400
Quaternary Ca/Li/Na/K//NO3	May intensify fire - H272 Causes serious eye irritation -H319
Oil Diathermic (THERMINOL® 66)	Skin Irrit. - H315 Eye Irrit. - H319 Suspected of damaging fertility- H361f Aquatic Acute - H400 Aquatic Chronic - H410

4) Material costs

[1]

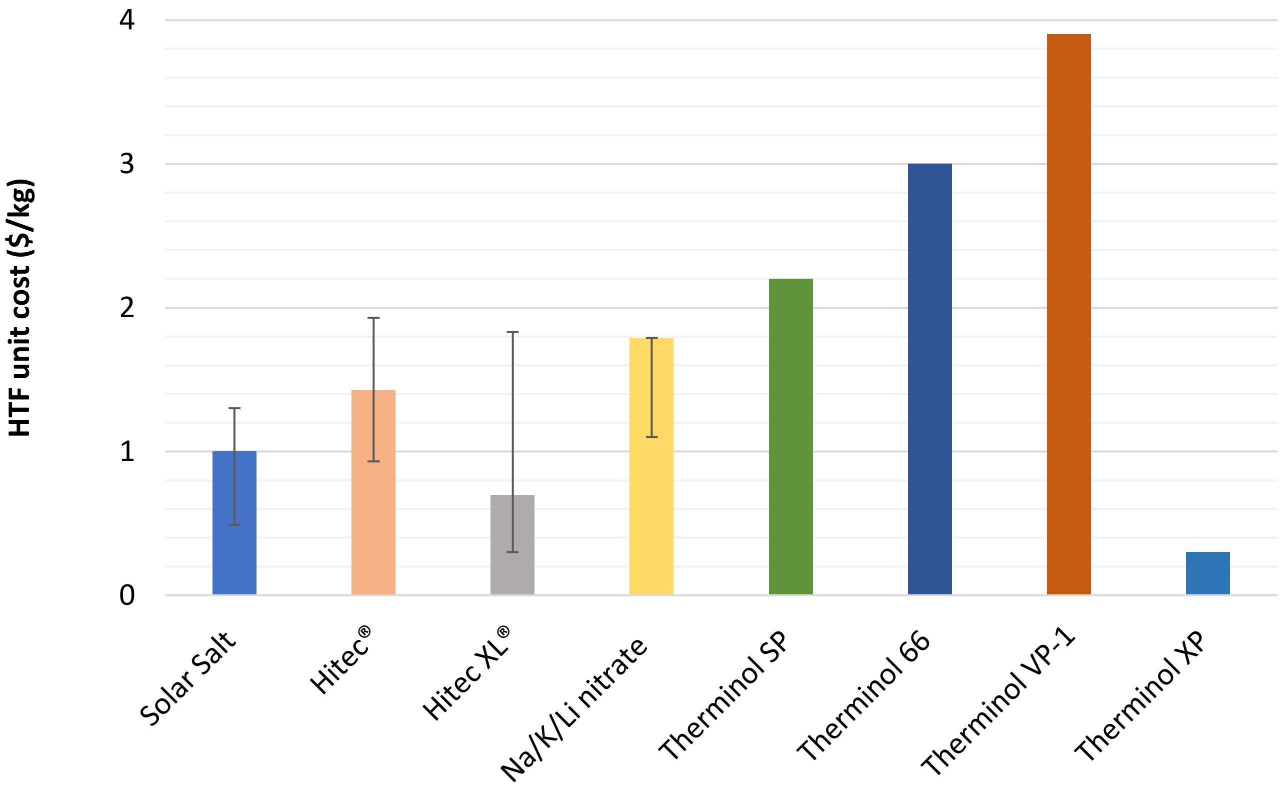

- **Ternary with calcium** is the less expensive material can be an alternative especially with respect to thermal oil, which is stable at the same temperature.
- Addition of **lithium nitrate** makes the cost of the mixture more or less comparable to the"Hitech® salt“
- **Ternary with lithium** has very good thermo-physical features, including thermal stability, but can be considered **too expensive**

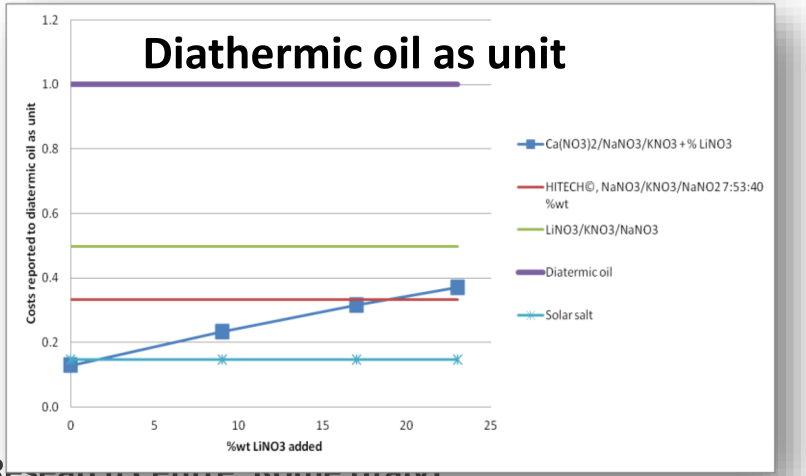

5) Construction materials compatibility

There are two mechanisms by which materials corrode in the presence of in molten salts: metal dissolution of the material constituents and oxidation of the metal to ions.

- ✓ The oxidation is the main degradation mechanism which causes uniform corrosion when a material is subject to molten salts like nitrate mixtures.
- ✓ The corrosion behaviour depends on the formation and stability of protective oxide layers over the material surface which impedes the material oxidation.

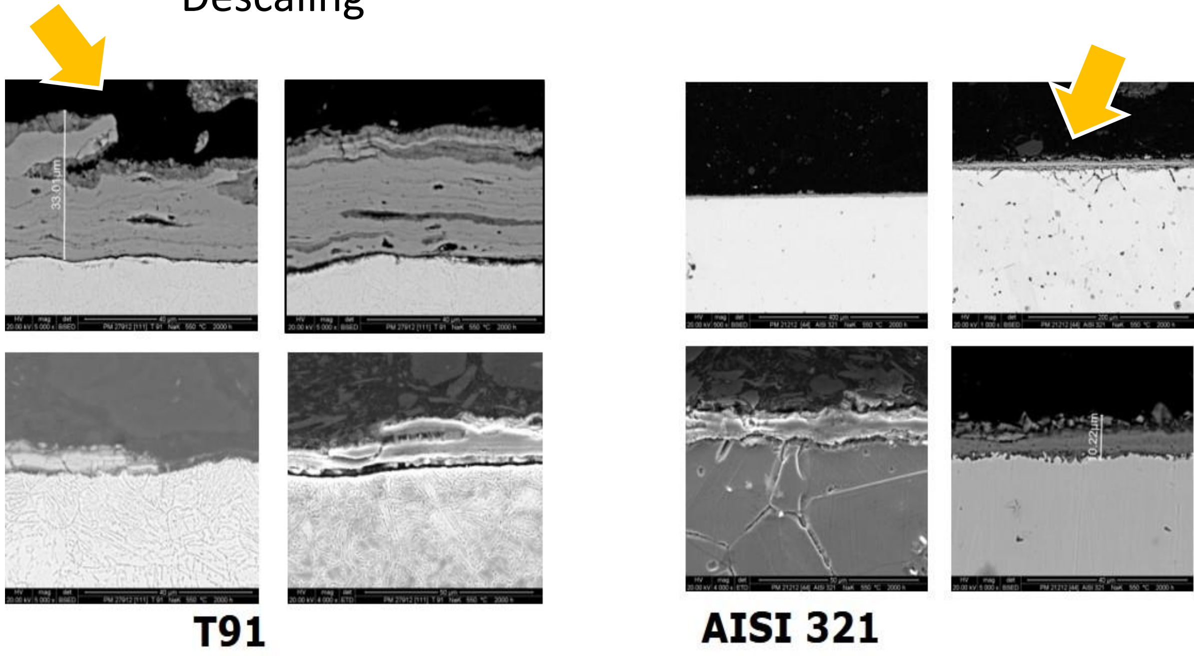

SEM images for the cross section of a specimen of T91 and AISI 321 after isothermal oxidation test (2000h) at 550°C in a molten salt mixtures.

HTFs and HSMs critical review

[2]

- **Binary $NaNO_3/KNO_3$ mixtures (M1).**

They present low cost along with good thermophysical properties and are not toxic.

- **Ternaries with lithium nitrate (M2).**

The advantages are a low freezing point and a thermal stability comparable with solar salt. The main disadvantage is the high price of lithium nitrate.

- **The addition of calcium nitrate to $NaNO_3$ and KNO_3** (M3)

decreases the mixture freezing point to about 110 °C, but also the upper temperature limit to around 450 °C .

- **Mixtures containing $NaNO_2$.** By far, the most used one is a commercial product named "Hitec©", here indicated as **M4,** but they are relatively costly and toxic.

- **Quaternary mixtures.**

The choice is limited to $Ca/Li/Na/K//NO_3$ or $Li/Na/K//NO_3/NO_2$ systems. The former seems more significant and investigated and one formulation is taken into account **(M5).** Calcium nitrate and sodium nitrite cannot be mixed together given the formation and rapid reoxidation of calcium nitrite even at low temperatures.

HTFs and HSMs critical review

		Tliquidus (°C)	Tdegradation (°C)	ΔT (°C)
Solar salt	M1	238	550*	312
Ternary Li/Na/K//NO3	M2	100-120	550*	440
Ternary Ca/Na/K//NO3	M3	133	450	317
Hitech®	M4	141	450	309
Quaternary Ca/Li/Na/K//NO3	M5	95	520	425
Oil Diathermic (THERMINOL® 66)	M6	-12	345	357

[2]

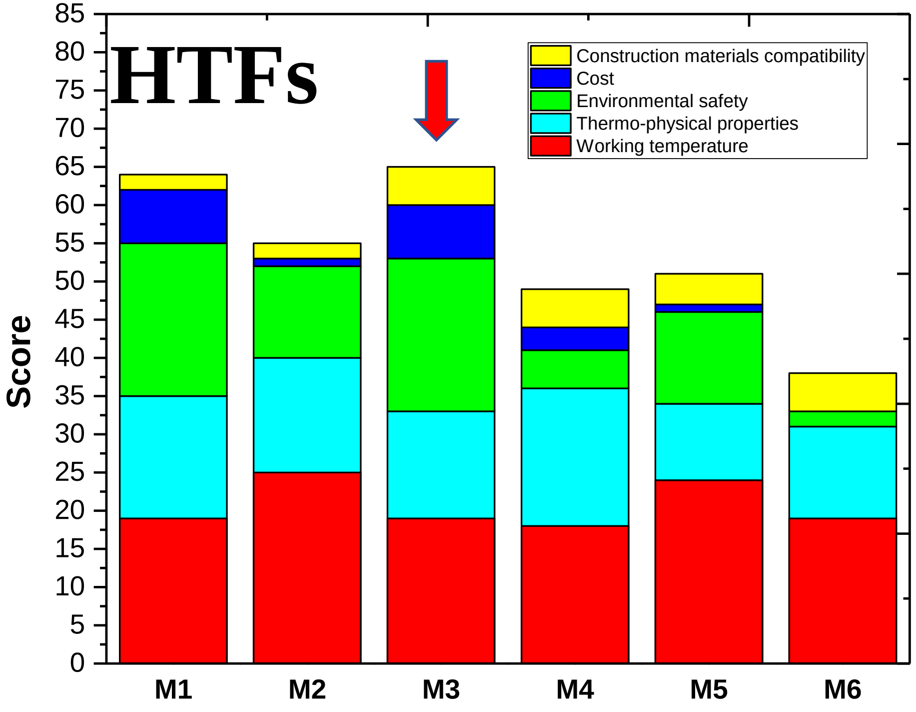

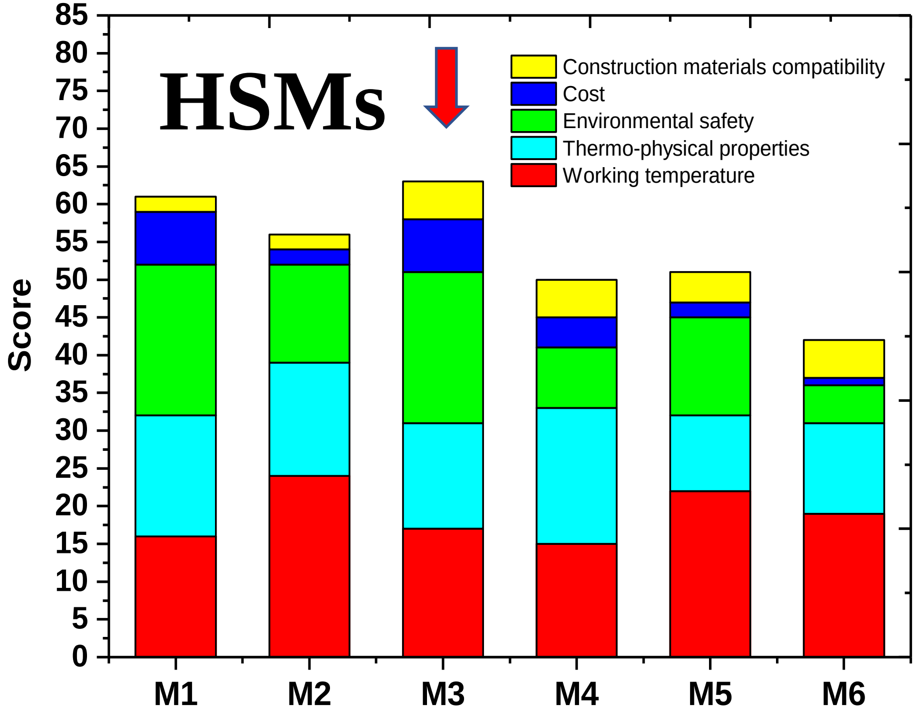

✓Mixtures with **Calcium nitrate** are very promising both as HSM and HTF.

[1] Giaconia, A.; Tizzoni, A.C.; Sau, S.; Corsaro, N.; Mansi, E.; Spadoni, A.; Delise, T. Assessment and Perspectives of Heat Transfer Fluids for CSP Applications. Energies 2021, 14, 7486.

[2] Delise, T., Tizzoni, A.C., Ferrara, M., Corsaro, N., D'Ottavi, C., Sau, S., Licoccia, S. Thermophysical, environmental, and compatibility properties of nitrate and nitrite containing molten salts for medium temperature CSP applications: A critical review (2019)
Journal of the European Ceramic Society, 39 (1), pp. 92-99.

SFERA-III
Solar Facilities for the European Research Area

Annarita SPADONI
ENEA
TERIN-STSN-SCIS
annarita.spadoni@enea.it

Anna Chiara TIZZONI
ENEA
TERIN-STSN-SCIS
annachiara.tizzoni@enea.it

GOBIERNO DE ESPAÑA MINISTERIO DE CIENCIA, INNOVACIÓN Y UNIVERSIDADES · Ciemat Centro de Investigaciones Energéticas, Medioambientales y Tecnológicas · ENEA · DLR Deutsches Zentrum für Luft- und Raumfahrt · UNIVERSIDADE DE ÉVORA · ESTELA · The Cyprus Institute · instituto imdea energía · Fraunhofer ISE · euronovia · LNEG · METU · ETH zürich · UNIVERSIDAD DE ALMERÍA · cnrs · cea

4th Training for Industries 07th-11th November 2022 – ENEA Casaccia Research Centre, Rome (Italy)

Solar Facilities for the European Research Area

References

- https://www.energy.gov/eere/solar/concentrating-solar-thermal-power
- Giaconia, A.; Tizzoni, A.C.; Sau, S.; Corsaro, N.; Mansi, E.; Spadoni, A.; Delise, T. Assessment and Perspectives of Heat Transfer Fluids for CSP Applications. Energies 2021, 14, 7486.
- Delise, T., Tizzoni, A.C., Ferrara, M., Corsaro, N., D'Ottavi, C., Sau, S., Licoccia, Thermophysical, environmental, and compatibility properties of nitrate and nitrite containing molten salts for medium temperature CSP applications: A critical review (2019) Journal of the European Ceramic Society, 39 (1), pp. 92-99.

SFERA-III

Solar Facilities for the European Research Area

4th Training for Industries

7-11th November 2022, Cr ENEA Casaccia Rome (Italy)

Predictive tools for molten salts mixtures

Salvatore Sau/Anna Chiara Tizzoni (ENEA, TERIN-STSN-SCIS)

JOINT RESEARCH ACTIVITIES

THIS PROJECT HAS RECEIVED FUNDING FROM THE EUROPEAN UNION'S HORIZON 2020 RESEARCH AND INNOVATION PROGRAMME UNDER GRANT AGREEMENT NO **823802**

Outline

- Since the multicomponent MS mixtures of possible practical interest are particularly numerous, it is practically impossible to determine the chemical-physical parameters for each of them.
- Development and validation of **predictive models** which, starting from the properties of the individual components, allow to establish the thermophysical characteristics of nitrate and nitrite mixtures according to their composition.
- An **experimental campaign** was preliminarily carried out aimed at:
  - filling the gaps present in the scientific literature regarding these data
  - obtaining a minimum number of values, which, would allow an appropriate validation of the predictive systems proposed.

Moreover, an **open-source database** has been developed, available and easy to consult, to make the results usable quickly and effectively, and allowing the integration the new data obtained with scientific literature.

The following work has been funded in the framework of the "Concentrating Solar Power" project, research activity lines on solar "process heat for industrial processes", under the "Electric System Research" Programme 2019-2021, with the financial support of Italian Ministry for Economic Development.

The results are going to be published in public domain, online available, reports (in Italian language)

Outline

- The mixtures of binary and ternary salts reported, with known composition, have been characterized from a chemical and physical point of view, experimentally measuring their heat capacity, viscosity and density.
- The mixtures have been studied in the temperature range that goes from values close to the solidification temperature up to the maximum values for which there is thermal stability.

	KNO_3	$NaNO_3$	$NaNO_2$	$Ca(NO_3)_2$
	Molar fraction			
KNO_3	1			
$NaNO_3$		1		
$NaNO_2$			1	
Solar Salt - $NaNO_3$-KNO_3 (60/40 % w/w)	0.36	0.64		
$NaNO_3$-$NaNO_2$ (45/55 % w/w)		0.40	0.60	
KNO_3-$NaNO_2$ (49/51 % w/w)	0.40		0.60	
$NaNO_3$-$Ca(NO_3)_2$ (55/45 % w/w)		0.70		0.30
KNO_3-$Ca(NO_3)_2$ (59/41 % w/w)	0.70			0.30
Hitec® $NaNO_3$-KNO_3-$NaNO_2$ (7/53/40 %w/w)	0.44	0.07	0.49	
Hitec XL® $NaNO_3$-KNO_3-$Ca(NO_3)_2$ (15/43/42 % w/w)	0.50	0.21		0.30

Specific Heat
Theory and experimental

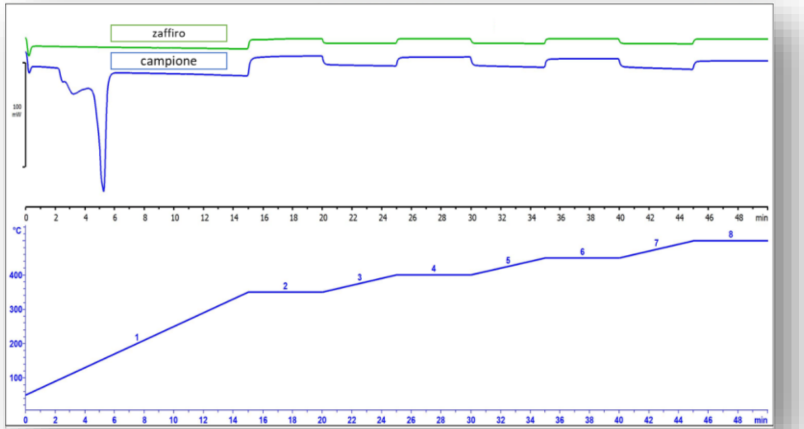

	cp (J/g*°C)	error %
KNO_3	1.335	2.61
$NaNO_3$	1.653	5.19
$NaNO_2$	1.586	1.22
Solar Salt	1.525	4.03
$NaNO_3$-$NaNO_2$	1.548	1.06
KNO_3-$NaNO_2$	1.468	4.28
$NaNO_3$-$Ca(NO_3)_2$	1.345	9.89
KNO_3-$Ca(NO_3)_2$	1.478	0.94
Hitec® $NaNO_3$-KNO_3-$NaNO_2$	1.475	1.67
Hitec XL® $NaNO_3$-KNO_3-$Ca(NO_3)_2$	1.342	15.07

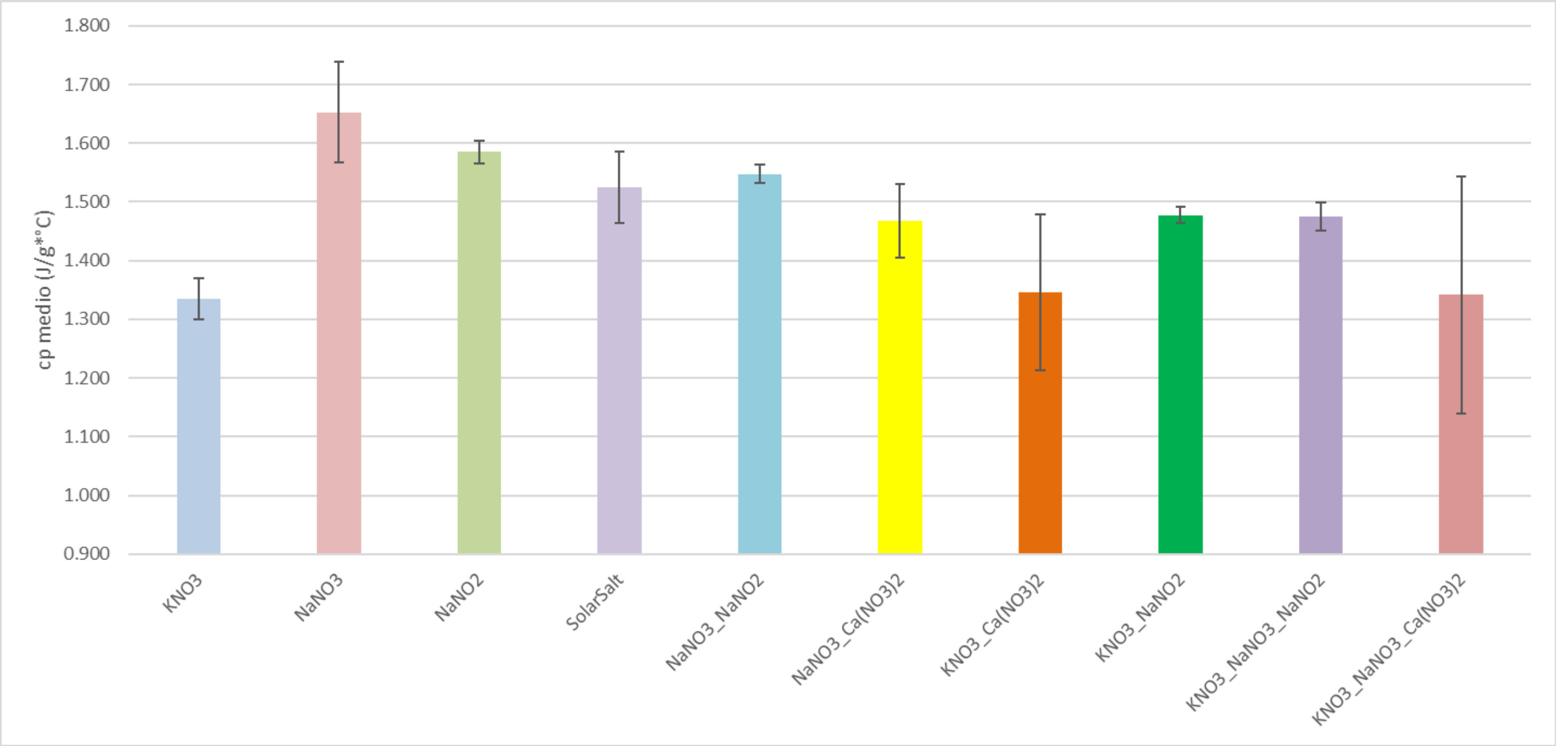

Specific Heat
Modelling

Modelling of multicomponent mixtures selected and comparison with literature and experimental data

Starting from the values of pure salts, the specific heat of a mixture can be estimated using the **additivity rule**, based on the molar contributions of the individual constituents.

The specific heat of a multicomponent mixture can therefore be derived from the following equation:

$$cp_x = \sum X_j * cp_j$$

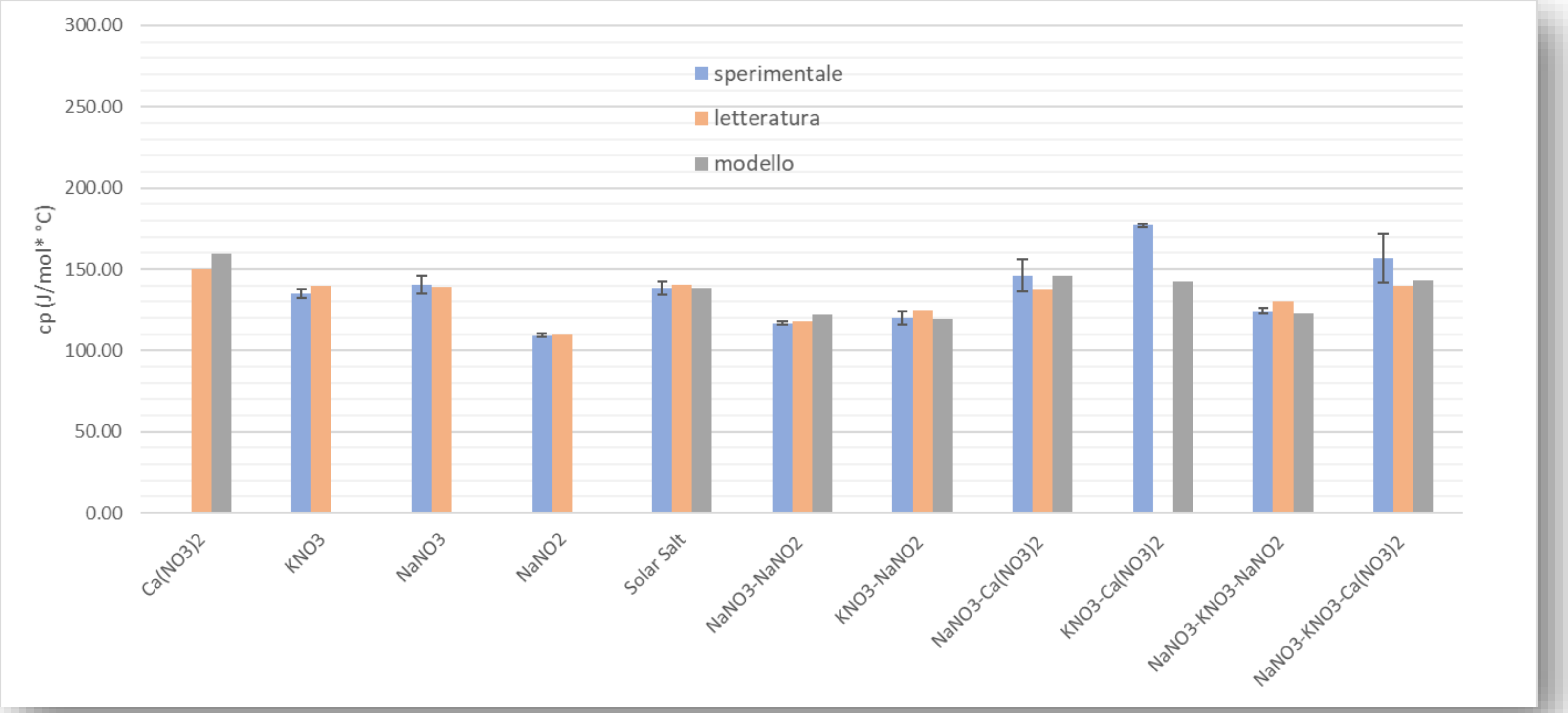

Specific Heat
Modelling

Modelling of other multicomponent mixtures

The specific heat of unknown multicomponent mixtures can be calculated using an additivity rule based on the properties of the individual constituents.

Having obtained all the specific heat values of the pure components, the cp of the mixtures in have been calculated with the model according and compared with the literature.

The deviation between the model data and the literature values is about 5%.

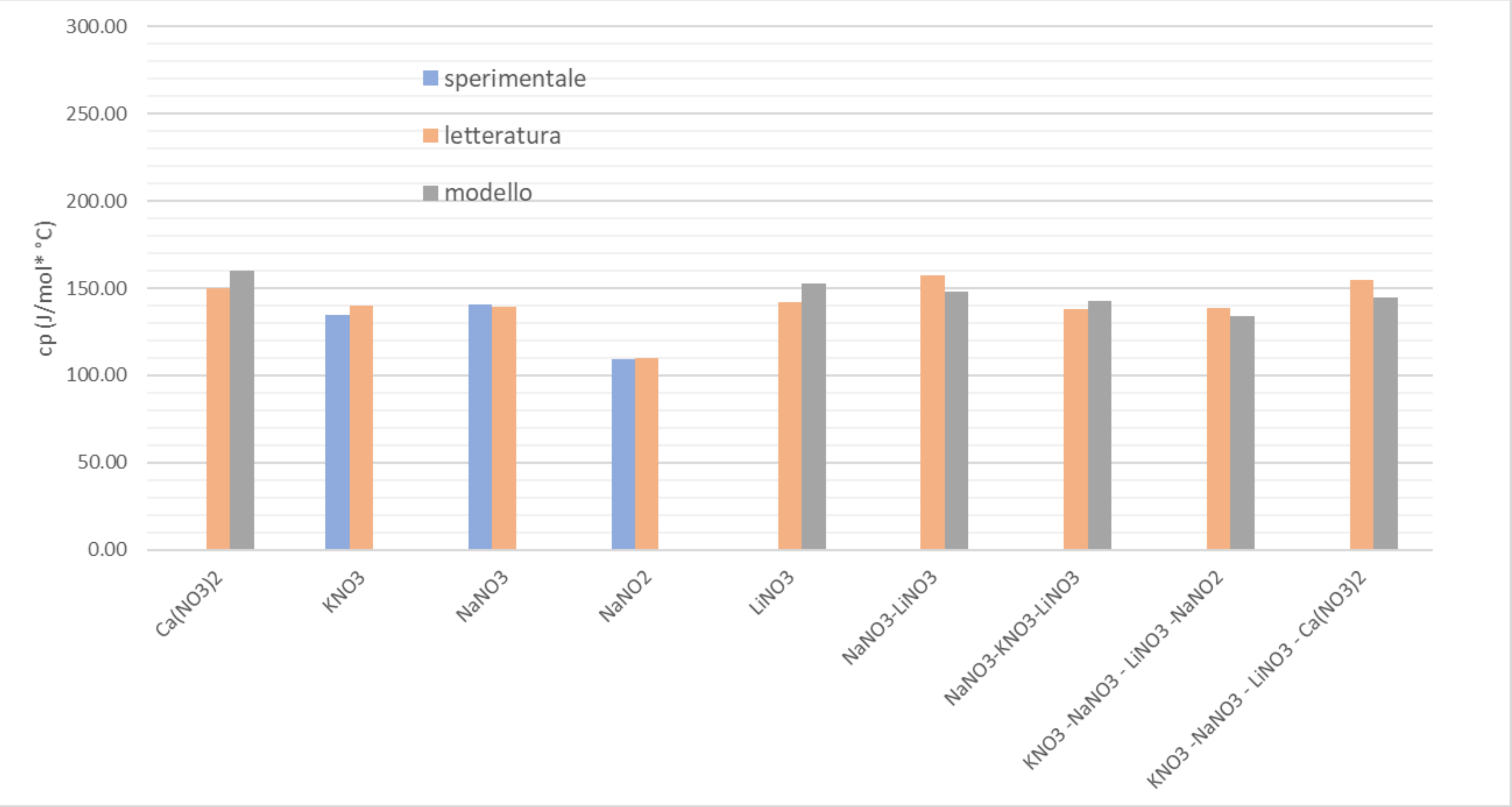

Density
Theory and experimental

Correlating density with the composition of a molten nitrate salt mixture has a practical application and, possibly, fundamental significance.

✓ From a practical aspect, a correlation enables density to be calculated for mixtures other than those subject to measurements and establishes this property for design purposes.

✓ With regard to fundamental characteristics of molten salt behaviour, the correlation may also indicate if mixtures behave ideally.

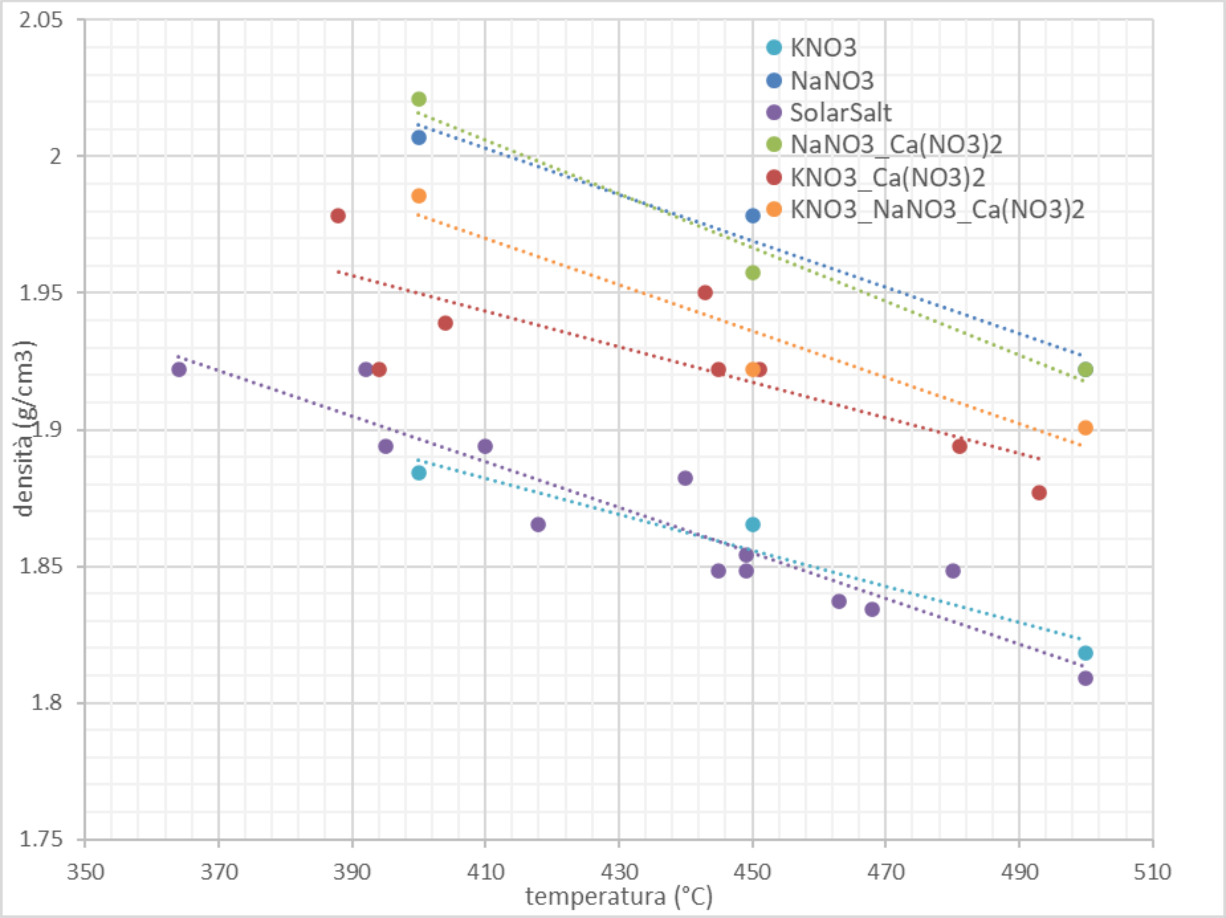

ENEA experimental density MS data

Density
Modelling

The molar volume of binary mixtures of molten salts can be obtained by a "volumetric additivity rule" based on the molar volumes of the individual constituents:

$$V_{m,x} = \sum X_j * V_{m,j}$$

Such a molar volume additivity rule can be applied to calculate the density of multi-component nitrate salts as a function of both composition and temperature.

Density is related to molar volume and molecular weight, MW:

$$\rho = \frac{\mathrm{MW}}{V_m} \qquad MW_x = \sum X_j * PM_j$$

Given the molar volumes of the constituents, the density of a mixture can be then calculated:

$$V_m = A_v + B_v \ * \ T$$

$$\rho = \frac{\sum X_j * PM_j}{\sum X_j * (A_{vj} + B_{vj} \ * \ T)}$$

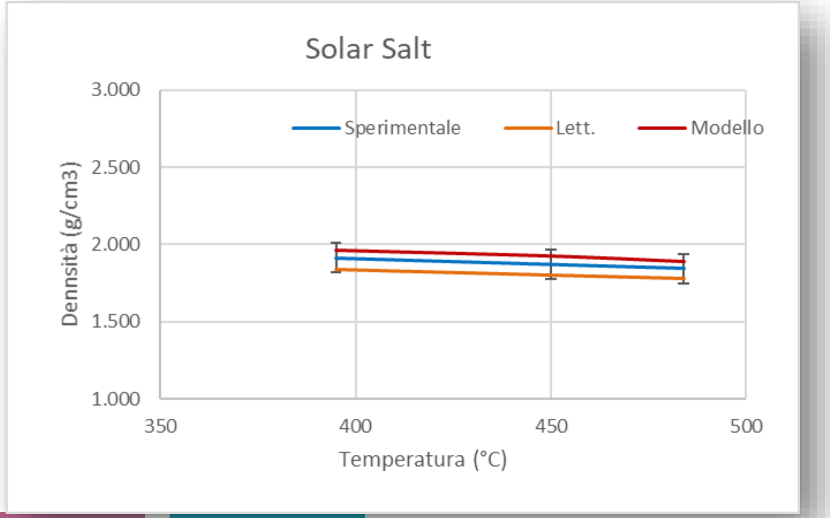

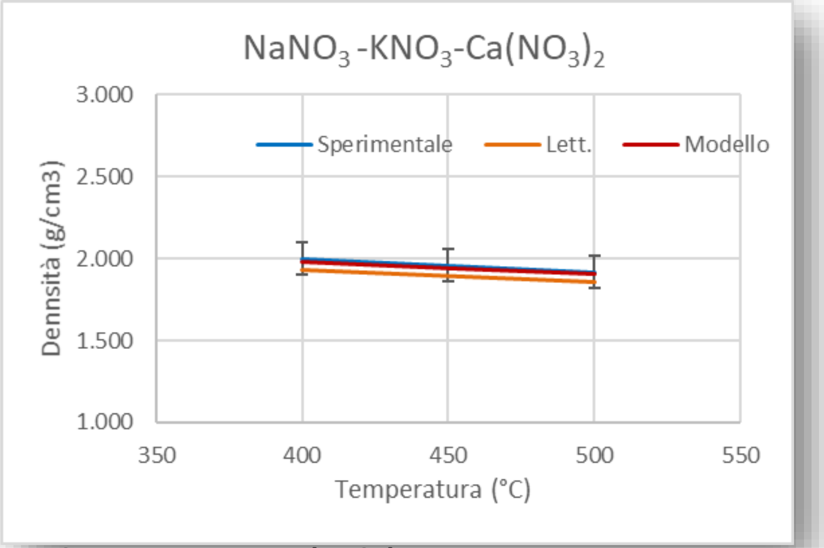

Caratterizzazione altre miscele con modello

The molar volume and therefore the density of **unknown multicomponent** mixtures can be calculated using an additivity rule based on the properties of the individual constituents.

From literature data, it has been possible to derive the molar volumes and therefore the densities also of other pure components, and their trends have been compared with the scientific literature.

The deviation of the modelling with respect to the literature data is about 6%.

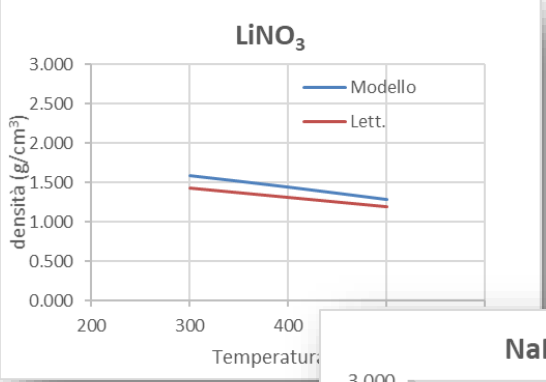

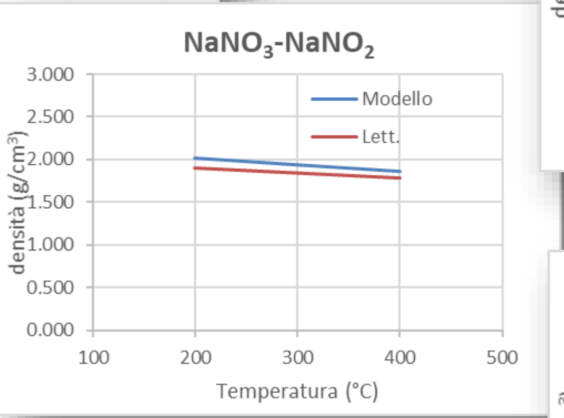

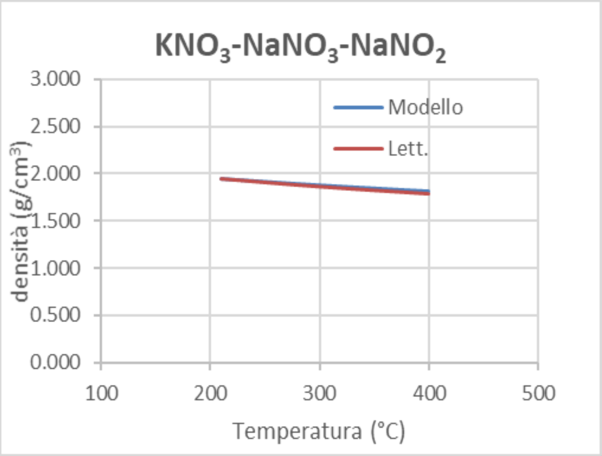

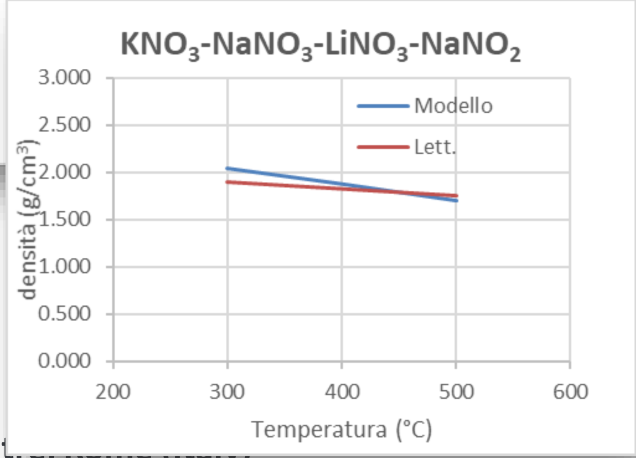

Viscosity
Theory and experimental

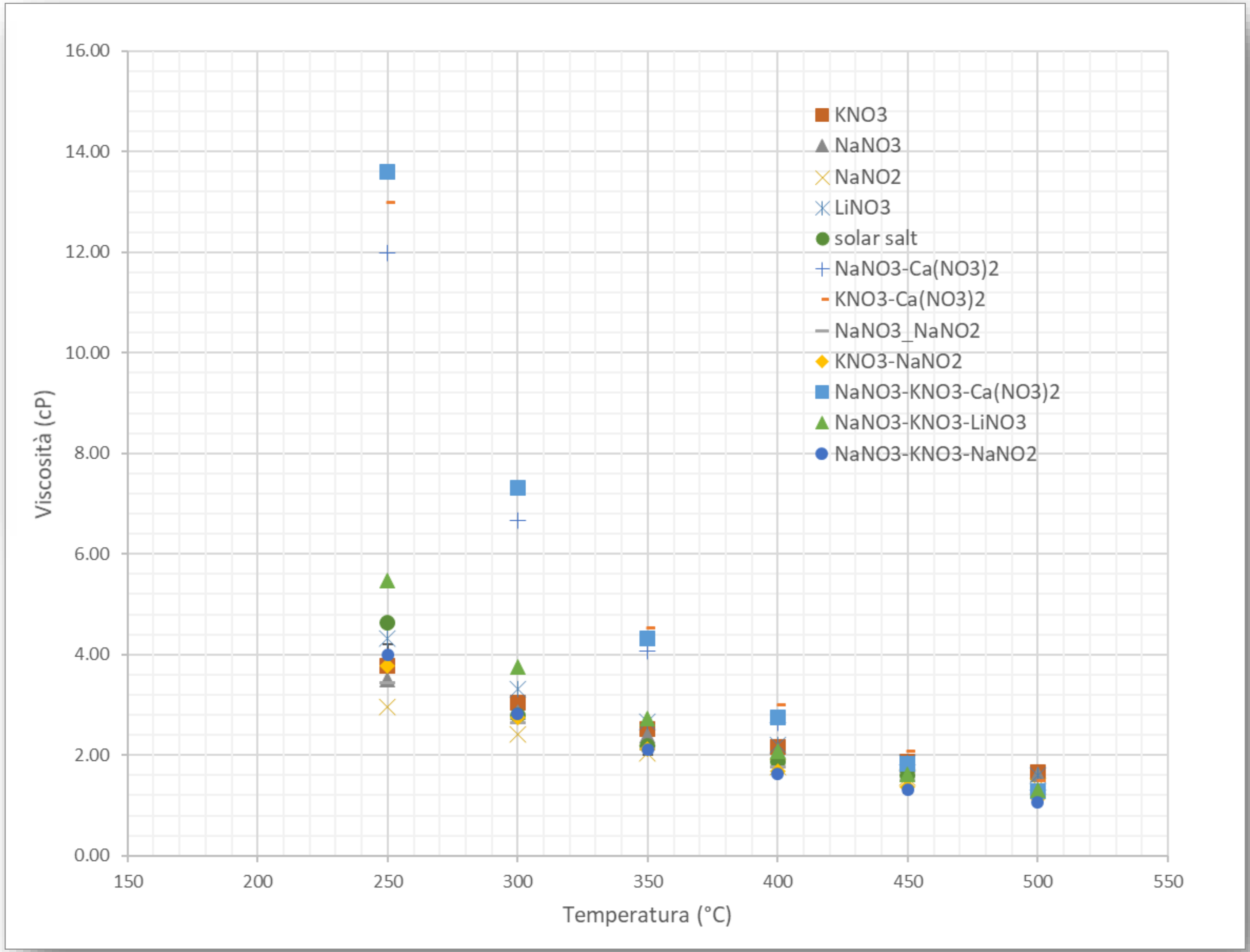

Viscosity
Modelling

- For the calculation of the resulting viscosity of the mixture of liquids, the following relationship can be used:

$$\mu_{mixture} = \frac{\sum_i \chi_i \rho_i}{\sum_i \chi_i \frac{\rho_i}{\mu_i}}$$

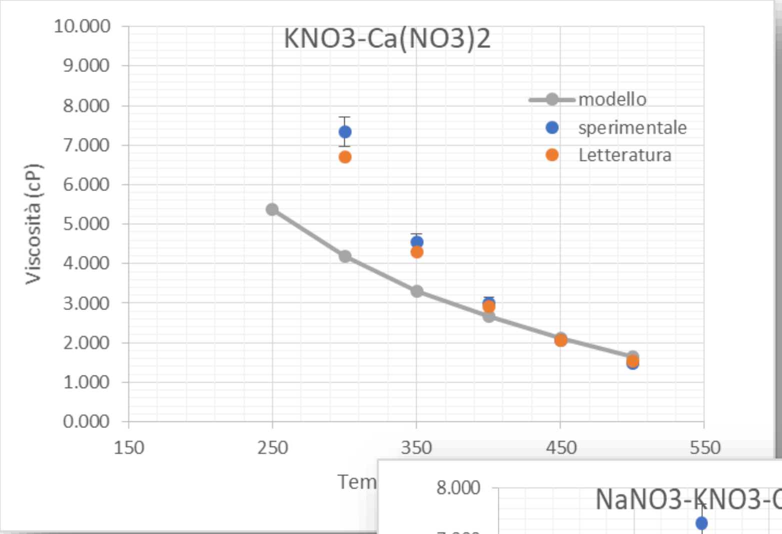

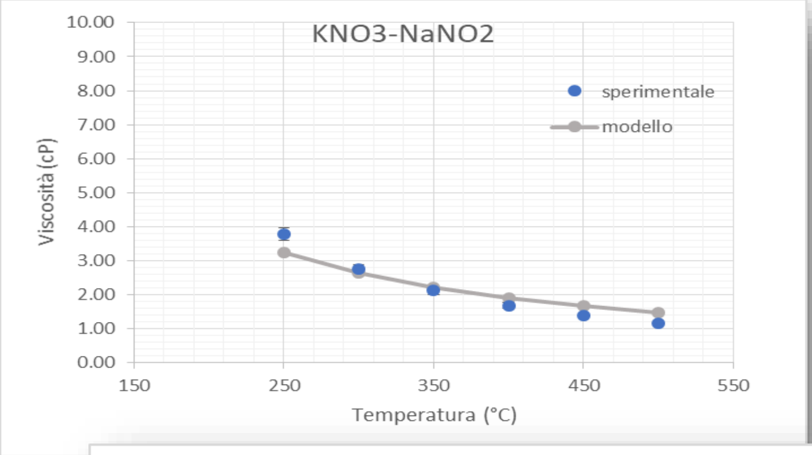

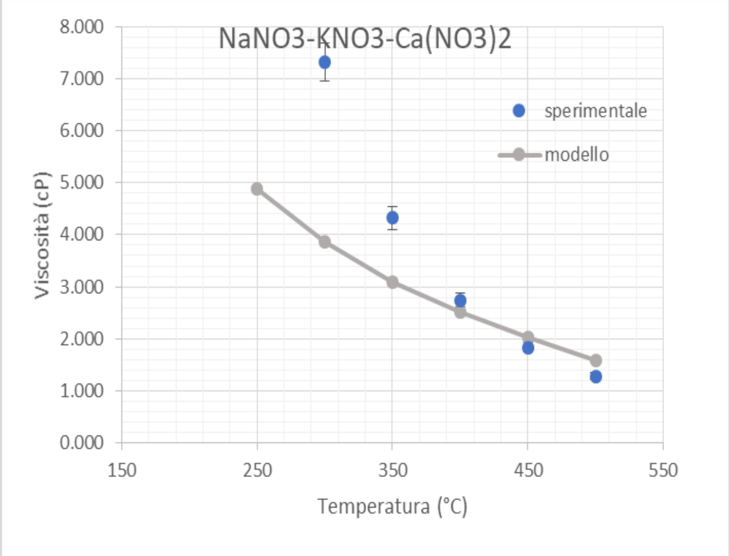

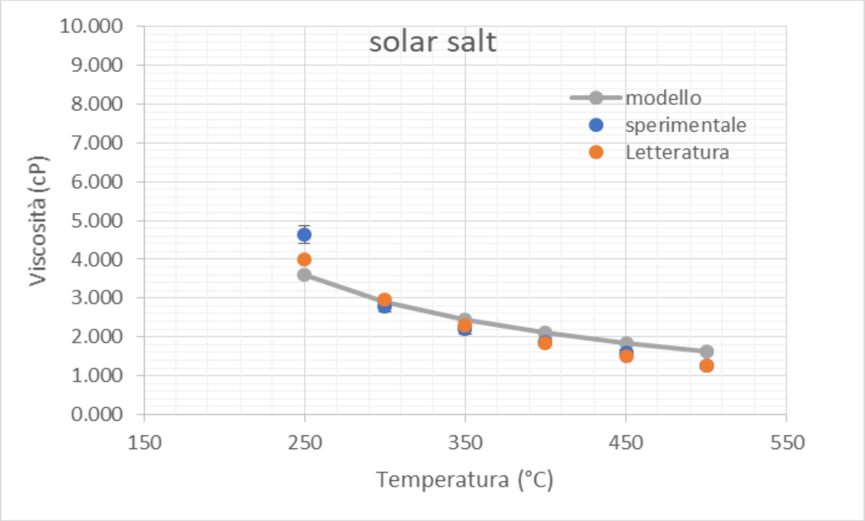

Viscosity
Modelling

- In mixtures containing calcium (**for molar fractions of calcium above 0.25**), a different approach was preferred, applying a model that considered the interaction between solute and solvent in an electrolyte solution, based on the theory of the liquid state.

The viscosity of a pure solvent at temperature T is expressed by: $\mu/\mu_0 = e^{\frac{f}{RT}}$

Where f is the Helmholtz activation energy, which can in turn be expressed as the sum of an ideal mixing and an excess contribution: $f = f_I + f_{EX}$

The viscosity for the ideal mixing contribution is expressed by: $\mu_I/\mu_0 = e^{\frac{f_I}{RT}}$
with μ_0 is the viscosity of the pure solvent.
It is possible to consider the ideal mixing contribution with a simpler equation as:

$$\mu/\mu_0 = (1 + a\sqrt{c} + bc)e^{\frac{f_{EX}}{RT}}$$

with a and b fitting parameters that can be varied and c the mole fraction of the solute.

The Helmholtz activation energy is approximated to the mixing energy, and the parameters in the equations **have physical significance and are related to the degree of ionic hydration.**

Viscosity
Modelling

The simplicity and precision of this model make it particularly suitable for practical applications.

$$\mu / \mu_0 = (1 + a\sqrt{c} + bc)e^{\frac{f_{EX}}{RT}}$$

Figure shows the good agreement between the trend of the experimental viscosity data for the mixtures containing calcium nitrate considered and their modeling, for molar fractions of calcium above 0.25.

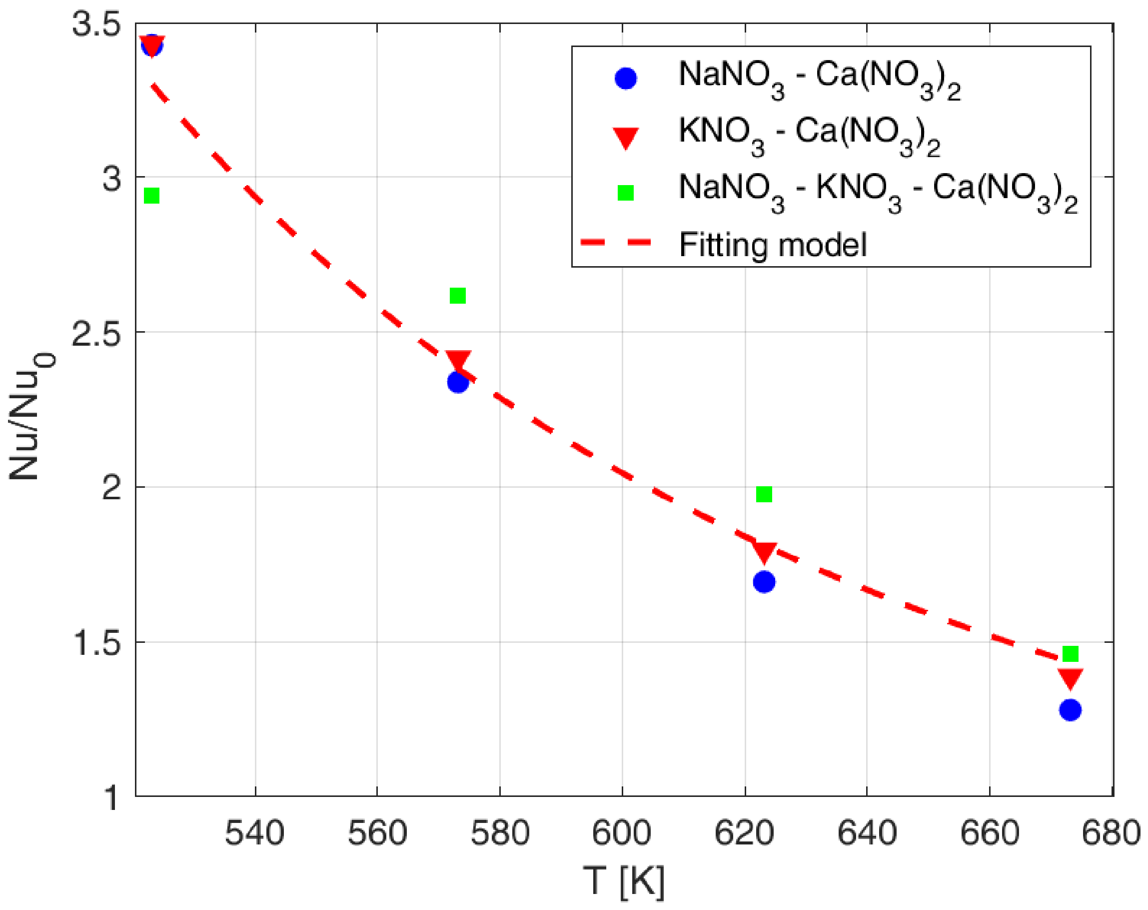

Thermal conductivity
Theory and modelling

For binary mixtures:
The thermal conductivity of the has not been evaluated experimentally, but methods to estimate it have been studied and validated.

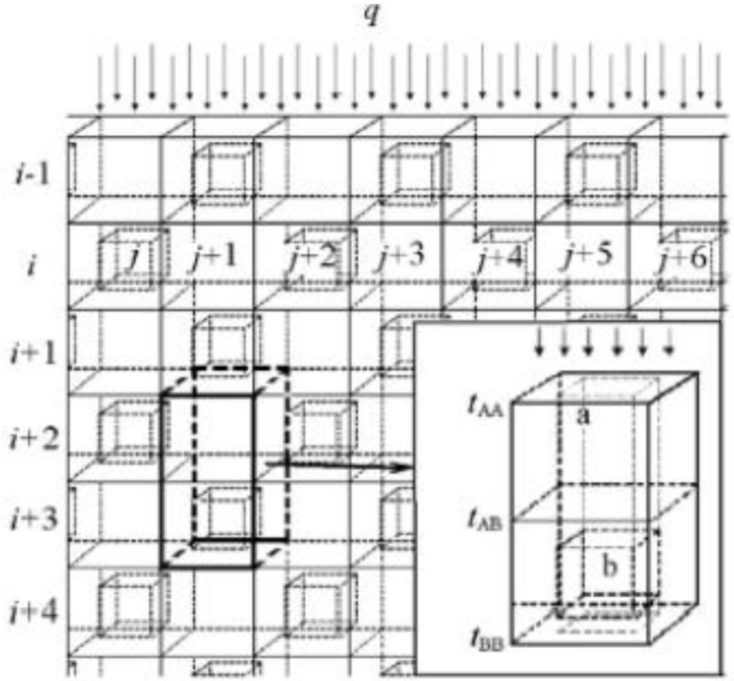

The thermal conductivity in a fluid at the macroscopic level can be simplified by assuming a flow of heat q through two types of unitary cells in series, because conduction at the macroscopic level is simply the repeated sum of the phenomenon at the microscopic level.

In them, infinitely small unit cells are considered, and it is assumed that the components of a mixture of molten salts **have been so thoroughly mixed that the mixture macroscopically behaves as a uniform phase.**
Starting from the density measurements and the calculation of the molar volume previously described for the binary mixtures:

$$\frac{b}{a} = \left(\frac{2\,\frac{\rho_A w_B}{\rho_B w_A}}{1 + \frac{\rho_A w_B}{\rho_B w_A}} \right)^{1/3}$$

$$\boxed{\lambda_e = \lambda_A \left\{ \left[1 - \left(\frac{b}{a}\right)^2 \right] + \frac{\left(\frac{b}{a}\right)^2}{1 + \left(\frac{\lambda_A}{\lambda_B} - 1\right)\frac{b}{2a}} \right\}}$$

Thermal conductivity
Theory and modelling

For multicomponent mixtures:

For multicomponent mixtures it is possible to use a simplified approach; *DiGuilio and Teja* demonstrated that the linear additivity rule for obtaining the thermal conductivity of mixtures of molten chlorates and nitrates produces good results with a still acceptable deviation.

In this work the following equation was therefore applied to extend the model to the ternary and quaternary mixtures of interest:

$$\lambda_{mix} = \sum_{i=0}^{m} \chi_i \, \lambda_i$$

The modeling results were compared with experimental values found in the scientific literature.

Thermal conductivity
Modelling

Comparisons with experimental data present in scientific literature, where present, stating that the model predicts expected thermal conductivity with errors of less than 2% for the **binary mixtures** considered.

		Molar volumes	Experimental density	Modelled Density	Thermal conductivity (literarture)
	°C	cm^3/mol	(g/cm^3)	(g/cm^3)	W/m*°C
$Ca(NO_3)_2$	400	78.646		2.086	0.5900
KNO_3	400	53.907	1.873		0.4047
$NaNO_3$	400	41.865	2.031		0.5277
$NaNO_2$	200	34.208		2.017	0.5382
$LiNO_3$	300	43.546		1.583	0.5856

						Thermal conductivity (W/m*°C)	Thermal conductivity (W/m*°C)
	KNO_3	$NaNO_3$	$NaNO_2$	$Ca(NO_3)_2$	°C		
						Letteratura	Modello
Solar salt	0.36	0.64			395	0.460 [38]	0.415
	A	B					
$NaNO_3$-$Ca(NO_3)_2$		0.70		0.30	400	0.559 [39]	0.583
		B		A			
KNO_3-$Ca(NO_3)_2$	0.70			0.30	388	-	0.416
	B			A			
$NaNO_3$-$NaNO_2$		0.40	0.60		200	-	0.529
		A	B				
KNO_3-$NaNO_2$	0.40		0.60		200	-	0.415
	A		B				

							Thermal conductivity (W/m*°C)	Thermal conductivit y (W/m*°C)
	KNO$_3$	NaNO$_3$	NaNO$_2$	$Ca(NO_3)$$_2$	LiNO$_3$	°C		
							Literature	Modello
$NaNO_3$-KNO_3-$NaNO_2$	0.44	0.07	0.49			400	0.510 [40]	0.479
$NaNO_3$-KNO_3-$LiNO_3$	0.45	0.18			0.37	400	0.416[40]	0.494
$NaNO_3$-KNO_3-$Ca(NO_3)_2$	0.50	0.20		0.30		300	0.519[28]	0.485
KNO_3 -$NaNO_3$ - $LiNO_3$ - $Ca(NO_3)_2$	0.22	0.53		0.07	0.18	200	0.480 [3]	0.515

The linear mixing rule gives results with an error of approximately 3%.

In general, it can be stated that accurate prediction of the thermal conductivity of molten salt mixtures, even at elevated temperatures, can be obtained if the measurement of pure compounds is measured with sufficient accuracy.

Thermal stability
experimental*

Nitrate/Nitrite salts chosen to be analyzed (%wt)	$NaNO_3$	$NaNO_2$	$LiNO_3$	KNO_3	$Ca(NO_3)_2$	T melting (°C)	T max? (°C)
$NaNO_3$	1					308	
$NaNO_2$		1				271	
$LiNO_3$			1			255	
KNO_3–$Ca(NO_3)_2$				0.59	0.41	143.2	
$NaNO_3$-KNO_3-$Ca(NO_3)_2$	0.15			0.43	0.42	140	
$NaNO_3$-KNO_3-$Ca(NO_3)_2$-$LiNO_3$	0.05		0.07	0.47	0.42	95	
$NaNO_3$-KNO_3-$NaNO_2$-$LiNO_3$	0.14	0.18	0.17	0.50		<100	

Very few data are currently available in the scientific literature about the chemical stability of nitrite and nitrates pure salts and their mixtures;

✓ it is very important to establish a criterion on the lifespan of these fluids and broaden the knowledge of promising low-melting mixtures, defining their actual **upper working temperature**.

****Paper: «Thermal stability investigation of molten salt mixtures for CSP applications» to be submitted to «Applied Energy»***

Thermal stability
experimental

The salt heating system was built up in ENEA lab consists of **a stainless-steel reactor** characterized by two concentric cylinders:

- ✓ the internal one in metal where the salt is placed
- ✓ the external one in refractory material that contains the heating system.

The reactor is thermally insulated and sealed by a final layer of steel.

Thermal stability
experimental

- Each salt was **heated up to three isotherms T_1, T_2 and T_3** and it is kept at these temperatures for 48 hours, in air.
- During each isothermal step, for each salt **5 sampling** were carried out .
- Once the sampling has been carried out, it must be processed before it can be analyzed


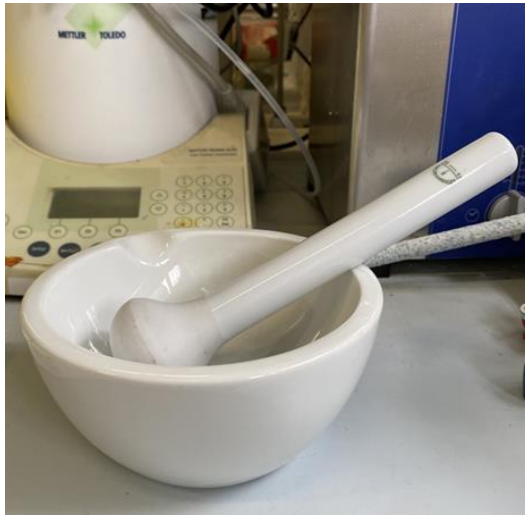
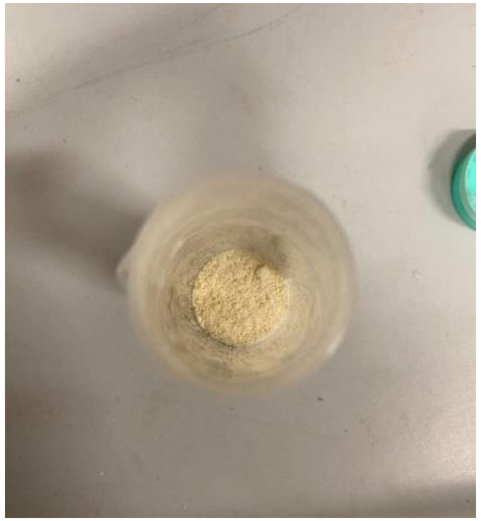

After each isothermal test few grams of molten salt is sampled to investigate the presence of:

- **NO_2^- (by ion chromatography)**
- **Oxides (by automatic acid/base titration)**

Thermal stability
experimental- Nitrites

❖ NO_2^- (by Ion Chromatography)

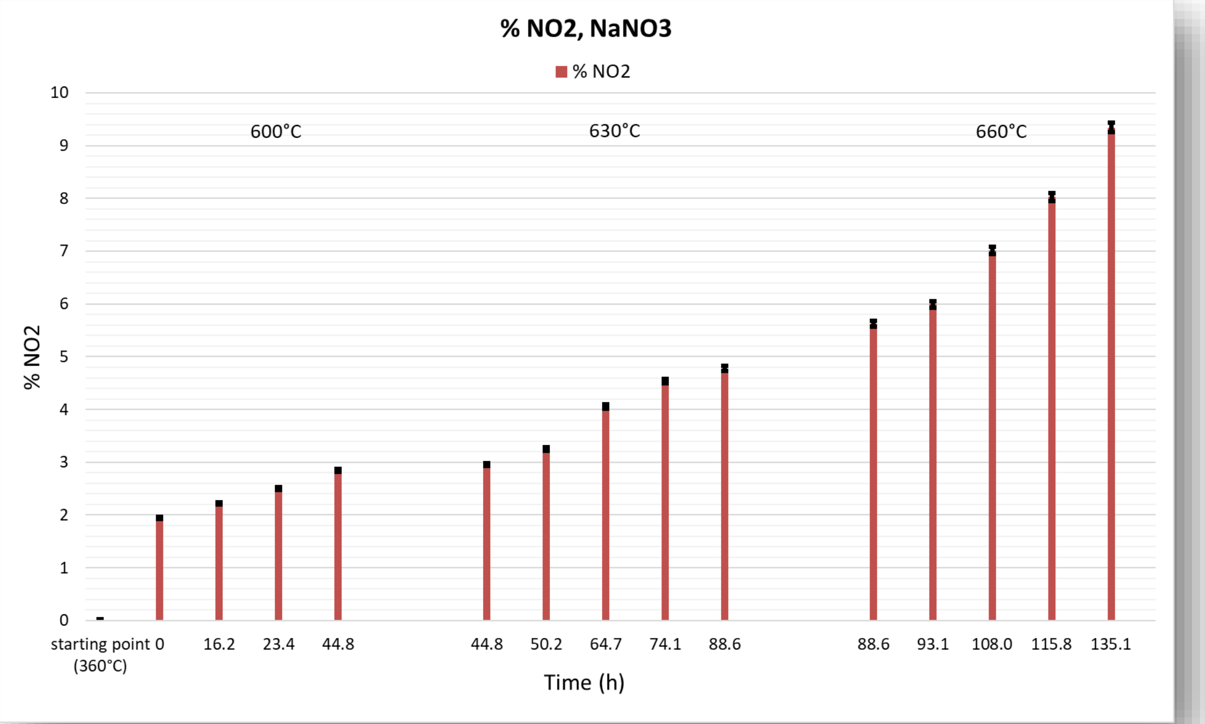

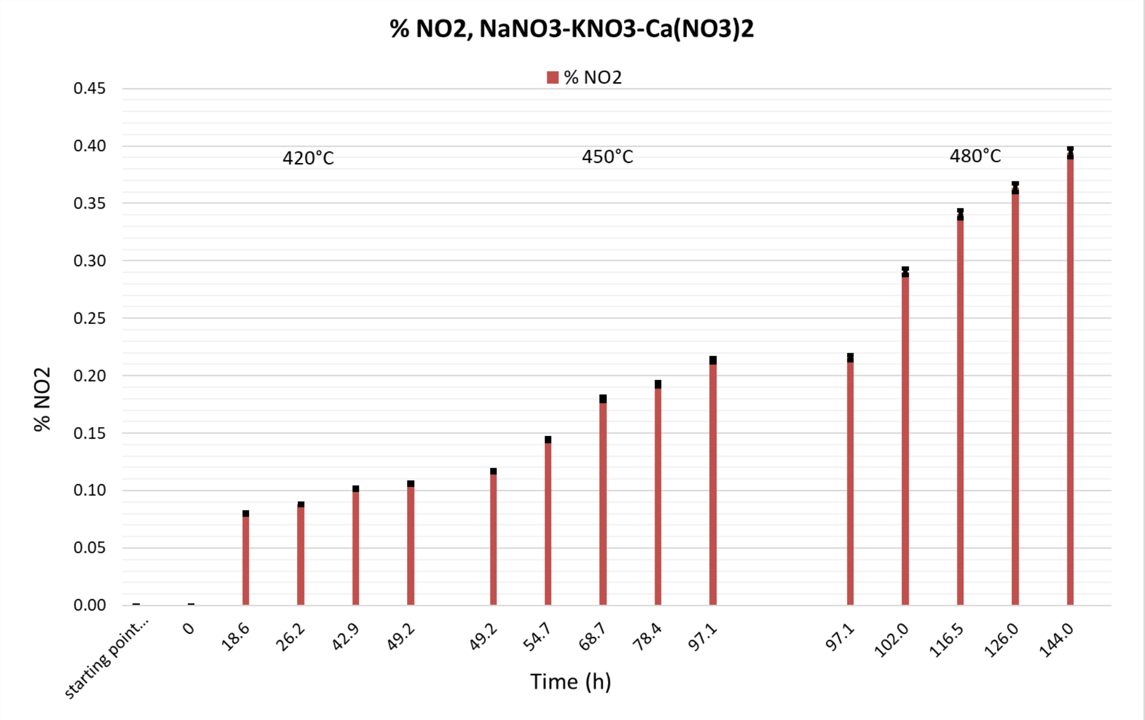

Thermal stability
experimental- Oxides

❖ **Oxides (by automatic acid/base titration)**

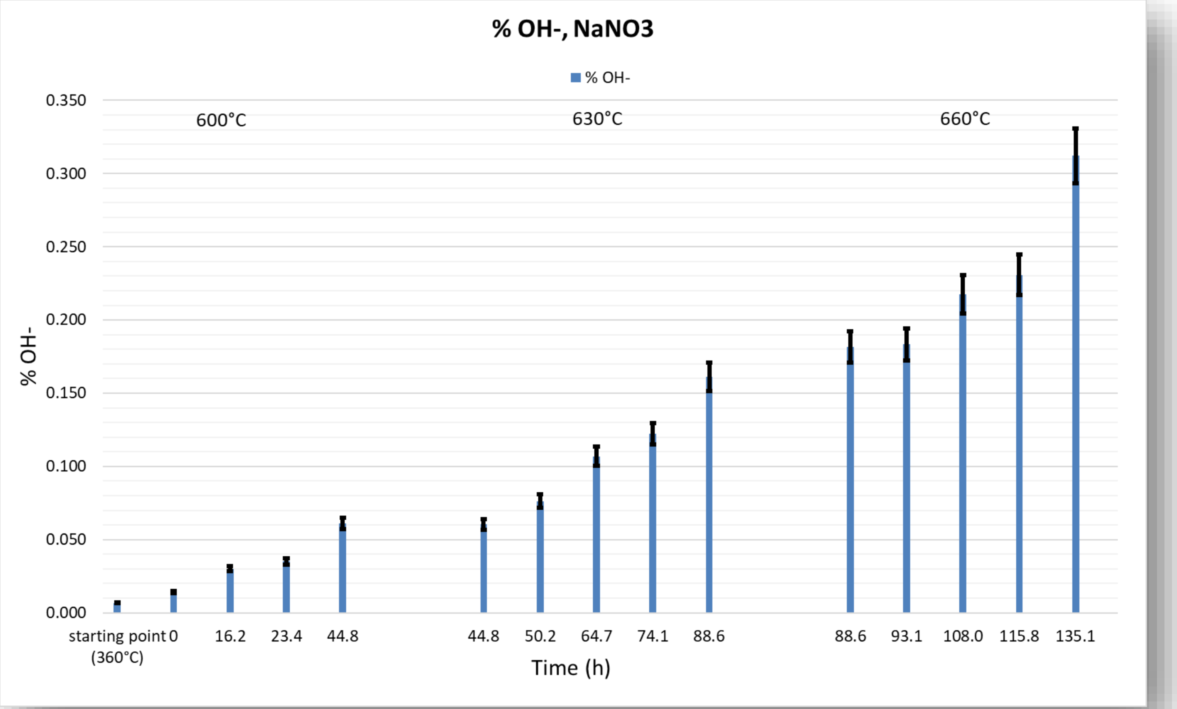

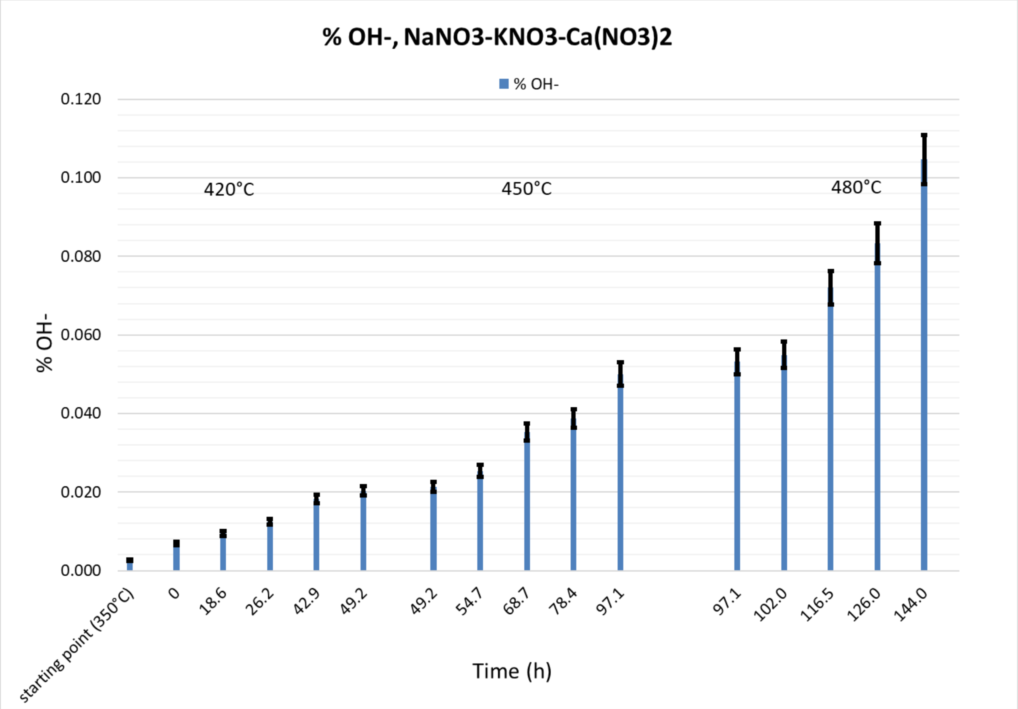

Thermal stability

Kinetic model: comparison at different temperatures

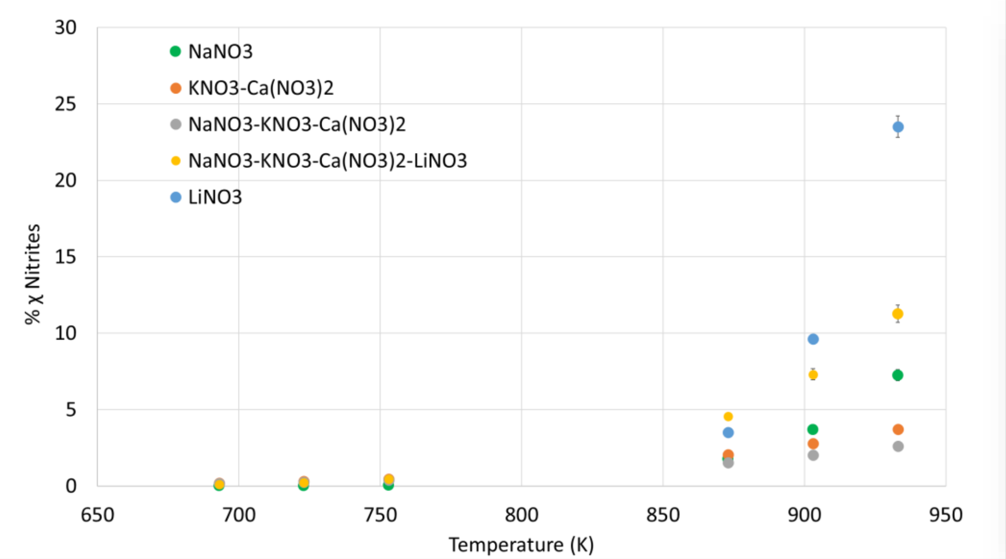

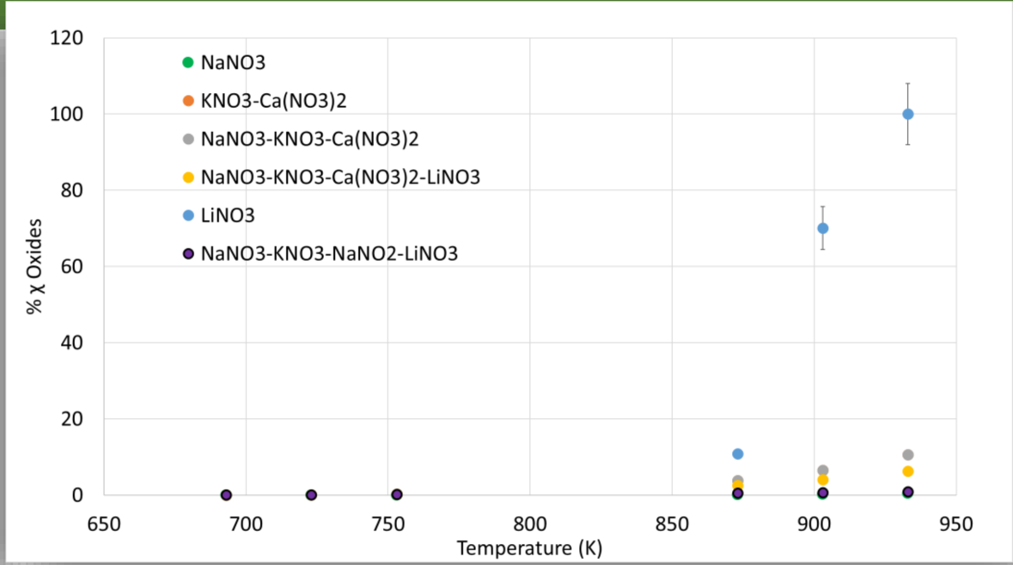

- Testing different kinetic models
- Lack of long-term experimental values
- Data useful for a comparison

Have a stabilizing effect

- $NaNO_3$ ✓
- KNO_3 ✓

Have a non-stabilizing effect

- $NaNO_2$ ✗
- $LiNO_3$ ✗
- $Ca(NO_3)_2$ ✗

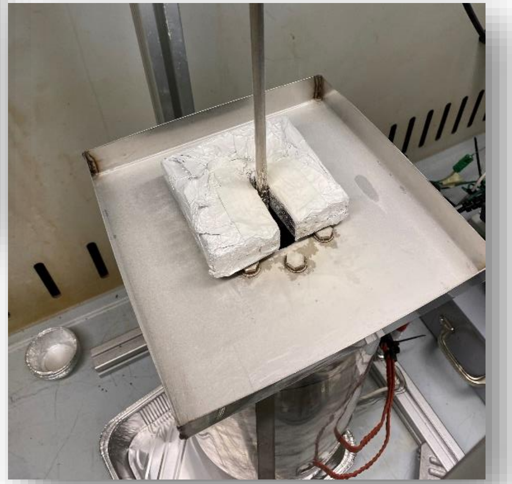

- Correlation between salts instability and volatility.
- Impossibility in predicting the behavior of a mixture based on the individual components, there are **Group contributions to be considered**.

Thermal stability

Kinetic model: predictive tool

The aim of this procedure is to have **a predictive tool** to determine, **for each temperature**, **how long will it take for the formation of a set oxide percentage .**

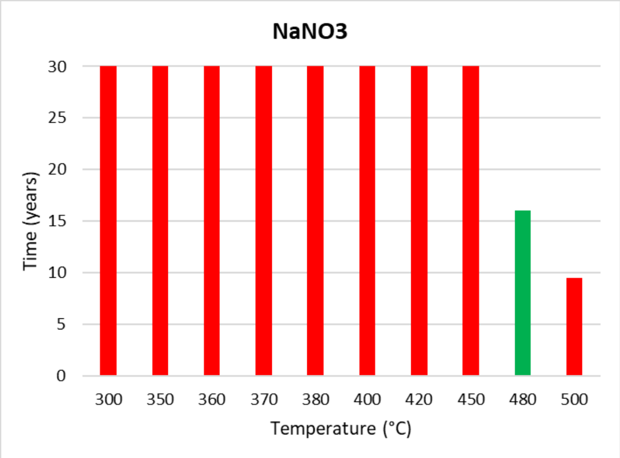

- A maximum value **<u>of 5% formation</u>** of oxides is set, considering a 15-year depreciation of the salts in a CSP system (parabolic trough solar plants, PTSP);

- We suppose equilibrium is not reached

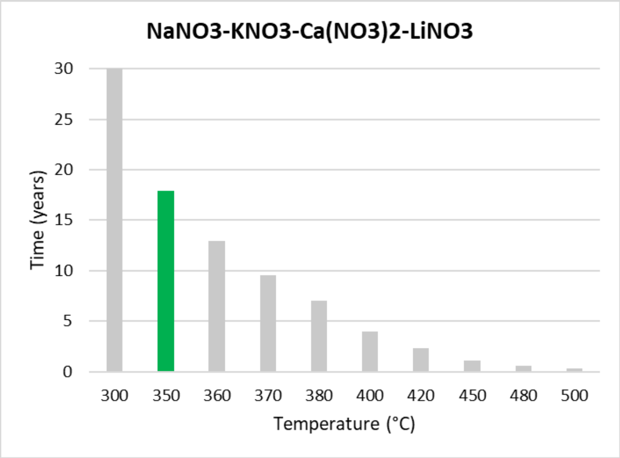

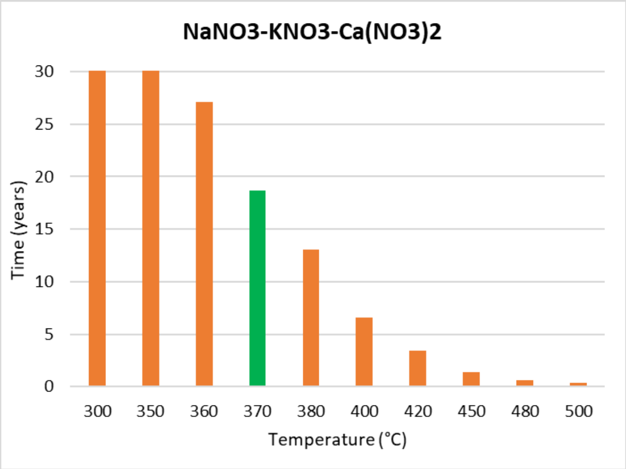

Thermal stability
conservative comparison

- **$NaNO_3$**, component of the largely used in "Solar Salt" (60/40% wt $NaNO_3$/KNO_3), the hypothesized model reflects the values found in the literature (**250°C-550°C**).
- **$NaNO_3$-KNO_3-$Ca(NO_3)_2$** which is used in CSP systems with a temperature range of **240 °C - 420 °C** is perfectly usable.
- The **Quaternary mixture with calcium nitrate**, which has the advantage of being low melting, is recommended to work with a range of temperatures from **300 °C to 350 ° C.**
- On the contrary, the **Quaternary mixture with sodium nitrite**, does not find application in plants CSP because the degradation mechanism is too high.

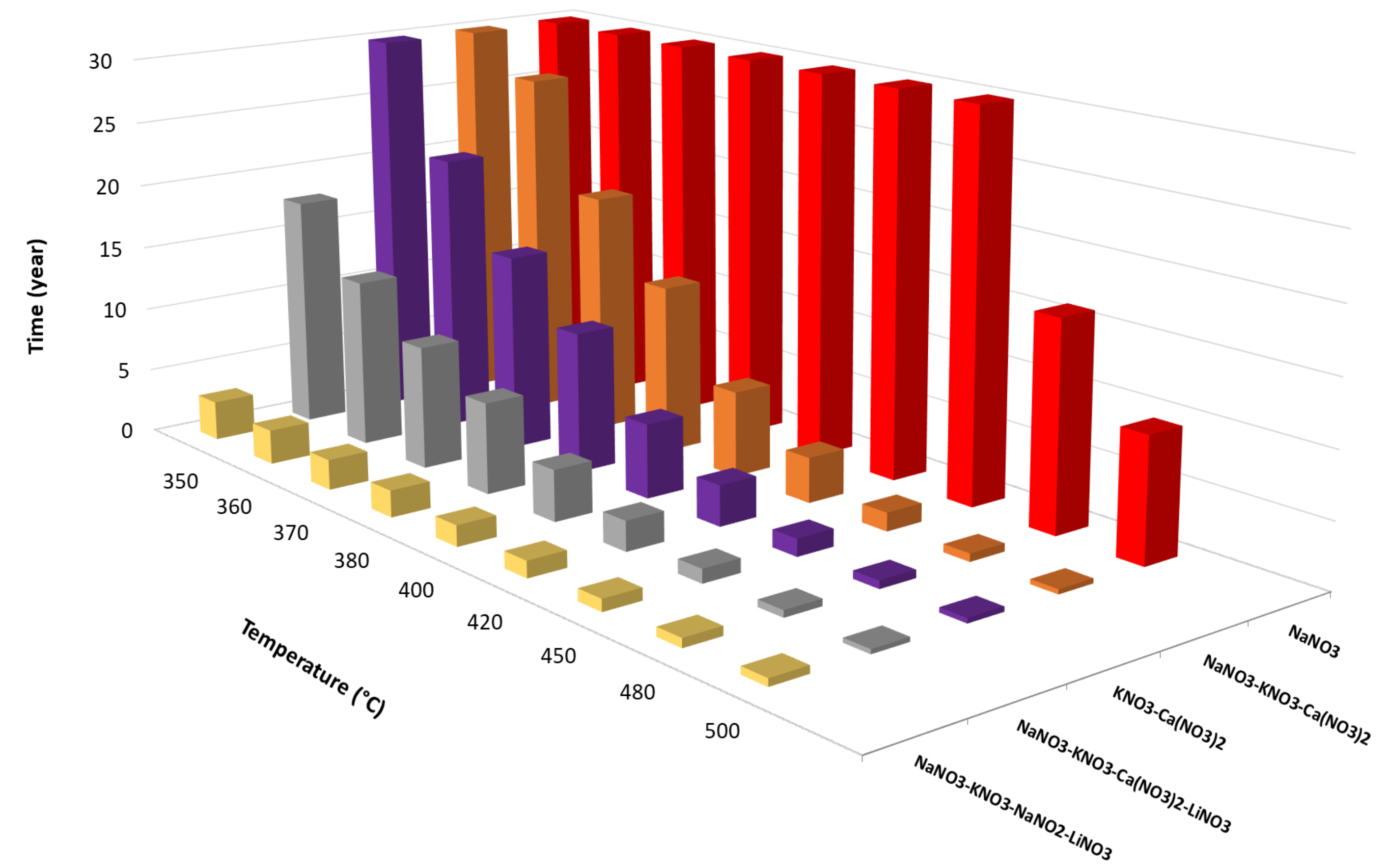

Thermophysical MS and thermal oil database

This database consents a quick and easy search of the properties of different thermal fluids, allowing their appropriate selection for practical applications, thanks to the possibility of setting search filters.

The models developed made possible to calculate the main thermophysical properties of a mixture of nitrates and nitrites starting from the individual components, to the molar composition and to the temperature desired.

The possibility of entering new data, depending on the heat transfer fluid being considered, makes this database an “open” and interactive tool, and can be expanded and improved by each user.

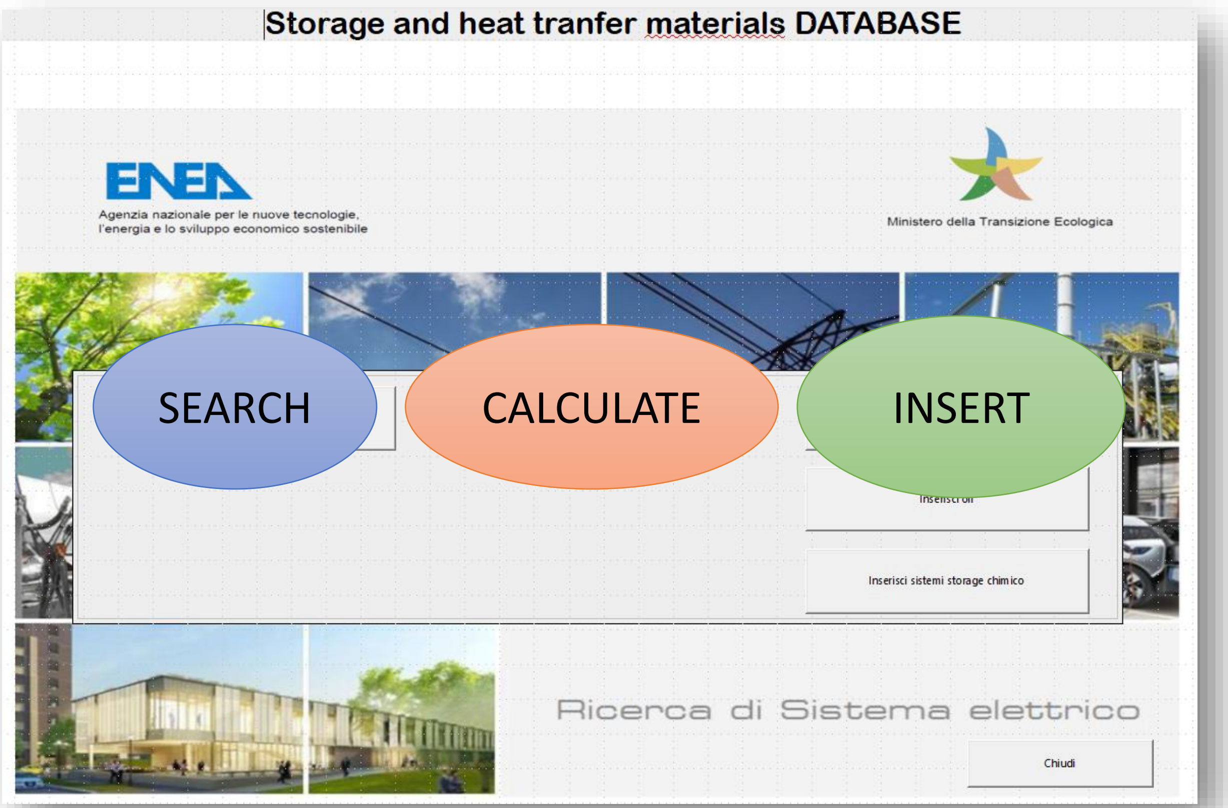

Thermophysical MS and thermal oil database: **search**

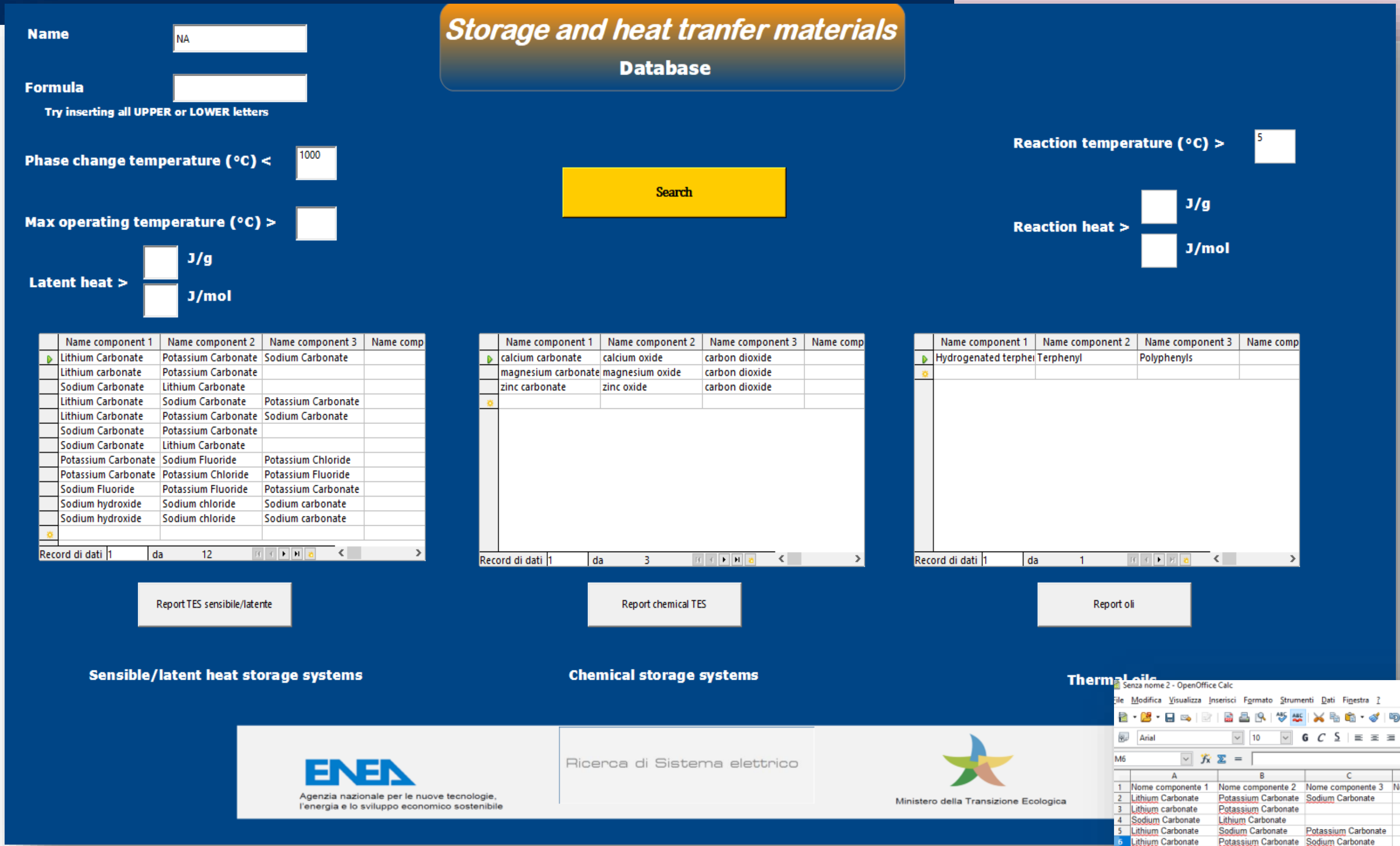

SEARCHING can be carried out by name or by chemical formula of the compound.

It is possible to insert search "filters" such as the maximum temperature of use, the melting point, the minimum value of latent heat or heat and reaction temperature for chemical storage

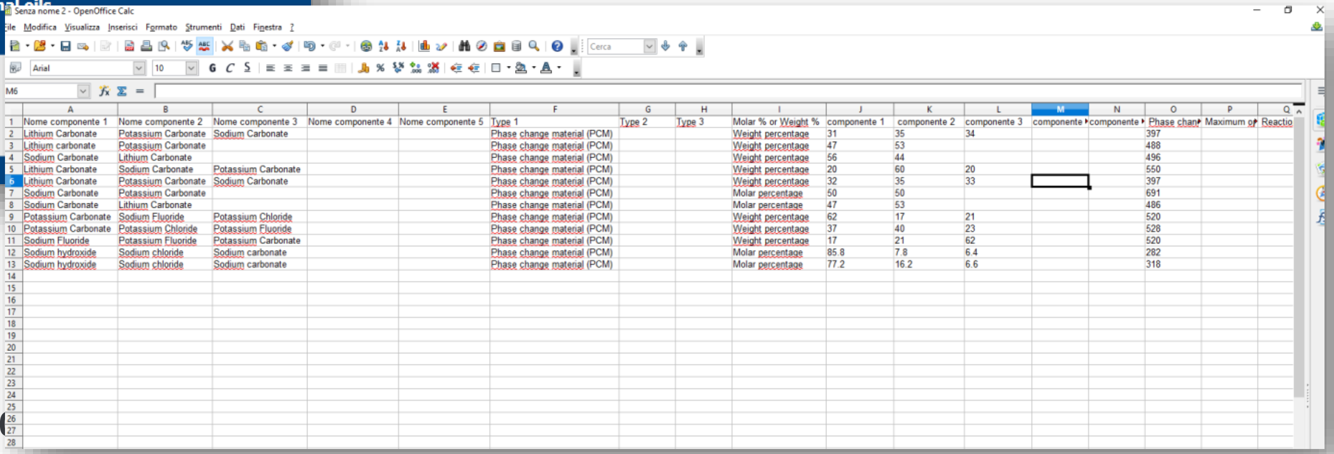

Thermophysical MS and thermal oil database: calculate

In the "Calculate" section it is possible to obtain the thermophysical properties of a mixture of nitrates and nitrites, starting from the individual components in percentage and at the desired temperature, by means of models studied and developed.

By choosing the individual components from the drop-down menu and entering the desired value of their molar composition and temperature, it is possible to obtain the **specific heat, density and viscosity values of the desired mixture.**

The single selected nitrates and nitrites, from which the multicomponent mixtures can be obtained, are: $NaNO_3$, KNO_3, $Ca(NO_3)_2$, $LiNO_3$, $NaNO_2$.

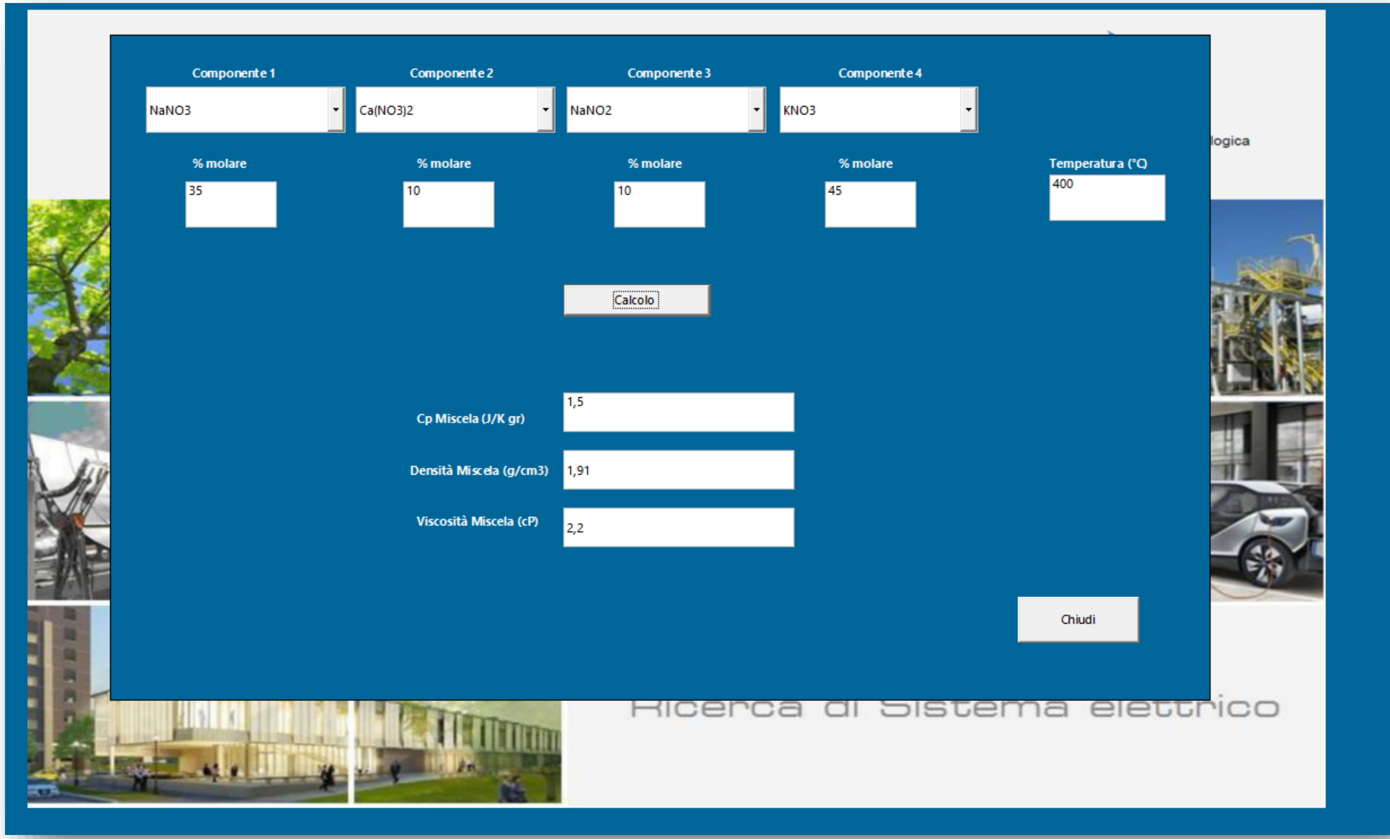

Thermophysical MS and thermal oil database: <u>insert</u>

Since this database is an **accessible and expandable tool**, it is possible to increase the database with new entries by all operators.

The possibility of entering new data, depending on the heat transfer fluid being considered, makes this database an **"open" and interactive tool**, that can be expanded and improved by each user.

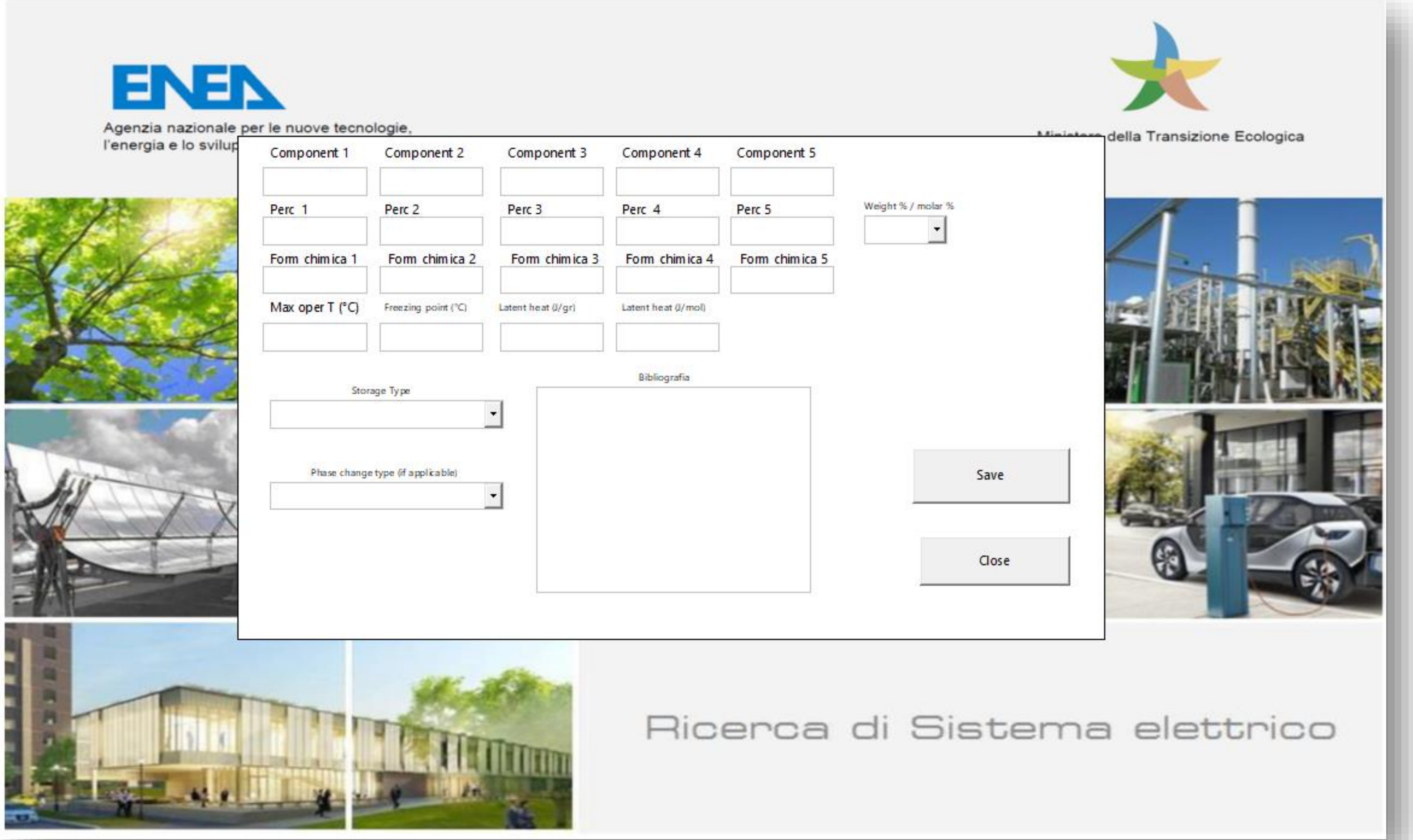

SFERA-III
Solar Facilities for the European Research Area

Anna Chiara TIZZONI
ENEA
TERIN-STSN-SCIS
annachiara.tizzoni@enea.it

Salvatore SAU
ENEA
TERIN-STSN-SCIS
salvatore.sau@enea.it

GOBIERNO DE ESPAÑA · MINISTERIO DE CIENCIA, INNOVACIÓN Y UNIVERSIDADES · Ciemat Centro de Investigaciones Energéticas, Medioambientales y Tecnológicas
ENEA
DLR Deutsches Zentrum für Luft- und Raumfahrt
UNIVERSIDADE DE ÉVORA
ESTELA
The Cyprus Institute
instituto imdea energía
Fraunhofer ISE
euronovia
LNEG
METU
ETH zürich
UNIVERSIDAD DE ALMERÍA
cnrs
cea
SFERA – Solar Facilities for the European Research Area

SFERA-III

Solar Facilities for the European Research Area

4th Training for Industries

7-11th November 2022, Cr ENEA Casaccia Rome (Italy)

Corrosion aspect and materials compatibility in molten salt plants

Elisabetta Veca (ENEA, TERIN-STSN-SCIS)

Stefano Frangini, Livia della Seta, Giuseppe Canneto, Salvatore Sau, Anna Chiara Tizzoni, Annarita Spadoni

Solar Facilities for the European Research Area

JOINT RESEARCH ACTIVITIES

THIS PROJECT HAS RECEIVED FUNDING FROM THE EUROPEAN UNION'S HORIZON 2020 RESEARCH AND INNOVATION PROGRAMME UNDER GRANT AGREEMENT NO **823802**

- General overview on literature about isothermal corrosion in static conditions
- Isothermal corrosion tests at 550-590°C

The following work (*) has been funded in the framework of the “Concentrating Solar Power” project, research activity lines on solar “process heat for industrial processes”, under the “Electric System Research” Programme 2019-2021, with the financial support of Italian Ministry for Economic Development.

	DelcoTerm	Therminol 66	Paratherm NF	Solar salt	HITEC XL
operative range	100-280°C	100-300 °C	100-300°C	290-550°C	150-425°C
ΔT	200	200	200	260	276
Cp [J /kg °C]	2200	1840	2302	1494	1494
ρ [kg/m3]	770	955	830	1902	2116
kg, oil, salts	9818182	11739130	9383145	11121409	10476689
ton, oil, salts	**9818**	**11739**	**9383**	**11121**	**10477**
Volume [m³]	12751	12292	11305	5847	4951
% Vol.	**ref**	**-4**	**-11**	**-54**	**-61**
Diameter [m]	**37**	**36**	**35**	**25**	**23**
Height [m]	**12**	**12**	**12**	**12**	**12**
thickness [cm]	**6**	**6**	**6**	**6**	**6**
stainless steel	**ton, steel**	**ton, steel**	**ton, steel**	**ton, steel**	**ton, steel**
321	1699	1650	1544	927	819
347	1672	1624	1519	912	806
304	1672	1624	1519	912	806
430	1630	1583	1481	889	785
316L	1706	1657	1550	931	822
	M€	**M€**	**M€**	**M€**	**M€**
321	***7,8***	***7,6***	***7,1***	***4,3***	***3,8***
347	***8,0***	***7,8***	***7,3***	***4,4***	***3,9***
304	***6,9***	***6,7***	***6,3***	***3,8***	***3,3***
430	***3,4***	***3,3***	***3,1***	***1,8***	***1,6***
316L	***9,8***	***9,5***	***8,9***	***5,3***	***4,7***

50 MW

Stainless steel	€/kg (wire rod)	
430	0.55	Jan 2020
	1.02	Sept2021
	1.95	Sept 2022
304	1.53	Jan 2020
	2.67	Sept 2021
	3.87	Sept 2022
316L	2.22	Jan 2020
	3.63	Sept 2021
	5.26	Sept 2022
321	1.72	Jan 2020
	2.65	Sept 2021
	4.30	Sept 2022
347	1.84	Jan 2020
	2.83	Sept 2021
	4.47	Sept 2022

Stainless steel	€/kg PEELED, oct 2022
430	2.06
304	4.14
316L	5.72
321	4.59
347	4.78

https://www.eureinox.it/extra-lega/
Steel price trend for italian market.

Mark Mehos, Craig Turchi, Clifford Ho, William Kolb, Alan Kruizenga, **"Concentrating Solar Power Gen3 Demonstration Roadmap"**, Technical Report NREL/TP-5500-67464, January 2017

Corrosion literature, 10MW Solar Two power tower pilot plant

- Several metal alloys are reported to be suitable for CSP applications up to 600 °C. In particular, the AISI 300 stainless steels series exhibited good corrosion properties; type **AISI 316** was proposed for the **receiver in the Solar Two system** [14] and type **AISI 304 for the hot salt storage tank and piping**[14] , **the cold tank on Solar Two was built of carbon steel ASTM A516-70**, and they basically maintains their features in dynamic HTF flow conditions, during thermal cycling and in presence of anionic impurities (chloride, for instance).

- However, from the experience developed by the Solar Two plant [15], it was noticed that these compatibility properties are maintained only when molten nitrates are in contact with the steel; during certain typical plant **maintenance procedures** an **aqueous environment** can be present on interior surfaces of receiver tubes and hot-salt piping, and **in this case conditions for a intergranular corrosion (IGC) attack can be attained**, leading to leakage problems when molten salts are recirculated again into the pipelines.

- This is due to **chromium depletion** at grain boundaries caused by **chromium carbide** formation between 530 and 590 °C; eventually, during the described operations, water together with chlorides (present as impurities in the solar salt mixture) can come in contact with the steel surface, and corrosion can occur [16]. As a consequence, 321H and 347 H are instead used, therefore, other elements (Titanium, Niobium) are added, which preferably precipitate as carbide.

AISI (321) stabilised with Titanium

AISI (347) stabilised with Niobium

Considering that a typical 30 years lifetime can be expected for a CSP plant [12], it is of a fundamental importance to employ materials presenting an acceptable corrosion compatibility with the solar salt employed as HTF and HSM.

- **Low carbon steel, T≤ 450°C, ex. P11**
- **Stainless Cr-Ni steel (≤ 500°C) , ex. 321H, 347H (with Nb, Ti)**
- **Ni-alloys (≤ 650°C), Alloy 800**

The most important parameters to investigate the corrosion phenomena

- Nitrate salt impurities (Cl), the chloride content is considered critical if >0.1%wt., although in literature there are data up to 1% [12][13];
- Nitrate salt decomposition (stability);
- Presence of water in molten salts;
- corrosion test conditions: static or dynamic immersion, thermal cycling, temperature, nitrogen or air atmosphere, duration;
- Stress corrosion cracking (SCC), mechanical stress (tensile loading) and corrosion reaction;
- oxides produced by corrosion;
- corrosion rate (CR), expressed as thickness change per year;

Chemical composition specifications of molten-salt [18]

Name	Mix potassium nitrate + sodium nitrate	
Composition	Sodium nitrate $NaNO_3$	60 %
	Potassium nitrate KNO_3	40 %
	Minimum nitrate %	99 %
MAX PERCENTAGE OF IMPURITIES		
Nitrite		0.20 %
Chloride		0.03 %
Carbonates		0.05 %
Sulfates		0.15 %
Alcalinity hidroxile		0.04 %
Perclorates		0.04 %
Magnesium		0.04 %
Calcium		0.04 %
Insoluble		0.06 %

Parameter **BASF**	unit	**specification**	**% wt**
NaNO3	g/100 g	min. 99,5	**99,7**
water	g/100 g	max 0,2	**0,20**
Sodium nitrite	mg /kg	max 50	**0,005**
Sodium carbonate	mg /kg	max 400	**0,04**
Sodium chloride	mg /kg	max 250	**0,025**
Sodium sulfate	mg /kg	max50	**0,005**
Insolubles	mg /kg	max 50	**0,005**

HAIFA	UNITS	**TYPICAL**	**TYPICAL %wt**	**SPECIFICATION**	**SPECIFICATION %wt**
Assay (as KNO3)	%	99.7	99,9	99.4 min	**99,9**
pH (10% sol.)	7	7	7	7	**7**
Sodium (Na)	ppm	150	0,015	300 max	**0,03**
Calcium (Ca)	ppm	13	0,0013	25 max	**0,0025**
Magnesium (Mg)	ppm	5	0,0005	10 max	**0,001**
Iron (Fe)	ppm	3	0,0003	10 max	**0,001**
Chloride (Cl)	ppm	160	0,016	300 max	**0,03**
Water Insolubles	ppm	180	0,018	350 max	**0,0352**

Methodology of corrosion tests

- gravimetric analysis
- SEM/EDS morphological and structural analysis corrosion
- products X-ray diffraction analysis

ISO 17245:2015 Corrosion of metals and alloys — Test method for high temperature corrosion testing of metallic materials by immersing in molten salt or other liquids under static conditions
ISO 8407 Corrosion of metals and alloys — Removal of corrosion products from corrosion test specimens
Guidelines for material selection and testing [19]

corrosion rate CR

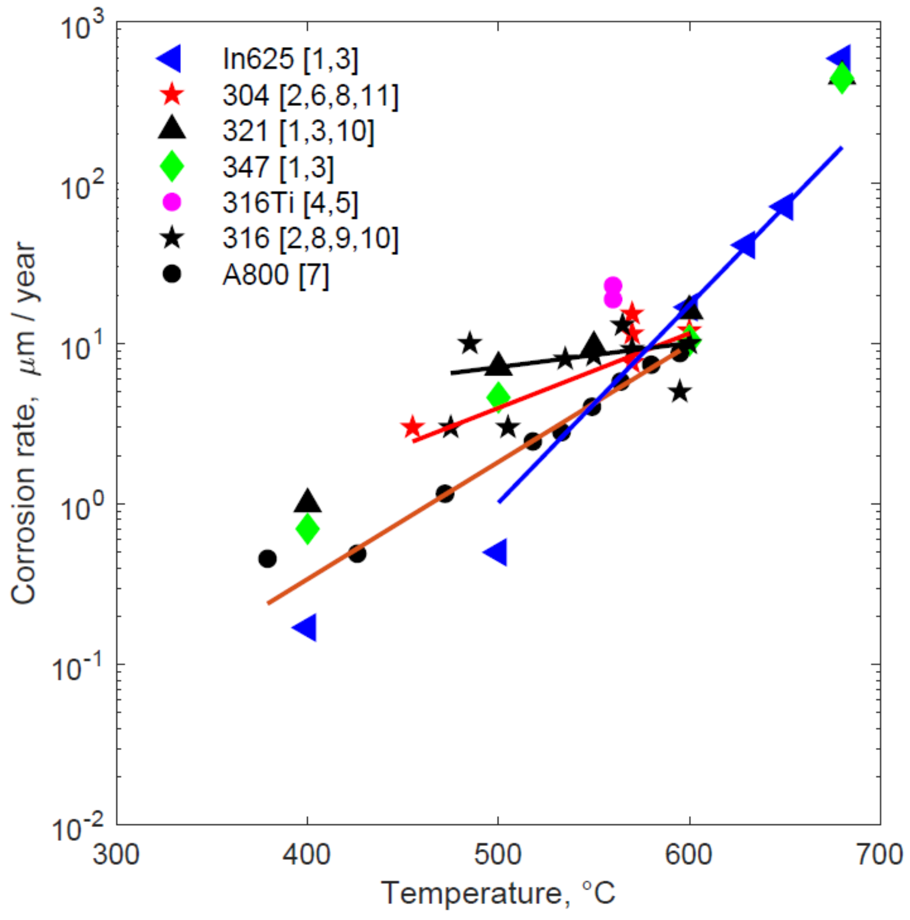

$$CR = \frac{86700 \cdot \Delta m}{\rho_s\, t} \quad Corrosion\ rate\ [\mu m/y]$$

$$\Delta m = \frac{m_i - m_d}{S} \quad descaled\ mass\ loss\ [mg/cm^2]$$

- ρ_s *alloy density* $[g/cm^3]$
- t *testing time* $[h]$
- m_i *initial mass of the specimen before the test* $[mg]$
- m_t *mass of the specimen before chemical descaling* $[mg]$
- m_d *mass of the specimen after chemical descaling* $[mg]$

$$\Delta mo_{xide} = \frac{m_t - m_d}{S} \quad mass\ of\ descaled\ oxide\ [mg/cm^2]$$

$$t_{oxide} = \frac{\Delta m_{oxide}}{\rho_{oxide}} \ [\mu m]\ average\ thickness\ of\ oxide\ layer\ \ \rho_{oxide}(Fe,Cr)$$

Technical drawings, stirred vessel for dynamic corrosion tests

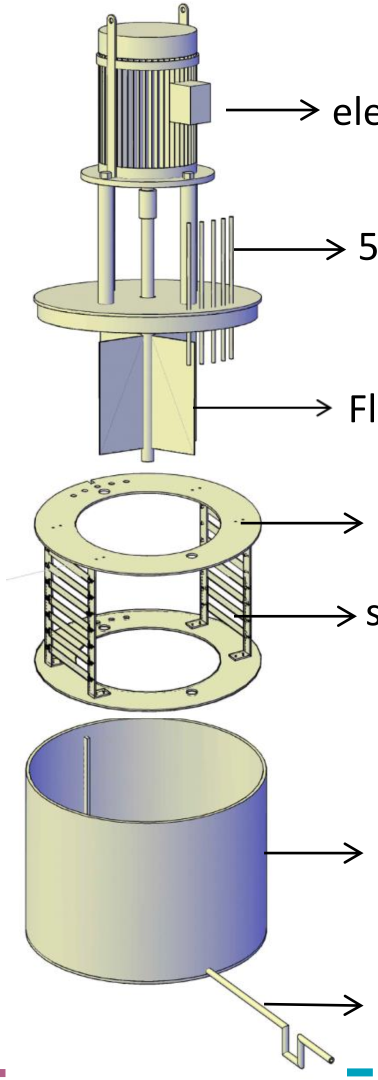

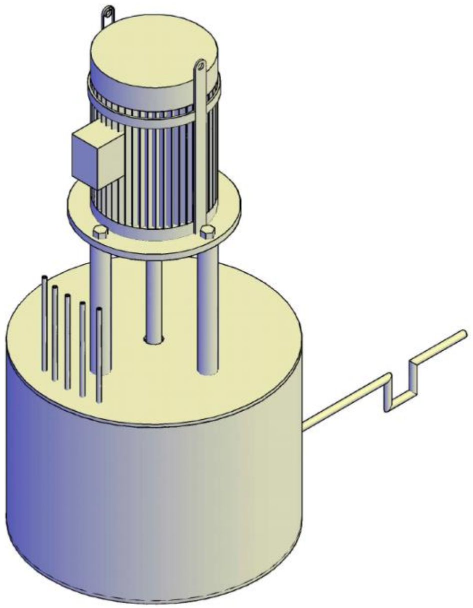

D_{ex}=410 mm

H=300 mm

Thickness =5 mm

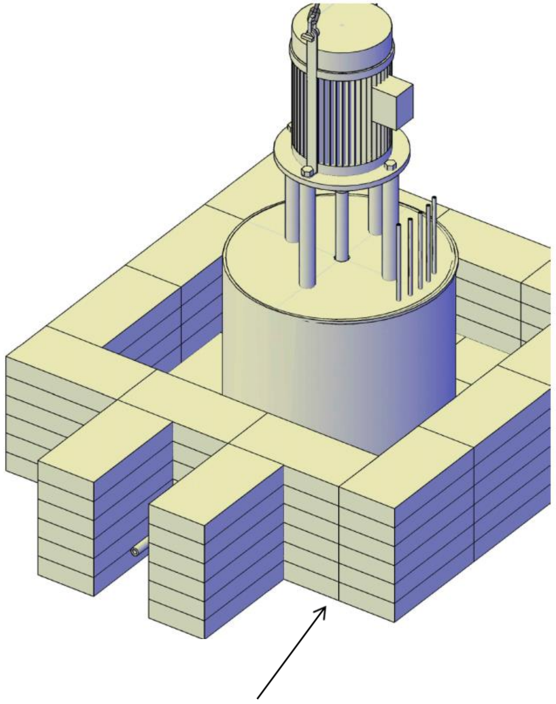

electrical heater

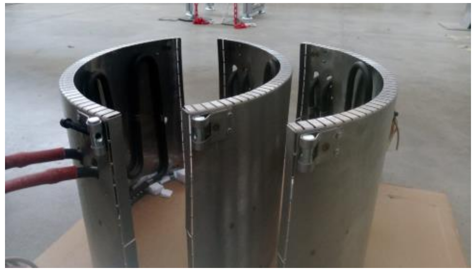

Features

- Allow Unattended operation, data logging
- external electrical heater up to 7 kW
- electrical motor 1 kW, 1500 rpm max
- **30-60 kg of salts**
- **Salts temperature monitoring** : 5 TC
- **V_{vessel}= 37 liters**

impeller

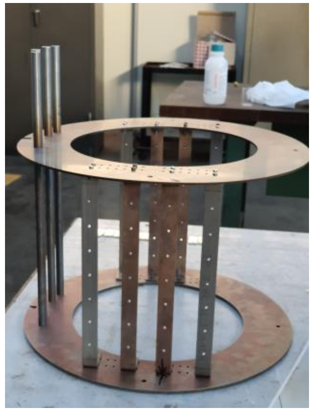

sample holder

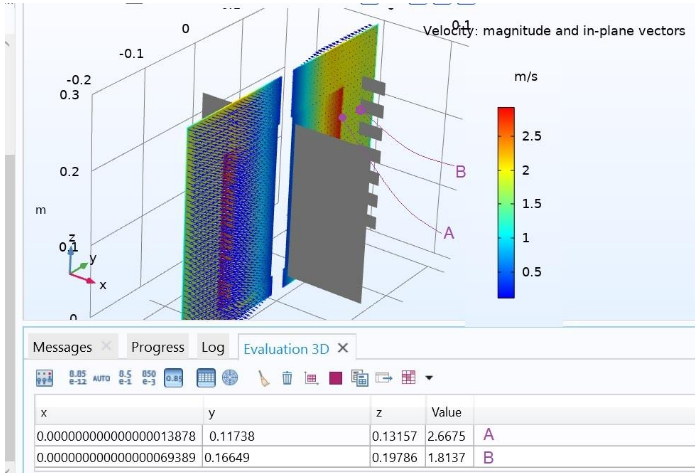

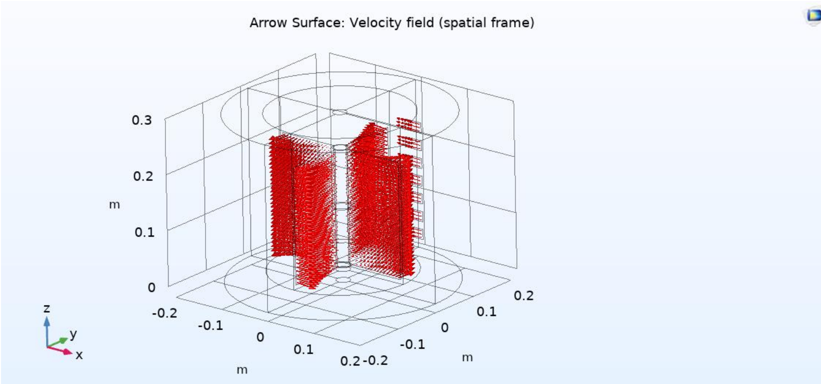

WP 6 task 6.1 stirred vessel dynamic corrosion tests

D_{ex}=410 mm

H=300 mm

Thickness =5 mm

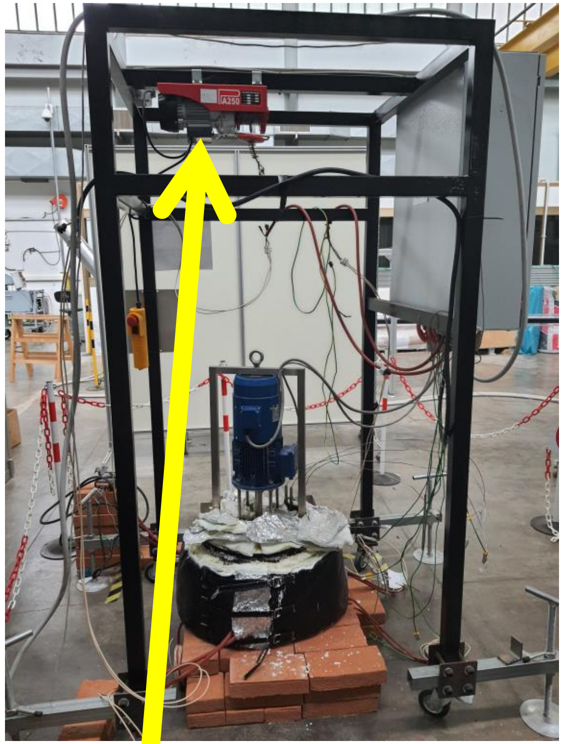

hoist

SFERA III WP 6 task 6.1 SEM results 3000 h

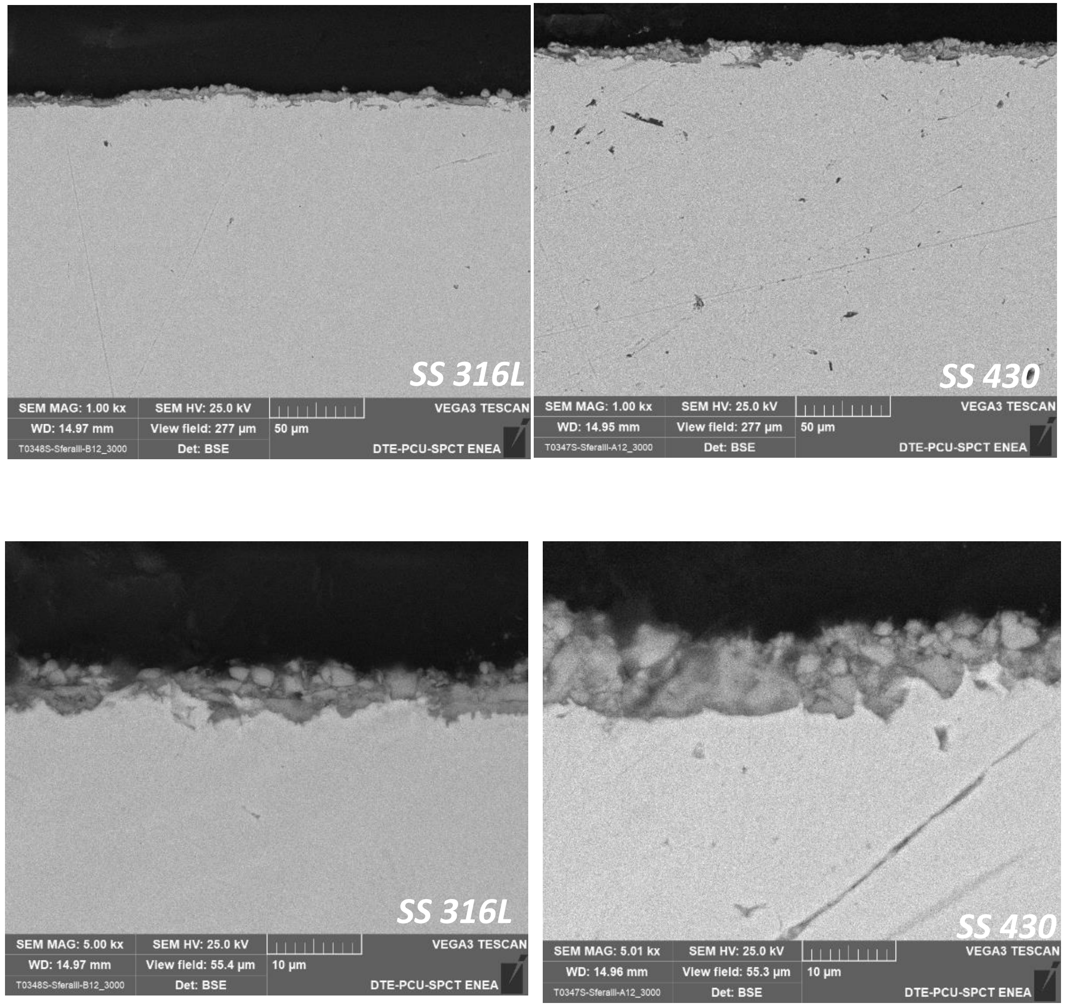

316L SS, 430 SS

3000 h in solar salt

550°C, v=0.7 m/sec

XRD patterns

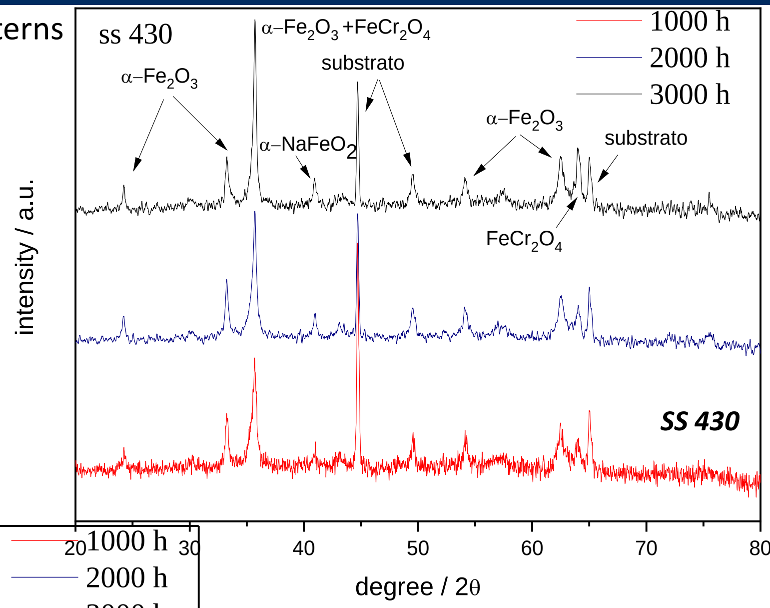

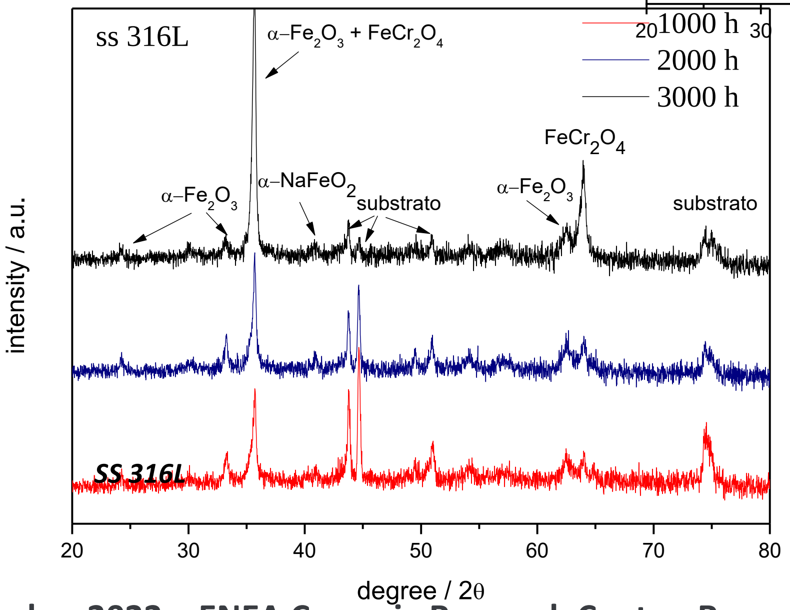

Corrosion product

$FeCr_2O_4$

Fe_2O_3

$NaFeO_2$

SFERA-III
Solar Facilities for the European Research Area

316 L T91 solar salt 1500 h at 550°C (*)

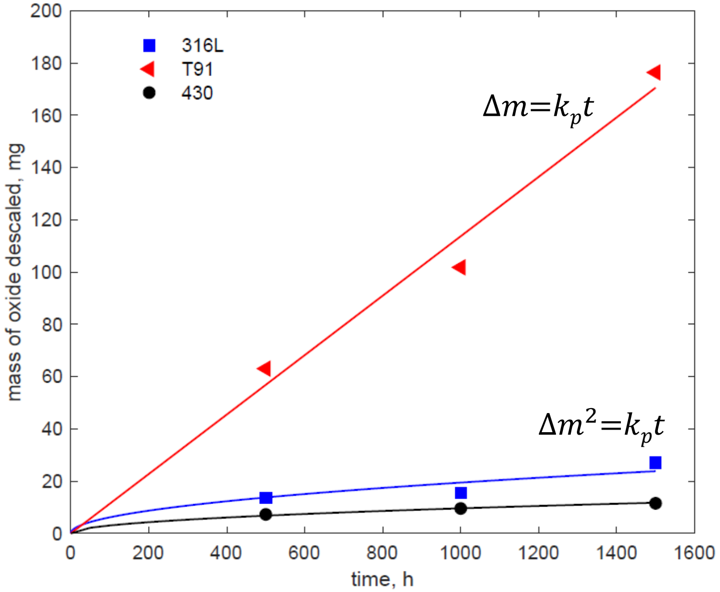

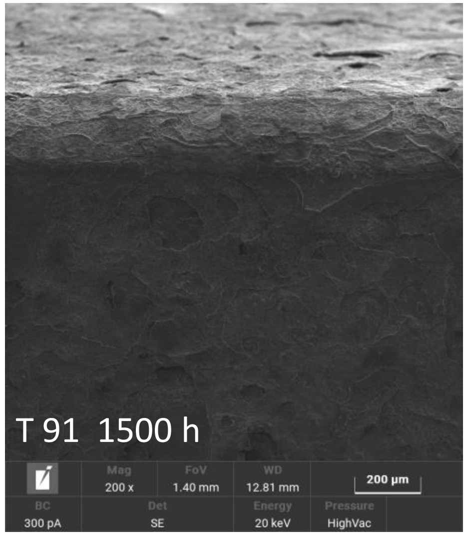

SEM /EDS analysis

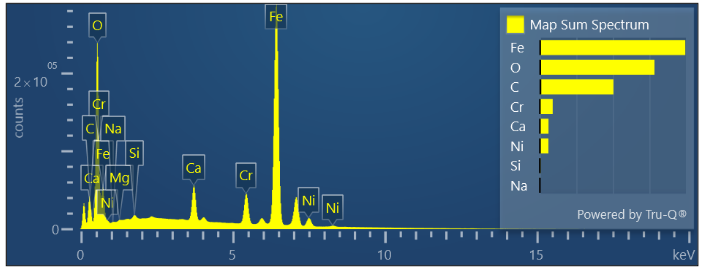

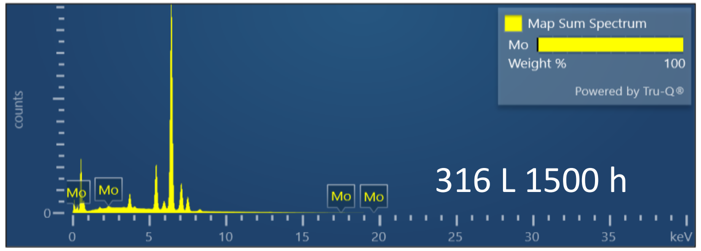

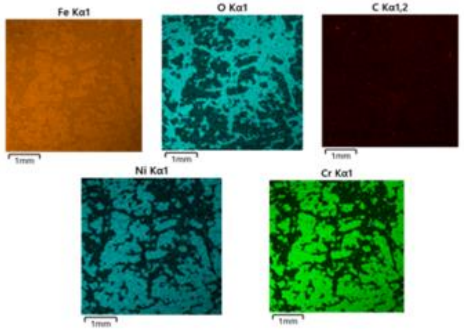

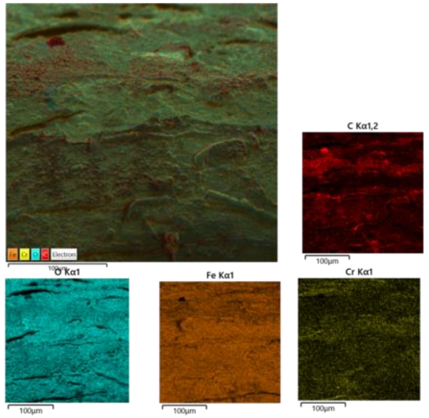

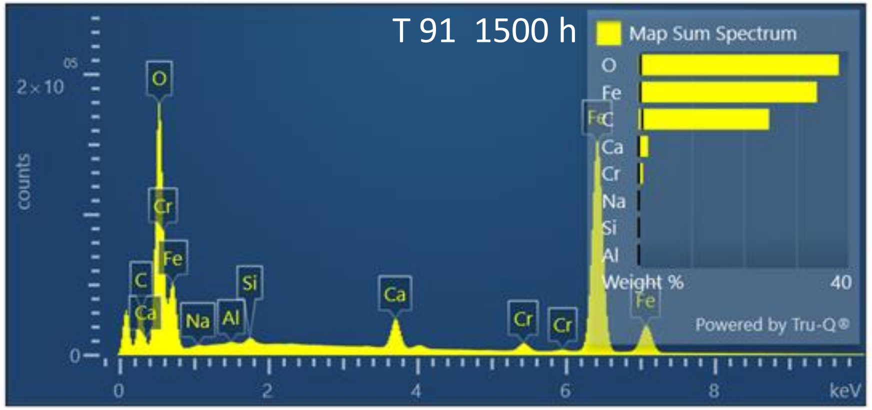

isothermal corrosion 550-590°C(**)

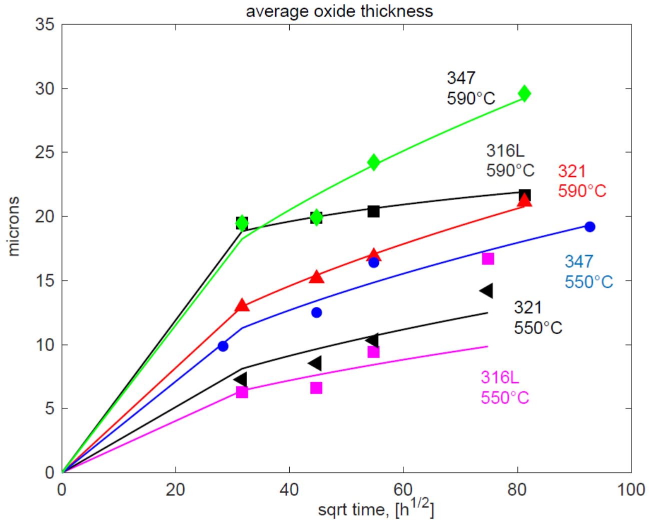

$$z^2(t)=k_p t$$

$$z(t) = k_p \log(t)$$

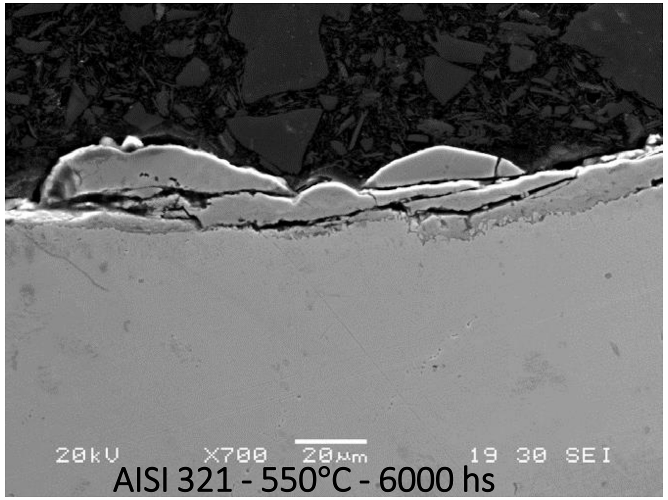

AISI 321 - 550°C - 6000 hs

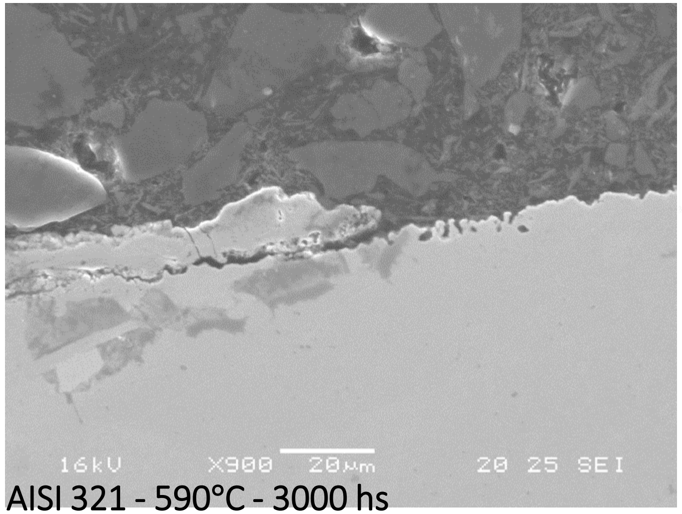

AISI 321 - 590°C - 3000 hs

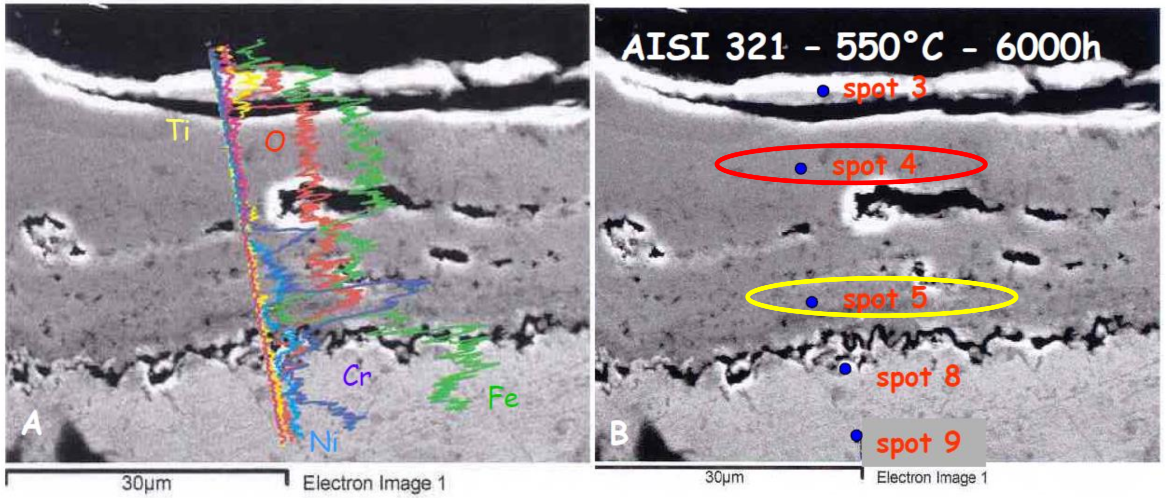

element	Cr	Mn	Ni	Si (tot)	O	Fe	Na	Ti	Zn
virgin (wt.%)	17,9	1,48	9,4	0,6	---	ddr	---	---	---
Weld stick (wt.%)	12,35	0,6	4,23						
spot 3	0,35				43,07	38,8	3,02	7,25	7,51
spot 4	0,54	0,69			37,63	53,45		0,44	7,24
spot 5	34,2		7,33	0,6	40,44	17,43			
spot 8	4,9		7,26			87,83			
spot 9	18,03	1,47	8,62	0,73		71,14			

isothermal corrosion 550-590°C (**)

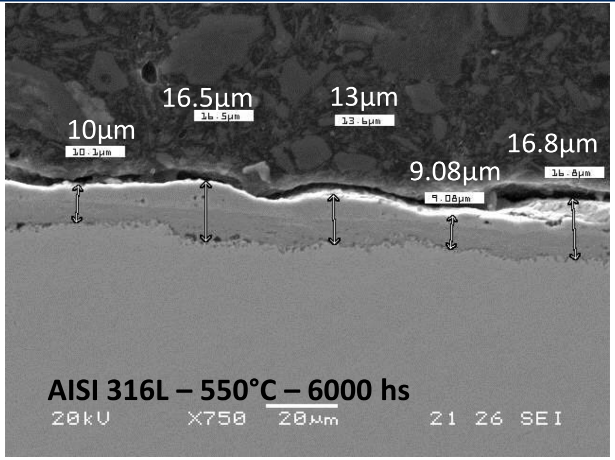

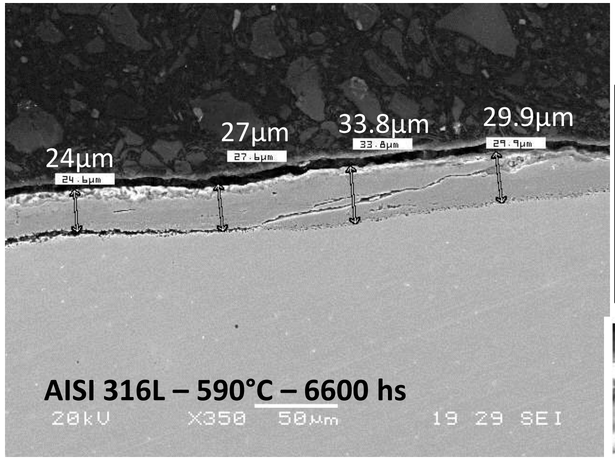

elemental composition analysis AISI 316L -590°C - 1000 hs

position	Fe	Cr	O	Ni	Na	Mo	Si	Mn
spot 1: matrix	68.52	17.94	--	11.06	--	1.98	0.51	--
spot 2: inner layer	21.69	31.43	37.59	3.96	--	1.72	0.99	2.63
spot 3: middle layer	46.12	7.11	42.86	1.38	--	0.54	0.62	1.37
spot 4: outer layer	37.87	1.39	55.36	--	1.82	1.29	0.66	1.61

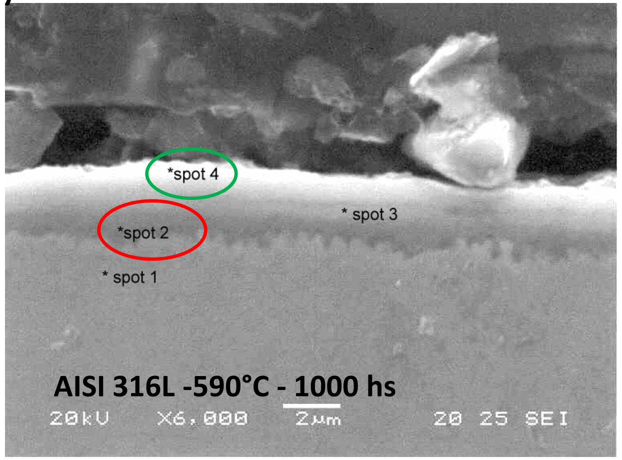

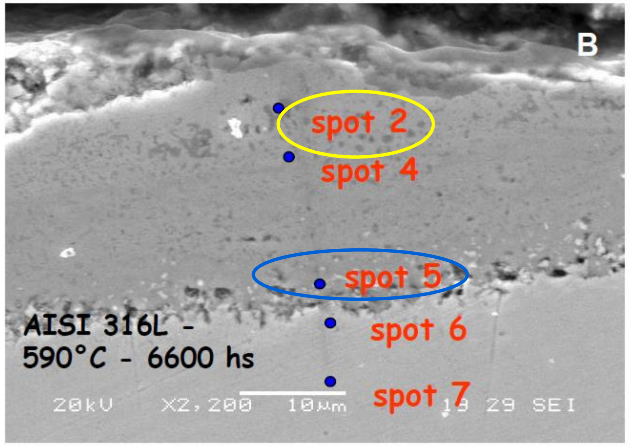

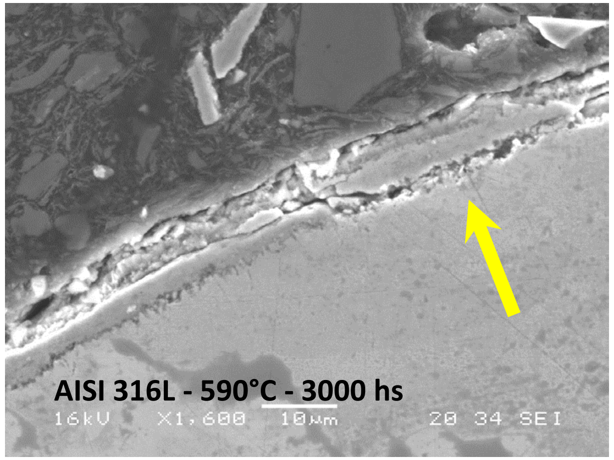

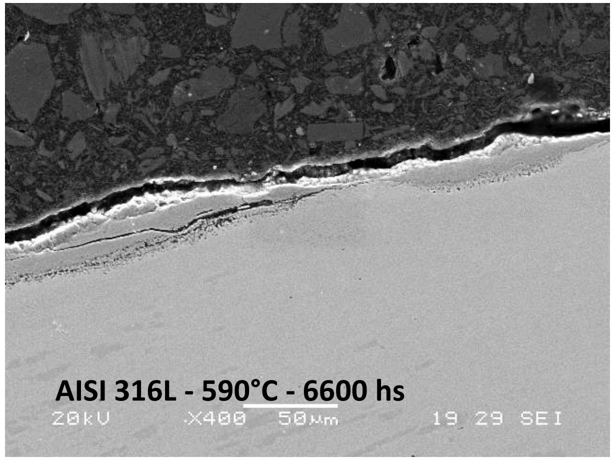

alloy element	Cr	Mn	Mo	Ni	Si (tot)	O	Fe
as received (wt.%)	16.09	1.53	2.18	11.03	0.05	---	ddr
spot 2	0,63				0,41	40,2	58,77
spot 4	23,68	1,73		5,58	0,79	37,94	30,29
spot 5	26,32			4,84	0,94	38,18	29,72
spot 6	8,71		5,62	26,71	1,53		57,54
spot 7	17,67	1,45	2,27	11,78	0,65		66,19

elemental composition analysis AISI 316L - 590°C - 6600 hs

isothermal corrosion 550-590°C (**)

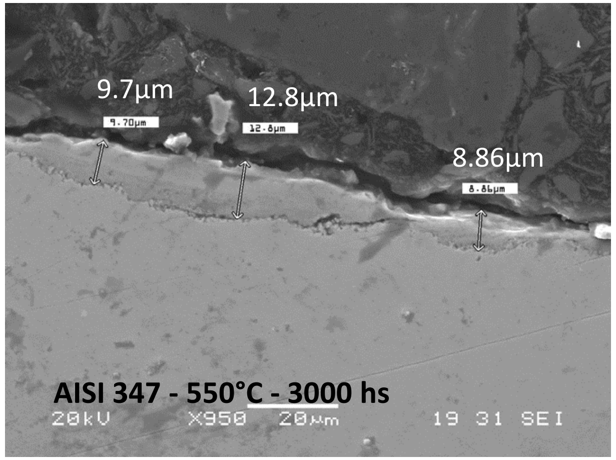

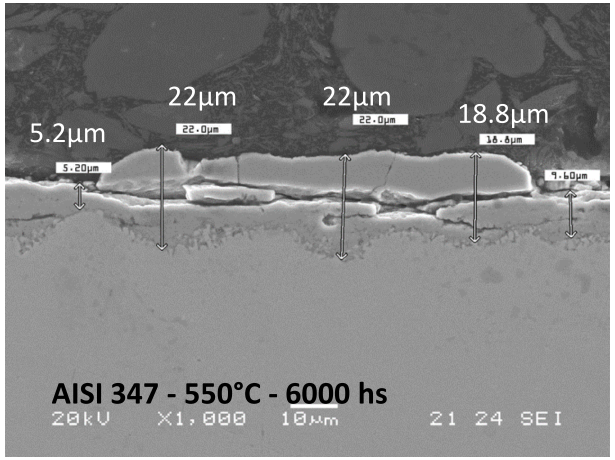

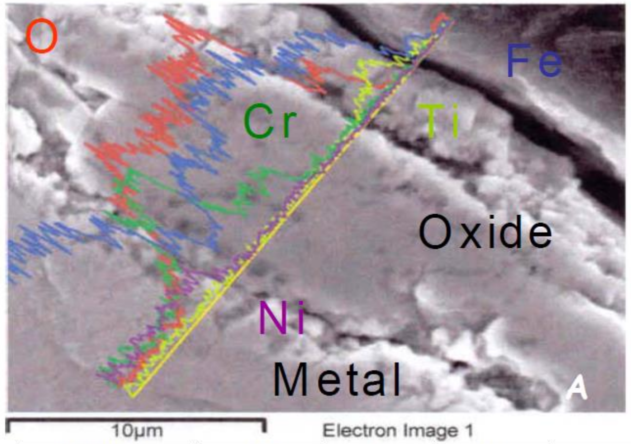

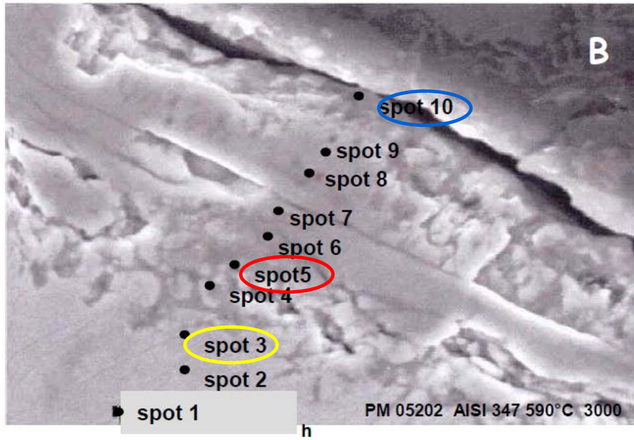

Specimen	Spot	O	Fe	Cr	Na	Ni	Mn	Si	Mo	Ti
AISI 347 3000 h 590°C	1		71.34	17.78		9.27	1.6			
	2		73.92	12.01		11.83		2.24		
	3	20.21	52.54	11.62		12.28	2.33	0.83		
	4	20.21	50.19	13.46		3.42	1.39	0.78		
	5	31.53	22.36	60.54		4.40	2.62	0.60		
	6	36.62	18.89	37.86		3.95	1.74	0.94		
	7	40.26	32.52	25.42			1.04	0.78		
	8	42.8	54.89	11.20	0.89					
	9	40.36	57.31	0.59			1.07			0.66
	10		78.82		2.23		4.77			14.18

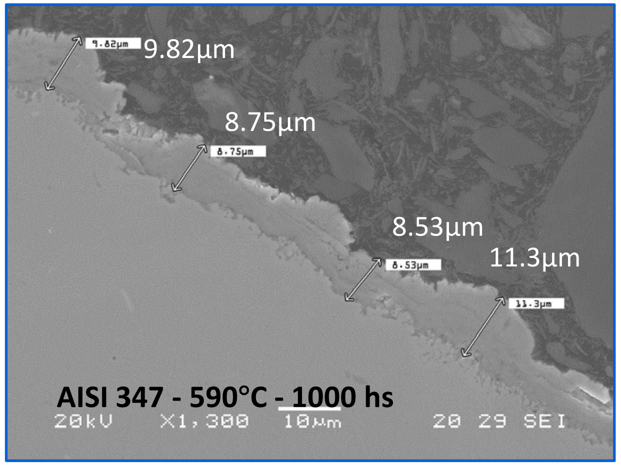

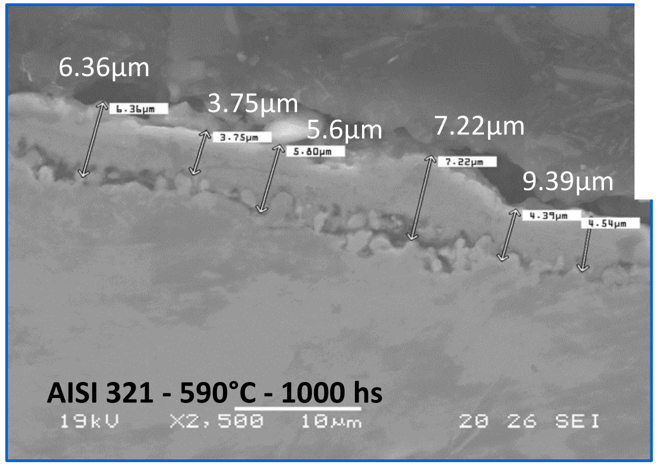

Line Scanning analysis (A) and spot elemental composition analysis performed by EPMA (B) of a specimens of AISI 347 exposed for 3000 h at 590°C.

isothermal corrosion 550-590°C (**)

comparison of the results about the weight loss in mg/cm2, metal loss observed for the austenitic specimens with the results of the SANDIA Laboratory [20]

ENEA results

material	T [°C]	hour	weight loss [mg/cm^2]	Metal loss [µm]	Average ox. thick. [µm]
AISI 316L	550	1000	2,93	3,68	6,31
		2000	2,97	3,73	6,62
		3000	4,21	5,28	9,41
		5600	8,11	10,19	16,70
	590	1000	9,6	12,07	19,48
		2000	9,9	12,50	19,99
		3000	9,8	12,34	20,40
		6600	10,23	12,85	21,65
AISI 321	550	1000	3,50	4,43	7,27
		2000	4,02	5,09	8,54
		3000	4,73	5,98	10,32
		5600	6,53	8,27	14,2
	590	1000	6,48	8,20	12,96
		2000	7,41	9,38	15,16
		3000	8,92	11,29	16,87
		6600	11,23	14,21	21,13
AISI 347	550	800	4,17	5,26	9,87
		2000	5,64	7,11	12,50
		3000	7,45	9,40	16,40
		8600	8,33	10,50	19,19
	590	1000	9,37	11,82	19,46
		2000	9,61	12,12	19,92
		3000	11,78	14,86	24,22
		6600	15,30	19.29	29.59

SANDIA Laboratory results

material	T [°C]	hour	weight loss [mg/cm^2][1]	
AISI 316	570	432	0,89	
			1,78	
		864	1,52	
			2,48	
		1608	2,48	
			3,43	
		2952	2,88	3,83
			3,59	4,68
		4008	3,43	3,14
			4,01	3,95
		7008	5,15	
			5,76	
AISI 304	570	432	1,63	
			2,46	
		864	2,19	
			4,40	
		1608	3,89	
			5,34	
		2952	4,49	7,19
			4,71	8,47
		4008	4,83	5,49
			5,20	6,33
		7008	7,31	
			9,52	

conclusions

isothermal corrosion 550-590°C (**)

- The thickness of the oxide layer rises with the test temperature and the time of exposition. Especially for long time of exposition the oxidized layer shows the spallation phenomenon and some localized cracking;

- The oxide scale grow adherent and changes into more porous with the increasing of exposure time. This phenomenon can induce the total lack of adherence of the oxide scale, that sometimes occurs;

- The rising of the scale thickness and its structure is similar for all the three kind of austenitic steels exposed at 550°C and 590°C;

- The structure of the oxide film on the austenitic specimens exposed at 550°C and 590°C of temperature have a complex, multiphase structure, divided in three layer. The **outer layer**, that is in direct contact with the molten salt, is a chromium-free iron based oxide and the sodium is also detected in this layer; the **middle layer** consist mainly of iron and oxygen with a minor amount of chromium and much less sodium than the outer layer; the **inner** is an iron oxide which contains a significant amount of chromium.

[1] Alan M. Kruizenga, David D. Gill, SANDIA REPORT SAND 2013-2526 Unlimited Release March 2013 Materials Corrosion of High Temperature Alloys Immersed in 600°C Binary Nitrate Salt.

[2] P. F. Tortorelli, J. H. DeVan, December 1982, Thermal Convection Loop Study of the Corrosion of Fe-Ni-Cr Alloys by Molten NaNO3 –KNO3.

[3] Alan M. Kruizenga, David D. Gill et al. , SANDIA REPORT SAND 2013-8256, September 2013 Corrosion of High Temperature Alloys in Solar Salt at 400, 500, and 680°C.

[4] Alexander Bonk et al., Solar Energy Materials and Solar Cells 203 **(2019)** 110162, Impact of Solar Salt aging on corrosion of martensitic and austenitic steel for concentrating solar power plants, https://doi.org/10.1016/j.solmat.2019.110162

[5] Dr. K. Federsel et al., Energy Procedia 69 **(2015)** 618 – 625, High-temperature and corrosion behavior of nitrate nitrite molten salt mixtures regarding their application in concentrating solar power plants, https://doi.org/10.1016/j.egypro.2015.03.071

[6] R. W. Bradshaw and R. W. Carling 1987 Proc. Vol. 1987-7 959, A Review of the Chemical and Physical Properties of Molten Alkali Nitrate Salts and Their Effect on Materials Used for Solar Central Receivers.

[7] R. W. Bradshaw; Thermal Convection Loop Study of the Corrosion of Incoloy 800 in Molten NaNO3-KNO3. CORROSION 1 **March 1987**; 43 (3): 173–178. doi: https://doi.org/10.5006/1.3583131

[8] Goods S.H.; Bradshaw R.W. Goods, S.H., Bradshaw, R.W., 2004. Corrosion of stainless steels and carbon steel by molten mixtures of commercial nitrate salts. J. Mater. Eng. Perform. 13, 78–87.

[9] A. Gomes, M. Navas, N. Uranga, T. Paiva, I. Figueira, T.C. Diamantino, High-temperature corrosion performance of austenitic stainless steels type AISI 316L and AISI 321H, in molten Solar Salt, Solar Energy, Volume 177, **2019**, Pages 408-419, ISSN 0038-092X, https://doi.org/10.1016/j.solener.2018.11.019

[10] Alan Kruizenga, David Gill , Corrosion of iron stainless steels in molten nitrate salt, SolarPACES 2013, Energy Procedia 49 (**2014**) 878 – 887.

[11] Xiaoming Zhang, Cancan Zhang, et al. Experimental research of high temperature dynamic corrosion characteristic of stainless steels in nitrate eutectic molten salt, Solar Energy, Volume 209, **2020**,Pages 618-627, https://doi.org/10.1016/j.solener.2020.09.034

[12] Carling R.W., Kramer C.M., Bradshaw R.W., Nissen D.A., Goods S.H., et al. - Molten nitrate salt technology development status report - **SANDIA report SAND80-8052, March 1981**

[13] Giaconia, A.; Tizzoni, A.C.; Sau, S.; Corsaro, N.; Mansi, E.; Spadoni, A.; Delise, T. Assessment and Perspectives of Heat Transfer Fluids for CSP Applications. **Energies 2021**, 14, 7486. https://doi.org/10.3390/en14227486

[14] P. F. Tortorelli, J. H. DeVan, December 1982, Thermal Convection Loop Study of the Corrosion of Fe-Ni-Cr Alloys by Molten NaNO3 –KNO3.

[15] Reilly H.E., Gregory G.J. - An Evaluation of Molten-Salt Power Towers Including Results of the Solar Two Project - **SANDIA report SAND2001-3674, November 2001**

[16] Kelly B., Fabrizi F. et al. - Nitrate and Nitrite/Nitrate Salt Heat Transport Fluids – Nexant, Parabolic Trough Technology Workshop, Golden, **Colorado, March 8th and 9th, 2007**

[17] S. H. Goods & R. W. Bradshaw Corrosion of stainless steels and carbon steel by molten mixtures of commercial nitrate salts Journal of Materials Engineering and Performance volume 13, pages 78–87 **(2004)**, DOI: 10.1361/10599490417542

[18] R12.4 Guidelines for Testing of CSP components, Chemical composition specifications of molten-salt **SFERA Solar Facilities for the European Research Area**

[19] Francisco Javier Pérez Trujillo, Victor Encinas Sanchez, Isabel Lasanta , Deliverable: D4.7 Best practice for material selection for molten salt plants and guideline on material testing in molten salt environment, RAISELIFE **H2020-NMP-16-2015 Nanotechnologies, Advanced Materials and Production**

[20] SANDIA REPORT (SAND2000-8727) R.W. Bradshaw, S.H. Goods. "Corrosion of Alloys and Metals by Molten Nitrates". August 2001

(*)The following work has been funded in the framework of the "Concentrating Solar Power" project, research activity lines on solar "process heat for industrial processes", under the "Electric System Research" Program 2019-2021, with the financial support of Italian Ministry for Economic Development.

(**) M.Agostini M. Azzati et al., **COMPATIBILITY TESTS FOR STAINLESS AND CARBON STEELS IN STAGNANT AND ISOTHERMAL MOLTEN NITRATES, FINAL TESTS REPORT,** ST-A-R-002 19/12/2003.

Elisabetta VECA, PhD
ENEA
TERIN-STSN-SCIS
elisabetta.veca@enea.it

THANK YOU FOR YOUR ATTENTION!
ANY QUESTIONS?

SFERA-III
Solar Facilities for the European Research Area

Solar Facilities for the European Research Area

4th Training for Industries
7-11 November 2022, Cr ENEA Casaccia Rome (Italy)

Instrumentation for molten salt plants
PhD Walter Gaggioli

JOINT RESEARCH ACTIVITIES

THIS PROJECT HAS RECEIVED FUNDING FROM THE EUROPEAN UNION’S HORIZON 2020 RESEARCH AND INNOVATION PROGRAMME UNDER GRANT AGREEMENT NO **823802**

Temperature

Pressure

Molten salts flow

Level

Temperature measurement

Thermocouples

Thermocouples are temperature sensors that use two different metals to produce a voltage that is proportional to the temperature.

Cheaper
robustness,
measurement speed,
large range of temperatures up to 1830°C.
more resilient
react faster to temperature changes.

Compensation cables for thermocouple:
They are cables composed of rigid or flexible conductive materials different from the materials of the thermocouple but with identical or very similar thermoelectric characteristics. They are tested from 0 ° C to 200 ° C.

Temperature measurement

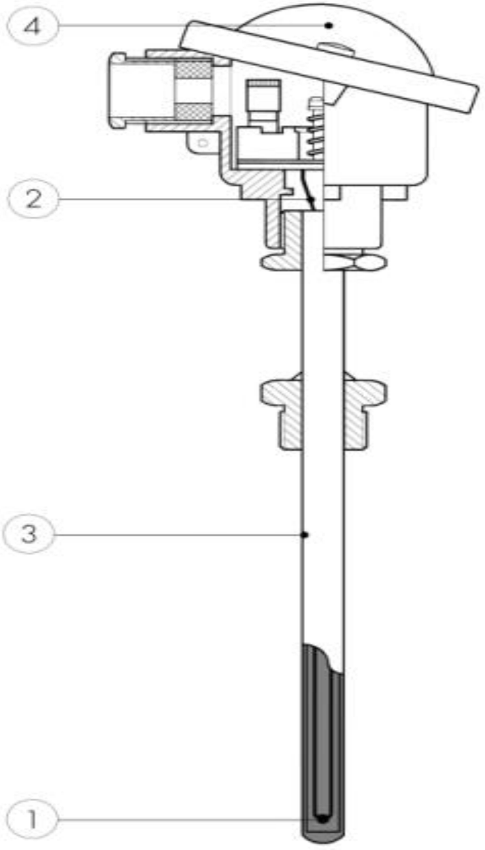

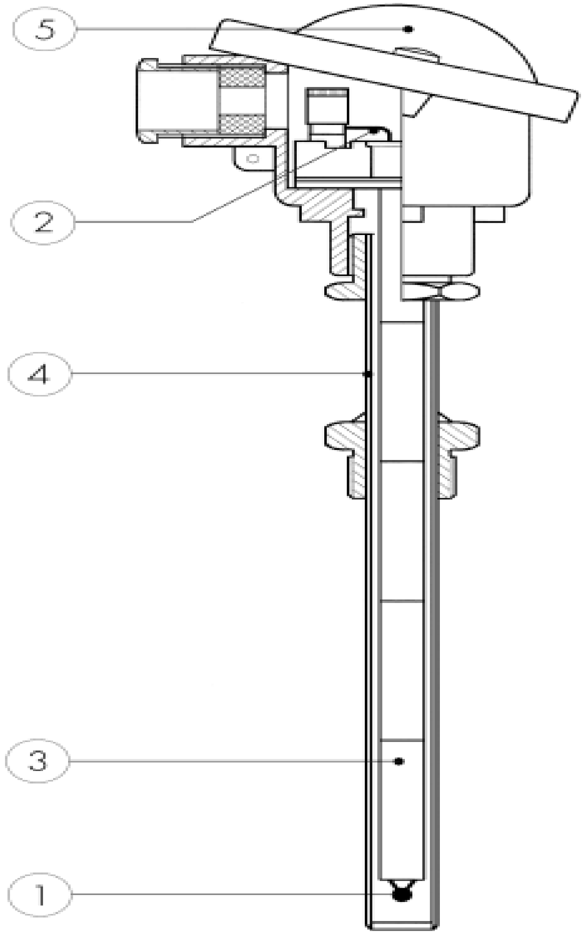

1- **Measuring junction** The measuring junction or hot junction is the area in which the two conductors of the thermocouple are joined together

2- Thermocouple wires The thermocouple wires must be adequately sized according to the conditions of use; it is possible to insert two or more thermocouples in the same probe.

3- Ceramic insulators The ceramic insulators are used to keep the thermocouple wires isolated for the entire length of the probe from each other and towards the outer sheath.

4- Protection sheath The protection sheath has the purpose of protecting the thermocouple wires

5- Connection head The connection head contains a terminal block made of insulating material (normally ceramic) which allows the electrical connection of the thermocouple. Depending on the conditions of use, explosion-proof enclosures can be used. In place of the terminal block it is possible to install a converter with 4-20mA output.

Temperature measurement

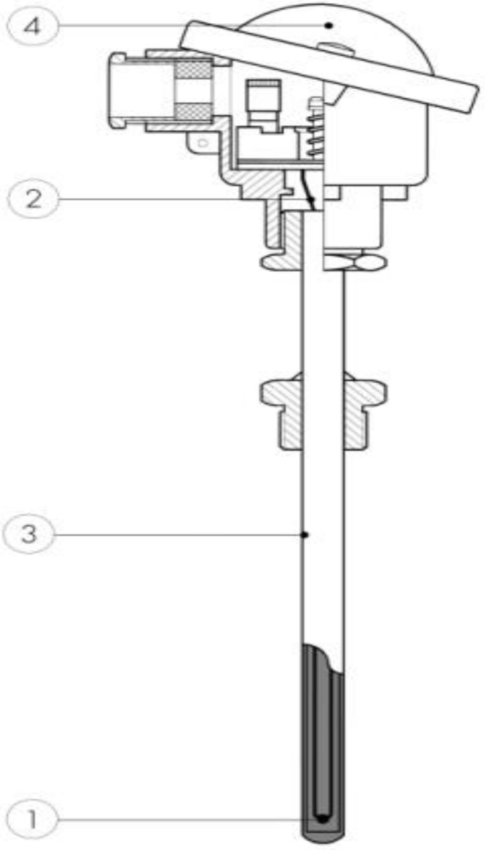

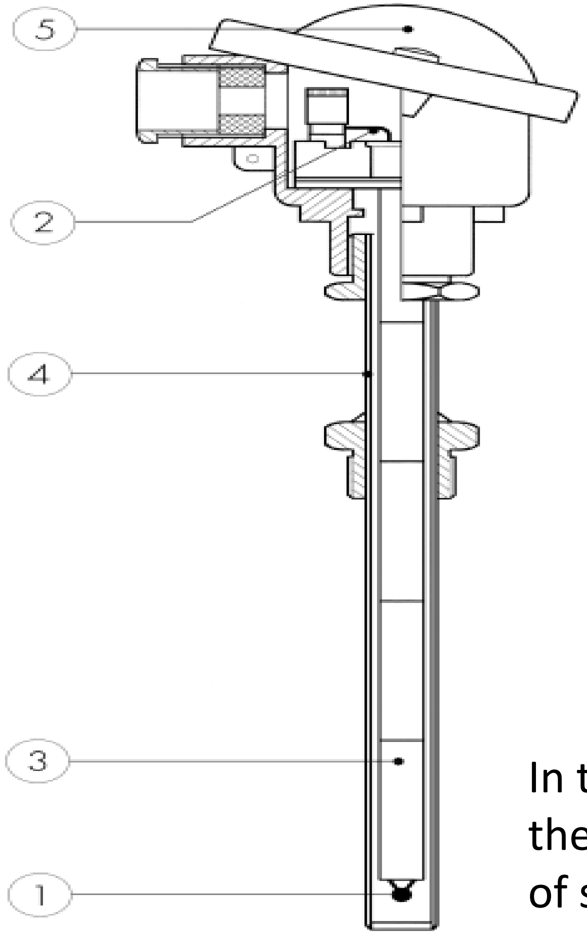

Insulated thermocouples (the standard insulation is magnesium oxide MgO)

This particular type of construction allows the creation of high performance thermocouples with excellent mechanical characteristics.
The main construction features of this type of construction can be summarized as follows:

- possibility of making very small thermocouples (starting from 0.5mm in diameter)
- possibility of bending the sheath with very narrow radii of curvature
- considerable increase in duration average of the thermocouple
- possibility of making very long thermocouples.

In thermocouples with traditional insulation, the limit of use of the different thermocouples is determined not only by the type of sheath, but also by the size of the wires of the same

Temperature measurement

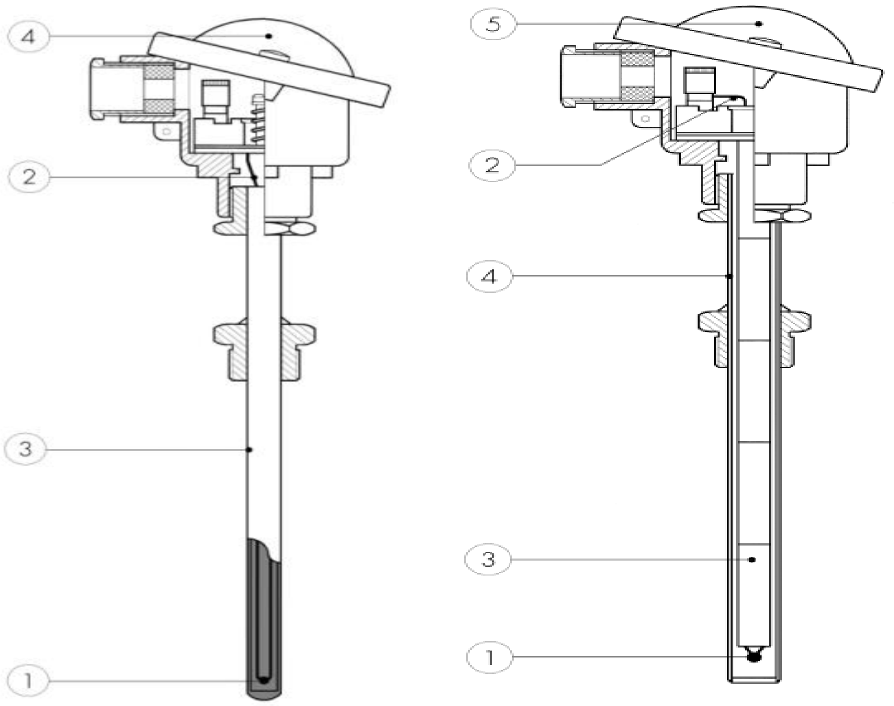

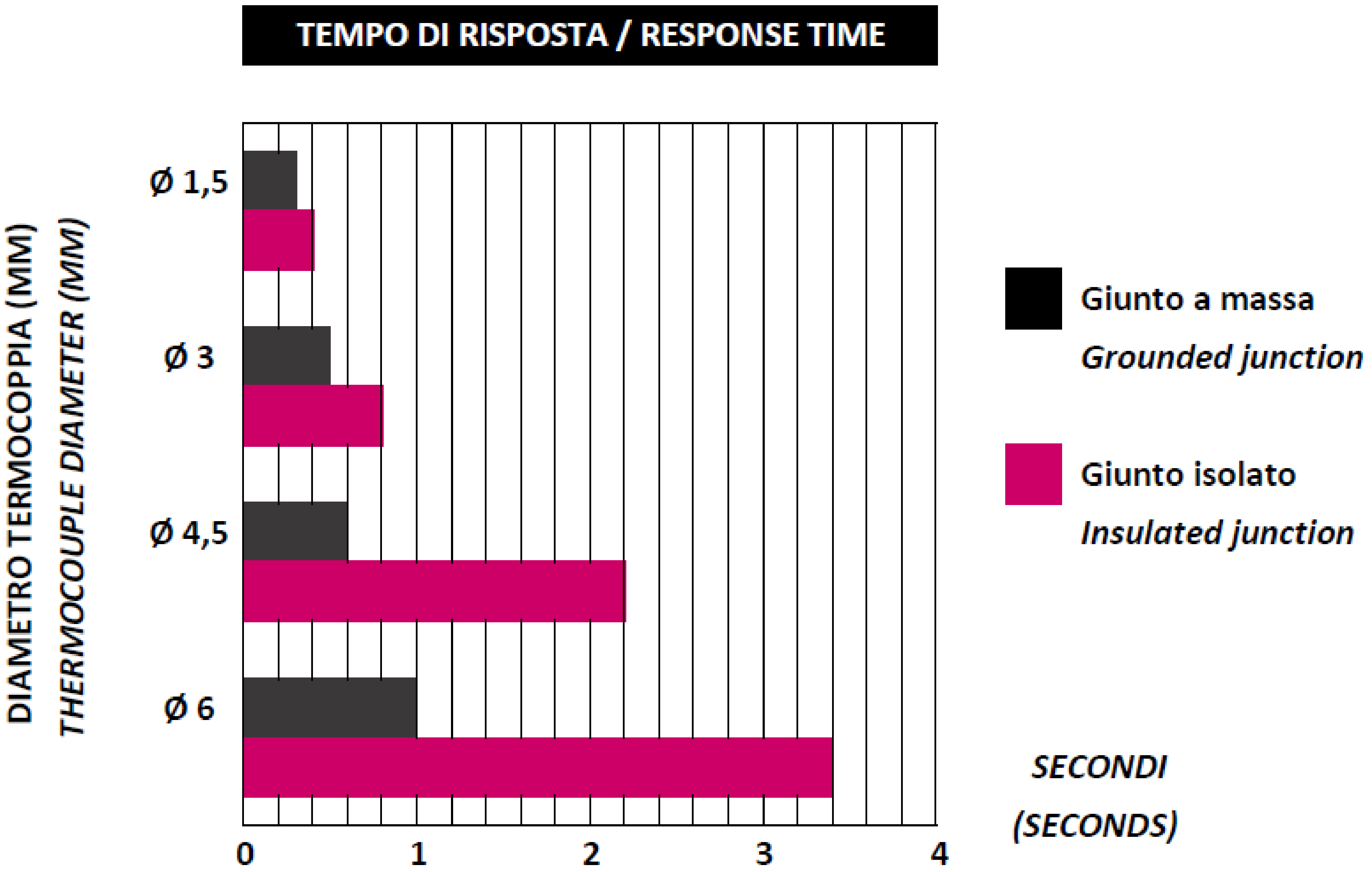

Temperature measurement

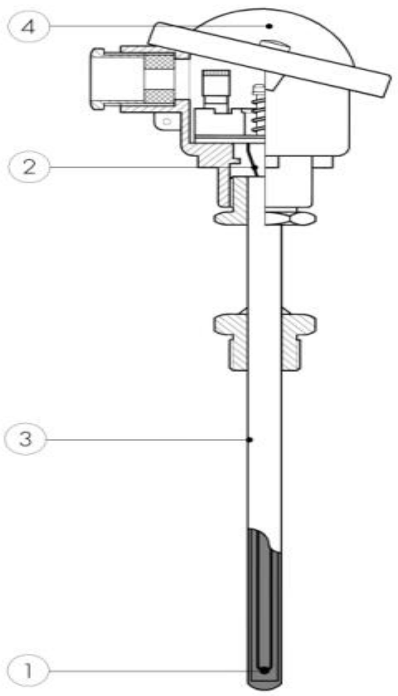

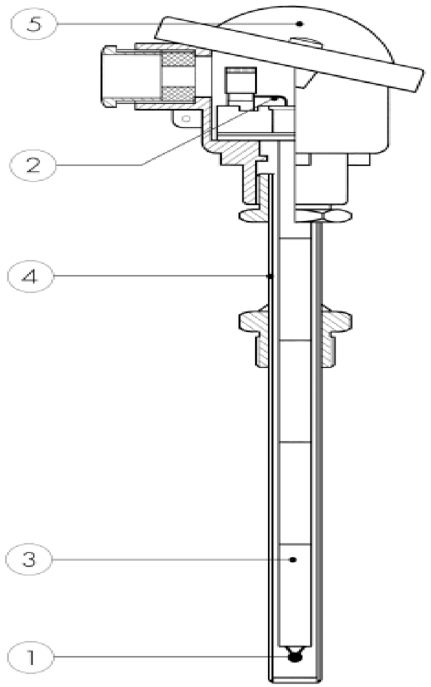

type		Working Range temperature °C	
J	Fe-Co	-210/1200	suitable for measurements of medium temperatures in reducing atmospheres and with the presence of hydrogen and coal, the presence of iron compromises its good functioning in oxidizing atmospheres
K	Cr-AL	-270/1370	suitable for high temperatures in oxidizing atmospheres, not suitable for reducing atomospheres

MAIN CAUSES OF ERROR IN MEASUREMENTS WITH THERMOCOUPLES

- Connecting the thermocouple to the measuring instrument with an unsuitable cable
- Polarity inversions in the various connections
- parasitic electromagnetic forces
- Wrong compensation of the reference junction.

All connections between thermocouples and measuring instruments must be made with suitable compensated cables

There are compensated cables for each type of thermocouple

The choice of the type of insulation and the dimensions depend solely on the conditions of use

The measurement with thermocouples requires compensation of the reference junction; it is therefore important that this is carried out correctly by the measuring instrument

Good practice, in the connections between thermocouples and measuring instruments, make as few junctions as possible and in any case use special devices with compensated contacts that also prevent polarity inversions.

Thermoresistances: ***R**esistance **T**emperature **D**etector (RTD)*

a Pt100 probe is a platinum resistance thermometer with nominal resistance defined according to IEC 751 (EN 60751) equal to 100 Ω at a temperature of 0 ° C.

The resistance thermometers are superior to the thermocouples in terms of:

accuracy,
the repeatability of the readings.
ease in calibration.

Measuring element	Connection method	Tolerance class	Measuring error in °C
Pt100	2-wire	B	5,25
	2-wire	A	4,65
	4-wire	B	1,05
	4-wire	A	0,45
Pt1000	2-wire	B	1,47
	2-wire	A	0,87
	4-wire	B	1,05
	4-wire	A	0,45

Thermoresistances: ***R**esistance **T**emperature **D**etector (RTD)*

a Pt100 probe is a platinum resistance thermometer with nominal resistance equal to 100 Ω at a temperature of 0 ° C.

Difference between Pt100 and Pt1000 The Pt100s have a nominal resistance of 100 Ω at the melting point of ice (0 ° C).

The nominal resistance of the Pt1000 at 0 ° C is instead of 1.000 Ω. The linearity of the characteristic curve, the operating temperature range and the response time are the same for both. The temperature coefficient of the resistance is also the same.

The readings of the Pt1000 probes are greater by a factor of 10 compared to the Pt100.

This difference becomes evident when comparing 2-wire configurations, in which the measurement error occurs. For example, the measurement error in a Pt100 could be + 1.0 ° C, and that of a Pt1000 with the same execution could be + 0.1 ° C.

Thermoresistances: ***R**esistance **T**emperature **D**etector (RTD)*

Pt100 advantages

- Pt100 probe is available in both wire wound and thin film execution (flexibility)
- Pt1000 probes are almost always thin film only
- Pt100 probes are compatible with a wide range of tools and processes

Pt1000 advantages

- Pt1000 probe is best in 2-wire configuration and when used with longer cable lengths.

The fewer wires and the longer they are, the more resistance is added to the readings, thereby causing inaccuracies.
(The higher rated resistance of the Pt1000 probe compensates for these added errors)

- Pt1000 probe is best for battery powered applications.

- Pt1000 consumes less energy, self-heating is lower. This means fewer read errors due to higher than ambient temperatures

Pressure sensors: diaphragm seal

Typically connected to a pressure gauge, process transmitter, or pressure switch, **a diaphragm seal is a thin, flexible wall that separates the media being measured from the pressure measuring instrument**.

The space between the diaphragm and the measuring instrument is filled with a system fluid (transmitting fluid), which hydraulically transmits pressure from the flexible diaphragm.

The contact surface between the media and the diaphragm is relatively large, which ensures more accurate pressure measurements – especially for very low pressures (< 600 mbar.) (−90 to +399°C)

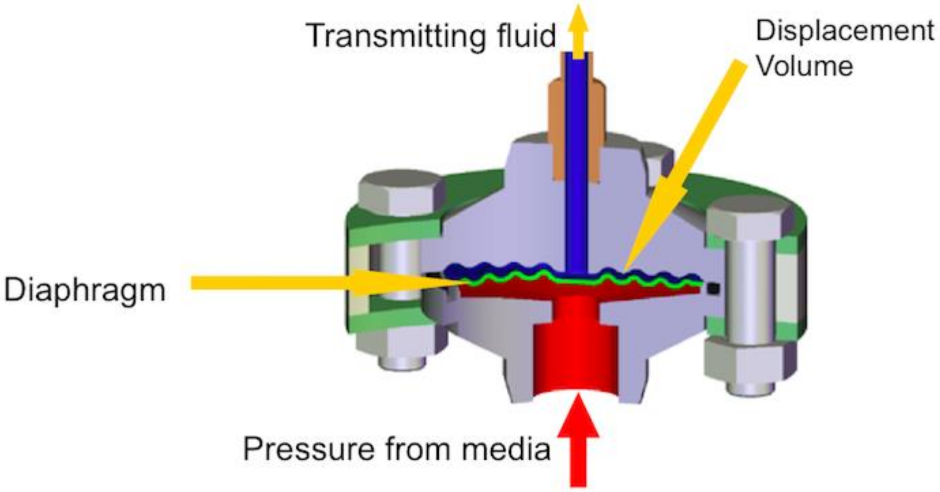

Diaphragm Seal with Flange Connection
Flush Diaphragm with Raised Face
Model: 8207

Pressure sensors: diaphragm seal

diaphragm seals extend the operating life of pressure measurement instruments – saving users significant time and money in the long run but …..

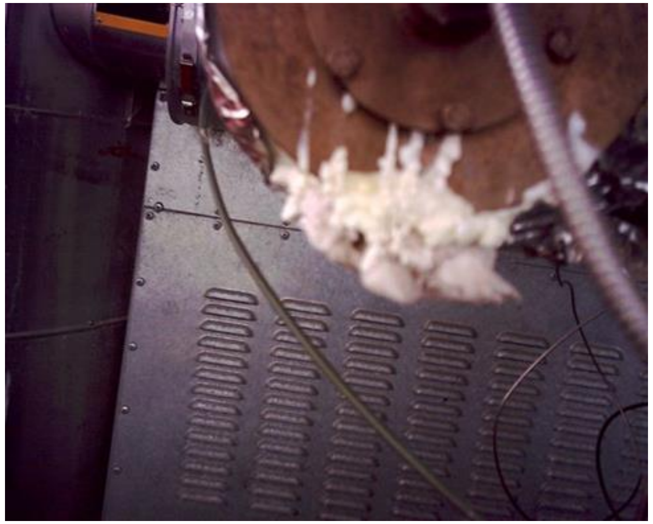

Ultrasonic flowmeters

Ultrasonic flowmeters from KROHNE work according to the time-of-flight method. For this method, two diagonally opposed ultrasonic sensors alternately function as transmitters and receivers.

Thus, the sound signal, which is alternately sent by both of them, is both accelerated by the flow and braked against the flow.

The differences in the times that the signal needs to travel the measured sections is directly proportional to the mean flow rate from which the volumetric flow is calculated.

Through the use of several ultrasonic paths, flow profile aberrations can be compensated.

Potential Supplier: KRONE, ITAL CONTROL METERS s.r.l

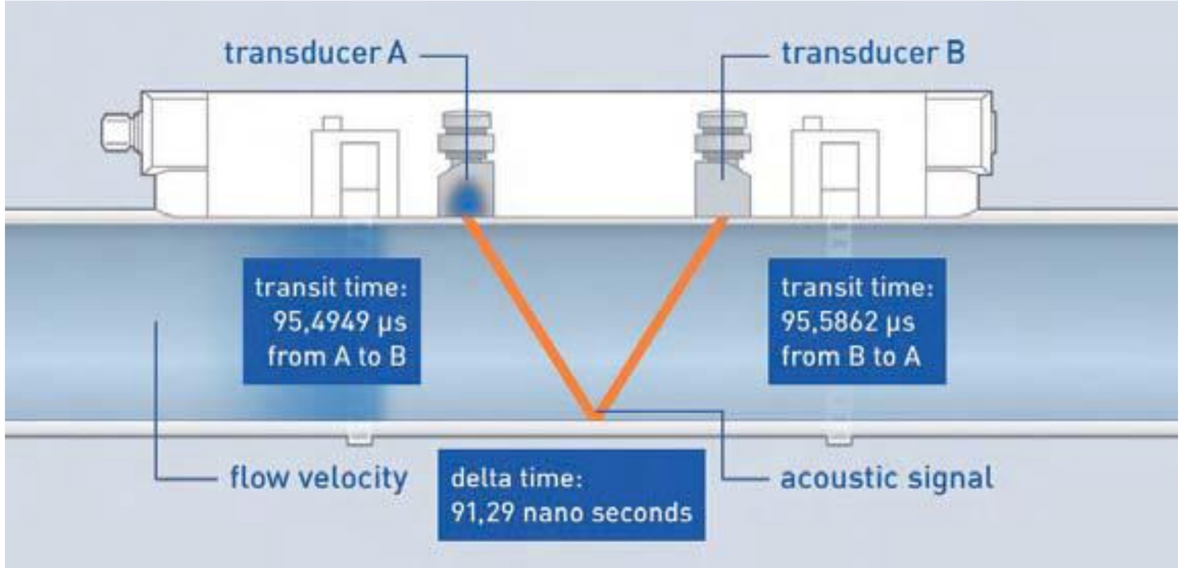

- The highest degree of accuracy and reproducibility
- No moving parts or parts that protrude into the measurement pipe
- Low operating costs because of nonwearing and maintenance-free propertie;
- Excellent long-term stability, no re-calibration
- High reliability due to several redundant measuring paths

calibrate flange

The Calibrated Flange is a Flow Element, and is in contact with the process fluid,

the calibrated flange by narrowing the fluid passage section creates a local increase in speed thus creating a pressure drop

the differential pressure existing between upstream and downstream of the flow element is sensed by a differential pressure transmitter which generates a 4 ÷ 20 mA signal managed by the local display, by a remote flow computer or by a DCS.

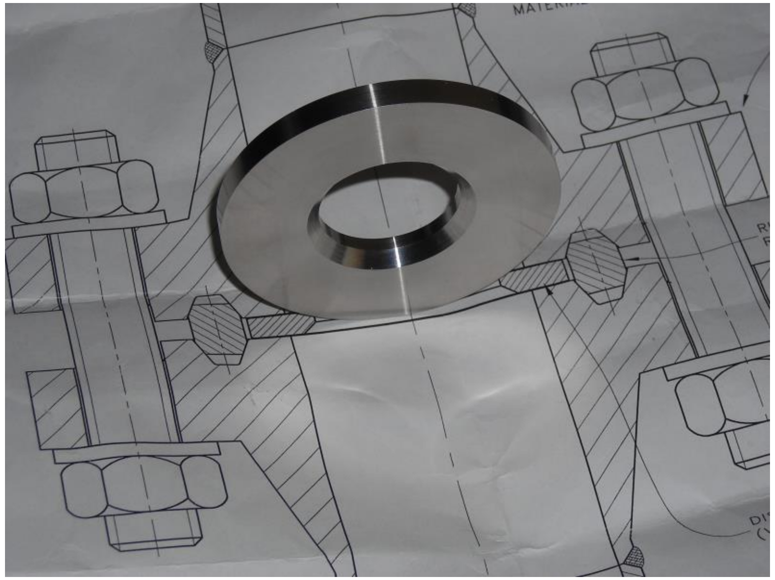

- No moving parts or parts that protrude into the measurement pipe
- easy to assemble
- cheaper;
- No professional installation

Radar/ultrasonic Level meters

Potential Supplier: VEGACAL, KRONE

radar, a high-frequency signal is used, the transmitting frequency of which increases
linearly during the measurement (frequency sweep). The signal is sent out, reflected back from the
surface of the measured product and received with a time delay. The difference Tf is formed from the
current transmitting and receiving frequency for further signal processing. It is directly proportional
to the distance, i.e. a large frequency difference means a large distance and vice versa

Walter GAGGIOLI, PhD
ENEA
TERIN-STSN
walter.gaggioli@enea.it

THANK YOU FOR YOUR ATTENTION!
ANY QUESTIONS?

SFERA-III

Solar Facilities for the European Research Area

4th Training for Industries

7-11th November 2022, ENEA Casaccia Research Center, Rome (Italy)

Basic design criteria for molten salt storage in CSP plants

Raffaele Liberatore (ENEA, TERIN-STSN-SCIS)

JOINT RESEARCH ACTIVITIES

THIS PROJECT HAS RECEIVED FUNDING FROM THE EUROPEAN UNION'S HORIZON 2020 RESEARCH AND INNOVATION PROGRAMME UNDER GRANT AGREEMENT NO **823802**

Outline:

Use of different heat transfer fluid

Solar field sizing

Thermal Energy Storage sizing

Trough technology with oil

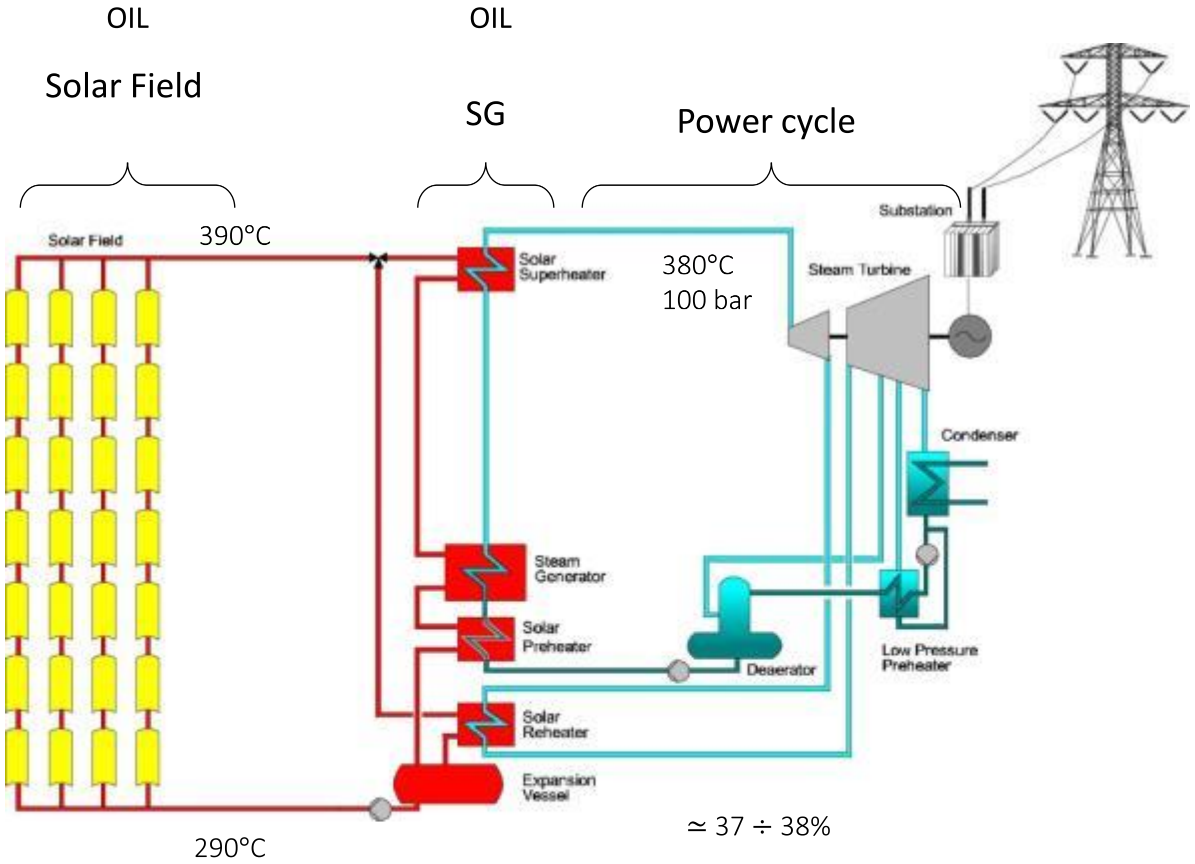

Temperature		Liquid density	Liquid heat capacity	Heat of vaporization	Liquid enthalpy[b]	Liquid thermal conductivity	Liquid viscosity[c]		Vapor pressure[d]
°C	°F	kg/m³	kJ/(kg·K)	kJ/kg	kJ/kg	W/(m·K)	cP (mPa·s)	cSt (mm²/s)	kPa
220	428	895	2.101	313.0	378.0	0.1106	0.345	0.385	41.5
230	446	886	2.128	308.0	399.1	0.1089	0.324	0.366	53.6
240	464	877	2.154	303.0	420.5	0.1072	0.305	0.348	68.4
250	482	867	2.181	297.9	442.2	0.1055	0.288	0.332	86.3
260	500	857	2.207	292.7	464.1	0.1038	0.272	0.317	108
270	518	848	2.234	287.5	486.3	0.1020	0.258	0.304	133
280	536	838	2.260	282.2	508.8	0.1002	0.244	0.292	163
290	554	827	2.287	276.8	531.6	0.0983	0.232	0.281	198
300	572	817	2.314	271.2	554.6	0.0964	0.221	0.271	239
310	590	806	2.341	265.6	577.8	0.0945	0.211	0.262	286
320	608	796	2.369	259.7	601.4	0.0925	0.202	0.254	340
330	626	784	2.397	253.8	625.2	0.0905	0.193	0.246	401
340	644	773	2.425	247.6	649.3	0.0885	0.185	0.239	470
350	662	761	2.454	241.3	673.7	0.0864	0.177	0.233	548
360	680	749	2.485	234.7	698.4	0.0843	0.170	0.227	635
370	698	736	2.517	227.8	723.4	0.0822	0.164	0.222	732
380	716	723	2.551	220.7	748.7	0.0800	0.158	0.218	840
390	734	709	2.588	213.2	774.4	0.0778	0.152	0.214	959
400	752	694	2.628	205.3	800.5	0.0756	0.146	0.211	1090
410	770	679	2.674	197.0	827.0	0.0733	0.141	0.208	1230
420	788	662	2.729	188.0	854.0	0.0710	0.137	0.206	1390

Molten salts 300°C
ρ= 1803 kg/m^3
Cp = 1.546 kJ/(kg*K)
k = 0.55 W/m^2
μ = 3.86 mPa*s

Trough technology with oil

WITH INTEGRATION

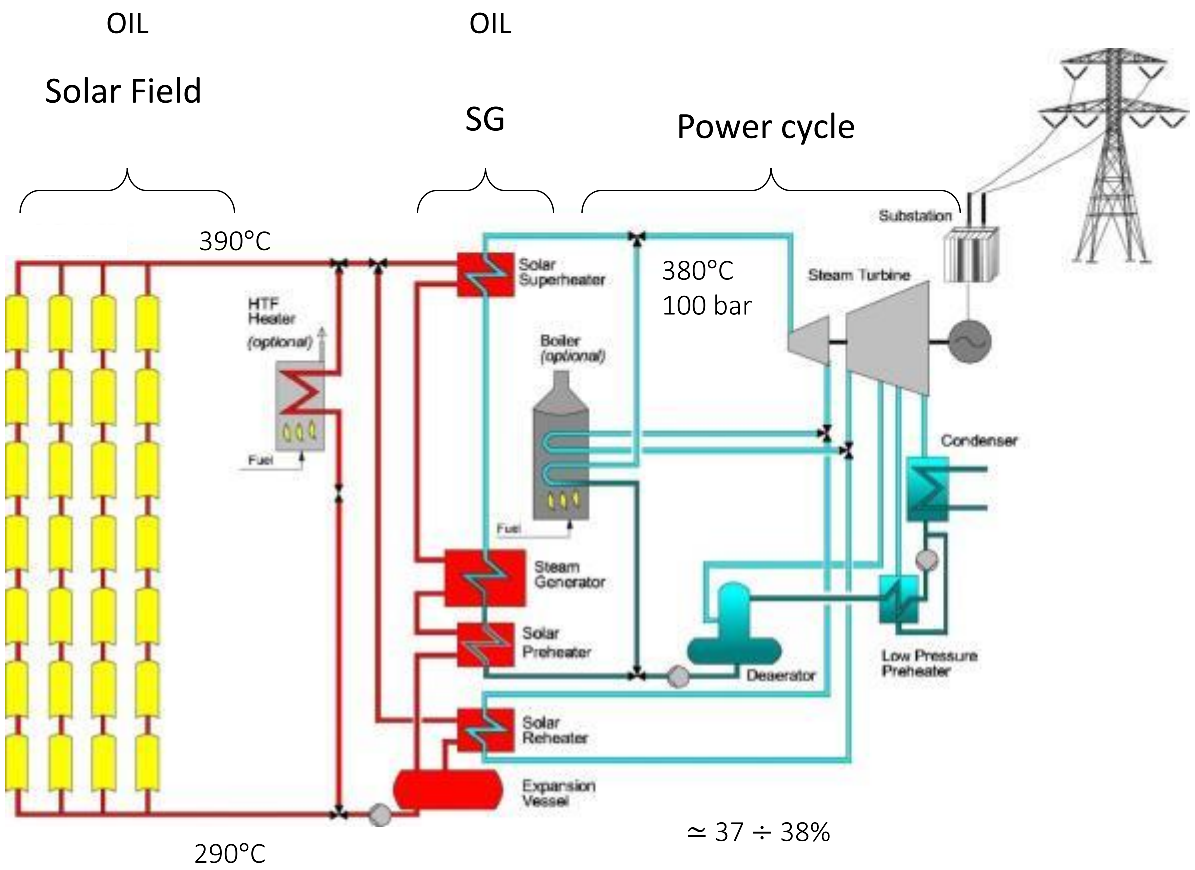

Trough technology with oil

WITH THERMAL ENERGY STORAGE

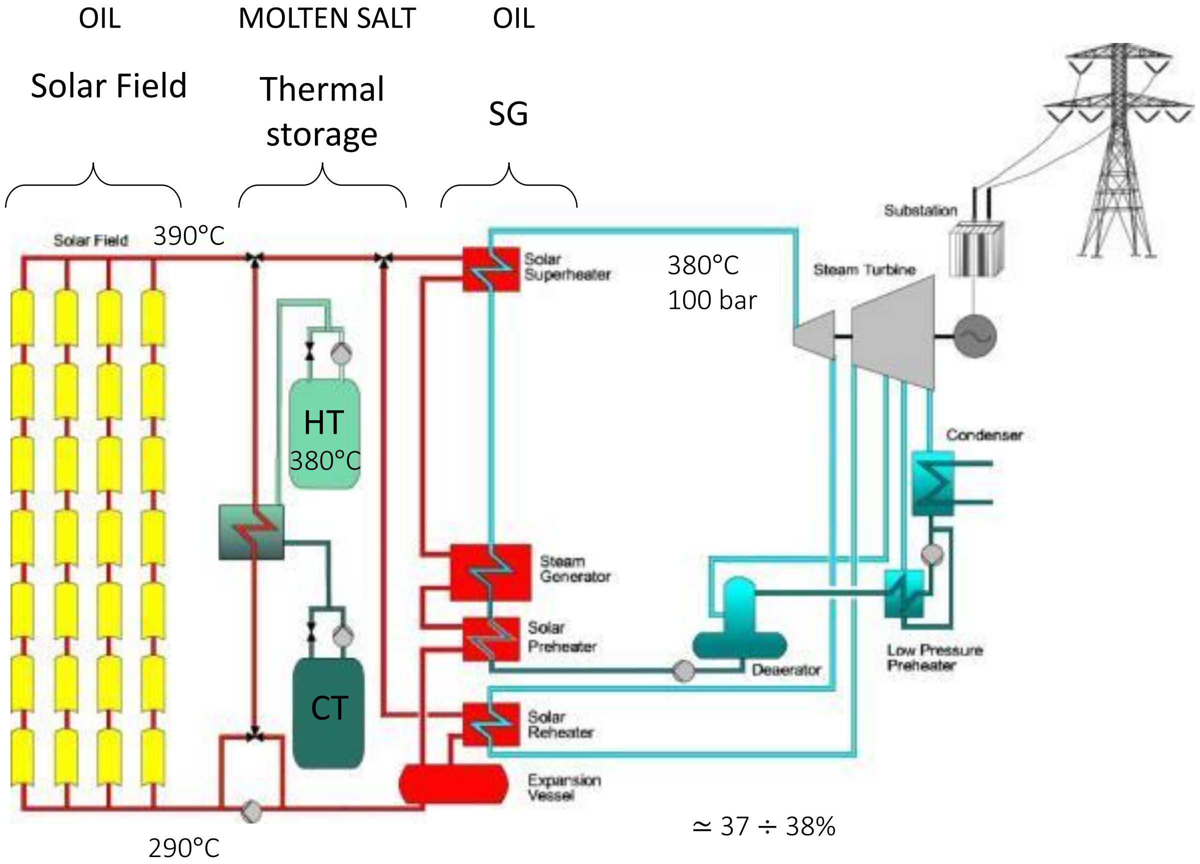

Trough technology with molten salt

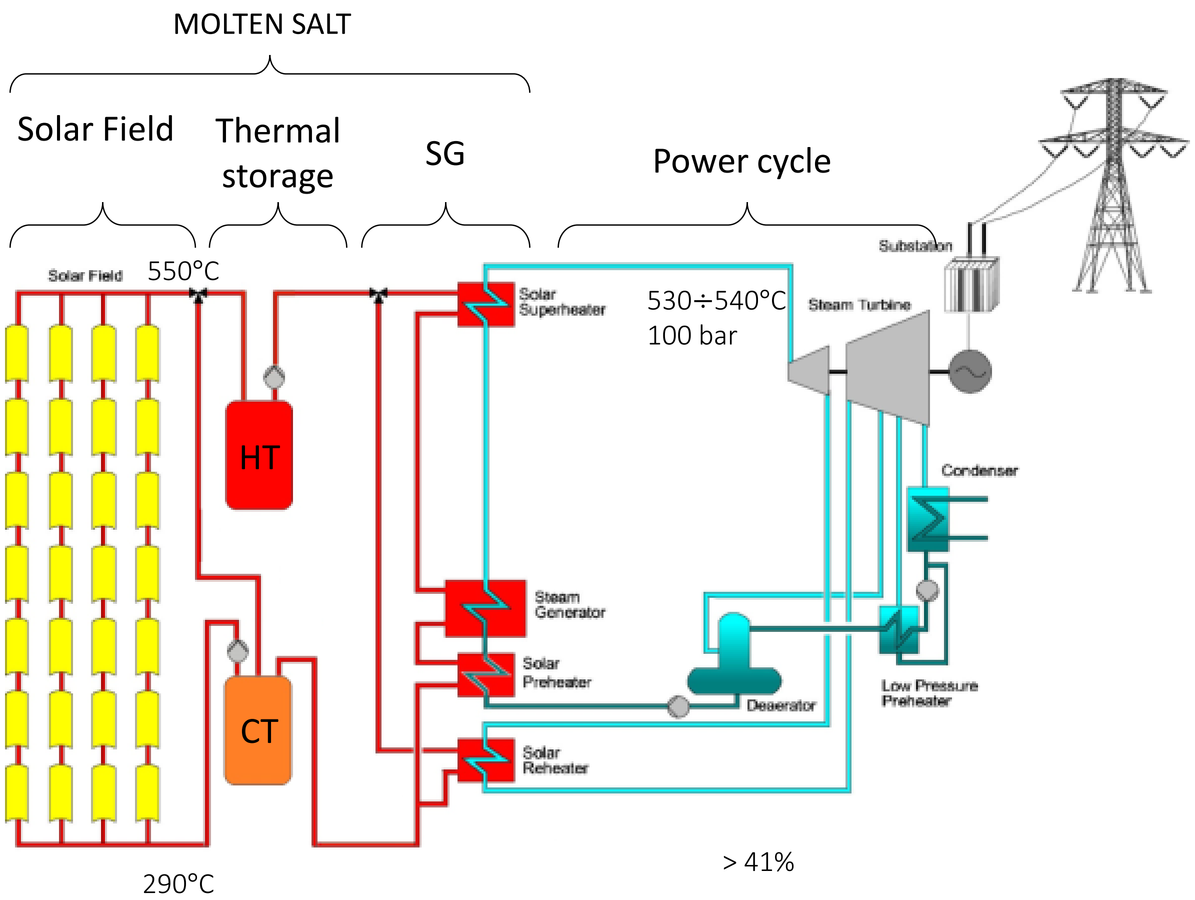

OIL vs MOLTEN SALT

OIL with Thermal Storage

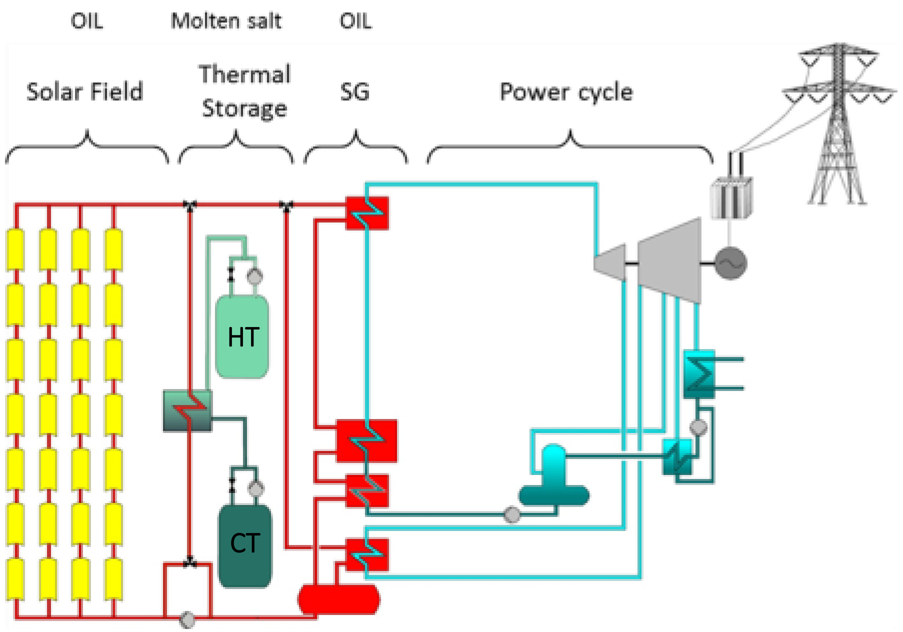

MOLTEN SALT

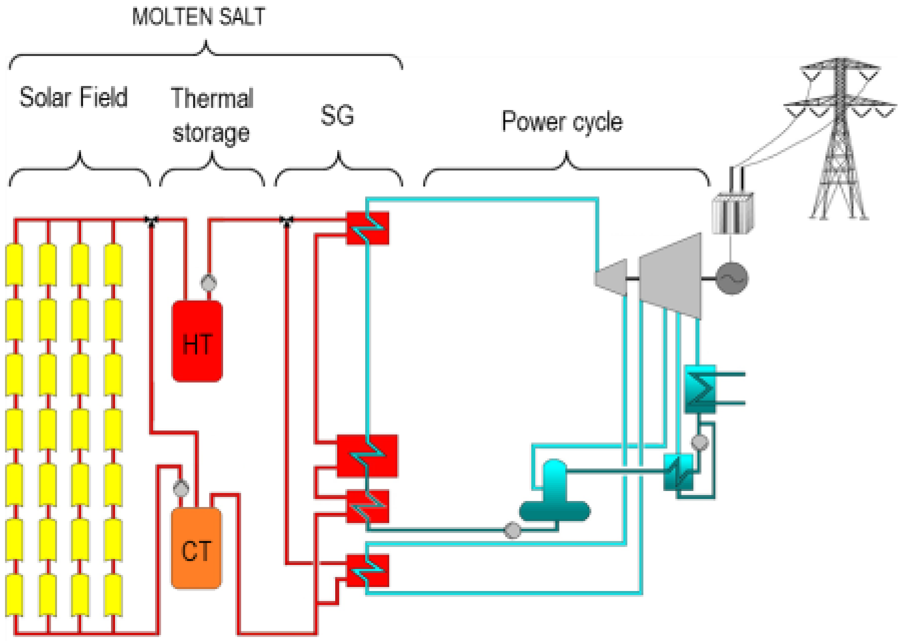

Synthetic oil - Therminol VP1, Dowtherm A
eutectic mixture: 73.5% diphenil oxide , 26.5% biphenil
range 12 - 400°C

Molten salt:
mixture: 60% $NaNO_3$, 40% KNO_3
range 240 - 600°C

OIL vs MOLTEN SALT

OIL with Thermal Storage

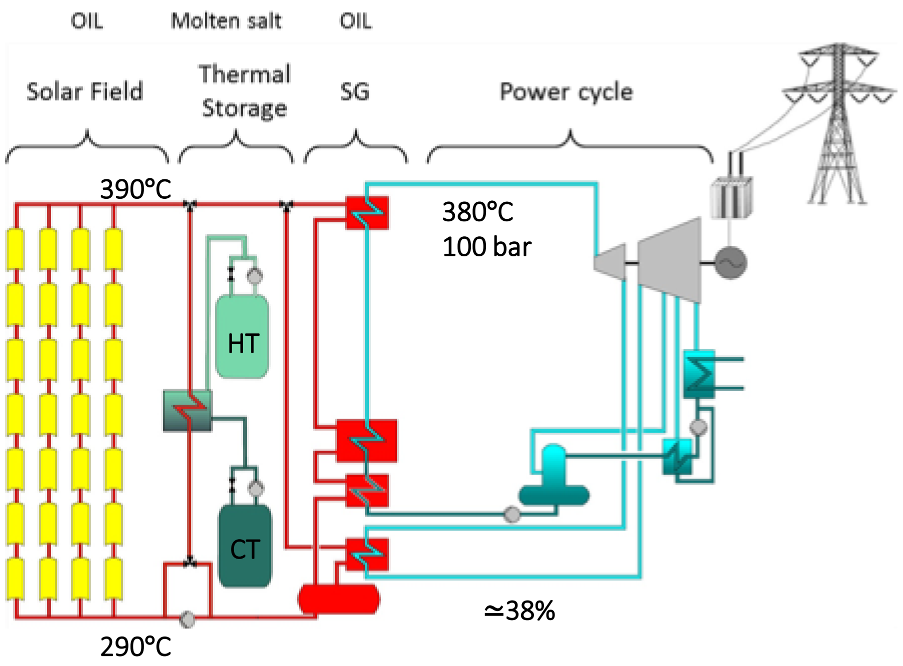

Oil/Salt heat exchangers

Expansion vessel

Indirect TES

14.42 m^3/MWh_t ~70 kWh/m^3

MOLTEN SALT

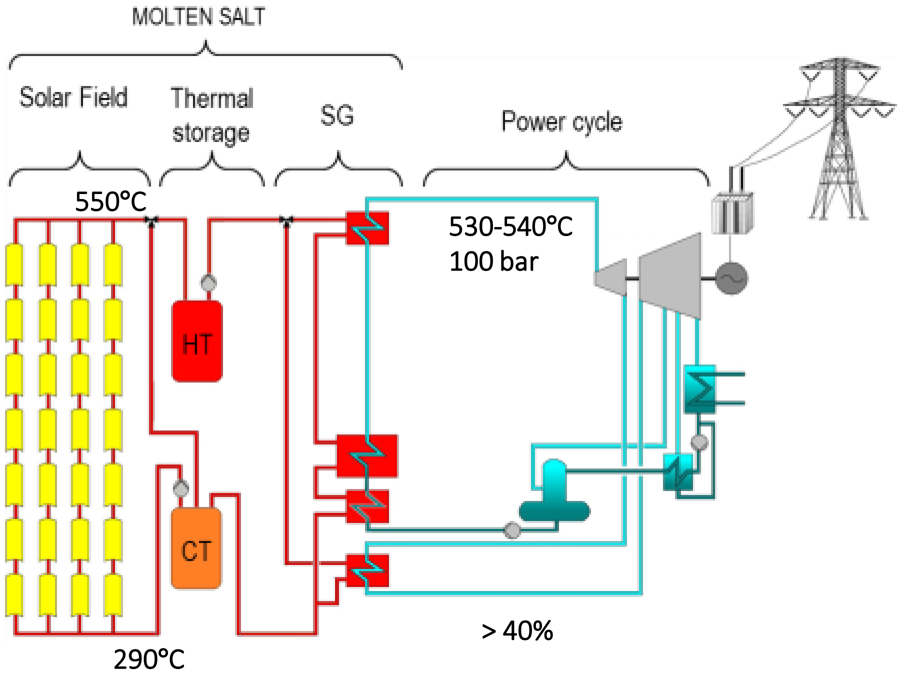

Direct TES

5.25 m^3/MWh_t ~190 kWh/m^3

$$Q \approx M \cdot Cp \cdot (T_{fin} - T_{in})$$

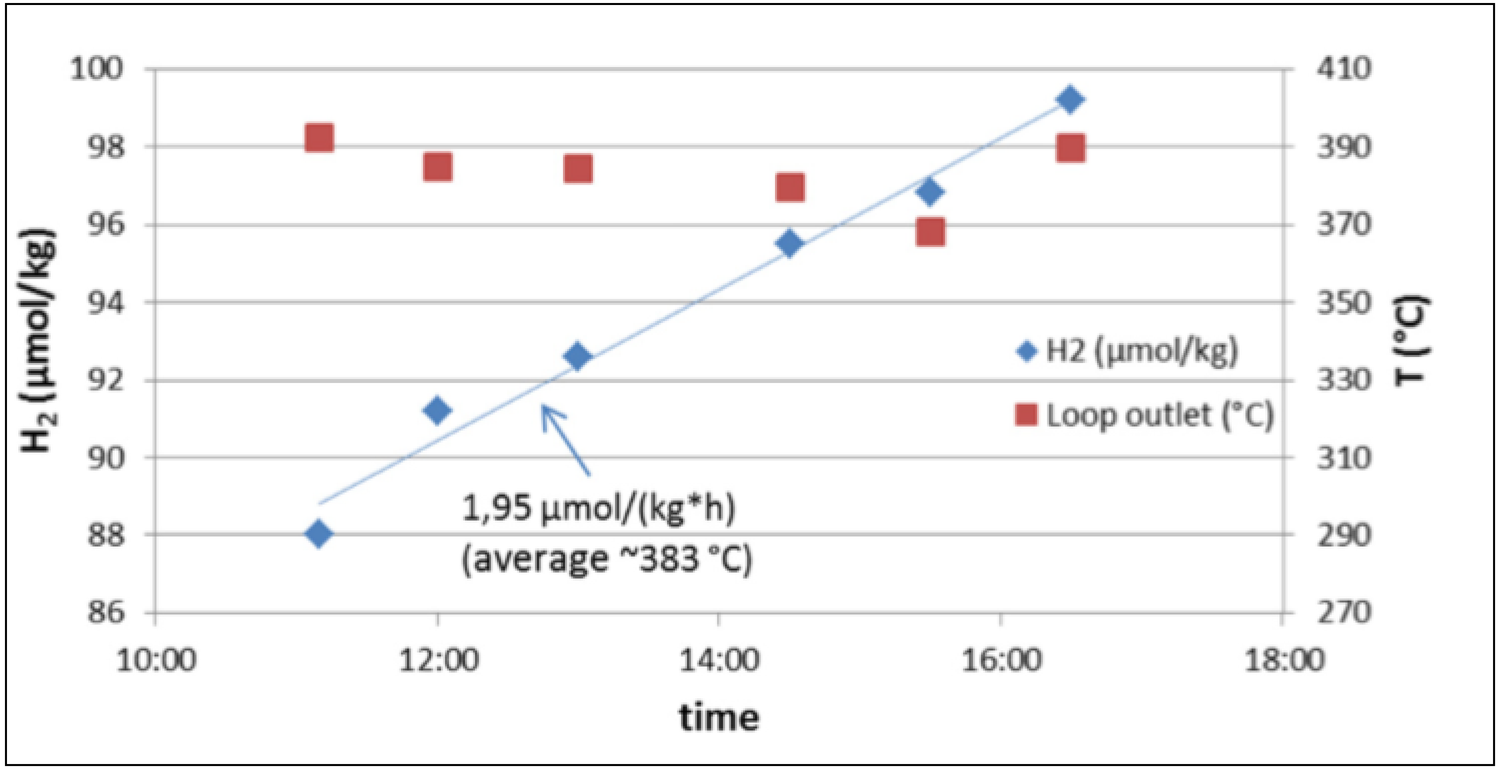

*At elevated temperatures, the organic components of the oil undergo **degradation** reactions that produce hydrogen.*

OIL vs MOLTEN SALT

Thermal decomposition

Hydrogen permeates through the receiver tube walls and establishes an equilibrium partial pressure within the annulus of the receiver. The thermal losses increases.

Heat losses with or without H_2 presence

Heat losses increase the glass temperature

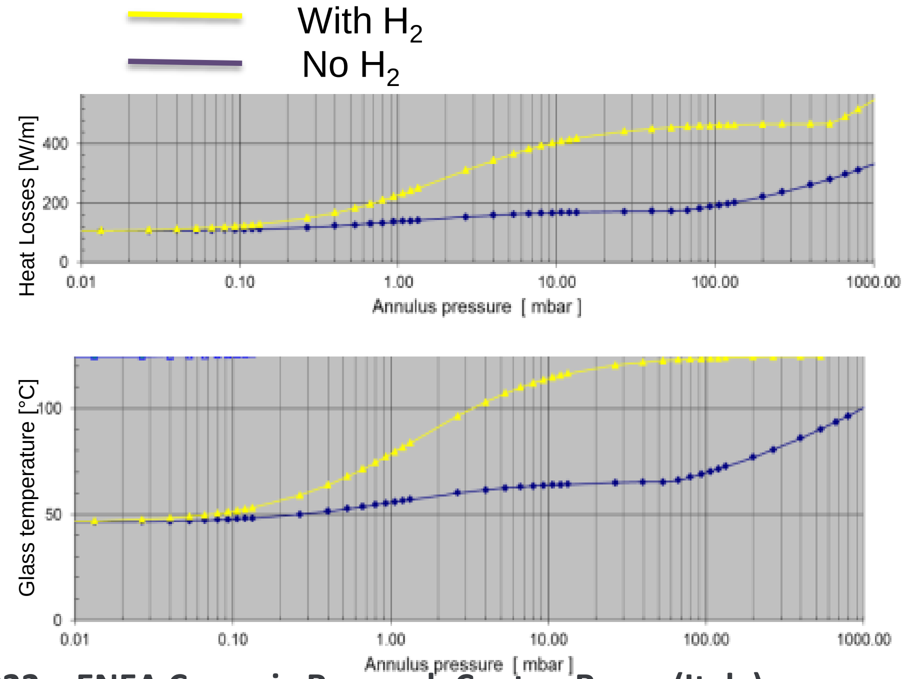

Electric heating system

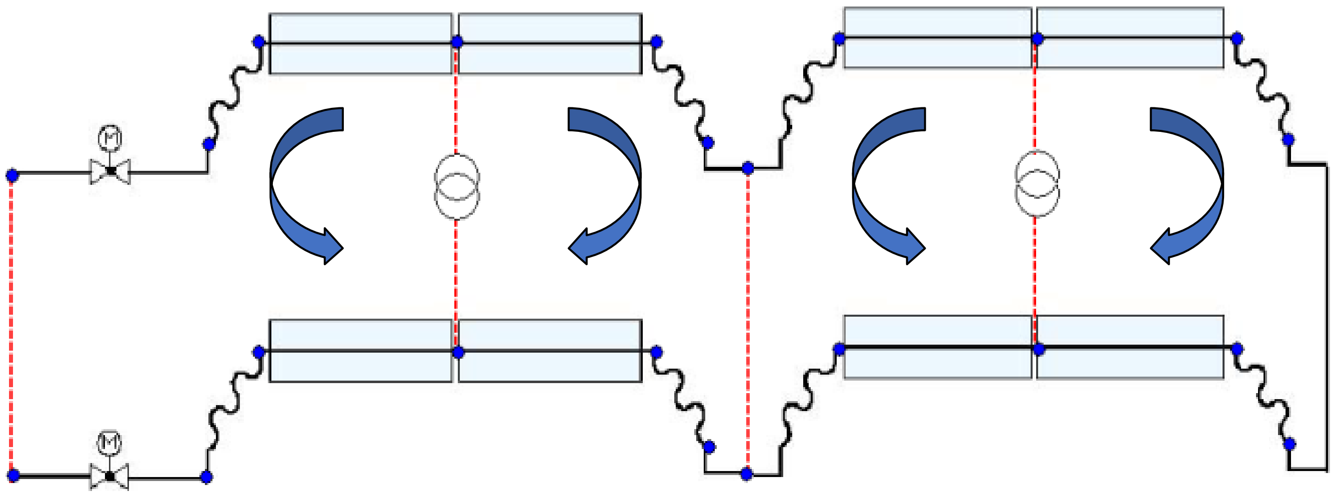

Heating power considers in particular the Heat Collection Element HCE.
In order to heat the pipelines and the receivers, it is applied a DV of +- 35 V (70 in total) with 400 A. This way, it is possible to use the ***Joule effect*** *because at 300 °C molten salt is dielectric.*

Take care with:

- Loss of vacuum, or else the necessary heating power increases
  - Heat loss at 270°C: 80 W/m with vacuum and 295 W/m without vacuum

OIL vs MOLTEN SALT

Advantages:

- Low freezing temperature (~ 12°C)
- High thermal stability (12 ÷ 400°C)
- Low viscosity
- No corrosivity

Disadvantages:

- Limited maximum temperatures > 400°C
- Chemical contamination, air oxidation, thermal decomposition (H_2)
- Working under pressure to prevent evaporation at operating temperature (~10 bar at 393°C)
- Problems of toxicity & fire
- High cost (~5÷8 €/kg)

Advantages:

- High maximum temperature (~600°C)
- High thermal stability (240 ÷ 600°C)
- No toxicity problems
- Low working pressure
- Low cost (~1.5÷1 €/kg)

Disadvantages:

- Low corrosivity
- High freezing temperature (~238°C)

Temperature		Liquid density	Liquid heat capacity	Heat of vaporization	Liquid enthalpy[b]	Liquid thermal conductivity	Liquid viscosity[c]		Vapor pressure[d]
°C	°F	kg/m³	kJ/(kg·K)	kJ/kg	kJ/kg	W/(m·K)	cP (mPa·s)	cSt (mm²/s)	kPa
220	428	895	2.101	313.0	378.0	0.1106	0.345	0.385	41.5
230	446	886	2.128	308.0	399.1	0.1089	0.324	0.366	53.6
240	464	877	2.154	303.0	420.5	0.1072	0.305	0.348	68.4
250	482	867	2.181	297.9	442.2	0.1055	0.288	0.332	86.3
260	500	857	2.207	292.7	464.1	0.1038	0.272	0.317	108
270	518	848	2.234	287.5	486.3	0.1020	0.258	0.304	133
280	536	838	2.260	282.2	508.8	0.1002	0.244	0.292	163
290	554	827	2.287	276.8	531.6	0.0983	0.232	0.281	198
300	572	817	2.314	271.2	554.6	0.0964	0.221	0.271	239
310	590	806	2.341	265.6	577.8	0.0945	0.211	0.262	286
320	608	796	2.369	259.7	601.4	0.0925	0.202	0.254	340
330	626	784	2.397	253.8	625.2	0.0905	0.193	0.246	401
340	644	773	2.425	247.6	649.3	0.0885	0.185	0.239	470
350	662	761	2.454	241.3	673.7	0.0864	0.177	0.233	548
360	680	749	2.485	234.7	698.4	0.0843	0.170	0.227	635
370	698	736	2.517	227.8	723.4	0.0822	0.164	0.222	732
380	716	723	2.551	220.7	748.7	0.0800	0.158	0.218	840
390	734	709	2.588	213.2	774.4	0.0778	0.152	0.214	959
400	752	694	2.628	205.3	800.5	0.0756	0.146	0.211	1090
410	770	679	2.674	197.0	827.0	0.0733	0.141	0.208	1230
420	788	662	2.729	188.0	854.0	0.0710	0.137	0.206	1390

Molten salts 300°C
ρ= 1803 kg/m^3
Cp = 1.546 kJ/(kg*K)
k = 0.55 W/m^2
μ = 3.86 mPa*s

Aereal view of Andasol1
51 ha mirrors→200ha land area

OIL vs MOLTEN SALT

Aereal view of Andasol1

Nameplate capacity	50MWe
Capacity factor	0.41
Storage capacity	7.5 hours
Annual output	165 GWh

TES system is 13% Andasol's initial cost

OIL vs MOLTEN SALT

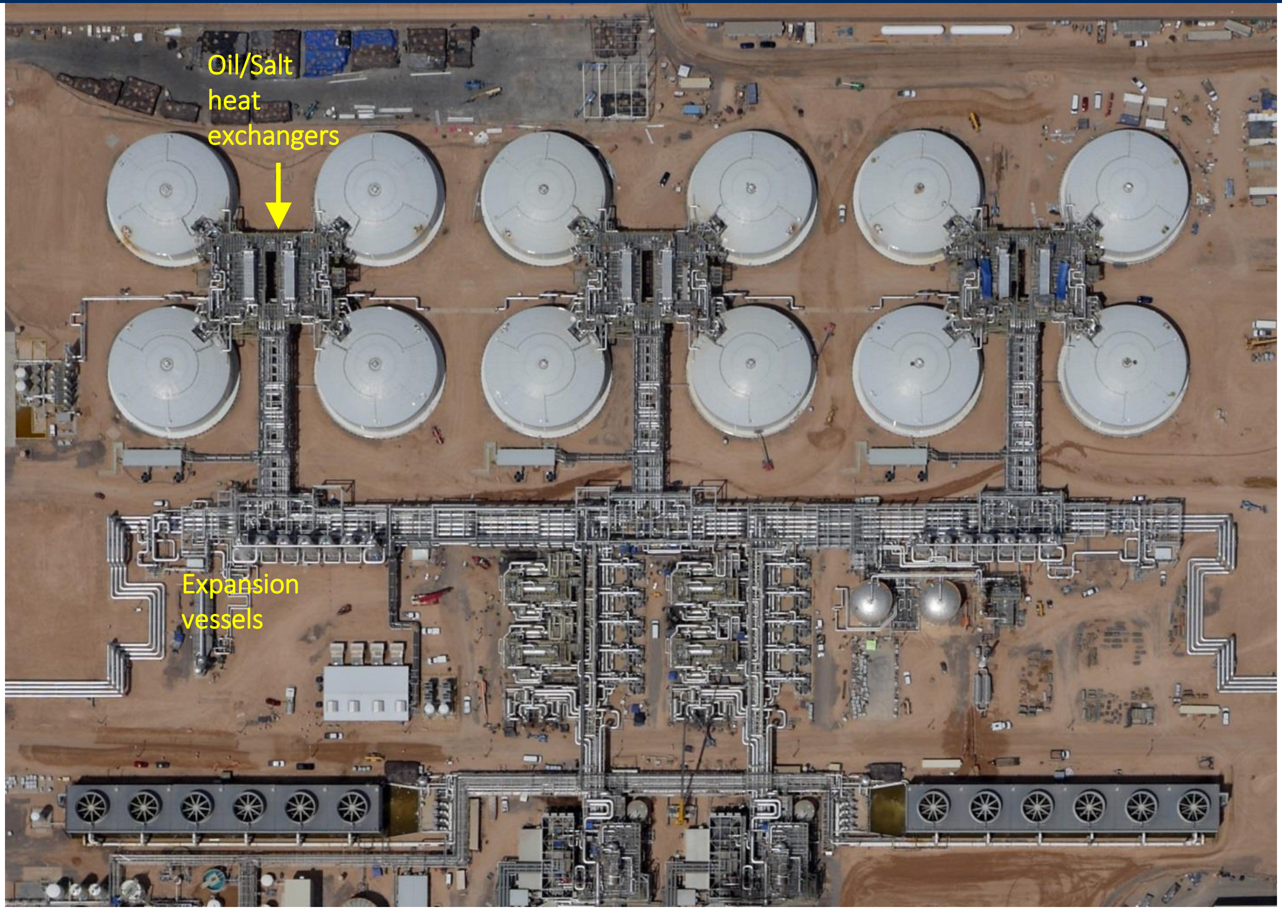

Aereal view of Solana Plant (280 MWe 6 h)

Expansion vessels

Gila Bend, Arizona
Solar field 223 ha
Site area: 780 ha
Production (2016 output) 644 GW·h
Cost: 2 G$
CF: 26.26%

Archimede: storage tanks (front view)

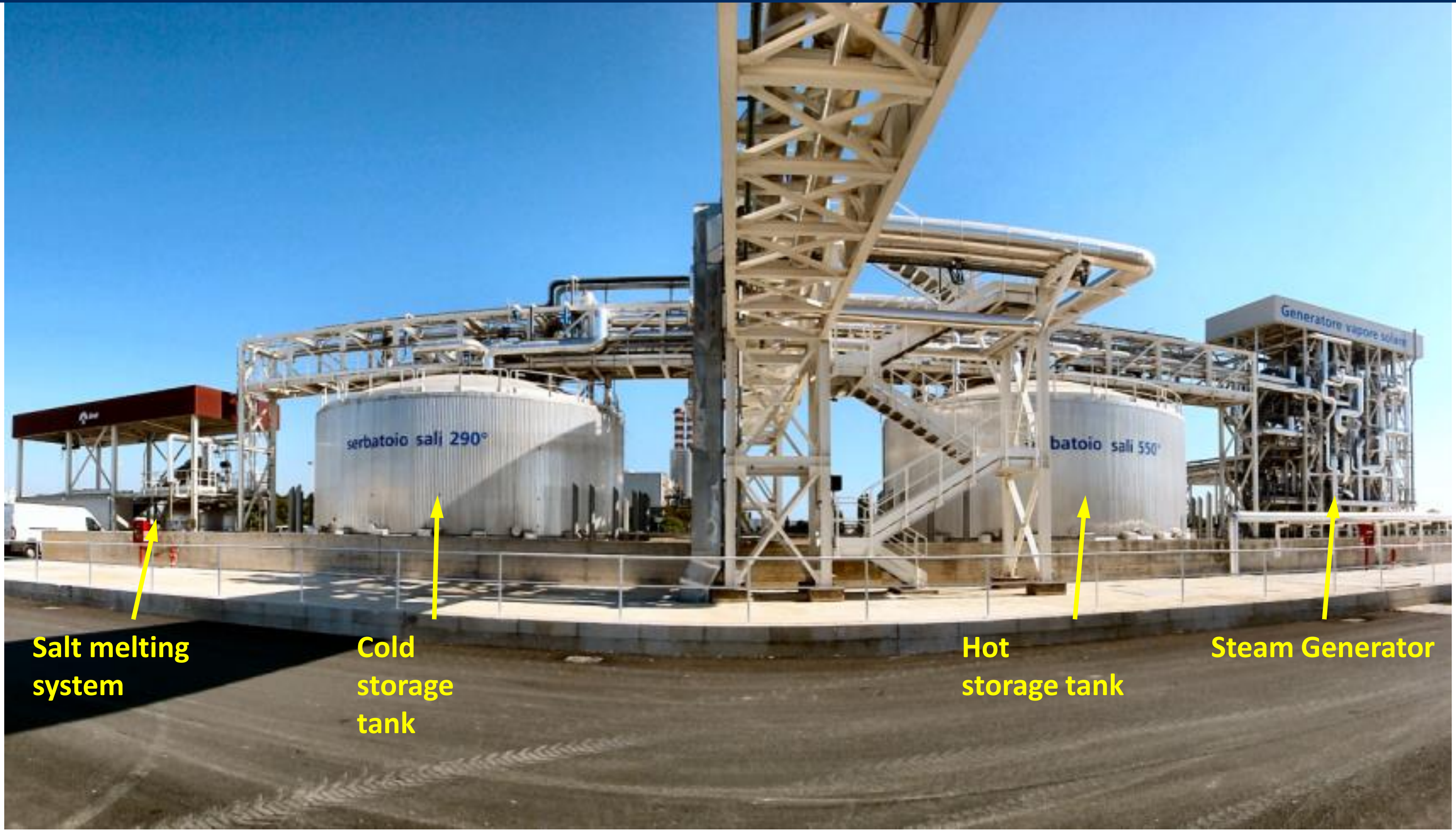

Archimede: Steam Generator

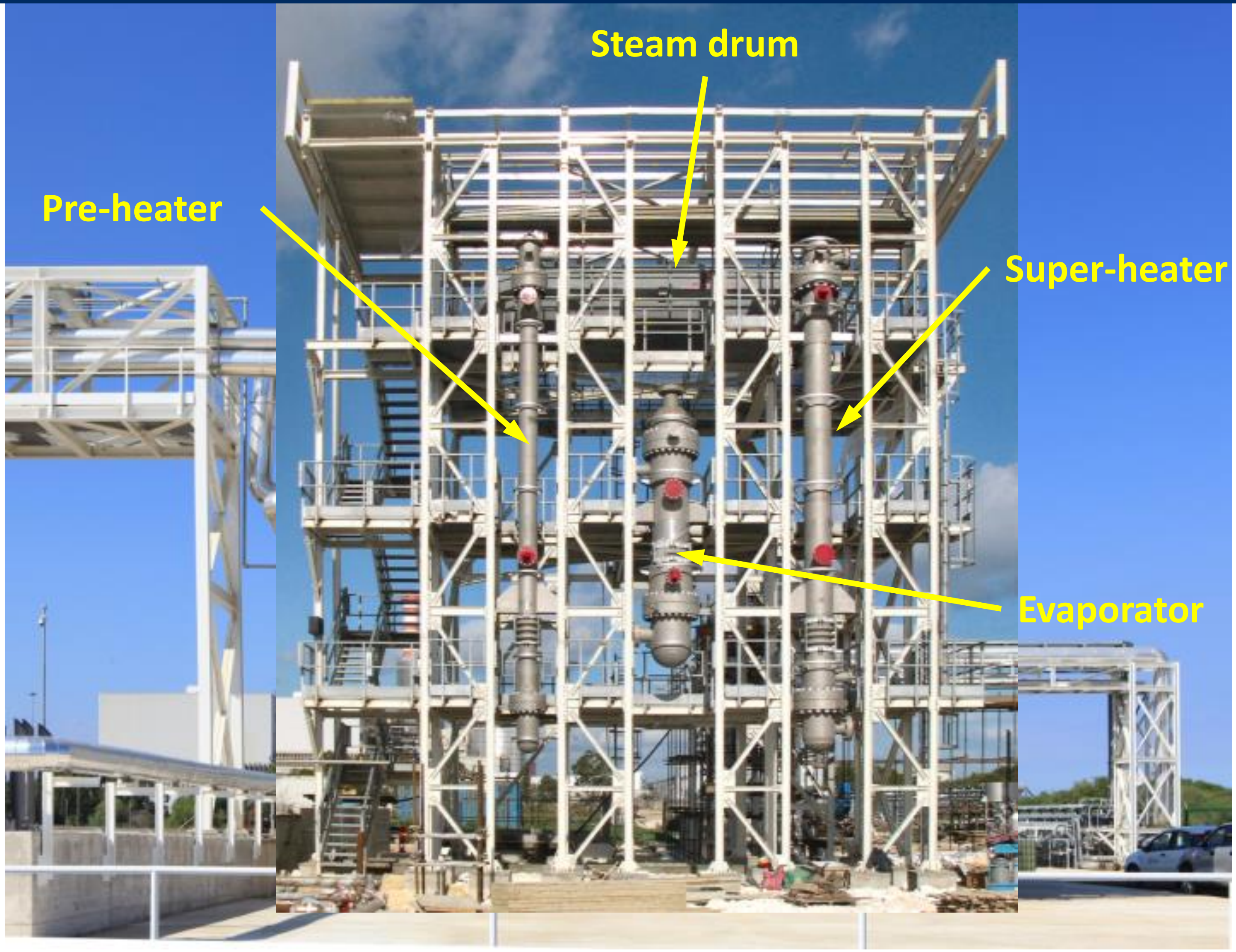

Archimede: solar field

MATS plant at Borg El Arab (Egypt)

Main features of the Solar Field:

- ❑ Lanaro collectors, Reflex mirrors, receiver tubes from Archimede Solar Energy, flex tubes from Astroflex
- ❑ Self-draining configuration
- ❑ Connected in series with gas back-up unit

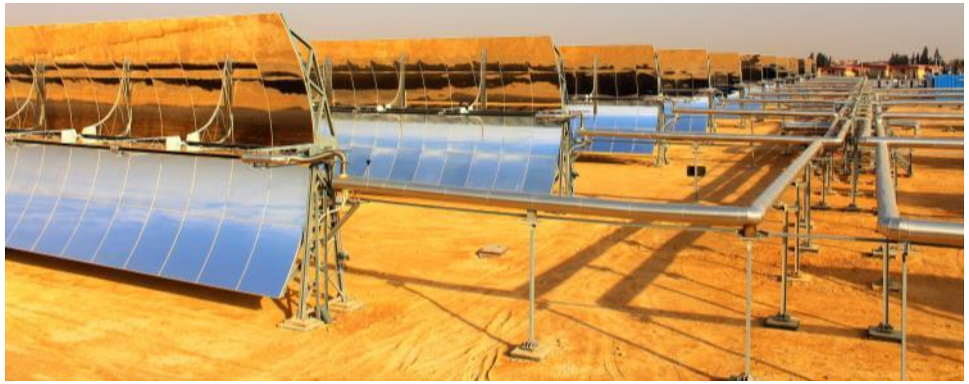

Solar field images

The size of a solar field depends mainly on:

- Electric capacity of the plant
- Thermal to electric conversion efficiency of the power cycle
- Distribution of the solar radiation
- Solar field efficiency
- Thermal Energy Storage system capacity

Solar field sizing

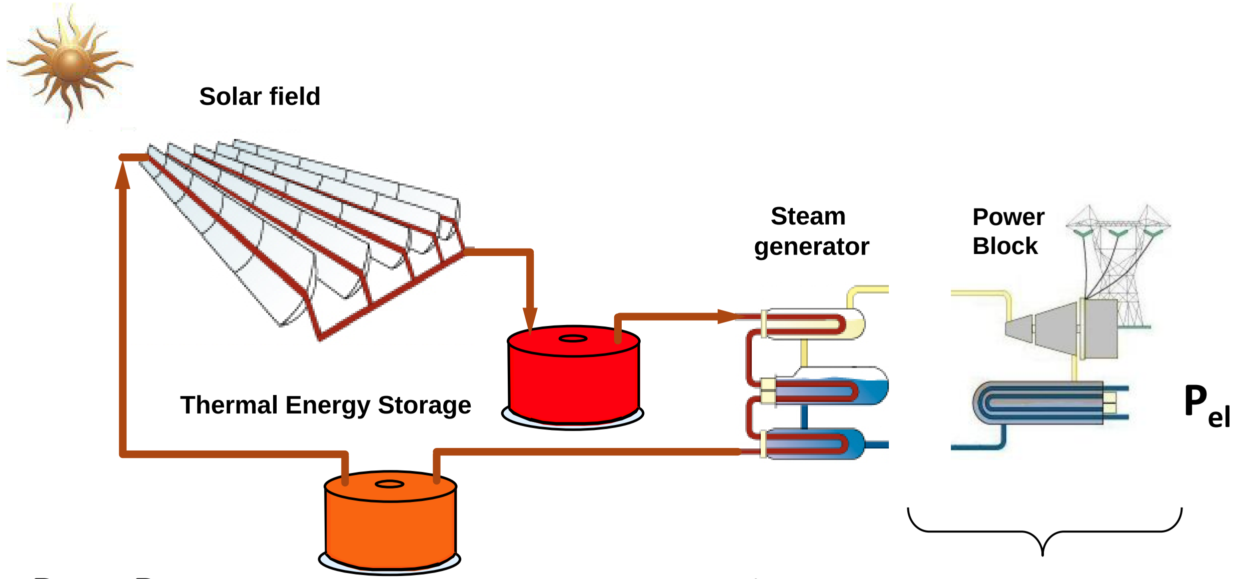

$\mathbf{P_{SF} = P_{SG}}$

$P_{SG} = P_{el}/\eta$

η

$P_{SF} = SF_{area} \cdot DNI_{des} \cdot \boldsymbol{\eta_{SF}}$

Solar field sizing

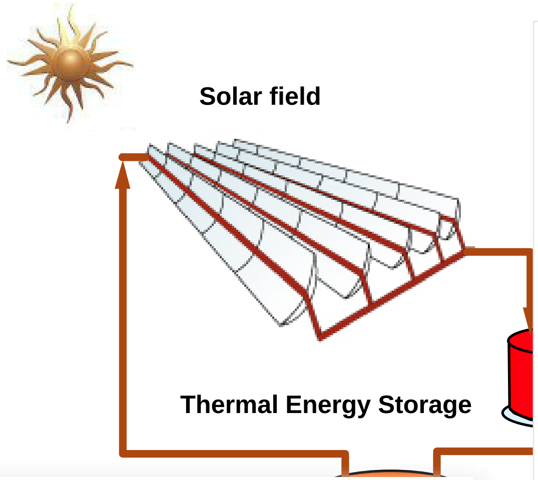

- DNI_{des} is the DNI design value used to calculate the aperture area required to drive the power cycle at its design capacity.
  - high value results in an undersized solar field that produces sufficient thermal energy to drive the power block at its design point only few hours
  - low value results in a large solar field and in excessive dumped energy.
- For systems in the Mojave Desert (CA), DNI >2700 kWh/m^2 y, a value of 920 W/m^2 is suggested, while for systems in the southern of Spain, DNI > 2100 kWh/m^2 y, a value of 800 W/m^2 is reasonable.

$P_{GV} = P_{el}/\eta$ η

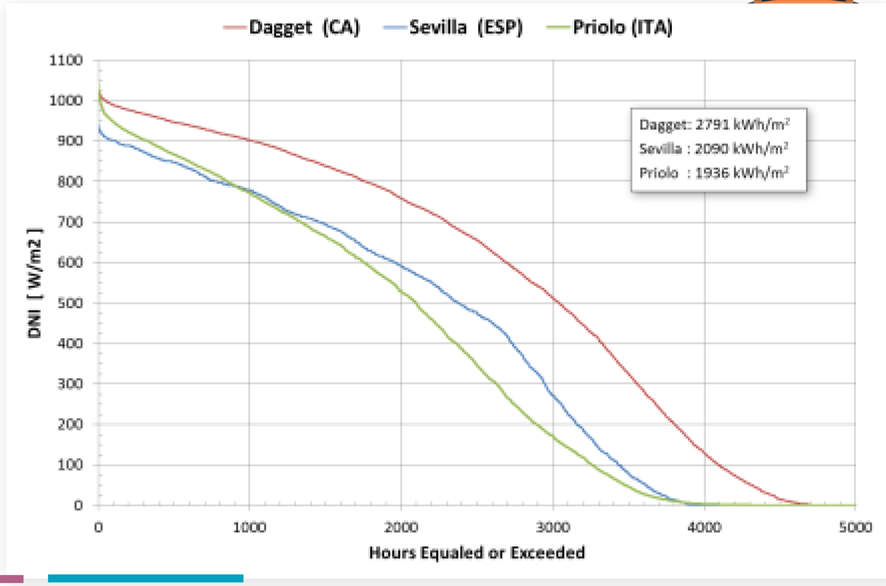

Solar Collector Assembly (SCA)

SCA

More SCAs linked

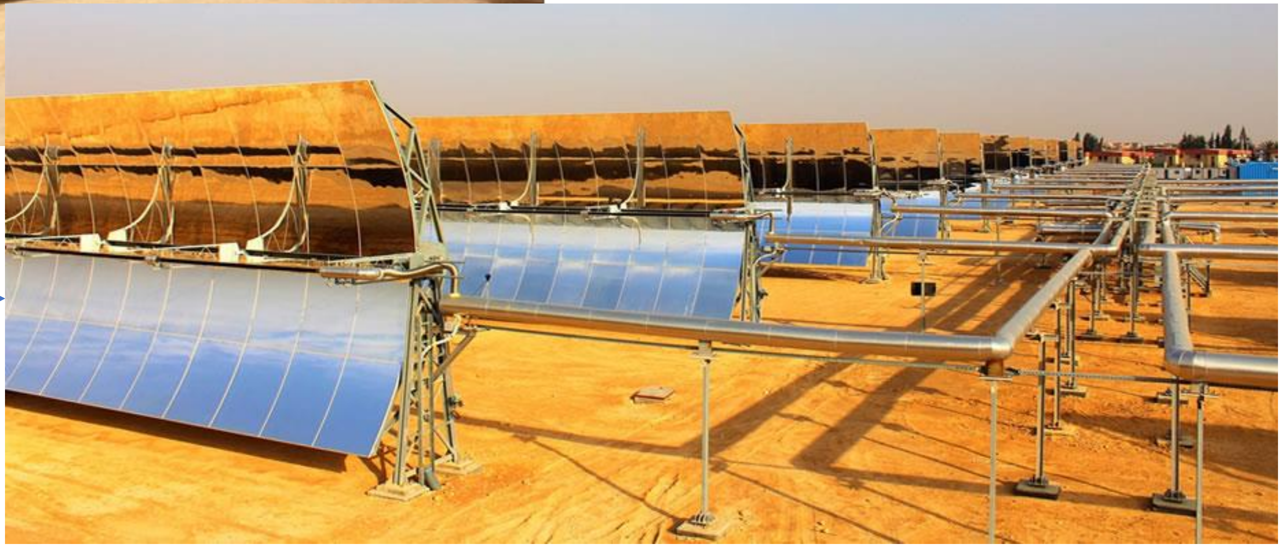

Solar field efficiency

- Solar field configuration is modular
- The module is not a single SCA but several SCA connected in series to form a loop
- The loops are then connected in parallel
- The length of a loop (number of SCA) depends on the operating temperatures

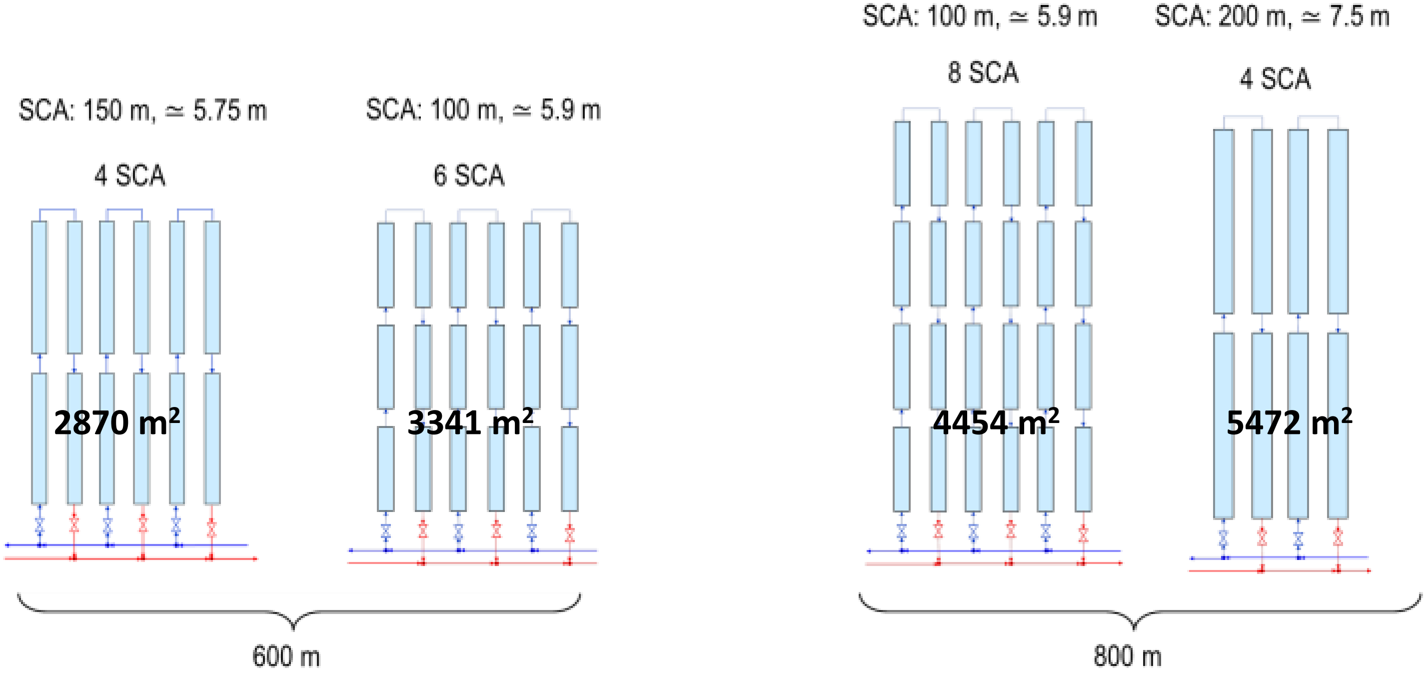

- With molten salt with a temperature range of 290÷550°C, we need at least 600 m

Solar field efficiency

- 6 SCA, T in = 290, Tout = 550°C

$$P \approx F \cdot Cp \cdot (T_{fin} - T_{in})$$

$$P_{SF} = SF_{area} \cdot DNI_{des} \cdot \eta_{SF}$$

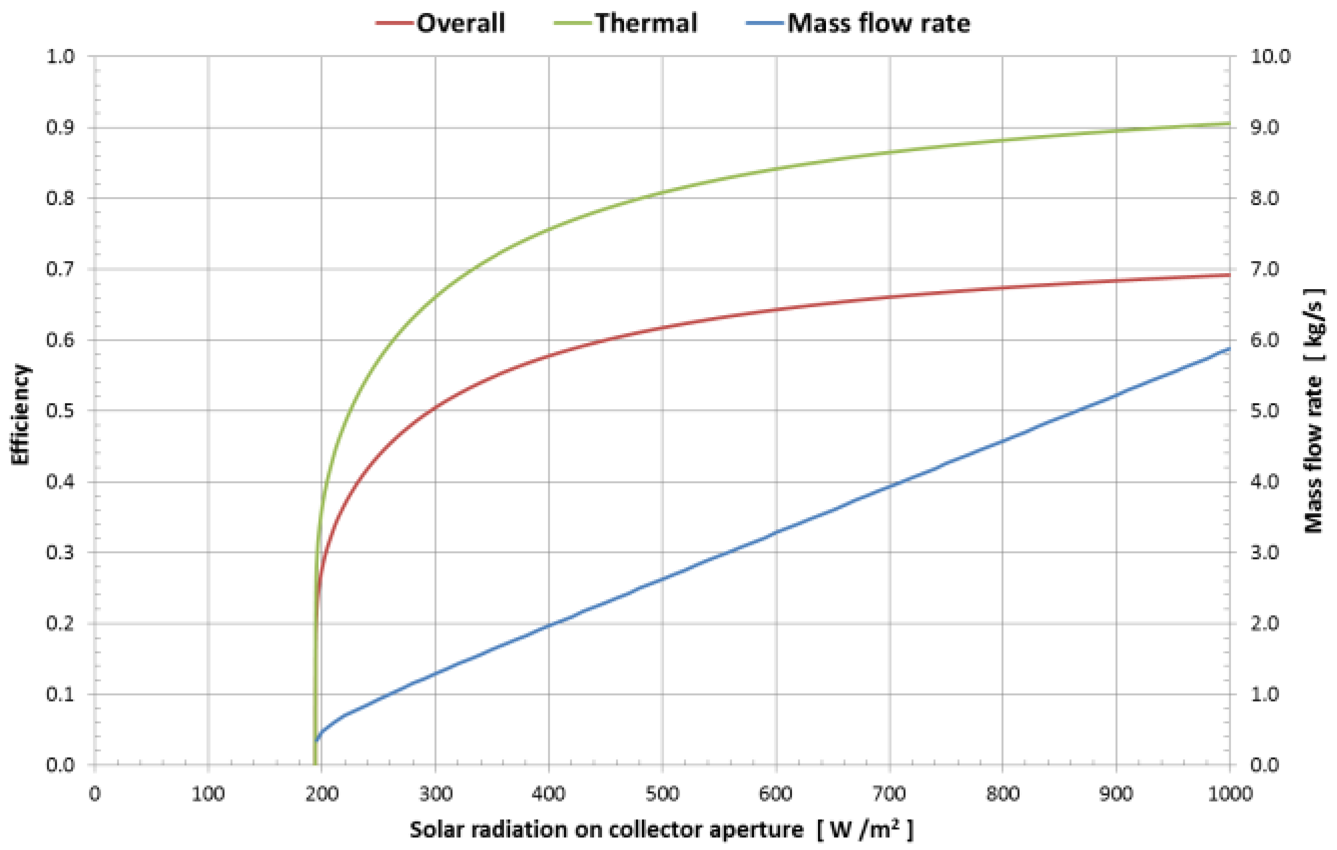

P: thermal power [W_t]
F: flow [kg/s]

Solar field efficiency

- 6 SCA, T in = 290, Tout = 550°C

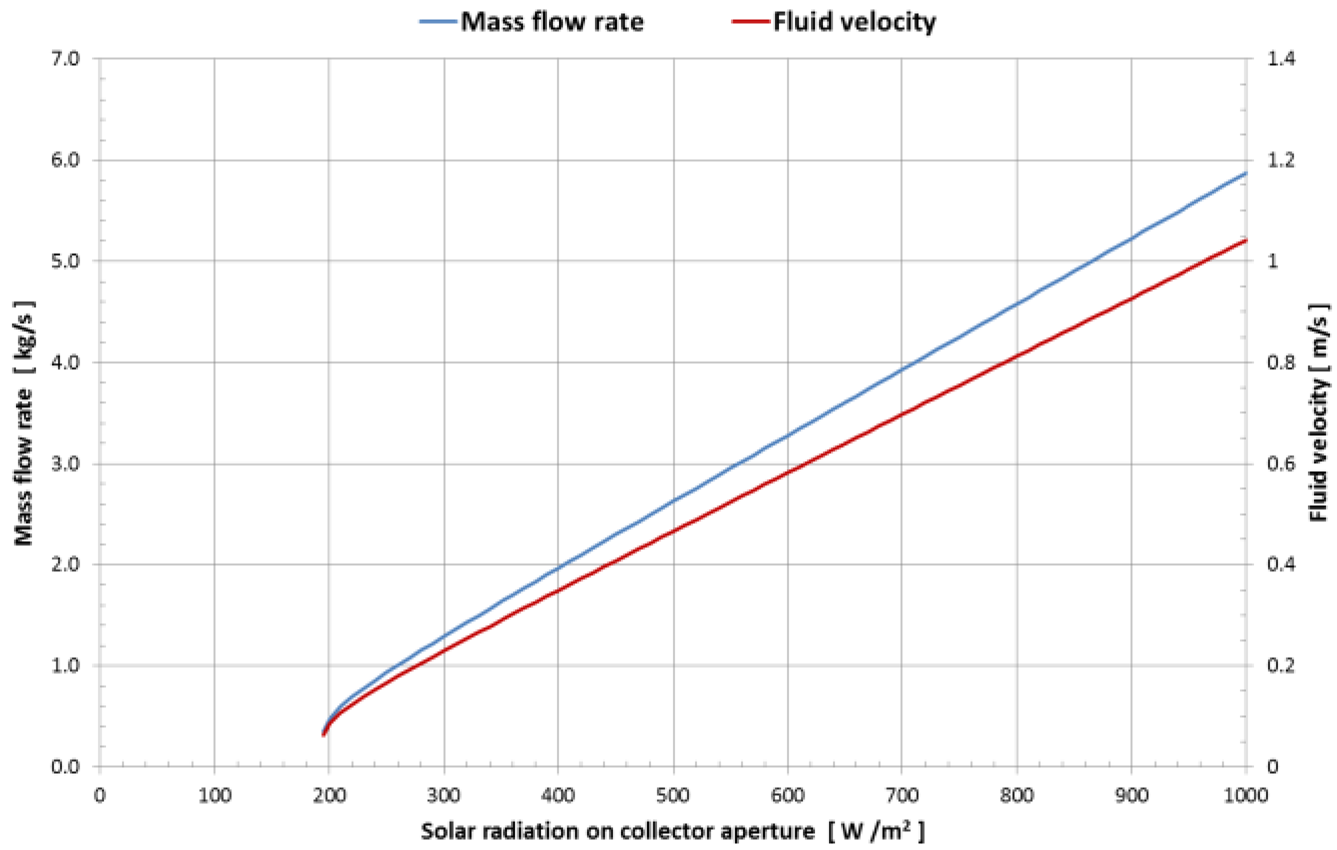

Solar field efficiency

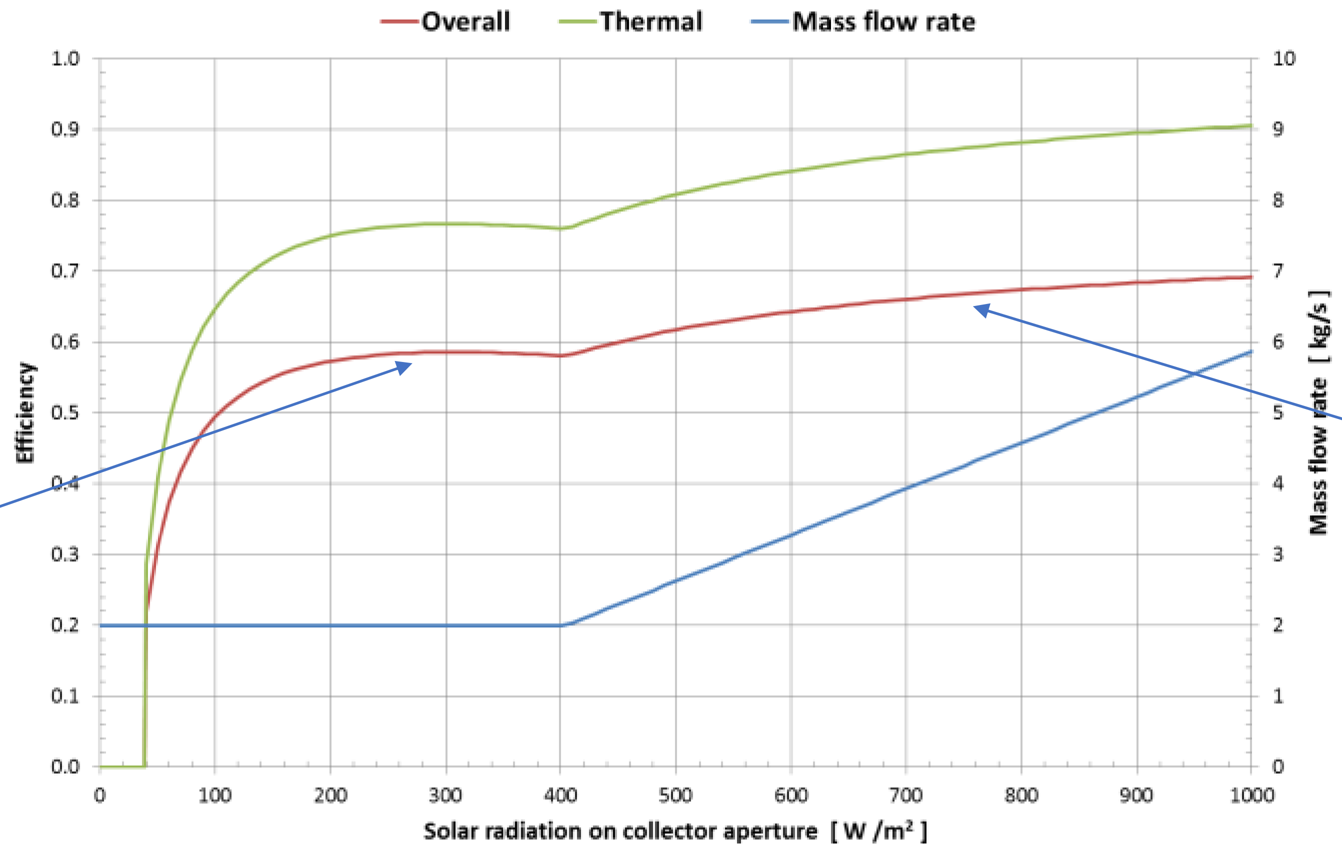

Outlet temperature decreases with the decrease of DNI.

Outlet temperature remains constant with the decrease of the mass flow.

Solar field efficiency

- 6 SCA, T in = 290, Tout = 550°C

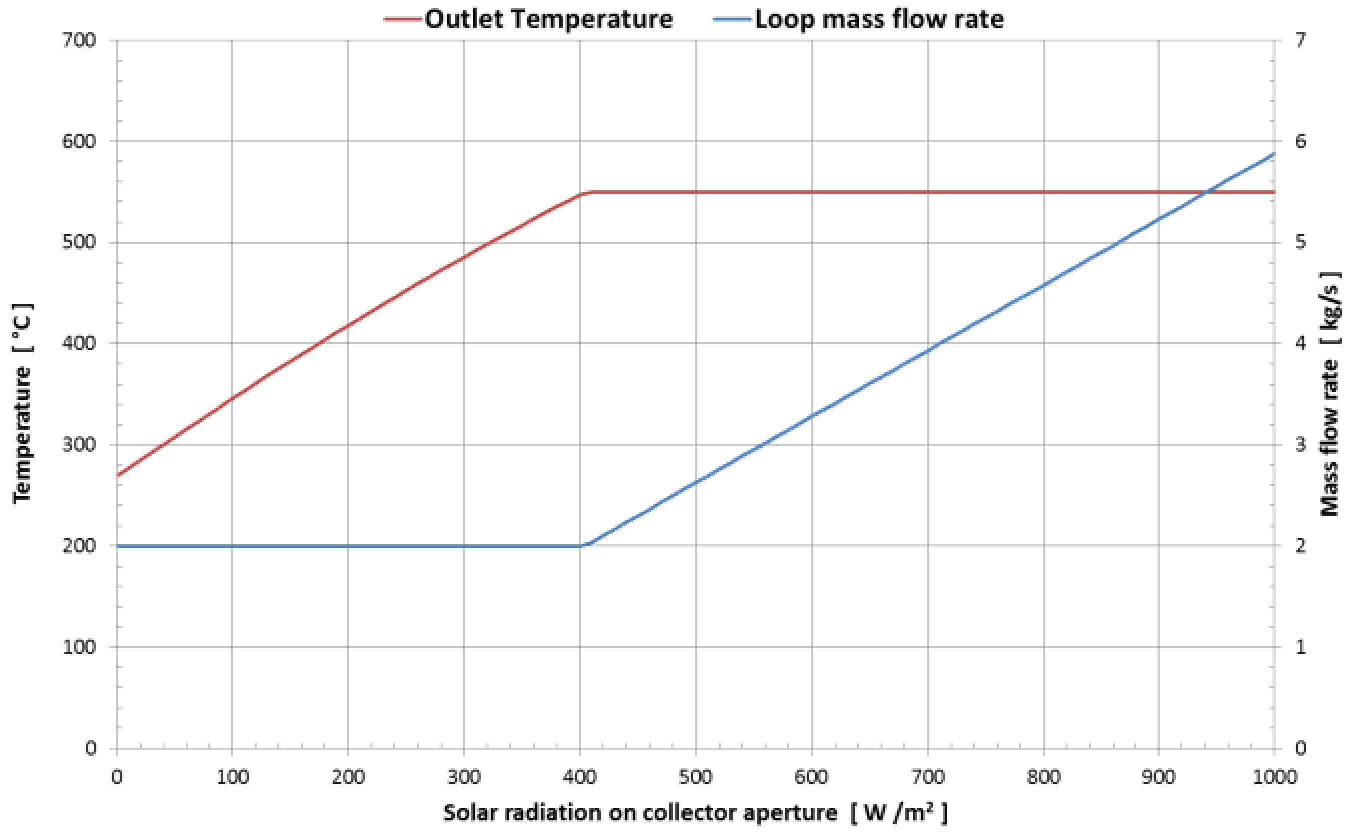

Solar field efficiency

- Increasing the length of the loop, extends the operation at nominal temperature

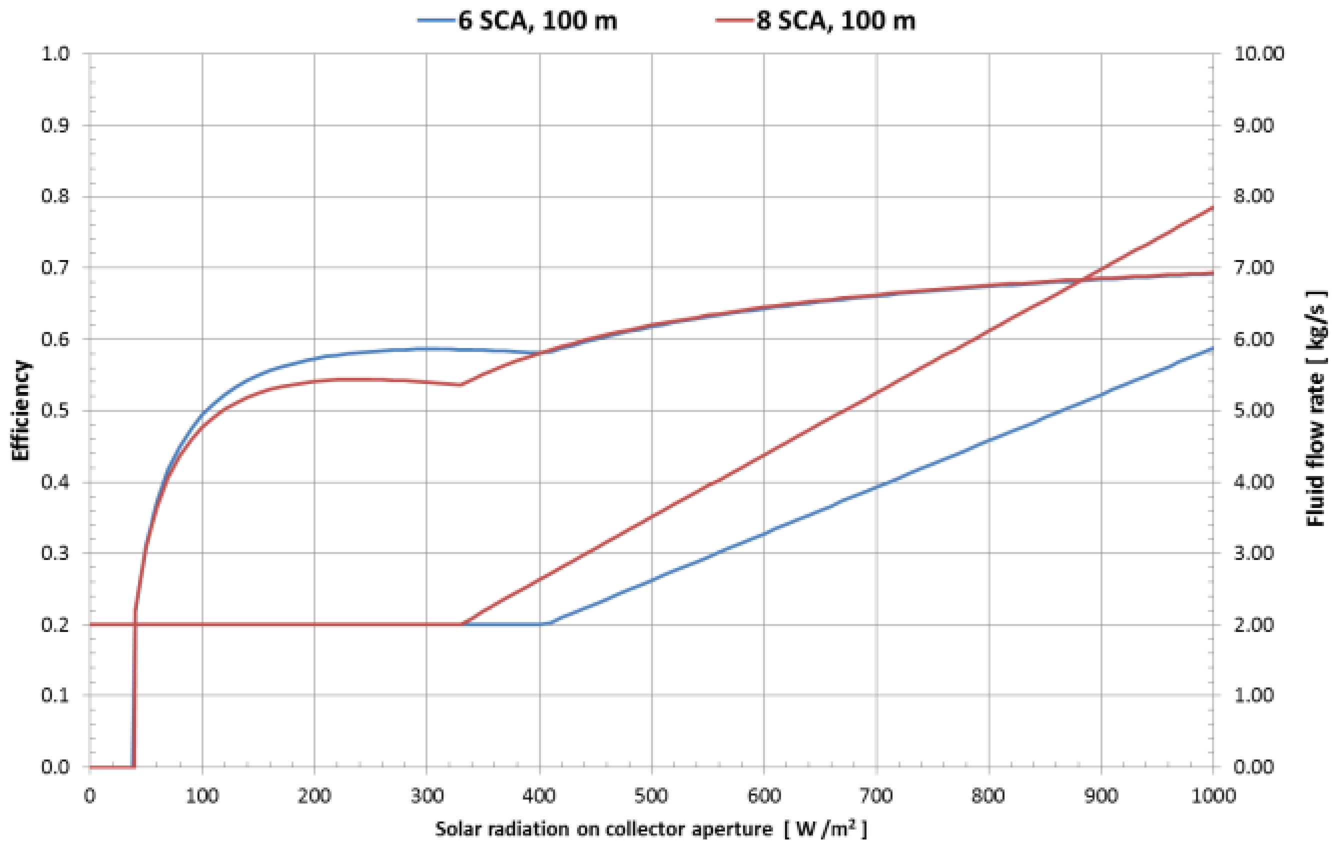

Solar field efficiency

- Increasing the length of the loop, extends the operation at nominal temperature

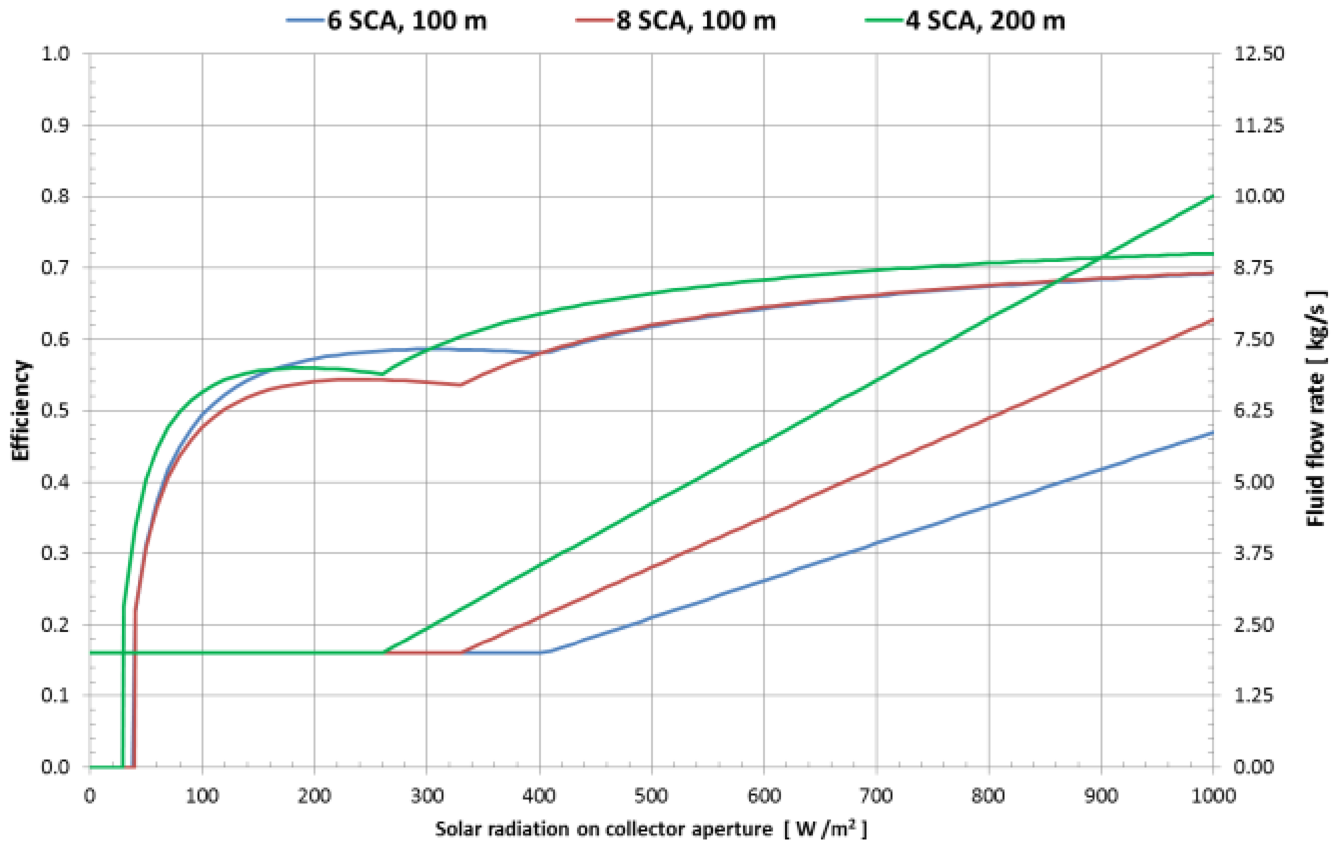

Solar field efficiency

- Increasing the length of the loop, extends the operation at nominal temperature

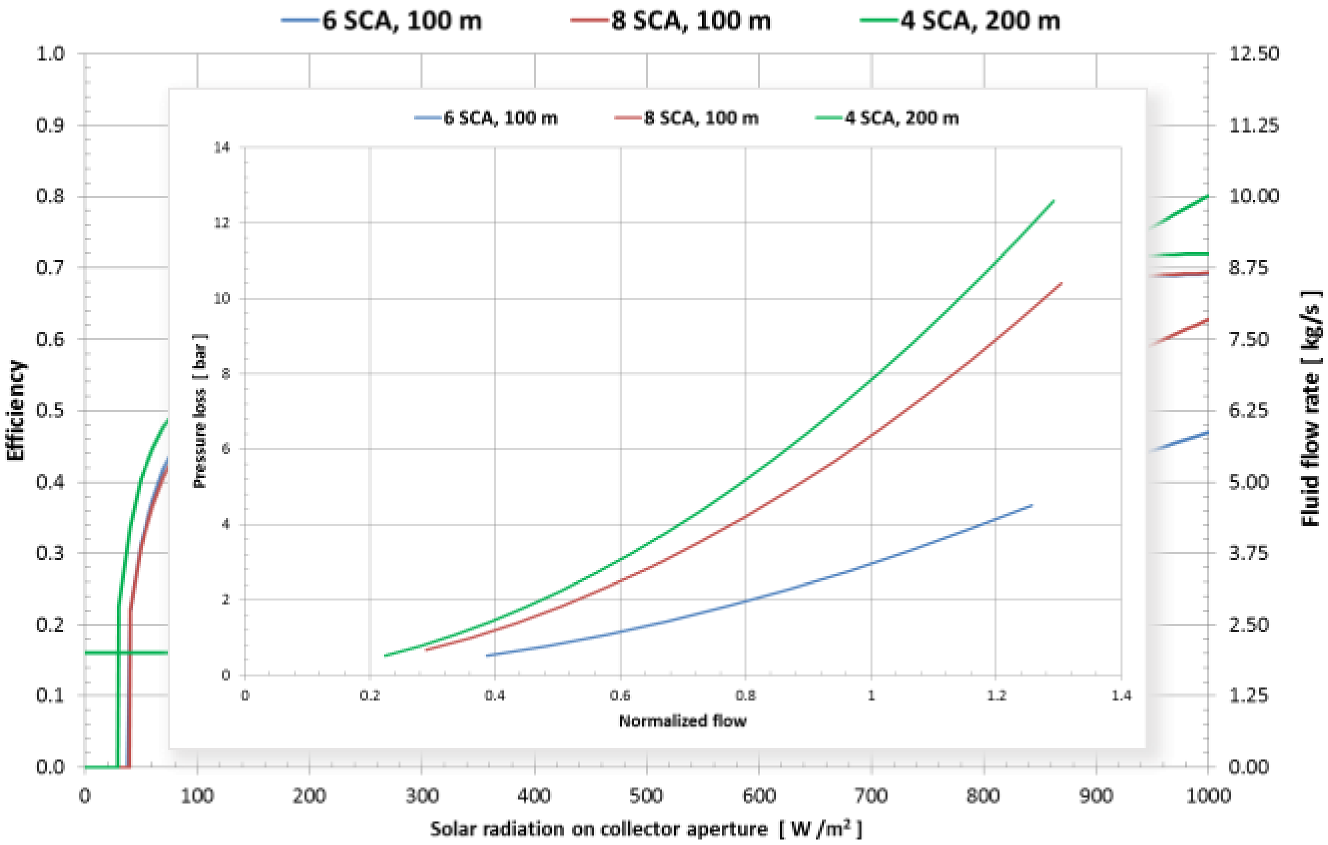

Solar field sizing

Solar multiple

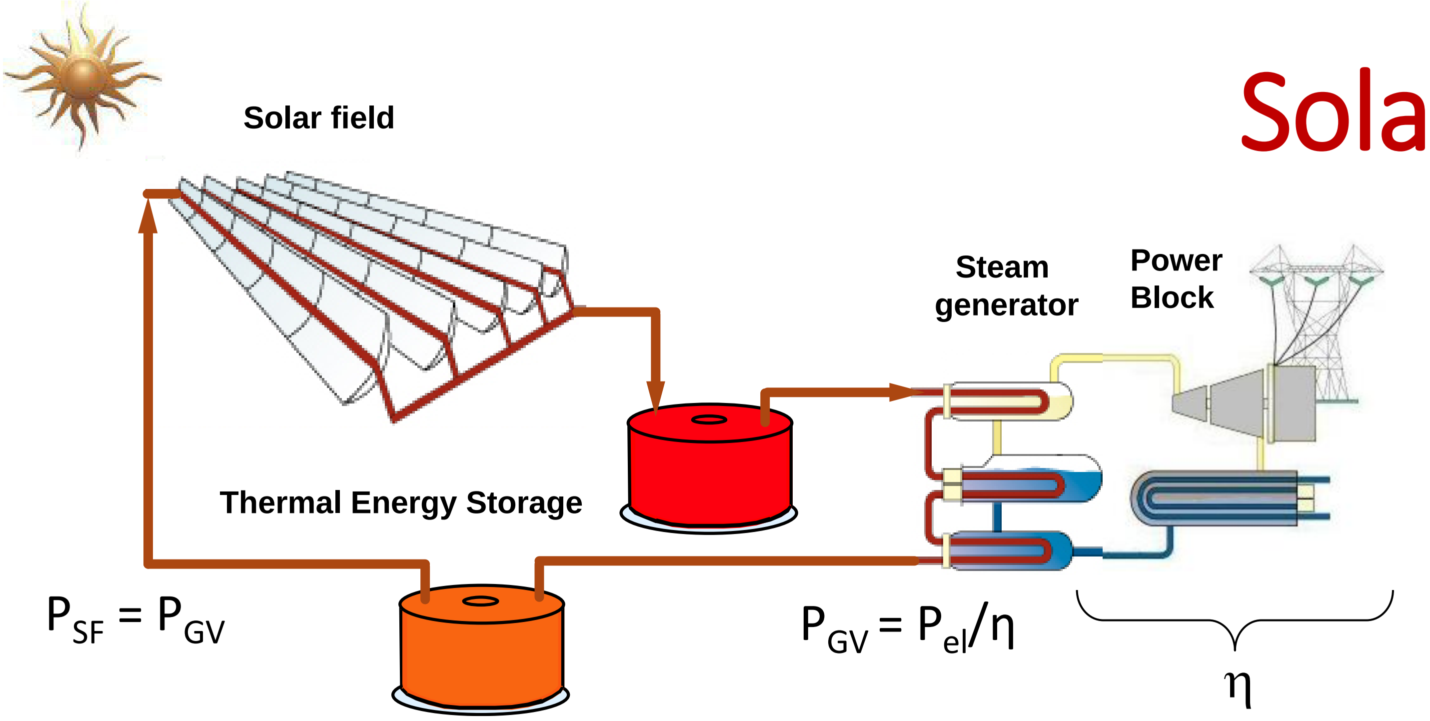

$P_{SF} = P_{GV}$

$P_{GV} = P_{el}/\eta$

$P_{SF} = SF_{area}\ DNI_{des} \cdot \eta_{SF}\ /\ SM$

SM = Solar Multiple

SM depends on the TES capacity (Full load hours of TES), and on location

for TES capacity of 6÷8 h SM 2 ÷ 2.5

Solar field sizing

The solar field size should be evaluated by an optimization analysis which minimize the cost of energy.

Full load hours of TES = 7 h

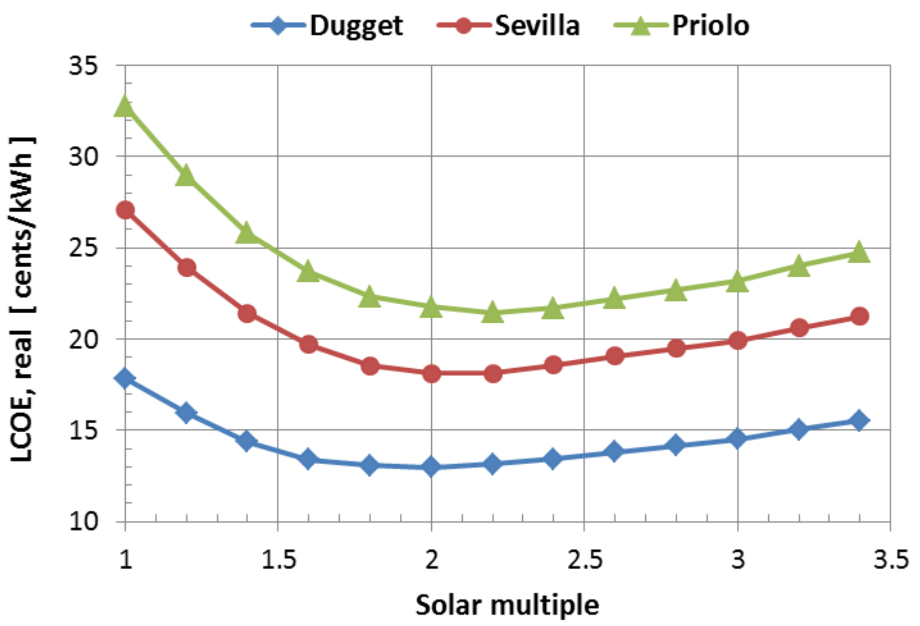

- Dugget: 2791 kWh/m^2
- Sevilla : 2090 kWh/m^2
- Priolo : 1936 kWh/m^2

SAM 2015.1.30

Solar field sizing

The solar field size should be evaluated by an optimization analysis which minimize the cost of energy.

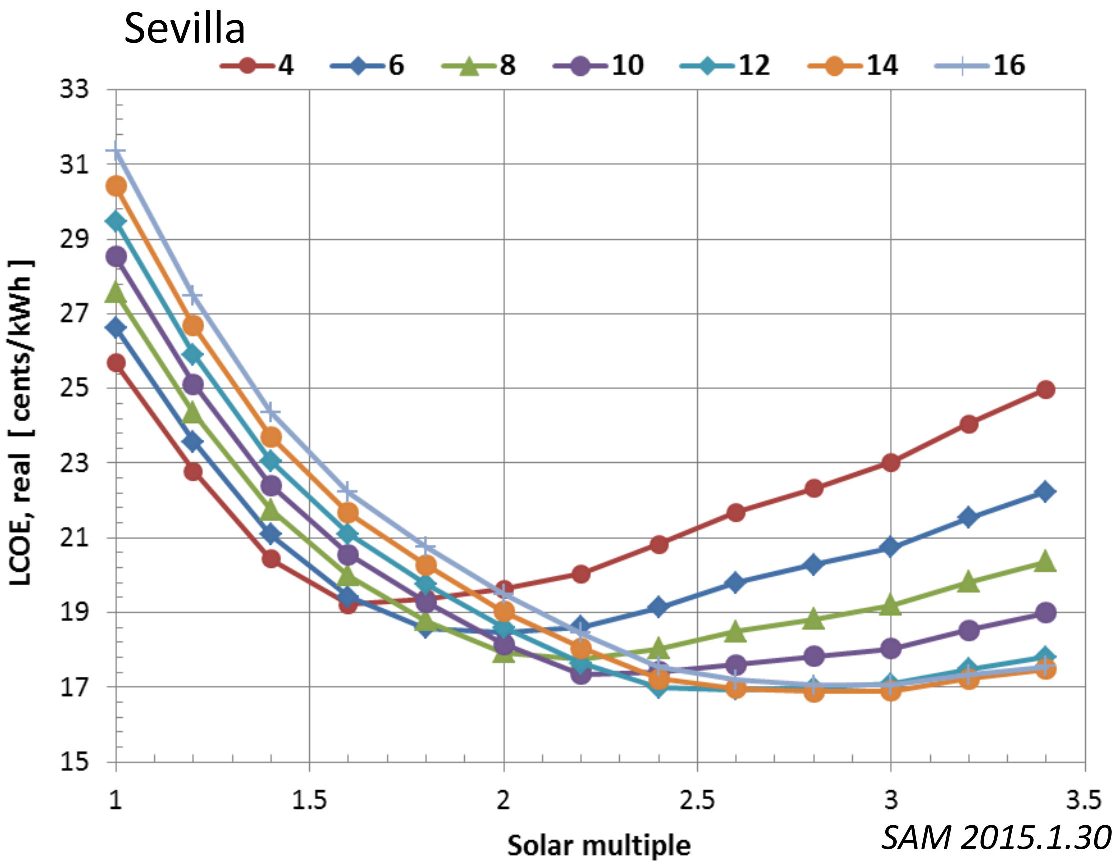

Solar field sizing

P_{el} = 50 MWe η_{el} = 0.41   8 SCA/loop A_{loop} = 4454 m^2 DNI_{des} = 800 W/m^2

TES = 7 h => 854 MWh η_{SF} = 0.675

SM = 2

$$A_{SF} = \frac{P_{el} / \eta_{el}}{DNI_{des} \cdot \eta_{SF}} = 225926\, m^2$$

$$N_{loop} = \frac{A_{SF}}{A_{loop}} = 50.7 = 51 \cdot 2 = 102$$

$$A_{SF} = 454308\, m^2$$

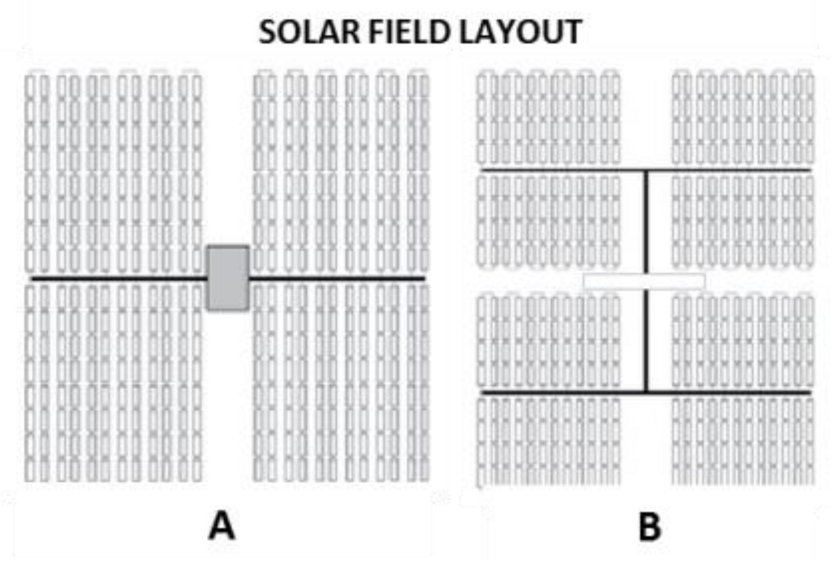

A

$$N_{loop/block} = 102/4 = 25.5 = 26$$

$$N_{loop} = 26 \cdot 4 = 104 \qquad N_{SCA} = 832$$

B

$$N_{loop/block} = 102/8 = 12.75 = 13$$

$$N_{loop} = 13 \cdot 8 = 104 \qquad N_{SCA} = 832$$

$$A_{SF} = 463258\, m^2$$

Thermal Energy Storage tanks sizing

For each MW to the steam generator, the fluid mass flow rate from the hot tank is:

$$m_{GV} = \frac{1000}{C_p(T_m) \times \Delta T} \text{ [kg/s]}$$

- T_m = (290+550)/2 = 420°C
- $C_p(T_m)$ = 1.515 kJ /(kg °C)
- ΔT = 550-290 = 260°C

Then for each MWh of energy to the steam generator, the volume of fluid transferred from the hot tank to the cold tank is:

$$V_1 = \frac{m_{GV} \times 3600}{\rho(550°C)} = 5.25 \ m^3$$

- $\rho(550°C)$ = 1740 kg/m^3

In this way we can calculate the volume of the fluid in the hot storage tank to have the TES capacity expected:

V_{TES} = $TES_{capacity}$ x V_1 = 854 MWh x 5.25 m^3/MWh = **4483** m^3

854 MWh x 14.42 m^3/MWh = **12315** m^3

Thermal Energy Storage tanks sizing

The real volume of the hot tank (and of the fluid) will be greater of V_{TES} :

- there is a minimum operating level, H_1, that depends on the pump suction head
- there is an upper level, H_2, to mitigate liquid sloshing

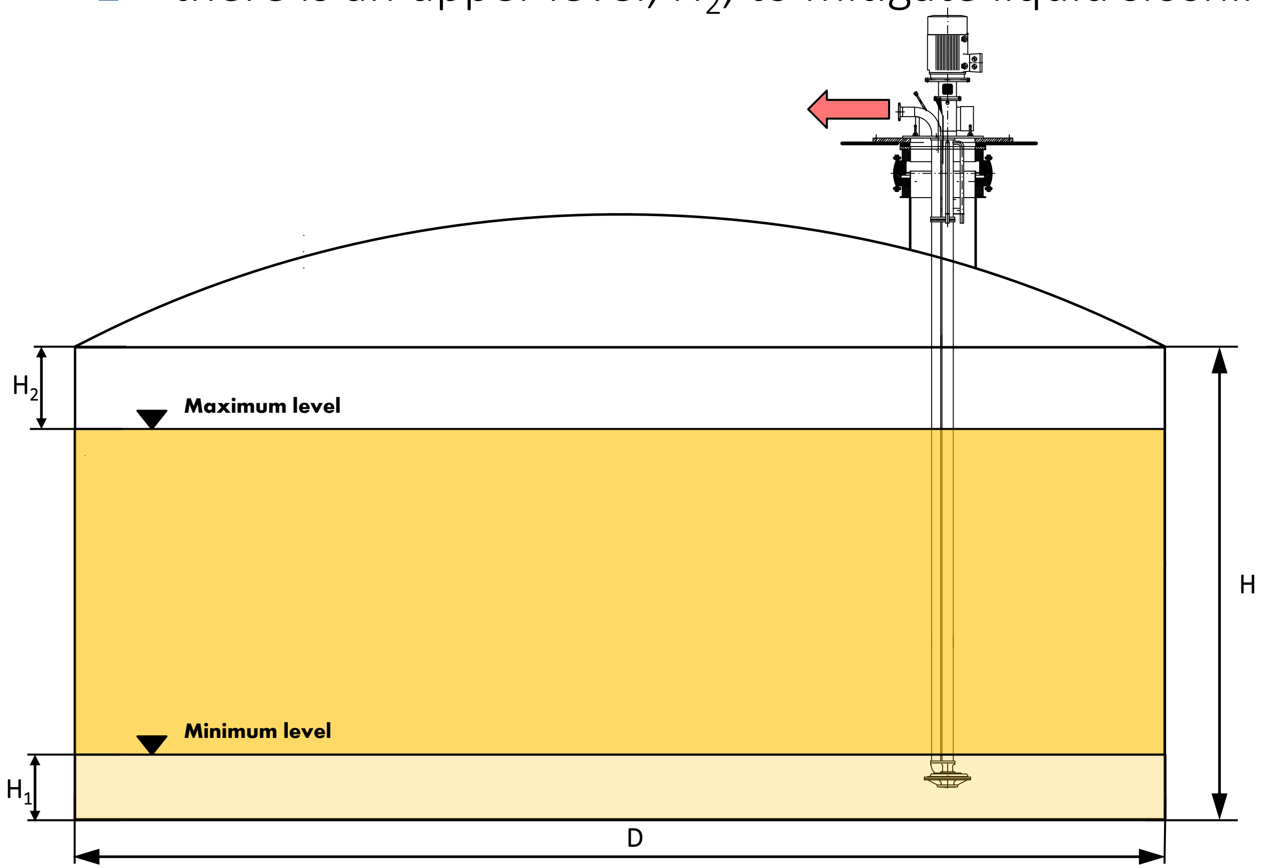

- $H_1 \lesssim 1$ m (0.75 m)
- $H_2 \simeq 1$ m

$$V_{TES} = \frac{D^2 \times \pi}{4} \times (H - H_1 - H_2)$$

H = 12 m D ≃ 23.6 m

H = 10 m D ≃ 26.3 m

H = 8 m D ≃ 30.2 m

Thermal Energy Storage tanks sizing

- there is a minimum operating level, H_1, that depends on the pump suction head

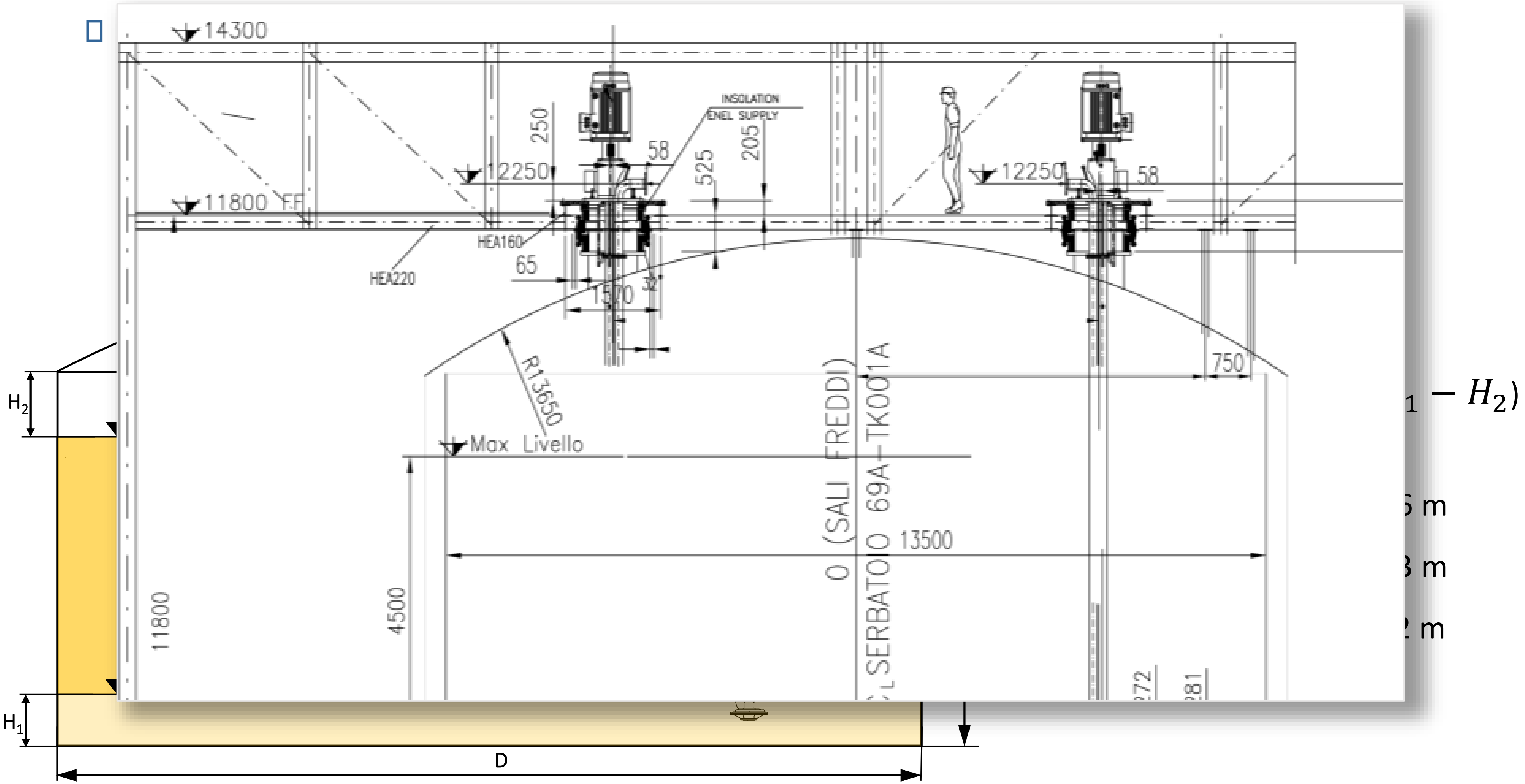

Thermal Energy Storage tanks sizing

To calculate the volume of the cold tank we have to consider that, initially, this will contain all the fluid in the system: solar field, piping and steam generator, TES system:

- $V_{solar\ field} = V_{loop} \times N_{loop} = 2.8 \times 104 = \mathbf{291}\ m^3$
- $V_{piping} = 1.4 \cdot V_{solar\ field} = \mathbf{436}\ m^3$ (estimated from a 152 loop solar field)
- $V_{SG} \simeq \mathbf{61}\ m^3$ (estimated from Archimede SG: 0.5 m^3/MW)
- $V_{CT} = V_{solar\ field} + V_{piping} + V_{SG} + (V_{TES} + V_{min}) \dfrac{\rho(550°C)}{\rho(290°C)} + V_{min} =$
- $291 + 436 + 61 + (4483 + 407)\ \ 0.913 + 407 = 5601\ m^3$

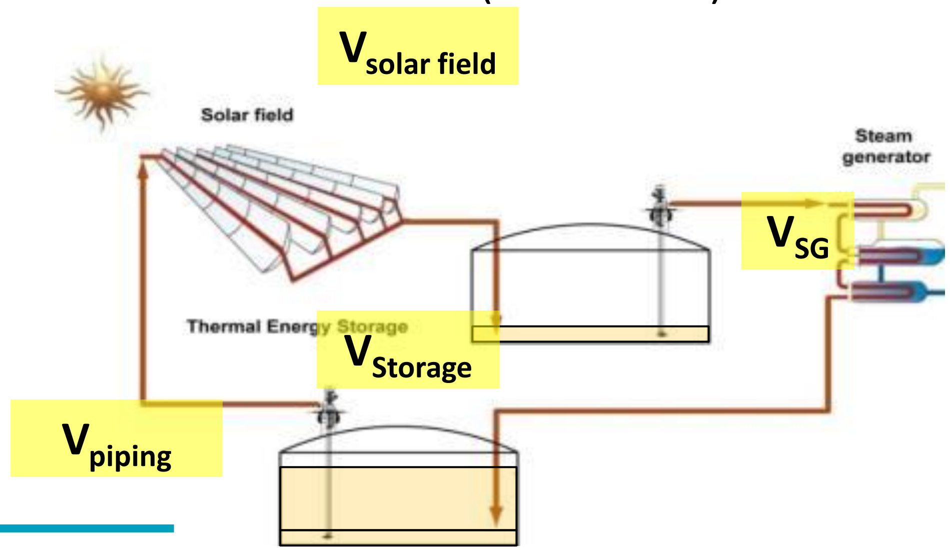

$H = 10$ m, $H_1 = 0.75$ m, $H_2 = 1$ m

$D = 26.3$ m

The total fluid volume is:

$V_{liq} = \mathbf{5601}\ m^3$ $\quad M_{salt} = 10672$ t

$H_{liq} = 10.3$ m => $H = 11.3$ m

$H_{liq} = 9$ m => $D_{cold} = 28.3$ m

$V_{liq} = \mathbf{5665}\ m^3$ $\quad M_{salt} = 10795$ t

Tank temperture, stored energy

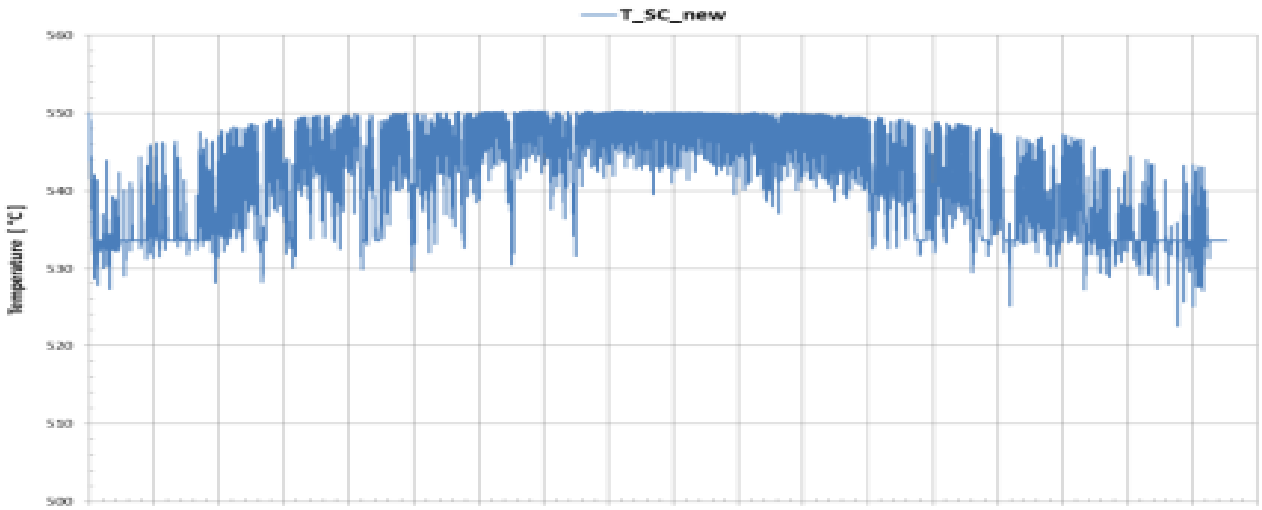

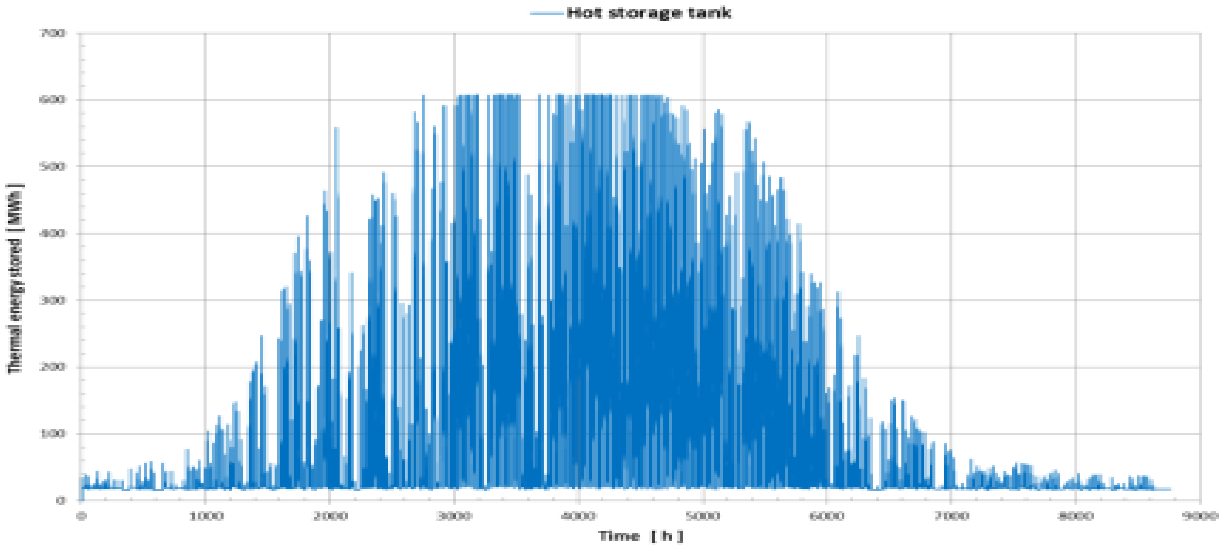

Capacity factor

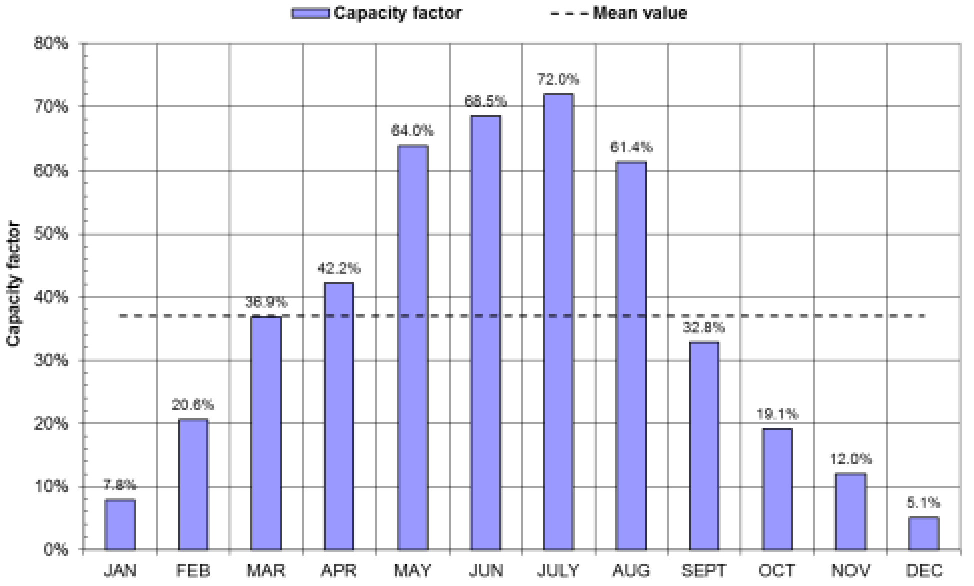

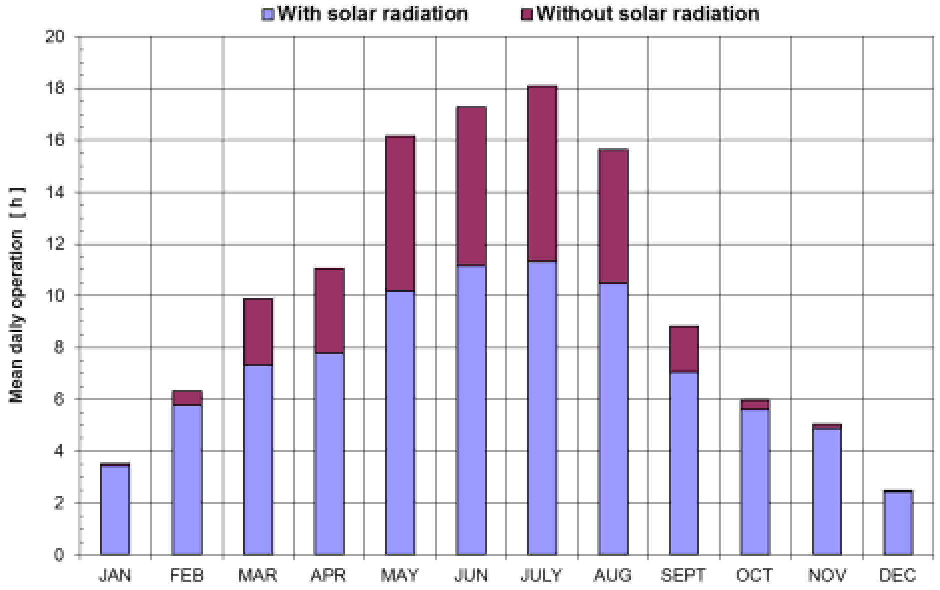

Thermal power distribution

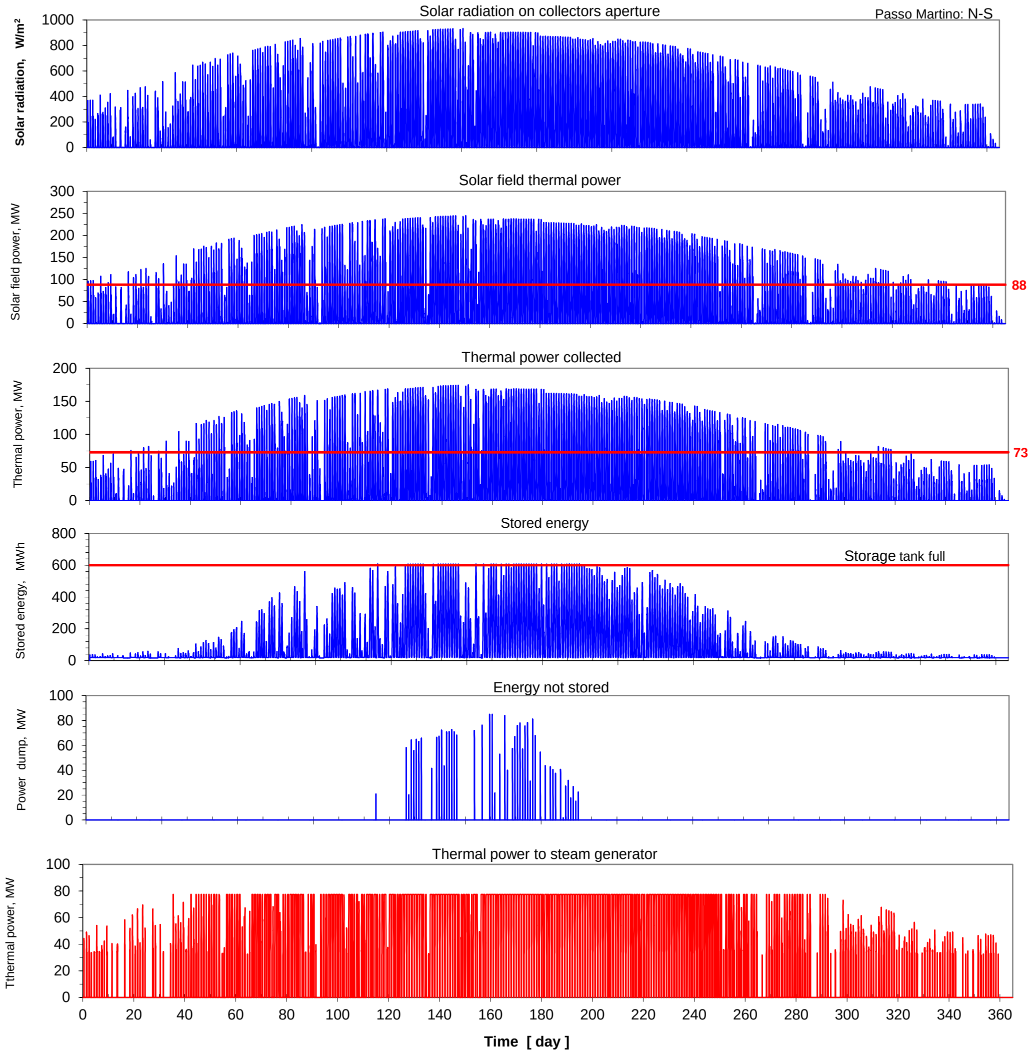

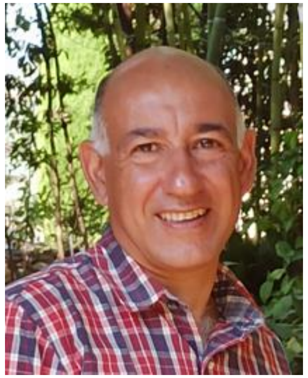

Raffaele LIBERATORE
ENEA
TERIN-STSN-SCIS
raffaele.liberatore@enea.it

THANK YOU FOR YOUR ATTENTION!
ANY QUESTIONS?